Contents

**Elliptic Functions of the Worst Kind: Non-linear Quantisation
of the Classical Spherical Pendulum**

John W. Perram and Edgar R. Smith

**Theoretical NMR $^nJ(^{13}C,^{13}C)$ Scalar Couplings as Probes to Study
Diamagnetic Ring Currents in Fullerenes**   **127**

Rubén H. Contreras, Juan E. Peralta, Verónica Barone
and Gustavo E. Scuseria

**The Dipole Polarizability of F^- in Aqueous Solution. A Sequential
Monte Carlo/Quantum Mechanics Study**   **141**

Sylvio Canuto, Kaline Coutinho and Prasanta K. Mukherjee

**In Search for the Negative Polarizability States – the EF $^1\Sigma_g^+$ State
of Hydrogen Molecule**   **151**

Jacek Komasa

The Rotational g Tensor of HF, H$_2$O, NH$_3$, and CH$_4$: A Comparison of Correlated Ab Initio Methods

Stephan P. A. Sauer

Contributors

Numbers in parentheses indicate the pages where the authors' contributions can be found.

S. Ajith Perera (435), Quantum Theory Project, University of Florida, Gainesville, FL 32611-8435, USA

Gustavo A. Aucar (161), Department of Physics, University of Northeastern, Av. Libertad 5500, W 3404 AAS Corrientes, Argentina

Verónica Barone (127), Department of Chemistry, Rice University, Houston, TX 77005-1892, USA

Rodney J. Bartlett (435), Quantum Theory Project, University of Florida, Gainesville, FL 32611-8435, USA

Zsolt Bihary (23), Department of Chemistry, Northwestern University, Evanston, IL 60208, USA

Remigio Cabrera-Trujillo (47, 335), Departments of Physics and Chemistry, University of Florida, Gainesville, FL, 32611-8435, USA

Sylvio Canuto (141), Instituto de Física, Universidade de São Paulo, CP 66318, 05315-970, São Paulo, SP, Brazil

Miguel Carvajal (209), Departamento de Fisica Aplicada, Facultad de Ciencias Experimentales, Avda. de las FF.AA. s/n, Universidad de Huelva, 21071, Huelva, Spain

Rubén H. Contreras (127), Department of Physics, FCEyN, University of Buenos Aires and CONICET, Buenos Aires, Argentina

Kaline Coutinho (141), Instituto de Física, Universidade de São Paulo, CP 66318, 05315-970, São Paulo, SP, Brazil

S. A. Cruz (335), Departamento de Fisica, Universidad Autonoma Metropolitana, Iztapalapa, Apdo. Postal 55-534, 09340, Mexico, D. F., Mexico

Erik Deumens (47), Departments of Physics and Chemistry, University of Florida, Gainesville, FL, USA

Geerd H. F. Diercksen (59), Max-Planck-Institut für Astrophysik, Karl-Schwarzschild-Straße 1, D-85741 Garching, Germany

Frank E. Harris (407), Department of Physics, University of Utah, Salt Lake City, UT, USA; Quantum Theory Project, University of Florida, Gainesville, FL, USA

Christof Hättig (9), Forschungszentrum Karlsruhe, Institute of Nanotechnology, P.O. Box 3640, D-76021 Karlsruhe, Germany

Per Jensen (209), FB C – Theoretische Chemie, Bergische Universität, D-42097 Wuppertal, Germany

Hans Jørgen Aa. Jensen (319), Department of Chemistry, University of Southern Denmark, Campusvej 55, DK-5230 Odense M, Denmark

Poul Jørgensen (9), Department of Chemistry, University of Århus, DK-8000 Århus C, Denmark

Mariusz Klobukowski (59), Department of Chemistry, University of Alberta, Edmonton, Alta., Canada T6G 2G2

Jacek Komasa (151), Department of Chemistry, A. Mickiewicz University, Grunwaldzka 6, 60-780 Poznań, Poland

Hai Lin (209), Department of Chemistry, University of Minnesota, 207 Pleasant Street SE, Minneapolis, MN 55455, USA

Jan Linderberg (1), Department of Chemistry, Aarhus University, Aarhus, Denmark

John M. H. Lo (59), Department of Chemistry, University of Alberta, Edmonton, Alta., Canada T6G 2G2

Hendrik J. Monkhorst (35), Quantum Theory project, University of Florida, Gainesville, FL 32611-8435, USA

Prasanta K. Mukherjee (141), Instituto de Física, Universidade de São Paulo, CP 66318, 05315-970, São Paulo, SP, Brazil; Department of Spectroscopy, Indian Association for the Cultivation of Science, Jadavpur, Kolkata 700 032, India

Lene B. Oddershede (xvii), The Niels Bohr Institute, Blegdamsvej 17, Copenhagen Ø, Denmark

J. Oddershede (253), Syddansk Universitet, Campusvej 55, DK-5230 Odense M, Denmark

Yngve Öhrn (47), Departments of Physics and Chemistry, University of Florida, Gainesville, FL, USA

John F. Ogilvie (253, 319), Escuela de Quimica, Universidad de Costa Rica, San Pedro de Montes de Oca, San Jose 2060, Costa Rica

Ivana Paidarová (185), J. Heyrovský Institute of Physical Chemistry, Academy of Sciences of the Czech Republic, Dolejškova 3, Prague 8, 182 23 Czech Republic

Filip Pawłowski (9), Department of Chemistry, University of Århus, DK-8000 Århus C, Denmark

Juan E. Peralta (127), Department of Chemistry, Rice University, Houston, TX 77005-1892, USA

John W. Perram (111), The Maersk Mc-Kinney Moller Institute for Production Technology, University of Southern Denmark, Odense, Denmark

Patricio F. Provasi (161), Department of Physics, University of Northeastern, Av. Libertad 5500, W 3404 AAS Corrientes, Argentina

Juraj Raab (421), Department of Theoretical Chemistry, Chemical Center, P.O. Box 124, S-221 00 Lund, Sweden

Mark A. Ratner (23), Department of Chemistry, Northwestern University, Evanston, IL 60208, USA

Björn O. Roos (421), Department of Theoretical Chemistry, Chemical Center, P.O. Box 124, S-221 00 Lund, Sweden

John R. Sabin (xvii, 47), Departments of Physics and Chemistry, University of Florida, Gainesville, FL, USA; Kemisk Institut, Syddansk Universitet, Odense, Denmark

Marina Sanchez (161), Department of Physics, University of Northeastern, Av. Libertad 5500, W 3404 AAS Corrientes, Argentina

Trond Saue (383), UMR 7751 CNRS/Université Louis Pasteur, Laboratoire de Chimie Quantique et de Modélisation Moléculaire, 4 rue Blaise Pascal, 67000 Strasbourg, France

Stephan P. A. Sauer (161, 185, 319, 469), Department of Chemistry, University of Copenhagen, Universitetsparken 5, DK-2100 København Ø, Denmark

Gustavo E. Scuseria (127), Department of Chemistry, Rice University, Houston, TX 77005-1892, USA

Peter Sigmund (91), Department of Physics, University of Southern Denmark, DK-5230 Odense M, Denmark

Jack Simons (239), Chemistry Department, Henry Eyring Center for Theoretical Chemistry, University of Utah, Salt Lake City, UT 84112, USA

Piotr Skurski (239), Chemistry Department, Henry Eyring Center for Theoretical Chemistry, University of Utah, Salt Lake City, UT 84112, USA; Department of Chemistry, University of Gdansk, 80-952 Gdansk, Poland

Edgar R. Smith (111), School of Mathematics, La Trobe University, Bundoora, Australia

Vedene H. Smith Jr. (407), Department of Chemistry, Queen's University, Kingston, Ont., Canada

Monika Sobczyk (239), Chemistry Department, Henry Eyring Center for Theoretical Chemistry, University of Utah, Salt Lake City, UT 84112, USA; Department of Chemistry, University of Gdansk, 80-952 Gdansk, Poland

J. Soullard (335), Instituto de Fisica, UNAM, Apdo. Postal 20-364, 01000, Mexico, D. F., Mexico

Walter Thiel (209), Max-Planck-Institut für Kohlenforschung, Kaiser-Wilhelm-Platz 1, D-45470 Mülheim an der Ruhr, Germany

Lucas Visscher (369), Theoretical Chemistry Section, Faculty of Sciences, Vrije Universiteit Amsterdam, 1081 HV Amsterdam, The Netherlands

Sergei N. Yurchenko (209), Max-Planck-Institut für Kohlenforschung, Kaiser-Wilhelm-Platz 1, D-45470 Mülheim an der Ruhr, Germany

Jens Oddershede – Adventurer in Quantum Chemistry

Lene B. Oddershede[1] and John R. Sabin[2,3]

[1]*The Niels Bohr Institute, Blegdamsvej 17, Copenhagen Ø, Denmark*
[2]*Department of Physics, University of Florida, Gainesville, FL, USA*
[3]*Kemisk Institut, Syddansk Universitet, Odense, Denmark*

Contents

1. DEDICATION

It is appropriate that this volume is named Jens Oddershede – Adventurer in Quantum Chemistry, as Jens has always viewed his sojourn through quantum chemistry as an adventure rather than a job. His enthusiasm for, and dedication to, good and interesting science has been an inspiration to all of us who have worked together with him over the years.

This volume is made up of contributions from Jens' friends and collaborators, all of whom have benefited from interaction with him. Most of the names of the senior authors of these chapters appear as well on the list of Jens' publications which follows this piece.

Rather than grouping chapters according to subject matter, the chapters in this volume are ordered according to when Jens first published with the author of the chapter. (You are left to sort out the details of contributions bearing the names of several of Jens' earlier collaborators!)

For all of us, it is a pleasure and an honor to contribute to this volume which is published to celebrate Jens' 60th birthday. May the coming years be equally as full of adventure as the first 60 have been.

2. BIOGRAPHY

Jens Oddershede grew up on the country side in the province of Thy, northwestern Denmark. As the oldest son it would have been natural for him to overtake/inherit the family farm in Kåstrup, however, Jens preferred to do chemistry experiments in the attic rather than participating in the farm life (by all accounts, it was only by extraordinary luck that the house survived). Therefore, after having completed

gymnasium in Thisted, he started his scientific career at Århus University as a student of physics and chemistry. The thesis for his Cand. Scient. degree was done in quantum chemistry in the newly established group headed by Prof. Jan Linderberg. The thesis ended up as a publication together with Jan Linderberg (#1 in the list of publications, following) entitled 'First Order Calculations of Spin Densities in ClO_4^{2-} and ClO_4.' This was to be the first of nearly 170 publications by Jens and his collaborators so far. It was in Århus that he met many of the people that would play a significant role in his future scientific life, as well as where he first developed, together with Poul Jørgensen and Jan Linderberg, the polarization propagator approximation for response properties of molecules that has played a central role in Jens' scientific life for the past 30 years.

While at Århus, Jens spent two years from 1971–1973 at the University of Utah with Prof. Frank Harris' group, where he worked on the problem of describing metallic hydrogen using a Hartree–Fock methodology. He then returned to Århus and continued his collaboration with Poul Jørgensen on propagator methods. He completed his Dr. Scient. degree in 1978 at Århus University with a dissertation entitled 'Polarization propagator calculations'.

In 1977, Jens moved to Odense University (since 1998 called the University of Southern Denmark), where he became a Lector (Associate Professor) of chemistry. At this time he began a collaboration with Prof. Geerd H. F. Diercksen at the Max-Planck-Institute für Astrophysik. This collaboration resulted in the adding the capability of polarization propagator calculations to the **MUNICH** system of programs; a powerful general molecular electronic structure program. Jens also visited the University of Florida's Quantum Theory project during these years. He was made Adjunct Professor of Chemistry at the University of Florida in 1984, and continues this affiliation today.

Jens Oddershede was appointed Professor of Chemistry at Odense University in 1988, and remains so. In 1992, he supplemented his scientific career with administrative tasks when he became Dean of Science, which, however, did not keep him from being active in Science. In 2001, he was elected Rector (President) of the University of Southern Denmark, a position which he continues to serve. However, he is still an active participant in theoretical chemistry and presently among the most cited scientists at the University of Southern Denmark.

3. SCIENCE

When Jens Oddershede was elected a Fellow of the American Physical Society in 1993, the citation read 'For contribution to the theory, computation, and understanding of molecular response properties, especially through the elucidation implementation of the Polarization Propagator formalism.' Although written more than a decade ago, it is still true today. The common thread that has run through Jens' work for the past score of years is development of theoretical methods for studying the response properties of molecules. His primary interest has been in the development and applications of polarization propagator methods for direct calculation of electronic spectra, radiative lifetime and linear and non-linear response properties such as dynamical dipole polarizabilities and

hyperpolarizabilities, spin−spin coupling constants, nuclear magnetic shieldings and magnetizabilities, using both fully relativistic (4-component) and non-relativistic methods. Jens has also been involved in the properties of energy deposition by swift molecules in molecular targets such as the calculation of stopping powers and shell corrections. This work led him to calculations, again using the polarization propagator formalism, of moments of the dipole oscillator strength distributions such as mean excitation energies. This and various dipole and generalized oscillator strength sum rules are among his current research interests.

Considering the success with which Jens Oddershede has developed the polarization propagator formalism and applied it to calculation of various response properties, it is not surprising that his most cited paper (#44 in the list of publications) is a didactic review which lays out the polarization propagator formalism in detail. This paper is one which is necessary reading for anyone who wishes to implement the polarization propagator formalism, and that necessity is reflected in the citation count for this paper. It, along with other highly cited papers, is the result of Jens' early and lasting collaboration with Prof. Poul Jørgensen.

In his professional capacity, he is a member of the Danish Physical Society, serving as the board member of the Division of Atomic and Molecular Physics from 1980 to 1989, and as Chairman from 1987 to 1989. Jens is a member of The Danish Chemical Society where he was a board member from 1989 to 1992, and served as Chairman of the Division for Theoretical Chemistry from 1981 to 1985. He is also a member of The European Physical Society, The American Physical Society (fellow), and The Danish Natural Science Academy.

Jens has won the research prize awarded each year by Fyens Stiftstidene in 1981.

Jens Oddershede is, a member of the advisory editorial boards of Advances in Quantum Chemistry and Theoretical Chemistry Accounts, and has served on the boards of Theoretica Chemica Acta and The International Journal of Quantum Chemistry.

Outside the academy, Jens is also active. He was designated Årets Fynbo in 1996 and has been a member of more than a dozen boards of trustees.

Jens Oddershede is surely a man of many talents.

Bonding in the Perchlorate Anion and Radical

Jan Linderberg

Department of Chemistry, Aarhus University,
Aarhus, Denmark

Abstract

Electron distributions are studied in the perchlorate anion and in the radical in order to elucidate the pattern of bonding in these systems. Qualitative considerations are supplemented with numerical calculations. Comparison with other efforts supports the previously suggested interpretation of the radical as a weakly exchange coupled complex of an oxygen diatom and a chloryl radical.

Contents

1. INTRODUCTION

Paramagnetic centers in perchlorate crystals were a topic of detailed experimental investigation when Jens Oddershede begun his graduate studies at Aarhus University [1]. He (and I) found it interesting to attempt a calculation of the spin density parameter associated with the Fermi contact interaction term for the perchlorate radical, ClO_4 and a species identified as ClO_4^{2-}. The technique to be used was based on the electron propagator or Green function for the anion, which contains information on the states of the radical as well as on the doubly negative species [2]. Induced spin densities were required since neither the highest occupied nor the lowest unoccupied molecular orbital had any zeroth order amplitude on the central chlorine nucleus according to the contemporary analysis by Manne [3]. Perturbation theory of the kind used by McLachlan *et al.* [4] to derive proton spin densities in aromatic hydrocarbons gave a satisfactory result [5].

Oddershede's calculations were limited by the computational facilities and more recent calculations indicate that while Manne's ordering of the occupied molecular orbitals stays unchallenged, there is little significance to assign to virtual orbitals for an anion [6]. It was pointed out [5] that ionization from a degenerate state would lead to a distortion in the system due to the Jahn–Teller theorem.

No effort to examine this possibility was undertaken until Byberg observed a similarity between the quadrupole coupling tensors in chloryl and perchlorate radicals. The species ClO_4 could be interpreted as an exchange coupled complex of ClO_2 and O_2 [7].

Van Huis and Schaefer [8] found that ClO_4 has a minimum electronic energy structure of C_{2v} symmetry in contrast with an experimental assignment from infrared spectra by Grothe and Willner [9]. These authors arrived at C_{3v} as the appropriate symmetry group for ClO_4 in a neon matrix. The continued interest in the perchlorate radical has prompted the present small study of its electronic features and bonding characteristics.

It will be illustrated in the next section that the favored distortion of ClO_4 from a tetrahedral symmetry is in the direction towards the C_{3v} rather than the form deduced by Van Huis and Schaefer [8]. The electronic structure of the open shell is analyzed from the results of electronic structure calculation for structure with small but finite distortions in Section 3 and a different conclusion is reached. Fourthly, a juxtaposition of the findings from the previous sections supports the Van Huis–Schaefer case. Additional remarks appear in the final section.

2. MOLECULAR ORBITALS

Regular Hartree–Fock calculations within a 'triple-zeta-valence' atomic basis were performed with the program system GAMESS [10] which is freely available and gives an optimized chlorine–oxygen bond length of 1.464 Å in a tetrahedral conformation and a set of three highest occupied molecular orbitals of t_1 symmetry. These are nonbonding orbitals and are not overlapping with orbitals on the central chlorine in a basis lacking f-orbitals there. Removal of an electron will then create a degenerate state, which cannot be stable according to the Jahn–Teller theorem.

A suitable frame for the discussion places the tetrahedral molecular ion so that the two-fold rotation axes are the coordinate axes. We choose to represent the three degenerate t_1-orbitals by their f-orbital equivalents:

$$\{f_x f_y f_z\} \propto \{x(y^2 - z^2)y(z^2 - x^2)z(x^2 - y^2)\}$$

Distortions need to have their symmetry contained in the direct product $t_1 \otimes t_1 = a_1 + e + t_1 + t_2$ and we will consider only such displacements that leave the Cl–O bonds invariant. This leaves only e-type and t_2-type to be of concern. An e-deformation shortens or lengthens opposite edges of the tetrahedron and does little to split the t_1 degeneracy. The t_2 modes will be classified as d-orbitals and the perturbing potential will have the form $V = \xi V_{yz} + \eta V_{zx} + \zeta V_{xy}$ with the matrix representation

$$\langle f_x f_y f_z | V | f_x f_y f_z \rangle = \begin{bmatrix} 0 & \zeta & \eta \\ \zeta & 0 & \xi \\ \eta & \xi & \end{bmatrix} \langle f \| V \| f \rangle$$

Relative weights of the three equivalent changes are given by the coefficients and an appropriate reduced matrix element determines the magnitude of the perturbation.

The t_1 degeneracy is cancelled, to first order, by the perturbation and the orbital energy changes are determined by the eigenvalues of the matrix above. They are expressed as

$$V_j = 2\langle f\|V\|f\rangle \cos\left(\gamma + \frac{2\pi j}{3}\right); \quad j = 1, 2, 3$$

$$\xi^2 + \eta^2 + \zeta^2 = 3; \quad \cos(3\gamma) = \xi\eta\zeta.$$

where a convenient normalization is chosen. Extrema for the eigenvalues occur at $\pm\xi = \pm\eta = \pm\zeta = 1$.

'Scissoring' modes occur when two of the basic weights vanish, one edge shortens while the opposite one lengthens. 'Umbrella' modes have equal basic weights. It should be observed that there remains a two-fold degeneracy for umbrella modes and that the gradient of the energy is not analytic. The ratio of the orbital energies of the highest occupied molecular orbital in the scissoring mode to the umbrella mode is $\cos(\pi/6) = 1/2(\sqrt{3})$ or 87%.

It is the closing umbrella that causes the highest occupied molecular orbital energy level to be nondegenerate and localized on a set of three oxygens as an a_2-type, antibonding species (see Fig. 1). An opening umbrella will have a degenerate e-type molecular orbital level as the highest occupied one. Both orbitals have their main amplitude on the oxygen that defines the handle of the umbrella.

Modifications of the scissoring type concentrate the amplitude of the relevant orbital to the two oxygens that are brought closer together (see Fig. 2). Antibonding results from the increased overlap and eases the effort to remove an electron.

No localization of the t_1 orbitals takes place when e-forms of distortion are induced; the density is equally distributed over all the ligands in every one of the three orbitals. Marginal energy shifts are found.
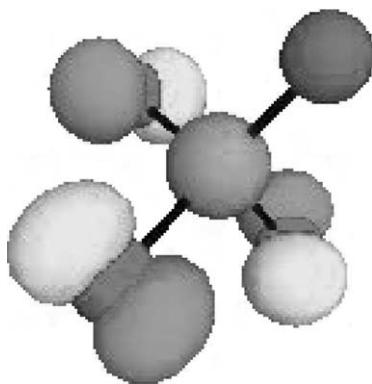
Fig. 1. The highest occupied molecular orbital for the closing umbrella mode.
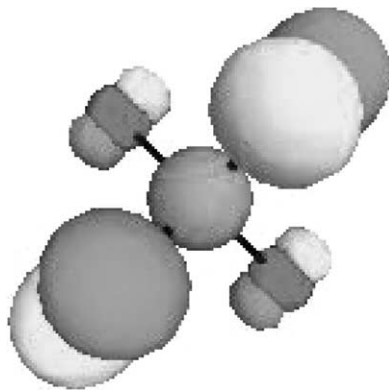
Fig. 2. The highest occupied molecular orbital for the scissoring mode.

3. FINITE DISPLACEMENTS

Infinitesimal changes of the atomic positions were analyzed above. An estimate of the magnitude of reduced matrix element $\langle f\|V\|f\rangle$ will be obtained from calculations at small, finite distortions. Table 1 presents essential data from the calculations with GAMESS [10]. Basic displacements were introduced and bond length renormalizations were effected in order to avoid stretching contributions. This process will make it more difficult to ensure that the various forms have moved an equal amount.

A measure of the distance between molecular conformations has been introduced [11] in order to gauge the amount of movement required to transform one structure into another disregarding relative translations and

Table 1. Perchlorate Hartree–Fock calculations for somewhat distorted tetrahedral conformations

Entity[a]	Closing umbrella	Opening umbrella	Closing scissoring	Opening scissoring	Tetrahedral
$R(\text{Cl–O})$	1.464 Å	1.464 Å	1.464 Å	1.464 Å	1.464 Å
$R(\text{O}_a\text{–O}_b)$	2.441 Å	2.338 Å	2.320 Å	2.458 Å	2.391 Å
$R(\text{O}_a\text{–O}_c)$	2.441 Å	2.338 Å	2.389 Å	2.389 Å	2.391 Å
$R(\text{O}_a\text{–O}_d)$	2.441 Å	2.338 Å	2.389 Å	2.389 Å	2.391 Å
$R(\text{O}_c\text{–O}_d)$	2.335 Å	2.438 Å	2.458 Å	2.320 Å	2.391 Å
$R(\text{O}_b\text{–O}_d)$	2.335 Å	2.438 Å	2.389 Å	2.389 Å	2.391 Å
$R(\text{O}_b\text{–O}_c)$	2.335 Å	2.438 Å	2.389 Å	2.389 Å	2.391 Å
E_{rel}	$0.0065 E_{\text{h}}$	$0.0063 E_{\text{h}}$	$0.0038 E_{\text{h}}$	$0.0038 E_{\text{h}}$	0
ε_{-3}	$-0.2801 E_{\text{h}}$	$-0.2868 E_{\text{h}}$	$-0.2834 E_{\text{h}}$	$-0.2834 E_{\text{h}}$	$-0.2787 E_{\text{h}}$
ε_{-2}	$-0.2801 E_{\text{h}}$	$-0.2713 E_{\text{h}}$	$-0.2775 E_{\text{h}}$	$-0.2775 E_{\text{h}}$	$-0.2787 E_{\text{h}}$
ε_{-1}	$-0.2688 E_{\text{h}}$	$-0.2713 E_{\text{h}}$	$-0.2712 E_{\text{h}}$	$-0.2712 E_{\text{h}}$	$-0.2787 E_{\text{h}}$
E_{est}	$0.2753 E_{\text{h}}$	$0.2776 E_{\text{h}}$	$0.2750 E_{\text{h}}$	$0.2750 E_{\text{h}}$	$0.2787 E_{\text{h}}$

[a] $E_0 = -758.6971 E_{\text{h}}$, $E_{\text{rel}} = E_{\text{tot}}(\text{RHF}) - E_0$; $E_{\text{est}} = E_{\text{rel}} - \varepsilon_{-1}$.

rotations. Each conformation is characterized by a set of mass points, $\{m_j, \vec{r}_j | j = 1, 2, \ldots N, \ \sum m_j \vec{r}_j = 0\}$, with their center of gravity at the origin. The distance between two conformations is defined from the least value of the functional

$$d_{AB}^2 \left(\sum m_j \right) = \min_{\Omega \in SO(3)} \sum m_j |\vec{r}_{Aj} - \Omega \vec{r}_{Bj}|^2;$$

The extreme value is found from a real symmetric eigenvalue equation [11].

Five conformations have been studied here and their displacements from one another are given in Ångström in the matrix

$$\{d_{AB}\} = \left\{ \begin{array}{cccccc} & \text{CU} & \text{OU} & \text{CS} & \text{OS} & \text{Td} \\ \text{CU} & 0 & 0.0939 & 0.0742 & 0.0396 & 0.0472 \\ \text{OU} & 0.0939 & 0 & 0.0393 & 0.0738 & 0.0468 \\ \text{CS} & 0.0742 & 0.0393 & 0 & 0.0724 & 0.0362 \\ \text{OS} & 0.0396 & 0.0738 & 0.0724 & 0 & 0.0362 \\ \text{Td} & 0.0472 & 0.0468 & 0.0362 & 0.0362 & 0 \end{array} \right\}$$

where the rows and columns are labeled CU for closing umbrella and so on. The two pairs (CU, OU) and (CS, OS) can be pictured as defining straight lines through the Td as the crossing point. These lines form an angle of 49° as compared with the angle between the (1,1,1) direction and a coordinate axis of 54°. Such close similarity justifies a mapping on to the infinitesimal model.

Closing or opening the scissoring mode refers only to which pair of Cl–O bonds that is considered and the symmetry is reflected in the identical result for the orbital energies. Closing an umbrella is not the mirror image of opening one and the difference comes out in the orbital energies.

Scissoring-mode orbital energies are well represented by the expression

$$\varepsilon_j = \varepsilon_s + 2\langle f\|V\|f\rangle \cos\left(\frac{2\pi j}{3} - \frac{\pi}{6}\right); \quad j = -3, -2, -1;$$

$$\varepsilon_s = -0.2774 E_h; \quad \langle f\|V\|f\rangle\sqrt{3} = 0.0061 E_h.$$

while the umbrella modes have two forms. The closing form gives

$$\varepsilon_j = \varepsilon_c + 2\langle f\|V\|f\rangle \cos\left(\frac{2\pi j}{3} + \frac{2\pi}{3}\right); \quad j = -3, -2, -1;$$

$$\varepsilon_c = -0.2763 E_h; \quad 2\langle f\|V\|f\rangle = 0.0125 E_h.$$

and the opening one provides

$$\varepsilon_j = \varepsilon_o + 2\langle f\|V\|f\rangle \cos\left(\frac{2\pi j}{3}\right); \quad j = -3, -2, -1;$$

$$\varepsilon_o = -0.2765 E_h; \quad 2\langle f\|V\|f\rangle = -0.0103 E_h.$$

Thus, there are three estimates for the matrix elements.

We assume a linear dependence of the reduced matrix element on the displacement and find that

$$\langle f\|dv/dd\|f\rangle \approx \begin{cases} \dfrac{\langle f\|V\|f\rangle}{d_{\mathrm{OS,Td}}\sqrt{3}} = 0.10(E_h/\text{Å}) & \text{scissor mode} \\[2ex] -\dfrac{\langle f\|V\|f\rangle}{2d_{\mathrm{OU,Td}}} = 0.11(E_h/\text{Å}) & \text{opening umbrella mode} \\[2ex] \dfrac{\langle f\|V\|f\rangle}{2d_{\mathrm{CU,Td}}} = 0.13(E_h/\text{Å}) & \text{closing umbrella mode} \end{cases}$$

with a satisfactory agreement from a rather primitive model.

4. A WINNING ALTERNATIVE

The analyses in the previous sections support the notion that there will be an initial force in the direction termed the closing umbrella mode on the tetrahedral structure when an electron is removed from the perchlorate anion. Infinitesimal changes favor a change to a C_{3v}-form as suggested by Grothe and Willner [9]. Finite displacements indicate, however, that the effect of the orbital splitting is overcome by a uniform shift of the orbital energies and the cost of bending the original structure. This is seen in the last line of Table 1 where a Koopmans theorem estimate is given for the energy of the neutral radical.

A distortion in the scissoring mode affects only two $O-O$ distances while the other changes all six. Thus, it is reasonable that the overall energy change is less. It is also what Van Huis and Schaefer [8] deduced by extensive electronic structure studies. Their optimized C_{2v} conformer is further indicated by the localization of the highest occupied molecular orbital on the two approaching oxygen atoms that results in an increase in bonding between these atoms when an electron is removed. Geometry optimization on the neutral species leads to increased $Cl-O$ bond lengths here as well.

It seems that the weakening of the bond between the chloryl species and the oxygen diatom leaves room for the view that a coupling between the two is not dissimilar to the situation in the crystalline environment where a good interpretation is offered by an antiferromagnetic exchange interaction giving a doublet from a chloryl doublet and a triplet dioxygen [7]. Such a description is based on three singly occupied orbitals, one on the chlorine and two on the dioxygen. Thus, it would be ineffective to attempt an accurate

calculation without proper account of the possible electronic valence bond like structures.

Grothe and Willner argue for a C_{3v} structure where the 'umbrella' would open and the odd oxygen ligand be moved away from the central atom [9]. Their suggestion involving electron transfer between σ^* orbitals seems unlikely as the source of a change in geometric structure. There is no support for this view in the present analysis. The initially promising suggestion is not corroborated by even modest theoretical efforts.

5. FINAL REMARKS

Attempts to establish the existence and structure of chlorine tetraoxide have not led to a unique and undisputed situation. Byberg identified the species in his comprehensive studies on crystalline forms such as irradiated potassium perchlorate and was led to the exchange coupled interpretation [7]. Studies of the species in a neon matrix suggested the C_{3v} form to Grothe and Willner [9]. Somewhat elaborate calculations by Van Huis and Schaefer [8] favor the C_{2v} geometry as an optimized structure of the isolated radical.

The analysis in this note lends credibility to the findings of Van Huis and Schaefer and indicates a relation to the complex formation of the chloryl and the oxygen molecule. It will be necessary to include an environment in theoretical calculations to bring this matter further.

REFERENCES

[1] J. R. Byberg, S. J. Knak Jensen and L. T. Muus, *J. Chem. Phys.*, 1967, **46**, 131.
[2] J. Linderberg and Y. Öhrn, *Propagators in Quantum Chemistry*, Academic, London, 1973, New improved edition Wiley, New York, 2004.

[3] R. Manne, *J. Chem. Phys.*, 1967, **46**, 4645.

[4] A. D. McLachlan, H. H. Dearman and R. Lefèbre, *J. Chem. Phys.*, 1960, **33**, 65.

[5] J. Oddershede and J. Linderberg, *Chem. Phys. Lett.*, 1971, **8**, 165.

[6] A. I. Boldyrev, M. Gutowski and J. Simons, *Acc. Chem. Res.*, 1996, **29**, 497.

[7] J. R. Byberg and J. Linderberg, *Chem. Phys. Lett.*, 1975, **33**, 612.

[8] T. J. Van Huis and H. F. Schaefer III., *J. Chem. Phys.*, 1997, **106**, 4028.

[9] H. Grothe and H. Willner, *Angew. Chem. Int. Ed.*, 1996, **35**, 768.

[10] M. W. Schmidt, K. K. Baldridge, J. A. Boatz, S. T. Elbert, M. S. Gordon, J. H. Jensen, S. Koseki, N. Matsunaga, K. A. Nguyen, S. J. Su, T. L. Windus, M. Dupuis and J. A. Montgomery, *J. Comput. Chem.*, 1993, **14**, 1347.

[11] J. Linderberg, *J. Chem. Soc. Faraday Trans.*, 1997, **93**, 893.

[12] G. G. Hall, *Rep. Prog. Phys.*, 1959, **22**, 1.

[13] B. M. Bode and M. S. Gordon, *J. Mol. Graphics Modell.*, 1998, **16**, 133.

Cauchy Moments of Ne, Ar, and Kr Atoms Calculated Using the Approximate Coupled Cluster Triples Model CC3

Filip Pawłowski,[1] Poul Jørgensen[1] and Christof Hättig[2]

[1]*Department of Chemistry, University of Århus, DK-8000 Århus C, Denmark*
[2]*Forschungszentrum Karlsruhe, Institute of Nanotechnology, P.O. Box 3640, D-76021 Karlsruhe, Germany*

Abstract

The Cauchy moments are derived and implemented for the approximate triples model CC3 with the proper N^7 scaling (where N denotes the number of basis functions). The Cauchy moments are calculated for the Ne, Ar, and Kr atoms using the hierarchy of the coupled-cluster models CCS, CC2, CCSD, CC3 and a large correlation-consistent basis sets augmented with diffuse functions. A detailed investigation of the one- and N-electron errors shows that the CC3 results have the accuracy comparable to the experimental results.

Contents

1. INTRODUCTION

The calculation of frequency-dependent linear-response properties may be an expensive task, since first-order response equations have to be solved for each considered frequency [1]. The cost may be reduced by introducing the Cauchy expansion in even powers of the frequency for the linear-response function [2]. The expansion coefficients, or Cauchy moments [3], are frequency independent and need to be calculated only once for a given property. The Cauchy expansion is valid only for the frequencies below the first pole of the linear-response function,

however, most experiments are also carried out in this frequency region. Moreover, using analytical continuation techniques in the complex plane the Cauchy expansion may be extended beyond this limit [4].

The Cauchy moments are thus very useful in describing molecular properties like dynamic polarizabilities at real and imaginary frequencies [5], inelastic scattering cross sections [6], Verdet constants of atoms [7], dispersion interactions between atoms and molecules [5], and the paramagnetic contribution to the Cotton–Mouton constants of atoms [8]. Cauchy moments have been implemented for the wavefunction models: Hartree–Fock (HF) [9–11], multi-configurational self-consistent field (MCSCF) [12], and second-order polarization propagator approach (SOPPA) [13,14]. Using the time-averaged quasi-energy Lagrangian techniques [1] Cauchy moments have also been determined for the coupled cluster (CC) hierarchy of models CCS, CC2, CCSD [4]. We extend in this chapter the latter implementation to the approximate triples model CC3. CCS stands for the CC singles model, where all the single excitations from a reference wavefunction are taken into account. In CCSD [15] all the single and double excitations are treated; and in CCSDT all the triples are further added. CC2 model is obtained from CCSD by approximating the doubles equations [16]. Similarly, CC3 is an approximation to CCSDT, where approximations are introduced in the triples equation [17]. The computational cost of the CC2 and CC3 models is reduced compared to CCSD and CCSDT, respectively, and the cost across the hierarchy scales as N^4 (CCS), N^5 (CC2), N^6 (CCSD), N^7 (CC3), where N is the number of basis functions.

The CCS, CC2, CCSD, CC3 hierarchy has been designed specially for the calculation of frequency-dependent properties. In this hierarchy, a systematic improvement in the description of the dynamic electron correlation is obtained at each level. For example, comparing CCS, CC2, CCSD, CC3 with FCI singlet and triplet excitation energies showed that the errors decreased by about a factor 3 at each level in the coupled cluster hierarchy [18]. The CC3 error was as small as 0.016 eV and the accuracy of the CC3 excitation energies was comparable to the one of the CCSDT model [18].

Frequency-dependent polarizabilities and first hyperpolarizabilities have also been calculated to high accuracy using the CC3 model [19–21]. Recently, we have shown that oscillator strengths calculated using the CC3 model are practically gauge invariant [22] and that the accuracy of the CC3 frequency-dependent second hyperpolarizability of the Ne atom is at least the same as the accuracy of the latest experiments [23]. This outstanding accuracy of the CC3 model reflects the importance of the inclusion of triple excitations in the CC wavefunction for accurate description of molecular properties – a fact that has been observed a number of times for static properties calculated using CCSD(T) model [24]. Contrary to the CCSD(T) model, the CC3 model may be used to calculate both static and frequency-dependent properties [17]. The CC3 and CCSD(T) [25] models have comparable accuracy and the same formal computational scaling, N^7, with the CC3 model being iterative and the CCSD(T) model non-iterative.

The results presented in this chapter are complementary to the ones of Ref. [4], where the Cauchy moments were calculated for the Ne atom using the CCS, CC2, CCSD hierarchy. A systematic improvement in the quality of the Cauchy

moments was found in Ref. [4] when increasing the level of the hierarchy; in particular, the CCSD Cauchy moments were in a very good agreement (0.04–3%) with the empirical constrained dipole oscillator strength distribution (DOSD) values [6] which are believed to be accurate within $\pm 1\%$. We here investigate the improved accuracy of the Cauchy moments when going from CCSD to CC3.

In the next section, we recapitulate the derivation of the Cauchy moment expressions for CC wavefunction models and give the CC3-specific formulas; we also outline an efficient implementation of the CC3 Cauchy moments. Section 3 contains computational details. In Section 4, we report the Cauchy moments calculated for the Ne, Ar, and Kr gases using the CCS, CC2, CCSD, CC3 hierarchy and correlation-consistent basis sets augmented with diffuse functions. In particular, we consider the issues of one- and N-electron convergence and compare with the Cauchy moments obtained from the DOSD approach and other experiments.

2. THEORY

The Cauchy moments have been derived in Ref. [4] for CC wavefunctions, using the time-dependent quasi-energy Lagrangian technique [1]. In Section 2.1 we recapitulate the important points of that derivation and use it in Section 2.2 to derive the CC3-specific formulas.

2.1. Cauchy moments for coupled cluster wavefunctions

The oscillator strength sums, or Cauchy moments, $S_{AB}(k)$, for an exact state are defined by the sum-over-states formula [3]:

$$S_{AB}(k) = \sum_{n \neq 0} \omega_{0n}^k f_{0n}^{AB}, \tag{1}$$

where ω_{0n} is the excitation energy for the transition from the reference state $|0\rangle$ to the excited state $|n\rangle$, f_{0n}^{AB} is the oscillator strength:

$$f_{0n}^{AB} = 2\omega_{0n}\langle 0|A|n\rangle\langle n|B|0\rangle, \tag{2}$$

and A and B denote the perturbation operators. The Cauchy moments enter the expansion of the polarizability [2, 4]:

$$\alpha_{AB}(-\omega; \omega) = \sum_{n \neq 0} \frac{f_{0n}^{AB}}{\omega_{0n}^2 - \omega^2} = \sum_{k=0}^{\infty} \omega^{2k} S_{AB}(-2k - 2), \tag{3}$$

where ω denotes the frequency of the external perturbation. The last equality in equation (3) is fulfilled for $|\omega| < \min\{\omega_{0n}\}$ [4].

For the non-variational CC wavefunctions, the polarizability is the negative of the linear-response function and may therefore be identified as the second

derivative of the real part of the time-averaged quasi-energy Lagrangian, L (for the definition of the Lagrangian see, for example, Section II B in Ref. [21]), with respect to the field strengths $\varepsilon_X(\omega_X)$ [1]:

$$\alpha_{AB}(\omega_A; \omega_B) = -\frac{1}{2} C^{\pm\omega} \left\{ \eta^A t^B(\omega_B) + \eta^B t^A(\omega_A) + \mathbf{F} t^A(\omega_A) t^B(\omega_B) \right\}, \quad (4)$$

where $\omega_A = -\omega_B$ and where $C^{\pm\omega}$ is the complex conjugation and frequency sign inversion operator defined by

$$C^{\pm\omega} g^{AB\cdots}(\omega_A, \omega_B, \ldots) = g^{AB\cdots}(\omega_A, \omega_B, \ldots) + (g^{AB\cdots}(-\omega_A, -\omega_B, \ldots))^*. \quad (5)$$

The $\mathbf{F}$ matrix and η^A vector in equation (4) are defined as the second partial derivatives of the Lagrangian, taken at the zero perturbation strength:

$$\eta^A_{\mu_i} = \left(\frac{\partial^2 L}{\partial \varepsilon_A(\omega_A) \partial t_{\mu_i}} \right)_0, \quad (6)$$

$$F_{\mu_i \nu_j} = \left(\frac{\partial^2 L}{\partial t_{\mu_i} \partial t_{\nu_j}} \right)_0, \quad (7)$$

where t denotes the unperturbed wavefunction parameters (e.g., the coupled-cluster amplitudes). $t^A(\omega_A)$ in equation (4) denote the first-order response of the wavefunction parameters to an external perturbation A oscillating with the frequency ω_A. They are determined from the first-order response equation:

$$t^A(\omega_A) = -(\mathbf{A} - \omega_A \mathbf{I})^{-1} \xi^A, \quad (8)$$

where $\mathbf{I}$ denotes a unit matrix. The Jacobian, $\mathbf{A}$, and the ξ^A vector in equation (8) are defined as the second partial derivatives of the Lagrangian:

$$A_{\mu_i \nu_j} = \left(\frac{\partial^2 L}{\partial \bar{t}_{\mu_i} \partial t_{\nu_j}} \right)_0, \quad (9)$$

$$\xi^A_{\mu_i} = \left(\frac{\partial^2 L}{\partial \bar{t}_{\mu_i} \partial \varepsilon_A(\omega_A)} \right)_0, \quad (10)$$

where $\bar{t}$ denotes the unperturbed Lagrange multipliers.

Applying the matrix identity

$$(\mathbf{X} - \mathbf{Y})^{-1} = \mathbf{X}^{-1} + \mathbf{X}^{-1} \mathbf{Y} (\mathbf{X} - \mathbf{Y})^{-1} \quad (11)$$

recursively to equation (8) we obtain an expansion of the first-order wavefunction parameters:

$$t^A(\omega_A) = (-\mathbf{A}^{-1} - \omega_A \mathbf{A}^{-2} - \omega_A^2 \mathbf{A}^{-3} - \omega_A^3 \mathbf{A}^{-4} - \cdots) \xi^A, \quad (12)$$

which may be rewritten in terms of Cauchy vectors, $C^A(n)$:

$$t^A(\omega_A) = C^A(0) + \omega_A C^A(1) + \omega_A^2 C^A(2) + \cdots = \sum_{n=0}^{\infty} \omega_A^n C^A(n). \qquad (13)$$

Comparing equations (12) and (13) we obtain the recursive procedure for calculating the Cauchy vectors:

$$C^A(-1) = -\xi^A \qquad (14)$$

$$C^A(0) = \mathbf{A}^{-1} C^A(-1) \qquad (15)$$

$$C^A(1) = \mathbf{A}^{-1} C^A(0) \qquad (16)$$

$$\vdots \qquad (17)$$

$$C^A(n) = \mathbf{A}^{-1} C^A(n-1) \quad \text{for } n \geq 0. \qquad (18)$$

Inserting equation (13) into equation (4) we obtain the polarizability expansion:

$$\alpha_{AB}(-\omega;\omega) = -\sum_{k=0}^{\infty} \omega^{2k} \left\{ \eta^A C^B(2k) + \eta^B C^A(2k) + \sum_{n=0}^{2k} (-1)^n \mathbf{F} C^A(2k-n) C^B(n) \right\}, \qquad (19)$$

where we have introduced explicitly the terms resulting from the $C^{\pm\omega}$ operator. Comparing equations (3) and (19) we identify the Cauchy moments as

$$S_{AB}(-2k-2) = -\left\{ \eta^A C^B(2k) + \eta^B C^A(2k) + \sum_{n=0}^{2k} (-1)^n \mathbf{F} C^A(2k-n) C^B(n) \right\}. \qquad (20)$$

Calculation of the Cauchy moments, $S_{AB}(-2k-2)$, thus only requires solving a set of frequency-independent linear equations, equation (18), up to order $2k$ and carrying out the linear transformations involving η^A vector and $\mathbf{F}$ matrix (see equation (20)). Note, that contrary to equation (1) no sum over states is involved in this formulation of the Cauchy moments.

2.2. Cauchy moments for the CC3 model

To calculate the Cauchy moments we first need to solve the equations for the Cauchy vectors (equation (18)). In the CC3 model this equation may be written as

$$\begin{pmatrix} C_{\text{SD}}^A(n) \\ C_{\text{T}}^A(n) \end{pmatrix} = \begin{pmatrix} \mathbf{A}_{\text{SD,SD}} & \mathbf{A}_{\text{SD,T}} \\ \mathbf{A}_{\text{T,SD}} & \mathbf{A}_{\text{T,T}} \end{pmatrix}^{-1} \begin{pmatrix} C_{\text{SD}}^A(n-1) \\ C_{\text{T}}^A(n-1) \end{pmatrix}, \qquad (21)$$

where the Cauchy vectors and the Jacobian have been partitioned into the contributions originating from the singles-and-doubles (SD) and the triples (T) spaces. The pure triples contribution to the Jacobian is represented by the diagonal matrix consisting of the triple excitation energies, ω_{μ_3}:

$$\mathbf{A}_{\mathrm{T,T}} = \delta_{\mu_3 \nu_3} \omega_{\mu_3}, \tag{22}$$

with μ_3 referring to a triples excitation. To keep the CC3 storage demands within acceptable limits, the triples components of the Cauchy vectors cannot be written to the disk or put to the memory and, therefore, no explicit reference to the triples space can be made when solving equation (21). The explicit reference to the triples space may be avoided by projecting all the triples components into the singles-and-doubles space.

To achieve this we write the inverse of the CC3 Jacobian in the form

$$\begin{pmatrix} \mathbf{A}_{\mathrm{SD,SD}} & \mathbf{A}_{\mathrm{SD,T}} \\ \mathbf{A}_{\mathrm{T,SD}} & \mathbf{A}_{\mathrm{T,T}} \end{pmatrix}^{-1}$$

$$= \begin{pmatrix} (\mathbf{A}_{\mathrm{SD,SD}}^{\mathrm{eff}})^{-1} & -(\mathbf{A}_{\mathrm{SD,SD}}^{\mathrm{eff}})^{-1} \mathbf{A}_{\mathrm{SD,T}} \mathbf{A}_{\mathrm{T,T}}^{-1} \\ -\mathbf{A}_{\mathrm{T,T}}^{-1} \mathbf{A}_{\mathrm{T,SD}} (\mathbf{A}_{\mathrm{SD,SD}}^{\mathrm{eff}})^{-1} & \mathbf{A}_{\mathrm{T,T}}^{-1} + \mathbf{A}_{\mathrm{T,T}}^{-1} \mathbf{A}_{\mathrm{T,SD}} (\mathbf{A}_{\mathrm{SD,SD}}^{\mathrm{eff}})^{-1} \mathbf{A}_{\mathrm{SD,T}} \mathbf{A}_{\mathrm{T,T}}^{-1} \end{pmatrix}, \tag{23}$$

where

$$\mathbf{A}_{\mathrm{SD,SD}}^{\mathrm{eff}} = \mathbf{A}_{\mathrm{SD,SD}} - \sum_{\mu_3} \frac{\mathbf{A}_{\mathrm{SD},\mu_3} \mathbf{A}_{\mu_3,\mathrm{SD}}}{\omega_{\mu_3}} \tag{24}$$

is the effective Jacobian in the singles-and-doubles space. Using equation (23) we may express equation (21) as a set of two equations:

$$(\mathbf{A}_{\mathrm{SD,SD}}^{\mathrm{eff}}) C_{\mathrm{SD}}^A(n) = C_{\mathrm{SD}}^{\mathrm{eff}}(n-1) \tag{25}$$

$$C_{\mathrm{T}}^A(n) = \mathbf{A}_{\mathrm{T,T}}^{-1} (C_{\mathrm{T}}^A(n-1) - \mathbf{A}_{\mathrm{T,SD}} C_{\mathrm{SD}}^A(n)) \tag{26}$$

with the effective Cauchy vectors defined as

$$C_{\mathrm{SD}}^{\mathrm{eff}}(n-1) = C_{\mathrm{SD}}^A(n-1) - \sum_{\mu_3} \frac{\mathbf{A}_{\mathrm{SD},\mu_3} C_{\mu_3}^A(n-1)}{\omega_{\mu_3}} \tag{27}$$

Only equation (25), which is the counterpart of equation (21) in the subspace of $\mathbf{A}_{\mathrm{SD,SD}}$, is solved iteratively. In this equation all the triples components have been projected into the singles-and-doubles space. Once equation (25) has been solved the $C_{\mathrm{SD}}^A(n)$ solution vector is stored on disk. The triples component of the solution vector, $C_{\mathrm{T}}^A(n)$, may then be constructed *on the fly* (see equation (26)), whenever it is needed. In this way, the storage of the triples components is avoided.

The effective singles-and-doubles equation for the Cauchy vectors, equation (25), has the same structure as the effective singles-and-doubles equation for the first-order CC3 amplitudes (see equation (26) of Ref. [21]), the main difference being that now the right-hand side depends on the solution vector of lower order. Equation (25) may thus be implemented following the scheme described in Ref. [21] with an extra external loop over n (i.e., the Cauchy vectors order).

Let us now consider the calculation of the triples part of the Cauchy vector, $C_T^A(n)$, according to equation (26). Expanding $C_T^A(n-1)$ on the right-hand side of equation (26) recursively, we obtain:

$$C_{\mu_3}^A(n) = -\left\{ \frac{\xi_{\mu_3}^A}{\omega_{\mu_3}^{n+1}} + \sum_{m=0}^{n} \frac{\sum_{\nu_i; i=1,2} A_{\mu_3,\nu_i} C_{\nu_i}^A(m)}{\omega_{\mu_3}^{n+1-m}} \right\} \tag{28}$$

Equation (28) leads to the following computational scheme for the triples part of the CC3 Cauchy vectors with $n \geq 0$:

$C_T^A(n) \leftarrow \xi_T^A$
loop $m = 0, n$
    $C_T^A(n) \leftarrow C_T^A(n) + \mathbf{A}_{T,SD} C_{SD}^A(m)$
    $C_T^A(n) \leftarrow C_T^A(n)/\omega_T$
end loop m
turn sign: $C_T^A(n) \leftarrow -C_T^A$

where ω_T is a vector with ω_{μ_3} elements.

The equation for the triples part of the (frequency-independent) first-order amplitudes, $t_T^A(0)$, has a form:

$$t_T^A(0) = -\mathbf{A}_{T,T}^{-1}(\xi_T^A + \mathbf{A}_{T,SD} t_{SD}^A(0)) \tag{29}$$

and may be viewed as the special case of equation (26); indeed, $t_T^A(0)$ is obtained in the first iteration ($m=0$) of the above computational scheme. The calculation of the $C_{\mu_3}^A(n)$ vectors may thus be implemented as a straightforward generalization of the implementation of equation (29) (an extra loop over m and some reorganization are only required). The efficient implementation of equation (29) has been described in detail in Ref. [21]; the calculations are carried out for two fixed virtual MO indexes leading to the triples vector intermediates of the form $W^{BC}(aijk)$, where B and C are the two fixed virtual indexes, a is the third virtual index, and i, j, k are three occupied indexes – see Ref. [21] for details.

Once the equations for the Cauchy vectors have been solved, the Cauchy moments can be calculated according to equation (20), which for the CC3 model may be written as

$$S_{AB}(-2k-2) = -\eta^A_{SD}C^B_{SD}(2k) - \eta^B_{SD}C^A_{SD}(2k)$$

$$-\sum_{n=0}^{2k}(-1)^n \mathbf{F}_{SD,SD} C^A_{SD}(2k-n) C^B_{SD}(n)$$

$$-\eta^A_T C^B_T(2k) - \eta^B_T C^A_T(2k)$$

$$-\sum_{n=0}^{2k}(-1)^n \mathbf{F}_{SD,T} C^A_{SD}(2k-n) C^B_T(n)$$

$$-\sum_{n=0}^{2k}(-1)^n \mathbf{F}_{SD,T} C^B_{SD}(2k-n) C^A_T(n), \qquad (30)$$

where the $\mathbf{F}$ matrix and the η^X and C^X vectors have been partitioned into the contributions from the singles-and-doubles and the triples spaces.

Since the Cauchy moments formula, equation (20), has the same structure as the CC linear-response function, equation (4), the contractions in equation (30) may be implemented by a straightforward generalization of the computational procedures described in Section III B of Ref. [21] for the calculation of the CC3 linear-response function.

3. COMPUTATIONAL DETAILS

In the next section, we present the Cauchy moments, $S(k)$, for the Ne, Ar, and Kr gases calculated using the hierarchy of models CCS, CC2, CCSD, and CC3. We consider the orders $k = -2, -4, -6, -8, -10$.

All the calculations have been carried out using a local version of the Dalton program package [26]. The implementation of the Cauchy moments for the CCS, CC2, and CCSD models has been described in Ref. [4]. The CC3 Cauchy moments have been implemented by us following the outline presented in the previous section.

Dunning's correlation consistent basis sets cc-pVXZ [27] augmented with diffuse functions [28] were used in the calculations. We considered cardinal numbers $X =$ D, T, Q, 5, 6 and single (s), double (d), triple (t), and quadruple (q) augmentations. The orbitals were not allowed to relax in the coupled cluster response calculations.

4. RESULTS

4.1. Neon

In Table 1 we have collected the Cauchy moments, $S(k)$, calculated for the Ne atom using the CCSD model and the n-aug-cc-pVXZ basis-set family. As can be seen from the table, single augmentation is not sufficient for the calculation of the Cauchy moments. On the other hand, going beyond the double augmentation

Table 1. The basis-set convergence of the Cauchy moments $S(k)$ [a.u.] for Ne calculated with CCSD model and the n-aug-cc-VXZ basis-set family (all electrons correlated)

	aug	d-aug	t-aug	q-aug
$k=-2$				
DZ	2.003	2.707	2.715	2.715
TZ	2.433	2.698	2.699	2.699
QZ	2.598	2.680	2.680	2.680
5Z	2.643	2.668	2.668	2.668
6Z	2.650	2.662	2.662	2.662
$k=-4$				
DZ	1.711	2.916	3.015	3.019
TZ	2.148	2.922	2.943	2.943
QZ	2.485	2.880	2.882	2.882
5Z	2.678	2.858	2.858	2.857
6Z	2.741	2.845	2.845	2.845
$k=-6$				
DZ	3.009	4.997	5.391	5.404
TZ	3.496	5.072	5.193	5.196
QZ	3.925	4.999	5.018	5.019
5Z	4.328	4.948	4.948	4.948
6Z	4.524	4.915	4.914	4.913
$k=-8$				
DZ	6.041	10.817	11.890	11.915
TZ	7.110	10.832	11.261	11.272
QZ	7.818	10.637	10.740	10.746
5Z	8.683	10.522	10.535	10.537
6Z	9.235	10.433	10.436	10.437
$k=-10$				
DZ	12.315	26.571	29.036	29.076
TZ	15.252	25.825	26.975	27.001
QZ	16.944	24.984	25.350	25.372
5Z	19.143	24.636	24.718	24.730
6Z	20.779	24.386	24.426	24.431

practically does not change the results. In the following we will, therefore, report results obtained using the doubly augmented basis. The Cauchy moments in general converge smoothly with increasing cardinal number, X, toward the basis-set limit. Only for $k=-4$, -6, and -8 they first increase from $X=D$ to $X=T$, and then smoothly decrease. This might reflect the poor quality of the double-zeta basis.

The Cauchy moments of Ne at the CCSD/q-aug-cc-pV5Z level were found in Ref. [4] to be converged within 1% compared to the basis-set limit result. We have calculated the Cauchy moments also for the $X=6$ cardinal number. From the results in Table 1 it appears that the Cauchy moments at this level are significantly less than 1% from the basis-set limit result.

Table 2. The Cauchy moments $S(k)$ for Ne calculated at various levels of the CC hierarchy using the d-aug-cc-pV6Z basis-set (all electrons correlated). All numbers in a.u.

					Experiment	
k	CCS	CC2	CCSD	CC3	DOSD[a]	Other[b]
-2	2.461	2.791	2.662	2.665	2.669	2.663[c]
-4	2.137	3.218	2.845	2.859	2.886	2.938
-6	3.030	6.009	4.915	4.946	5.063	5.137
-8	5.328	13.759	10.433	10.485	10.86	10.95
-10	10.359	34.673	24.386	24.442	25.53	25.65

[a] Ref. [6].
[b] Ref. [30].
[c] Ref. [29].

The Cauchy moments calculated for the Ne atom using the d-aug-cc-pV6Z basis at the different levels of the CC hierarchy are compared in Table 2 to the DOSD results [6]. Other experimental results are also quoted [29,30]. A systematic improvement toward the DOSD results (which are believed to be accurate within $\pm 1\%$) is observed in the CC hierarchy. The CCS model underestimates, while the CC2 model overestimates the DOSD results. Both the CCSD and CC3 results approach the DOSD values from below. The CCSD Cauchy moments are in a very good agreement with the DOSD results: the discrepancies are between 0.2% ($S(-2)$) and 4.6% ($S(-10)$) and increase monotonically with k. This monotonic increase reflects that the error in the position of the first pole in the polarizability (i.e., the excitation energy to the first dipole-allowed transition) gets increasing weights in the power series expansion of the polarizability [4].

Turning our attention to the CC3 model we observe that the inclusion of triple excitations further improves the quality of the Cauchy moments in the sense that all the CC3 moments are closer to the DOSD results than the CCSD moments. The CC3 and DOSD Cauchy moments are in fact so close that it is worth investigating in more detail the errors associated with the CC3 results.

The excitation energy to the lowest dipole allowed state $2s^2 2p^5 3s^1 (P^O)$ was in a benchmark study [18] using the aug-cc-pVDZ basis found to be 19.041 eV (CCSD), 19.240 eV (CC3), 19.206 eV (CCSDT), 19.247 eV (FCI), showing that the CC3 excitation energy is converged, for all practical purposes, in N-electron space. Calculations of the excitation energy using the d-aug-cc-pV5Z and d-aug-cc-pV6Z basis gave 16.773 and 16.795 eV (CCSD), 16.811 and 16.826 eV (CC3). The CC3 results compare very favorable with the experimental result of 16.848 eV from Ref. [31]. The very small error in the excitation energy at the CC3 level suggests that this error may be neglected in CC3 calculations of the Cauchy moments.

Let us now consider the errors in the CC3 $S(-2)$ Cauchy moment (the static polarizability). From the monotonic convergence of the CCSD doubly augmented basis-set calculations of $S(-2)$ in Table 1 it appears that the difference between the 5Z and 6Z results should give a good estimate of the CCSD basis-set error at the 6Z level. CC3/d-aug-pV5Z $S(-2)$ Cauchy moment is 2.670 a.u. Using the

CC3/d-aug-pV6Z $S(-2)$ from Table 2 we may thus estimate the CC3 basis-set limit for $S(-2)$ to be 0.005 a.u. below the CC3/d-aug-pV6Z result. The errors resulting from correlation effects beyond CC3 may be estimated from the aug-cc-pVDZ calculations in Ref. [32] where it was found that the FCI static polarizability of Ne was 0.003 a.u. smaller than the corresponding CC3 result. Relativistic effects have been determined in Ref. [33] to increase $S(-2)$ by 0.004 a.u. Adding the basis set, correlation and relativistic contribution gives a decrease in $S(-2)$ of 0.004 a.u. The effects not accounted for in the CC3/d-aug-pV6Z calculation thus to a high degree cancel each other. For the Cauchy moments with the higher values of $|k|$ no relativistic contribution or correlation contribution beyond CC3 has been calculated and it is for that reason difficult to estimate the accuracy of these Cauchy moments. However, the above analysis makes us to believe that the reported Cauchy moments have the accuracy comparable to the experimental results.

4.2. Argon

The Cauchy moments calculated for the Ar atom at the different levels of the CC hierarchy using d-aug-cc-pV6Z basis are collected in Table 3 together with the empirical DOSD results [6] and other experimental results [34,35]. The behavior of the CCS and CC2 models is less systematic than for Ne: these models overestimate the Cauchy moments for the lower values of $|k|$ and then underestimate for higher $|k|$. As in the case of the Ne atom, the CCSD model systematically approaches the DOSD values from below. The CC3 Cauchy moments are first larger than the DOSD values (for $k = -2$ and -4) and then become smaller than the DOSD values (for the remaining k's). The CC3 model gives generally better agreement with the DOSD values than the CCSD model, the discrepancies being reduced by a factor of 4 ($k = -10$) to 20 ($k = -6$). In most cases the CC2 model is in better agreement with both the CC3 and DOSD values than is the CCSD model. This is due to a fortuitous cancellation of errors at the CC2 level. To make a more detailed analysis of the CC3 uncertainties, the

Table 3. The Cauchy moments $S(k)$ [a.u.] for Ar calculated at various levels of the CC hierarchy using the d-aug-cc-pV6Z basis-set (all electrons correlated)

					Experiment	
k	CCS	CC2	CCSD	CC3	DOSD[a]	Other[b]
-2	11.469	11.233	11.084	11.102	11.08	11.08[c]
-4	25.599	28.089	27.360	27.996	27.91	27.92
-6	78.942	94.068	90.761	94.846	95.06	95.26
-8	297.742	378.822	362.949	386.833	391.5	392.0
-10	1260.532	1702.508	1621.707	1760.880	1802	1800

[a] Ref. [6].
[b] Ref. [35].
[c] Ref. [34].

basis set and correlation error must be established and the relativistic contribution to the Cauchy moments might need to be taken into account.

4.3. Krypton

The Cauchy moments of Kr (Table 4) have been calculated using the largest currently available correlation-consistent basis augmented with diffuse functions – d-aug-cc-pV5Z basis. As for the Ar atom, the CCS and CC2 results overestimate the DOSD values for smaller $|k|$ and underestimate for larger $|k|$. The CCSD model behaves in the same manner. The CC3 model systematically

Table 4. The Cauchy moments $S(k)$ [a.u.] for Kr calculated at various levels of the CC hierarchy using the d-aug-cc-pV5Z basis-set (all electrons correlated)

					Experiment	
k	CCS	CC2	CCSD	CC3	DOSD[a]	Other[b]
-2	17.627	17.119	16.918	16.861	16.79	16.80[c]
-4	52.631	56.665	55.386	56.002	56.32	56.51
-6	216.762	249.399	242.394	248.098	256.7	258.7
-8	1079.250	1302.841	1263.398	1306.458	1404	1419
-10	6002.085	7554.571	7321.634	7639.949	8558	8669

[a] Ref. [6].
[b] Ref. [35].
[c] Ref. [34].

approaches the DOSD values from below. As observed for Ne and Ar, the discrepancy between the CC3 and DOSD results for Kr is smaller than the discrepancy between CCSD and DOSD. For most of the values of k, the CC2 Cauchy moments are in better agreement with both the CC3 and DOSD values than is the CCSD results. This unexpected good performance of CC2 is again the result of a fortuitous cancellation of errors. For $k = -6$ the situation is extreme – the CC2 result is in better agreement with DOSD than is the CC3 results. Again, any more detailed judgments of the uncertainty of the CC3 Cauchy moments are not possible at this stage.

5. CONCLUSION

The high quality of the CC3 model and the convergence in one-electron space have allowed us to determine the Cauchy moments for Ne which have the accuracy comparable to the experimental results. To arrive at the similar conclusion for the Ar and Kr atoms a more detailed investigation of the convergence in one-electron and N-electron space is required. The relativistic contribution to the Cauchy moments may also need to be taken into account for these two atoms.

ACKNOWLEDGEMENTS

REFERENCES

[1] O. Christiansen, P. Jørgensen and C. Hättig, *Int. J. Quantum Chem.*, 1998, **68**, 1.
[2] P. Lazzeretti, in (ed. S. Wilson), World Scientific/Wiley, Singapore/New York, Vol. 3, 2002, p. 53.
[3] J. O. Hirschfelder, W. B. Brown and S. T. Epstein, *Adv. Quantum Chem.*, 1964, **1**, 255.
[4] C. Hättig, O. Christiansen and P. Jørgensen, *J. Chem. Phys.*, 1997, **107**, 10592.
[5] A. Kumar and W. J. Meath, *Mol. Phys.*, 1985, **54**, 823.
[6] A. Kumar and W. J. Meath, *Can. J. Chem.*, 1985, **63**, 1616.
[7] W. A. Parkinson, S. P. A. Sauer, J. Oddershede and D. M. Bishop, *J. Chem. Phys.*, 1993, **98**, 487.
[8] M. J. Jamieson, *Chem. Phys. Lett.*, 1991, **183**, 9.
[9] H. Hettema and P. E. S. Wormer, *J. Chem. Phys.*, 1990, **93**, 3389.
[10] B. Silvi and N. Fourati, *Mol. Phys.*, 1984, **52**, 415.
[11] G. H. F. Diercksen, J. Oddershede, I. Paidarova and J. R. Sabin, *Int. J. Quantum Chem.*, 1991, **39**, 755.
[12] P. W. Fowler, P. Jørgensen and J. Olsen, *J. Chem. Phys.*, 1990, **93**, 7256.
[13] M. J. Packer, S. P. A. Sauer and J. Oddershede, *J. Chem. Phys.*, 1994, **100**, 8969.
[14] S. P. A. Sauer, G. H. F. Diercksen and J. Oddershede, *Int. J. Quantum Chem.*, 1991, **39**, 667.
[15] G. D. Purvis III and R. J. Bartlett, *J. Chem. Phys.*, 1982, **76**, 1910.
[16] O. Christiansen, H. Koch and P. Jørgensen, *Chem. Phys. Lett.*, 1995, **243**, 409.
[17] H. Koch, O. Christiansen, P. Jørgensen, A. M. Sanchez de Merás and T. Helgaker, *J. Chem. Phys.*, 1997, **106**, 1808.
[18] H. Larsen, K. Hald, J. Olsen and P. Jørgensen, *J. Chem. Phys.*, 2001, **115**, 3015.
[19] O. Christiansen, J. Gauss and J. F. Stanton, *Chem. Phys. Lett.*, 1998, **292**, 437.
[20] O. Christiansen, J. Gauss and J. F. Stanton, *Chem. Phys. Lett.*, 1999, **305**, 147.
[21] K. Hald, F. Pawłowski, P. Jørgensen and C. Hättig, *J. Chem. Phys.*, 2003, **118**, 1292.
[22] F. Pawłowski, P. Jørgensen and C. Hättig, *Chem. Phys. Lett.*, 2004, **389**, 413.
[23] F. Pawłowski, P. Jørgensen and C. Hättig, *Chem. Phys. Lett.*, 2004, **391**, 27.
[24] T. Helgaker, P. Jørgensen and J. Olsen, *Molecular Electronic-Structure Theory*, Wiley, New York, 2000.
[25] K. Raghavachari, G. W. Trucks, M. A. Pople and M. Head-Gordon, *Chem. Phys. Lett.*, 1989, **157**, 479.
[26] T. Helgaker *et al.*, DALTON, *A Molecular Electronic Structure Program*, Release 1.2, 2001, see http://www.kjemi.uio.no/software/dalton/dalton.html
[27] T. H. Dunning, *J. Chem. Phys.*, 1989, **90**, 1007.
[28] R. A. Kendall, T. H. Dunning and R. J. Harrison, *J. Chem. Phys.*, 1992, **96**, 6796.
[29] U. Hohm and K. Kerl, *Mol. Phys.*, 1990, **69**, 803.
[30] W. F. Chan, G. Cooper, X. Guo and C. E. Brion, *Phys. Rev. A*, 1992, **45**, 1420.
[31] C. E. Moore, *Atomic Energy Levels as Derived from the Analysis of Optical Spectra*, United States Department of Commerce, National Bureau of Standards, Circular 467.
[32] H. Larsen, J. Olsen, C. Hättig, P. Jørgensen, O. Christiansen and J. Gauss, *J. Chem. Phys.*, 1999, **111**, 1917.
[33] W. Klopper, S. Coriani, T. Helgaker and P. Jørgensen, *J. Phys. B: At. Mol. Opt. Phys.*, 2004, **37**, 3753.
[34] U. Hohm, *Mol. Phys.*, 1994, **81**, 157.
[35] W. F. Chan, G. Cooper, X. Guo, G. R. Burton and C. E. Brion, *Phys. Rev. A*, 1992, **46**, 149.

Density of States and Transmission in Molecular Transport Junctions

Zsolt Bihary and Mark A. Ratner

Department of Chemistry, Northwestern University,
Evanston, IL 60208, USA

Abstract

Electron transport through molecular junctions (a molecule coordinated to two electrodes) is a non-equilibrium phenomenon, and corresponds to a current/voltage spectroscopy. We discuss such transport in two different limits. In the scanning tunneling microscope limit, where the coupling to one electrode is very much stronger than that to the other, the density of states (DOS) along the molecule effectively dominates the transport. However, when the couplings to the two electrodes are comparable, then the DOS itself is inadequate to determine either mechanism or magnitude of transport. The DOS still describes the quantum interference effects and the statistical aspects of transport, but the actual mechanism is described by another factor, that we call the transmittance. This transmittance function modulates the DOS, due to the effects of electronic structure changes (and, though not explored here, other couplings through interelectronic correlations or vibronic coupling). In the limit of transport outside of the band, the superexchange-type exponential decay with length enters not through the DOS, but through the transmittance function.

Contents

1. INTRODUCTION

The electronic spectrum and the current/voltage spectrum of molecular systems are related, since transmission through a molecular junction is greatly enhanced if the conduction electrons are injected at energies close to the molecular resonances. This relationship is even more pronounced in Scanning Tunneling Microscopy (STM). Indeed the modeling and the interpretation of such experiments is most simply expressed by the Tersoff–Hamann formula which gives the STM current as proportional to the density of states (DOS) at the tip location and at the Fermi energy [1–6].

Molecular transmission, the measure of the probability that an electron with a given energy transmits current through the molecular junction, is clearly related to the electronic structure of the molecule. At energies close to resonances, transmission (differential conductance) shows peaks, reminiscent of the electronic spectra of the molecule. In this chapter, we explore the relationship between the (local) DOS of the molecule and the transmission function that characterizes its transport properties. To keep the discussion as simple and transparent as possible, we shall describe the molecular system with a single-band tight-binding Hamiltonian and treat the contacts as locally coupled, site-wise incoherent point sources, within the wide-band limit. We will use the standard non-equilibrium Green function formalism in the energy representation. Only elastic currents will be discussed, within the single-electron picture, therefore we neglect any internal interactions, such as electron–phonon coupling and electron–electron Coulomb repulsion. We find that while the current is indeed proportional to a scaled DOS, an additional factor, called the transmittance and describing the mechanism of the transport, enters as a proportionality factor, and can dominate the behavior in some situations.

2. FORMALISM AND MODEL

In this section, we describe our model, and give a brief, self-contained account on the equations of the non-equilibrium Green function formalism. This is closely related to the electron and particle–hole propagators, which have been at the heart of Jens' electronic structure research [7,8]. For more detailed and more general analysis, see some of the many excellent references [9–15]. We restrict ourselves to the study of stationary transport, and work in energy representation. We assume the existence of a well-defined self-energy. The aim is to solve the Dyson and the Keldysh equations for the electronic Green functions:

$$G^{\mathrm{r}}(E) = (E - H_{\mathrm{el}} - \Sigma^{\mathrm{r}}(E))^{-1} \tag{1}$$

$$G^{\mathrm{a}}(E) = (E - H_{\mathrm{el}} - \Sigma^{\mathrm{a}}(E))^{-1} = [G^{\mathrm{r}}(E)]^{+} \tag{2}$$

$$G^{<}(E) = G^{\mathrm{r}}(E)\Sigma^{<}(E)G^{\mathrm{a}}(E) \tag{3}$$

$$G^{>}(E) = G^{\mathrm{r}}(E)\Sigma^{>}(E)G^{\mathrm{a}}(E). \tag{4}$$

H_{el} is the Hamiltonian, $G^{\mathrm{r}}(E)$, $G^{\mathrm{a}}(E)$, $G^{<}(E)$ and $G^{>}(E)$ are the retarded, advanced, lesser and greater Green functions, and $\Sigma^{\mathrm{r}}(E)$, $\Sigma^{\mathrm{a}}(E)$, $\Sigma^{<}(E)$ and $\Sigma^{>}(E)$ are the corresponding self-energies. We use the Huckel (tight-binding) model to describe the molecular system. The basis for electronic states is a set of spatially localized orbitals that may be considered atomic orbitals, or orbitals associated with different groups of atoms, 'sites' within the molecule.

The Hamiltonian in second quantized notation is

$$\hat{H}_{\text{el}} = \sum_{i,j} t_{ij} \hat{a}_i^+ \hat{a}_j, \tag{5}$$

where $\hat{a}_i^+$ ($\hat{a}_i$) describes the creation (annihilation) of an electron at site i in the molecule. In this chapter, we will investigate homogeneous, one-dimensional, single-band models defined by the Hamiltonian

$$\hat{H}_{\text{1D}} = \varepsilon \sum_{i=1}^{n} \hat{a}_i^+ \hat{a}_i - t \sum_{i=1}^{n-1} (\hat{a}_i^+ \hat{a}_{i+1} + \hat{a}_{i+1}^+ \hat{a}_i). \tag{6}$$

Here, n is the number of sites, ε is the energy of the sites, t is the hopping parameter. The conventional negative sign is used in the Hamiltonian to energetically favor long wavelength molecular states. The Hamiltonian, the Green functions, and the self-energies are all represented by matrices, using the atomic (site) basis (this corresponds to real-space representation). Within the elastic, non-interacting model we are considering here, the self-energy stems purely from the coupling to the leads (contacts). We shall study two-terminal arrangements, so the self-energies contain two terms: $\Sigma^{\text{r,a},<,>} = \Sigma_1^{\text{r,a},<,>} + \Sigma_2^{\text{r,a},<,>}$, referring to the source and the emitter. As we are concerned about the effect of the molecular energy structure on the transmission, and not about effects due to the band structure of the leads, we simply take the contacts into account with self-energy terms in the wide band limit:

$$\Sigma_{1(2)}^{\text{r}} = -\frac{i}{2} \Gamma_{1(2)} \tag{7}$$

$$\Sigma_{1(2)}^{\text{a}} = +\frac{i}{2} \Gamma_{1(2)} \tag{8}$$

$$\Sigma_{1(2)}^{<} = +i\Gamma_{1(2)} f_{1(2)}(E) \tag{9}$$

$$\Sigma_{1(2)}^{>} = -i\Gamma_{1(2)}[1 - f_{1(2)}(E)] \tag{10}$$

where $\Gamma_{1(2)}$ is the escape rate matrix and $f_{1(2)}(E)$ is the Fermi–Dirac distribution characterized by the chemical potential in the corresponding leads. Certain combinations of the self-energies yield the escape rate matrices: $i(\Sigma_{1(2)}^{\text{r}} - \Sigma_{1(2)}^{\text{a}}) = i(\Sigma_{1(2)}^{>} - \Sigma_{1(2)}^{<}) = \Gamma_{1(2)}$, as can be easily verified using equations (7)–(10). We define the total escape rate matrix as the sum $\Gamma = \Gamma_1 + \Gamma_2 = i(\Sigma^{\text{r}} - \Sigma^{\text{a}}) = i(\Sigma^{>} - \Sigma^{<})$. The self-energy terms due to the contacts do not depend on the Green functions themselves, therefore equations (1)–(4) can be solved in a straightforward manner; no self-consistent calculation is needed.

Once the Green functions have been obtained, together with the self-energies, they allow calculation of the quantities of interest. In particular, the spectral function is given as

$$A(E) = i(G^{\text{r}}(E) - G^{\text{a}}(E)) = i(G^{>}(E) - G^{<}(E)), \tag{11}$$

or, combining the expressions (3) and (4) and noting the definition of Γ, we can also write:

$$A(E) = G^{\mathrm{r}}(E)\Gamma G^{\mathrm{a}}(E). \tag{12}$$

The diagonal elements of the spectral function yield the local DOS at the corresponding site, while their sum, the trace, yields the DOS:

$$N(i, E) = \frac{1}{2\pi}[A(E)]_{ii}, \tag{13}$$

$$N(E) = \frac{1}{2\pi}\mathrm{Tr}[A(E)]. \tag{14}$$

The current transmitted through the junction is given as an integral of the flux of electrons at the source (or, equivalently, at the emitter) over different energies:

$$i(E) = \frac{e}{h}\mathrm{Tr}[\Sigma_1^<(E)G^>(E) - \Sigma_1^>(E)G^<(E)] \tag{15}$$

$$I = \int \mathrm{d}Ei(E). \tag{16}$$

When internal interactions are neglected, the current is purely coherent (elastic), and the formalism yields expressions that are consistent with the Landauer formula. The current can be rewritten as

$$I = \frac{e}{h}\int \mathrm{d}E(f_1(E) - f_2(E))T(E), \tag{17}$$

where T is the transmission function. The expression $f_1(E) - f_2(E)$ in equation (17) can be viewed as the window function for transmission; it assumes non-zero (unity) value only at energies where one of the contacts is occupied, but the other has a hole. The transmission function describes the probability for such an electron to indeed transfer through the molecular junction. It is related to the differential conductance as $G = (2e^2/h)T$, and hence is a primary observable in experiments. In what follows, we will characterize the (energy-dependent) transport of the molecular system with the function $T(E)$ and compare it with the (local) DOS. From the equations introduced in this section, the transmission function can be derived as [16–25]:

$$T = \mathrm{Tr}[\Gamma_1 G^{\mathrm{r}}\Gamma_2 G^{\mathrm{a}}]. \tag{18}$$

3. TRANSMISSION IN STM EXPERIMENTS

Let us consider a molecule absorbed on a metallic surface with an STM tip positioned at site k. This arrangement is schematically shown in Fig. 1a. One of the 'leads' in this case is the tip, the other one is the metal itself. The escape rate matrix for the tip can be modeled as a local contact, only coupling the molecule at site k:

$$[\Gamma_1]_{ij} = \Gamma_1\delta_{ij}\delta_{ik}, \tag{19}$$
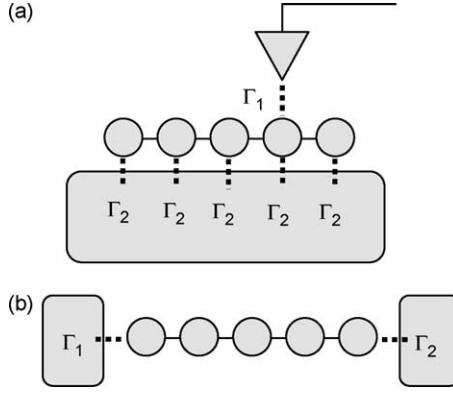
Fig. 1. Two limiting cases for transport. The upper figure represents the scanning tunneling microscope limit, where the molecular structure coupling to the electrode is much stronger than that to the scanning tip. The lower figure shows the molecular wire junction, where the interactions with the two electrodes are comparable in magnitude.

where Γ_1 now is simply the escape rate through the tip junction. The metallic surface interacts with each site, along the entire molecular chain, and we model its rate matrix as

$$[\Gamma_2]_{ij} = \Gamma_2 \delta_{ij}, \tag{20}$$

where Γ_2 is the escape rate to the metal at any given site. Figure 1a illustrates this coupling scheme. Plugging the assumed forms for the Γ matrices (equations (19) and (20)) into the general formula equation (18), we obtain the transmission function for the STM arrangement:

$$T = \Gamma_1 \Gamma_2 \sum_j Q_{kj}, \tag{21}$$

where the Q matrix is defined as [26]

$$[Q]_{ij} = |G^{\mathrm{r}}_{ij}|^2. \tag{22}$$

Using equation (12) we can express the diagonal elements of the spectral function and calculate the local DOS at site i:

$$2\pi N(i, E) = \Gamma_1 Q_{ik} + \Gamma_2 \sum_j Q_{ij}. \tag{23}$$

If we make the very reasonable assumption that the (overall) coupling strength to the metal is much stronger than that to the tip, the RHS of equation (23) is dominated by the second term. In this limit, expressing the local DOS at site k, where the tip is coupled, we obtain

$$2\pi N(k, E) = \Gamma_2 \sum_j Q_{kj}. \tag{24}$$

Comparing this result with equation (21), we can express T with the local DOS:

$$T = \Gamma_1 2\pi N(k, E). \tag{25}$$

Our simple calculation thus reflects the well-known result [1–6] that the differential resistance measured in the tunneling current through an STM tip is proportional to the local DOS of the molecule at the tip. In this section, we did not use any concrete model for the Hamiltonian, the only assumption we needed to make was that the molecule is much more strongly coupled to the metal surface than to the tip, which, at least for metallic surfaces, is always the case.

4. TRANSMISSION THROUGH A MOLECULAR JUNCTION

In this section, we consider a molecular junction [9–15]. The molecular chain is sandwiched between two metallic leads, and it is only coupled to them at its terminal sites. This arrangement is illustrated in Fig. 1b. The escape rate matrices now can be modeled as

$$[\Gamma_1]_{ij} = \Gamma_1 \delta_{ij} \delta_{i1}, \tag{26}$$

$$[\Gamma_2]_{ij} = \Gamma_2 \delta_{ij} \delta_{in}, \tag{27}$$

where once again Γ_1 and Γ_2 are now the escape rates to the source and emitter contacts. Using equation (18), we can calculate the transmission function:

$$T = \Gamma_1 \Gamma_2 Q_{1n} = \Gamma_1 \Gamma_2 |G_{1n}^r|^2. \tag{28}$$

This is a well-known result [16–25], the transmission of a molecular chain is related to the $1-n$ element of the Green function. Using equation (12), we can also calculate the local DOS and the DOS:

$$2\pi N(i, E) = \Gamma_1 Q_{1i} + \Gamma_2 Q_{ni}, \tag{29}$$

$$2\pi N(E) = (\Gamma_1 + \Gamma_2) \sum_i Q_{1i}. \tag{30}$$

In equation (30) we used the fact that our molecular Hamiltonian is mirror symmetric. Again, in the limit of very different couplings $\Gamma_2 \gg \Gamma_1$, the transmission function can be related to the local DOS at the weak coupling terminal: $T = \Gamma_1 2\pi N(1, E)$. This is a natural and rather general result noted by many authors: Due to the strong coupling on one end, the molecule essentially becomes part of the corresponding lead, the transmission is limited and determined by the junction at the other terminal [27–29]. In the case when the couplings are comparable, however, no such simple result is available. We shall discuss this case next.

For a single-site model (and, more generally, in the case of proportionate couplings, even for interacting central regions), a very general relationship exists

between the transmission and the spectral function [30]:

$$T = \frac{\Gamma_1 \Gamma_2}{\Gamma_1 + \Gamma_2} A. \tag{31}$$

To generalize this relation for the multi-site model, we define the *transmittance function τ*, whose physical meaning we will shortly discuss, as

$$T = \frac{\Gamma_1 \Gamma_2}{\Gamma_1 + \Gamma_2} \tau \bar{A}, \tag{32}$$

where $\bar{A}$ is the averaged spectral function, basically the size-scaled DOS:

$$\bar{A} = \frac{1}{n} \text{Tr}[A] = \frac{N(E)}{2\pi n}. \tag{33}$$

The transmittance is a dimensionless function of energy, just like the transmission. By definition, for a single-site model it equals unity, and is independent of energy. Using our simple model, we shall now calculate it for arbitrarily long chains.

To keep the calculation tractable, we will only consider the weak-coupling limit $(\Gamma_1, \Gamma_2 \ll t)$, in this case the advanced (and retarded) Green functions do not depend on the Γs, and for the model defined by equation (6) they are given as

$$[G^{\text{r}}(E)]_{ij} = -\frac{1}{t} \frac{\sin i\theta}{\sin \theta} \frac{\sin(n + 1 - j)\theta}{\sin(n + 1)\theta}, \tag{34}$$

$$\cos \theta = -\frac{(E - \varepsilon)}{2t}, \tag{35}$$

if $i \leq j$, and G^{r}, just like H_{1D}, is symmetric. These formulae yield real θ values for energies such that $|E - \varepsilon| < 2t$, i.e., for energies within the molecular band. Outside of the band the formulae are still valid, but θ becomes purely imaginary. In this parameter regime, substituting the trigonometric functions with their hyperbolic counterparts retains the above forms with real θ. Using equations (12) and (18) once again, we can readily calculate the transmission function and the averaged spectral function:

$$T = \frac{\Gamma_1 \Gamma_2}{t^2} \frac{\sin^2 \theta}{\sin^2(n + 1)\theta}, \tag{36}$$

$$\bar{A} = \frac{\Gamma_1 + \Gamma_2}{4nt^2 \sin^2(n + 1)\theta} \left(2n + 1 - \frac{\sin(2n + 1)\theta}{\sin \theta} \right). \tag{37}$$

The rapidly changing trigonometric denominator gives rise to divergences that correspond to the molecular resonances [16,27,28]. We can see that the DOS contains the same divergent term as the transmission, therefore, at least close to the molecular resonances, the transmission seems to be proportional to the scaled DOS, as suggested by the equation defining τ (equation (32)). The spectral function (see equation (37)) contains the term $\Gamma_1 + \Gamma_2$, which refers to the contacts

rather than to the molecule itself. This is already apparent in equation (12). Indeed, the spectral function in the sense of quantum transport should and does depend on the arrangement of the leads. In the case when the contact self-energies are purely imaginary (such as in the case studied here, see equations (7)–(10)), the effect of the contacts is to broaden the molecular resonant lines, without shifting them. When the weak coupling limit is taken, all the lines remain very narrow, and the spectral function is essentially that of a free molecule. This feature is somewhat disguised in equation (37), a more careful analysis around the poles of the Green function (that takes into account the small but non-zero self-energies) shows the proper limiting behavior.

Comparing equations (36) and (37), and taking into consideration equation (32), we can write the transmittance function as

$$\tau = \frac{4n \sin^2\theta}{2n + 1 - \sin(2n + 1)\theta/\sin\theta}. \tag{38}$$

No divergences and dependence on the contact parameters $\Gamma_{1,2}$ remain in the form for τ. It shows the transmittance function (at least in the weak-coupling limit) is indeed a well-defined *molecular* quantity. We can rewrite equation (38), taking into account the definition of θ (see equation (35)) and the definition of the Chebyshev polynomials of the second kind $U_n(\cos\theta) = \sin[(n+1)\theta]/\sin\theta$ as

$$\tau = \frac{4n(1 - ((E - \varepsilon)/2t)^2)}{2n + 1 - U_{2n}((E - \varepsilon)/2t)}. \tag{39}$$

For even indices, $U_n(x)$ is an even function, therefore the transmittance is a symmetric function of energy. For $n=1$, τ is constant and equals unity by definition, as we have mentioned. When $n=2$, we obtain:

$$\tau(n = 2) = \frac{2t^2}{(E - \varepsilon)^2 + t^2}. \tag{40}$$

The transmittance function is now a Lorentzian, having its maximum at the middle of the molecular band (at $E=\varepsilon$). The DOS for the two-site model is also a combination of two Lorentzians, peaking at the resonances of the molecule (at $\varepsilon \pm t$), but it is important to realize that *the width of these peaks is determined by the coupling to the leads which can be very small (indeed, in our derivations we have taken such limit), while the range of the transmittance function is determined by t, the band-width parameter*. We can already see a behavior that is quite general (as we shall demonstrate later): The sharp peaks in the transmission function are due to its being proportional to the DOS, but the proportionality factor, the transmittance, is a slowly varying function that assumes large values within the entire molecular band. On a more physical note we may say that the transmittance function characterizes the *mechanism* of the transition (ballistic within the band *vs.* tunneling out of the band), while the resonance structure, characterized by the DOS, reflects instances of *quantum interference* of the transferring electron which can greatly enhance or inhibit the transmission.

Figure 2 shows the scaled DOS (solid black line), the transmission function (dashed line) and the transmittance function (solid gray line) for a six-site chain. The functions were calculated numerically, directly applying equations (1), (2), (12), (18) and (32). The hopping parameter t was taken as the unit of energy, and the on-site energy was chosen as the energy reference ($\varepsilon = 0$). To avoid divergence in the DOS and transmission function, a small value was chosen for the leakage rates to the electrodes ($\Gamma_1/t = \Gamma_2/t = 0.1$). In order to show the large changes of the functions, the plot is semi-logarithmic. Inspection of Fig. 2 confirms our conclusions: The DOS and the transmission function show the six resonance peaks within the molecular band. The transmittance function does not change significantly within the band, but it drops sharply at the band edge. The diminishing transmission function outside of the band is mainly a consequence of the drop in the transmittance, not in the DOS.

We now investigate the long chain limit. In this case ($n \to \infty$), within the molecular band ($|E - \varepsilon| < 2t$), the denominator in equation (39) is dominated by the term proportional to n, and we obtain:

$$\tau_{\text{inband}}(n \to \infty) = 2(1 - ((E - \varepsilon)/2t)^2). \tag{41}$$

Transmittance within the band is a simple quadratic function of energy. Its maximum is at the middle of the band, and it goes to zero at the edges of the band. In the long chain limit, transmittance (like the band width) becomes independent of system size. Within the molecular band, sudden changes in the conductance
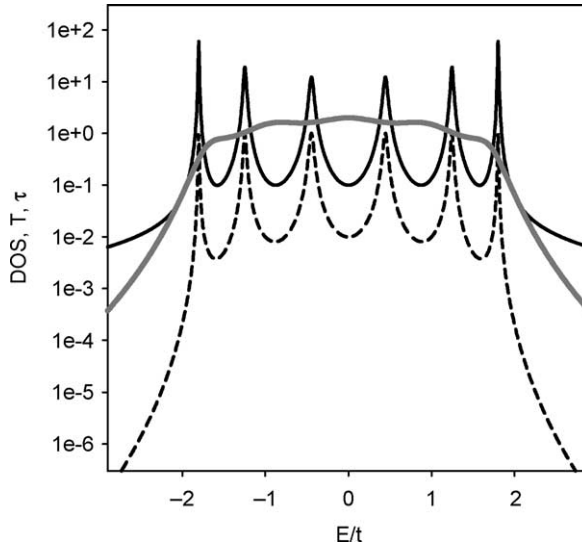
Fig. 2. Density of states, transmission and transmittance for the six site chain, as described in the text. The scaled state density (solid black line) exhibits resonances arising from eigenstates on the bridge. The transmittance (solid gray line) drops beyond the limits of the band, and shows only minimal oscillations within the band itself. The behavior of the overall resulting transmission function (dashed line) is determined by the scaled DOS within the band, and by the transmittance outside of the band.

(either due to size changes or by changing the Fermi energy) are dominated by the instances of *quantum interference*, while the mechanism is always ballistic transmission, signified by the slowly changing transmittance function.

Far outside of the molecular band ($|(E - \varepsilon)| \gg 2t$), the situation is very different. The DOS is proportional to $(t/E - \varepsilon)^2$ and is independent of system size. The denominator in equation (39) is now dominated by the highest order term of the Chebyshev polynomial $2^{2n}((E - \varepsilon)/2t)^{2n}$, and the numerator by $((E - \varepsilon)/2t)^2$. Taking the limit, we obtain

$$\tau_{\text{offband}}(n \to \infty) = n\left(\frac{t}{E - \varepsilon}\right)^{2(n-1)}, \tag{42}$$

and the transmission function is proportional to $(t/(E - \varepsilon))^{2n}$. This is the standard McConnell super-exchange result [10,31,32]. Transmittance now falls exponentially with system size, and the decrease is stronger when the energy is farther from the molecular band. We can see, that *in the off-resonant case it is the transmittance and not the DOS that is mostly responsible for the exponential size-dependence of conduction*. Indeed, it is the tunneling *mechanism*, and not the (missing) instances of *quantum interference* that limits conductance in this regime. We defined the transmittance as the proportionality factor between transmission and the *scaled* DOS, and indeed, within the molecular band it was a natural choice. In the off-band regime, the DOS is independent of system size, therefore the transmittance contains an additional n factor.
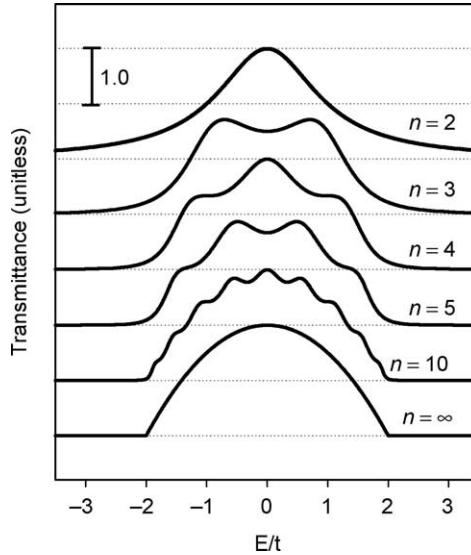
Fig. 3. The transmittance function and its variation with length for the tight binding model. For the two-site case, the exact result demonstrates the transmittance as a Lorentzian. However, for longer chains the transmittance (as in Fig. 2) varies weakly within the band, and drops quite sharply outside the band – this latter dependence dominates the overall transport in this region.

Figure 3 shows the transmittance function for molecular chains with various lengths using the same parameters as in Fig. 2. The functions are shifted for better visibility. For $n=2$, it is a Lorentzian as suggested by the exact result (equation (40)). With growing chain length, the transmittance function shows weak modulations within the band, and drops sharply outside of the band. We also show the exact result obtained in the limit of infinite chain length (equation (41)).

5. CONCLUSIONS

It was realized long ago that conductance properties of a molecule are strongly related to the (local) DOS of the system [1,2]. We rederived the known relationship for an STM arrangement within the non-equilibrium Green function (Keldysh) formalism, using a simple tight-binding model for the molecule, and an empirical description for the contacts. We tried to generalize and explore the conductance-energy level relation also for a molecular junction arrangement. We found it to be both useful and productive of insight to dissect the transmission function into the DOS and a proportionality factor we called transmittance. This way, two very different but equally important aspects of molecular conductance can be individually considered. Transmission can be enhanced or suppressed by instances of quantum interference of the transmitting electron, and is also greatly influenced by the conduction mechanism. We argue that the former is characterized by the DOS, while the latter is determined by the transmittance.

A rough but instructive analogy exists between our formulation of the transmittance τ and the introduction of the transmission coefficient, k, in the activated complex theory of chemical reactions [33]. There one writes the rate constant as $k = kK_{\nu}^{\ddagger}$, with $K_{\nu}^{\ddagger}$ the quasi-equilibrium constant relating concentration at the barrier top to that of the reactants. The analogy arises because in both situations a time rate of change (current or rate constant) is the product of a statistical factor $((\Gamma_1\Gamma_2/\Gamma_1+\Gamma_2)\bar{A}$ or $K_{\nu}^{\ddagger})$ and a dynamical, mechanistic factor $(\tau$ or $k)$. In both cases limits exist in which the dynamical correction is unimportant, so that the statistics $(\Gamma_1\Gamma_2/\Gamma_1+\Gamma_2$ (*scaledDOS*) or $K_{\nu}^{\ddagger})$ completely determines the rate. The essential point of the present chapter is that this limit is appropriate for the STM experiment of Fig. 1a, but not, in general, for the transport junction experiment in Fig. 1b.

While we have limited our discussion to a tight-binding chain, very similar considerations are relevant to interacting electron models as well as electron/environment interactions such as vibronic coupling or dephasing. The general factorization into a scaled state density (describing the energetics of the molecule) and a transmittance that characterizes the transmission mechanism should remain valid and constructive for such more general, more realistic models.

ACKNOWLEDGEMENTS

this research. This paper is dedicated to Jens Oddershede with love, with thanks and with respect for 35 years of science and friendship.

REFERENCES

[1] J. Tersoff and D. R. Hamann, *Phys. Rev. Lett.*, 1983, **50**, 1998.
[2] J. Tersoff and D. R. Hamann, *Phys. Rev. B*, 1985, **31**, 805.
[3] H.-J. Guntherodt and R. Wiesendanger (eds) *Scanning Tunneling Microscopy I: General Principles and Applications to Clean and Adsorbate-Covered Surfaces*, Springer, Berlin, 1992.
[4] R. Wiesendanger and H.-J. Güntherodt (eds) *Scanning Tunneling Microscopy II: Further Applications and Related Scanning Techniques*, Springer, Berlin, 1992.
[5] R. Wiesendanger and H.-J. Güntherodt (eds) *Scanning Tunneling Microscopy III: Theory of STM and Related Scanning Probe Methods*, Springer, Berlin, 1993.
[6] C. J. Chen, *Introduction to Scanning Tunneling Microscopy*, Oxford University Press, New York, 1993.
[7] J. Linderberg and Y. Ohrn, *Propagators in Quantum Chemistry*, Academic Press, New York, 1973.
[8] (a) J. Oddershede, *Adv. Quantum Chem.*, 1978, **11**, 275; (b) J. Oddershede, Adv. Chem. Phys., 1987, **69**, 201.
[9] C. Joachim, J. K. Gimzewski and A. Aviram, *Nature*, 2000, **408**, 541.
[10] A. Nitzan, *Annu. Rev. Phys. Chem.*, 2001, **52**, 681.
[11] A. Nitzan and M. A. Ratner, *Science*, 2003, **300**, 1384.
[12] M. Di Ventra, S. Evoy and J. R. Heflin (eds) *Introduction to Nanoscale Science and Technology*, Kluwer Academic Publishers, Norwell, 2004.
[13] M. A. Reed and T. Lee (eds) *Molecular Nanoelectronics*, American Scientific Publishers, Valencia, CA, 2003.
[14] (a) See in *Mol. Electron.: Sci. Technol.* (Ann. NY Acad. Sci.), **852**; (b) *Mol. Electron. II* (Ann. NY Acad. Sci.), **960**; (c) *Mol. Electron. III* (Ann. NY Acad. Sci.), **1006**.
[15] S. Datta, *Quantum Transport, Atom to Transistor*, Cambridge University Press, Cambridge, in press.
[16] V. Mujica, M. Kemp and M. A. Ratner, *J. Chem. Phys.*, 1994, **101**, 6849.
[17] Y. Q. Xue, S. Datta and M. A. Ratner, *Chem. Phys.*, 2002, **281**, 151.
[18] A. W. Ghosh, P. Damle, S. Datta and A. Nitzan, *MRS Bull.*, 2004, **29**, 391.
[19] S. Datta, *Electronic Transport in Mesoscopic Systems*, Cambridge University Press, Cambridge, 1995.
[20] T. Seideman and W. H. Miller, *J. Chem. Phys.*, 1992, **97**, 2499.
[21] E. G. Emberly and G. Kirczenow, *Mol. Electron.: Sci. Technol. (Ann. NY Acad. Sci.)*, 1998, **852**, 54.
[22] H. Ness and A. J. Fisher, *Phys. Rev. Lett.*, 1999, **83**, 452.
[23] N. S. Hush, *Mol. Electron. III (Ann. NY Acad. Sci.)*, 2003, **1006**, 1.
[24] K. Stokbro, J. Taylor, M. Brandbyge and P. Ordejon, *Mol. Electron. III (Ann. NY Acad. Sci.)*, 2003, **1006**, 212.
[25] M. Buttiker, *IBM J. Res. Dev.*, 1988, **32**, 63.
[26] Z. Bihary and M. A. Ratner, *Phys. Rev. B*, submitted.
[27] V. Mujica, M. Kemp, A. Roitberg and M. A. Ratner, *J. Chem. Phys.*, 1996, **104**, 7296.
[28] M. Kemp, A. Roitberg, V. Mujica, T. Wanta and M. A. Ratner, *J. Phys. Chem.*, 1996, **100**, 8349.
[29] S. Datta, W. D. Tian, S. H. Hong, R. Reifenberger, J. I. Henderson and C. P. Kubiak, *Phys. Rev. Lett.*, 1997, **79**, 2530.
[30] Y. Meir and N. S. Wingreen, *Phys. Rev. Lett.*, 1992, **68**, 2512.
[31] H. McConnell, *J. Chem. Phys.*, 1961, **35**, 508.
[32] M. A. Ratner, *J. Phys. Chem.*, 1990, **94**, 4877.
[33] An elementary but enlightening discussion is given by D. G. Truhlar and the authors in R. S. Berry, S. A. Rice, J. Ross, *Physical Chemistry*, 2nd edn., Oxford, 2000, sec. 30.6.

GW Method for Extended, Periodic Systems with a Mixed Slater-Orbital/Plane-Wave Basis and Fourier Transform Techniques

Hendrik J. Monkhorst

Quantum Theory project, University of Florida,
Gainesville, FL 32611-8435, USA

Abstract

A pitch is made for a renewed, rigorous and systematic implementation of the GW method of Hedin and Lundquist for extended, periodic systems. Building on previous accurate Hartree–Fock calculations with Slater orbital basis set expansions, in which extensive use was made of Fourier transform methods, it is advocated to use a mixed Slater-orbital/plane-wave basis. Earlier studies showed the amelioration of approximate linear dependence problems, while such a basis set also holds various physical and analytical advantages. The basic formalism and its realization with Fourier transform expressions is explained. Modern needs of materials by precise design, assisted by the enormous advances in computational capabilities, should make such a program viable, attractive and necessary.

Contents

1. REMINISCENCES AS PROLOGUE

It was in March (or April) of 1972 when Jens and I first met, in Salt Lake City. We had arranged that he and his family lived in our house from about October 1971 till then, while I spent a 'mini-sabbatical' in Croatia. Jens spent his first postdoctoral study in the group of Frank Harris and me. We hit it off immediately, and decided to collaborate on the electron-correlation problem in rigorous solid-state calculations. Jens was (understandably) full of Green's functions at the time, and he educated me about its powers and elegance. Frank Harris and I had reached the point of 'near-perfection' in calculating the first, very accurate Hartree–Fock (HF) energies and wavefunctions for solid atomic hydrogen [1]. We were using Fourier transform

techniques with a Slater orbital basis. Jens and I set out to use these results and, at the random-phase approximation (RPA) level, got total correlation energies for various lattice constants. I remember that we had trouble getting our first paper accepted to *Phys. Rev. Lett.* We met Jim Krumhansl, then the PRL Editor-in-Chief, on one of his many ski visits, ostensibly to meet Gale Dick in the Physics Department of the University of Utah. We convinced him (maybe it was just Jens, he was and is known to be quite persuasive!) that this was a very significant paper on the outstanding problem of rigorous correlation treatment in solids. At the time, only very approximate treatments were in vogue, all based on the electron gas model. We were essentially the first ones to implement the RPA with very accurate HF bands and energies. We could show that the total energies had much more realistic values and variation with the lattice constant. At the time, it caught the attention of experimentalists attempting to metallize hydrogen under megabar pressures.

So, we got the paper published in PRL [2], and two more papers resulted from our collaboration [3,4]. I still remember fondly those youthful, upbeat and inspiring days in Utah, when our science seemed limitless and all fun, Jens' pipe tobacco smelled good, and our discussions (often very political) were vigorous, and opiniated. Can we go back to those days, Jens? Happy birthday!

What follows can be rightly seen as a (long-delayed) afterthought to our happy Utah sojourns.

2. MOTIVATION

When considering truly rigorous, *ab initio* studies of periodic systems one implicitly adopts a number of criteria that the needed methods and numerical techniques have to satisfy. These are

1. Adoption of a many-body theory that is systematically improvable (at least in principle) and testable for its numerical convergence;
2. Avoidance of unphysical, analytical 'pathologies' intrinsic to a particular truncation of the hierarchy of sophistication levels in that theory;
3. Realization with basis sets for Bloch orbital expansions that are physically, analytically and/or practically motivated, and also systematically improvable and testable;
4. Computability of quantities that enable the extraction of properties specific for extended systems, such as density of states, bandwidths and gaps, and other spectral properties, i.e., response properties physically and conceptually most directly associated with experiments;
5. Adoption of numerical techniques that maximally exploit space group symmetry, the periodic boundary condition, and the nature of the basis set;
6. Possibility of a practical, yet again systematically improvable introduction of temperature via phonons, so central to condensed matter properties.

Criterion 1 seems to exclude the DFT-based methods, because systematic improvements are elusive, and we cannot state, in any precise manner, which many-body effects have been included. Criterion 2 suggests only limited use of

'pure' Hartree–Fock calculations. Although Hartree–Fock provides a variational upper bound to the total crystal energy, this property is not of primary interest to solid-state physics. In addition, the infamous 'Hartree–Fock pathology' [5] causes problems for the response properties under criterion 4.

Typical Bloch orbital basis sets are made up from plane waves, Gaussians or Slater-type functions. Plane wave basis sets, albeit analytically and numerically attractive, suffer from the need for very large sizes. This results from their inadequacy of describing atom-like behavior near nuclei, often overlooked (or down-played) in solid-state theory. Gaussian basis sets have the advantage of easy computability of all crystal integrals, whether in momentum ($\mathbf{p}$) or configuration ($\mathbf{r}$) space, as in quantum chemistry. However, their ability to describe accurate orbital behavior near nuclei is also limited because of their analytical behavior for all finite $\mathbf{r}$ or $\mathbf{p}$. Only Slater functions are capable to describe the correct cusp behavior, at least in principle. To the extent that one needs, or desires 'good nuclear cusps', even with limited basis set sizes, such functions are essentially mandatory.

Traditional evaluation of integrals involving Slater functions is notoriously difficult and time consuming. Uniform accuracy control is also a problem. As a result, only diatomic quantum chemical calculations are sometimes performed with Slater bases. On the other hand, when solid-state calculations are performed in $\mathbf{p}$ space, all crystal integrals can be expressed as reciprocal lattice sums. This is described in a series of papers by Harris, Monkhorst and coworkers; a summary is provided in 'Hartree–Fock density of states for extended systems', by Monkhorst [5], and references therein. In this formulation, the reciprocal lattice sums are over terms involving Fourier transforms of basis functions only. Therefore, the advantages of using Gaussians over Slater functions largely disappear: Fourier transforms are in closed form, and simple for either functions. In this formulation, full exploitation of space group symmetries is also possible. It carries the additional advantage of rigorously handling the conditionally convergent lattice sums (see Ref. [5]).

Brillouin zone integrations, pervasive in any solid-state calculation, are best performed with the Monkhorst–Pack scheme [6]. These integrations are essentially equally demanding in any representation and with any basis set. This satisfies criterion 5.

In our opinion, the use of and calculations for one-particle Green's functions are uniquely suitable for solid-state systems periodic in any number of dimensions. When faithfully implemented, it satisfies all criteria above. Green's functions offer analytically compact and physically rich tools for representing many properties for extended, periodic systems. They satisfy powerful and elegant relations for quantities such as density of states, lifetimes for excitations, dielectric functions, photo-emission and absorption spectra, total crystal energies, and many more.

This position is nothing new; it was succinctly and convincingly laid out in a pair of papers by Hedin [7] and Hedin and Lundquist [8], now well over 30 years ago. Particularly, the second paper is an impressive, and valuable review of the full powers of the Green's function method. Frankly, we believe that most, if not all important theoretical aspects have been identified in these papers.

What is new is the modern computer capability of better dealing with needed speed and memory for the substantial effort to implement the Green's function

method faithfully, accurately and systematically. In addition, the analytical and numerical advances made by us (Refs. [5,6]) should allow a more efficient organization of the calculations.

A specific incarnation of the Green's function method is its so-called *GW* approximation (because of the form of the self-energy), first proposed by Hedin [7]; it is often referred to as the *GW* method. Its formal structure, and possible extensions if needed, will be reviewed in the next section. A realization by representation in **p** space, with attendant reciprocal lattice sums, will then be given. Notation and derivation follow closely that given in Ref. [5]. Next, calculation of the so-called self-energy, screened potential, dielectric and irreducible polarization propagator matrices is discussed. Calculation of the last matrix is the core of the computational effort; all other matrices depend on it, and are computationally much less demanding. We conclude with a summary, pointing out challenges and possibilities ahead, as well as questions with regard to incorporation in existing solid-state program packages.

3. THE GW METHOD

Many-body perturbation theory (MBPT) for periodic electron systems produces many terms. All but the first-order term (the exchange term) diverges for the electron gas and metallic systems. This behavior holds for both the total and self-energy. Partial summations of these MBPT terms must be made to obtain finite results. It is a well-known fact that the sum of the most divergent terms in a perturbation series, when convergent, leads often to remarkably accurate results [9–11].

The GW method, defined by Hedin in 1965 [7] (see also Ref. [8]), accomplishes such a partial sum for Σ. The GW method is thoroughly reviewed in Aryasetiawan and Gunnarsson (AG) [13] and Aulburn *et al.* (AJW) [14] in publications through 2000. Much of previous work relies heavily on DFT-zeroth order calculations, and few attempts are made to achieve convergence. As expected, Aissing and Monkhorst [12] could show that the pathology in the HF DOS at the Fermi level is absent in the GW method, regardless of the shape of the Fermi surface, and for any dimensionality of periodic systems. It was also found [12] that using HF as a zeroth order state will *not* remove this (unphysical) vanishing of the DOS at the Fermi surface, even after iterations towards a converged solution of Σ. This singularity is weakened, but not removed.

We start by sketching the formal structure of the GW method. This is followed by a realization with a AO-PW basis set.

3.1. Formal structure

We closely follow Hedin [7], and the notation of Monkhorst [5]. The *one-particle Green's function operator* $\hat{G}$ satisfies the equation

$$(E - \hat{T} - \hat{V} - \hat{C})\hat{G}(E) - \hat{\Sigma}(E)\hat{G}(E) = \hat{I} \tag{1}$$

$\hat{T}$, $\hat{V}$ and $\hat{C}$ are the kinetic, nuclear potential and Hartree-like, electron–electron repulsion potential operators, respectively. $\hat{\Sigma}(E)$ is the *self-energy* operator. The *crystal quasi-particle states* are denoted by $|\mu\mathbf{k}\rangle$ and their energies by $E_\mu(\mathbf{k})$, with μ the band index, and $\mathbf{k}$ the Bloch vector. With these quantities $\hat{G}(E)$ can be given the *spectral resolution*

$$\hat{G}(E) = \sum_{\mu\mathbf{k}} \frac{|\mu\mathbf{k}\rangle\langle\mu\mathbf{k}|}{E - E_\mu(\mathbf{k}) - i\delta_\mu(\mathbf{k})}, \tag{2}$$

where

$$\delta_\mu(\mathbf{k}) = \begin{cases} 0^+, & E_\mu(\mathbf{k}) < E_{\mathrm{F}} \\ 0^-, & E_\mu(\mathbf{k}) \geq E_{\mathrm{F}} \end{cases} \tag{3}$$

with E_{F} the Fermi energy. As a result the $|\mu\mathbf{k}\rangle$ satisfy [7]

$$(E_\mu(\mathbf{k}) - \hat{T} - \hat{V} - \hat{C})|\mu\mathbf{k}\rangle - \hat{\Sigma}(E_\mu(\mathbf{k})|\mu\mathbf{k}\rangle = 0 \tag{4}$$

Given an expression for the self-energy operator, equations (2) and (4) must be solved self-consistently. $\hat{\Sigma}(E)$ is also called the *exchange-correlation potential*; it is manifestly non-local and energy dependent.

$E_\mu(\mathbf{k})$ can be, and in fact are generally complex. Their real part corresponds to the average of some group of excited states, and their imaginary part to their spread (related to life times of quasi-particles).

The self-energy determines the many-body accuracy for $\{|\mu\mathbf{k}\rangle, E_\mu(\mathbf{k})\}$, thus $\hat{G}(E)$. Following Hedin [7] and Hedin and Lundqvist [8], $\hat{\Sigma}(E)$ is expanded in terms of a *screened potential* $\hat{W}$, rather than the bare Coulomb potential $\hat{v}$ (atomic units are used throughout):

$$\hat{\Sigma}(E) = i\hat{G} \otimes \hat{W}(E) + O(\hat{W}^2) \tag{5}$$

where

$$f \otimes g(E) = \int \frac{\mathrm{d}E'}{2\pi} f(E - E')g(E')\exp(-i\Delta E') \tag{6}$$

with $\Delta = 0^+$. $\hat{W}(E)$ can be obtained from an integral equation, expressed formally

$$\hat{W}(E) = \hat{v} + \hat{W}(E)\hat{P}(E)\hat{v} \tag{7}$$

The kernel $\hat{P}$ can be expanded as

$$\hat{P}(E) = -i\hat{G} \otimes \hat{G}(E) + O(\hat{G}^2\hat{W}\hat{G}^2) \tag{8}$$

$\hat{P}(E)$ is called the *irreducible polarization propagator*, and $\hat{W}(E)$ the *dielectrically screened interaction*.

The *GW* method of Hedin [7] amounts to approximating $\hat{\Sigma}(E)$ with the first terms of equations (5) and (8). To the extent it was implemented faithfully to solid-state problems, the approximation was found to be very satisfactory. Below we will argue why this should be so.

A formal solution for $\hat{W}(E)$ of equation (7) is

$$\hat{W}(E) = \hat{v}(\hat{I} - \hat{P}(E)\hat{v})^{-1} \equiv \hat{v}\hat{\varepsilon}^{-1}(E) \tag{9}$$

with the *dielectric 'matrix'* $\hat{\varepsilon} = \hat{I} - \hat{P}\hat{v}$.

$\hat{P}$ is the central quantity in the *GW* method, and carries many-body effects beyond the *HF* approximation. In the limit $\hat{P} \to 0$, the self-energy limits to

$$\hat{\Sigma}(E) \to \hat{\Sigma}_{\text{HF}} = i\hat{G}_{\text{HF}} \otimes \hat{v} \tag{10}$$

$\hat{\Sigma}_{\text{HF}}$ is energy independent, but non-local.

Note that in equations (1) and (4), $(\hat{V} + \hat{C})$ is a multiplicative operator in **r** representation, and a convolution operator in **p** representation. $\hat{\Sigma}(E)$ is neither convolution nor multiplicative-like in either representation because

$$\langle \mathbf{r}|\hat{\Sigma}(E)|\mathbf{r}'\rangle \neq f(\mathbf{r} - \mathbf{r}') \tag{11}$$

Moreover, because of its energy dependence, it is not Hermitian, so that

$$\langle \mu\mathbf{k}|\nu\mathbf{k}\rangle \neq \delta_{\mu,\nu}. \tag{12}$$

Of course, due to the energy independence of $\hat{\Sigma}_{\text{HF}}$,

$$\hat{\Sigma}_{\text{HF}}^{\dagger} = \hat{\Sigma}_{\text{HF}}. \tag{13}$$

Thus, orthonormality of $|\mu\mathbf{k}\rangle_{\text{HF}}$ is assured, and $E_\mu(\mathbf{k})$ are real.

The *GW* method seems very limited, given the very large number of perturbative terms that are omitted. However, experience has shown great improvements, and predictive precision over Hartree–Fock calculations. The reason is that, with the Coulomb potential

$$\langle \mathbf{r}|\hat{v}|\mathbf{r}'\rangle = \frac{1}{|\mathbf{r} - \mathbf{r}'|}, \tag{14}$$

$\hat{W}(E)$ from equation (7) contains the sum of the most divergent terms in each order of MBPT, *regardless of $|\mu\mathbf{k}\rangle$ describing a localized or delocalized state in* **r** *representation*. It is well known in mathematical physics that the sum of convergent or lesser divergent terms in each order is often smaller, and in fact generally small, compared to this 'leading sum' [9]. This is also true for $\hat{P}(E)$. Of course, to the extent that we find the results for $|\mu\mathbf{k}\rangle$ and $E_\mu(\mathbf{k})$ wanting, we can add terms of order $\hat{W}^2$ to $\hat{\Sigma}$, and/or terms of order $\hat{W}$ to $\hat{P}(E)$. (Vertex corrections may also be important).

3.2. Total energy expression

With a converged $\hat{G}(E)$ we can calculate the total energy of the system. Writing

$$\mathbf{x} = (\mathbf{r}, \zeta), \quad \mathbf{x}' = (\mathbf{r}', \zeta'), \tag{15}$$

for space-spin coordinates, the total energy is given by [7]

$$E_{\text{tot}} = -i \int \frac{\mathrm{d}E}{2\pi} \exp(i\Delta E) \mathrm{Tr}\left(\hat{T} + \hat{V} + \frac{1}{2}\hat{C} + \frac{1}{2}\hat{\Sigma}(E) \right) \hat{G}(E) + R$$

$$= -i \int \frac{\mathrm{d}E}{2\pi} \exp(i\Delta E) \int \mathrm{d}\mathbf{x} \left\langle \mathbf{x} \left| \left(\hat{T} + \hat{V} + \frac{1}{2}\hat{C} + \frac{1}{2}\hat{\Sigma}(E) \right) \hat{G}(E) \right| \mathbf{x} \right\rangle + R, \tag{16}$$

with $\Delta = 0^+$. R is the nuclear repulsion term. Note that, because of $\Sigma_{\mathbf{k}}$ in $\hat{G}$ (see equation (2)), E_{tot} is proportional to the number of unit cells N.

Since $\hat{T}$, $\hat{V}$ and $\hat{C}$ are spin independent, and since

$$-i \int \frac{\mathrm{d}E}{2\pi} \exp(i\Delta E) \hat{G}(E) = \sum_{\mu\mathbf{k}} |\mu\mathbf{k}\rangle n_\mu(\mathbf{k}) \langle\mu\mathbf{k}| \tag{17}$$

where

$$n_\mu(\mathbf{k}) = \begin{cases} 1, & E_\mu(\mathbf{k}) < E_{\text{F}} \\ 0, & E_\mu(\mathbf{k}) \geq E_{\text{F}} \end{cases} \tag{18}$$

we can also write

$$E_{\text{tot}} = 2 \sum_{\mu\mathbf{k}} n_\mu(\mathbf{k}) \left\langle \mu\mathbf{k} \left| \hat{T} + \hat{V} + \frac{1}{2}\hat{C} \right| \mu\mathbf{k} \right\rangle + R$$

$$- i \int \frac{\mathrm{d}E}{2\pi} \int \mathrm{d}\mathbf{r} \exp(iE\Delta) \langle \mathbf{r}|\hat{\Sigma}(E)\hat{G}(E)|\mathbf{r}\rangle \tag{19}$$

The $(\mu\mathbf{k})$ sum represents the Hartree-like contribution to E_{tot}. As explained in Ref. [5], the $\hat{V}$, $\frac{1}{2}\hat{C}$ and R terms exhibit singularities that cancel. When expressed in $\mathbf{p}$ representation, the result is a lattice structure constant (equation (27) of Ref. [5]), and reciprocal lattice sums for $\langle\mu\mathbf{k}|\hat{V}|\mu\mathbf{k}\rangle$ and $\langle\mu\mathbf{k}|\frac{1}{2}\hat{C}|\mu\mathbf{k}\rangle$, omitting $\mathbf{K} = 0$.

Notice that

1. The factors '2' for both terms in equation (19) are due to spin integration.
2. The $|\mu\mathbf{k}\rangle$ are *not orthogonal*, but *are assumed normalized*:

$$\langle\mu\mathbf{k}|\mu\mathbf{k}\rangle = 1 \tag{20}$$

3. E_{tot} is not variational, i.e., not an upper bound to the exact energy. Because the $\{|\mu\mathbf{k}\rangle, E_\mu(\mathbf{k})\}$ are solved self-consistently, the propagator lines in diagrams are so-called dressed.

4. Both terms will be proportional to N because of

$$\sum_{\mathbf{k}} \rightarrow \frac{N v_0}{(2\pi)^3} \int d^3 k,$$

with v_0 the volume of the unit cell.

4. IMPLEMENTATION

During the 1970s Harris and I developed Fourier transform methods and programs to perform *ab initio* HF calculations with Slater-type basis orbitals. For a review of the formalism and references to earlier work, see Ref. [5]. The key findings were that the formalism handles the Madelung summations problem, and the calculation of rigorous exchange and all central Fourier quantities, in an efficient, transparent and accurate manner. All quantities are expressed as reciprocal lattice sums involving Fourier transforms of the Slater functions only. This is true for core and valence-type functions. Formulas can be interpreted in terms of deviations of real crystals from the electron gas model. All singularities arising from the Coulomb potential are removed explicitly.

Approximate linear dependence of AO-based sets is always a numerical problem, especially in 3D extended systems. Slater functions are no exceptions. We studied and recommended the use of mixed Slater/plane-wave (AO–PW) basis sets [15]. It offers a good compromise of local accuracy (nuclear cusps can be correctly described), global flexibility (nodes in $|\mu\mathbf{k}\rangle$ outside primitive unit cell can be correct) and reduced PW expansion lengths. It seems also beneficial for GW calculations that need low-lying excited bands (not available with AO bases), yet limited numbers of PWs. Computationally the AOs and PWs mix perfectly: mixed AO–PW matrix elements are even easier to calculate than those involving AO–AO combinations.

The expansion of the quasi-particle states thus assumes the form

$$|\mu\mathbf{k}\rangle = \sum_{p} |p\mathbf{k}\rangle C_{p\mu}(\mathbf{k}) + \sum_{\mathbf{K}} |\mathbf{K} + \mathbf{k}\rangle C_{\mathbf{K}\mu}(\mathbf{k}) \qquad (21)$$

The AO-basis Bloch functions are, as sum over reciprocal lattice vectors,

$$|p\mathbf{k}\rangle = \frac{N^{-1/2}}{v_0} \sum_{\mathbf{K}'} |\mathbf{K}' + \mathbf{k}\rangle \langle \mathbf{K}' + \mathbf{k}|p\rangle \qquad (22)$$

v_0 is the unit cell volume, $\langle \mathbf{r}|\mathbf{Q}\rangle = \exp[-i\mathbf{Q}\cdot\mathbf{r}]$, and

$$\langle \mathbf{Q}|p\rangle = \int d\mathbf{r} \langle \mathbf{Q}|\mathbf{r}\rangle \langle \mathbf{r}|p\rangle \qquad (23)$$

is the Fourier transform (FT) of AO $|p\rangle$. The equations for $\mathbf{C}(\mathbf{k})$ can be written as [12]

$$[\mathbf{T}(\mathbf{k}) + \mathbf{V}(\mathbf{k}) + \mathbf{C}(\mathbf{k}) + \Sigma(E_\mu(\mathbf{k}), \mathbf{k}) - E_\mu(\mathbf{k})\mathbf{S}(\mathbf{k})]\mathbf{C}_\mu(\mathbf{k}) = 0 \qquad (24)$$

where

$$O_{ij}(\mathbf{k}) \equiv \langle i\mathbf{k}|\hat{O}|j\mathbf{k}\rangle, \quad \hat{O} = \hat{T}, \hat{V}, \hat{C}, \hat{I} \text{ or } \hat{\Sigma}(E) \qquad (25)$$

and $|i\mathbf{k}\rangle = |p\mathbf{k}\rangle$ or $|\mathbf{K}\mathbf{k}\rangle = |\mathbf{K}+\mathbf{k}\rangle$. See Ref. [5] for detailed working expressions for $\hat{O} = \hat{T}, \hat{V}, \hat{C}$ and $\hat{I}$. $\mathbf{V}(\mathbf{k})$ and $\mathbf{C}(\mathbf{k})$ have singularities that cancel; it amounts to the removal of $\mathbf{K}=0$ from the reciprocal lattice sums. Σ is the self-energy matrix, and presents the main computational challenge. For details we again refer to Ref. [12]. For example, at the GW level, $\Sigma_{pq}(\mathbf{k})$ can be written as

$$\Sigma_{pq}(E, \mathbf{k}) \equiv \langle p\mathbf{k}|\hat{\Sigma}(E)|q\mathbf{k}\rangle$$
$$= \frac{1}{v_0^2} \sum_{\mathbf{K},\mathbf{K}'} \langle p|\mathbf{K}+\mathbf{k}\rangle\langle\mathbf{K}+\mathbf{k}|\hat{\Sigma}(E)|\mathbf{K}'+\mathbf{k}\rangle\langle\mathbf{K}'+\mathbf{k}|q\rangle \qquad (26)$$

with

$$\langle\mathbf{Q}_1|\hat{\Sigma}(E)|\mathbf{Q}_2\rangle$$
$$= \frac{i}{(2\pi)^3} \int d\mathbf{k}' \sum_{\mathbf{K},\mathbf{K}'} \langle\mathbf{K}+\mathbf{k}'|\hat{G}|\mathbf{K}'+\mathbf{k}'\rangle \otimes \langle\mathbf{K}+\mathbf{k}'-\mathbf{Q}_1|\hat{W}(E)|\mathbf{K}'+\mathbf{k}'-\mathbf{Q}_2\rangle$$

$$(27)$$

Of course, major simplifications occur when i and/or j in equation (25) are plane waves $|\mathbf{K}\mathbf{k}\rangle$. With the expression (9) for $\hat{W}(E)$ we derive

$$\langle\mathbf{Q}_1|\hat{W}(E)|\mathbf{Q}_2\rangle = \frac{4\pi}{Q_1^2}\langle\mathbf{Q}_1|\hat{\varepsilon}^{-1}(E)|\mathbf{Q}_2\rangle \qquad (28)$$

where we can write for the reciprocal space vectors $\mathbf{Q}_1 \equiv \mathbf{K}_1 + \mathbf{q}$, $\mathbf{Q}_2 \equiv \mathbf{K}_2 + \mathbf{q}$, with $\mathbf{K}_1$, $\mathbf{K}_2$ reciprocal lattice vectors and $\mathbf{q}$ within the first Brillouin zone (FBZ). Also writing

$$\varepsilon^{-1}_{\mathbf{K}_1\mathbf{K}_2}(\mathbf{q}, E) \equiv \langle\mathbf{Q}_1|\hat{\varepsilon}^{-1}(E)|\mathbf{Q}_2\rangle, \qquad (29)$$

the inverse of the dielectric matrix $\varepsilon(\mathbf{q})$ (see equation (9)),

$$\varepsilon_{\mathbf{K}\mathbf{K}'}(\mathbf{q}, E) = \delta_{\mathbf{K}\mathbf{K}'} - P_{\mathbf{K}\mathbf{K}'}(\mathbf{q}, E)\frac{4\pi}{|\mathbf{K}'+\mathbf{q}|^2} \qquad (30)$$

The real work goes into calculating $P_{\mathbf{K}\mathbf{K}'}$ (see equation (8)) and the convolution of equation (27). The latter also can be performed with FT techniques [14,16].

The former can be expressed, among other forms, as

$$P_{\mathbf{K}\mathbf{K}'}(\mathbf{q}, E) = -\frac{2v_0}{(2\pi)^3} \sum_{\mu,\nu} \int d\mathbf{k}\, n_\mu(\mathbf{k})(1 - n_\nu(\mathbf{k}-\mathbf{q}+\mathbf{K}_1))$$
$$\times \frac{E_\nu(\mathbf{k}-\mathbf{q}+\mathbf{K}_1) - E_\mu(\mathbf{k})}{(E_\nu(\mathbf{k}-\mathbf{q}+\mathbf{K}_1) - E_\mu(\mathbf{k}))^2 - E^2} \Psi_{\mu\nu}(\mathbf{K}+\mathbf{q}, \mathbf{k})\Psi^*_{\mu\nu}(\mathbf{K}'+\mathbf{q}, \mathbf{k})$$

$$(31)$$

$n_\mu(\mathbf{k})$ are band occupation numbers, and

$$\Psi_{\mu\nu}(\mathbf{Q},\mathbf{k}) = \frac{1}{v_0} \sum_{\mathbf{K}''} \langle\mu|\mathbf{K}'' + \mathbf{k}\rangle \langle\mathbf{K}'' + \mathbf{k} + \mathbf{Q}|\nu\rangle \qquad (32)$$

and $\mathbf{K}_1$ in equation (31) is chosen such that $(\mathbf{k} - \mathbf{q} + \mathbf{K}_1)$ is within the FBZ. With equation (21) the $\Psi_{\mu\nu}$ can be reduced to corresponding quantities involving the basis functions $|p\rangle$ and PWs; we leave out details, except to stress that all the terms in equation (31) are analytic, converge well and for core–core-like elements real space evaluation can be done accurately. When equidistant special reciprocal space grids are chosen [6], sums/differences of vectors on this grid also are on this grid. Thus, there is no need for lattice interpolations. We may want to obtain Padé approximants for the E dependence to enable the convolution integrals of equation (27).

5. DISCUSSION

The core of the computational effort is the calculation of the self-energy matrix $\Sigma(E,\mathbf{k})$. Quite obviously, the rate-determining step is the evaluation of the irreducible polarization propagator matrix $\mathbf{P}(\mathbf{q},E)$, equation (31). This is needed for as many $(\mathbf{K},\mathbf{K}')$ reciprocal lattice vectors, and E and $\mathbf{q}$ points as possible, and required for convergence. It is well known that total energies are quite insensitive to details of band energies and wave functions. On the other hand, the latter quantities determine most of the interesting solid-state properties, such as density of states, bandwidths and gaps, transition probabilities and the like. It is therefore important to monitor the convergence of such properties as a function of basis sets, $\mathbf{k}$, E, $\mathbf{q}$ integration points and $\mathbf{K}$ summations.

New insights should be sought, and numerical experimentation will be necessary. For example, 'clever' interpolations or Padé functions can be 'invented' to give global expressions for some matrix elements. We could also consider the evaluation of the convolution-type E integrals with a Fourier transform technique. In addition, much of existing solid-state computational technology can be brought to bear.

As pointed out above, we can equally easily use Slater-type bases. The only expense is the somewhat slower convergence in $\mathbf{K}$ summations. As discussed in Ref. [5], and references therein, we can use a mixture of configuration and momentum space sums when core-like basis functions are involved.

6. EPILOGUE

Jens and I started an attempt at a systematic, rigorous inclusion of electron correlation effects on solid-state properties. We hailed both from a quantum chemistry tradition of formal clarity, analytical and numerical care, and attention for efficient programming techniques. On the other hand, the solid-state theory tradition followed, and continues to travel a very different route. This path is

characterized by reliance on semi-quantitative concepts such as the electron gas-based and pseudo-potential model descriptions. Much less attention is being paid to quantitative rather than qualitative results such as trends, power laws of properties, etc. As a result, notions of high accuracy and/or many-body or numerical convergence are of considerably lesser interest. The arrival of density functional theory on the solid-state calculational scene perpetuated, if not solidified this trend. Although great computational effort is expended on evermore complicated crystals using a number of widely available programs, it is fair to state that no significant theoretical advances are pursued. The schism between the quantum chemistry and band-theoretical approaches remains. Jens's and my start went cold.

And yet, the desire for designing materials with specific properties is only gaining. Examples are semi-conducting behavior, laser action at particular wave-lengths, magnetic properties, super-conduction at high temperatures, etc. Most, if not all of these properties are subtly determined by electron correlation and phonon effects. Just having the right trends of their quantitative behavior is then not sufficient, instead a full recognition of the crystal's stoichiometry is required; after all, atoms and/or molecules make up such systems.

It is therefore my conviction that, rather sooner then later, we will see a resurgence of the precise many-body approach to solid-state theory as we envisioned. Almost assuredly the GW method will be the tool of choice. I hope to see those days, and maybe Jens and I can enjoy them together.

REFERENCES

[1] (a) F. E. Harris and H. J. Monkhorst, in *Computational Methods in Band Theory* (eds P. M. Marcus, J. F. Janak and A. R. Williams), Plenum Press, New York, 1971, pp. 517–541; (b) F. E. Harris and H. J. Monkhorst, *Solid State Commun.*, 1971, **9**, 1449; (c) F. E. Harris, L. Kumar and H. J. Monkhorst, *Int. J. Quantum Chem.*, 1971, **6**, 601; (d) see also references to earlier, Fourier transform treatments of the Madelung problem.
[2] H. J. Monkhorst and J. Oddershede, *Phys. Rev. Lett.*, 1973, **30**, 797.
[3] J. Oddershede, L. Kumar and H. J. Monkhorst, *Int. J. Quantum Chem.*, 1974, **S8**, 447.
[4] L. Kumar, H. J. Monkhorst and J. Oddershede, *Int. J. Quantum Chem.*, 1977, **12**, 145.
[5] H. J. Monkhorst, *Phys. Rev.*, 1979, **B20**, 1504.
[6] H. J. Monkhorst and J. D. Pack, *Phys. Rev.*, 1976, **B13**, 5188.
[7] L. Hedin, *Phys. Rev.*, 1965, **139**, A796.
[8] L. Hedin and S. Lundquist, *Solid State Phys.*, 1969, **23**, 2.
[9] C. M. Bender and S. A. Orszag, *Advanced Mathematical Methods for Scientists and Engineers I – Asymptotic Methods and Perturbation Theory*, Springer, Berlin, 1999.
[10] (a) M. Gell-Mann and K. Brueckner, *Phys. Rev.*, 1957, **106**, 364; (b) M. Gell-Mann, *Phys. Rev.*, 1957, **106**, 369.
[11] D. M. Ceperley and B. J. Alder, *Phys. Rev. Lett.*, 1980, **45**, 566.
[12] G. Aissing and H. J. Monkhorst, *Int. J. Quantum Chem.*, 1993, **S27**, 81.
[13] F. Aryasetiawan and O. Gunnarsson, *Rep. Prog. Phys.*, 1998, **61**, 237.
[14] W. G. Aulburn, L. Jönsson and J. W. Wilkins, *Solid State Phys.*, 2000, **54**, 1.
[15] G. Aissing and H. J. Monkhorst, *Int. J. Quantum Chem.*, 1992, **43**, 733.
[16] W. Ku and A. G. Eguiluz, *Phys. Rev. Lett.*, 2002, **89**, 126401.

Orientational Effects in Energy Deposition by Protons in Water

Remigio Cabrera-Trujillo,[1] John R. Sabin,[1,2] Erik Deumens[1] and Yngve Öhrn[1]

[1]*Departments of Physics and Chemistry, University of Florida, Gainesville, FL, USA*
[2]*Kemisk Institut, Syddansk Universitet, Odense, Denmark*

Abstract

We consider here the orientational aspects of the stopping of swift protons by the water molecule. The calculations are dynamical in nature, and they are compared to the electronic structure-based calculations made by Oddershede *et al.* on similar quantities. The comparisons, although qualitative, show good agreement between the two approaches.

Contents

1. DEDICATION

Over the years, Jens Oddershede has written extensively on various aspects of energy deposition by swift ions in material targets. In many cases, he has been concerned with the orientational effects of target molecules with respect to the projectile beam direction, and has explained these differences in the context of the relevant oscillator strength distribution of the target [1–8]. It is in the spirit of Jens' work that we carried out this study of the orientational aspects of the energy deposition by swift protons in water, and we report them now in celebration of his the-third-times-twentieth birthday.

2. INTRODUCTION

We consider the linear energy loss, or stopping power [9–12], of a non-relativistic swift ion as it passes through matter. The energy transfer (loss) from the ion to the target atoms or molecules is usually represented as $-dE/dx$. From simple conservation of energy and momentum, it is clear that at all but the lowest collision energies, the bulk of the energy transfer will be to target electrons, leading to electronic excitation and/or ionization. That transfer involves only matrix elements corresponding to polarizations (momentum transfer) perpendicular to the direction of the projectile velocity [4]. Consequently, as directions are important here, and as it is now becoming possible to make a target molecule orientationally homogeneous with respect to the projectile beam, understanding of the details of the effects of target orientation in ion–molecule collisions becomes important.

   We will restrict our considerations to electronic stopping where energy transfer is from the kinetic energy of the projectile to the target *via* electronic excitation. It should be noted, however, there are other modes of energy transfer that can be studied, for example, energy transfer to target nuclei kinetic energy (known as nuclear stopping, and effective only at low projectile energy), and to vibrational and rotational modes of polyatomic systems.

   Much of the work of Jens Oddershede on energy deposition has been done from the viewpoint of the calculation of the oscillator strength distribution, either the generalized oscillator strength distribution (GOSD) or the dipole approximation to it (DOSD). In these cases, a perturbative treatment which is based on the assumption that the scattering is sufficiently weak, i.e., that the projectile–target interaction is weak enough that one may apply first-order perturbation theory in the interaction, is normally used. The most fundamental quantity describing such an interaction in the first Born approximation is the generalized oscillator strength (GOS) distribution of the target system [13–15]. The GOS distribution completely determines the differential cross section for inelastic scattering of swift projectiles from target atoms or molecules (or any other target, for that matter) at the level of the first Born approximation.

   The method used to obtain the results presented here is quite different, and is based in scattering theory rather than in perturbation theory.

   In the scattering theory approach, the stopping power, or energy loss per unit length for a projectile of energy E_p, can be written in terms of a differential scattering cross section $d\sigma/d\Omega$ as

$$-\frac{1}{n}\frac{dE}{dx} = S(E_p) = -\int \Delta E(E_p, \Omega)\frac{d\sigma}{d\Omega}d\Omega = -\int b\Delta E(E_p, b)db\,d\varphi \qquad (1)$$

where n is the density of target scattering centers and ΔE is the kinetic energy loss of the projectile. Here, we have used the deflection function, $\Theta(b)$ to transform the angular integral to the impact parameter (b) representation. The energy-dependent stopping power normalized by the density of scattering centers, n, is the stopping cross section ($S(E_p)$).

Calculation of many trajectories at different impact parameters for each given incident energy yields the energy-dependent deflection function and energy loss, which can then, through equation (1), be used to calculate the stopping cross section.

Our goal in this work is to understand the process of energy loss suffered by protons when they collide with water, and by which modes energy is transferred to the target. In particular, we are interested in the orientational dependence of the stopping power.

3. METHODOLOGY

The scheme we employ uses a Cartesian laboratory system of coordinates which avoids the spurious small kinetic and Coriolis energy terms that arise when center of mass coordinates are used. However, the overall translational and rotational degrees of freedom are still present. The unconstrained coupled dynamics of all participating electrons and atomic nuclei is considered explicitly. The particles move under the influence of the instantaneous forces derived from the Coulombic potentials of the system Hamiltonian and the time-dependent system wave function. The time-dependent variational principle is used to derive the dynamical equations for a given form of time-dependent system wave function. The choice of wave function ansatz and of sets of atomic basis functions are the limiting approximations of the method. Wave function parameters, such as molecular orbital coefficients, $z_i(t)$, average nuclear positions and momenta, $\mathbf{R}_k(t)$ and $\mathbf{P}_k(t)$, etc., carry the time dependence and serve as the dynamical variables of the method. Therefore, the parameterization of the system wave function is important, and we have found that wave functions expressed as generalized coherent states are particularly useful. A minimal implementation of the method [16,17] employs a wave function of the form:

$$|\Psi(t)\rangle = |\mathbf{R}(t), \mathbf{P}(t)\rangle|z(t), \mathbf{R}(t), \mathbf{P}(t)\rangle = |\phi\rangle|z\rangle \tag{2}$$

where the first term contains the nuclear coordinates, and is coupled to the second term, which contains the electronic coordinates. Here, the electronic wave function is expressed as a complex, spin unrestricted, single determinant:

$$|z\rangle = \det\{\chi_i(\mathbf{x}_j)\} \tag{3}$$

where $\mathbf{x}_j$ is the three-dimensional position coordinate and spin of electron j. The determinantal wave function is built from non-orthogonal dynamical spin orbitals:

$$\chi_i = \phi_i + \sum_{j=N+1}^{K} \phi_j z_{ji}, \quad i = 1, 2, ..., N \tag{4}$$

which, in turn, are expressed in terms of a basis of atomic spin orbitals $\{\phi_i\}$ of rank K. These, in turn, are expanded in a basis of traveling Gaussian, centered on the average nuclear positions $\mathbf{R}$ and moving with momentum $\mathbf{P}$ [17]. The time-dependent variational principle requires the action to be stationary under

variations of the wave function, yielding, in the narrow nuclear wave packet limit, the Lagrangian for the composite system [17]. One should also note that the molecular orbital coefficients z are complex.

The Euler–Lagrange equations can be formed for the dynamical variables $q = R_{jl}, P_{jl}, z_{ph}, z_{ph}^*$ and collected into a matrix equation which, when solved, yields the wave function for the compound system at each time step.

This level of theory outlined above is implemented in the *ENDyne* code [18]. The explicit time dependence of the electronic and nuclear dynamics permits illustrative animated representations of trajectories and of the evolution of molecular properties. These animations reveal reaction mechanisms and details of dynamics otherwise difficult to discern, making the approach particularly suitable for the study of the subtleties of contributions to the stopping cross section.

We emphasize that in this treatment trajectories are neither preselected nor restricted: thus, they need not be straight. Although the total charge of the projectile/target system is fixed, charge exchange between the projectile and target may happen. Molecular bonds are not fixed: the target, or the projectile, in appropriate cases, may fragment. Total system energy is fixed and conserved, but conversion among translational, electronic, vibrational, and rotational energy is not restricted. Total momentum and angular momentum are also conserved.

Details of the method and its implementation can be found in Refs. [16,17,19,20].

3.1. Deflection function

Once we have calculated the dynamics of the collision, we obtain the final electronic wave function, as well as the final nuclear momenta and positions. We observe that even for relatively large impact parameters, the projectile suffers an appreciable deflection.

At the terminus of each trajectory, we obtain the final momentum of the projectile, $\hbar\mathbf{k}_f(E_p, b)$, which defines the deflection function for the projectile when projected on the initial momentum, $\hbar\mathbf{k}_i$, i.e.,

$$\Theta(E_p, b) = \arccos[\mathbf{k}_f(E_p, b) \cdot \mathbf{k}_i / k_f(E_p, b)k_i] \tag{5}$$

for each impact parameter b, which describes the dynamical interaction between projectile and target. The scattering angle is defined as the absolute value of the deflection function for the projectile, i.e., $\theta = |\Theta(E_p, b)|$.

3.2. Direct differential cross section

From the deflection function we calculate the differential cross section which is needed in equation (1). We note that there could be several different trajectories (two different impact parameters) that produce the same scattering angle, leading to quantum mechanical interference of their nuclear wave functions. We thus

introduce semiclassical corrections to the narrow nuclear width approximation (classical nuclei) used in the minimal implementation of electron nuclear dynamics.

We have implemented semiclassical corrections *via* the Schiff approximation [21] for small scattering angles. The direct differential cross section in the Schiff approximation within the END approximation is given by [22]

$$\frac{d\sigma}{d\Omega} = \frac{k_f}{k_i} |f(\theta, \varphi)|^2 \tag{6}$$

with the scattering amplitude

$$f(\theta, \varphi) = ik_i \int_0^\infty J_0(qb)(e^{2i\delta(b)} - 1)b \, db \tag{7}$$

Here, $J_0(x)$ is the Bessel function of zero order, $q = |\mathbf{k}_f - \mathbf{k}_i|$ is the momentum transfer, which depends on the scattering angle θ, and $\delta(b)$ is the semiclassical phase shift, which is given in terms of the deflection function as $\Theta(b) = d\delta(b)/2k_i \, db$.

Using the deflection function, we then obtain the direct differential cross section. Note that for high energies, the direct differential cross section typically shows Rutherford scattering, characteristic of a heavy ion scattering process. However, for low projectile energies, the long collision time and the changing electronic structure of the ion can modify the interaction potential dynamically, producing a rainbow angle, and thus interference in the direct differential cross section.

In other words, the classical direct differential cross section

$$\frac{d\sigma}{d\Omega} = \frac{b}{\sin\theta \left|\frac{d\Theta}{db}\right|} \tag{8}$$

will diverge at the rainbow angle, as at that point $|d\Theta/db| = 0$. Furthermore, we note that the Schiff approximation takes into account the quantum effects of forward scattering.

3.3. Electron transfer cross section

During a projectile–target collision, the possibility of charge exchange exists. One might expect that either of the collision partners might gain or lose electrons through charge exchange or ionization. (We note that although ionization is included in the electron nuclear dynamics theory, it is not part of the current implementation. Thus, we restrict out studies to projectile energies below the ionization threshold, which occurs at about 100 keV, which is approximately the peak in the stopping cross section.) From the evolving molecular state wave function, we can determine the number of electrons associated with a projectile and/or target by the use of the Mulliken population analysis [23], and from this we can extract the probability of electron capture

or loss. From equations (3) and (4), the total number of electrons in the system is [24]

$$N = \sum_{\nu,\mu} P_{\nu\mu} \varDelta_{\mu\nu} = \sum_{\nu} (\mathbf{P}\varDelta)_{\nu\nu} = \mathrm{Tr}(\mathbf{P}\varDelta) \tag{9}$$

where $P_{\nu\mu} = \sum_i z_{i\nu} z_{i\mu}$ and $\varDelta_{\mu\nu}$ is the atomic orbital overlap matrix. It is possible to interpret $(\mathbf{P}\varDelta)_{\mu\mu}$ as the number of electrons to be associated with the basis function u_μ. Thus, $n_A = \sum_{\mu \in A} (\mathbf{P}\varDelta)_{\mu\mu}$ is the number of electrons associated with nuclei A. Knowing the initial number of projectile electrons allows one to calculate the probability for electron capture or loss.

From the probability for charge exchange, the charge exchange cross section can be obtained from

$$\sigma_{\mathrm{exch}}(E_{\mathrm{p}}) = 2\pi \int_0^\infty P_{\mathrm{exch}}(b, E_{\mathrm{p}}) b \, \mathrm{d}b \tag{10}$$

4. COMPUTATIONAL DETAILS

In order to calculate a stopping cross section for a molecule using a dynamics method, one sets the molecule in a lab-fixed coordinate frame with a specific orientation specified by the Euler angles and internal coordinates of the molecule. In this study the target water molecule was placed with the oxygen atom at the origin of a Cartesian laboratory. We then specify sets of orientations by the relation of the dipole moment vector of water to the velocity vector of the incoming beam (along the z-axis).

We consider three sets of orientations:

Orientation a. The molecule is lined up with the dipole moment vector either parallel or antiparallel to the z-axis. The molecule is rotated about the dipole vector. The molecule is rotated about the z-axis.
Orientation b. The molecule is aligned with the dipole vector along the x-axis, and the molecule in the xz-plane. The dipole vector is then rotated about the z-axis in the xy-plane.
Orientation c. The molecule is aligned with the dipole vector along the x-axis and the molecule in the xy-plane. The dipole vector is then rotated about the z-axis with the dipole vector in the xy-plane.

Each of these orientations is depicted in Fig. 1.

For each of the three orientations depicted in Fig. 1, calculations were made for the molecule rotated about the z-axis by 0, 90, 180, and 270° with respect to the original position. For each position the initial projectile velocity was parallel to the z-axis, and directed toward the target with an impact parameter b, measured perpendicular to the z-axis. A total of 72 impact parameters were used for each position. The projectile was started 30 a.u. from the target and the trajectory was followed until the projectile was 30 a.u. past the target, or until there were no longer changes in the energy or charge of the projectile.

(a) x

H

In the xz-plane, rotation about the z-axis

z

H

(b)

H   H   In the xz-plane, rotation about the z-axis

z

(c)   H H

In the xy-plane, rotation about the z-axis

z
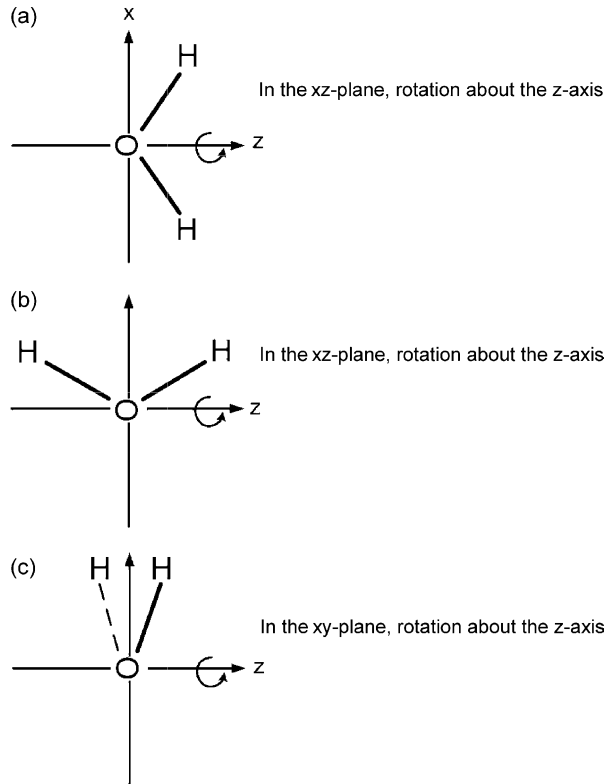
Fig. 1. Orientations of molecules used for determining the stopping power of oriented water.

The basis functions used for the atomic orbital expansion were derived from those of Dunning [25], and were centered on the moving nuclei. For O a [10s5p/3s2p] was used [26], while for H a [5s1p/3s1p] basis [27] with an added diffuse s-orbital was used. The combination of these basis sets on the determinant describing the total system (supermolecule description), as required by equation (3), produces a set of 24 accessible virtual orbitals for the target in its Hartree–Fock ground state. The electronic ground state of water is $^1A_1$ so the supermolecule will remain a singlet throughout the calculations.

The computations yielding the positions, momentum, and wave function coefficients were performed using our ENDyne code [18].

5. RESULTS AND DISCUSSION

Oddershede's earlier results [3–5] calculate the directional values of the dipole oscillator strength distribution for use in the Bethe theory [9], which is valid for high-energy projectiles. Our approach, since we have not implemented the possibility of treating unbound electrons, is restricted to calculating stopping cross

sections for projectile energies below the ionization threshold. Although this makes comparison of the two approaches difficult, one might expect the same qualitative results in the region of the stopping maximum. It is in this region that we will make the connection.

The total electronic stopping cross sections for the three independent directions in which the water molecule has been oriented with respect to the beam axis are presented in Fig. 2, along with the experimental results of Reynolds *et al.* [28] for comparison.

Although the calculated directional stopping cross sections in the region of the maximum differ among themselves by amount only something less than 10%, it is clear that they are clearly distinct in this region, and with order $S_t(a) > S_t(c) > S_t(b)$. Oddershede's earlier results [3,5] give the mean excitation energies in the order $I_0^x > I_0^z > I_0^y$ which, since in Bethe's theory $S \propto 1/I_0$, would result in $S_y > S_z > S_x$.

To compare to Oddershede's earlier result, one must realize that contributions to the excitation spectrum of the target molecule can only come from momentum transfers perpendicular to the projectile momentum [4]. Thus, the identification between Oddershede's polarization directions and the orientational directions used here can be made, and the results are, as expected, in qualitative agreement.

The orientational average of the directional stopping cross sections can also be taken, in which case the total stopping cross section, S_t, is obtained, and is presented here in Fig. 3, again, along with the results of Reynolds *et al.*, indicated by the filled circles. The agreement of our result with that of Reynolds *et al.* is quite good on the lower projectile energy end of the experiments, but begins to diverge from, and become larger than, the experiments at the higher energy end. This can be attributed to the fact that we do not treat ionization correctly, and that
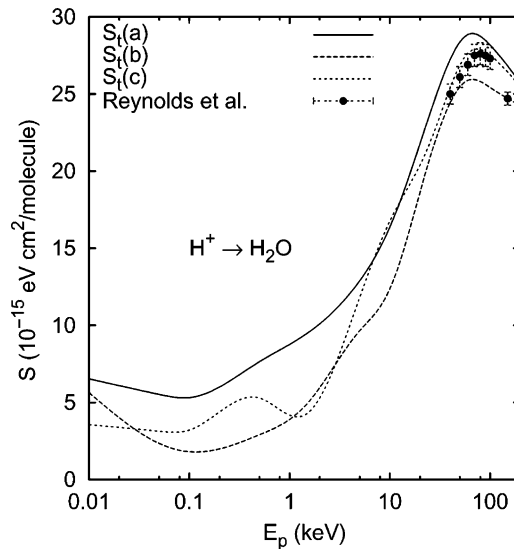
Fig. 2. Stopping cross section for protons impinging on oriented H_2O as a function of proton velocity. See Fig. 1 for the definition of target orientations.
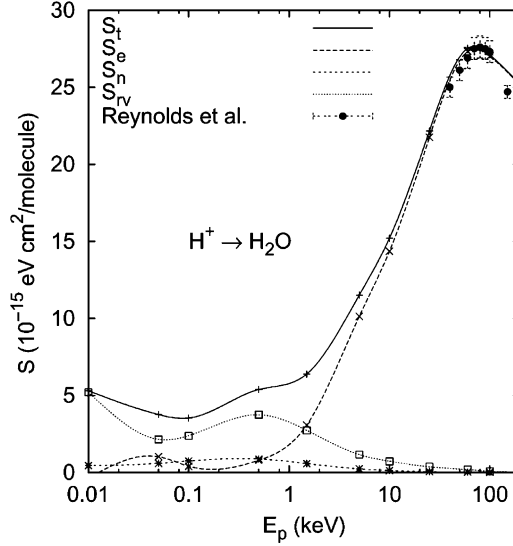
Fig. 3. Orientationally averaged total stopping cross section S_t for protons impinging on H_2O as a function of proton velocity along with the experimental results of Reynolds *et al.* (filled circles) [28]. S_e, S_n, and S_{rv} represent the electronic, nuclear, and rovibrational contributions to the stopping, respectively.

the advent of the ionization threshold at around $E_p = 100$ keV gives an additional contribution to the stopping that we do not represent properly.

In addition to the total stopping cross section (S_t), we present the electronic (S_e), nuclear (S_n), and rovibrational (S_{rv}) contributions to the stopping in Fig. 3. In all cases, the symbols represent the projectile energies where the stopping was calculated. We note that next to the electronic stopping, the largest contribution to the total stopping for projectile energies above 1 keV or so is the rovibrational stopping. The water molecule has two high-frequency vibrational modes (the symmetric stretch at 3657 cm^{-1} and the asymmetric stretch at 3756 cm^{-1}) which have maxima in their cross sections around the projectile energy $E_p < 1$ keV. The bump in $S_{rv}(E_p)$ is reflected in the total stopping cross section. At very low energies, one expects no electronic stopping, due to the relatively high energy of the first electronic transition in water (7.5 eV). The rovibrational energy transfer channel is still open, however, even at low energies, which causes a rise in the total stopping at low energy. As the molecular mass is large compared to that of a proton, the nuclear stopping is small, and negligible at projectile energies above 10 keV.

In the simplest case, one expects $S(v) = (1/3) \sum S_i(v)$ where i identifies one of the three orientations. Although this identity is not obeyed exactly in this calculation, as the orientational grid used is somewhat coarse, it is nearly satisfied.

More interesting, perhaps, is the observation that $S_t(c)$ is very close to the total stopping cross section, S_t. This would imply that in the Bethe formulation, the mean excitation energy associated with the random orientation and that associated

with Oddershede's *z*-polarization should be nearly identical, which is indeed the case.

6. FINAL REMARKS

The results reported here stem from a very different approach to stopping theory from that used by Oddershede *et al.* in their various excursions into the calculations of stopping cross sections. While all of their work has been done in the context of electronic structure calculations with stopping cross sections extracted *via* oscillator strength distributions, the results presented here are dynamical. While Oddershede *et al.* calculate average electronic properties of target (and occasionally projectile) molecules, we have concentrated on the properties of individual projectile/target collisions, and then averaged them. It is gratifying to see that the two approaches give consistent results, although they are vastly different in inception.

Finally, Jens Oddershede has contributed to many branches of atomic and molecular theory, and all of us are proud to have been associated with him over the years. Two of us (RCT and JRS) have been privileged to be called *et al.*!

ACKNOWLEDGEMENTS

REFERENCES

[1] J. Geertsen, J. Oddershede and J. R. Sabin, *Phys. Rev. A*, 1986, **34**, 1104.
[2] P. Jensen, J. Oddershede and J. R. Sabin, *Phys. Rev. A*, 1991, **43**, 4040.
[3] S. P. A. Sauer, J. R. Sabin and J. Oddershede, *Phys. Rev. A*, 1993, **47**, 1123.
[4] H. H. Mikkelsen, J. Oddershede, J. R. Sabin and E. Bonderup, *Nucl. Instrum. Methods B*, 1995, **100**, 451.
[5] S. P. A. Sauer, J. R. Sabin and J. Oddershede, *Nucl. Instrum. Methods B*, 1995, **100**, 458.
[6] J. R. Sabin and J. Oddershede, *Nucl. Instrum. Methods B*, 1996, **115**, 79.
[7] E. K. Dalskov, J. Oddershede and J. R. Sabin, *Proc. Am. Phys. Soc.*, 1997, **CP392**, 1373.
[8] R. Cabrera-Trujillo, J. R. Sabin and J. Oddershede, *Adv. Quantum Chem.*, 2004, **46**, 121.
[9] E. Bonderup, *Penetration of Charged Particles Through Matter*, 2nd edn., Fysisk Instituts Trykkeri, Aarhus Universitet, Aarhus, Denmark, 1981.
[10] P. Sigmund, *Stopping of Heavy Ions, A Theoretical Approach*, Springer, Karlsruhe, 2004.
[11] R. Cabrera-Trujillo and J. R. Sabin (eds.) *Theory of the Interaction of Swift Ions with Matter. Part 1. Advances in Quantum Chemistry*, Elsevier, Amsterdam, 2004.
[12] R. Cabrera-Trujillo and J. R. Sabin (eds.) *Theory of the Interaction of Swift Ions with Matter. Part 2. Advances in Quantum Chemistry*, Elsevier, Amsterdam, 2004.
[13] H. Bethe, *Ann. Phys. (Leipzig)*, 1930, **5**, 325.
[14] M. Inokuti, *Rev. Mod. Phys.*, 1971, **43**, 297.
[15] M. Inokuti, Y. Itakawa and J. E. Turner, *Rev. Mod. Phys.*, 1978, **50**, 23.
[16] E. Deumens, A. Diz, H. Taylor and Y. Öhrn, *J. Chem. Phys.*, 1992, **96**, 6820.
[17] E. Deumens, A. C. Diz, R. Longo and Y. Öhrn, *Rev. Mod. Phys.*, 1994, **66**, 917.

[18] E. Deumens, T. Helgaker, A. Diz, H. Taylor, B. Mogensen, J. Morales, M. Coutinho, A. Blass, R. Cabrera-Trujillo and D. Jacquemin, *ENDyne Version 5 Software for Electron Nuclear Dynamics*, Quantum Theory Project, University of Florida, Gainesville, FL, 2002, http://www.qtp.ufl.edu/endyne.html

[19] Y. Öhrn, E. Deumens, A. Diz, R. Longo, J. Oreiro and H. Taylor, in *Time Dependent Molecular Dynamics* (eds J. Broeckhove and L. Lathouwers), Plenum Press, New York, 1992, pp. 272.

[20] R. Cabrera-Trujillo, J. R. Sabin, E. Deumens and Y. Öhrn, *Adv. Quantum Chem.*, 2004, **45**, 99.

[21] L. I. Shiff, *Phys. Rev.*, 1956, **103**, 443.

[22] R. Cabrera-Trujillo, J. R. Sabin, Y. Öhrn and E. Deumens, *Phys. Rev. A*, 2000, **61**, 032719.

[23] R. S. Mulliken, *J. Chem. Phys.*, 1962, **36**, 3428.

[24] R. Cabrera-Trujillo, Y. Öhrn, E. Deumens and J. R. Sabin, *Nucl. Instrum. Methods B*, 2000, **168**, 484.

[25] T. H. Dunning, *J. Chem. Phys.*, 1989, **90**, 1007.

[26] T. H. Dunning and P. J. Hay, in (ed. H. F. Schaefer III.), Plenum Press, New York, 1977.

[27] L. T. Redmon, G. D. Purvis III. and R. J. Bartlett, *J. Am. Chem. Soc.*, 1979, **101**, 2856.

[28] H. K. Reynolds, D. N. Dunbar, W. A. Wenzel and W. Whaling, *Phys. Rev.*, 1953, **92**, 742.

Low-Lying Excited States of the Hydrogen Molecule in Cylindrical Harmonic Confinement

John M. H. Lo,[1] Mariusz Klobukowski[1] and Geerd H. F. Diercksen[2]

[1]*Department of Chemistry, University of Alberta, Edmonton, Alta., Canada T6G 2G2*
[2]*Max-Planck-Institut für Astrophysik, Karl-Schwarzschild-Straße 1, D-85741 Garching, Germany*

Abstract

The low-lying excited states of the hydrogen molecule confined in the harmonic potential were studied using the configuration interaction method and large basis sets. Axially symmetric harmonic oscillator potentials were used. The effect of the confinement on the geometry and spectroscopic constants was analyzed. Detailed analysis of the effect of confinement on the composition of the wavefunction was performed.

Contents

1. INTRODUCTION

The study of atoms and molecules in external fields is a fascinating area of research that has attracted much attention from different areas of science and engineering. Following the influential work of Loudon in 1959, in which he performed the quantum mechanical analysis of the behavior of a one-dimensional hydrogen atom in various Coulomb potentials [1], many studies have been carried out to understand the physics of excitons (hydrogen-like electron–hole pair) and some related systems [2–5]. The discovery of neutron stars and white dwarf stars further motivated rapid development of this field since it stimulated the interest of studying the variation of electronic structure and behavior of atomic and

molecular systems when they are under the magnetic field in which the Lorentz force outweighs the Coulombic interaction [6,7]. Besides the exploration of the process of star evolution, several areas of condensed-matter physics, in particular the studies of quantum Hall effects and quantum dots, also require an in-depth theoretical framework that explains the motion of electrons and particles in strong electric and magnetic fields [8]. Electrons, when being spatially localized in either quasizero-, one-, or two-dimensions by means of an applied electric or magnetic field, exhibit unique properties that are absent without external confinement [9]. Extensive investigations, both theoretical and experimental, have been performed, and some useful results have been obtained. The advances in the technology of lithographic etching [10] allow for the facile creation of quantum dots, wires, and wells of various sizes and numbers of electrons, which greatly assist the intense experimental research of these intriguing objects. To date, quantum dots and wells have already been widely used in electronic and opto-electronic devices, such as compact discs and microwave antennas, as well as in medical science, for instance, as imaging biosensors of living cells [11].

Despite being the simplest neutral molecule, dihydrogen molecule (H_2) is of great importance to astrophysics, atomic and molecular physics, solid-state physics, plasma physics, catalysis, and fuel cell studies. Hydrogen is the first element synthesized in the formation of a star, and is found to exist in the interstellar space and in a wide range of cosmic objects. It is the most abundant molecular species and constitutes approximately 92% of the matter in the Universe [12,13]. Hence, the studies of magnetized hydrogen provide a vital information for the mapping of the life-cycle of a star and the evolution of the universe. From the theoretical viewpoint, hydrogen molecule is the best candidate for the benchmarking calculations when testing new theories due to its structural simplicity and the availability of highly accurate experimental spectroscopic constants [14]. Since the first qualitative quantum mechanical calculation performed in 1927 [15], hydrogen molecule has been extensively studied using various methods, in which the computation carried out by Kolos and Wolniewicz was the most remarkable [16].

In contrast to a large number of studies on H_2 in field-free environment, the investigations of H_2 in the presence of strong fields are rather limited. Most of these calculations center on the H^+ molecular ion [17–20]. Recently, the behavior of H_2 in strong to superstrong magnetic fields has became a topic of considerable interest, and several calculations have been performed concerning the explanation of some unusual phenomena of hydrogen molecules in superstrong fields ($B \geq 10^{11}$ G) [21,22]. Calculations performed by Lai *et al.* using Hartree–Fock method suggested the existence of long-chain polymers of hydrogen on the surface of neutron stars where the magnetic field is as strong as 10^{12} G [23]. A subsequent study by Demeur *et al.* also supported the stability of finite chains of hydrogen in very intense magnetic fields [24]. In addition, a number of changes in both the electronic structure and geometry of H_2 were proposed. Korolev and Liberman found that the total spin of the hydrogen molecule in an ultra-high magnetic field becomes one as a result of a triplet ground state [22]. The analysis by Ortiz *et al.* using variational quantum Monte Carlo method proved that the hydrogen molecule possesses the ground state symmetry of $^3\Pi_0$ in superstrong

magnetic fields [25]. On the other hand, the studies conducted by Detmer *et al.* using configuration interaction method predicted that the $^3\Sigma_u$ state would be the ground state when the magnetic field strength is moderate ($B \approx 0.2$ a.u.) [26]. These investigations also showed that both the ground and excited states of H_2 will be more strongly bound and in certain circumstances local maxima appear at large internuclear distances which have no counterparts in the field-free situation [26–28]. Moreover, different vibrational excitation levels were obtained when the orientation of the applied magnetic field was changed, which gives rise to a continuum opacity in the photoionization of excited-state H_2 on neutron star [29]. The chaotic behavior of the energy levels of H_2 in Rydberg state may also result from the linear and quadratic Zeeman interaction induced by the application of a magnetic field [30].

The laterally confining potential of a small quantum dot can be approximated by a smooth parabolic well in the cases where the scattering states are to be neglected due to the generalized Kohn theorem [31]. Maksym and Chakraborty [32], and Bakshi *et al.* [33] demonstrated, using far-infrared spectroscopy (FIR), that the resonance energy of a quantum dot is independent of the number of confined electrons, which is a unique characteristic of a parabolic potential. The Hartree–Fock modeling of a GaAs quantum dot (300×300 nm) with $N \leq 10$ electrons revealed that the parabolic confining potential that is approximately circularly symmetric, with the diameter of about 100 nm, leads to the observed magnetic-field-dependence of energy levels [34].

In the present work a cylindrical harmonic potential has been adopted as a model potential of a 2-dimensional quantum well. The potential energy curves (PEC) of the ground and low-lying excited states of H_2 aligned along the axis of the potential have been calculated using the method of configuration interaction with single and double substitutions (CISD) (in the case of H_2 this corresponds to full configuration interaction method) and the results of computations are reported below together with the analysis of the associated wavefunctions. Comparison with the results from the studies of hydrogen molecule in a parallel magnetic field [22,25–27] has been made. Several similarities as well as differences are observed for the excited states of hydrogen molecule when it is embedded in the two potentials and they are discussed in the following sections.

2. METHOD OF COMPUTATION

Within the Born–Oppenheimer approximation, the non-relativistic electronic Hamiltonian of an N-electron molecular system in the presence of an external potential can be written (in atomic units) as

$$\mathcal{H}_{\mathrm{el}}(\vec{r}) = -\frac{1}{2} \sum_{i=1}^{N} \nabla_i^2 - \sum_{\alpha=1}^{K} \sum_{i=1}^{N} \frac{Z_\alpha}{|\vec{R}_\alpha - \vec{r}_i|} + \sum_{i>j}^{N} \frac{1}{|\vec{r}_i - \vec{r}_j|} + \mathcal{V}(\vec{r}) \quad (1)$$

$$\mathcal{H}_{\mathrm{el}}(\vec{r}) = \mathcal{H}(\vec{r}) + \mathcal{V}(\vec{r}). \quad (2)$$

$\vec{r} \equiv \{\vec{r}_1, \vec{r}_2, \ldots, \vec{r}_N\}$ represents the spatial coordinates of the electrons while $\vec{R} \equiv \{\vec{R}_1, \vec{R}_2, \ldots, \vec{R}_K\}$ denotes the nuclear coordinates. The first two terms in equation (1) describe, respectively, the electronic kinetic energy and electron–nuclear attraction and the third term is a two-electron operator that represents the electron–electron repulsion. These three operators comprise the electronic Hamiltonian in free space. The term $\mathcal{V}(\vec{r})$ is a generic operator for an external potential. One of the common ways to express $\mathcal{V}(\vec{r})$, when it is affecting electrons only, is to expand it as a sum of one-electron contributions

$$\mathcal{V}(\vec{r}) = \sum_{i=1}^{N} V(\vec{r}_i), \tag{3}$$

in which the one-electron operators may be written as

$$V(\vec{r}_i) = \frac{1}{2}[\omega_x^{n_x+1}(x_i - b_x)^{2n_x} + \omega_y^{n_y+1}(y_i - b_y)^{2n_y} + \omega_z^{n_z+1}(z_i - b_z)^{2n_z}] \tag{4}$$

where $r_i = (x_i, y_i, z_i)$. The form of equations (3) and (4) provides great flexibility for the description of potentials of various forms. The potential $\mathcal{V}(\vec{r})$ will be reduced to a 3-dimensional anisotropic harmonic oscillator when $n_x = n_y = n_z = 1$. In the present work, it was assumed that $\omega_z = 0$ and $\omega_x = \omega_y = \omega$ in order to model an approximate lateral parabolic potential which is co-axial to the hydrogen molecule aligned along the z-axis. In addition, the center of confining potential was chosen to coincide with the center of mass of the molecule, i.e., $b_x = b_y = b_z = 0$. Hence, the resulting one-electron interaction potential is

$$V(\vec{r}_i) = \frac{\omega^2}{2}[x_i^2 + y_i^2], \tag{5}$$

and the complete electronic Hamiltonian used in the present work is

$$\mathcal{H}_{el}(\vec{r}_1, \vec{r}_2) = -\frac{1}{2}\sum_{i=1}^{2}\nabla_i^2 - \sum_{i=1}^{2}\sum_{\alpha=1}^{2}\frac{1}{|\vec{r}_i - \vec{R}_\alpha|} + \frac{1}{|\vec{r}_1 - \vec{r}_2|} + \frac{\omega^2}{2}\sum_{i=1}^{2}(x_i^2 + y_i^2). \tag{6}$$

The potential of equation (5) acts only on electrons and, in consequence, affects the electronic wavefunctions, electron density, as well as the PECs.

The PECs of hydrogen molecule were calculated using the configuration interaction (CI) method implemented in the modified version of GAMESS-US program [35]. Preliminary calculations were carried out using the object-oriented OPENMOL program [36]. The configuration state functions (CSFs) were generated by the Graphical Unitary Group Approach (GUGA) [37] in which all possible single and double excitations from the occupied to virtual one-electron orbitals were included. The canonical orbitals obtained by solving the Hartree–Fock–Roothaan equations were used. The total energies of the molecule in different symmetry states were computed as the eigenvalues of the full CI matrix. The virtual space was not truncated.

The basis set adopted in the calculations was optimized to yield good values of both the ground and excited state energies of hydrogen atom. Detailed analysis of the basis set will be given in the following section. In addition

to the atom-centered Gaussian basis set, a set of basis functions (1s1p1d), with the exponents of $\omega/2$, was added at the mid-bond position of the hydrogen molecule in order to appropriately account for the distortion of electron density due to the external harmonic potential. This mixed basis set strategy has been tested on numerous atomic systems such as confined two-electrons quantum dots, negative hydrogen ion, helium atom and lithium atom [38,39], and satisfactory results have been obtained. It is expected that these confinement functions should behave equally well in the molecular cases. The recent study of lithium dimer confined in an ellipsoidal harmonic potential [40] showed that the use of the confinement functions ensures the proper description of avoided crossings between the electronic states and of their correct dissociation limits.

3. RESULTS AND DISCUSSION

3.1. Basis set

One of the bottlenecks of the modern quantum chemical calculations is the large number of integrals that have to be evaluated. Depending on the nature of the formalism, the scaling may vary from K^5 to K^{10}, where K is the number of basis functions, which makes the calculations including explicit treatment of electron correlation very expensive computationally. The full CI method, which is size-consistent, can yield the variationally exact eigenvalues within the space spanned by the given basis set. However, it suffers from the fact that a tremendous number of determinants will be generated and this number grows factorially with respect to the number of basis functions. Therefore, the application of full CI calculations is limited to very small systems. As a two-electron system, hydrogen molecule is the best candidate for the benchmark calculation of different sophisticated post-Hartree–Fock methods because rather small number of integrals must be computed even when a comparatively large basis set is used. Another advantage of employing hydrogen molecule in calculations is that experimental data of high precision are available that allow for verification of a method. Consequently, hydrogen molecule has been extensively studied by various quantum chemical methods [16,41–47], and an enormous number of basis sets have been designed for accurate computations of structures and properties of hydrogen-containing compounds.

Recently, Tachikawa and Osamura have applied the fully variational molecular orbital method (FVMO), combined with the full CI wavefunctions, to obtain very accurate geometries and excitation energies of the ground and excited states of hydrogen molecule [48]. Their study also showed that full CI calculations using large correlation-consistent basis sets do not necessarily yield results that agree very well with the experiment. Severe problems appeared in the estimations of excitation energies T_e, which for the $^1\Pi_u$ state was about $6325\,\mathrm{cm}^{-1}$ ($\sim 6.3\%$) overestimated. Due to the limitations of the correlation-consistent basis sets for the excited state studies, a new atomic basis set has been designed in the present work for the accurate calculation of the PECs of the low-lying excited states as

Table 1. H-73 basis set of Hydrogen

Symmetry	Exponent	Coefficient
s	418.55081	1.00
	62.745349	1.00
	14.279584	1.00
	4.0418170	1.00
	1.3163895	1.00
	0.47346186	1.00
	0.18279991	1.00
	0.072884362	1.00
	0.039056541	1.00
	0.019077672	1.00
	0.0097350280	1.00
p	65.554593	1.00
	4.4119074	1.00
	1.4101801	1.00
	0.31641648	1.00
	0.10161790	1.00
	0.038707113	1.00
	0.015936506	1.00
d	22.213281	0.15854785
	2.5916309	0.47406581
	0.41870791	0.71413682
	0.67153126	1.00
	0.12927862	1.00
	0.034247992	1.00
f	7.2151367	0.40231477
	0.88389643	0.79963606
	0.33897511	1.00
	0.063826911	1.00

well as the ground state of hydrogen molecule. The exponents and coefficients of the basis set were obtained by the least-square fitting to the radial distribution functions of the 1s, 2s, 2p, 3d, and 4f orbitals. The basis set, denoted by H-73, consists of 11s-, 7p-, 6d-, and 4f-type basis functions contracted to [11s7p4d3f]. The s- and p-type functions are fully uncontracted to allow for the greatest flexibility in the molecular calculations. The exponents and coefficients are given in Table 1.

The H-73 basis set has been tested in the atomic calculation for hydrogen. The total energy of hydrogen atom in ^2S state was -0.4999951 a.u., which is superior to the results obtained by employing aug-cc-pVTZ and aug-cc-pVQZ basis sets, and comparable to the values from aug-cc-pV5Z and aug-cc-pV6Z calculations. To test the validity of the basis set in molecular calculations, CI calculations for the ground and several low-lying excited states of the hydrogen molecule have been performed. Figure 1 depicts the *ab initio* PECs of H_2 and H_2^+ ion and Tables 2 and 3 show the calculated equilibrium bond distances and excitation energies of different electronic states of the hydrogen molecule.
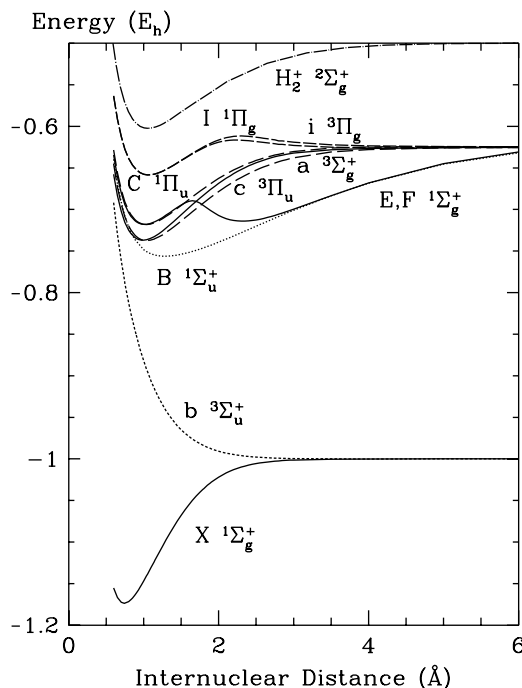
Fig. 1. Potential energy curves of the ground and low-lying excited states of H_2 and of the ground state of H_2^+. Solid lines: Σ_g^+ states; dotted lines: Σ_u^+ states; short-dashed lines: Π_g states; long-dashed lines: Π_u state; dotted-short-dashed line: H_2^+ ground state. For the Π_g manifold, the $^3\Pi_g$ state lies slightly above the $^1\Pi_g$ state. The opposite is observed for the Π_u manifold.

It may be seen that the bond distances calculated using H-73 basis set agree better with experiment than those obtained using aug-cc-pVQZ or aug-cc-pVTZ basis set, and are close to the highly accurate values computed using FVMO method.

It is noticeable that correlation-consistent basis sets are not able to accurately reproduce the bond distances and energies of the excited states in Π symmetry, which may be attributed to the relatively inadequate p-space. The problem was eliminated in the case of H-73 basis set. The polarization set that was purposefully optimized to correlate with the 2p orbitals of hydrogen atoms greatly improved the bond lengths and excitation energies, and reduced the errors to be within $100 \, \text{cm}^{-1}$ of exact values.

3.2. General features of the potential energy curves

Due to the superior performance of the H-73 basis set in the CI calculations of structures and energies for the excited states of hydrogen molecule, it was used in the subsequent studies of H_2 enclosed in a cylindrical harmonic potential. The PECs of the ground and eight low-lying excited states of H_2 encapsulated

Table 2. Equilibrium geometries of selected electronic states of H_2 (in Å)

Basis set	$X\ ^1\Sigma_g^+$	$B\ ^1\Sigma_u^+$	$C\ ^1\Pi_u$	$a\ ^3\Sigma_g^+$	$c\ ^3\Pi_u$
6-31++G**[a]	0.7389	1.1232	0.7846	0.9502	0.7215
6-311++G**[a]	0.7434	1.1567	0.8944	0.9726	0.8136
aug-cc-pVDZ[a]	0.7617	1.2670	0.9838	0.9884	1.0197
aug-cc-pVTZ[a]	0.7431	1.2822	0.9976	0.9870	1.0211
aug-cc-pVQZ[a]	0.7419	1.2845	1.0245	0.9874	1.0476
FV-OPT/[8s4p2d][a]	0.7417	1.2828	1.0330	0.9887	1.0375
H-36[b]	0.7419	1.2747	1.0287	0.9857	1.0321
H-73	0.7414	1.2840	1.0319	0.9887	1.0375
Numerical limit[a]	0.7408	1.2859	1.0330	0.9885	
Experiment[c]	0.7414	1.2928	1.0327	0.9887	1.0370

[a] Ref. [48].
[b] Ref. [50].
[c] Ref. [14].

in a cylindrical potential have been calculated. Several confining potential strengths ω have been utilized: 0.00, 0.05, 0.10, 0.15, and 0.20 a.u. The mapping of PECs was done in the range from 0.6 to 8.0 Å so as to capture the dissociation limits.

Figure 2(a)–(d) displays the PECs of several electronic states of H_2 and of the ground state of the H_2^+ ion in the presence of a confining potential. Several features may be observed when compared to the situation where no potential is applied. Firstly, the energy corresponding to a dissociation limit, $E_{\lim} = E(r \to \infty)$, shifts up for all the states when the strength of the potential increases. For instance, in the dissociation channel for the $X\ ^1\Sigma_g^+$ and $b\ ^3\Sigma_u^+$ (channel I), $E_{\lim} = -1.0000$ a.u. for $\omega = 0.00$ a.u.

This value increases to -0.9808 a.u. for $\omega = 0.10$ a.u., and -0.9292 a.u. for $\omega = 0.20$ a.u. In other words, all the dissociation channels are destabilized by

Table 3. Excitation energies of selected electronic states of H_2 (in cm^{-1})

Basis set	$B\ ^1\Sigma_u^+$	$C\ ^1\Pi_u$	$a\ ^3\Sigma_g^+$	$c\ ^3\Pi_u$
aug-cc-pVQZ[a]	91,660.9	10,6414.5	95,935.4	99,095.4
FV-OPT/[8s4p2d][a]	91,670.1	100,067.1	95,884.3	95,828.4
H-36[b]	91,372.4	99,964.9	95,437.5	95,603.5
H-73	91,612.4	99,990.6	95,844.3	95,763.8
Numerical limit[a]	91,694.2	100,104.3	95,981.4	
Experiment[c]	91,700.0	100,089.8	95,936.1	95,838.5

[a] Ref. [48].
[b] Ref. [50].
[c] Ref. [51].

Fig. 2. Potential energy curves of H_2 and H_2^+ in confinement. Solid lines: Σ_g^+ states; dotted lines: Σ_u^+ states; short-dashed lines: Π_g states; long-dashed lines: Π_u states; dotted-short-dashed line: H_2^+ ground state. (a) For the Π_g manifold, the $^3\Pi_g$ state lies slightly above the $^1\Pi_g$ state. The opposite is observed for the Π_u manifold. (b) For the Π_u manifold, the $^1\Pi_u$ state lies above the $^3\Pi_u$ state.

the harmonic repulsive potential that acts on electrons. The electron density of H_2 is compressed by the potential and the increased Coulomb interaction destabilizes the molecule. Secondly, the dissociation channel that leads to $H(1s) + H(2s$ or $2p)$ in a field-free environment (channel II) splits into two when the potential is turned on. The states of Σ symmetry correlate to the channel, which is lower in energy, that corresponds to $H(1s) + H(2p_z)$, while those of Π symmetry correlate to the higher channel that leads to the limit of $H(1s) + H(2p_x/2p_y)$. The energy separation between these two channels becomes

Fig. 3. Atomic energies of hydrogen atom in confinement.

larger when a stronger potential is used. The peculiar nature of the channel II within the harmonic potential can be rationalized *via* the atomic calculations of hydrogen atom for various confining potential strengths. Figure 3 shows the energies corresponding to different configurations of the hydrogen atom (see also Table 4).

The data show that $H(2p_z)$ configuration becomes more stable relative to the $H(2p_x)$ and $H(2p_y)$ counterparts in the harmonic potential. It can be attributed to the fact that the potential is laterally circular about the z-axis which enhances the electrostatic interaction along the x- and y-directions. As a consequence, the p-shell degeneracy is removed, and the channel II splits, with the one corresponding to $H(1s)$ and $H(2p_z)$ becoming lower in energy.

Finally, it should be noticed that the energy of the one-electron system H_2^+ increases less rapidly than the system of the states of the two-electron H_2. In consequence, for the larger values of ω, the energy of the ionized system H_2^+ will be lower than the energy of some of the excited electronic states of H_2.

Table 4. Atomic calculations of hydrogen atom in confinement

Configura-tion	$\omega = 0.00$	$\omega = 0.05$	$\omega = 0.10$	$\omega = 0.15$	$\omega = 0.20$
1s	-0.499995	-0.497521	-0.490376	-0.479179	-0.464588
2s	-0.124999	-0.097968	-0.047714	0.006649	0.062849
$2p_x/2p_y$	-0.124991	-0.100749	-0.050135	0.011405	0.081274
$2p_z$	-0.124991	-0.112215	-0.084665	-0.050641	-0.012044

All values are in a.u.

In cylindrical confinement, in contrast to spherical [49] or ellipsoidal [38] confinements, there is a possibility of escape of an electron when the repulsive influence of confinement exceeds the attractive interaction with the nuclei. In the following sections, in order to compare qualitative behavior of our results with those previously published, we sometimes discuss the results obtained for very large values of ω. However, in tables and figures we show only those data that relate to the excited states whose energies are below the ground-state energy of H_2^+ in the confinement of a given strength ω.

3.2.1. $X\,^1\Sigma_u^+$ and $b\,^3\Sigma_u^+$ states

Both the $X\,^1\Sigma_g^+$ and $b\,^3\Sigma_u^+$ states of the H_2 molecule correlate to the limit of $H(1s) + H(1s)$ (channel I). The ground state $X\,^1\Sigma_g^+$ arises from the configuration $|1\sigma_g^2\rangle$ while the $b\,^3\Sigma_u^+$ state results from the configuration $|1\sigma_g 1\sigma_u\rangle$. The configurations of these states remain the same for the applied potential with various strengths. It has been suggested that the hydrogen molecule, under the influence of a parallel ultrastrong magnetic field, undergoes a transition of the ground state symmetry from $^1\Sigma_g$ to $^3\Pi_0$ [22–26]. In the intermediate regime, Detmer *et al.* [26] and Kravchenko and Liberman [52] showed, using numerical Hartree–Fock approach, that the $^3\Sigma_u$ state would appear as the ground state, although the existence of this weakly bound Bose-particle superfluid phase is still controversial. Nevertheless, such transitions do not happen in the present case even up to the field strength of 0.20 a.u. The ground state retains the symmetry $^1\Sigma_g^+$ and the PECs of these two states still lead to the same dissociation limit of channel I. The difference between these two situations can be accounted for by considering the different nature of the external fields. The potential adopted in the present study is purely electrostatic and repulsive to the electrons. The first-order Stark effect will not split the species in channel I because it corresponds to a non-degenerate ground-state hydrogen atoms whose orbital angular momentum is zero. In the case of magnetic field, however, the spin–orbit interaction and the coupling between the canonical momentum and the vector field have to be taken into account. As a result, the influence of the magnetic field on the electronic structures of different states of H_2 becomes orientation-dependent, and the Zeeman effects (linear and quadratic) split the dissociation channel I according to the different spin states of $^1\Sigma_g$ and $^3\Sigma_u$.

Despite the difference in the asymptotic limits, some features characteristic for molecules in magnetic fields can also be seen in the present work. Table 5 shows that the binding energy of the ground state H_2 increases with the strength of the potential and the equilibrium internuclear distance r_e decreases. Meanwhile, the monotonically increasing ν_e suggests that the potential well becomes more steeper.

Similar observations have been made when H_2 was placed in a parallel magnetic field [26]. The shorter bond distance and stronger binding interaction in the ground state H_2 are the consequences of the increased electron density between the two nuclei that is induced by the potential.

Table 5. Spectroscopic parameters of $X\ ^1\Sigma_+^g$ and $b\ ^3\Sigma_+^u$ states

State	Parameter	$\omega=0.00$	$\omega=0.05$	$\omega=0.10$	$\omega=0.15$	$\omega=0.20$
$X\ ^1\Sigma_g^+$	r_e	0.7414 (0.7414)[a]	0.7368	0.7273	0.7202	0.7156
	ν_e	4404.6 (4401.2)[a]	4428.4	4503.3	4635.5	4737.8
	B_e	60.857 (60.853)[a]	61.620	63.242	64.491	65.318
	$\nu_e x_e$	147.262 (121.336)[a]	145.819	150.791	233.272	123.788
	α_e	3.2393 (3.0622)[a]	3.2497	3.2325	4.1626	3.1167
	D_e	38,111.9 (38,292.8)[b]	38,328.4	39,103.2	40,072.8	41,328.1
$b\ ^3\Sigma_u^+$	r_e	4.1608 (4.13)[c]	4.1379	4.0842	4.0305	3.9846
	ν_e	34.65	35.17	36.02	35.53	35.31
	B_e	1.932	1.954	2.005	2.059	2.107
	$\nu_e x_e$	102.005	106.100	110.776	116.817	122.854
	α_e	3.8806	3.8700	3.8589	4.3257	4.4514
	D_e	4.148(4.20)[c]	4.280	4.236	3.995	3.622

Experimental values are given in parentheses; all values are in cm^{-1}.
[a] Ref. [51].
[b] Ref. [16].
[c] Ref. [55].

The lowest triplet state, $b\ ^3\Sigma_u^+$, possesses interesting characteristics that are worth noting. According to the early work of Kolos and Wolniewicz [53], the $b\ ^3\Sigma_u^+$ state is predominantly repulsive except for a shallow van der Waals minimum around $R\approx7.8$ a.u. (4.1 Å) with the estimated binding energy of about 4 cm^{-1}. Other computations [54–56], that included electron correlation, confirmed the existence of a van der Waals minimum. In the present work a minimum was also found and its parameters are shown in Table 6. The analysis of the PEC in the region of $3.0\leq R\leq5.0$ Å including the correction for the basis set superposition error (BSSE), which is significant for such a weak binding, yielded $r_e=4.1608$ Å and $D_e=4.15$ cm^{-1}, as illustrated by Fig. 4. The results are in good agreement with the available theoretical values. Similarly to the situation of the ground state, the application of an external potential causes the contraction of the internuclear distance. However, the change of dissociation energy is drastically different. Initially, the potential well depth increases when a potential of $\omega=0.05$ a.u. is imposed. However, the potential becomes shallower when the potential strength exceeds 0.10 a.u. and the binding energy decreases monotonously. Same situation has also been seen for the hydrogen molecule in a magnetic field [26], in which the van der Waals minimum eventually vanished when the magnetic field strength became greater than 100 a.u. (corresponding to about 10^{11} G).

Table 6. Spectroscopic parameters of van der Waals minima of selected states

State	Parameter	$\omega=0.00$	$\omega=0.05$	$\omega=0.10$	$\omega=0.15$	$\omega=0.20$
$b\ ^3\Sigma_u^+$	r_e	4.1608 $(4.13)^a$	4.1379	4.0842	4.0305	3.9846
	ν_e	34.65	35.17	36.02	35.53	35.31
	B_e	1.932	1.954	2.005	2.059	2.107
	$\nu_e x_e$	102.005	106.100	110.776	116.817	122.854
	α_e	3.8806	3.8700	3.8589	4.3257	4.4514
	D_e	4.148 $(4.20)^a$	4.280	4.236	3.995	3.622
$a\ ^3\Sigma_g^+$	r_e		5.5335	5.0862	4.7692	
	ν_e		83.21	104.68	129.09	
	B_e		1.092	1.293	1.471	
	D_e		94.1	156.6	194.2	
$I\ ^1\Pi_g$	r_e	4.3089 $(4.2)^b$	4.0112			
	ν_e	123.1	154.2			
	B_e	1.802	2.079			
	D_e	173.3 $(177)^b$	214.7			

Experimental values are given in parentheses; all values are in cm^{-1}.
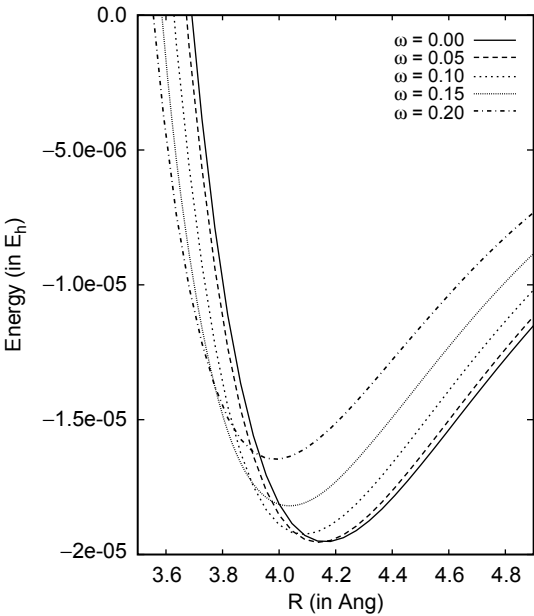[a] Ref. [55].
[b] Ref. [88].

Fig. 4. $b\ ^3\Sigma_u^+$ state in confinement.

3.2.2. $B\,^1\Sigma_u^+$ and $a\,^3\Sigma_u^+$ states

Being the lowest stable excited state, the electronic structure of the $B\,^1\Sigma_u^+$ state of H_2 has been of considerable interest. The calculation of Kolos and Wolniewicz using the variational method with elliptic coordinates [57] showed that the wavefunction is well represented by a mixture of three configurations: ionic, $|1s2s\rangle$ and $|1s2p_\sigma\rangle$. The analysis of the wavefunction indicated that for the region of $3 \le R \le 7$ a.u. the nature of the $B\,^1\Sigma_u^+$ state is essentially ionic. For the small internuclear distances, however, the most important contribution comes from the Heitler–London type $|1s2p_\sigma\rangle$ function. Yet for the large values of R both the $|1s2s\rangle$ and $|1s2p_\sigma\rangle$ functions become important, leading to the asymptotic limit of $H(1s) + H(2p)$ in the field-free space. Because of the strong ionic character, the B state PEC exhibits a very broad minimum. The dihydrogen molecule in the $B\,^1\Sigma_u^+$ state is paramagnetic [58] and can form stable compounds with noble gases [59].

The spectroscopic constants obtained by polynomial fitting to the calculated *ab initio* PECs for the $B\,^1\Sigma_u^+$ state are given in Table 7. The values are in a very good agreement with the experiment except for the binding energy being underestimated by about 1%. The relatively large discrepancy of r_e results from the flat minimum of the potential which increases the uncertainty in the evaluation of r_e. Change of configurations with R was noticed in the wavefunction analysis. The contribution from the ionic wavefunction drops from about 80% at $R \approx 4.00$ a.u. to about 20% at $R \approx 12$ a.u.; meanwhile, the contribution of $|1s2p_\sigma\rangle$ wavefunction grows from 5 to 62%.

Under the influence of the external harmonic potential, two changes occur: an elongation of the internuclear distance and the accompanying reduction of the vibrational constant. These variations could be attributed to the increasing contribution of $|1s2s\rangle$ wavefunction with the strength of the potential, which diminishes the ionic interaction and stretches the internuclear separation. Similar to the case where no potential is applied, when $R \to \infty$, the configuration of $|1s2p_\sigma\rangle$ dominates and leads to $H(1s) + H(2p_z)$ as this is the function that gives non-vanishing dispersion at the dissociation limit. For $\omega \ge 0.15$ a.u. unusual changes occur in the B state, in which the equilibrium internuclear distance starts to decrease and the vibrational constant increases. These unexpected differences have also been predicted for the hydrogen molecule placed in a parallel magnetic field of strength larger than 0.20 a.u. [26], although the effect is more pronounced in the latter case. The shortening of r_e could be a consequence of the induced interaction due to the polarized electron density, within the internuclear vicinity, caused by the harmonic potential.

In contrast to channel I, which remains non-degenerate in the field, channel II splits into three dissociation branches due to the Stark effect. Atomic calculations of the H atom in a cylindrical potential oriented along the z-axis show that the energy levels of 2p-orbitals split and $H(2p_z)$ becomes more stable relative to $H(2p_x)$ and $H(2p_y)$. Because of the lateral symmetry of the potential, the degeneracy of $H(2p_x)$ and $H(2p_y)$ persists. For small values of ω, $H(2s)$ is slightly less stable than $H(2p_x)$ and $H(2p_y)$ while the ordering reverses when ω exceeds 0.15 a.u. As a result, there exist three dissociation limits for channel II, with a non-zero cylindrical potential, which correspond to $H(2s)$, $H(2p_z)$, and $H(2p_x)/H(2p_y)$.

Table 7. Spectroscopic parameters of $B\,^1\Sigma_u^+$ and $a\,^3\Sigma_g^+$ states

State	Parameter	$\omega = 0.00$	$\omega = 0.05$	$\omega = 0.10$	$\omega = 0.15$	$\omega = 0.20$
$B\,^1\Sigma_u^+$	r_e	1.2840 (1.2928)[a]	1.3163	1.3383	1.3469	1.3413
	v_e	1365.8 (1358.1)[a]	1472.3	1360.4	1423.6	1507.0
	B_e	20.290 (20.015)[a]	19.305	18.675	18.438	18.593
	$v_e x_e$	24.330 (20.888)[a]		10.548	8.403	6.739
	α_e	1.3219 (1.1845)[a]	0.9516	0.5665	0.3622	0.2584
	D_e	28,812.3 (28,852.7)[b]	29,956.7	32,331.8	34,904.0	37,630.0
	T_e	91,612.4 (91,700)[a]	92,908.8	95,710.5	99,113.8	102,927.2
$a\,^3\Sigma_g^+$	r_e	0.9887 (0.9887)[a]	0.9736	0.9625	0.9634	
	v_e	2664.8 (2664.8)[a]	2747.9	2778.7	2719.4	
	B_e	34.219 (34.216)[a]	35.286	36.109	36.036	
	$v_e x_e$	82.061 (71.65)[a]	80.943	96.870	99.888	
	α_e	1.7192 (1.671)[a]	1.8673	2.0239	2.2410	
	D_e	24,581.4 (24,615.3)[c]	22,246.5	18,584.4	15,727.3	
	T_e	95,844.3 (95,936.1)[a]	100,635.8	109,471.3	118,310.0	

Experimental values are given in parentheses; all values are in cm^{-1}.
[a] Ref. [51].
[b] Ref. [91].
[c] Ref. [92].

Besides the $B\,^1\Sigma_u^+$ state, the $a\,^3\Sigma_g^+$ state also possesses the asymptotic limit of $H(1s) + H(2p_z)$ in the presence of a harmonic electrostatic potential. The PEC of the $a\,^3\Sigma_g^+$ state has already been extensively studied [60–64], and both highly accurate adiabatic and non-adiabatic *ab initio* PECs have been calculated. The PEC and the corresponding spectroscopic constants determined in the present study are in very good agreement with the experiment except for the excitation energy where the calculated value is about 90 cm^{-1} smaller than the experimental one. Zung and Duncan, using orthonormal molecular orbitals with variable orbital parameters, showed that the contribution of $|1s2p_z\rangle$ to the total energy near the potential minimum is negligible [61]. On the other hand, Mulliken has demonstrated that for $R \geq r_e$ the MO configuration becomes a mixture of $|1s2s\rangle$

and $|1s2p_z\rangle$ and when $R \rightarrow \infty$ the function $|1s2p_z\rangle$ predominates and correlates to the dissociation of H(1s)+H(2p) [65]. A detailed analysis of the relative contributions of various configurations in the $a\,^3\Sigma_g^+$ state wavefunction confirms their conclusions. It is found that the main component of the state at the region around the minimum is a mixture of $|1s2s\rangle$ and $|1s3s\rangle$ which then changes to $|1s2s\rangle$ and $|1s2p_z\rangle$ when R increases. For very large R, the predominant configuration is $|1s2p_z\rangle$ which leads to the appropriate dissociation limit of H(1s)+H(2p).

In the presence of the confining harmonic potential, several interesting changes of the $a\,^3\Sigma_g^+$ state occur. In contrast to the other states, where the binding energy increases with the stronger potential strength, the dissociation energy for the $a\,^3\Sigma_g^+$ state exhibits a decreasing trend. The D_e value reduces from 24,578 cm^{-1} for $\omega = 0.00$ a.u. to 15,727 cm^{-1} for $\omega = 0.15$ a.u. For $\omega = 0.20$ a.u., the energy of the $a\,^3\Sigma_g^+$ state is greater than the energy of the ground state of H_2^+. Detmer *et al.* have observed similar behavior of the $a^3\Sigma_g^+$ state of H_2 in a parallel magnetic field with the strength below 0.5 a.u. [26] and they have found that upon further increasing the field, the well starts becoming deeper and more pronounced. In order to verify the existence of the same phenomenon in the present case, the dissociation energy has been evaluated for the potential strength of 1.0, 2.0, and 5.0 a.u., respectively. The calculations show that the binding energy further reduces to about 9060 cm^{-1} when $\omega \approx 1.0$ a.u. However, a turnover appears for $\omega \geq 1.0$ a.u. in which the dissociation energy drastically increases to about 30,000 cm^{-1} for $\omega = 2.0$ a.u. and 68,000 cm^{-1} for $\omega = 5.0$ a.u. The development of $a\,^3\Sigma_g^+$ state under an extremely strong potential can be rationalized by considering the variation of configurations with the confinement strength. For the field-free and weak-field regime (i.e., $\omega \leq 1.0$ a.u.) the contribution from the function $|1s2s\rangle$ increases progressively from 60% ($\omega = 0.00$ a.u.) to 98% ($\omega = 1.0$ a.u.) while that from the function $|1s2p_z\rangle$ diminishes very rapidly. The domination of the configuration of $|1s2s\rangle$ weakens the exchange interaction between the two parallel-spin electrons in 1s and 2s orbitals, respectively [66], which counteracts the enhanced binding due to the applied potential. For the strong-field regime, however, the contribution from the function $|1s2p_z\rangle$ suddenly increases and dominates the state wavefunction. The better orbital overlap between 1s and $2p_z$ orbitals under the influence of an applied potential increases the exchange energy [67] which in turn strengthens the binding interaction. On the other hand, the main configuration for the $a^3\Sigma_g^+$ state at large R is $|1s2p_z\rangle$ and its contribution grows very rapidly when the potential strength increases. For $\omega \geq 0.20$ a.u. the configuration becomes exclusively $|1s2p_z\rangle$. As mentioned, the larger involvement of the $2p_z$ orbital can increase the binding interaction *via* the enhanced exchange energy contribution. Consequently, the dissociation limit of H(1s)+H2p_z) is stabilized relative to the potential minimum, and the binding energy is reduced.

Besides the abrupt change of binding energy, Detmer *et al.* have observed the development of a second minimum at large R which has no counterpart in the field-free space [26]. This additional minimum becomes more pronounced when the magnetic field increases to 1.0 a.u. The further increase in the field starts to diminish the potential well. The minimum eventually vanishes when the field is greater than 50.0 a.u. The calculated PEC of the $a\,^3\Sigma_g^+$ state in the present study

also exhibits a shallow minimum. As shown in Table 6, for a confining potential of $\omega = 0.05$ a.u., the second minimum appears at about 5.5 Å with the binding energy of 94.1 cm^{-1} which accommodates one vibrational level. The position of this minimum moves towards a smaller value of R, accompanying the increase of the binding energy and number of vibrational levels when the potential strength increases. Using the above-mentioned argument, the existence of the second minimum and the increase of its binding energy with the increasing ω can be accounted for by the strong exchange interaction of 1s and 2p$_z$ orbitals which constitute the major contribution to the $a\,^3\Sigma_g^+$ state at large R.

3.2.3. $C\,^1\Pi_u$, $c\,^3\Pi_u$, $I\,^1\Pi_g$, and $i\,^3\Pi_g$ states

Experimental studies of the Π-manifold excited states of H$_2$ began with the extensive investigations of the emission spectra of molecular hydrogen from the near infrared to extremely ultraviolet regions [68–71]. After the observation by Lichten, using molecular beam resonance spectroscopy technique, that the $c\,^3\Pi_u$ state is metastable [72,73], a lot of work has been devoted to accurate theoretical calculations of the Π_u PECs of H$_2$ which helped to assist the assignments and confirmation of emission bands. Meanwhile, the studies of the Π_g counterparts emerged rapidly because of the problem of 3d $\Sigma\Pi\Delta$ complex of states that leads to the breakdown of Born–Oppenheimer approximation in the computation of the excited states involving 3d orbitals [74]. The wrong prediction of singlet–triplet splitting for Π_g states also stimulated the calculations of reliable PECs that cover very wide range of R [75]. Up to now highly accurate PECs for these states have already been obtained [75–78] and precise spectroscopic constants have been determined which are in excellent agreement with the experiment [79–81]. All of these states are found correlated to the dissociation limit of H(1s)+H(2p) as $R \rightarrow \infty$. Despite the same asymptotic behavior, they exhibit very different characteristics for the small to medium-R region that are of interest to discuss.

The $C\,^1\Pi_u$ state has attracted much attention from spectroscopists because the state was believed to be the upper state of the ultraviolet absorption band which can help establish the accurate dissociation energy of the ground state of H$_2$ [82]. Therefore, several attempts have been made to obtain the complete PEC for the C state [53,76,83,84]. The calculations by Browne revealed that there exists a suspicious maximum at $R \approx 8$ a.u. which is about 160 cm^{-1} above the dissociation limit [76]. This observation was consistent with the conclusion of Herzberg and Monfils that a maximum might exist in the vicinity of $R \approx 13$ a.u. [82]. The subsequent calculations by Kolos and Wolniewicz [53], and Namioka [77] refined the barrier to be about 105.5 cm^{-1} at $R \approx 9$ a.u. The computed PEC for the $C\,^1\Pi_u$ state and the fitted spectroscopic parameters (r_e, v_e, $v_e x_e$, α_e) in the present study agree well with the experiment, as demonstrated by Table 8.

The hump is located at $R \approx 9.03$ a.u. being 106.3 cm^{-1} higher than the dissociation limit, which differs by only 1 cm^{-1} from the value determined by Kolos and Wolniewicz. The estimated excitation energy for the C state is far superior than the value obtained by CI calculation using aug-cc-pVQZ basis set [48], which overestimated T_e by 6300 cm^{-1}.

Table 8. Spectroscopic parameters of $C\ ^1\Pi_u$ and $c\ ^3\Pi_u$ states

State	Parameter	$\omega=0.00$	$\omega=0.05$	$\omega=0.10$	$\omega=0.15$
$C\ ^1\Pi_u$	r_e	1.0319 (1.0327)[a]	1.0202	1.0033	
	ν_e	2445.3 (2443.8)[a]	2497.0	2584.2	
	B_e	31.346 (31.363)[a]	31.964	32.977	
	$\nu_e x_e$	79.039 (69.524)[a]	79.113	96.862	
	α_e	1.6616 (1.6647)[a]	1.7640	1.7889	
	D_e	20,435.1 (20,488.6)[b]	19,932.2	19,383.7	
	T_e	99,990.6 (100,089.8)[a]	105,600.8	116,397.0	
$c\ ^3\Pi_u$	r_e	1.0358 (1.037)[a]	1.0274	1.0105	0.9896
	ν_e	2466.7 (2466.9)[a]	2522.4	2633.1	2765.8
	B_e	31.077 (31.07)[a]	31.545	31.583	33.968
	$\nu_e x_e$	71.365 (63.51)[a]	77.493	75.341	54.905
	α_e	1.525 (1.425)[a]	1.477	1.515	1.480
	D_e	24,666.6 (24,816.8)[a]	25,604.0	27,437.3	29,437.1
	T_e	95,763.8 (95,838.5)[a]	99,836.9	108,257.5	118,264.0

Experimental values are given in parentheses; all values are in cm^{-1}.
[a] Ref. [51].
[b] Ref. [91].

The PEC of the $c\ ^3\Pi_u$ state has been studied, although less thoroughly than the C state, in order to get insight into the metastable behavior of the $\nu=0$ vibrational level that decays to the $B\ ^1\Sigma_u^+$ with the lifetime in the range of milliseconds [73]. Browne [76] and Hoyland [78] have computed the PEC for the $c\ ^3\Pi_u$ state and showed that it resembles very much that for the singlet counterpart except that there is no local maximum at large R. Same observations have been made in the present study where, due to the different electron–nuclear interaction [85], the triplet state is lower in energy than the singlet state by about 4232 cm^{-1} at r_e, which is comparable to the experimental value of 4251.3 cm^{-1} [51]. The spectroscopic constants determined using the calculated PEC have excellent agreement with the experimental values. Similarly to the $C\ ^1\Pi_u$ state, the calculated T_e for the c state is closer to the experiment than that obtained by using aug-cc-pVQZ basis set [48].

The natural orbital analysis indicated that the major configuration for both Π_u states is $|1s_{\sigma_g}2p_{\pi_u}\rangle$ near the minimum [86]. While this configuration remains dominant for the $c\,^3\Pi_u$ state throughout the whole range of R, the $C\,^1\Pi_u$ state undergoes a configuration mixing at large R where the repulsive $|1s_{\sigma_u}2p_{\pi_g}\rangle$ dominates, resulting in the small potential maximum [87]. Wavefunction analysis in the present work corroborates these observations. A drastic change of the relative contributions of $|1s_{\sigma_g}2p_{\pi_u}\rangle$ and $|1s_{\sigma_u}2p_{\pi_g}\rangle$ states along the potential curve is observed. The former one is paramount ($\sim 50\%$) while the latter one is absent in the region close to the minimum. For the region of large R, however, a sharp increase of the contribution from $|1s_{\sigma_u}2p_{\pi_g}\rangle$ is noticed, especially at $7.00 \leq R \leq 12.00$ a.u. where its weight raises from 5 to 20%. Simultaneously, the contribution from the attractive term $|1s_{\sigma_g}2p_{\pi_u}\rangle$ drops rapidly to 25%. Interestingly, the higher excitation terms, such as $|1s3p_\sigma\rangle$, have a significant interaction with these states ($\sim 46\%$ at $R = 20.00$ Å). Therefore, a basis set that is optimized not only for 2p space but also for 3p space is necessary for the proper description of the Π states at large internuclear distances.

Accurate PECs of $I\,^1\Pi_g$ and $i\,^3\Pi_g$ states have been computed using highly flexible wavefunctions in elliptical coordinates containing explicit r_{12} terms [88]. The presently calculated potential curves for these states, as illustrated by Fig. 1 and Table 9, are in good agreement with those results except for $v_e x_e$ which are all overestimated by 10%. The estimated singlet–triplet splitting for the Π_g states at r_e is about 12.7 cm^{-1}, with the triplet state being lower in energy, which is consistent with the value of 10.8 cm^{-1} determined by Kolos and Rychlewski. A crossing between the states is found at $R \approx 1.25$ Å where the triplet state becomes higher in energy than the singlet state. For both states a maximum appears at $2.25 \leq R \leq 2.30$ Å which are 1870 cm^{-1}, for the singlet state, and 2942 cm^{-1}, for

Table 9. Spectroscopic parameters of $I\,^1\Pi_g$ and $i\,^3\Pi_g$ states

State	Parameter	$\omega = 0.00$	$\omega = 0.05$
$I\,^1\Pi_g$	r_e	1.0658 (1.0693)[a]	1.0839
	v_e	2252.8 (2259.2)[a]	2114.8
	B_e	29.445 (29.259)[a]	28.473
	$v_e x_e$	91.675 (78.41)[a]	111.864
	α_e	1.919 (1.584)[a]	2.208
	D_e	7324.4 (7576.8)[b]	2853.3
	T_e	113,096.5 (113,142)[a]	122,523.8
$i\,^3\Pi_g$	r_e	1.0653 (1.0700)[a]	1.0805
	v_e	2260.8 (2253.6)[a]	2154.9
	B_e	29.475 (29.221)[a]	28.653
	$v_e x_e$	89.075 (67.05)[a]	100.194
	α_e	1.880 (1.506)[a]	2.021
	D_e	7373.5 (7493.4)[c]	2957.6
	T_e	113,083.8 (113,132)[a]	122,502.4

Experimental values are given in parentheses; all values are in cm^{-1}.
[a] Ref. [51].
[b] Ref. [89].
[c] Ref. [93].

the triplet state, above the asymptote. These values match the values estimated by Kolos and Rychlewski [88], Dressler and Wolniewicz [80] and Wolniewicz [89]. The existence of maxima for the two Π_g states is attributed to the avoided crossing between the $|1\sigma_g1\pi_g\rangle$ and $|1\sigma_u1\pi_u\rangle$ states where the latter one is repulsive [87]. To verify this argument the wavefunctions for the Π_g states have been analyzed. For the singlet state, the contribution of $|1\sigma_g1\pi_g\rangle$ function declines quickly from 73% at r_e to 18% at 6.00 Å, while the that for the $|1\sigma_u1\pi_u\rangle$ function increases from 0 to 25%. A similar variation of configurations is observed as well for the triplet state although the change is slightly more significant, which is anticipated due to the fact that the valence repulsion in the triplet state is enhanced by the repulsive resonance interaction, giving rise to the broader and higher hump at large R [88]. Therefore, this strong configuration interaction at large internuclear distances is indicative of the crossing between $|1\sigma_g1\pi_g\rangle$ and $|1\sigma_u1\pi_u\rangle$ for the Π_g states that leads to the local maxima.

The attractive resonance interaction for the $^1\Pi_g$ state overcomes the valence repulsion at large R and causes the formation of a second minimum, which is not found in the triplet state [88]. The resonance interaction in the triplet state is instead repulsive which further strengthens the valence repulsion at large internuclear distances. The second minimum for the $^1\Pi_g$ state is found at 8.14 a.u. which has the depth of 173 cm^{-1} and accommodates several vibrational levels in the present study. These values are only moderately different from the values reported by Wolniewicz including the adiabatic corrections [89], who found the second minimum at $R \approx 8.25$ a.u. with the depth of 178 cm^{-1}.

The four Π states behave in substantially different ways in accordance to the applied confining potential. For these highly excited states, the Π_g energies are above the energy of the $^2\Sigma_g^+$ state of H_2^+ already for $\omega = 0.10$ a.u., while the lower Π_u energies are placed above that of H_2^+ at $\omega = 0.15$ a.u. For the potential strength $\omega \leq 0.10$ a.u. the equilibrium internuclear distance of the $^1\Pi_u$ state decreases from 1.0319 to 1.0033 Å. Simultaneously, the binding energy drops from 20,435 cm^{-1}, for $\omega = 0.00$ a.u., to 19,384 cm^{-1}, for $\omega = 0.10$ a.u. On the other hand, a trend opposite to the change of binding energy is noticed for the well-known maximum at large R. While this hump is shifted towards smaller values of R, its height with respect to the dissociation limit increases rapidly for $0.00 \leq \omega \leq 0.15$ a.u. and then decreases. Detmer *et al.* have also observed similar behavior of the $^1\Pi_u$ state in the presence of a parallel magnetic field [27]. The inverse relation between ω and D_e could be accounted for by considering the deformation of π orbitals within a repulsive cylindrical potential. Due to the symmetry restriction exerted by the applied potential, the np orbital sets lose the degeneracy, with p_x and p_y components being more destabilized. The distorted $1\pi_u$ MO, which is more localized in the region between the two nuclei, has better overlap with the $1\sigma_g$ MO, thus strongly enhancing the Coulomb interaction. However, the overlap between $1\sigma_u$ and $1\pi_g$ is remarkably diminished. Consequently, the dissociation limit is greatly stabilized with respect to the potential minimum, giving rise to the decreasing binding energy for the $^1\Pi_u$ state. The induced stabilization effect on the repulsive $|1\sigma_u1\pi_g\rangle$ function also explains the larger barrier of the large-R maximum for $\omega \geq 0.00$ a.u. since it intensifies the coupling between the $|1\sigma_u1\pi_g\rangle$ and $|1\sigma_g1\pi_u\rangle$ configurations, resulting in a higher potential hump. When ω

increases, the single-reference $|1\sigma_u 1\pi_g\rangle$ potential curve is more stabilized and crosses the single-reference $|1\sigma_g 1\pi_u\rangle$ potential curve at smaller R. This explains the shift of the maximum towards smaller R with the increasing ω.

On the contrary, the PEC of the $^3\Pi_u$ state evolves in a way similar to that of the $X\,^1\Sigma_g^+$ state: the potential well becomes increasingly deeper, and the equilibrium internuclear distance contracts continuously. As in the case of the singlet $C\,^1\Pi_u$ state, the overlap between $1\sigma_g$ and $1\pi_u$ MOs is enhanced due to the distortion from the confining potential. Apart from the stronger Coulomb interaction, the exchange energy between the two parallel electrons is introduced which cancels out the Coulomb repulsion [65]. Therefore, the $|1\sigma_g 1\pi_u\rangle$ configuration, which dominates in the region near the minimum, is more stabilized than the $|1\sigma_u 1\pi_g\rangle$ configuration in which the orbital overlap is less efficient, and this exchange effect contributes towards the increasing well depth of the $^3\Pi_u$ state when an external potential is applied.

The PECs of the highest states in the Π manifold, $^1\Pi_g$ and $^3\Pi_g$ states, exhibit drastic changes in the presence of a cylindrical potential. The changes of the PECs of these states with confinement are shown in Figs 5 and 6. For both cases, the equilibrium internuclear distances increase with ω. Concurrently, the binding energies of both states decrease, with the change in the singlet state being more pronounced. Both of the Π_g states correlate to the united-atom limit of He(1s3d) [65]. For $R \approx r_e$, the wavefunctions of $^1\Pi_g$ and $^3\Pi_g$ are composed of $|1\sigma_g 3d_{\pi_g}\rangle$, which is treated as a Rydberg state, and $|1\sigma_g 2p_{\pi_g}\rangle$, respectively. The latter function becomes more important when R is larger until eventually it dominates at very large R and leads to the asymptote of H(1s)+H(2p). When the hydrogen molecule is encapsulated in a cylindrical potential, not only the p-shell but also
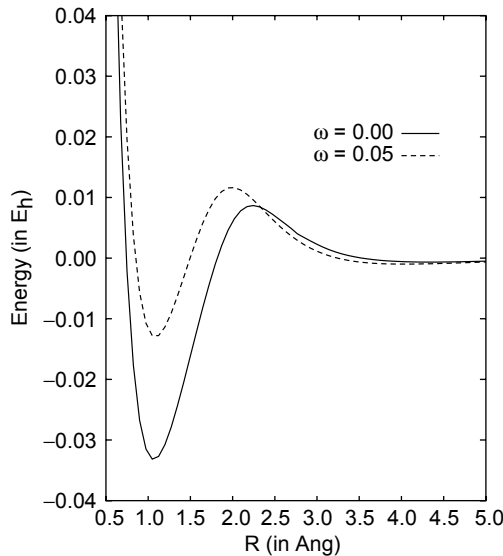

Fig. 5. $I\,^1\Pi_g$ state in confinement. The energy is shown with respect to the dissociation limit.
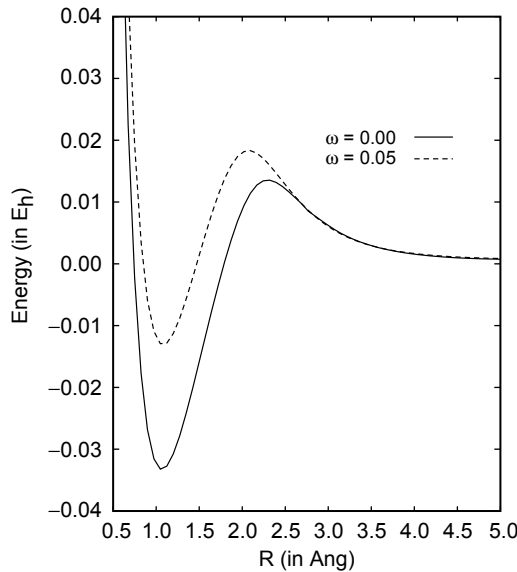
Fig. 6. $i\,^3\Pi_g$ state in confinement. The energy is shown with respect to the dissociation limit.

the d-shell orbital degeneracy is removed, and those involved in $3d_{\pi_g}$ MOs, i.e., $3d_{xz}$ and $3d_{yz}$ orbitals which are very diffuse, will be very intensely destabilized. As a consequence, in the region close to the minimum, their contribution to the $^1\Pi_g$ and $^3\Pi_g$ states, as measured by squares of coefficients in the CI expansion, is reduced. The destabilization of 3d orbitals causes the attractive potential of $|1\sigma_g 3d_{\pi_g}\rangle$ to be shifted upward in energy relative to the repulsive potential of $|1\sigma_g 2p_{\pi_g}\rangle$, resulting in the decreasing binding energy. Simultaneously, the maximum is shifted towards smaller values of R and becomes higher in energy with respect to the dissociation limit due to the fact that the two potential curves of $|1\sigma_g 2p_{\pi_g}\rangle$ and $|1\sigma_g 3d_{\pi_g}\rangle$ cross at smaller R. The slight stretching of the equilibrium internuclear distances also reflects a larger contribution of the $|1\sigma_g 2p_{\pi_g}\rangle$ function.

It may be seen from Figs 5 and 6 that the $^1\Pi_g$ state is more susceptible to the influence of the external potential than the $^3\Pi_g$ state. Unlike the first minimum at small R the second van der Waals minimum of the $^1\Pi_g$ becomes more pronounced with the increasing strength of the harmonic potential. The corresponding binding energy (see Table 6) increases from 173 cm^{-1} for $\omega = 0.00$ a.u. to 215 cm^{-1} for $\omega = 0.05$ a.u. and the minimum moves to smaller values of R. Detmer *et al.* have observed a similar trend [27] and they found that the second minimum will vanish when the magnetic field strength is larger than 10.0 a.u. Mulliken ascribed the second minimum to the first-order London dispersion interaction between H(1s) and H(2p$_\pi$) which yields a net stabilization for the $^1\Pi_g$ state at large R [90]. As the contribution of $|1\sigma_g 2p_{\pi_g}\rangle$ function to the $^1\Pi_g$ state increases with the application of a cylindrical confining potential, this long-range attraction is significantly enhanced, giving rise to a deeper potential well in the region $6 \leq R \leq 8$ a.u.

3.2.4. E, F $^1\Sigma_g^+$ state

The first excited $^1\Sigma_g^+$ state is characterized by the double-minimum potential which is manifested in a very complicated vibrational–rotational spectrum [94]. The PEC of the E, F $^1\Sigma_g^+$ state has been extensively studied by Davidson [95,96], Gerhauser and Taylor [62], and Kolos and Wolniewicz [97]. The peculiar double minimum is the result of an avoided crossing of the potential curves for the, in MO notation, $|1\sigma_g 2\sigma_g\rangle$ and $|1\sigma_u^2\rangle$ configurations. The inner minimum originates from the covalent $|1\sigma_g 2\sigma_g\rangle$ configuration while the outer minimum is composed mainly of ionic $|1\sigma_u^2\rangle$ configuration. These configurational alterations along R and multiple-minimum potential have also been observed for higher excited $^1\Sigma_g^+$ states, and were attributed to the H^+H^- separate atom level that intervenes in all the $|1sns\rangle$ levels below $|1s5s\rangle$ [95]. The calculated PEC of E, F $^1\Sigma_g^+$ state is plotted in Fig. 1 and the corresponding spectroscopic constants are summarized in Table 10. Very good agreement with the experiment is achieved except that the discrepancies in vibrational frequencies are moderately large. The detailed analysis of the CI wavefunction has been performed in order to comprehend the nature of the state, and it reveals a complicated change of configurations with R. Figure 8(a) illustrates the variation of contributions of configurations involved in the E, F $^1\Sigma_g^+$ state. For $R \leq 1.5$ Å the state is well represented by the covalent $|1\sigma_g 2\sigma_g\rangle$ configuration ($\sim 90\%$) whose PEC rises very rapidly to the asymptote corresponding to H(1s) + H(2s). When R approaches the point of avoided crossing

Table 10. Spectroscopic parameters of E, F $^1\Sigma_g^+$ states

State	Parameter	$\omega = 0.00$	$\omega = 0.05$	$\omega = 0.10$	$\omega = 0.15$	$\omega = 0.20$
$E\ ^1\Sigma_g^+$	r_e	1.0114 (1.011)[a]	0.9966	0.9940	0.9986	
	ν_e	2541.1 (2588.9)[a]	2626.8	2615.2	2542.9	
	B_e	32.698 (32.68)[a]	32.679	33.853	33.542	
	$\nu_e x_e$	124.879 (130.5)[a]	148.904	146.964	167.952	
	α_e	1.909 (1.818)[a]	1.969	1.961	2.226	
	T_e	100,018.9 (100,082)[a]	106,018.4	115,651.0	124,419.7	
$F\ ^1\Sigma_g^+$	r_e	2.3227 (2.31)[a]	2.3193	2.2913	2.2491	2.2039
	ν_e	1248.1 (1199)[a]	1289.1	1349.9	1419.9	1486.2
	B_e	6.198	6.218	6.372	6.613	6.886
	$\nu_e x_e$	30.365	26.909	26.993	27.574	27.957
	α_e	0.1202	0.1529	0.1657	0.1701	0.17841
	T_e	100,879.7 (100,911)[a]	102,488.6	105,999.7	110,231.2	114,884.1

Experimental values are given in parentheses; all values are in cm^{-1}.
[a] Ref. [51].

(~ 1.65 Å), an intrusion of the ionic potential happens that causes a drastic increase in the weight of $|1\sigma_u^2\rangle$ and forms a deep minimum at fairly large R (~ 2.3 Å).

These observations confirm the molecular orbital analysis of the $E, F\ ^1\Sigma_g^+$ state carried out by Kolos and Wolniewicz in which the ionic part of the total wavefunction dominates the region from 3 to 6 a.u. [97]. At still larger R, the $|1\sigma_g 2\sigma_g\rangle$ configuration, which is a mixture of $|1s2s_\sigma\rangle$ and $|1s2p_\sigma\rangle$, becomes predominant again due to a second avoided crossing with the ionic potential. This avoided crossing allows for the proper dissociation of the state into the separate atom limit of H(1s) and H(2s) [65].

The evolution of the PEC of $E, F\ ^1\Sigma_g^+$ state under the effect of a cylindrical harmonic potential is illustrated in Fig. 7. The two minima have considerably different behavior in response to the applied potential, and several characteristics are noticeable. The inner minimum becomes less pronounced when the potential strength is increased from 0.00 to 0.15 a.u. However, this monotonous change is not seen in r_e, which first decreases for $\omega \leq 0.10$ a.u. and then increases for larger ω. On the other hand, the outer minimum is shifted monotonically towards the inner minimum accompanied by the increasing potential depth. Schmelcher *et al.* have studied the $^1\Sigma$ excited states of hydrogen molecule in a parallel magnetic field for the field strength ranging from 0 to 100 a.u. [98], and they observed qualitatively very similar trends of the inner and outer minima evolving in the field with strengths smaller than 0.5 a.u. The unusual behavior can be explained in terms of the different extent of configuration mixing with respect to the strength of confining potential. Figure 8(b)–(d) displays the weight of each configuration in the total CI wavefunction that corresponds to the $E, F\ ^1\Sigma_g^+$ state when a harmonic potential is present. At the region close to the inner minimum $|1\sigma_g 2\sigma_g\rangle$ remains as the dominant configuration. However, the associated potential well becomes more shallow because the $|1\sigma_g 2\sigma_g\rangle$ configuration is strongly destabilized due to the involvement of 2s orbitals and the PEC is shifted up relative to the ionic
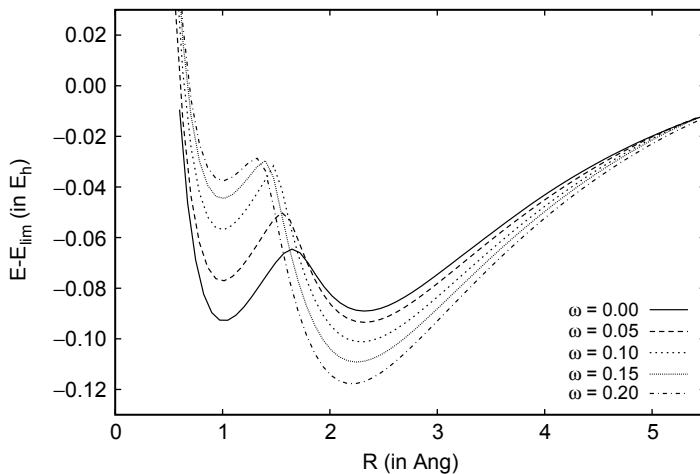

Fig. 7. $E, F\ ^1\Sigma_g^+$ state in confinement. The energy is shown with respect to the dissociation limit.
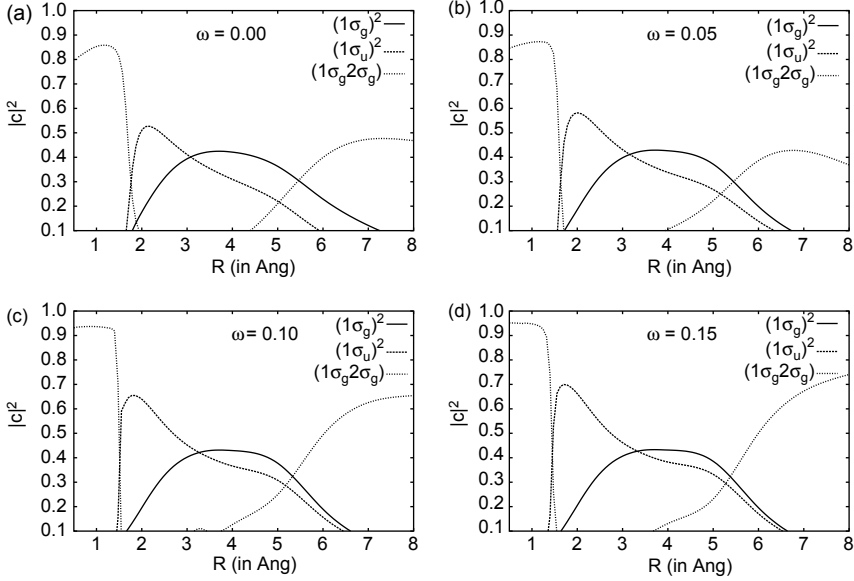
Fig. 8. Decomposition of waveform of $E, F\,^1\Sigma_g^+$ state in confinement.

PEC. This PEC shifting leads to the transition point where the $|1\sigma_g2\sigma_g\rangle$ PEC crosses the ionic PEC moving to smaller R, as implied by the observation that the contribution of $|1\sigma_g2\sigma_g\rangle$ configuration vanishes more rapidly for $\omega = 0.15$ a.u. (Fig. 8(d)) when compared to the field-free case (Fig. 8(a)).

Another feature of the $E, F\,^1\Sigma_g^+$ state wavefunction is the increase in weight of the ionic character in the intermediate-R region. The contribution of ionic wavefunction raises from 50 to 70% when a potential of the strength $\omega = 0.20$ a.u. is applied. This is not unexpected because the competing $|1\sigma_g2\sigma_g\rangle$ configuration becomes less and less important due to the 2s destabilization. Furthermore, the $|1\sigma_u^2\rangle$ configuration is less destabilized as the smaller electron density within the internuclear vicinity reduces the repulsive interaction between electrons. Thus, the depth of the outer minimum which is formed from the $|1\sigma_u^2\rangle$ configuration increases monotonically for $\omega \leq 0.15$ a.u. The greater ionic character of the $E, F\,^1\Sigma_g^+$ state enhances the coupling with the $G, K\,^1\Sigma_g^+$ state, as shown in Fig. 9, giving
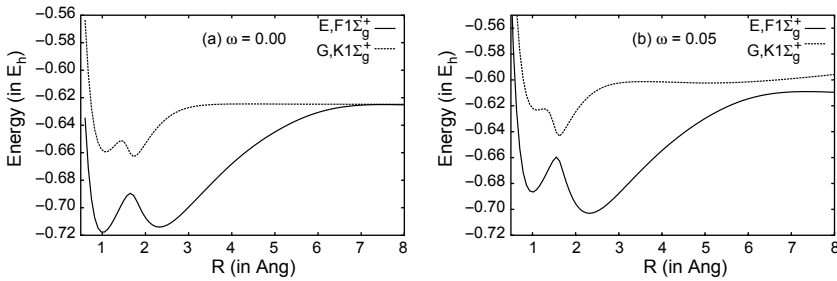

Fig. 9. The E, F and $G, K\,^1\Sigma_g^+$ states in confinement.

rise to a smaller energy difference between these two state at the point of avoided crossing, that may indicate a possibility of the failure of the Born–Oppenheimer approximation in the calculations of low-lying excited states in the presence of a confining potential. Shi *et al.* have shown recently that for a diatomic molecule two electronic states of the same spatial symmetry may intersect in multi-parameter space because additional symmetry elements appear in the perturbation operator in the adiabatic approximation that may result in zero off-diagonal matrix elements even though the two states have the same spatial symmetry [99]. In the present case, the external harmonic potential can be viewed as a perturbation to the Hamiltonian of the hydrogen molecule in free space. Hence, the perturbation operator will be expressed in terms of not only the internuclear distance R but also the strength of confining potential ω, and the assumption that the off-diagonal coupling matrix elements are non-zero if two states are of the same symmetry may no longer be valid. A thorough understanding of this phenomenon requires a more detailed analysis of conical intersection in both theoretical and experimental aspects, a subject of intensive recent studies [100,101].

Compared to the wavefunction in free space, the role of the $|1\sigma_g 2\sigma_g\rangle$ configuration is of greater significance at large R when confining potential is present. Its contribution progressively increases from 45 to 80% when ω is increased from 0.00 to 0.20 a.u. It suggests that the dissociation channel leading to $H^+ + H^-$ will be strongly destabilized relative to the covalent channels and will lie higher in energy, which confirms the contention of Sako and Diercksen that negative hydrogen ion possesses a fragile electron density that is easily affected by the confinement [38]. Surprisingly, a closer look at the composition of $|1\sigma_g 2\sigma_g\rangle$ configuration at large values of R discloses that the configuration comprises $|1s2s_\sigma\rangle$ and $|1s2p_\sigma\rangle$ (in Heitler–London convention) and the latter one predominates for $\omega \neq 0.00$ a.u., in contrast to the situation without confinement, where the former one dominates the state throughout a wide range of R till the asymptote. Concurrently, the dissociation limit of the $E, F\ ^1\Sigma_g^+$ state merges to that of $B\ ^1\Sigma_u^+$ and $^3\Sigma_g^+$ states that corresponds to $H(1s) + H(2p_z)$ for $\omega \geq 0.00$ a.u. These observations can be explained by noting the fact that the 2s and 2p energy levels of the hydrogen atom, which are degenerate when there is no external field, split in a cylindrical harmonic potential, as depicted by Fig. 3, and $2p_z$ orbital becomes lower in energy relative to 2s orbital, resulting in the splitting of the channel II into three routes: $1s2p_z \leq 1s2s \leq 1s2p_x,\ 1s2p_y$.

3.3. Molecules in magnetic fields

The results of calculations carried out in the present study show similarity to the results obtained using the cylindrical harmonic potential and those obtained from the numerical calculations of hydrogen molecule in parallel magnetic field. On the other hand, there exist a number of differences between these two models such as the switch of ground state symmetry in an intermediate- to ultrahigh-field regime. In order to understand the origin of the interesting similarities, it is worthwhile to review the basic formalism of a molecule in magnetic field.

From the classical electrodynamics, the Dirac Hamiltonian of a hydrogen molecule moving in a constant magnetic field $\vec{B}$ is [102]

$$\mathcal{H}_{\text{mag}} = \sum_{i=1}^{2} \frac{1}{2m_e} \left[\sigma_i \cdot \left(\vec{p}_i + \frac{e}{c}\vec{A} \right) \right]^2 - \sum_{i=1}^{2} \sum_{\alpha=1}^{2} \frac{Ze^2}{R_{i\alpha}} + \frac{e^2}{r_{12}} + \frac{Z^2 e^2}{R} \qquad (7)$$

Here the adiabatic approximation is employed (to assume that the kinetic energy of nuclei is zero), and it is assumed that $4\pi\varepsilon_0 = 1$ for simplicity. R is the internuclear distance, r_{12} is the distance between the two electrons, and $R_{i\alpha}$ is the distance between the ith electron and the αth nucleus. $\vec{A}$ is the vector potential of the magnetic field that obeys the relation

$$\vec{B} = \nabla \times \vec{A}, \qquad (8)$$

and σ_i is the Pauli spin matrix. It is assumed that the molecular axis is along the z-direction and $\vec{B} = B\hat{z}$ where $\hat{z}$ is the corresponding unit vector. The Schrödinger equation is gauge-invariant and any gauge can be selected if equation (8) is fulfilled. Hence, a symmetric Coulomb gauge, $\nabla \cdot \vec{A} = 0$, is used which is defined as $\vec{A} = (B/2)(-y, x, 0)$. The substitution of $\vec{A}$ into equation (7) yields the Hamiltonian

$$\mathcal{H}_{\text{mag}} = \frac{1}{2m_e} \sum_{i=1}^{2} \left\{ \left(p_{ix} - \frac{eBy}{2c} \right)^2 + \left(p_{iy} + \frac{eBx}{2c} \right)^2 + p_{iz}^2 \right\} + \sum_{i=1}^{2} \sum_{j=1}^{2} \frac{Ze^2}{R_{ij}}$$

$$+ \frac{e^2}{r_{12}} + \frac{Z^2 e^2}{R} - \sum_{i=1}^{2} \mu_{is} \cdot \vec{B} \qquad (9)$$

where the last term deals with the interaction between an electron spin and the field $\vec{B}$. The simplification of equation (9) is straightforward; expanding and rearranging the terms leads to the following:

$$\mathcal{H}_{\text{mag}} = \sum_{i=1}^{2} \frac{p_i^2}{2m_e} - \sum_{i=1}^{2} \sum_{j=1}^{2} \frac{Ze^2}{R_{ij}} + \frac{e^2}{r_{12}} + \frac{Z^2 e^2}{R} + \frac{e^2 B^2}{8m_e c^2} \sum_{i=1}^{2} (x_i^2 + y_i^2)$$

$$+ \frac{eB}{2m_e c} \sum_{i=1}^{2} l_{iz} + \frac{eB}{m_e c} \sum_{i=1}^{2} S_{iz} \qquad (10)$$

$$\mathcal{H}_{\text{mag}} = \sum_{i=1}^{2} \frac{p_i^2}{2m_e} - \sum_{i=1}^{2} \sum_{j=1}^{2} \frac{Ze^2}{R_{ij}} + \frac{e^2}{r_{12}} + \frac{Z^2 e^2}{R} + \frac{1}{2} m_e \gamma^2 \sum_{i=1}^{2} (x_i^2 + y_i^2)$$

$$+ \gamma \left(\sum_{i=1}^{2} \ell_{iz} + 2 \sum_{i=1}^{2} S_{iz} \right), \qquad (11)$$

where $\gamma = eB/2m_e c$. The first part of equation (11) is the Hamiltonian of a hydrogen molecule in free space, while the second part deals with the interaction of the molecule with the field. Comparing equation (11) and equations (1)–(6), it is seen that the two Hamiltonians are very similar except that equation (11) contains two extra terms which constitute the longitudinal kinetic energy Hamiltonian [24]

$$\mathcal{H}_1 = \sum_{i=1}^{2} T_{iz} = \gamma \sum_{i=1}^{2} (\ell_{iz} + 2S_{iz}) \tag{12}$$

that corresponds to the Zeeman effect [103]. The transverse magnetic Hamiltonian

$$\mathcal{H}_2 = \sum_{i=1}^{2} h_i^{\perp} = \frac{1}{2} m_e \gamma^2 \sum_{i=1}^{2} (x_i^2 + y_i^2) \tag{13}$$

is equivalent to equation (5) when $\omega^2 = \gamma^2$ in atomic units.

Hence, the Hamiltonian constructed from equations (1) and (5) is suitable for the evaluation of the transverse magnetic effect on a hydrogen molecule, due to the presence of a parallel magnetic field, that gives rise to the fine features of PECs. Since equation (12) commutes with the total Hamiltonian $\mathcal{H}_{\text{mag}}$, the correction for the longitudinal component of the total magnetic effect on the molecule can be calculated as the energy eigenvalue of the Hamiltonian $\mathcal{H}_1$ acting on the hydrogen molecular wavefunction, and the corrected total energy is given by

$$E^{\mathcal{H}_{\text{mag}}} = E^{\mathcal{H}_{\text{el}}} + \Delta E^{\mathcal{H}_1} \tag{14}$$

The GUGA-CI wavefunctions are spatial and spin symmetry-adapted, thus the projections of total orbital angular momentum and total spin of a hydrogen molecule in a particular electronic state are conserved for all the values of R. Therefore, the term $\Delta E^{\mathcal{H}_1}$ remains constant for an electronic state, and it causes a shift of the corresponding PEC depending on the spin configuration. For the Σ states the orbital contribution to $\Delta E^{\mathcal{H}_1}$ is zero since the total orbital angular momentum is zero. Similarly, for the singlet states the spin contribution is zero as $S_z = 0$. Accordingly, it is expected that the ground $X\,^1\Sigma_g^+$ state would be identical if either the Hamiltonian $\mathcal{H}$ or $\mathcal{H}_{\text{mag}}$ is used because the term $\Delta E^{\mathcal{H}_1}$ vanishes. However, the term becomes non-zero for the triplet states, and the spin configuration has to be taken into account. A triplet state will be split into three sub-levels since there are three possible values of $S_z = -1$, 0, 1. If only the lowest state, i.e., $S_z = -1$ is considered, the term $\Delta E^{\mathcal{H}_1}$ will become negative, thus lowering the complete PEC. This explains the change of ground-state symmetry of hydrogen molecule in magnetic field. Since the term $\Delta E^{\mathcal{H}_1}$ is always negative for both $b\,^3\Sigma_u^+$ and $c\,^3\Pi_u$ states, for a sufficiently strong magnetic field, these states would be lowered in energy until they cross successively the $X\,^1\Sigma_g^+$ state and become the ground state.

4. FINAL REMARKS AND CONCLUSIONS

Molecules exhibit versatile behavior in response to the application of various forms of external potentials. In the present study, different electronic states of a hydrogen molecule enclosed in a cylindrical harmonic potential have been investigated and it has been found that states with different spatial symmetry and spins behave in different manner. In general, the applied potential shrinks the molecule and makes the minima on the PECs more pronounced. However, the symmetries of atomic orbitals that constitute the configuration of an electronic state also play a crucial role, and some unexpected shallow van der Waals minima and interchanges of dissociation limits that are caused by the orbital reordering under the influence of confinement have been observed. Moreover, a near intersection has been seen between the excited $^1\Sigma_g^+$ states through which a possible breakdown of the Born–Oppenheimer approximation may occur. Interestingly, it is found that a hydrogen molecule, when confined in a cylindrical potential, behaves in a very similar way as it does under the influence of a parallel magnetic field, which stimulates a further study regarding the use of this model potential to the electrodynamic studies of molecules in external fields.

REFERENCES

[1] R. Loudon, *Am. J. Phys.*, 1959, **27**, 649.
[2] H. Hasegawa and R. E. Howard, *J. Phys. Chem. Solids*, 1961, **21**, 179.
[3] D. Cabib, E. Fabri and G. Fiorio, *Solid State Commun.*, 1971, **9**, 1517.
[4] E. R. Smith, R. J. W. Henry, G. L. Surmelian, R. F. O'Connell and A. K. Rajagopal, *Phys. Rev. D*, 1972, **6**, 3700.
[5] G. H. Garstang and S. B. Kemic, *Astrophys. Space Sci.*, 1974, **31**, 103.
[6] J. R. P. Angel, E. F. Borra and J. D. Landstreet, *Astrophys. J. Suppl. Ser.*, 1981, **45**, 457.
[7] J. Trümper, W. Pietsch, C. Reppin, W. Voges, R. Staubert and E. Kendziorra, *Astrophys. J.*, 1978, **219**, L105.
[8] D. Yoshioka, *The Quantum Hall Effect*, Springer, New York, 2002.
[9] L. Jacak, P. Hawrylak and A. Wójs, *Quantum Dots*, Springer, New York, 1998.
[10] M. Reed, R. T. Bate, K. Bradshaw, W. M. Duncan, W. M. Frensley, J. W. Lee and H. D. Smith, *J. Vacuum Sci. Technol. B*, 1986, **4**, 358.
[11] J. K. Jaiswal, H. Mattoussi, J. M. Mauro and S. M. Simon, *Nature Biotech.*, 2003, **21**, 47.
[12] F. Combes and G. Pineau des Forêts, *Molecular Hydrogen in Space*, Cambridge University Press, Cambridge, 2000.
[13] A. G. Massey, *Main Group Chemistry*, 2nd edn., Wiley, New York, 2000.
[14] G. Herzberg, *Phys. Rev. Lett.*, 1969, **23**, 108.

[15] W. Heitler and F. London, *Z. Physik*, 1927, **44**, 455.
[16] W. Kolos and L. Wolniewicz, *J. Chem. Phys.*, 1968, **49**, 404.
[17] D. M. Larsen, *Phys. Rev. A*, 1982, **25**, 1295.
[18] U. Wille, *J. Phys. B: At. Mol. Phys.*, 1987, **20**, L417.
[19] U. Kappes and P. Schmelcher, *Phys. Rev. A*, 1995, **51**, 4542.
[20] U. Kappes and P. Schmelcher, *Phys. Rev. A*, 1996, **54**, 1313.
[21] S. Basile, F. Trombetta and G. Ferrante, *Nuovo Cimento*, 1987, **9**, 457.
[22] A. V. Korolev and M. A. Liberman, *Phys. Rev. A*, 1992, **45**, 1762.
[23] D. Lai, E. E. Salpeter and S. L. Shapiro, *Phys. Rev. A*, 1992, **45**, 4832.
[24] M. Demeur, P. H. Heenen and M. Godefroid, *Phys. Rev. A*, 1994, **49**, 176.
[25] G. Ortiz, M. D. Jones and D. M. Ceperley, *Phys. Rev. A*, 1995, **52**, R3405.
[26] T. Detmer, P. Schmelcher, F. K. Diakonos and L. S. Cederbaum, *Phys. Rev. A*, 1997, **56**, 1825.
[27] T. Detmer, P. Schmelcher and L. S. Cederbaum, *Phys. Rev. A*, 1998, **57**, 1767.
[28] K. Runge and J. R. Sabin, *Int. J. Quantum Chem.*, 1997, **64**, 561.
[29] D. Lai and E. E. Salpeter, *Phys. Rev. A*, 1996, **53**, 152.
[30] T. S. Monteiro and K. T. Taylor, *J. Phys. B: At. Opt. Phys.*, 1990, **23**, 427.
[31] W. Kohn, *Phys. Rev.*, 1961, **123**, 1242.
[32] P. Maksym and T. Chakraborty, *Phys. Rev. Lett.*, 1990, **65**, 108.
[33] P. Bakshi, D. A. Broido and K. Kempa, *Phys. Rev. B*, 1990, **42**, 7416.
[34] A. Kumar, S. E. Laux and F. Stern, *Phys. Rev. B*, 1990, **42**, 5166.
[35] M. W. Schmidt, K. K. Baldridge, J. A. Boatz, S. T. Elbert, M. S. Gordon, J. H. Jensen, S. Koseki, N. Matsunaga, K. A. Nguyen, S. J. Su, T. L. Windus, M. Dupuis and J. A. Montgomery, *J. Comput. Chem.*, 1993, **14**, 1347.
[36] G. H. F. Diercksen and G. Hall, *Comput. Phys.*, 1994, **8**, 215.
[37] B. R. Brooks and H. F. Schaefer, *J. Chem. Phys.*, 1979, **70**, 5092.
[38] T. Sako and G. H. F. Diercksen, *J. Phys. B: At. Mol. Opt. Phys.*, 2003, **36**, 1681.
[39] T. Sako and G. H. F. Diercksen, *J. Phys. B: At. Mol. Opt. Phys.*, 2003, **36**, 1433.
[40] T. Sako, I. Cernusak and G. H. F. Diercksen, *J. Phys. B: At. Mol. Opt. Phys.*, 2004, **37**, 1091.
[41] U. Kaldor, *J. Chem. Phys.*, 1975, **62**, 4634.
[42] L. Wolniewicz, *J. Chem. Phys.*, 1998, **109**, 2254.
[43] R. Bukowski, B. Jeziorski and K. Szalewicz, *J. Chem. Phys.*, 1999, **110**, 4165.
[44] O. V. Gritsenko, S. J. A. van Gisbergen, A. Görling and E. J. Baerends, *J. Chem. Phys.*, 2000, **113**, 8478.
[45] K. Yokoyama, H. Nakano, K. Hirao and J. P. Finley, *Theor. Chem. Acc.*, 2003, **110**, 185.
[46] P. R. Surjan, D. Kohalmi and A. Szabados, *Collect. Czech. Chem. Commun.*, 2003, **68**, 331.
[47] B. O. Roos (ed.) *Lecture Notes in Quantum Chemistry*, Springer, New York, 1992, pp. 177–255.
[48] M. Tachikawa and Y. Osamura, *J. Chem. Phys.*, 2000, **113**, 4942.
[49] D. Bielińska-Wąż, G. H. F. Diercksen and M. Klobukowski, *Chem. Phys. Lett.*, 2001, **349**, 215.
[50] E. W. S. Schreiner, PhD Thesis, Max-Planck-Institut für Astrophysik, 1996.
[51] K. P. Huber and G. Herzberg, *Molecular Spectra and Molecular Structure Constants of Diatomic Molecules*, Van Nostrand Reinhold, New York, 1979.
[52] Y. P. Kravchenko and M. A. Liberman, *Phys. Rev. A*, 1998, **57**, 3403.
[53] W. Kolos and L. Wolniewicz, *J. Chem. Phys.*, 1965, **43**, 2429.
[54] J. W. Liu and S. Hagstrom, *J. Phys. B: At. Mol. Opt. Phys.*, 1994, **27**, L729.
[55] D. Frye, G. C. Lie and E. Clementi, *J. Chem. Phys.*, 1989, **91**, 2366.
[56] F. Borondo, F. Martin and M. Yanez, *J. Chem. Phys.*, 1986, **86**, 4982.
[57] W. Kolos and L. Wolniewicz, *J. Chem. Phys.*, 1966, **45**, 509.
[58] J. Rychlewski and W. T. Raynes, *Mol. Phys.*, 1983, **50**, 1335.
[59] S. C. Farantos, G. Theodorakopoulos and C. A. Nicolaides, *Chem. Phys. Lett.*, 1983, **100**, 263.
[60] H. M. James and A. S. Coolidge, *J. Chem. Phys.*, 1939, **6**, 730.
[61] T. Zung and A. B. F. Duncan, *J. Chem. Phys.*, 1962, **36**, 2140.
[62] J. Gerhauser and H. S. Taylor, *J. Chem. Phys.*, 1965, **42**, 3621.
[63] W. Kolos and J. Rychlewski, *Chem. Phys. Lett.*, 1978, **59**, 183.

[64] D. M. Bishop and L. M. Cheung, *Chem. Phys. Lett.*, 1981, **79**, 130.
[65] R. S. Mulliken, *J. Am. Chem. Soc.*, 1966, **88**, 1849.
[66] P. Schmelcher, M. V. Ivanov and W. Becken, *Phys. Rev. A*, 1999, **59**, 3424.
[67] J. E. Avron, I. W. Herbst and B. Simon, *Phys. Rev. A*, 1979, **20**, 2287.
[68] T. Hori, *Zeits. F. Physik*, 1927, **44**, 838.
[69] G. H. Dieke and J. J. Hopfield, *Phys. Rev.*, 1927, **30**, 400.
[70] H. H. Hyman, *Phys. Rev.*, 1930, **36**, 187.
[71] C. R. Jeppesen, *Phys. Rev.*, 1933, **44**, 165.
[72] W. Lichten, *J. Chem. Phys.*, 1957, **26**, 306.
[73] W. Lichten, *Phys. Rev.*, 1960, **120**, 848.
[74] Y. N. Chiu, *J. Chem. Phys.*, 1964, **41**, 3235.
[75] W. M. Wright and E. R. Davidson, *J. Chem. Phys.*, 1965, **43**, 840.
[76] J. C. Browne, *J. Chem. Phys.*, 1964, **40**, 43.
[77] T. Namioka, *J. Chem. Phys.*, 1965, **43**, 1636.
[78] J. R. Hoyland, *J. Chem. Phys.*, 1966, **45**, 3928.
[79] L. Y. Chow Chiu, *Phys. Rev.*, 1965, **137**, A384.
[80] K. Dressler and L. Wolniewicz, *Can. J. Phys.*, 1984, **62**, 1706.
[81] K. Dressler, L. Wolniewicz and P. Quadrelli, *Int. J. Quantum Chem.*, 1986, **29**, 185.
[82] G. Herzberg and A. Monfils, *J. Mol. Spectr.*, 1960, **5**, 482.
[83] G. H. Brigman, S. J. Brient and F. A. Matsen, *J. Chem. Phys.*, 1961, **34**, 958.
[84] A. Amemiya, *Proc. Phys. Math. Soc. (Jpn)*, 1939, **21**, 394.
[85] E. R. Davidson, *J. Chem. Phys.*, 1965, **42**, 4199.
[86] S. Rothenberg and E. R. Davidson, *J. Chem. Phys.*, 1966, **45**, 2560.
[87] W. T. Zemke, P. G. Lykos and A. C. Wahl, *J. Chem. Phys.*, 1969, **51**, 5635.
[88] W. Kolos and J. Rychlewski, *J. Mol. Spectrosc.*, 1977, **66**, 428.
[89] L. Wolniewicz, *J. Mol. Spectrosc.*, 1995, **169**, 329.
[90] R. S. Mulliken, *Phys. Rev.*, 1960, **120**, 1674.
[91] G. Herzberg and L. L. Howe, *Can. J. Phys.*, 1957, **37**, 636.
[92] W. Kolos, *J. Mol. Struct.*, 1978, **46**, 73.
[93] J. Rychlewski, *Theor. Chim. Acta*, 1995, **83**, 249.
[94] G. H. Dieke, *J. Mol. Spectrosc.*, 1958, **2**, 494.
[95] E. R. Davidson, *J. Chem. Phys.*, 1960, **33**, 1577.
[96] E. R. Davidson, *J. Chem. Phys.*, 1961, **35**, 1189.
[97] W. Kolos and L. Wolniewicz, *J. Chem. Phys.*, 1969, **50**, 3228.
[98] P. Schmelcher, T. Detmer and L. S. Cederbaum, *Phys. Rev. A*, 2000, **61**, 043411.
[99] Q. Shi, S. Kais, F. Remacle and R. D. Levine, *J. Chem. Phys.*, 2001, **114**, 9697.
[100] B. E. Applegate, T. A. Barckholtz and T. A. Miller, *Chem. Soc. Rev.*, 2003, **32**, 38.
[101] G. A. Worth and L. S. Cederbaum, *Annu. Rev. Phys. Chem.*, 2004, **55**, 127.
[102] A. Messiah, *Quantum Mechanics*, North-Holland, Amsterdam, 1986, Vol. II.
[103] E. U. Condon and G. H. Shortley, *The Theory of Atomic Spectra*, Cambridge University Press, Cambridge, 1991.

Interplay of Classical and Quantum Mechanics in the Theory of Charged-Particle Stopping

Peter Sigmund

Department of Physics, University of Southern Denmark,
DK-5230 Odense M, Denmark

Abstract

A quarter of a century ago the author stepped into Jens Oddershede's office and asked for support on a problem involving computation with atomic wave functions in connection with a new theoretical scheme to treat stopping of charged particles at intermediate speed. This visit resulted in two related publications, two joint papers and a number of follow-up studies by Jens and several others. In 1989 a Sanibel Symposium was devoted to aspects of the penetration of charged particles through matter, and since then, quite a few quantum chemists have joined the community of theoreticians dealing with particle penetration.

Niels Bohr, a pioneer in both disciplines, emphasized the significance of classical *vs.* quantal arguments in particle penetration. Not the least in view of the complexity of *ab initio* computations in this area, such considerations keep being relevant. This note adds new points to an old discussion based on recent developments.

Contents

1. INTRODUCTION

Swift charged particles penetrating through matter with kinetic energies in the keV/*u* regime and higher slow down primarily by interacting with the electrons of the stopping material. The simplest way to quantify the stopping process is to consider it as a random sequence of free-Coulomb scatterings with a cross section

$$\frac{\mathrm{d}\sigma(T)}{\mathrm{d}T} = \frac{2\pi Z_1^2 e^4}{mv^2} \frac{1}{T^2}, \quad 0 < T < T_{\max}, \tag{1}$$

where the projectile has been assumed to be a bare ion with speed v and atomic number Z_1. The quantity T is the energy transfer in an individual elastic collision with a target electron (charge $-e$, mass m) at rest,[1] and $T_{\max} = 2mv^2$ the maximum energy transfer compatible with energy and momentum conservation.[2]

With this we find the *stopping force*

$$-\frac{\mathrm{d}E}{\mathrm{d}R} = n \int T \, \mathrm{d}\sigma(T) = \frac{2\pi Z_1^2 e^4}{mv^2} n \int_{T_{\min}}^{T_{\max}} \frac{\mathrm{d}T}{T}, \tag{2}$$

where R is the travelled pathlength and n the mean number of electrons per volume.

Since the cross section for nonrelativistic Coulomb scattering is the same in classical and quantum mechanics, equation (2) must contain much of the essential physics in the slowing-down process. However, it also contains an undetermined minimum energy transfer $T_{\min}$ which is nominally zero and hence leads to an infinite stopping force.

Bohr [4], using purely classical arguments, found a solution to this problem which turned out to survive the emergence of quantum mechanics. To see what is going on, consider first Thomson's formula

$$T(p) = \frac{2mv^2}{1 + (pmv^2/Z_1 e^2)^2}, \tag{3}$$

which expresses the energy loss T as a function of the classical impact parameter p and from which equation (1) can easily be derived. Clearly, small values of T originate in large impact parameters p. In those distant collisions the time-dependent electric field induced by the projectile near the target electron varies slowly in space but rapidly in time. Hence, energy transfer in such collisions resembles the interaction between an electromagnetic wave and the target electrons. This process was well described by Drude's electron theory at Bohr's time.

Drude's theory characterizes the electron as a harmonic oscillator with a resonance frequency ω. Adopting this model, Bohr found that the Coulomb

---

[1] Although quantum chemists usually set $\hbar = m = e = 1$, this notation will be avoided here. Setting $\hbar = 1$ would compromise the use of classical arguments right from the beginning.

[2] For electron and positron projectiles, slight modifications are necessary [3].

interaction is effectively truncated at the *adiabatic radius*

$$p_{\max} \simeq a_{\mathrm{ad}} = \frac{v}{\omega}. \tag{4}$$

For $a_{\mathrm{ad}} \gg b$, where

$$b = \frac{2Z_1 e^2}{mv^2} \tag{5}$$

is the *classical collision radius*, equation (3) is readily seen to reduce to

$$T_{\min} \simeq T(p = p_{\max}) \simeq \frac{2(Z_1 e^2)^2}{mv^2} \frac{\omega^2}{v^2}. \tag{6}$$

In modern notation, Bohr's stopping formula then reads

$$-\frac{\mathrm{d}E}{\mathrm{d}R} = \frac{4\pi Z_1^2 e^4}{mv^2} N \sum_{\nu=1}^{Z_2} \ln \frac{Cmv^3}{Z_1 e^2 \omega_\nu}, \tag{7}$$

where ω_ν is the resonance frequency of the νth electron in a target atom of atomic number Z_2 and N the number of atoms per volume. The constant $C = 1.1229$ follows from a detailed evaluation [4] of the functional dependence of $T(p)$.

Bethe's quantum theory [5] changed surprisingly little in equation (7):

- Instead of one resonance frequency per individual electron, Bethe recovered the spectrum of resonance frequencies ω_ν for the atom, weighted by dipole oscillator strengths f_ν satisfying the sum rule

$$\sum_\nu f_\nu = Z_2, \tag{8}$$

  just as in the quantum theory of optical dispersion and absorption.[3]
- Being based on lowest-order perturbation theory, Bethe theory approximates equation (3) by $T = 2(Z_1 e^2/p)^2/mv^2$ so that

$$\frac{T_{\max}}{T_{\min}} = \left(\frac{p_{\max}}{p_{\min}}\right)^2. \tag{9}$$

- The effective minimum impact parameter becomes

$$p_{\min} \simeq \frac{\hbar}{2mv} \tag{10}$$

  in Bethe theory. In other words, de Broglie's wavelength replaces the classical collision radius b.

---

[3] Having recognized the close quantitative connection between optical properties and collision dynamics at this stage of development of atomic theory is a remarkable example of Bohr's physical intuition.

Bethe's formula [5] then reads

$$-\frac{dE}{dR} = \frac{4\pi Z_1^2 e^4}{mv^2} N \sum_\nu f_\nu \ln \frac{2mv^2}{\hbar\omega_\nu} \tag{11}$$

in standard form. Note that in both equations (7) and (11) the only material property entering is the *I*-value given by

$$Z_2 \ln I = \sum_\nu f_\nu \ln(\hbar\omega_\nu). \tag{12}$$

A most remarkable feature of Bethe's theory, pointed out by Bloch [8], is that p_{max} is the same in Bohr and Bethe theory, not only in the present, simplified picture but also in the more detailed mathematical form.

Figure 1 shows a comparison between experimental stopping data and equations (7) and (11). It is seen that over a broad range of beam energies, Bohr's classical formula is superior to Bethe's when the same *I*-value is inserted.

Figure 1 also makes it clear that there must be a fairly wide variety of systems and bombardment conditions where neither equation (7) nor (11) can provide accurate predictions of stopping forces. A considerable number of improvements of the theory can be made and has been made, and the main purpose of this paper is to identify to what extent such improvements can be based safely on classical, Bohr-type arguments. For simplicity of notation, reference will be made in the following to the *stopping number L* defined by

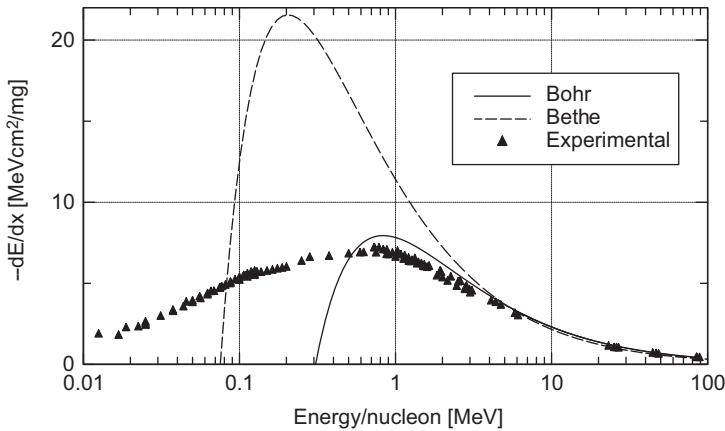$$-\frac{dE}{dR} = \frac{4\pi Z_1^2 e^4}{mv^2} N Z_2 \cdot L, \tag{13}$$

Fig. 1. Stopping force on oxygen ions in aluminium: Comparison of Bohr and Bethe formulae with measurements from numerous laboratories compiled in Ref. [6]. From Ref. [7].

i.e., a quantity which reduces to $L_{\text{Bohr}} = \ln(Cmv^3/Z_1v_0I)$ and $L_{\text{Bethe}} = \ln(2mv^2/I)$, respectively, where $v_0 = e^2/\hbar$ is the Bohr velocity.

2. GENERAL CONSIDERATIONS

I like to emphasize that Fig. 1 is not meant to indicate any fundamental limitation of quantum mechanics: both Bohr's and Bethe's formulae invoke mathematical approximations to the underlying physical models, and Bethe's formula in particular relies on first-order perturbation theory for both distant and close collisions.

On the other hand, Fig. 1 demonstrates the power of classical collision theory. In view of the complexity of a complete quantal treatment of the stopping of a point charge in a many-electron target, or even a many-electron projectile in a many-electron target, utilizing the power of classical collision theory whereever justified, and knowing its limitations, is nothing less than a necessity from a practical point of view.

It appears appropriate here to distinguish between two aspects of quantum mechanics, the stationary states of an isolated target atom or molecule on the one hand, and the physical processes during collision on the other. The former will be considered as intrinsically quantal. No attempt will be made to turn the wheel backward and to estimate dipole oscillator strengths on the basis of the correspondence principle or the like. After all, atomic data for energy levels, transition frequencies, orbital velocities, and oscillator strengths are available in numerous tabulations and computer codes, albeit of varying accuracy. The question to be addressed here is to what extent *additional* quantal arguments need to enter *via collision theory*.

It was seen in the previous section that the main difference between Bethe's and Bohr's descriptions lies in the dynamics of *close collisions*, in which electron binding is unimportant. This feature is beautifully illustrated by Bethe's sum rule [5] which expresses the mean energy transfer to a target electron at a given momentum transfer $\hbar\mathbf{q}$ as

$$\frac{1}{Z_2} \sum_\nu (\varepsilon_\nu - \varepsilon_0)|F_{\nu 0}(\mathbf{q})|^2 = \frac{\hbar^2 q^2}{2m}, \qquad (14)$$

where ε_0 and ε_ν represent the energies of the ground state and an arbitrary excited state of a target atom and

$$F_{\nu 0}(\mathbf{q}) = \left(\sum_{\ell=1}^{Z_2} e^{i\mathbf{q} \cdot \mathbf{r}_\ell} \right)_{\nu 0} \qquad (15)$$

a transition amplitude. While the left-hand side in equation (14) contains the energies of all bound and continuum states, the right-hand side represents the energy transfer to a free electron.

The reason for the difference between Bethe's and Bohr's formulae, despite the identity of the nonrelativistic cross sections for Coulomb scattering in classical and quantum mechanics, was identified by Bloch [8], who ascribed it to the connection between energy transfer and impact parameter. This difference drops out during integration over impact parameter if the range of energy transfers is unlimited, but it becomes significant once a limiting impact parameter is set by electron binding.[4]

The Bloch correction[5]

$$\Delta L_{\mathrm{Bloch}} = \mathrm{Re}\left[\psi(1) - \psi\left(1 + \mathrm{i}\frac{Z_1 e^2}{\hbar v}\right)\right], \tag{16}$$

when added to the Bethe logarithm $L = \ln(2mv^2/I)$, reproduces Bohr's formula (7) and Bethe's formula (11) at low and high-projectile speed, respectively.

The Bloch correction is independent of target properties, and its magnitude is governed by the *Bohr parameter*

$$\kappa = \frac{2Z_1 e^2}{\hbar v}. \tag{17}$$

For $\kappa \gg 1$, de Broglie's wavelength is small enough compared to the classical collision radius b so that a wave packet can be constructed which, approximately, follows the classical Coulomb trajectory [3]. The opposite limit, where the *Sommerfeld parameter* $Z_1 e^2/\hbar v \ll 1$, denotes the case of weak Coulomb interaction where the Born approximation may be expected to be valid.

As it stands, $\Delta L_{\mathrm{Bloch}}$, equation (16), when added to the Bethe formula, extends its range of validity into the classical regime. Alternatively one may introduce an inverse-Bloch correction [10,11]

$$\Delta L_{\mathrm{inv\ Bloch}} = \ln \frac{Z_1 e^2}{\hbar v} - \mathrm{Re}\,\psi\left(1 + \mathrm{i}\frac{Z_1 e^2}{\hbar v}\right) \tag{18}$$

which, when added to the Bohr formula, extends its range of validity into the Bethe regime.

2.1. Electrons and positrons

The Bohr criterion $\kappa \gg 1$ depends on the projectile *speed* rather than its *kinetic energy*. This, together with the fact that $|Z_1| = 1$, implies that for electrons or positrons the validity of semiclassical collision theory becomes

---

[4] Bloch employed what chemists call the semiclassical model, where the motions of the projectile and the target nucleus are treated classically while target electrons obey quantum mechanics. In this model the impact parameter p refers to the target *nucleus* rather than an electron. In genuine quantum mechanics, angular momentum takes over the role of an impact parameter [9].

[5] $\psi(\xi)$ denotes the logarithmic derivative of the gamma function in conventional notation.

questionable at projectile energies above ~ 50 eV. For electrons in particular, the Pauli principle is known to introduce an additional feature that is absent in classical scattering theory and that is particularly important at lower energies. Altogether, the tradition to avoid classical arguments in the computation of atomic stopping parameters for impinging electrons and positrons appears well founded.

3. SHELL CORRECTION

Electrons belonging to a target atom or molecule are not only bound, they also move. This motion is ignored in Bohr stopping theory. Although the same is not true in Bethe theory as far as the fundamental relations are concerned, orbital motion is not taken properly into account in equation (11): it is lost at the point where accessible energy transfers are classified into dipole excitations and free-particle collisions.[6] Indeed, equation (11) represents the leading term in an expansion in powers of v_ν/v, where v_ν is a characteristic electron speed in the νth orbital. This deficiency is repaired by including the *shell correction*.

In Bethe theory the shell correction $\Delta L_{\mathrm{Shell}}$ is conveniently defined as the difference between the stopping number L_{Born} in the Born approximation and the Bethe logarithm $L_{\mathrm{Bethe}} = \ln(2mv^2/I)$. Fano [12] wrote the leading correction in the form

$$\Delta L_{\mathrm{shell}} \sim -\frac{\langle v_e^2 \rangle}{v^2} + \mathcal{O}\left(\frac{1}{v^4}\right), \tag{19}$$

i.e., the leading shell correction reflects the orbital motion of the target electrons. However, the subsequent term ($\propto v^{-4}$) does not allow such a simple interpretation, and terms of order $\propto v^{-6}$ and higher can be shown to diverge for atomic and molecular targets.

Shell corrections can also be evaluated without recourse to an expansion in powers of v^{-2}, but existing calculations such as Refs. [13,14] are based on specific models for the target atom and, unlike equation (19), do not end up in expressions that would allow to identify the physical origin of various contributions. It is clear, however, that orbital motion cannot be the sole cause of shell corrections: The fact that the Bethe logarithm turns negative at $2mv^2/I < 1$ cannot be due to the neglect of orbital motion but must be of a purely mathematical nature. Unfortunately, the uncertainty principle makes it impossible to eliminate orbital motion in an atom from the beginning.

There is, however, an exception: in an infinite homogeneous electron gas, electrons are delocalized. Neglecting their orbital motion does not contradict quantum mechanics, and lacking localization is unproblematic when only cross

---

[6] For details the reader is referred to Ref. [12].

sections are of interest. For this system the stopping number reads [15]

$$L = \ln\frac{2mv^2}{\hbar\omega_P} - \frac{3}{5}\frac{v_F^2}{v^2} - \frac{3}{14}\frac{v_F^4}{v^4} - \cdots; \tag{20}$$

where ω_P is the plasma frequency representing a binding force exerted by the surrounding electrons and v_F the Fermi velocity representing their zero-point motion. In other words, the two leading correction terms in equation (20) are of a purely kinematic nature.[7]

Unlike for an atom, a shell correction expansion up to high orders is possible for an electron bound in a harmonic-oscillator potential [16]. However, this system is characterized by only one parameter and, hence, does not readily allow to separate kinetic from other contributions.

Conceptionally the situation is much clearer in classical theory because the cross-over toward negative stopping numbers of the Bohr logarithm $L_{Bohr} = \ln(Cmv^3/Z_1v_0I)$ can easily be avoided [11]. Orbital motion can be incorporated into the initial conditions [17], although the actual evaluation in Ref. [17] was carried through only to the leading term in v^{-2}.

A fairly general way to evaluate shell corrections is based on *kinetic theory* [1]. Here it is assumed that shell corrections account for orbital motion and nothing else. The theoretical basis is a relation between the stopping number L_0 for a target at rest and the stopping number L for a moving target [1],

$$L(v) = v\left\langle \frac{\mathbf{v}\cdot(\mathbf{v} - \mathbf{v}_e)}{|\mathbf{v} - \mathbf{v}_e|^3} L_0\big(|\mathbf{v} - \mathbf{v}_e|\big) \right\rangle_{\mathbf{v}_e}, \tag{21}$$

where the average is taken over the spectrum of orbital velocities. This relation is exact for free, binary elastic collisions, and since it only relies on conservation laws, it is equally valid in classical and quantal collision theory. The relation may be taken to be approximately valid when binding is of minor significance. Equation (21) was shown [1] to reproduce the leading term in the shell correction expansion (19).

A complete numerical evaluation [2] of equation (21) requires a choice of L_0. The most feasible choice, readily available in 1982, was the Bethe logarithm $L_0 = \ln(2mv^2/I)$ or, better, $L_{0\nu} = \ln(2mv^2/\hbar\omega_\nu)$, allowing proper association of orbital velocities with transition frequencies. In order to avoid artifacts originating in negative stopping numbers, $L_{0\nu}$ was set to zero for $2mv^2/\hbar\omega_\nu < 1$. The missing interval must be significant in the integral due to the factor $|v - v_e|^{-3}$ and hence lead to an error of unknown magnitude. To this adds the more fundamental problem of the precise physical significance of the shell correction in the Bethe theory mentioned above. Nevertheless, this seemed to be the best available option at the time.

As indicated, these problems can be eliminated consistently within Bohr theory, where a nonnegative expression for L_0 or $L_{0\nu}$, valid approximately down to

---

[7] Note that $3v_F^2/5$ is the mean-square electron speed in a Fermi gas, i.e., equation (20) is consistent with (19).
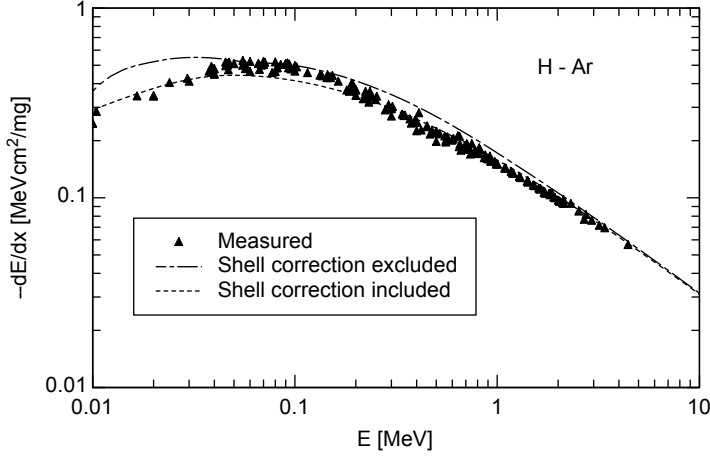
Fig. 2. Stopping cross section for hydrogen in argon. Calculated from binary theory with and without shell correction. Experimental data from numerous laboratories compiled in Ref. [6].

velocity zero, has been found [11]. The transition into the Bethe regime can then be achieved by adding the inverse-Bloch correction (18). Note that also the Bloch correction ignores orbital motion, and therefore, needs shell correction. That correction, however, is unproblematic: the Bloch theory operates with free binary collisions, hence the transformation (21) is exact.

Figure 2 shows the stopping force of argon gas on protons. Experimental data are compared to two predictions of binary stopping theory to be discussed below, excluding and including shell correction, respectively. The difference is seen to be substantial.

3.1. Higher moments

Higher moments of the energy-loss spectrum such as straggling

$$\langle (\Delta E - \langle \Delta E \rangle)^2 \rangle = N \int T^2 \, \mathrm{d}\sigma(T) \tag{22}$$

or the third cumulant[8]

$$\langle (\Delta E - \langle \Delta E \rangle)^3 \rangle = N \int T^3 \, \mathrm{d}\sigma(T) \tag{23}$$

are increasingly determined by contributions from large energy transfers T, i.e., close collisions. Energy transfers between moving collision partners may exceed the kinematic limit $T_{\mathrm{max}} = 2mv^2$. Therefore, the shell correction becomes

---

[8] Although equations (22) and (23) look compellingly similar, the reader is warned against undue generalization: The fourth cumulant does not follow the same pattern.

increasingly significant in the higher moments. It is, in fact, the leading correction to what would follow from straight free-Coulomb scattering [18].

4. BARKAS–ANDERSEN EFFECT

The *Barkas effect* denotes the observation that the stopping cross section of a material is typically greater for a positive particle than for its negative antiparticle under otherwise identical conditions. This effect, first reported in 1953 [19] and confirmed in numerous later experiments, is not predicted by Bethe theory where, independent of the inclusion or omission of shell corrections, the stopping cross section is proportional to the square of the projectile charge. That this effect is also important for swift ions was pointed out by Andersen *et al.* [20] who found that the ratio of stopping cross sections for alphas and protons exceeded the value four predicted by the Bethe formula. Clearly, the *Barkas–Andersen effect* indicates the presence of higher order terms in the projectile charge. Unlike the Bloch correction, the Barkas–Andersen correction must include terms of uneven order in Z_1.

The theoretical literature on the Barkas–Andersen effect is extensive. The present discussion focuses on the role of quantal *vs.* classical arguments.

Traditionally the effect is incorporated into stopping theory *via* expansion in powers of Z_1. As pointed out by Lindhard [21], there are two independent dimensionless parameters containing Z_1, namely, the Bohr parameter κ (equation (17)) and the Barkas parameter

$$B = \frac{Z_1 e^2 \omega}{m v^3}. \tag{24}$$

While the Bloch correction represents a series expansion in powers of κ^2, the leading term in the Barkas–Andersen correction was found [22] to be $\propto B$.

It is important to note here that B is the inverse of the dimensionless variable entering Bohr's stopping formula equation (7). Lindhard [21] concluded from this that the Barkas effect is basically a classical phenomenon. In particular, this implies that within Bohr stopping theory, in the absence of a shell correction, the stopping number can depend only on the variable $m v^3 / Z_1 e^2 \omega$. The validity of this simple scaling relationship in modified Bohr theory – allowing for shell and inverse-Bloch correction as well as projectile screening – has been tested recently [23]. Although not exact, the relation is well fulfilled over a wide range of ion-target combinations and beam energies. An example is shown in Fig. 3.

One must expect the presence of mixed terms of the form $\kappa^\alpha B^\beta$ in the expansion. The term of lowest order ($\alpha = 2$, $\beta = 1$), contributing $\propto Z_1^5$ to the stopping cross section, would indicate a difference between the Barkas–Andersen correction evaluated from the Born series and the Bohr model, respectively. While such a comparison has not been performed in general terms, a numerical evaluation for the specific case of Li in C revealed a negligible difference [24].

In practice, series expansions of the stopping cross section in powers of Z_1 are only useful at high beam velocities where neither the Bloch nor
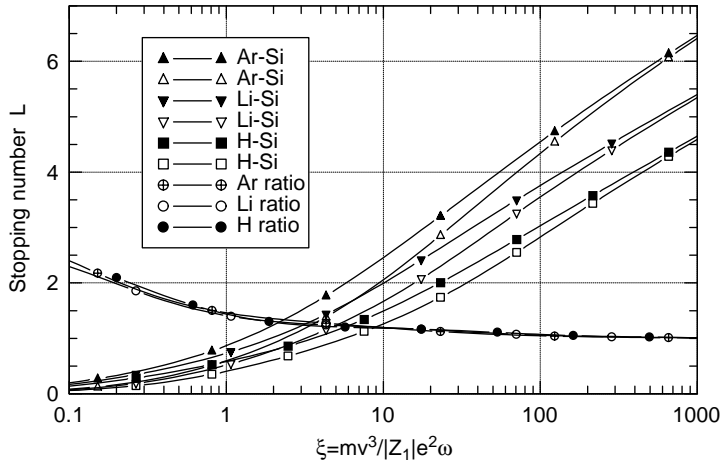
Fig. 3. Barkas–Andersen effect predicted by binary stopping theory. Plotted are stopping numbers for singly charged Ar, Li, and H ions and for their anti-ions in Si. Also shown are the respective ion/anti-ion ratios. From Ref. [23].

the Barkas–Andersen effect exceed a few per cent in relative magnitude. Experiments with antiproton beams at energies down to 1 keV [30] and comparison with standard proton data [31] revealed much larger proton–antiproton differences.

While more than a handful theoretical schemes are available to nonperturbatively evaluate the Barkas–Andersen correction quantum mechanically, *binary stopping theory* developed recently [32] fulfills the task on the basis of the Bohr stopping model[9]; the only quantum feature added is the inverse-Bloch correction (18) which does not differentiate between particle and antiparticle. Figure 4 demonstrates that with regard to comparison with experimental antiproton stopping data, classical theory is fully competitive with various quantum theories.

Clever schemes have been developed to treat the Barkas–Andersen effect for light ions in an electron gas ([27,34] and others) in what is called the *nonlinear quantum regime*. While there is little doubt that there must be a lower velocity limit for the validity of Bohr-like stopping theory, a reliable estimate of this limit does not seem available, nor is there a demonstration of where and in what manner quantum mechanics is an indispensable feature.

Moreover, estimates for an electron gas can hardly be representative for *insulating materials*. There have been speculations on the relevance of promotion effects [35], but theoretical estimates of the Barkas–Andersen effect in insulating solid materials have been performed only on the basis of classical theory so far

---

[9] The essential point in binary stopping theory is the avoidance of an expansion of $T(p)$ in powers of Z_1; this is achieved by mapping the Bohr model on a binary-collision problem involving a screened interaction potential, following a suggestion by Lindhard [21] but with an additional term that generates exact equivalence in the limit of distant collisions. The theory has been implemented in the PASS code [33] which allows incorporation of several features that were either unknown or of no interest at Bohr's time.
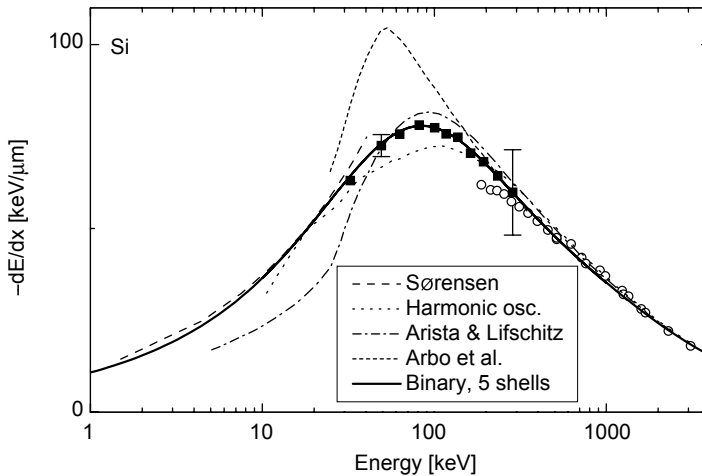
Fig. 4. Stopping of antiprotons in Si: comparison of experimental data [25] with theoretical predictions [25–29]. From Ref. [29].

[36,37]: to the extent that electron promotion contributes significantly, classical theory will be inadequate in the respective velocity regime.

5. DRESSED IONS

Dressed ions carry electrons while slowing down. This feature is important for all ions below some characteristic speed v_c. A rough estimate for v_c is

$$v_c \simeq v_0 Z_1^{2/3} \tag{25}$$

for ions in charge equilibrium [3]. Until less than 10 years ago, generally accepted theoretical descriptions of the stopping of dressed ions were only available for the low-speed regime, $v \ll v_c$, where the stopping cross section was predicted to be proportional to the projectile speed. The estimates by Firsov [38] and Lindhard and Scharff [39] are classical as far as the collisional aspects are concerned, and employ Thomas–Fermi electron densities.

Lacking progress in the theory of stopping of *swift dressed ions* had two serious reasons:

- It was a fairly common belief that such a theory should be a modification of the Bethe theory. Although the fact that the screening regime ($v \lesssim v_c$) lies entirely within the classical domain was presumably recognized, the implication that classical theory must be more powerful than the Born approximation in this regime was evidently not taken at face value.
- A large Barkas–Andersen correction had to be expected for $Z_1 \gg 1$. Available estimates referred to the first term in a perturbation expansion in Z_1. Such an estimate could not be expected to apply to higher-Z_1 ions.

The field of stopping of heavy ions is under rapid development [40]. Several powerful theoretical schemes have been proposed, with varying reliance on classical and quantal arguments. Interestingly, where until a decade ago, classical estimates dominated the low-speed regime while modified Bethe theory was taken to apply to swift ions, the situation has reversed: classical estimates have proven successful to quantify stopping of swift ions, while recent schemes addressing the low-speed regime such as [41] and numerous follow-up papers rely on quantum theory.

5.1. Charge states

Based on the Z_1^2 dependence of the Bethe stopping cross section (equation (11)) it was a widespread assumption that the stopping cross section for a dressed ion could be found by replacing Z_1 in the Bethe formula by the charge number q_1, i.e., the number of electrons missing from a neutral projectile. Specifically, stopping in charge equilibrium was assumed to be determined by an effective charge q_{eff}. More or less drastic differences between q_{eff}, so defined and extracted from measured stopping cross sections, and the charge state of ions emitted from foils, were discussed extensively. This *charge-state paradox* was resolved stepwise:

1. Bethe theory was reevaluated on the basis of screened instead of unscreened Coulomb interaction [42],
2. Bethe theory was replaced by Bohr theory [43],
3. New concepts were developed [32,44–46].

In the present context the most important conclusion emerging from all theoretical schemes, whether classical or quantal, is that the dependence of the stopping cross section on the ion charge tends to be *weaker* than q_1^2. This dependence is sensitive primarily to the ratio Z_1/Z_2 and less pronouncedly so to the projectile speed [43].

Although an accurate theory of equilibrium and nonequilibrium charge-state populations must presumably be based on a quantal description of electron capture and loss, a simple estimate of the equilibrium charge state

$$q_{\text{equil}} \simeq Z_1 \left(1 - e^{-v/Z_1^{2/3} v_0} \right),\tag{26}$$

based on an argument by Bohr [47] – involving little more than the Thomas–Fermi model of the atom combined with physical reasoning – has been used successfully to predict stopping cross sections for a wide variety of systems [33,48]. More accurate expressions for equilibrium charge states [49,50] rely on empirical charge-state data rather than theory.

5.2. Pitfalls

A dressed ion will repeatedly change identity due to charge exchange while penetrating through a medium. Therefore, precise definition of the stopping force

is essential both in a classical and a quantal description of the stopping process. As long as one deals with stopping, it is the *change in kinetic energy of the projectile nucleus* that is the pertinent parameter T entering the stopping cross section $\int T\, d\sigma$ [40,51]. If one deals with energy deposition or ionization, other quantities may be more relevant.

The point may be illustrated by an example. A highly charged ion contains a significant amount of potential energy when interacting with a material. For N^{7+} this would be ~ 1.5 keV, which is the energy required to strip all electrons, one by one, from a neutral nitrogen atom. Neutralization of this ion proceeds *via* electron capture into excited states ('hollow atoms') and subsequent decay *via* Auger and photon emission. As a result one observes radiation effects such as electron emission, sputtering, etc. even if the ion has negligible kinetic energy. Even at sizable beam velocities, effects caused by neutralization may dominate over those due to slowing down. Depending on the precise definition of energy loss, the calculated stopping cross section may become anything between exceedingly large and negative. An unambiguous definition is

$$T = \left\langle \frac{P^2}{2M_1} \right\rangle_{t=-\infty} - \left\langle \frac{P^2}{2M_1} \right\rangle_{t=\infty} \tag{27}$$

for an individual event, where $\mathbf{P}$ and M_1 are the momentum and the mass of the projectile nucleus, respectively. Such a definition applies equally well to quantal, semiclassical, and classical estimates in the nonrelativistic regime. Of course it does not preclude a projectile from gaining kinetic energy in an individual collision event.

Another, more subtle consequence of ignoring the difference between the energy of an atom and the kinetic energy of the nucleus was pointed out recently [52]: a dressed projectile may get electronically excited in a collision; the energy consumed in such a process will be taken from the kinetic energy of the nucleus and hence contribute to T. On the other hand, if the projectile gets *ionized*, the excess kinetic energy of the emitted electron will *not* contribute to T since, in the laboratory frame of reference, the emitted electron is likely to move *more slowly* after the collision than before. Following a pioneering paper in this area [53], several authors[10] overestimated the stopping force on dressed ions by including *all* energy consumed in projectile ionization as seen from a moving reference frame.

5.3. Screening

The prime effect on the stopping of a dressed ion is the *static screening* due to its accompanying cloud of bound electrons. This effect can be estimated by assigning a screened-Coulomb potential to the projectile with a screening function depending on the charge state. Since Bohr's kappa criterion (17) defining

---

[10] For details see Ref. [52].

the limits of the classical-orbit picture was derived for unscreened Coulomb interaction, it does not strictly apply to dressed ions. Although Bohr's estimate can be extended to screened potentials [54], a more heuristic argument may serve the present purpose: model calculations on the basis of a Yukawa screening function have been performed both on the basis of Bethe and Bohr stopping theory [42,43, 55]. Identical expressions were found for the energy loss *vs.* impact parameter in distant interactions. Conversely, screening is unimportant in close collisions.

There may be an intermediate regime of impact parameters where the effect of screening depends on whether the description is quantal or classical. This could be found by reevaluation of the Bloch correction for a screened potential.

6. RELATIVITY

The relativistic regime differs fundamentally from what has been discussed so far, in that the cross sections for Coulomb scattering are not the same in quantum as in classical mechanics. Therefore, with the exception of the Fermi density effect – which is classical as far as the collision physics is concerned – classical arguments are less powerful in this regime.

While this has been known for a long time, recent developments in heavy-ion stopping [56] stimulated a reevaluation of the Bloch theory which resulted in a major revision of relativistic stopping theory, giving rise to substantial changes in quantitative predictions, in particular for the heaviest ions [9].

A particularly interesting feature of the theory [9] is the incorporation of deviations from Coulomb scattering due to the nonvanishing size of the projectile nucleus. The very fact that the theory is based on the Dirac equation and that spin dependences enter nontrivially indicates that quantum mechanics is essential here. Moreover, at the highest energies considered, pair production becomes important, i.e., an effect that does not have a classical equivalent [57].

7. DISCUSSION

Quantum chemistry is a discipline on its own, and its development is presumably determined at least as much by its inherent dynamics as by the needs of experimental chemistry. This is even more likely to be the case with regard to the relation between quantum chemistry and particle stopping. Nevertheless, some conclusions may be drawn from the above discussion on what sort of information is most urgently needed in particle penetration from quantum chemists, and, what might be interesting challenges for ambitious quantum chemists on the more esoteric side. I shall conclude this survey by expressing a few personal views that may not necessarily be shared by all those active in the field.

I tried to consistently distinguish between the quantum mechanics of atomic and molecular properties on the one hand and quantum collision theory on the other. The present discussion follows the same pattern.

7.1. Atomic and molecular properties

Here is a list of quantities needed as input in particle stopping:

- Atomic and molecular velocity distributions for evaluation of shell corrections. As discussed above, this need is even accentuated once interest is directed toward higher moments such as straggling and skewness, where the shell correction constitutes the leading deviation from standard forms following from straight Coulomb scattering. An unsolved fundamental problem in this context is of a conceptual kind: a pronounced difference has been found between shell corrections determined from Hartree–Fock-type [59,60] and hydrogenic velocity spectra [37], cf. Fig. 5.
- Dipole oscillator strengths form important input into all stopping models based on Bethe or Bohr theory. Emphasis has frequently been on total I-values which show only little sensitivity to the specific input. More important are differential oscillator-strength spectra, in particular at projectile speeds where inner-shell excitation channels are closed. Spectra bundled into principal or subshells [60] are sufficient for many purposes, but the best available tabulations are based on analysis of optical data rather than on theory, and such data are unavailable for numerous elements and compounds [61].

There have been several brave attempts to evaluate *generalized oscillator strengths* which involve matrix elements of the type of equation (15). Such computations are quite laborious [62] because of numerous high-lying states involved, and much computation time is employed to confirm the validity of Rutherford's law although that may not be evident. More seriously, such calculations can at best serve a complete evaluation of a stopping cross section in
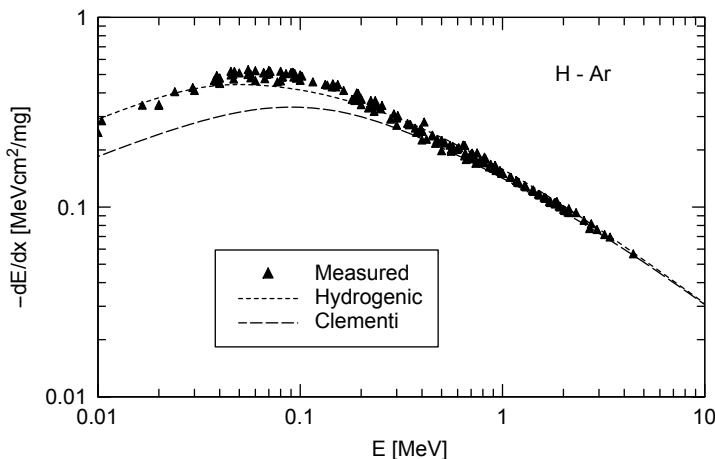

Fig. 5. Stopping cross section for hydrogen in argon. Calculated from binary theory with shell correction based on Clementi [58] and hydrogenic wave functions. Experimental data from numerous laboratories compiled in Ref. [6].

the Born approximation. Inclusion of the Barkas–Andersen effect requires computation of generalized oscillator strengths connecting numerous excited states with each other rather than just with the ground state.

Other atomic data needed, such as electronic charge distributions and screened potentials for partially stripped ions can presumably be based on available tabulations, although existing theoretical treatments have been based on simple and not necessarily accurate scaling relations.

7.2. Quantal collision theory

From the above discussion of the relative merits of quantal and classical collision theory one may extract that

- Quantal collision theory is indispensable in the relativistic regime.
- An accurate treatment of the role of charge exchange, in particular in nonequilibrium stopping in dense media, can hardly be based on classical theory alone.[11]
- There is a widespread opinion that stopping of projectiles at velocities below the Bohr velocity is essentially quantal. The claim appears plausible for insulators to the extent that electron promotion may be an essential sink of energy.

Apart from these items, classical theory appears to do an adequate job whenever reliable input is available.

7.3. Simulation

Straight simulation of collision processes relevant to stopping by solution of the classical equations of motion has been common for about two decades [64]. Although the necessary computational effort is considerable, remarkable results have been found in comparisons with experimental results such as emitted-electron spectra [65]. The main application area of this method refers to very heavy ions at not too high speeds where the Bohr criterion is well satisfied yet relativistic effects are insignificant.

Straight simulations based on Schödinger's equation are coming up slowly, as far as penetration problems are concerned. They appear most promising in case of simple collision systems and allow to test the validity of theoretical models. Such calculations have been performed on the interaction of a point charge with a harmonic oscillator [66] and on the penetration of hydrogen ions or antiprotons in hydrogen or helium gas [67]. The latter are particularly useful to illustrate the role of electron capture in the stopping of light ions at low and intermediate velocities.

---

[11] Apart from the atomistics of charge exchange, especially electron capture, there is also a statistical aspect which has been studied extensively within a classical approach [51] which appears adequate for gases but less obvious for penetration through solids [63].

An interesting recent development is the application of an electron–nuclear-dynamics code [68] to penetration phenomena [69]. The scheme is capable of treating multi-electron systems and may be particularly useful for low-velocity stopping in insulating media, where alternative treatments are essentially unavailable. However, conceptional problems in the data analysis need attention, such as separation of nuclear from electronic stopping and, in particular, the very definition of stopping force as discussed in Section 5.2.

As a general rule, simulations based on classical or quantal equations of motion may serve a useful purpose as benchmarks for model calculations. The days where such simulations may be used for routine calculations of stopping parameters are likely to lie quite a few years ahead, even with the present pace of hardware development in mind. Stopping data are potentially needed for 92×92 elemental ion-target combinations over almost ten decades of beam energy and for a considerable number of charge states, and to this adds an unlimited number of compounds and alloys. It seems wise to keep this in mind in a cost–benefit analysis of one's effort.

ACKNOWLEDGEMENTS

REFERENCES

[1] P. Sigmund, *Phys. Rev. A*, 1982, **26**, 2497–2517.
[2] J. R. Sabin and J. Oddershede, *Phys. Rev. A*, 1982, **26**, 3209–3219.
[3] N. Bohr, *Mat. Fys. Medd. Dan. Vid. Selsk.*, 1948, **18** (8), 1–144.
[4] N. Bohr, *Phil. Mag.*, 1913, **25**, 10–31.
[5] H. Bethe, *Ann. Physik.*, 1930, **5**, 324–400.
[6] H. Paul, Stopping power graphs, www.exphys.uni-linz.ac.at/stopping/
[7] P. Sigmund and A. Schinner, in *Fundamental and Applied Aspects of Modern Physics* (eds S. H. Connell and R. Tegen), World Scientific, Singapore, 2001, p. 178.
[8] F. Bloch, *Ann. Physik*, 1933, **16**, 285–320.
[9] J. Lindhard and A. H. Sørensen, *Phys. Rev. A*, 1996, **53**, 2443–2456.
[10] L. de Ferrariis and N. R. Arista, *Phys. Rev. A*, 1984, **29**, 2145–2159.
[11] P. Sigmund, *Phys. Rev. A*, 1996, **54**, 3113–3117.
[12] U. Fano, *Ann. Rev. Nucl. Sci.*, 1963, **13**, 1–66.
[13] M. C. Walske, *Phys. Rev.*, 1952, **88**, 1283–1289.
[14] H. Bichsel, *Phys. Rev. A*, 2002, **65**, 052709-1–052709-11.
[15] J. Lindhard and A. Winther, *Mat. Fys. Medd. Dan. Vid. Selsk.*, 1964, **34** (4), 1–22.
[16] P. Sigmund and U. Haagerup, *Phys. Rev. A*, 1986, **34** (2), 892–910.
[17] P. Sigmund, *Eur. Phys. J. D*, 2000, **12**, 111–116.
[18] P. Sigmund and K. Johannessen, *Nucl. Instrum. Methods B*, 1985, **6**, 486–495.
[19] F. M. Smith, W. Birnbaum and W. H. Barkas, *Phys. Rev.*, 1953, **91**, 765–766.
[20] H. H. Andersen, H. Simonsen and H. Sørensen, *Nucl. Phys.*, 1969, **A125**, 171–175.
[21] J. Lindhard, *Nucl. Instrum. Methods*, 1976, **132**, 1–5.
[22] J. C. Ashley, R. H. Ritchie and W. Brandt, *Phys. Rev. B*, 1972, **5**, 2393–2397.

[23] P. Sigmund and A. Schinner, *Nucl. Instrum. Methods B*, 2003, **212**, 110–117.

[24] A. Schinner and P. Sigmund, *Nucl. Instrum. Methods B*, 2000, **164/165**, 220–229.

[25] S. P. Møller, E. Uggerhøj, H. Bluhme, H. Knudsen, U. Mikkelsen, K. Paludan and E. Morenzoni, *Phys. Rev. A*, 1997, **56**, 2930–2939.

[26] A. H. Sørensen, *Nucl. Instrum. Methods B*, 1990, **48**, 10–13.

[27] N. R. Arista and A. F. Lifschitz, *Phys. Rev. A*, 1999, **59**, 2719–2722.

[28] D. G. Arbó, M. S. Gravielle and J. E. Miraglia, *Phys. Rev. A*, 2000, **62**, 032901-1-7.

[29] P. Sigmund and A. Schinner, *Eur. Phys. J. D*, 2001, **15**, 165–172.

[30] S. P. Møller, A. Csete, T. Ichioka, H. Knudsen, U. I. Uggerhøj and H. H. Andersen, *Phys. Rev. Lett.*, 2002, **88**, 193201.

[31] ICRU, Stopping powers and ranges for protons and alpha particles, Vol. 49, ICRU Report, International Commission of Radiation Units and Measurements, Bethesda, Maryland, 1993.

[32] P. Sigmund and A. Schinner, *Eur. Phys. J. D*, 2000, **12**, 425–434.

[33] P. Sigmund and A. Schinner, *Nucl. Instrum. Methods B*, 2002, **195**, 64–90.

[34] T. D. Gaztelurrutia and J. M. Pitarke, *J. Phys. A*, 2001, **34**, 7607–7620.

[35] K. Eder, D. Semrad, P. Bauer, R. Golser, P. Maier-Komor, F. Aumayr, M. Peñalba, A. Arnau, J. M. Ugalde and P. M. Echenique, *Phys. Rev. Lett.*, 1997, **79**, 4112.

[36] P. Sigmund and A. Schinner, *Nucl. Instrum. Methods B*, 2002, **193**, 49–55.

[37] A. Sharma, A. Fettouhi, A. Schinner and P. Sigmund, *Nucl. Instrum. Methods B*, 2004, **218**, 19–28.

[38] O. B. Firsov, *Zh. Eksp. Teor. Fiz.*, 1959, **36**, 1517–1523.

[39] J. Lindhard and M. Scharff, *Phys. Rev.*, 1961, **124**, 128–130.

[40] P. Sigmund, *Stopping of Heavy Ions. Vol. 204 of Springer Tracts of Modern Physics*, Springer, Berlin, 2004.

[41] P. M. Echenique, R. M. Nieminen and R. H. Ritchie, *Solid State Commun.*, 1981, **37**, 779–781.

[42] W. Brandt and M. Kitagawa, *Phys. Rev. B*, 1982, **25**, 5631–5637.

[43] P. Sigmund, *Phys. Rev. A*, 1997, **56**, 3781–3793.

[44] G. M. Azevedo, P. L. Grande and G. Schiwietz, *Nucl. Instrum. Methods B*, 2000, **164/165**, 203–211.

[45] G. Maynard, M. Chabot and D. Gardès, *Nucl. Instrum. Methods B*, 2000, **164/165**, 139–146.

[46] N. R. Arista, *Nucl. Instrum. Methods B*, 2002, **195**, 91–105.

[47] N. Bohr, *Phys. Rev.*, 1941, **59**, 270–275.

[48] ICRU, Stopping of Heavy Ions. *J. ICRU*, 2005.

[49] K. Shima, T. Ishihara and T. Mikumo, *Nucl. Instrum. Methods*, 1982, **200**, 605–608.

[50] G. Schiwietz and P. L. Grande, *Nucl. Instrum. Methods B*, 2001, **175–177**, 125–131.

[51] P. Sigmund and L. Glazov, *Nucl. Instrum. Methods B*, 1998, **136–138**, 47–54.

[52] P. Sigmund and L. G. Glazov, *Eur. Phys. J. D*, 2003, **23**, 211–215.

[53] Y. K. Kim and K. T. Cheng, *Phys. Rev. A*, 1980, **22**, 61–67.

[54] J. Lindhard, *Mat. Fys. Medd. Dan. Vid. Selsk.*, 1965, **34** (14), 1–64.

[55] P. L. Grande and G. Schiwietz, *Nucl. Instrum. Methods B*, 2002, **195**, 55–63.

[56] C. Scheidenberger, H. Geissel, H. H. Mikkelsen, F. Nickel, T. Brohm, H. Folger, H. Irnich, A. Magel, M. F. Mohar, G. M. M. Pfützner, E. Roeckl, I. Schall, D. Schardt, K. H. Schmidt, W. Schwab, M. Steiner, T. S. K. Sümmerer, D. J. Vieira, B. Voss and M. Weber, *Phys. Rev. Lett.*, 1994, **73**, 50–53.

[57] A. H. Sørensen, *Nucl. Instrum. Methods B*, 2005, **230**, 12–16.

[58] E. Clementi and C. Roetti, *At. Data Nucl. Data Tables*, 1974, **14**, 177.

[59] V. H. Ponce, *At. Data Nucl. Data Tables*, 1977, **19**, 63–82.

[60] J. Oddershede and J. R. Sabin, *At. Data Nucl. Data Tables*, 1984, **31**, 275–297.

[61] E. D. Palik, *Electronic Handbook of Optical Constants of Solids – version 1.0. SciVision*, Academic Press, London, 2000.

[62] O. H. Mortensen, J. Oddershede and J. R. Sabin, *Nucl. Instrum. Methods B*, 1992, **69**, 24–32.

[63] Z. L. Miskovic, F. O. Goodman, W. K. Liu and Y. N. Wang, *Phys. Rev. A*, 2003, **67**, 012902.

[64] R. E. Olson, *Atomic Molecular and Optical Physics Handbook*, AIP, New York, 1996, pp. 664–668.

[65] L. H. Toburen, R. D. Dubois, C. O. Reinhold, D. R. Schultz and R. E. Olson, *Phys. Rev. A*, 1990, **42**, 5338–5347.

[66] H. H. Mikkelsen and H. Flyvbjerg, *Phys. Rev. A*, 1992, **45** (5), 3025–3031.
[67] G. Schiwietz, *Phys. Rev. A*, 1990, **42**, 296–306.
[68] E. Deumens, A. Diz, R. Longo and Y. Öhrn, *Rev. Mod. Phys.*, 1994, **73**, 917–983.
[69] R. Cabrera-Trujillo, J. R. Sabin, E. Deumens and Y. Öhrn, *Phys. Rev. A*, 2002, **66**, 022706.

Elliptic Functions of the Worst Kind: Non-linear Quantisation of the Classical Spherical Pendulum

John W. Perram[1] and Edgar R. Smith[2]

[1]*The Maersk Mc-Kinney Moller Institute for Production Technology, University of Southern Denmark, Odense, Denmark*
[2]*School of Mathematics, La Trobe University, Bundoora, Australia*

Abstract

This chapter considers a problem much studied by the pioneers of quantum mechanics at the beginning of the 20th century, the motion of the spherical pendulum, for which the equations of motion are the same as those of the symmetric top, reporting a number of new results. An accurate approximation to the variation of the frequency of vertical oscillations with the initial angular displacement from the downward vertical direction is obtained on the basis of physical approximations to the equation of motion, rather than mathematical, approximations to the solution. This formula predicts that for angular displacements less than about 70°, the frequency of vertical oscillations first becomes smaller as the energy is increased, passes through a minimum and thereafter rises again. This effect is confirmed by numerical simulation of the exact equations.

In general, the 3D motion of the spherical pendulum is very complex, but for fixed initial angular displacements, values of the kinetic energy can be found (by trial and error) for which this motion is periodic. The approximation discussed above leads to the approximate description of the horizontal motion in terms of Mathieu functions, for which Flocquet analysis determines periodic solutions in terms of two integers k and n, which can be thought of as quantum numbers.

Contents

1. INTRODUCTION

As only one of us has but a single joint article [1] with Jens, not surprisingly because we are not quantum chemists, we are honoured to have been invited to contribute to this special issue in his honour. In all the 25 or so years we have known him, being professors of applied mathematics, we have had to listen to cheap jibes about special functions, asymptotic expansions and other things of beauty, so this invitation gives us the opportunity for some revenge, because, knowing how conscientious Jens is, we are sure that he will read the article.

Theoretical chemists learn about a number of special functions, the Hermite functions in connection with the quantisation of the harmonic oscillator, Legendre and associated Legendre functions in connection with multipole expansions, Bessel functions in connection with Coulomb Greens' functions, the Coulomb wave functions and a few others. All these have in common that they are the solutions of second order linear equations with a parameter. It is usually the case that solutions of boundary value problems for these equations only exist for countable sets of values of the parameter. This is how quantisation crops up in the Schrödinger picture. Quantum chemists are very comfortable with this state of affairs, but rarely venture outside the linear world where everything seems to be ordered.

The spherical pendulum, which consists of a mass attached by a massless rigid rod to a frictionless universal joint, exhibits complicated motion combining vertical oscillations similar to those of the simple pendulum, whose motion is constrained to a vertical plane, with rotation in a horizontal plane. Chaos in this system was first observed over 100 years ago by Webster [2] and the details of the motion discussed at length by Whittaker [3] and Pars [4]. All aspects of its possible motion are covered by the case, when the mass is projected with a horizontal speed V in a horizontal direction perpendicular to the vertical plane containing the initial position of the pendulum when it makes some acute angle with the downward vertical direction. In many respects, the motion is similar to that of the symmetric top with one point fixed, which has been studied *ad nauseum* by many of the early heroes of quantum mechanics [5].

These two systems are examples from non-linear physics, where the equations can be solved in terms of elliptic functions and elliptic integrals. The reader who is not familiar with these functions, which do not arise in the same way as the previously mentioned special functions, is referred to the excellent book by Whittaker and Watson [6]. In that book, the reader will see that there are two flavours of elliptic functions, the Weierstrass and Jacobi representations, three kinds of elliptic integrals, and six kinds of pseudo-periodic functions, the Weierstrass zeta and sigma functions and the four kinds of Jacobi theta functions. Of historical interest for theoretical chemists is the fact that Jacobi's imaginary transformation of the theta functions is the same as the Ewald transformation of crystal physics [7].

Related to the elliptic integral of the third kind are the Lamé functions, which arise in the generalisation of spherical harmonics to confocal ellipsoidal coordinates. Applications of these in molecular electrostatics can be found

in Ref. [8]. In this day of computers, all these functions have fallen into disuse and are candidates for extinct knowledge.

So how is the spherical pendulum quantised? The answer is that its motion is generally chaotic, except for discrete values of the initial projection speed, for which it is periodic. The precise details of this phenomenon are difficult to get a handle on, because, although the vertical motion is always described by periodic elliptic functions, the horizontal motion is described in terms of Lamé functions, which are very difficult to study and for which periodicity is difficult to diagnose.

At this point, we had better get back to how Jens Oddershede fits into the picture. Apart from his fame as a leading quantum chemist whose contributions we celebrate in this volume, Jens is recognised amongst the leading academic administrators in Denmark, first as Dean of the Faculty of Science and Engineering and now as President of the University of Southern Denmark. One of his major achievements was to put the 'engineering' in 'science and engineering', which partly occurred because he, with a bit of assistance from me, was able to convince the owner of a ship building company with which I had been involved in a robotics research project, to make the largest recorded donation to a Danish university to fund the institute to which I am attached. The key ingredient in the robotics project was to use some advanced analytical mechanics from the world of molecular dynamics to do collision-avoiding trajectory planning for welding and painting robots.

In this version of mechanics, we model mechanical systems as assemblies of point masses connected by massless rigid rods, so we operate with redundant coordinates and constraints, rather than eliminating the constraints using generalised coordinates. Linear algebra is then used to compute the forces of constraint. When I began to teach our course in analytical mechanics to the engineering students, I started to ask whether this way of looking at mechanics also had pedagogical apart from computational advantages. If one looks at the treatment of the pendulum in any modern freshman physics textbook [9], one begins to grasp why no one wants to study physics anymore. To get around the problem that the motion of the pendulum is usually described in terms of the angular displacement of the pendulum from the downward vertical direction, which is a generalised coordinate and not a mechanical variable, a fictitious tangential equation of motion is introduced, fictitious because it is relative to an accelerating (rotating) frame. Since first year physics students have not been introduced to generalised coordinates and analytical mechanics, it is no wonder that they are confused.

At this point, I was on sabbatical at La Trobe University in Australia, where my host was Professor Edgar Smith, a frequent visitor to Odense and so well known to Jens, that he is well qualified as a co-author of this article. We began to speculate that students might find more convincing set of arguments which led them from Newton's second law to the motion of the pendulum, shown in Fig. 1.

The motion of the spherical pendulum for general values of its initial vertical coordinate and horizontal velocity can be quite complex, as can be seen in Fig. 2 which shows the projection of three trajectories onto the horizontal plane, where
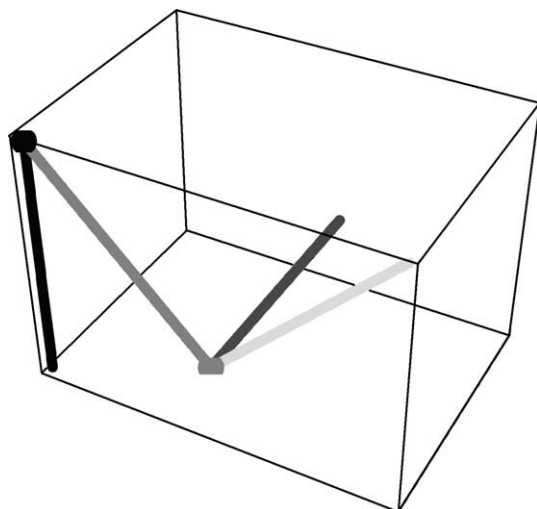
Fig. 1. The geometry of the pendulum (the stick and balls). In the case of the simple pendulum, the system is displaced from its downward position released from rest with the initial value of its vertical coordinate $z[0]$ measured from the support point, as shown. The most general motion involves giving the mass an initial velocity V in the plane formed by the two lines, which are perpendicular to the pendulum and thus tangent to the sphere on which the pendulum moves. It is sufficiently general to consider the initial velocity V to be horizontal (in the direction of the vector perpendicular to the vertical plane containing the pendulum).

the pendulum starts from a horizontal position but with different horizontal speeds, increasing from left to right. The middle case is much simpler than the other two, indicating a periodic trajectory.

There is a considerable literature [10–13] devoted to finding approximate formulas for the frequency of the simple pendulum for non-zero amplitudes, usually based on mathematical arguments designed to approximate elliptic functions.

Fig. 2. The horizontal projection of three trajectories of the spherical pendulum with different initial horizontal velocities, increasing from left to right.

In this chapter, we will derive the approximate formula

$$\sqrt{\frac{g}{L}\left(1 - \frac{1}{2}\sin^2\left[\frac{\Theta}{2}\right]\right)} \tag{1}$$

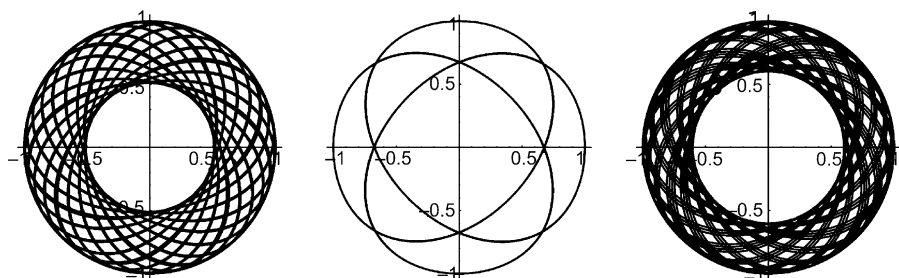where g is the gravitational acceleration and L the length of the pendulum, for the angular frequency as a function of the initial angular deviation Θ of the pendulum from the downward vertical direction, which is accurate up to angles as large as $90°$. This formula is obtained by finding the optimal symbolic linear approximation to the vertical force on the pendulum, using computer algebra. Interestingly enough, my main input to Ref. [1] involved using the computer algebra system REDUCE running on a mainframe to compute the asymptotic expansion of the solution to an algebraic equation.

For the case of spherical pendulum, it is relevant to ask how the frequency of vertical oscillations changes as the initial horizontal velocity V increases from zero, in terms of the dimensionless kinetic energy K defined by

$$K = \frac{V^2}{2gL} \tag{2}$$

The authors invite physical explanations of the fact that for angles less than about $67°$, the frequency decreases, goes through a minimum, before rising again. For larger angular deviations, the frequency increases. The same approximation predicts that the critical angle is given by

$$\arccos[1/3] \tag{3}$$

whose numerical value is about $70.5°$.

In this approach, the horizontal coordinates $x[t]$ and $y[t]$ both satisfy linear, second order equations. The exact trajectories satisfy Lamé's equation of order two, which is extremely difficult to analyse. The corresponding equation for the linear approximation is Mathieu's equation, which is known to have both periodic and aperiodic solutions.

2. NEWTON'S EQUATIONS FOR THE PENDULUM IN CARTESIAN COORDINATES

In the absence of friction, there are two forces acting on the mass m whose position vector at time t is denoted by the vector $\mathbf{r}[t]$ measured relative to the support point, which is the origin of a set of Cartesian axes with three-component $\mathbf{k}$ in the upward vertical direction. The first is the force of gravity on the mass, which acts downwards with a value $-mg\mathbf{k}$. The second is the centripetal force, unknown for the moment, which is directed along the support towards the universal point. We denote this force by $-T\mathbf{r}[t]$, where T is a scalar function of time to be found. The Newtonian equations of motion can then be written as

$$m\mathbf{r}''[t] = -mg\mathbf{k} - T\mathbf{r}[t] \tag{4}$$

Another way of thinking of the centripetal force is that it is a force arising because the mass is constrained to move on the surface of a sphere, expressed by the constraint

$$\mathbf{r}[t]^2 = L^2 \tag{5}$$

This equation can be differentiated with respect to time to obtain the equations

$$\mathbf{r}[t] \cdot \mathbf{r}'[t] = 0, \quad \mathbf{r}[t] \cdot \mathbf{r}''[t] = -\mathbf{r}'[t]^2 \tag{6}$$

The first of these expresses the condition that the centripetal constraint force does no work, because the velocity is perpendicular to the radius. The second states that the radial component of the acceleration is directed inwards and equal to the square of the speed. This relation can be used to calculate the constraint force by taking the scalar product of the equation of motion (2) with the vector function $\mathbf{r}[t]$, and using the constraint and its time derivatives to obtain

$$m\mathbf{r}[t] \cdot \mathbf{r}''[t] = -mg\mathbf{r}[t] \cdot \mathbf{k} - TL^2 = -mgz[t] - TL^2 = -m\mathbf{r}'[t]^2 \tag{7}$$

This can be solved for T to obtain

$$T = \frac{m\mathbf{r}'[t]^2 - mgz[t]}{L^2} \tag{8}$$

Although this equation is derived in the classic works of Webster [2] and Sommerfeld [5], only Webster notes that the equation of conservation of energy

$$\frac{1}{2}m\mathbf{r}'[t]^2 + mgz[t] = H = \frac{1}{2}mV^2 + mgZ \tag{9}$$

where Z is the initial value $z[0]$ of the vertical coordinate, can be used to eliminate the velocity from the expression for T to obtain

$$T = \frac{2H - 3mgz[t]}{L^2} \tag{10}$$

so that the equation of motion becomes

$$m\mathbf{r}''[t] = -mg\mathbf{k} - \frac{2H - 3mgz[t]}{L^2}\mathbf{r}[t] \tag{11}$$

Webster, however, does not notice that we may take the scalar product of the equation of motion with the vector $\mathbf{k}$ and use the resulting expression to obtain

$$mz''[t] = -mg - z[t]\frac{2H - 3mgz[t]}{L^2} \tag{12}$$

which is a second order differential equation for the vertical coordinate z. This equation is exact and applies equally well for the simple and spherical pendulums. For the case of the simple pendulum, released from rest, this becomes

$$mz''[t] = -mg - z[t]\frac{2mgZ - 3mgz[t]}{L^2} \tag{13}$$

The vertical equation of motion in both cases can be simplified by dividing out the mass m and defining new variables w, W and τ by

$$w[\tau] = \frac{z[t]}{L}, \quad W = \frac{Z}{L}, \quad \tau = t\sqrt{\frac{g}{L}} \tag{14}$$

to obtain

$$\frac{d^2 w}{d\tau^2} = w''[t] = 3w[\tau]^2 - 2(W + K)w[\tau] - 1 \tag{15}$$

where K is the dimensionless initial kinetic energy, previously defined as

$$K = \frac{V^2}{2gL} \tag{16}$$

If we could solve this equation to find $w[t]$ and hence $z[t]$ we could insert the result into the equation of motion and take the scalar product with a horizontal unit vector, **i** say, to obtain

$$mx''[t] = -\frac{2H - 3mgz[t]}{L^2} x[t] \tag{17}$$

which is a linear differential equation for one of the horizontal coordinates $x[t]$. The other coordinate $y[t]$ satisfies the same equation.

3. FIRST INTEGRAL AND SOLUTION FOR THE VERTICAL COORDINATE

3.1. The first integral

If we multiply the differential equation for the vertical coordinate $z[t]$ by the vertical velocity $z'[t]$ and integrate, we obtain

$$w'[\tau]^2 = 2(W - w[\tau])\bigl(1 - w[\tau]^2 + K(W + w[\tau])\bigr) \tag{18}$$

since the initial vertical velocity is assumed to be zero.

3.2. Behaviour of the solution

The right-hand sided is a cubic polynomial in $w[\tau]$ which is shown in Fig. 3, plotted as a function of w for $W = -1/2$ (corresponding to an initial angular displacement from the downward vertical of 60°) and three values of K.

Since the first integral must be non-negative, the motion is restricted to the region above the horizontal axis. The three values of w for which the first integral is zero are given symbolically by

$$\left\{ W, \ \frac{1}{2}\left(K - \sqrt{4 + K^2 + 4KW}\right), \ \frac{1}{2}\left(K + \sqrt{4 + K^2 + 4KW}\right) \right\} \tag{19}$$
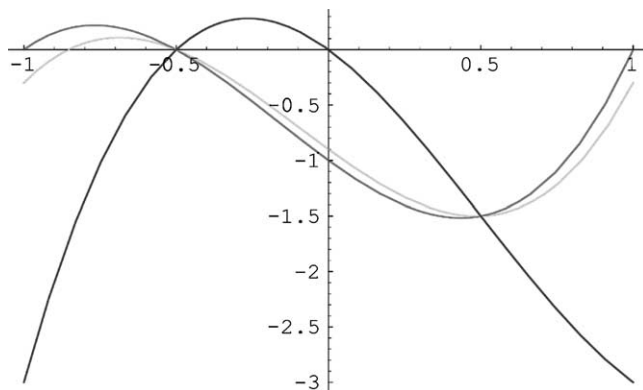
Fig. 3. The first integral of the equation of motion for vertical coordinate $z[t]$ of the pendulum, plotted for three values of the kinetic energy K. In the case of the simple pendulum ($K=0$, the curve cutting the horizontal axis at $z=-1$), we see that the first integral is only non-negative if $z[t]$ lies between -1, its lowest possible value and W, the vertical coordinate of the point from which it is released. As K increases, the zero at $z=-1$ moves to the right. For small values of K (0.2), the left zero of the first integral, representing the lower limit of the vertical coordinate, lies to the left of the initial value, so that the initial vertical motion is downwards. As K increases, this zero moves above the initial value, and the initial motion is upwards.

The value of the third zero is never less than 1, so that the motion is restricted to the interval bounded by the first two zeros. If the two zeros are equal, which occurs when

$$K = \frac{-1 + W^2}{2W} \tag{20}$$

there are no vertical oscillations and the pendulum moves in a horizontal circle (this case is called the conical pendulum).

3.3. Transformation of the first integral to Weierstrassian form

This cubic can be transformed to canonical form (with the quadratic term missing) by means of the linear transformation

$$w[\tau] = 2\wp[\tau] + \frac{K + W}{3} \tag{21}$$

to give

$$\wp'[\tau]^2 = 4\wp[\tau]^3 - \frac{2}{27}(54 + 18K^2 + 36KW + 18W^2)\wp[\tau]$$

$$- \frac{2}{27}(9K + 2K^3 - 18W + 6K^2W - 21KW^2 + 2W^3) \tag{22}$$

which is precisely the differential equation for the Weierstrass elliptic P-function, whose solution can be written as

$$w[\tau] = 2\wp[\tau + a] + \frac{K + W}{3} \tag{23}$$

where a is a constant to be found from the initial conditions, which, since the initial vertical velocity is zero, indicates that the constant a is one of the semi-periods of the Weierstrass elliptic function.

4. EQUATIONS FOR THE HORIZONTAL COORDINATES

If we define the dimensionless horizontal coordinates by

$$X[\tau] = \frac{x[t]}{L}, \quad Y[\tau] = \frac{y[t]}{L} \tag{24}$$

and use the formal solution for w in terms of the Weierstrass functions, then X satisfies

$$X''[\tau] = -(2W + 2K - 3w[\tau])X[\tau] \tag{25}$$

which, on inserting the solution, becomes

$$X''[\tau] = -(W + K - 6\wp[\tau + a])X[\tau] \tag{26}$$

the same equation as is satisfied by Y. These equations have solutions in terms of Lamé functions of the second kind. Very little is known about these functions and the solutions of this equation: in fact, it is a highly non-trivial task to compute the details of the solution, so that it is very difficult to extract much physics out of the solution even when it is found.

5. APPROXIMATE EQUATION OF MOTION

The right-hand side of the equation of motion is a quadratic expression in w, which is plotted in Fig. 4 for the same parameter values as in Fig. 2.

   The curvature of all three is moderate, which suggests that it might be possible to approximate this acceleration by a straight line over the interval over which the first integral is non-negative, to a function of the form

$$w''[t] = aw[t] + b \tag{27}$$

Modern mathematical software, such as *Mathematica*, allows us to compute symbolically the mean square deviation of this approximation from the exact acceleration, integrated over the feasible region, differentiate the resulting expression symbolically with respect to the parameters a and b, set the results to zero and solve the equations symbolically, and simplify the whole lot to find the following remarkably simple expressions

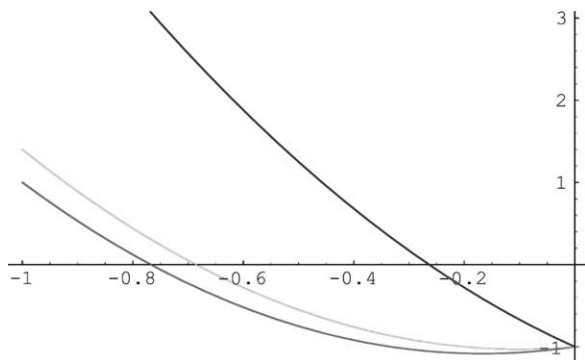$$a = -\frac{K}{2} + W - \frac{3}{2}\sqrt{4 + K^2 + 4KW} \tag{28}$$

Fig. 4. The acceleration associated with the vertical coordinate for the simple pendulum (the lowest curve), the slow spherical pendulum (the middle curve) and the fast spherical pendulum (the upper curve).

$$b = \frac{1}{4}\left(-6 - K^2 - 2W^2 + 4W\sqrt{4 + K^2 + 4KW} \right.$$
$$\left. + K(-6W + \sqrt{4 + K^2 + 4KW}) \right) \tag{29}$$

The value of a is always negative, so that the solutions will always be oscillatory and expressible in terms of the normal circular functions, with a frequency equal to the square root of $-a$, namely

$$\Omega = \sqrt{\frac{K}{2} - W + \frac{3}{2}\sqrt{4 + K^2 + 4KW}} \tag{30}$$

To our knowledge, this is the first analytical estimate of the frequency of the spherical pendulum to have been published.

For the case of the simple pendulum ($K=0$), the value of a simplifies to

$$\Omega = \sqrt{3 - W} \tag{31}$$

leading to the remarkably simple and accurate formula equation (1) for the approximate amplitude dependence of the frequency. Note that when $W = -1$ and the oscillations are infinitesimal, this has the value of 2. The explanation for this is that the vertical coordinate goes through two periods as the pendulum swings back and forth through one oscillation in the angular displacement.

There is actually a considerable literature on the approximate amplitude dependence of the simple pendulum [9–11], although this is the only one we know of which is based on approximating the physics rather than the mathematics. The formula is remarkably accurate even for initial angular displacements of 90° from the downward vertical. The corresponding equations for the spherical pendulum in generalised coordinates are altogether more complicated, very
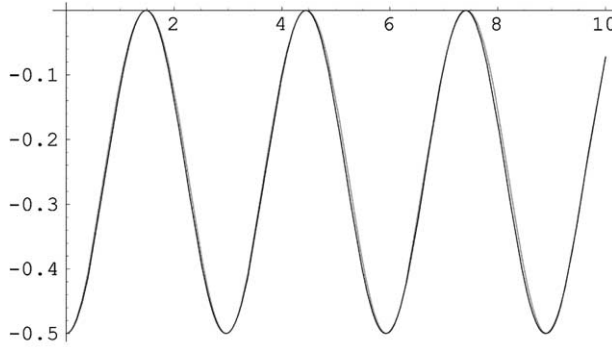
Fig. 5. The solution $w[t]$ of the linear approximation superimposed on the exact solution for $K=2$ and $W=-1/2$.

similar to those of the spinning top [12], and thus rarely discussed in the educational literature [13,14].

5.1. Solution of the approximate equation of motion

The solution satisfying the initial conditions $w[0]=W$, $w'[0]=0$ is found to be

$$w[t] = \frac{K + 2W - \sqrt{4 + K^2 + 4KW}}{4}$$

$$- \frac{K - 2W - \sqrt{4 + K^2 + 4KW}}{4} \cos\left[\Omega\sqrt{\frac{g}{L}}t\right] \qquad (32)$$

Figure 5 shows the solution $w[t]$ of the linear approximation superimposed on the exact solution for $K=2$ and $W=-1/2$. Again the agreement is quantitative.

6. APPROXIMATE FREQUENCY DEPENDENCE OF THE SPHERICAL PENDULUM ON THE KINETIC ENERGY

Figure 6 shows the approximate frequency of the spherical pendulum relative to the ideal value for the simple pendulum, plotted as a function of the dimensionless kinetic energy.

These curves reveal an apparently new and surprising phenomenon. For small initial angular displacements from the downward vertical (the curve with the most pronounced minimum), the frequency apparently decreases as the kinetic energy K increases from zero, and passes through a minimum, before increasing. For larger initial angular displacements (the middle curve), the minimum is less pronounced and occurs at lower values of K. In the last curve, the minimum has
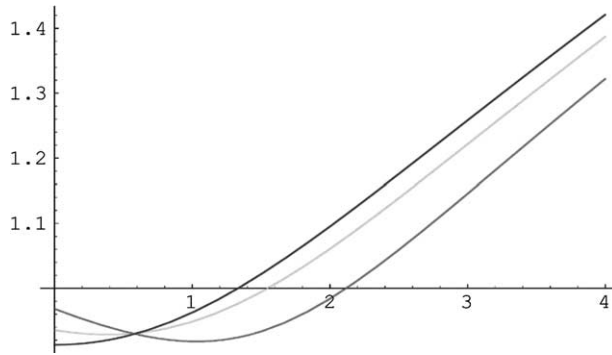
Fig. 6. The approximate frequency of the spherical pendulum plotted as a function of the kinetic energy K for initial vertical coordinates $W = -3/4$ (the curve with the most pronounced minimum), $W = -1/2$ (the middle curve) and $W = -1/4$ (the monotonic curve).

disappeared. The critical value of W for which the minimum occurs when $K = 0$ can be computed symbolically to be $-1/3$, corresponding to about $72°$. Exact calculations using the Weierstrassian functions implemented in *Mathematica*, reveal that this effect is real, with the critical angular displacement estimated to be about $67°$.

7. APPROXIMATE HORIZONTAL MOTION

Whittaker [3] has given an expression for the azimuthal angle of the spherical pendulum in terms of elliptic functions of the third kind, so that, not surprisingly, there has been very little numerical discussion of its motion. Instead, we see if our approximate theory can be used to obtain a simpler picture of the motion.

7.1. Equation of motion for the horizontal coordinates

If we insert the approximate solution for w into the equation of motion for X, we obtain

$$X''[\tau] = -\frac{1}{4}\left(5K + 2W + 3\sqrt{4 + K^2 + 4KW} \right.$$

$$\left. - 3\left(-K + 2W + \sqrt{4 + K^2 + 4KW}\right)\cos\left[2\tau\frac{\Omega}{2}\right]\right)X[\tau] \qquad (33)$$

which can be put in the form of Mathieu's equation [6,15–17]

$$X''[T] = -(a - 2q\cos[2T])X[T] \qquad (34)$$

where

$$T = \frac{\tau \Omega}{2} \tag{35}$$

$$a = \frac{2(5K + 2W + 3\sqrt{4 + K^2 + 4KW})}{(K - 2W + 3\sqrt{4 + K^2 + 4KW})} \tag{36}$$

$$q = \frac{3(-K + 2W + \sqrt{4 + K^2 + 4KW})}{(K - 2W + 3\sqrt{4 + K^2 + 4KW})} \tag{37}$$

The initial conditions for $X[\tau]$ are

$$X[0] = \sqrt{1 - W^2}, \quad X'[0] = 0 \tag{38}$$

The solution for X is then

$$X[\tau] = \frac{\sqrt{1 - W^2}}{C[a, q, 0]} C\left[a, q, \frac{\Omega \tau}{2}\right] \tag{39}$$

where $C[a,q,t]$ is the even Mathieu function.

The corresponding initial conditions for $Y[\tau]$, which satisfies the same Mathieu's equation, are

$$Y[0] = 0, \quad Y'[0] = \sqrt{2K} \tag{40}$$

The solution for Y is then given by

$$Y[\tau] = \frac{2\sqrt{2K}}{\Omega S'[a, q, 0]} S\left[a, q, \frac{\Omega \tau}{2}\right] \tag{41}$$

where $S[a,q,t]$ is the odd Mathieu function.

7.2. Periodic Mathieu functions

Numerical simulations of the spherical pendulum for arbitrary values of K and W will usually reveal a very complicated, a periodic motion of the type shown in Fig. 2, but in some cases the motion is periodic. The theory can be found in Refs. [9,11], but is summarised here. Let r be any integer or simple fraction (such as 3/2, etc.). Then solutions of Mathieu's equation of the form

$$\exp[\imath r T] f[T] = \exp\left[\imath r \frac{\Omega \tau}{2}\right] f\left[\frac{\Omega \tau}{2}\right] \tag{42}$$

where $f[T]$ is 2π-periodic, exist, and are thus periodic. Since both a and q depend on K and W, we can set a value for W and find K such that the so-called characteristic value $A[r,q]$ is equal to a. For example, for $W=0$ (the case
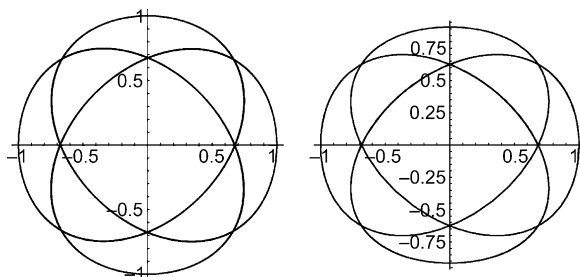
Fig. 7. The horizontal projection of the trajectories for the exact solution (the left curve) and the solution of the approximate equation of motion in terms of Mathieu functions (the right curve) for $n=1$, $k=2$.

studied in Fig. 2), the value of K for $r=3/2$ is about 0.359. The middle, periodic solution in Fig. 2 is found when $K=0.3972$. In fact, periodic solutions exist when r is any rational function of the form

$$r = \frac{n+k}{k} \tag{43}$$

Clearly the smaller the values of the integral quantum numbers n and k, the simpler the motion.

The horizontal projection of the approximate motion for $n=1$, $k=2$ is shown in Fig. 7 (the right curve), compared with the same curve from Fig. 2 for the exact motion (the left figure).

ACKNOWLEDGEMENTS

REFERENCES

[1] B. Crist, J. Oddershede, J. R. Sabin, J. W. Perram and M. A. Ratner, Polymer fracture – a simple model for chain scission. *J. Polym. Sci.*, 1984, **22**, 881–897.
[2] A. G. Webster, *The Dynamics of Particles, and of Rigid, Elastic and Fluid Bodies*, B. G. Teubner, Leipzig, 1925.
[3] E. T. Whittaker, *A Treatise on the Analytical Mechanics of Particles and Rigid Bodies*, 4th edn., Cambridge University Press, Cambridge, 1937.
[4] L. A. Pars, *A Treatise on Analytical Dynamics*, Heinemann, London, 1965.
[5] A. Sommerfeld, *Mechanics*, Academic Press, New York, 1964. This is a reprint of Sommerfeld's lecture notes, published many years after his retirement.
[6] E. T. Whittaker and G. N. Watson, *A Course of Modern Analysis*, 4th edn., Cambridge University Press, Cambridge, 1927.
[7] P. Ewald, *Ann. Phys.*, 1921, **64**, 253.

[8] J. W. Perram and P. J. Stiles, On the application of ellipsoidal harmonics to potential problems in molecular electrostatics and magnetostatics. *Proc. R. Soc. Lond. A*, 1976, **349**, 125–139.

[9] W. P. Ganley, Simple pendulum approximation. *Am. J. Phys.*, 1985, **53**, 73–76.

[10] L. H. Cadwell and E. R. Boyko, Linearization of the simple pendulum. *Eur. J. Phys.*, 2004, **59**, 37–39.

[11] R. R. Parwani, An approximate expression for the large angle period of a simple pendulum. *Am. J. Phys.*, 1991, **59**, 979–981.

[12] F. Klein and A. Sommerfeld, *Über die Theorie des Kreisels*, Band I–IV, B.G. Teubner, Leipzig, 1897–1910.

[13] M. G. Olsson, The precessing spherical pendulum. *Am. J. Phys.*, 1978, **46**, 1118–1120.

[14] M. G. Olsson, Spherical pendulum revisited. *Am. J. Phys.*, 1981, **49**, 531–534.

[15] F. M. Arscott, *Periodic Differential Equations*, Pergamon, Oxford, 1964.

[16] S. Wolfram, *The Mathematica Book*, Cambridge University Press, Cambridge, 1999.

[17] E. Weisstein, http://mathworld.wolfram.com/MathieuFunction.html

Theoretical NMR $^nJ(^{13}C,^{13}C)$ Scalar Couplings as Probes to Study Diamagnetic Ring Currents in Fullerenes

Rubén H. Contreras,[1] Juan E. Peralta,[2] Verónica Barone[2] and Gustavo E. Scuseria[2]

[1]*Department of Physics, FCEyN, University of Buenos Aires and CONICET, Buenos Aires, Argentina*
[2]*Department of Chemistry, Rice University, Houston, TX 77005-1892, USA*

Abstract

In this work $J(^{13}C,^{13}C)$ coupling constants and the principal components of nuclear magnetic shielding constants in the C_{60}, C_{70}, and $C_{60}^{(6-)}$ fullerenes are calculated at the B3LYP/cc-pCVDZ-sd level using optimized B3LYP/cc-pCVDZ geometries. Indirect spin–spin couplings are utilized to study local diamagnetic ring currents in fullerenes. In unsaturated carbon containing compounds, the Fermi contact (FC) contribution to long-range $^nJ(^{13}C,^{13}C)$ ($n > 4$) coupling constants is mainly transmitted through the mobile π-electronic system following a few simple rules: the alternating sign-rule and the pathway invariance. Besides, the absolute value of such a coupling decreases slowly when increasing the number of bonds separating the coupled nuclei. Without explicitly addressing the controversial topic of the aromaticity of fullerenes, we show that the π-transmitted components of the FC contribution provide information on factors affecting ring currents in fullerenes.

Contents

1. INTRODUCTION

High resolution NMR parameters are recognized as invaluable probes to detect fine details of the electronic molecular structure of different types of compounds when adequate combinations of theoretical and experimental approaches are adopted. Pioneer works of Professor Oddershede on the study of high resolution NMR parameters are very well recognized in the literature [1–6]. For this reason and for this occasion, the authors thought it pertinent to present a contribution

where calculated coupling constants are useful to study the behavior of diamagnetic ring currents in fullerenes.

Since the discovery of the C_{60} fullerene [7], the existence of ring current contributions to the magnetic susceptibility in this compound has been a rather controversial issue [8]. Smalley and co-workers [7] suggested that C_{60} is a spheroidal aromatic molecule and supported this assumption with π-electron and total energy calculations. On the other hand, the computation [8] of the π-electron ring-current susceptibility of C_{60} using the finite-field version of the original London theory [9] suggested that this is an aromatic molecule with vanishingly small ring current susceptibility. Fowler *et al.* [10] performed the first *ab initio* calculation on the polarizability and magnetizability of C_{60} and they predicted a C_{60} net diamagnetism as well as diamagnetic effects on the NMR chemical shift of an encapsulated atom. Commenting critically on the Fowler *et al.* paper, Haddon and Elser [11] argued that the magnetic susceptibility of C_{60} is incompatible with its description as a normal aromatic molecule. This controversy arose a renewed interest for quantifying the 'aromaticity' of a conjugated aromatic compound and several new criteria were established to quantify such a property. Among them, the following are worth mentioning: the 'nucleus-independent chemical shift' [12,13], the 'harmonic oscillator model of aromaticity' index [14], the 'para-delocalization index' [15], and the 'ring-current analysis' [16]. In a detailed review, Lazzeretti [17] gives an account of different magnetic criteria for aromaticity.

Spin–spin coupling constants, when properly analyzed, can provide insight into the fine details of the electronic molecular structure [18,19]. However, a good amount of information can frequently be obtained resorting only to some known features of these spectral parameters. In this work, an approach of this type is applied to study diamagnetic ring currents in C_{60} and in C_{70}. Our methodology is based on well-known transmission features of the Fermi contact (FC) contribution to long-range spin–spin couplings in conjugated systems [20].

When comparing the molecular electronic structures of C_{60} and C_{70}, one of the most striking differences is observed when considering the [3]He chemical shifts in endohedral [3]He at C_{60} and [3]He at C_{70}. In fact, [3]He atoms encapsulated in these endohedral compounds appear at, respectively, -6.4 and -28.8 ppm, relative to dissolved [3]He at 0.0 ppm [21,22]. Such differences in the [3]He shielding suggest that even though diamagnetic ring currents are significant in these two fullerene compounds, they are more important for shielding the encapsulated He atom in C_{70} than in C_{60} [23]. Saunders *et al.* [21] consider that C_{70} should be classified as aromatic, while the aromaticity of C_{60} is less well defined.

Several notably different features are observed in the ^{13}C NMR spectra of C_{60} [24] and C_{70} [25,26]. The former consists of only one line, at *ca.* 143 ppm down field from TMS, indicating that the 60 C atoms in C_{60} are all magnetically equivalent in agreement with its icosahedral symmetry. Because of its symmetry and the existence of only one C magnetic isotope, $J(^{13}C,^{13}C)$ spin–spin couplings are not amenable to measurement in C_{60}. On the other hand, the ^{13}C NMR spectrum of C_{70} consists of five lines [25], indicating that there are five magnetically non-equivalent ^{13}C nuclei, which is compatible with D_{5h} symmetry [27], and therefore there are only four $^{1}J(^{13}C,^{13}C)$ couplings amenable to

measurement [25]. To the best of the authors' knowledge, $^nJ(^{13}C,^{13}C)$ with $n>1$ have not been observed yet for C_{70}. Long-range couplings $(n>4)$ should be interesting probes to study several features of diamagnetic ring currents since they are known to be greatly dominated by the FC term, and they are mainly transmitted through the mobile π-bond systems [28–30]. It is well known that such long-range couplings follow simple rules, like for instance, the alternating sign rule, [i.e., $^nJ(^{13}C,^{13}C)>0$ if n is odd and $^nJ(^{13}C,^{13}C)<0$ if n is even], the pathway invariance, and the low sensitivity of its absolute value with n. For this reason, it is expected that such couplings provide valuable information on diamagnetic ring currents. As experimental $^nJ(^{13}C,^{13}C)$ $(n>1)$ have not yet been reported on fullerenes, theoretically calculated couplings supply helpful information, provided they are obtained at a high level of theory. Such a high level can be achieved with the DFT formalism if both adequate functional and basis set are used [31]. In a previous paper from our group, excellent agreement was reported between DFT-B3LYP/cc-pCVDZ-sd calculated [32] and experimental [25] $^1J(^{13}C,^{13}C)$ spin–spin coupling constants for C_{70}. This suggests that this level of theory is also adequate for calculating $^nJ(^{13}C,^{13}C)$ $(n>4)$ couplings in C_{60}, C_{70}, and $C_{60}^{(6-)}$. It is important to stress that calculated $^1J(^{13}C,^{13}C)$ couplings [32] were not only in excellent agreement with the experimental values, but they also provided an interesting rationalization of some aspects of the C_{70} diamagnetic ring currents along the borders of the belt [32]. This rationalization was found to be compatible with the experimental trends of its ^{13}C chemical shifts. The excellent agreement between calculated and measured $^1J(^{13}C,^{13}C)$ couplings in C_{70} supports the idea of relying on C_{60} calculated $J(^{13}C,^{13}C)$ couplings to obtain insight into C_{60} diamagnetic currents. Both one-bond as well as long-range $J(^{13}C,^{13}C)$ couplings are expected to be adequate probes for such study. Since the London theory predicts that the $C_{60}^{(6-)}$ anion is strongly diamagnetic because diamagnetic ring currents flow around its hexagons as well as its pentagons [8,33–36], $^nJ(^{13}C,^{13}C)$ spin–spin couplings in the anion are also calculated at the same level of theory in this work.

2. COMPUTATIONAL DETAILS

All calculations carried out in this work were performed with the Gaussian 03 [37] suite of programs. The geometries of C_{60} and $C_{60}^{(6-)}$ were optimized at the B3LYP/cc-pVDZ level assuming icosahedral symmetry. In both compounds, all four terms of isotropic $^nJ(^{13}C,^{13}C)$ coupling constants, namely, FC, spin-dipolar (SD), paramagnetic spin-orbital (PSO), and diamagnetic spin-orbital (DSO), were calculated at the B3LYP/cc-pCVDZ-sd level. The cc-pCVDZ-sd basis set is cc-pCVDZ [38] with all s functions fully decontracted. Isotropic and anisotropic nuclear magnetic shielding constants in C_{60}, $C_{60}^{(6-)}$, and C_{70} were calculated using the gauge-included atomic orbitals (GIAO) approach [39,40] at the same level of theory employed for the spin–spin couplings. For comparison, $^nJ(^{13}C,^{13}C)$ spin–spin couplings and the ^{13}C magnetic shielding tensor in benzene were also calculated using the cc-pCVDZ-sd basis set for C atoms and the

totally decontracted cc-pVDZ basis set for H atoms (its geometry was optimized at the same level).

3. RESULTS AND DISCUSSION

The calculated four isotropic contributions to the two different $^1J(^{13}C,^{13}C)$ spin–spin coupling constants in C_{60} are compared in Table 1 with the analogous contributions to $^1J(^{13}C,^{13}C)$ couplings in $C_{60}^{(6-)}$ and in C_{70} reported recently [32]. The numbering of carbon nuclei in C_{60} and $C_{60}^{(6-)}$ and in C_{70} is displayed in Schemes 1 and 2, respectively. Couplings in all these three compounds were calculated at the same level of theory. In the same Table 1, isotropic contributions to the calculated $^1J(^{13}C,^{13}C)$ coupling in benzene are also displayed and its total value is compared with the corresponding experimental value [41]. The two different $^1J(^{13}C,^{13}C)$ couplings in C_{60} correspond to a side shared by a pentagon ring and an hexagon ring ($J_a = 55.3$ Hz, bond length $B_a = 1.456$ Å, according to the optimized geometry), and to a side shared by two hexagon rings ($J_b = 68.5$ Hz, bond length $B_b = 1.397$ Å), respectively. Each hexagon ring contains three bonds of type B_b alternated with three bonds of type B_a. The FC, SD and PSO contributions to J_a and J_b are typical of a conjugating C–C bond sequence [42], and therefore π-electron delocalization along a sequence of type $-B_a-B_b-B_a-B_b-$ can be expected. Such an electron delocalization corresponds to a diamagnetic current and it represents an efficient pathway for transmitting the π-component of the FC contribution to long-range couplings. On the other hand, all pentagon rings are equilateral in C_{60}, and therefore, the above rationalization suggests that there are no diamagnetic currents along a pentagon, in agreement with assumptions commonly found in

Table 1. Different isotropic contributions to calculated $^1J(^{13}C,^{13}C)$ spin–spin couplings (Hz) in C_{60}, C_{70} and $C_{60}^{(6-)}$. They are compared with the corresponding values in benzene

Comp.	$^1J(C_i,C_j)$	FC	SD	PSO	DSO	Total
C_{60}	$^1J(C_1,C_2)$	73.6	1.6	−7.2	0.4	68.5
	$^1J(C_1,C_{13})$	58.8	0.7	−4.6	0.4	55.3
C_{70}	$^1J(C_1,C_2)$	58.5	0.7	−4.7	0.4	54.9
	$^1J(C_1,C_{11})$	73.6	1.5	−7.1	0.4	68.4[a]
	$^1J(C_{11},C_{36})$	58.6	0.7	−4.7	0.4	55.0[a]
	$^1J(C_{36},C_{22})$	70.9	1.5	−7.2	0.4	65.7
	$^1J(C_{36},C_{56})$	58.1	0.7	−4.5	0.4	54.7[a]
	$^1J(C_{56},C_{41})$	64.0	1.1	−5.9	0.4	59.7
	$^1J(C_{56},C_{66})$	65.7	1.0	−6.0	0.4	61.1[a]
	$^1J(C_{66},C_{62})$	59.7	0.6	−4.5	0.4	56.3
$C_{60}^{(6-)}$	$^1J(C_1,C_2)$	62.5	0.3	−5.2	0.4	58.0
	$^1J(C_1,C_{13})$	57.1	0.8	−5.2	0.4	53.1
C_6H_6		61.5	1.3	−6.7	0.2	56.3[b]

[a] Experimental values: $^1J(C_1,C_{11}) = 68$ Hz; $^1J(C_{11},C_{36}) = 55$ Hz; $^1J(C_{36},C_{56}) = 55$ Hz; $^1J(C_{56},C_{66}) = 62$ Hz (taken from Ref. [25]).
[b] Experimental value: 55.87 Hz (taken from Ref. [41]).
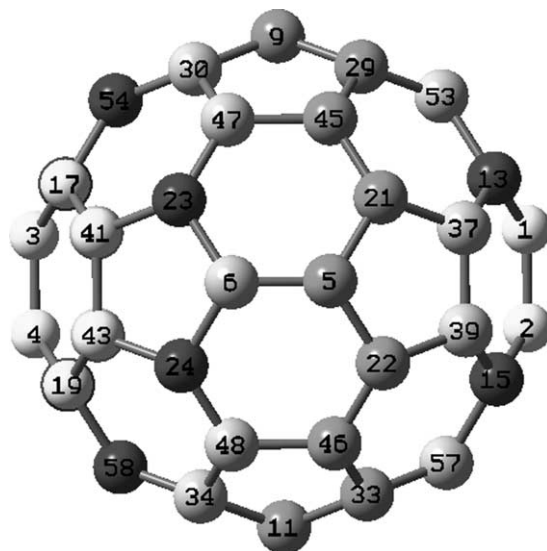
Scheme 1.

the literature [33]. The sequence along a C_{60} pentagon ring is B_a–B_a–B_a–B_a–B_a, and the corresponding total calculated one-bond coupling is 55.3 Hz.

^{13}C magnetic shielding constants for C_{60}, C_{70}, $C_{60}^{(6-)}$, and benzene are displayed in Table 2. The anisotropy of the corresponding magnetic shielding tensors increases along the fullerene series. It is observed that the calculated anisotropy of the benzene ^{13}C magnetic shielding tensor is somewhere between those of C_{60} and C_{70}. The experimental values of the principal components of the C_{60} chemical shift tensor are 220, 186, and 40 ppm [43]. Following Cioslowski [33], the known values of the ^{13}C chemical shift in C_{60} and the magnetic shielding constant in benzene can be used to calculate the 'experimental' shielding constant in C_{60} at

A   B
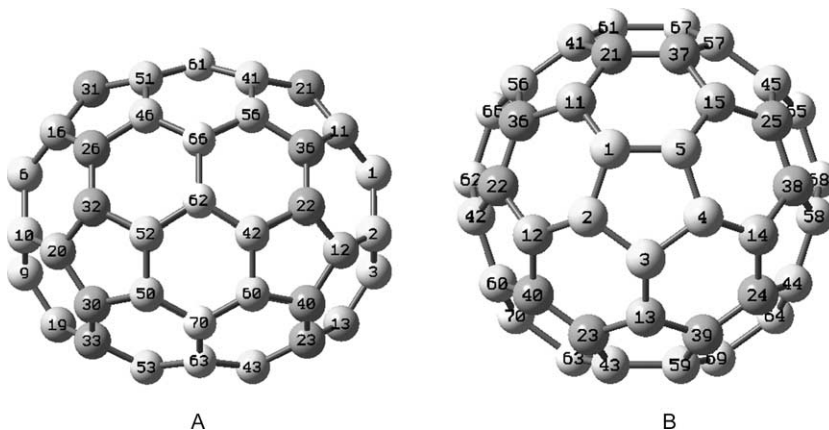
Scheme 2.

Table 2. GIAO-DFT-B3LYP/cc-pCVDZ-sd ^{13}C magnetic shielding tensors (in ppm) in C_{60}, C_{70} and $C_{60}^{(6-)}$

		Eigenvalues			Aniso	Iso
C_{60}[a]		−30.1	0.1	144.6	163.1	39.4
C_{70}[b]	C_1	−50.5	−15.6	157.1	190.1	30.3
	C_{11}	−40.7	−14.6	159.8	187.5	34.8
	C_{21}	−49.1	−11.7	161.4	191.8	33.5
	C_{41}	−37.9	−17.3	162.8	190.3	35.8
	C_{61}	−23.1	−1.7	177.3	190.3	51.0
$C_{60}^{(6-)}$		−59.0	−52.3	166.9	222.6	18.5
Benzene		−50.4	45.4	176.3	178.7	57.1

[a] Experimental principal values −34; 0 and 146 ppm (see Ref. [33]).
[b] Assignments made according to Ref. [25]. The numbering of C atoms is shown in Scheme 2.

43 ppm (39.4 ppm, according to Table 2), as well as the 'experimental' values of principal components of the shielding tensor, i.e., −34, 0, and 146 ppm [33] (−30.1, 0.1, and 144.6 ppm, according to Table 2). A few other calculated isotropic magnetic shielding constant for C_{60} found in the literature are 40.43 ppm [44] (HF); 51.3 ppm [45] (IGLO-DFTB), and 50.59 ppm [46] (B3LYP/6-31G*// GIAO-B3LYP/6-31G*).

In Table 3, the calculated chemical shifts in C_{70} are compared with those calculated by Sun and Kertesz [46] and the experimental values given by Taylor *et al.* [26]. Values in Table 3 are referred to C_{60} at 143.15 ppm [47]. The important shielding effect on C_e was attributed mainly to the shielding effect of diamagnetic ring currents circulating through the borders of the belt. Similarly, the important deshielding effect on C_a was attributed to the position of site *a* outside of the belt ring currents. The total shielding span of values shown in Table 3 is 20.70 ppm (this work), 19.17 ppm (Sun and Kertesz) and 19.79 ppm (experimental).

When comparing the magnetic shielding tensors in C_{60} and $C_{60}^{(6-)}$, it is observed that the six extra electrons in the latter yield an important increase in the anisotropy and a strong shielding effect in the isotropic part of the nuclear shielding.

Table 3. Comparison between calculated and experimental ^{13}C chemical shifts in C_{70} (in ppm) referred to C_{60} at 143.15 ppm (taken form Ref. [47])

C atom[a]	C atom[b]	This work	Ref.[c]	Exp.[d]
C_1	C_a	152.25	151.24	150.54
C_{21}	C_c	149.05	148.23	147.99
C_{11}	C_b	147.75	147.03	147.29
C_{41}	C_d	146.33	146.75	145.66
C_{61}	C_e	131.55	132.07	130.75

[a] Numbering of C atoms as in Scheme 2.
[b] Labeling of C atoms as in Ref. [25] (*a* to *e* are the distinct sites from cap to belt).
[c] Ref. [46].
[d] Experimental values taken from Ref. [26].

The potential of long-range couplings as probes to study diamagnetic ring currents is first exemplified considering the $^nJ(^{13}C,^{13}C)$ couplings in C_{70}. We emphasize that only the π-transmitted component of the FC contribution can provide insight into diamagnetic ring currents. Therefore, only long-range $^nJ(^{13}C,^{13}C)$ couplings with $n > 4$ are useful for this analysis since those with $n \leq 4$ may have substantial contributions transmitted through the σ-framework and, consequently, the π-contribution could be masked. For instance, if $n = 4$ and the coupled nuclei are connected by a 'W' pathway a positive σ-component of a larger absolute value than the respective π-component is expected. Rationalization of ring currents along the belt borders C_{41}–C_{56}–C_{36}–C_{22}–C_{42}… and its specular sequence, C_{51}–C_{46}–C_{26}–C_{32}–C_{52}… in C_{70} was based on $^1J(^{13}C,^{13}C)$ couplings [32]. These currents indicate that long-range couplings are efficiently transmitted along such pathways and the corresponding FC contributions are transmitted mainly by the mobile π-electronic system following well-known trends like the alternating sign rule and the pathway invariance [48]. However, when analyzing such couplings in C_{70} as well as in other fullerenes, it should be taken into account that in general, there are several pathways connecting a given pair of C atoms. Each of these pathways is efficient for transmitting the π-component of the FC contribution only if there is a diamagnetic ring current along this pathway. When two carbon atoms are connected by more than one pathway, like for instance some of type n and some of type $n + 1$, there should be a near cancellation of the resulting FC term, unless one of such pathways is not efficient in transmitting a diamagnetic ring current. The sign of the FC term of such coupling should indicate which one is the more efficient pathway. The diamagnetic ring currents along the border belt atoms in C_{70} transmit the FC contribution to long-range couplings along each border. A sequence of FC terms transmitted along the border belt is displayed in Table 4. This sequence is compared with another one involving pathways transversal to the borders of the belt. It is important to note that atoms C_{53} and C_{61} are connected by several pathways with some nine- and eight-bond pathways. Therefore, there is a competition between contributions transmitted through pathways containing odd and even number of bonds (i.e., they are of different 'parity'). The calculated FC term of $^{8,9}J(C_{53},C_{61})$ is $+0.24$ Hz. This suggests that the nine-bond pathways (e.g., C_{53}–C_{33}–C_{30}–C_{50}–C_{52}–C_{32}–C_{26}–C_{46}–C_{51}–C_{61}) are

Table 4. Comparison between the FC term of several long-range $^nJ(C_i,C_j)$ couplings (in Hz) in C_{70} transmitted along the belt and transversal to it

n	Belt		Transversal	
9	$J(C_{53},C_{61})$	$+0.24$	$J(C_{10},C_1)$	-0.05
8	$J(C_{63},C_{61})$	-0.20	$J(C_{20},C_1)$	$+0.04$
7	$J(C_{63},C_{41})$	$+0.21$	$J(C_{32},C_1)$	-0.02
6	$J(C_{63},C_{56})$	-0.24	$J(C_{52},C_1)$	-0.16
5	$J(C_{63},C_{56})$	$+0.41$	$J(C_{62},C_1)$	$+0.26$
4	$J(C_{63},C_{22})$	$+0.12$	$J(C_{42},C_1)$	-0.75
3	$J(C_{63},C_{42})$	$+3.14$	$J(C_{22},C_1)$	$+3.71$
2	$J(C_{63},C_{60})$	$+1.19$	$J(C_{36},C_1)$	$+1.29$
1	$J(C_{63},C_{70})$	$+59.74$	$J(C_{11},C_1)$	$+73.60$

more efficient for transmitting the FC term than the eight-bond pathways (e.g., C_{53}–C_{33}–C_{30}–C_{20}–C_{32}–C_{26}–C_{46}–C_{51}–C_{61}). It should be noted that, for symmetry reasons, $^1J(C_{30},C_{20})=\,^1J(C_{20},C_{32})=55.0$ Hz (calculated total couplings), and therefore the C_{30}–C_{20}–C_{32} fragment of the eight-bond pathway is not efficient for transmitting the FC term of the $^{8,9}J(C_{53},C_{61})$ coupling. On the other hand, the C_{30}–C_{50}–C_{52}–C_{32} fragment of a nine-bond pathway is efficient for transmitting the FC term of $^9J(C_{53},C_{61})$ since $^1J(C_{30},C_{50})=54.7$ Hz; $^1J(C_{50},C_{52})=59.7$ Hz and $^1J(C_{52},C_{32})=54.7$ Hz (calculated total couplings), which correspond to a conjugating sequence. Both fragment pathways are part of a pentagon, but only the latter is efficient for transmitting the π-component of the FC contribution to long-range couplings. A similar reasoning holds for the FC contribution to the $^{8,9}J(C_{63},C_{61})=-0.20$ Hz coupling. In this case, the nine-bond pathway involves the C_{30}–C_{20}–C_{32} fragment and therefore, this pathway is not efficient for transmitting the π-component of the FC term. Other couplings transmitted through pathways along the belt ($n>4$) (shown in Table 4) follow nicely the alternating sign rule. The example shown for $n=4$, i.e., $^4J(C_{63},C_{22})=+0.12$ Hz, does not follow the alternating sign rule since the shortest pathway corresponds to a 'W' arrangement of bonds and therefore, such coupling is expected to have a positive σ-transmitted component. It is noted that these two carbon atoms are also connected by the six-bond C_{63}–C_{43}–C_{23}–C_{40}–C_{60}–C_{42}–C_{22} pathway, which is also formed by an even number of bonds. The main pathway for $^3J(C_{63},C_{42})$ corresponds to a *trans*-arrangement, which should also transmit a positive σ-component. Note that the FC term of $^2J(C_{63},C_{60})$ is $+1.19$ Hz, while the FC term of $^2J(C,C)$ in benzene as calculated in this work is -1.15 Hz, i.e., they are of opposite signs. It is known [49–51] that the FC term of two-bond couplings becomes more positive when there are important hyperconjugative interactions into the antibonding orbitals belonging to the coupling pathway, this result suggests that $^2J(C_{63},C_{60})=+1.19$ Hz reflects the strain in the neighbor pentagon rings, which enhances hyperconjugative interactions like for instance, $(C_{42}$–$C_{22})\rightarrow(C_{70}$–$C_{63})^*$. At this point it is important to recall [52] that the cage-like structure of a fullerene consists of 12 pentagon rings with hexagon rings in an amount that depends on the total number of carbon atoms. The 'isolated pentagon rule' [53,54], which holds true for most synthesized fullerene compounds, states that pentagon rings should be separated from each other to minimize strain.

In Table 4, a few long-range couplings whose pathways are transversal to the belt are shown. As expected, pathways crossing the symmetry plane are not efficient for transmitting the FC term of long-range couplings. For instance, $^9J(C_{10},C_1)$ is small and negative, suggesting that the C_{10}–C_{20}–C_{32}–C_{52}–C_{62}–C_{42}–C_{22}–C_{36}–C_{11}–C_1 pathway is very inefficient in transmitting the spin information associated with the π-component of the FC term. Obviously, similar considerations can be applied to $^8J(C_{20},C_1)$ and $^7J(C_{32},C_1)$ couplings. In all these three cases the coupling pathway includes two equivalent bonds that are adjacent, e.g., C_{52}–C_{62} and C_{62}–C_{42}. Both bonds are equivalent for symmetry reasons. $^6J(C_{52},C_1)$ satisfies the alternating sign rule and is larger than the previous three. This shows that its main pathway is C_{52}–C_{62}–C_{66}–C_{56}–C_{36}–C_{11}–C_1, i.e., it does not involve two adjacent equal bonds. Similarly, one of the main pathways for $^5J(C_{62},C_1)$ is C_{62}–C_{66}–C_{56}–C_{36}–C_{11}–C_1. The four-bond pathway for $^4J(C_{42},C_1)$ is quite inefficient for transmitting

a σ-component and therefore, it is not surprising that it satisfies the alternating sign rule. The FC contribution to ^{3}J(C$_{22}$,C$_1$) is notably smaller than the similar coupling in benzene, where the FC term calculated in this work is 8.02 Hz (the experimental value of the ^{3}J(C,C) in benzene was reported by Kaski *et al.* [41] as 10.111 Hz). The FC contribution to ^{2}J(C$_{36}$,C$_1$) is calculated as positive, which is indicative of the strain of neighbor pentagon rings (*vide supra*).

The main features of diamagnetic ring currents in C$_{70}$ deduced from long-range J(C,C) couplings are nicely supported observing the different experimental ^{13}C chemical shifts reported by Johnson *et al.* [25], as discussed above. A similar analysis based on long-range J(C,C) couplings is carried out for C$_{60}$. A few examples are shown in Table 5, where several analogous couplings are compared for C$_{60}$ and C$_{60}^{(6-)}$. The numbering of C atoms is displayed in Scheme 1. Since it is accepted that diamagnetic ring currents along a pentagon ring are inhibited, it is expected that coupling constants transmitted through pathways involving two adjacent pentagon bonds are inefficient for transmitting the π-component of long-range couplings. This suggests that one of the main ^{10}J(C$_3$,C$_2$) coupling pathways is C$_3$–C$_{17}$–C$_{41}$–C$_{23}$–C$_{47}$–C$_{45}$–C$_{21}$–C$_{37}$–C$_{13}$–C$_1$–C$_2$, being inhibited the coupling pathways involving an odd number of bonds like, for instance, C$_3$–C$_{17}$–C$_{54}$–C$_{30}$–C$_9$–C$_{29}$–C$_{53}$–C$_{13}$–C$_1$–C$_2$ and   C$_3$–C$_4$–C$_{19}$–C$_{58}$–C$_{34}$–C$_{11}$–C$_{33}$–C$_{57}$–C$_{15}$–C$_2$. These last two pathways involve two adjacent pentagon bonds. Therefore, we expect their ability for transmitting the spin information associated with the π-component of the FC term in the C$_{60}^{(6-)}$ anion, to be enhanced. The result displayed in Table 5, ^{10}J(C$_3$,C$_2$) = +0.62 Hz, is compatible with such a rationalization. Similar considerations hold for ^{9}J(C$_3$,C$_1$), where in C$_{60}^{(6-)}$ the eight-bond pathways are operating. Another interesting case is ^{9}J(C$_{11}$,C$_9$) in C$_{60}$ where the eight-bond as well as the nine-bond pathways involve two-adjacent pentagon-bond sequence. Upon increasing in 6 the number of electrons, i.e., in

Table 5. Comparison between the FC contributions (in Hz) to several long-range couplings, ^{n}J(C$_i$,C$_j$), in C$_{60}$ and in C$_{60}^{(6-)}$

n	J(C$_i$,C$_j$)	C$_{60}$	C$_{60}^{(6-)}$
10	J(C$_3$,C$_2$)	−0.27	+0.62
9	J(C$_3$,C$_1$)	+0.35	−0.11
9	J(C$_{11}$,C$_9$)	−0.01	−0.10
8	J(C$_{33}$,C$_9$)	−0.00	+0.07
8	J(C$_{17}$,C$_1$)	−0.29	0.07
7	J(C$_{41}$,C$_1$)	+0.34	−0.12
7	J(C$_{46}$,C$_9$)	−0.00	+0.05
7	J(C$_{33}$,C$_{29}$)	+0.34	+0.04
6	J(C$_{23}$,C$_1$)	−0.34	+0.18
6	J(C$_{22}$,C$_9$)	−0.00	−0.07
5	J(C$_{47}$,C$_1$)	+0.51	−0.12
4	J(C$_{46}$,C$_{23}$)	−0.98	−0.43
3	J(C$_{21}$,C$_1$)	+3.63	+2.93
2	J(C$_{37}$,C$_1$)	+1.03	+2.51
1	J(C$_{13}$,C$_1$)	+58.8	+57.1

$C_{60}^{(6-)}$, both types of pathways are enhanced in their abilities for transmitting the π-component of the FC term. Since the calculated FC term is negative, $^9J(C_{11},C_9) = -0.10$ Hz, and its absolute value is smaller than expected, it seems that there is a strong competition between pathways of different parity. Similar considerations hold for $^8J(C_{33},C_9)$, $^7J(C_{46},C_9)$, and $^6J(C_{22},C_9)$ couplings. The behavior of $^8J(C_{17},C_1)$, $^7J(C_{41},C_1)$, $^7J(C_{33},C_{29})$, $^6J(C_{23},C_1)$, and $^5J(C_{47},C_1)$ couplings is quite similar to those of $^{10}J(C_3,C_2)$ and $^9J(C_3,C_1)$. For instance in C_{60}, $^6J(C_{23},C_1)$ is mainly transmitted by the six-bond C_{23}–C_{47}–C_{45}–C_{21}–C_{37}–C_{13}–C_1 coupling pathway and in $C_{60}^{(6-)}$ it is also transmitted through seven-bond coupling pathways like C_{23}–C_{47}–C_{30}–C_9–C_{29}–C_{53}–C_{13}–C_1. In the latter compound there seems to be a strong competition between the seven- and six-bond pathways, being more important the transmission through the pathways containing an odd number of bonds. The comparison between two different types of three-bond couplings in C_{60} and in $C_{60}^{(6-)}$ is also worthy of note. For instance, $^3J(C_{21},C_1)$ corresponds to a *trans*-pathway, C_{21}–C_{37}–C_{13}–C_1. In the former compound, pathways involving an even number of bonds like C_{23}–C_5–C_{22}–C_{39}–C_{15}–C_2–C_1 are inhibited since they contain adjacent pentagon bonds. In the latter compound, the transmission through such pathway is enhanced, corresponding to a negative contribution. The resulting FC term of $^3J(C_{21},C_1)$ is smaller in $C_{60}^{(6-)}$ than in C_{60} ($+2.93$ *vs.* $+3.63$ Hz). A similar effect is observed for a three-bond pathway involving the diagonal of an hexagon ring like the $^3J(C_{46},C_6)$ coupling. In $C_{60}^{(6-)}$ six-bond pathways like C_{46}–C_{22}–C_{39}–C_{37}–C_{21}–C_5–C_6 are enhanced, reducing the total FC term from $+3.94$ to $+2.48$ Hz. $^2J(C_{21},C_6)$ increases from $+1.03$ Hz in C_{60} to $+2.51$ Hz in $C_{60}^{(6-)}$. This effect is originated in both, an increase in the strain in a pentagon ring and an enhancement of a five-bond pathway like C_{21}–C_{37}–C_{39}–C_{22}–C_5–C_6, which should give a positive π-contribution to the FC term. The optimized pentagon bond length is somewhat shorter in the anion than in the neutral compound, 1.454 and 1.456 Å, respectively. It is important to point out that the π-transmitted contribution to the FC term of a two-bond coupling is negative.

4. CONCLUSIONS

Results presented in this work indicate that long-range $^nJ(^{13}C,^{13}C)$ are remarkable probes to gauge diamagnetic ring currents in fullerenes. Without addressing explicitly the controversial topic about the aromaticity of fullerenes, the π-transmitted components of the FC contributions to such long-range couplings provide useful information about factors that either inhibit or enhance the circulation of diamagnetic ring currents. For instance, the equilateral ring pentagons inhibit diamagnetic ring currents both in C_{60} and in C_{70}. This behavior is observed as an inhibition of π-coupling pathways involving two adjacent bonds belonging to sides of equilateral pentagon rings. It is interesting to note that this inhibition is not present in the $C_{60}^{(6-)}$ anion. In C_{70}, diamagnetic ring currents are notably more preferential for pathways along the belt. Transversal diamagnetic ring currents are greatly hindered by the C_1–C_2–C_3–C_4–C_5 equilateral pentagon ring (and its symmetrical pentagon ring).

The FC term of $^2J(^{13}C,^{13}C)$ couplings provides interesting information about the distribution of strain tension in fullerenes. As reported previously, the main distinction to be made of *geminal* couplings is twofold. (a) Those whose coupling pathway involves two adjacent C–C bonds of pentagon rings. They are positive ($\sim$6 Hz) and correspond to two-pathway couplings, one of them being geminal and the second one *cis-vicinal*. They do not provide fundamental information concerning the molecular structure of fullerenes. (b) Those corresponding to a pathway involving two adjacent hexagon-ring bonds. Their absolute value is in general smaller than 2 Hz. They can provide interesting information about the local strain in this type of compounds, particularly, around a pentagon ring. A case in point is the following pair of FC contributions to *geminal* J(C,C) couplings in C_{70}: $^2FC(C_{56},C_{46}) = 0.3$ Hz; and $^2FC(C_{36},C_{66}) = 1.6$ Hz [32]. This suggests that, e.g., the $(C_{41}–C_{21}) \rightarrow (C_{56}–C_{66})^*$ hyperconjugative interaction is weaker than the $(C_{11}–C_1) \rightarrow (C_{36}–C_{56})^*$ interaction. This indicates that the strain around the $C_1–C_2–C_3–C_4–C_5$ equilateral pentagon ring is stronger than around the $C_{11}–C_{21}–C_{41}–C_{56}–C_{36}$ non-equilateral pentagon ring.

ACKNOWLEDGEMENTS

REFERENCES

[1] J. Oddershede, in *Advances in Quantum Chemistry*, (ed. P.-O. Löwdin), Academic Press, New York, 1978, Vol. 11, p. 275.
[2] J. Oddershede, P. Jorgensen and D. L. Yeager, *Comput. Phys. Rep.*, 1984, **2**, 33.
[3] J. Oddershede, in *Methods in Computational Molecular Physics* (eds S. Wilson and G. H. F. Diercksen), Plenum Press, New York, 1992, p. 303.
[4] J. Geertsen, S. Eriksen and J. Oddershede, in *Advances in Quantum Chemistry*, (ed. P.-O. Löwdin), Academic Press, New York, 1991, Vol. 22, p. 167.
[5] R. D. Wigglesworth, W. T. Raynes, S. P. A. Sauer and J. Oddershede, *Mol. Phys.*, 1997, **92**, 77.
[6] G. A. Aucar and J. Oddershede, *Int. J. Quantum Chem.*, 1993, **47**, 425.
[7] H. W. Kroto, J. R. Heath, S. C. O'Brien and R. E. Smalley, *Nature*, 1985, **318**, 162.
[8] V. Elser and R. C. Haddon, *Nature*, 1987, **325**, 792, and references cited therein.
[9] F. London, *J. Phys. Rad.*, 1937, **8**, 397.
[10] P. W. Fowler, P. Lazzeretti and R. Zanasi, *Chem. Phys. Lett.*, 1990, **165**, 79.
[11] R. C. Haddon and V. Elser, *Chem. Phys. Lett.*, 1990, **169**, 362.
[12] P. v. R. Schleyer, C. Maerker, A. Dransfeld, H. Jiao and N. J. R. van Eikema Hommes, *J. Am. Chem. Soc.*, 1996, **118**, 6317.
[13] C. Corminboeuf, T. Heine, G. Seifert, P. v. R. Schleyer and J. Weber, *Phys. Chem. Chem. Phys.*, 2004, **6**, 273.
[14] T. M. Krygowski and M. K. Cyrañsky, *Chem. Rev.*, 2001, **101**, 1385.
[15] J. Poater, X. Fradera, M. Duran and M. Solà, *Chem.-Eur. J.*, 2003, **9**, 400.

[16] R. W. A. Havenith, J. H. van Lenthe, F. Dijkstra and L. W. Jenneskens, *J. Phys. Chem. A*, 2001, **105**, 3838.

[17] P. Lazzeretti, *Prog. NMR Spectrosc.*, 2000, **36**, 1.

[18] A. Wu, J. Gräfenstein and D. Cremer, *J. Phys. Chem. A*, 2003, **107**, 7043.

[19] J. Gräfenstein, T. Tuttle and D. Cremer, *J. Chem. Phys.*, 2004, **120**, 9552.

[20] J. A. Pople, W. G. Schneider and H. J. Bernstein, *High Resolution Nuclear Magnetic Resonance*, McGraw-Hill, New York, 1959.

[21] M. Saunders, H. A. Jiménez-Vázquez, R. J. Cross, S. Mroczkowski, D. I. Freedberg and F. A. L. Anet, *Nature*, 1994, **367**, 256.

[22] M. Saunders, R. J. Cross, H. A. Jiménez-Vázquez, R. Shimshi and A. Khong, *Science*, 1996, **271**, 1693.

[23] A. L. Balch, Fullerenes as encapsulating hosts: preparation, detection, and structures of endohedral fullerenes, in *Encyclopedia of Supramolecular Chemistry* (eds J. L. Atwood and J. W. Steed), Marcel Dekker, New York, 2004, p. 579.

[24] R. D. Johnson, G. Meijer and D. S. Bethune, *J. Am. Chem. Soc.*, 1990, **112**, 8983.

[25] R. D. Johnson, G. Meijer, J. R. Salem and D. S. Bethune, *J. Am. Chem. Soc.*, 1991, **113**, 3619.

[26] R. Taylor, J. P. Hare, A. K. Abdul-Sada and H. W. Kroto, *J. Chem. Soc. Chem. Commun.*, 1990, **20**, 1423.

[27] G. E. Scuseria, *Chem. Phys. Lett.*, 1991, **180**, 451.

[28] M. Barfield and B. Chakrabarti, *Chem. Rev.*, 1969, **69**, 757.

[29] J. Kowalewski, *Prog. NMR Spectrosc.*, 1977, **11**, 1.

[30] A. R. Engelman, G. E. Scuseria and R. H. Contreras, *J. Magn. Reson.*, 1982, **50**, 21.

[31] J. E. Peralta, G. E. Scuseria, J. R. Cheeseman and M. J. Frisch, *Chem. Phys. Lett.*, 2003, **375**, 452.

[32] J. E. Peralta, V. Barone, G. E. Scuseria and R. H. Contreras, *J. Am. Chem. Soc.*, 2004, **126**, 7428.

[33] J. Cioslowski, *Electronic Structure Calculations on Fullerenes and Their Derivatives*, Oxford University Press, Oxford, 1995.

[34] V. Elser and R. C. Haddon, *Nature*, 1987, **325**, 792.

[35] A. Pasquarello, M. A. Schlüter and R. C. Haddon, *Science*, 1992, **257**, 1660.

[36] A. Pasquarello, M. A. Schlüter and R. C. Haddon, *Phys. Rev. A*, 1993, **47**, 1783.

[37] M. J. Frisch, G. W. Trucks, H. B. Schlegel, G. E. Scuseria, M. A. Robb, J. R. Cheeseman, J. A. Montgomery, Jr., T. Vreven, K. N. Kudin, J. C. Burant, J. M. Millam, S. S. Iyengar, J. Tomasi, V. Barone, B. Mennucci, M. Cossi, G. Scalmani, N. Rega, G. A. Petersson, H. Nakatsuji, M. Hada, M. Ehara, K. Toyota, R. Fukuda, J. Hasegawa, M. Ishida, T. Nakajima, Y. Honda, O. Kitao, H. Nakai, M. Klene, X. Li, J. E. Knox, H. P. Hratchian, J. B. Cross, C. Adamo, J. Jaramillo, R. Gomperts, R. E. Stratmann, O. Yazyev, A. J. Austin, R. Cammi, C. Pomelli, J. W. Ochterski, P. Y. Ayala, K. Morokuma, G. A. Voth, P. Salvador, J. J. Dannenberg, V. G. Zakrzewski, S. Dapprich, A. D. Daniels, M. C. Strain, O. Farkas, D. K. Malick, A. D. Rabuck, K. Raghavachari, J. B. Foresman, J. V. Ortiz, Q. Cui, A. G. Baboul, S. Clifford, J. Cioslowski, B. B. Stefanov, G. Liu, A. Liashenko, P. Piskorz, I. Komaromi, R. L. Martin, D. J. Fox, T. Keith, M. A. Al-Laham, C. Y. Peng, A. Nanayakkara, M. Challacombe, P. M. W. Gill, B. Johnson, W. Chen, M. W. Wong, C. Gonzalez and J. A. Pople, Gaussian 03, Revision B.01, Gaussian, Inc., Pittsburgh PA, 2003.

[38] T. H. Dunning, Jr., *J. Chem. Phys.*, 1989, **90**, 1007.

[39] K. Wolinski, J. F. Hinton and P. Pulay, *J. Am. Chem. Soc.*, 1990, **112**, 8251.

[40] J. R. Cheeseman, G. W. Trucks, T. A. Keith and M. J. Frisch, *J. Chem. Phys.*, 1996, **104**, 5497.

[41] J. Kaski, J. Vaara and J. Jokisaari, *J. Am. Chem. Soc.*, 1996, **118**, 8879.

[42] R. H. Contreras, V. Barone, J. C. Facelli and J. E. Peralta, *Annu. Rep. NMR Spectrosc.*, 2003, **51**, 452.

[43] C. S. Yannoni, R. D. Jonson, G. Meijer, D. S. Bethune and J. R. Salem, *J. Phys. Chem.*, 1991, **95**, 9.

[44] U. Schneider, S. Richard, M. M. Kappes and R. Ahlrichs, *Chem. Phys. Lett.*, 1993, **210**, 165.

[45] T. Heine, G. Seifert, P. W. Fowler and F. Zerbetto, *J. Phys. Chem.*, 1999, **103**, 8738.

[46] G. Sun and M. Kertesz, *J. Phys. Chem. A*, 2000, **104**, 7398.

[47] A. G. Avent, D. Dubois and A. Pénicaud, *J. Chem. Soc., Perkin Trans.*, 1997, **2**, 1907.

[48] A. R. Engelmann, R. H. Contreras and J. C. Facelli, *Theor. Chim. Acta*, 1981, **59**, 17.

[49] R. H. Contreras and J. E. Peralta, *Prog. NMR Spectrosc.*, 2000, **37**, 321.

[50] V. Barone, J. E. Peralta and R. H. Contreras, in *Encyclopedia of Computational Chemistry* (eds P. v. R. Schleyer, W. L. Jorgensen, H. F. Schaefer III., P. R. Scheiner, W. Thiel and R. Glen), DOI 10.1002/0470845015.cu0020 May 15, 2004.

[51] C. F. Tormena, R. Rittner, R. H. Contreras and J. E. Peralta, *J. Phys. Chem. A*, 2004, **108**, 7762.

[52] G. Sun, Fullerenes: identification of isomers based on nuclear magnetic resonance spectra, in *Dekker Encyclopedia of Nanoscience and Nanotechnology.* (eds J. L. Atwood and J. W. Steed), Marcel Dekker, New York, 2004, p. 1223.

[53] H. W. Kioto, *Nature*, 1987, **329**, 529.

[54] P. W. Fowler and D. E. Manolopoulos, *An Atlas of Fullerenes*, Oxford University Press, New York, 1995.

The Dipole Polarizability of F⁻ in Aqueous Solution. A Sequential Monte Carlo/Quantum Mechanics Study

Sylvio Canuto,[1] Kaline Coutinho[1] and Prasanta K. Mukherjee[1,2]

[1]*Instituto de Física, Universidade de São Paulo, CP 66318,*
05315-970, São Paulo, SP, Brazil
[2]*Department of Spectroscopy, Indian Association for the Cultivation of Science,*
Jadavpur, Kolkata 700 032, India

Abstract

The sequential Monte Carlo/quantum mechanics methodology is employed to obtain the dipole polarizability of the atomic fluorine anion in an aqueous medium. Using Monte Carlo simulation, the structure of the water around the F⁻ anion is generated. Statistically relevant configurations are extracted for subsequent quantum mechanical calculations using the first solvent shell of water molecules and the density-functional theory, within an extensive basis set. The statistically converged result for the dipole polarizability of the F⁻ anion in the presence of the first solvation shell of water molecules is $10.56 \pm 0.66 a_0^3$. This value is considerably reduced compared to the free atomic anion calculated as $20.59 a_0^3$ but still very large compared to the free neutral atom calculated as $3.88 a_0^3$.

Contents

1. INTRODUCTION

The static dipole polarizability is the linear response of an atomic or molecular system to the application of a weak static electric field [1]. It relates to a great variety of physical properties and phenomena [2–5]. Because of its importance, there have been numerous *ab initio* calculations of isolated atomic and molecular polarizabilities [6–14]. Particular theoretical attention has been dedicated to the polarizability of free atomic anions [15–21] because of its fragility and difficulty in obtaining direct experimental results. In recent years theoretical studies have

been initiated to find the effect of surrounding medium on the electronic properties of atomic or molecular systems. Understanding these solvent effects is important for rationalizing experimental data in general. Some progress has been achieved by treating solvent effects using the so-called continuum models [22–26], where the solvent is described by its macroscopic constants such as the dielectric constant and index of refraction. Solvent effects in dipole polarizabilities and hyperpolarizabilities have been studied using continuum theories [27–31]. Although very successful in some contexts, the statistical nature of the liquid environment is not considered in such models. The proper treatment of liquid systems has to consider its statistical nature [32,33]. Indeed, for nonzero temperature there are many possible geometrical arrangements of the molecules of the liquid with equivalent probability. Thus, liquid properties are best described by a statistical distribution [34–37], and all properties are obtained from statistical averaging over an ensemble.

In this paper we use the sequential Monte Carlo/quantum mechanics (S-MC/QM) methodology [38–41] to obtain the dipole polarizability of the atomic fluorine anion in an aqueous medium. We first generate the water environment around F^- using Metropolis Monte Carlo. Next, statistically relevant configurations are separated and submitted to quantum mechanical calculations. Several QM calculations are necessary to obtain the ensemble average that is necessary to characterize the statistical nature of the liquid. Statistically converged results are obtained. In the present study the dipole polarizability of F^- in water is obtained using density-functional theory (DFT). We compare the dipole polarizability in the condensed liquid phase with that for the gas phase. Because of the diffuse nature of the ground state of the anionic system, it is expected that the confinement due to the condensed medium will decrease the dipole polarizability. Currently, confined states are of great interest [42,43]. Understanding this confining effect is also of interest in relation to the absorption spectra leading to excited Rydberg states [44].

2. METHODS

2.1. Monte Carlo simulation

The Monte Carlo (MC) simulation is performed using standard procedures [33] for the Metropolis sampling technique in the isothermal–isobaric ensemble, where the number of molecules N, the pressure P and the temperature T are fixed. As usual, we used the periodic boundary conditions and image method in a cubic box of size L. In our simulation, we use one F^- embedded in 1000 molecules of water in normal conditions ($T = 298$ K and $P = 1$ atm). The F^- and the water molecules interact by the Lennard–Jones plus Coulomb potential with three parameters for each interacting site i (ε_i, σ_i and q_i).

$$U_{ab} = \sum_i^{\text{on a}} \sum_j^{\text{on b}} 4\varepsilon_{ij} \left[\left(\frac{\sigma_{ij}}{r_{ij}} \right)^{12} - \left(\frac{\sigma_{ij}}{r_{ij}} \right)^6 \right] + \frac{q_i q_j e^2}{r_{ij}} \tag{1}$$

where i and j are the sites in system a and b, respectively, r_{ij} is the interatomic distance between the sites i and j, e is the elementary charge, $\varepsilon_{ij} = (\varepsilon_i \varepsilon_j)^{1/2}$ and

$\sigma_{ij} = (\sigma_i \sigma_j)^{1/2}$. For the water molecules we used the SPC [45] parameters and for the anion F⁻ the OPLS [46] parameters. In the calculation of the pair-wise energy, each molecule interacts with all other molecules within a center of mass separation that is smaller than the cutoff radius $r_c = L/2$. For separations larger than r_c, we use the long-range correction of the potential energy [33]. The initial configuration is generated randomly, considering the position and the orientation of each molecule. One MC step is concluded after selecting one molecule randomly and trying to translate it in all the Cartesian directions and also rotate it around a randomly chosen axis. The maximum allowed displacement of the molecules is auto-adjusted to give an acceptance rate of new configurations around 50%. The maximum rotation angle is fixed during the simulation in $\pm 15°$. The simulation was performed with the DICE program [47].

The full simulation involves a thermalization stage of about 15×10^6 MC step followed by an averaging stage of 60×10^6 MC steps. During the averaging stage, the density was calculated as 0.989 ± 0.007 g/cm³ in agreement with the result for liquid water. Radial distribution functions (RDFs) and liquid configurations are also generated during the averaging stage in the simulation. After completing the cycle over all 1000 molecules, a configuration of the liquid is generated and separated. Thus, the total number of configurations generated by the MC simulation is 60,000.

As quantum mechanical calculations will be performed on the configurations generated by the MC simulation, it is important to optimize the statistics. Configurations that are statistically very correlated will not give important additional information. Therefore, we calculate the auto-correlation function of the energy, $C(i)$ [38], to obtain the interval of correlation τ, where the configurations are statistically uncorrelated, i.e., have less than 13% of statistical correlation [38,39,48,49]. For Markovian processes, $C(i)$ follows an exponentially decaying function [50,51], that after integration gives the interval of correlation, τ. Figure 1 shows the calculated auto-correlation function of the
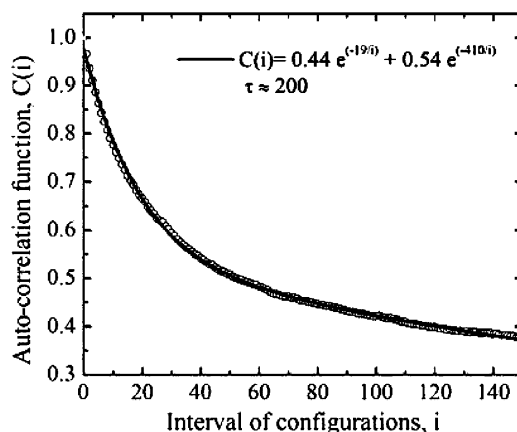
Fig. 1. Auto-correlation function of the energy and the best fit for a double exponential decay used to obtain the interval of statistical correlation.

energy calculated for the configurations generated by the anion F^- in water and the best fit of a doubly exponential decay function. From this exponential function, we obtain the interval of correlation $\tau \sim 200$. Therefore, from the 60,000 successive configurations generated by the MC simulation, we select 300 statistically uncorrelated configurations separated by an interval of 200 that represent the entire simulation [48]. As it will be seen (below) statistically converged result for the dipole polarizability of F^- is obtained using only 60 configurations.

2.2. Quantum mechanical calculations

The major interest of this paper is the calculation of the polarizability, α, of the anion F^- in an aqueous solution. Using the supermolecular approach, we calculated for several configurations obtained from the simulation, the polarizability of F^- surrounded by the first solvation shell (n water molecules) and subtracted the polarizability of these n water molecules without the F^-, i.e.,

$$\alpha(F^- \text{ in solution}) = \alpha(F^- + n H_2 O) - \alpha(n H_2 O) \tag{2}$$

Assuming this separability is an approximation that has been successfully used before [30,52].

As the appropriate Boltzmann weights are included in the Metropolis Monte Carlo sampling technique, the average value of the polarizability, or any other property calculated from the MC data, is given as a simple average over all the values calculated for each configuration.

The quantum mechanical polarizability is calculated using the DFT, with B3P86 (Becke's three-parameter functional [53] with the non-local correlation provided by Perdew [54]). The basis set used for the water molecules is $6\text{-}311++G$. Because of the very diffuse nature of the anion F^-, the basis set used is the specially designed, and very extensive, fully uncontracted 14s 9p 6d 2f Gaussian-type orbitals [55]. All the QM calculations were made with the Gaussian98 program [56].

3. RESULTS

3.1. Solvation shells and the hydrogen bonds

The molecular structure of liquids is best analyzed using the concept of RDF. This is of particular importance in solute–solvent structures as it defines the solvation shells around the solute molecule. Therefore, we analyzed the solvation of the anion F^- using the RDF between the anion and the oxygen of the water molecules, as shown in Fig. 2. At least three solvation shells are well defined. The integration of these peaks defines the coordination number, or the number of water molecules in each solvation shell. The first shell that ends at 3.15 Å with a maximum at 2.65 Å has, on average, 6.6 molecules of water. The second shell,
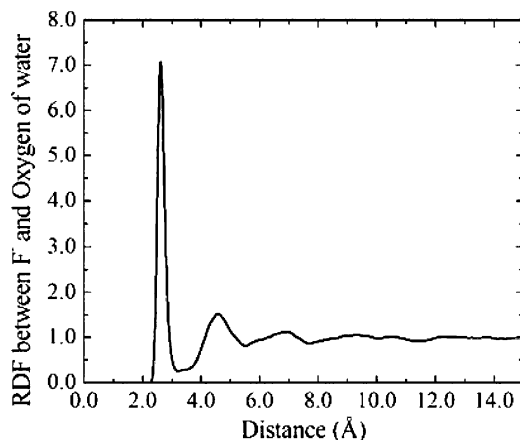
Fig. 2. The radial distribution function between F$^-$ and the oxygen atom of water.

ending on 5.50 Å with a maximum at 4.45 Å, has 25 molecules of water and the third, which goes to 7.60 Å with a maximum at 6.75 Å, has 64 molecules of water.

More detailed analysis of the first solvation shell of the F$^-$ can be obtained by the identification of the hydrogen bonds (HBs) formed between the water molecules and the anion. A very efficient procedure to identify the HBs in liquids is obtained using a geometric and energetic criteria [49,57–59]. We consider here a hydrogen-bonded structure when the distance $R_{F\cdots O} \leq 3.15$ Å, the angle $\Theta(FOH) \leq 35°$ and the binding energy is larger than 14.5 kcal/mol. This geometric criterion was obtained from the radial and angular distribution functions. The energetic criterion was obtained from the distribution of the pair-wise energy shown in Fig. 3. In this figure, there is a clear peak in the region of higher energy that characterizes the HBs for interacting energies larger than -14.5 kcal/mol. Thus, using the geometric and energetic criteria, in the 300 MC configurations we
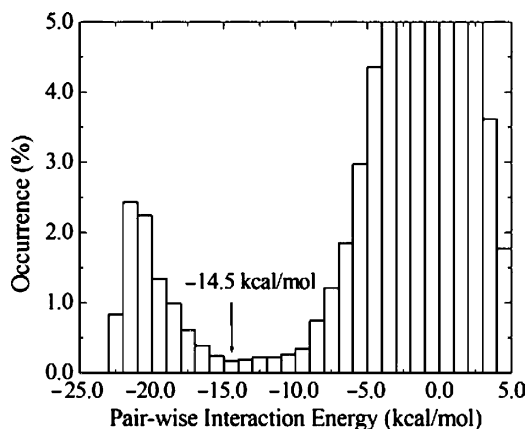
Fig. 3. Histogram of the pair-wise interaction energy between the F$^-$ and water molecules.
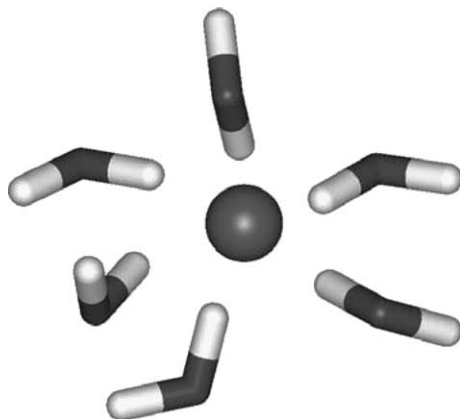
Fig. 4. Illustration of one structure of the F^- and 6 hydrogen-bonded water molecules obtained from the simulation of the aqueous solution.

find that in 7% of the configurations the F^- forms HB with 5 water molecules, in 52% forms 6 HBs, in 39% forms 7 HBs and in only 2% it forms 8 HBs. This gives an average of 6.3 HBs. Therefore, we used all the 156 most probable structures, one $F^- + 6H_2O$ hydrogen bonded, for the subsequent quantum mechanical calculations. Recent simulation of F^- in water suggested instead a number of 5 water molecules in the first shell [60]. Figure 4 shows, as an illustration, one of the structures obtained here for the first solvation shell. The calculated average of the distance $F \cdots H$ is 1.68 ± 0.13 Å, $F \cdots O$ is 2.66 ± 0.12 Å and the binding energy is 20.1 ± 2.6 kcal/mol.

3.2. Polarizability in solution

The dipole polarizability of the free F^- anion has been of substantial interest in the past [61–64] and the accurate result is estimated between 18 and $21a_0^3$, after inclusion of the very important electron correlation effects. The use of pre-fabricated basis is not recommended in this case. The Hartree–Fock (HF) and second-order MP2 results for the dipole polarizability of the free F^- anion, using the aug-cc-pVTZ basis [65], are only 7.09 and $8.89a_0^3$, respectively. All calculations described next were made with the 14s 9p 6d 2f basis set [55]. The HF result with this basis is $10.9a_0^3$, in good agreement with the estimated numerical HF result of $10.7a_0^3$ [66]. The MP2 result using the same basis is $17.2a_0^3$ [61]. The use of density-functional methods in this basis gave a better performance. Hybrid functionals, such as the popular B3LYP, B3PW91 and B3P86, gave results of 21.95, 21.20 and $20.59a_0^3$, respectively. For the calculations of the polarizability in solution we selected the B3P86 functional. Using the configurations extracted from the MC simulation, composed of the F^- anion and the six surrounding water molecules, corresponding to the first solvation shell, we calculated the dipole polarizability. Figure 5 shows the calculated results for the polarizability in solution. The converged result in water is $10.56 \pm 0.66a_0^3$. The uncertainty of $0.66a_0^3$ is the standard deviation As the result indicates, there is a considerable
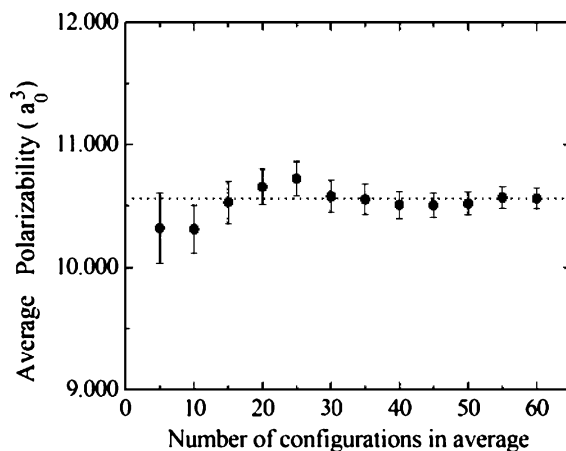
Fig. 5. Convergence of the average value of the polarizability of F$^-$ in aqueous solution with respect to the number of MC structures included in the quantum calculation. Statistical error is also shown.

reduction of the dipole polarizability compared to the free atomic anion. For reference, the calculated dipole polarizability of free neutral F, using the same theoretical method, is $3.88a_0^3$, in good agreement with the experimental value of $3.8a_0^3$ [5]. The polarizability change from $20.59a_0^3$ to $10.56 \pm 0.66a_0^3$ corresponds to a very large reduction ($\sim 49\%$). This reduction is similar to the case of Cl$^-$ studied by Morita and Kato [52] who obtained a reduction of 37%. Our theoretical estimate uses only the interaction with the first solvation shell. Inclusion of the outer shells may still affect the result. The standard deviation for the dipole polarizability in solution reflects the large variation seen in the liquid case. Figure 6 shows the statistical distribution of such values.
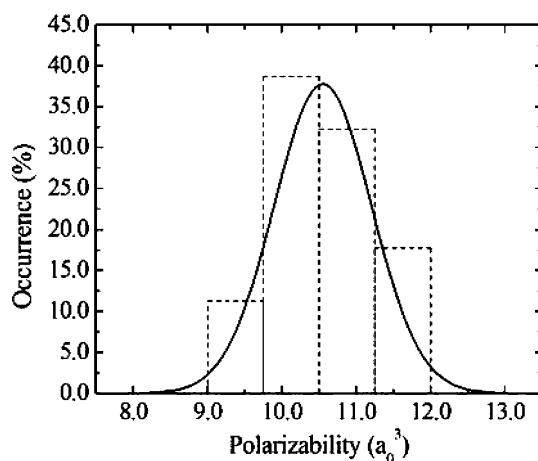
Fig. 6. Distribution of calculated polarizability of F$^-$ in aqueous solution and the normal distribution with average $\alpha = 10.56a_0^3$ and standard deviation $s = 0.66a_0^3$.

The changes in the dipole polarizabilities in solution using continuum theories have been questioned by van Duijnen *et al.* [67,68]. While most continuum theories yield an increase in the dipole polarizability, their studies suggest a reduction, compared to the isolated gas phase result. The present F^- anion case is interesting in this aspect because of the diffuse nature of this reference solute system. A considerable decrease is obtained here and the trend shows similarity with the results for the diffuse anionic atomic system Cl^- [52].

4. CONCLUDING REMARKS

The sequential Monte Carlo/quantum mechanics methodology has been employed to obtain the dipole polarizability of the atomic fluorine anion in liquid water. Using Monte Carlo simulation, the structure of the water around the F^- anion is generated. The auto-correlation function of the energy derived from the simulation is calculated and analyzed. From this, statistically relevant configurations are extracted for subsequent quantum mechanical calculations. Using the RDF we separate the first solvation shell of water molecules around the anion. Density-functional calculations within the hybrid B3P86 exchange correlation functional have been performed using an extensive basis set. Statistically converged result for the dipole polarizability of the F^- anion in the presence of the first solvation shell of water molecules is $10.56 \pm 0.66 a_0^3$. This value is considerably reduced compared to the calculated free atomic anion calculated as $20.59 a_0^3$ but still very large compared to the free neutral F calculated as $3.88 a_0^3$. This reduction can be understood in terms of liquid confinement, which in general reduces the diffuseness of the electronic charge cloud of the solute molecule.

ACKNOWLEDGEMENTS

REFERENCES

[1] J. Oddershede, P. Jorgensen and D. L. Yeager, *Comp. Phys. Rep.*, 1984, **2**, 33.
[2] T. M. Miller and B. Bederson, *Adv. At. Mol. Phys.*, 1988, **25**, 37.
[3] P. N. Prasad and D. J. Williams, *Introduction to Nonlinear Optical Effects in Organic Molecules and Polymers*, Wiley, New York, 1991.
[4] A. J. Stone, *The Theory of Intermolecular Forces*, Clarendon Press, Oxford, 1996.
[5] J. K. Nagle, *J. Am. Chem. Soc.*, 1990, **112**, 4741.
[6] D. M. Bishop, *Adv. Quantum Chem.*, 1994, **25**, 1.
[7] S. P. A. Sauer and J. Oddershede, *Int. J. Quantum Chem.*, 1994, **50**, 317.

[8] B. Kirtman, C. E. Dykstra and B. Champagne, *Chem. Phys. Lett.*, 1999, **305**, 132.

[9] G. Maroulis, *Chem. Phys. Lett.*, 2001, **334**, 207.

[10] W. A. Parkinson and J. Oddershede, *J. Chem. Phys.*, 1991, **94**, 7251.

[11] Y. Mochizuki and H. Ågren, *Chem. Phys. Lett.*, 2001, **336**, 451.

[12] R. J. Doerksen and A. J. Thakkar, *J. Phys. Chem. A*, 1999, **103**, 2141.

[13] P. Fuentealba, *Chem. Phys. Lett.*, 2004, **397**, 459.

[14] T. K. Ghosh, A. K. Das and P. K. Mukherjee, *Chem. Phys. Lett.*, 1994, **218**, 433.

[15] S. Canuto, W. Duch, J. Geertsen, F. Mueller-Plathe, J. Oddershede and G. Scuseria, *Chem. Phys. Lett.*, 1988, **147**, 435.

[16] S. Canuto, M. A. Castro and P. K. Mukherjee, *Phys. Rev. A*, 1994, **49**, 3315.

[17] G. H. F. Diercksen and A. J. Sadlej, *Chem. Phys. Lett.*, 1981, **84**, 390.

[18] E. F. Archibong and A. J. Thakkar, *Chem. Phys. Lett.*, 1990, **173**, 579.

[19] J. Pipin and D. M. Bishop, *J. Phys. B: At. Mol. Phys.*, 1992, **25**, 17.

[20] P. W. Fowler, P. Jorgensen and J. Olsen, *J. Chem. Phys.*, 1990, **93**, 7256.

[21] A. K. Das, T. K. Ghosh and P. K. Mukherjee, *Phys. Scr.*, 1994, **50**, 354.

[22] O. Tapia and O. Goscinski, *Mol. Phys.*, 1975, **29**, 1653.

[23] J. L. Rivail and D. Rinaldi, *Chem. Phys.*, 1976, **18**, 233.

[24] J. Tomasi and M. Persico, *Chem. Rev.*, 1994, **94**, 2027.

[25] M. M. Karelson and M. C. Zerner, *J. Phys. Chem.*, 1992, **96**, 6949.

[26] J. Tomasi, *Theor. Chem. Acc.*, 2004, **112**, 184.

[27] Y. Luo, H. Ågren, P. Jorgensen and K. V. Mikkelsen, *Adv. Quantum Chem.*, 1995, **26**, 165.

[28] K. V. Mikkelsen, P. Jorgensen and H. J. Aa. Jensen, *J. Chem. Phys.*, 1994, **100**, 6597.

[29] R. Cammi, M. Cossi and J. Tomasi, *J. Chem. Phys.*, 1996, **104**, 4611.

[30] K. V. Mikkelsen, Y. Luo, H. Ågren and P. Jorgensen, *J. Chem. Phys.*, 1995, **102**, 9362.

[31] A. Willettts and J. E. Rice, *J. Chem. Phys.*, 1993, **99**, 426.

[32] D. M. Heyes, *The Liquid State. Applications of Molecular Simulations*, Wiley, New York, 1998.

[33] M. P. Allen and D. J. Tildesley, *Computer Simulation of Liquids*, Clarendon Press, Oxford, 1987.

[34] J. T. Blair, K. Krogh-Jespersen and R. M. Levy, *J. Am. Chem. Soc.*, 1989, **111**, 6948.

[35] J. Gao, *J. Am. Chem. Soc.*, 1994, **116**, 9324.

[36] J. Zeng, N. S. Hush and J. R. Reimers, *J. Chem. Phys.*, 1993, **99**, 1496.

[37] K. Coutinho, S. Canuto and M. C. Zerner, *Int. J. Quantum Chem.*, 1997, **65**, 885.

[38] K. Coutinho and S. Canuto, *Adv. Quantum Chem.*, 1997, **28**, 89.

[39] K. Coutinho, S. Canuto and M. C. Zerner, *J. Chem. Phys.*, 2000, **112**, 9874.

[40] K. Coutinho and S. Canuto, *J. Chem. Phys.*, 2000, **113**, 9132.

[41] S. Canuto, K. Coutinho and D. Trzresniak, *Adv. Quantum Chem.*, 2002, **41**, 161.

[42] B. Saha, P. K. Mukherjee and G. H. F. Diercksen, *Astron. Astrophys.*, 2002, **41**, 337.

[43] S. Mandal, P. K. Mukherjee and G. H. F. Diercksen, *J. Phys. B: At. Mol. Phys.*, 2003, **396**, 4483.

[44] M. B. Robin, *Higher Excited States of Polyatomic Molecules*, Academic Press, New York, 1975.

[45] H. J. C. Berendsen, J. P. M. Postma and W. F. van Gunsteren, in *Intermolecular Forces* (ed. B. Pullman), Reidel, Dordrecht, 1981, pp. 331.

[46] J. Chandrasekhar, D. C. Spellmeyer and W. L. Jorgensen, *J. Am. Chem. Soc.*, 1984, **106**, 903.

[47] K. Coutinho and S. Canuto, *DICE: A General Monte Carlo Program for Liquid Simulation*, University of São Paulo, 2000.

[48] K. Coutinho, M. J. Oliveira and S. Canuto, *Int. J. Quantum Chem.*, 1998, **66**, 249.

[49] S. Canuto and K. Coutinho, *Int. J. Quantum Chem.*, 2000, **77**, 192.

[50] C. Chatfield, *The Analysis of Time Series. An Introduction*, 3rd edn., Chapman & Hall, London, 1984.

[51] R. Krätschmer, K. Binder and D. Stauffer, *J. Stat. Phys.*, 1976, **15**, 267.

[52] A. Morita and S. Kato, *J. Chem. Phys.*, 1999, **110**, 11987.

[53] A. D. Becke, *J. Chem. Phys.*, 1993, **98**, 5648.

[54] J. P. Perdew, *Phys. Rev. B*, 1986, **33**, 8822.

[55] S. Canuto, *J. Mol. Struct. (THEOCHEM)*, 1995, **335**, 45.

[56] M. J. Frisch, G. W. Trucks, H. B. Schlegel, G. E. Scuseria, M. A. Robb, J. R. Cheeseman, V. G. Zakrzewski, J. A. Montgomery, Jr., R. E. Stratmann, J. C. Burant, S. Dapprich, J. M. Millam, A. D. Daniels, K. N. Kudin, M. C. Strain, O. Farkas, J. Tomasi, V. Barone, M. Cossi, R. Cammi, B. Mennucci, C. Pomelli, C. Adamo, S. Clifford, J. Ochterski, G. A. Petersson, P. Y. Ayala, Q. Cui, K. Morokuma, D. K. Malick, A. D. Rabuck, K. Raghavachari, J. B. Foresman, J. Cioslowski, J. V. Ortiz, B. B. Stefanov, G. Liu, A. Liashenko, P. Piskorz, I. Komaromi, R. Gomperts, R. L. Martin, D. J. Fox, T. Keith, M. A. Al-Laham, C. Y. Peng, A. Nanayakkara, M. Challacombe, P. M. W. Gill, B. Johnson, W. Chen, M. W. Wong, J. L. Andres, M. Head-Gordon, E. S. Replogle, C. Gonzalez and J. A. Pople, Gaussian 98, Revision A.6, Gaussian, Inc., Pittsburgh PA, 1998.

[57] M. Mezei and D. L. Beveridge, *J. Chem. Phys.*, 1981, **74**, 622.

[58] W. L. Jorgensen, J. M. Briggs and M. L. Contreras, *J. Phys. Chem.*, 1990, **94**, 1683.

[59] T. Malaspina, K. Coutinho and S. Canuto, *J. Chem. Phys.*, 2002, **117**, 1692.

[60] A. Öhrn and G. Karlström, *J. Phys. Chem.*, 2004, **108**, 8452.

[61] S. Canuto, *Int. J. Quantum Chem. Symp.*, 1994, **28**, 265.

[62] T. Pluta, J. Noga and R. J. Bartlett, *Int. J. Quantum Chem. Symp.*, 1994, **28**, 379.

[63] L. Adamowicz, R. J. Bartlett and A. J. Sadlej, *J. Chem. Phys.*, 1988, **88**, 5749.

[64] R. Frank, H. Müller and J. Noga, *J. Chem. Phys.*, 2001, **114**, 7746.

[65] R. A. Kendal, T. H. Dunning Jr.. and R. J. Harrison, *J. Chem. Phys.*, 1992, **96**, 6796.

[66] P. C. Schmidt, A. Weiss and T. P. Das, *Phys. Rev. A*, 1979, **19**, 5525.

[67] P. Th. van Duijnen, A. H. De Vries, M. Swart and F. Grozema, *J. Chem. Phys.*, 2002, **117**, 8442.

[68] L. Jensen, M. Swart, P. Th. van Duijnen and J. G. Snijders, *J. Chem. Phys.*, 2002, **117**, 3316.

In Search for the Negative Polarizability States – the $EF\,^1\Sigma_g^+$ State of Hydrogen Molecule

Jacek Komasa

Department of Chemistry, A. Mickiewicz University,
Grunwaldzka 6, 60-780 Poznań, Poland

Abstract

The electric polarizability of the $EF\,^1\Sigma_g^+$ state of the hydrogen molecule is computed by means of the variation–perturbation method. The wave functions are expanded in exponentially correlated Gaussian (ECG) basis. The most accurate to date, 600-term ECG functions are employed to represent the unperturbed state and functions of similar quality are used as the first-order perturbation correction functions for parallel and perpendicular components of the dipole polarizability. In the lowest rovibrational state the computed components are 27 for the parallel and -9.6×10^3 a.u. for the perpendicular polarizability; consequently, the predicted total polarizability has large negative value.

Contents

1. INTRODUCTION

Recently, Romero and Andrews [1], and Lipiński [2] have shown that the calculated sum over states of a one-electron nonlinear optical property of a molecular system must vanish provided that the wave function employed satisfies the Hellmann–Feynman theorem. This statement applies, in particular, to the electric dipole polarizability and, as a consequence, there must exist systems which exhibit, most probably in excited states, a negative polarizability. Several examples of atomic and molecular systems with negative polarizability can be found in Refs. [3–8]. In search for such systems we study the $EF\,^1\Sigma_g^+$ state of the hydrogen molecule. An analysis of the Born–Oppenheimer (BO) curves of the closest states dipole-connected to the EF state leads to a presumption that this state might have a negative value of a polarizability component.

The $EF\,^1\Sigma_g^+$ is the lowest excited state of the same symmetry as the ground state. Its potential energy curve has two deep and well-separated minima (at $R = 1.91$ and 4.40 bohr), resulting from the avoided crossing of two

diabatic states, E and F [9]. In the united atom limit it has the ^1S (1s2s) symmetry. In the inner part of the potential the wave function is of $(1s\sigma_g2s\sigma_g)$ type, whereas in the outer part the $(2p\sigma_u)^2$ configuration dominates, although admixtures of the $(1s\sigma_g2s\sigma_g)$ and $(1s\sigma_g)^2$ configurations are also present. With $R \to \infty$, the EF state dissociates onto neutral 1s and 2s hydrogen atoms. The EF state has drawn significant interest and a number of variational calculations of increasing accuracy have been reported over the last 45 years [10–17]. The most accurate BO energy curves reported in literature were calculated using two different approaches. The first approach was presented by Wolniewicz and coworkers [13,14,16], who used the Kołos–Wolniewicz-type (KW) wave function [11]. The second, a bit more accurate curve was computed using the exponentially correlated Gaussian (ECG) wave function [17,18]. Historically, the most successful ansatz used in the studies of the hydrogen molecule was the KW function, which contains the terms linear in electron–nucleus and electron–electron distances and, in contrast to the ECGs, fulfills the necessary cusp conditions. Only in the last 15 years it was discovered that the ECG functions can surpass the accuracy provided by the KW functions [18–20] and these wave functions are employed in the present study to represent the unperturbed EF state.

2. METHOD OF CALCULATION

The time-dependent perturbation operator corresponding to the interaction of a molecule with an external oscillating electric field of an angular frequency ω is [21]

$$\hat{H}_\nu = \mu_\nu(\mathrm{e}^{i\omega t} + \mathrm{e}^{-i\omega t})F_\nu, \tag{1}$$

where μ_ν and F_ν represent components of the dipole moment and the electric field operators, respectively. We shall assume that the molecular axis either coincides with or is perpendicular to the external field direction and ν will be assigned $\parallel$ or $\perp$ for a parallel or perpendicular component, respectively. Let us further assume that the solution of the time-dependent Schrödinger equation

$$i\frac{\partial \Phi_\nu}{\partial t} = (\hat{H}^{(0)} + \hat{H}_\nu)\Phi_\nu \tag{2}$$

can be represented as a power series in variable F_ν

$$\Phi_\nu = \Phi^{(0)} + F_\nu \Phi_\nu^{(1)} + \dots. \tag{3}$$

This leads to the following time-dependent perturbation equations

$$i\frac{\partial \Phi^{(0)}}{\partial t} = \hat{H}^{(0)}\Phi^{(0)}, \tag{4}$$

$$i\frac{\partial \Phi_\nu^{(1)}}{\partial t} = \hat{H}^{(0)}\Phi_\nu^{(1)} + \mu_\nu(e^{i\omega t} + e^{-i\omega t})\Phi^{(0)}. \tag{5}$$

The first one has a solution

$$\Phi^{(0)} = \Psi^{(0)}e^{-iE^{(0)}t}, \tag{6}$$

where

$$\hat{H}^{(0)}\Psi^{(0)} = E^{(0)}\Psi^{(0)}, \tag{7}$$

and $\Psi^{(0)}$, $\hat{H}^{(0)}$, and $E^{(0)}$ are the known wave function, Hamiltonian, and energy, respectively, of the unperturbed system. The stationary solutions of the second equation can be expressed by

$$\Phi_\nu^{(1)} = \Psi_{\nu+}^{(1)}e^{-i(E^{(0)}-\omega)t} + \Psi_{\nu-}^{(1)}e^{-i(E^{(0)}+\omega)t}, \tag{8}$$

where $\Psi_{\nu\pm}^{(1)}$ are solutions of the first-order perturbation equations

$$(\hat{H}^{(0)} - E^{(0)} \pm \omega)\Psi_{\nu\pm}^{(1)} = -\mu_\nu\Psi^{(0)}. \tag{9}$$

Equation (9) can be solved variationally by minimizing the Hylleraas functionals [22,23]

$$J_{\pm\omega}[\Psi_{\nu\pm}^{(1)}] = \langle\Psi_{\nu\pm}^{(1)}|\hat{H}^{(0)} - E^{(0)} \pm \omega|\Psi_{\nu\pm}^{(1)}\rangle + 2\langle\Psi^{(0)}|\mu_\nu|\Psi_{\nu\pm}^{(1)}\rangle \tag{10}$$

with respect to the parameters of the first-order function. The functions $\Psi_\pm^{(1)}$ determined in this way enter the expression for $\alpha_{\nu\pm}$:

$$\alpha_{\nu\pm} = -\langle\Psi^{(0)}|\mu_\nu|\Psi_{\nu\pm}^{(1)}\rangle. \tag{11}$$

The final frequency-dependent polarizability is given by the sum of the *plus* and *minus* components

$$\alpha_\nu(\omega) = \alpha_{\nu+}(\omega) + \alpha_{\nu-}(\omega). \tag{12}$$

The variation–perturbation procedure is capable of yielding a lower bound to the exact polarizability provided that the exact $\Psi^{(0)}$ is known.

All the wave functions employed in this work were represented in the form of linear combinations of properly symmetrized two-electron basis functions $\psi_k^{(\kappa)}$ ($\kappa=0$ or 1):

$$\Psi^{(\kappa)}(\mathbf{r}) = (1 + \hat{\mathcal{P}}_{12})\left(\sum_{k=1}^{K^{(\kappa)}} c_k^{(\kappa)}\psi_k^{(\kappa)}(\mathbf{r})\right), \tag{13}$$

where, in general, the linear coefficients, $c_k^{(1)}$, of the expansion of the first-order function depend on the field frequency; $\mathbf{r}=(\mathbf{r}_1,\mathbf{r}_2)$ is a vector of electron position coordinates and $\hat{\mathcal{P}}_{12}$ is the electron exchange operator.

The EF state of H$_2$ has the Σ_g^+ symmetry. The first-order wave functions coupled to it by $\mu_\|$ and $\mu_\perp$ operators are of the Σ_u^+ and Π_u symmetry, respectively. The required symmetry of the wave function (13) was generated by an appropriate

choice of the spatial two-electron basis functions, $\psi_k(\mathbf{r})$. In the present work the following ECG functions of Singer [24,25] were used:

$$\sum_{\mathrm{g}}^{+}: \quad (1+\hat{\imath})\,\exp[-(\mathbf{r}-\mathbf{s}_k)\mathbf{A}_k(\mathbf{r}-\mathbf{s}_k)^T], \tag{14}$$

$$\sum_{\mathrm{g}}^{+}: \quad (1-\hat{\imath})\,\exp[-(\mathbf{r}-\mathbf{s}_k)\mathbf{A}_k(\mathbf{r}-\mathbf{s}_k)^T], \tag{15}$$

$$\Pi_{\mathrm{u}}: \quad (1-\hat{\imath})\,y_{m_k}\exp[-(\mathbf{r}-\mathbf{s}_k)\mathbf{A}_k(\mathbf{r}-\mathbf{s}_k)^T]. \tag{16}$$

The inversion operator $\hat{\imath}$ acts on the electronic coordinates ($\hat{\imath}\mathbf{r}=-\mathbf{r}$). It is employed to generate *gerade* and *ungerade* states. The pre-exponential factor, y_i, is the Cartesian component of the i-th electron position vector ($m_k=1$ or 2). Its presence enables obtaining Π symmetry of the wave function. The nonlinear parameters, collected in positive definite symmetric 2×2 matrices $\mathbf{A}_k$ and 2-element vectors $\mathbf{s}_k$, were determined variationally. The unperturbed wave function was optimized with respect to the second eigenvalue of the Hamiltonian using Powell's conjugate directions method [26]. The parameters of $\Psi_\nu^{(1)}$ were determined by minimization of the Hylleraas functional (10) at properly selected frequency ω also by means of the Powell algorithm. More details on the optimization of this type of the wave function can be found in Refs. [18,27,28].

3. RESULTS AND DISCUSSION

The 600-term wave functions of the form of equations (13) and (14) were generated for over 60 internuclear distances ranging from 0.0 to 20.0 bohr [17]. The extensive nonlinear optimization process was carried out separately at each distance. Table 1 presents the energies $E^{(0)}(R)$ for selected distances only. In Ref. [18] we analyzed the convergence of our ECG expansions for various two-electron systems, including the EF state of H_2 at $R=1.5$ bohr. We estimated the error of the present BO energies as about $0.01\ \mathrm{cm}^{-1}$ ($0.05\ \mu$ hartree) in the vicinity of $R=1.5$ bohr. Since our wave functions were fully optimized at each value of R, the error should not change dramatically along the potential energy curve, although we expect some gradual lowering of accuracy when moving from larger towards smaller internuclear distances. It is also worth noting that the variational optimization of all the linear and nonlinear parameters makes the ECG wave function satisfy the Hellmann–Feynman theorem.

There is a ladder of the excited states interacting with the $EF\ ^1\Sigma_{\mathrm{g}}^+$ state through the dipole moment operator. Among them the energetically nearest to the EF state are the $B\ ^1\Sigma_{\mathrm{u}}^+$ and $C\ ^1\Pi_{\mathrm{u}}$ states. Their BO energy curves are known with very high accuracy from calculations based on KW [29–31] and ECG [32] wave functions. The energy spacings $\Delta E(B-EF)$ and $\Delta E(C-EF)$ as functions of R are displayed in Fig. 1. When, for a fixed R, the external field frequency ω corresponds to ΔE,

Table 1. The Born–Oppenheimer energy and the parallel and perpendicular components of the polarizability for the $EF\ ^1\Sigma_g^+$ state of H_2 at selected distances R

R (bohr)	$E^{(0)}/E_h$	$\alpha_{\parallel}/e^2a_0^2E_h^{-1}$	$\alpha_{\perp}/e^2a_0^2E_h^{-1}$
0.000	–	$+800.317^a$	$+800.317^a$
0.010	97.854294759	$+800.636$	$+800.605$
0.250	1.958420900	$+951.949$	$+928.513$
0.500	0.127042176	$+1416.83$	$+1235.39$
0.750	-0.381959097	$+2979.38$	$+1743.94$
1.000	-0.580085574	-13382.3	$+2601.31$
1.250	-0.666021558	-1614.39	$+4218.63$
1.600	-0.710336960	-414.682	$+11624.0$
1.800	-0.717335853	-125.379	$+43285.0$
1.910	-0.718154650	-3.96026	$-192512.$
2.000	-0.717715240	$+82.5321$	-39741.6
2.500	-0.705475032	$+418.183$	-12454.5
3.000	-0.690747014	$+334.458$	$+14809.2$
3.500	-0.699079636	-221.937	$+306.718$
4.000	-0.711884469	-721.363	$+94.3393$
5.000	-0.710203357	-6949.14	$+67.3944$
6.000	-0.694267005	-71064.1	$+76.6692$
7.000	-0.677165620	$-441306.$	$+97.0209$
8.000	-0.662220979	$-330595.$	$+131.137$
10.000	-0.640254736	$-198117.$	$+327.412$
12.000	-0.628742051	-88288.2	$+1818.09$
15.000	-0.625202952	$+17897.8$	$+16210.9$

^{a} This value can be compared with the 'exact' atomic value $+800.31633(7)$ computed by Yan and Babb [33].

the energy is absorbed and the polarizability component $\alpha_\nu(\omega)$ has a pole. If two interacting states cross each other at some internuclear distance, then the polarizability has a singularity at zero frequency. In other words, the static polarizability considered as a function of R exhibits poles at those internuclear distances at which the EF state crosses one of the coupled states. From the known
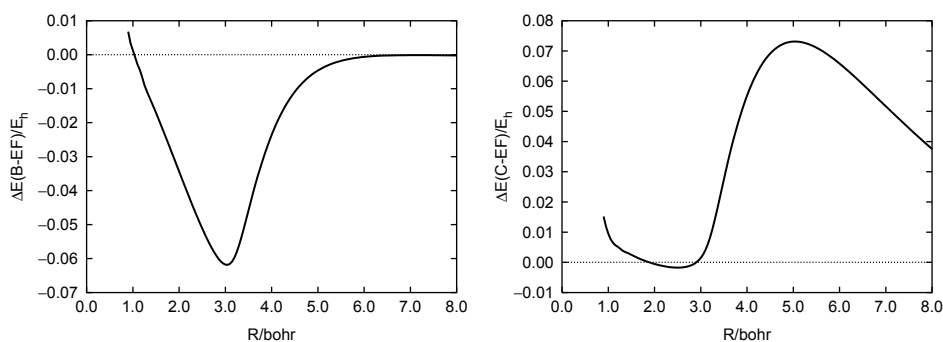
Fig. 1. Energy difference of B and EF and of C and EF states as a function of R.

BO energy curves of pertinent states we can expect the parallel component $\alpha_{\parallel}$ to have singularities at $R = 0.9873$ and 15.4482 bohr whereas the perpendicular $\alpha_{\perp}$ at $R = 1.8886$ and 2.9055 bohr. Because all three interacting states have the same dissociation limit, ΔE tends to zero when $R \to \infty$ and we can also expect that both polarizability components will escape to infinity with growing R.

In the present variation–perturbation calculations the first order corrections $\Psi_{\nu\pm}^{(1)}$ were expanded in 600-term ECG basis defined in equations (15) and (16). The components of the polarizability were computed from equation (11) using the optimized $\Psi_{\nu\pm}^{(1)}$. The optimization was performed separately for each component and internuclear distance. The values of $\alpha_{\nu}(\omega)$ are arithmetic sums of the *plus* and *minus* components (equation (12)) computed from two separate first-order corrections. For a given component ν (either $\parallel$ or $\perp$), $\Psi_{\nu+}^{(1)}$ and $\Psi_{\nu-}^{(1)}$ are expanded in the same basis but, because they are solutions to two different equations (equation (9)) they differ in the linear expansion coefficients. The computed components of the static polarizability $\alpha_{\parallel}(R)$ and $\alpha_{\perp}(R)$ are drawn in Fig. 2 and their numerical values at selected internuclear distances are listed in Table 1.

As far as the polarizability of the ground state is concerned, the $\alpha_{\nu+}(\omega)$ functions vary slowly with ω and exhibit no poles. The $\alpha_{\nu-}(\omega)$ components are responsible for large variations in the polarizability value and for the presence of the poles. The non-static optimization can then be performed with respect to the latter component at a frequency slightly smaller than the first resonance energy. If we are interested just in the static polarizability it is sufficient to perform optimization at $\omega = 0$. For an excited state, however, the interacting states can lie below a given state (see Fig. 1) and the poles are generated by the *plus* component as well. In such a case the optimization has to be performed at frequency larger than the value of the energy gap ΔE at given R.

In order to compute the polarizability for the lowest rovibrational level of the *EF* state we have to solve the radial nuclear Schrödinger equation.

$$-\frac{1}{2\mu}\frac{\mathrm{d}^2\chi_{vJ}(R)}{\mathrm{d}R^2} + V_J(R)\chi_{vJ}(R) = E_{vJ}\chi_{vJ}(R), \tag{17}$$
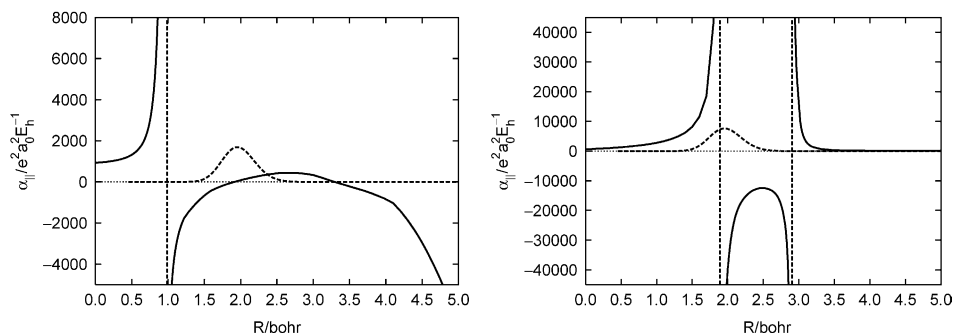
Fig. 2. $\alpha_{\parallel}$ and $\alpha_{\perp}$ as functions of R. The vibrational wave function $\chi_{00}(R)$ (dashed line) is drawn not in scale.

where μ is the reduced mass of the system, $V_J(R)$ is a sum of $E^{(0)}(R)$ and a centrifugal term $J(J+1)/(2\mu R^2)$, and where the eigenvalues, $E_{\nu J}$, and the eigenfunctions, $\chi_{\nu J}(R)$, are labeled by the vibrational and rotational quantum numbers ν and J, respectively. The solution was found numerically by means of Numerov–Cooley–Cashion [34] integration method as implemented in LeRoy's Level program [35]. The potential $V_J(R)$ was interpolated using 4-point piecewise polynomials and the integration step was 0.0189 bohr. The lowest rovibrational level E_{00} was found 19208.8522 cm^{-1} below the dissociation energy. The nuclear wave function $\chi_{00}(R)$ has a maximum at $R=1.96$ bohr. It vanishes quickly on both sides of the maximum so that $|\chi_{00}(R)|^2$ drops below 10^{-7} outside the (0.9,5.0) range of R/(bohr). A plot of $\chi_{00}(R)$ is shown as a dashed line in Fig. 2. This wave function was employed to compute the vibrationally averaged values of both polarizability components

$$\alpha_\nu^{00} = \int \chi_{00}^*(R)\alpha_\nu(R)\chi_{00}(R)\,\mathrm{d}R. \tag{18}$$

The integration was performed numerically in the range (0.9,5.0) with an assumption that the $|\chi_{00}|^2$ vanishes sufficiently fast to dump the whole integrand and the contribution to the integral from the outside of this range is negligible. The main difficulty in the integration origins from the poles located at the distances at which $|\chi_{00}|^2$ has meaningful values. In order to deal with the singularities appearing inside the integration domain, it was assumed that in the proximity of a pole R_p the polarizability curves can be modeled by

$$f(R) = A + \frac{B}{R-R_p} + \frac{C}{(R-R_p)^3} \tag{19}$$

with the parameters A, B, and C determined by fitting to the known $\alpha_\nu(R)$ points. For $A=0$ and $R_p=0$ the function $f(R)$ is antisymmetric i.e., it was assumed that the polarizability varies equally fast but with opposite signs on both sides of the pole. Within this model the polarizability growing to infinity on one side of the pole is compensated on the other side. The integration in equation (18) leads to

$$\alpha_\parallel^{00} = 27\mathrm{e}^2 a_0^2 E_\mathrm{h}^{-1} \quad \text{and} \quad \alpha_\perp^{00} = -9.6\times 10^3 \mathrm{e}^2 a_0^2 E_\mathrm{h}^{-1}, \tag{20}$$

and to the total polarizability α^{00} defined as one third of the trace of the polarizability tensor

$$\alpha^{00} = -6.4\times 10^3 \mathrm{e}^2 a_0^2 E_\mathrm{h}^{-1}. \tag{21}$$

4. CONCLUSIONS

Although the wave functions employed to compute polarizability at separate internuclear distances are of very high accuracy the presence of the singularities in the integration domain lowers significantly the precision of the final results. Nevertheless, the present computation reveals that the total polarizability of the

$EF\,{}^1\Sigma_g^+$ in the lowest vibrational state is negative. For this reason it would be interesting to study an interaction of the hydrogen molecule in the EF state with an external atomic or molecular system.

ACKNOWLEDGEMENTS

REFERENCES

[1] L. C. D. Romero and D. L. Andrews, *J. Opt. B: Quantum Semiclass. Opt.*, 2004, **6**, 59.
[2] J. Lipiński, *Chem. Phys. Lett.*, 2004, **394**, 397.
[3] M. Rerat and C. Pouchan, *Phys. Rev. A*, 1994, **49**, 829.
[4] M. Merawa and M. Rerat, *Eur. Phys. J. D*, 2001, **17**, 329.
[5] F. C. Grozema, R. Telesca, H. T. Jonkman, L. D. A. Siebbles and J. G. Snijders, *J. Chem. Phys.*, 2001, **115**, 10014.
[6] Z-C. Yan, *J. Phys. B*, 2002, **35**, 2713.
[7] M. Merawa, D. Bogue and A. Dargelos, *J. Phys. Chem. A*, 2003, **107**, 9628.
[8] F. C. Grozema, R. Telesca, J. G. Snijders and L. D. A. Siebbles, *J. Chem. Phys.*, 2003, **118**, 9441.
[9] T. E. Sharp, *Atomic Data*, 1971, **2**, 119.
[10] E. R. Davidson, *J. Chem. Phys.*, 1960, **33**, 1577.
[11] W. Kołos and L. Wolniewicz, *J. Chem. Phys.*, 1969, **50**, 3228.
[12] J. W. Liu and S. Hagstrom, *Phys. Rev. A*, 1993, **48**, 166.
[13] L. Wolniewicz and K. Dressler, *J. Chem. Phys.*, 1985, **82**, 3292.
[14] L. Wolniewicz and K. Dressler, *J. Chem. Phys.*, 1994, **100**, 444.
[15] L. Wolniewicz, *J. Chem. Phys.*, 1998, **109**, 2254.
[16] T. Orlikowski, G. Staszewska and L. Wolniewicz, *Mol. Phys.*, 1999, **96**, 1445.
[17] J. Komasa and W. Cencek, in *Computational Methods in Science and Technology* (eds J. Komasa, J. Wegharz and K. W. Wojciechowski), Scientific Publishers OWN, Poznań, 2003, Vol. 9, pp. 79–92.
[18] W. Cencek, J. Komasa and J. Rychlewski, *Chem. Phys. Lett.*, 1995, **246**, 417.
[19] J. Rychlewski, W. Cencek and J. Komasa, *Chem. Phys. Lett.*, 1994, **229**, 657.
[20] W. Cencek and W. Kutzelnigg, *J. Chem. Phys.*, 1996, **105**, 5878.
[21] J. O. Hirschfelder, W. Byers Brown and S. T. Epstein, *Adv. Quantum Chem.*, 1964, **1**, 255.
[22] E. Hylleraas, *Z. Phys.*, 1930, **65**, 209.
[23] S. T. Epstein, in *The Variation Method in Quantum Chemistry* (ed. E. M. Loebl), Academic Press, New York, 1974.
[24] K. Singer, *Proc. R. Soc. Lond. Ser. A*, 1960, **258**, 412.
[25] J. Rychlewski, Electron correlation in few-electron systems, in *Handbook of Molecular Physics and Quantum Chemistry* (ed. S. Wilson), Wiley, New York, 2003, Vol. 2, pp.199–218.
[26] M. J. D. Powell, *Comput. J.*, 1964, **7**, 155.
[27] J. Komasa and A. J. Thakkar, *Mol. Phys.*, 1993, **78**, 1039.
[28] J. Komasa, *Phys. Rev. A*, 2002, **65**, 012506.
[29] L. Wolniewicz and K. Dressler, *J. Chem. Phys.*, 1988, **88**, 3861.
[30] K. Dressler and L. Wolniewicz, *Ber. Bunsenges. Phys. Chem.*, 1995, **99**, 246.
[31] L. Wolniewicz, *Chem. Phys. Lett.*, 1995, **233**, 644.
[32] J. Komasa and A. J. Thakkar, *Chem. Phys. Lett.*, 1994, **222**, 65.

[33] Z-C. Yan and J. F. Babb, *Phys. Rev. A*, 1998, **58**, 1247.

[34] B. Numerov, *Publ. Observatoire Central Astrophys. Russia*, 1933, **2**, 188; J. W. Cooley, *Math.Comput.*, 1961, **15**, 363; J. K. Cashion, *J. Chem. Phys.*, 1963, **39**, 1872.

[35] R. J. Le Roy, 2002, LEVEL 7.5: a Computer Program for Solving the Radial Schrödinger Equations for Bound and Quasibound Levels, University of Waterloo Chemical Physics Research Report CP-655.

On the Usage of Locally Dense Basis Sets in the Calculation of NMR Indirect Nuclear Spin–Spin Coupling Constants: Vicinal Fluorine–Fluorine Couplings

Marina Sanchez,[1] Patricio F. Provasi,[1] Gustavo A. Aucar[1]
and Stephan P. A. Sauer[2]

[1]Department of Physics, University of Northeastern, Av. Libertad 5500,
W 3404 AAS Corrientes, Argentina
[2]Department of Chemistry, University of Copenhagen, Universitetsparken 5,
DK-2100 Copenhagen Ø, Denmark

Abstract

Locally dense basis sets (<DBSs) were developed for correlated *ab initio* calculations of vicinal fluorine–fluorine indirect nuclear spin–spin couplings in several saturated and unsaturated fluorinated hydrocarbons. We find that the choice of the basis set for each atom belonging to our studied model compounds depends on its location with respect to the coupled fluorine atoms and on the *cis/trans* or *synperiplanar/antiperiplanar* conformation of the molecule. Carbon atoms in the bonding path connecting the coupled fluorine atoms have to be described with better basis sets than the carbon atoms outside this path. For the hydrogen atoms directly connected to the coupling pathway in molecules with *trans* or *antiperiplanar* conformations and for all hydrogen atoms not directly connected to the coupling pathway one can employ a minimal basis set with only one s-function. Employing these type of LDBSs we can reduce the number of necessary basis functions by about 30% without losing more than about 1 Hz in accuracy. The analysis of the four contributions to the vicinal fluorine–fluorine coupling constants shows that the non-contact orbital paramagnetic term is the most important contribution followed by the also non-contact spin-dipolar term. The Fermi contact term is the largest contribution only in the *synperiplanar* conformations of 1,2-difluoroethane and -propane.

Contents

1. INTRODUCTION

The parameters of nuclear magnetic resonance (NMR) spectroscopy, i.e., chemical shift and indirect nuclear spin–spin coupling constant J, are useful tools in the analysis of chemical structures. As an example, important progress was recently made in the determination of three-dimensional structures of proteins and nucleic acids in solution by NMR spectroscopy [1]. Vicinal spin–spin coupling constants hereby play an important role in the determination of torsional angles. Theoretical predictions of chemical shifts and coupling constants can give the necessary insight into the physical mechanism involved.

However, accurate calculations of indirect nuclear spin–spin coupling constants are computationally very demanding. Jens Oddershede has contributed substantially to this field over the years [2–22]. One of the questions he addressed so far was the selection of an optimal basis set of Gaussian-type functions [10,20] which plays an important role in obtaining converged results within reasonable computational cost. The search for optimized basis sets which allow for the quantitative reproduction of experimental results has recently attracted much attention again [20,23–27]. The optimized basis sets turn out to be rather large, too large for accurate calculations on anything but small molecules. Provasi *et al.* [25] therefore proposed recently to make use of the old idea of locally dense basis sets (LDBSs) [28,29] also in the calculation of spin–spin couplings. This approach has in the meantime been used in several theoretical studies [30–40]. The evident advantages of this approach are: (i) the reduction of the computational cost without significant loss in the accuracy; (ii) the possibility of increasing the level of approximation, mainly of electronic correlation, in the calculations; and (iii) to obtain information about the way the coupling constants are transmitted in the molecule. Apart from the first LDBS study by Provasi *et al.* on the vicinal proton–proton couplings in monohalogen substituted ethane [25] no systematic investigation of couplings between other nuclei has been reported so far. The purpose of the present work is therefore to study the performance of LDBSs in the calculation of vicinal fluorine–fluorine coupling constants, $^3J_{F–F}$, in saturated and unsaturated hydrocarbons. As model systems we have chosen difluoroethyne (**1**), *trans*-1,2-difluoroethene (**2**), *trans*-1,2-difluoropropene (**3**), *cis*-1,2-difluoroethene (**4**), *cis*-1,2-difluoropropene (**5**), *antiperiplanar*-1,2-difluoroethane (**6**)[1], *antiperiplanar*-1,2-difluoropropane (**7**), *synperiplanar*-1,2-difluoroethane (**8**) and *synperiplanar*-1,2-difluoropropane (**9**). The study is focused on two main purposes:

(a) To analyze the sensitivity of this coupling on the basis set employed.
(b) To design optimized LDBSs for the calculation of vicinal F–F couplings

---

[1] The prefixes *synperiplanar* and *antiperiplanar* will often be abbreviated as *spp* and *app* in the following.

which maximize the ratio between the accuracy of the results and the size of the basis set.

Fluorinated organic compounds and their NMR spectra have recently attracted much attention due to their important biological activity and as promising candidates for quantum computers [41]. Fluorine has been incorporated into alpha-helices [42,43], proteins [44,45] and bioactive small molecules [46–49] as NMR probes for aggregation, microenvironmental structure and binding site interactions. Several classes of medicines contain fluorine atoms, which allow to monitor their transport *in vivo* in the human body by magnetic resonance imaging techniques [50]. Furthermore, unusually large F–F coupling constants have been predicted for conjugated systems [39].

We have employed the second-order polarization propagator approximation (SOPPA) in this study, a method which was mainly developed by Jens Oddershede and his co-workers [3,4,20,51–56]. Barone *et al.* [32] have recently shown that SOPPA reproduces the vicinal F–F couplings reasonably well in 1,2-difluoroethene.

The remaining chapter is divided into four sections. The following two sections review briefly the theory of spin–spin coupling constant calculations, report the computational details of the calculations and describe the nomenclature used in this work. In Section 4, the results of the LDBS study are discussed. It starts with a subsection on the converged results for the model systems studied here. Finally, the last section summarizes the conclusions of the present work.

2. THEORY

The non-relativistic theory of the indirect spin–spin coupling constant between two nuclei M and N was formulated by Ramsey, who proposed four contributions for it [57]. These four contributions arise from two different mechanisms by which a nuclear magnetic moment perturbs the surrounding electrons and the induced electronic current or spin polarization generates a magnetic field in the region close to the other nucleus that interacts with its nuclear magnetic moment. The interaction of the nuclear spin with the spin of the electrons is accounted for by the Fermi contact (FC) and spin dipolar (SD) contributions, while their interaction with the orbital angular momentum of the electrons is given by the orbital paramagnetic (OP) and orbital diamagnetic (OD) contributions.

The first three contributions, which depend on the first-order wave function, can be expressed as sum over states:

$$J_{MN}^{A} = \frac{2}{3} \frac{\gamma_M \gamma_N}{h} \sum_{\alpha=x,y,z} \sum_{n \neq 0} \frac{\langle 0|(\vec{O}_M^A)_\alpha|n\rangle \langle n|(\vec{O}_N^A)_\alpha|0\rangle}{E_0 - E_n} \tag{1}$$

$$(\vec{O}_M^{OP})_\alpha = \left(\frac{\mu_0}{4\pi}\right)\left(\frac{e\hbar}{m_e}\right) \sum_i \frac{(\vec{l}_{iM})_\alpha}{r_{iM}^3} \tag{2}$$

$$(\vec{O}_{\mathrm{M}}^{\mathrm{FC}})_\alpha = \left(\frac{\mu_0}{4\pi}\right)\left(\frac{4\pi g_{\mathrm{e}} e\hbar}{3m_{\mathrm{e}}}\right)\sum_i (\vec{s}_i)_\alpha \delta(\vec{r}_{i\mathrm{M}}) \tag{3}$$

$$(\vec{O}_{\mathrm{M}}^{\mathrm{SD}})_\alpha = \left(\frac{\mu_0}{4\pi}\right)\left(\frac{g_{\mathrm{e}} e\hbar}{2m_{\mathrm{e}}}\right)\sum_i \frac{3(\vec{s}_i\cdot\vec{r}_{iK})(\vec{r}_{iK})_\alpha - r_{iK}^2(\vec{s}_i)_\alpha}{r_{iK}^5} \tag{4}$$

The magnetogyric ratio of the nucleus M is γ_{M}, $\vec{r}_{i\mathrm{M}} = \vec{r}_i - \vec{r}_{\mathrm{M}}$ is the difference between the position vectors of the electron i and the nucleus M, $\vec{s}_i$ is the spin angular momentum operator and $\vec{l}_i$ the orbital angular momentum operator of the ith electron, $\delta(x)$ is the Dirac delta function and all the other symbols have their usual meaning [58].

The OD term is an average value of the ground state:

$$J_{\mathrm{MN}}^{\mathrm{OD}} = \frac{1}{3}\frac{\gamma_{\mathrm{M}}\gamma_{\mathrm{N}}}{h}\sum_{\alpha,\beta=x,y,z}\langle 0|(\vec{O}_{\mathrm{MN}}^{\mathrm{OD}})_{\alpha\beta}|0\rangle \tag{5}$$

with

$$(\vec{O}_{\mathrm{MN}}^{\mathrm{OD}})_{\alpha\beta} = \left(\frac{\mu_0}{4\pi}\right)^2\frac{e^2\hbar^2}{m_{\mathrm{e}}}\sum_i\left(\frac{\vec{r}_{i\mathrm{N}}\cdot\vec{r}_{i\mathrm{M}} - (\vec{r}_{i\mathrm{N}})_\alpha(\vec{r}_{i\mathrm{M}})_\beta}{r_{i\mathrm{N}}^3 r_{i\mathrm{M}}^3}\right) \tag{6}$$

although it can also be formulated as a sum over states [59].

Excited triplet states $|n\rangle$ with energy E_n are included in the sum for the FC and SD terms, while excited singlet states contribute to the OP term. Recalling the spectral representation of the polarization propagator for zero frequency ω [60]
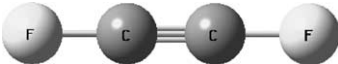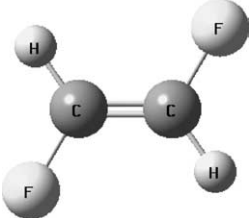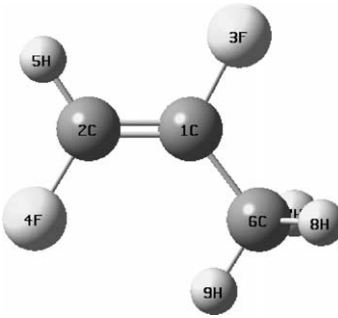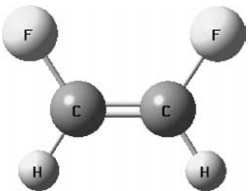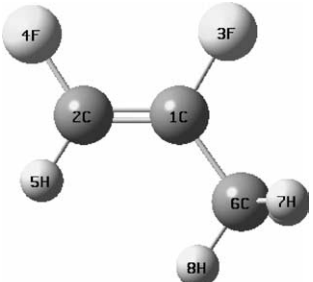
$$\langle\langle P;Q\rangle\rangle_{\omega=0} = 2\sum_{n\neq0}\frac{\langle 0|P|n\rangle\langle n|Q|0\rangle}{E_0 - E_n} \tag{7}$$

it can be seen that those three contributions can be calculated without knowing explicitly the excited states. Within the random phase approximation (RPA) [61] or time-dependent Hartree–Fock theory [62] the polarization propagator is evaluated consistently through first order in the fluctuation potential, i.e., the difference between the instantaneous interelectron interaction and the average interaction of the Hartree–Fock approximation. In the SOPPA [52] the single excitation contributions to the polarization propagator are evaluated through second order in Møller–Plesset perturbation theory [63,64]. Explicit expressions for SOPPA have been given elsewhere [4,20,53–56].

3. COMPUTATIONAL DETAILS AND NOMENCLATURE
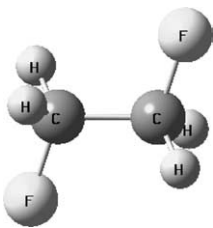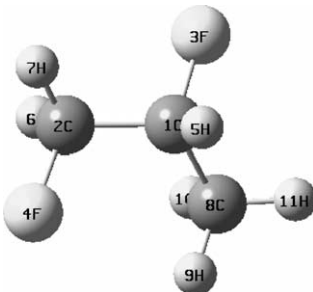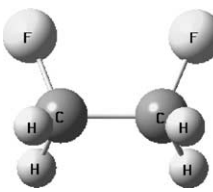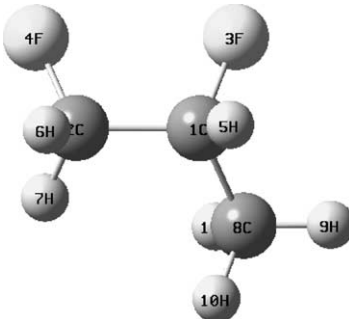
The geometry for all the studied model compounds was optimized with the Gaussian98 program [65] at the MP2/cc-pVTZ level using the very tight option. The internal coordinates of the optimized geometries are given in Table 1. The total $J_{\mathrm{F–F}}$ coupling constants and their four contributions were calculated with

Table 1. Geometries (in Å and degrees) calculated at MP2/cc-pVTZ level

Compound	Salient geometric parameters
(1)	$r(FF) = 3.7673$, $r(CF) = 1.2864$, $r(CC) = 1.1945$
(2)	$r(FF) = 3.5372$, $r(CF) = 1.3400$, $r(CC) = 1.3258$, $r(CH) = 1.0778$, $\angle(FCC) = 120.1701$, $\angle(FCH) = 115.1236$
(3)	$r(FF) = 3.5338$, $r(1C3F) = 1.3505$, $r(2C4F) = 1.3443$, $r(1C2C) = 1.3293$, $r(1C6C) = 1.4790$, $r(2C5H) = 1.0772$, $\angle(3F1C2C) = 117.1972$, $\angle(4F2C1C) = 120.6879$, $\angle(2C1C6C) = 128.1424$, $\angle(4F2C5H) = 114.9643$
(4)	$r(FF) = 2.7740$, $r(FC) = 1.3350$, $r(CC) = 1.3264$, $r(CH) = 1.0773$, $\angle(FCC) = 122.8302$, $\angle(FCH) = 115.2188$
(5)	$r(FF) = 3.5338$, $r(1C3F) = 1.3443$, $r(2C4F) = 1.3386$, $r(1C2C) = 1.3299$, $r(1C6C) = 1.4813$, $r(2C5H) = 1.0768$, $\angle(3F1C2C) = 119.9497$, $\angle(4F2C1C) = 122.3318$, $\angle(2C1C6C) = 125.5068$, $\angle(4F2C5H) = 114.9868$

Table 1. (*continued*)

Compound	Salient geometric parameters
(**6**)	r(FF) = 3.5419, r(CF) = 1.3838, r(CC) = 1.5107, r(CH) = 1.0878, ∠(FCC) = 108.1414, ∠(FCH) = 108.8924, ∠(HCH) = 109.5053
(**7**)	r(FF) = 3.5404, r(1C3F) = 1.3936, r(2C4F) = 1.3846, r(1C2C) = 1.5143, r(1C5H) = 1.0900, r(1C8C) = 1.5056, r(2C6H) = 1.0894, r(2C7H) = 1.0877, ∠(3F1C2C) = 105.8568, ∠(4F2C1C) = 109.1488, ∠(2C1C8C) = 112.9819, ∠(2C1C5H) = 109.7840, ∠(4F2C6H) = 108.6942, ∠(4F2C7H) = 108.7976
(**8**)	r(FF) = 2.5163, r(CF) = 1.3754, r(CC) = 1.5425, r(CH) = 1.0880, ∠(FCC) = 110.7310, ∠(FCH) = 108.0009, ∠(HCH) = 108.8507
(**9**)	r(FF) = 2.5022, r(1C3F) = 1.3832, r(2C4F) = 1.3754, r(1C2C) = 1.5453, r(1C5H) = 1.0901, r(1C8C) = 1.5079, r(2C6H) = 1.0887, r(2C7H) = 1.0897, ∠(3F1C2C) = 109.3907, ∠(4F2C1C) = 111.2098, ∠(2C1C8C) = 112.0529, ∠(2C1C5H) = 109.4548, ∠(4F2C6H) = 108.1834, ∠(4F2C7H) = 107.6864

the Dalton program package [66]. Electronic correlation was included in all calculations by the SOPPA method [4,20,52].

In the calculations of the F–F spin–spin couplings we employed the following basis sets:

(i) standard basis sets, cc-pVXZ (with X = D or T) and their augmented versions, aug-cc-pVXZ (which include diffuse functions) [67–69],
(ii) optimized NMR-*J* basis sets, aug-cc-pVTZ-J [26,70], which permit an adequate treatment of the cusp of the wave function at the nucleus and give therefore a very good description of the FC term (Ref. [26] and references cited therein),
(iii) a minimal basis set, containing only one s-type Gaussian function with coefficient 1.159 for hydrogen and two s-type Gaussian functions with co-efficients 3.319 and 0.9059 and one p-type Gaussian function with coefficient 0.3827 for carbon.

We have investigated several series of LDBSs which were generated as different combinations of these basis sets for the non-coupled atoms and the aug-cc-pVTZ-J basis set for the coupled fluorine atoms. The results are presented graphically in Figs 1–10.

In order to simplify the discussion of the different LDBSs we use the following acronyms for the basis sets:

apTJ : for aug-cc-pVTZ-J
apT : for aug-cc-pVTZ
pT : for cc-pVTZ
apD : for aug-cc-pVDZ
pD : for cc-pVDZ
m : for the minimal basis set of only one *s*-type function with coefficient 1.159 for hydrogen and two *s*-type Gaussian functions with coefficients 3.319 and 0.9059 and one *p*-type Gaussian function with coefficient 0.3827 for carbon

A LDBS is then identified by listing the labels for the basis sets separated by '/'. The first label is for the coupled fluorine atoms, the second is for the atoms in the structure of interest, i.e., in this work the coupling path (here always carbon), the third labels are for atoms directly bond to the atoms in the coupling path and the last is for atoms not directly bond to the coupling path. When more than one type of atoms belong to a group, e.g., '6C' and '5H' in (**3**), the basis set labels will then appear in order of decreasing atomic number. The label LDBS apTJ/apTJ/[pT/pD]/m for 1,2-difluoropropen (**3**) or (**5**), e.g., stands therefore for a LDBS with the aug-cc-pVTZ-J basis set on the fluorine atoms and on the doubly bonded carbon atoms, the cc-pVTZ basis set on the carbon atom in the methyl group, the cc-pVDZ basis set on the vinyl hydrogen and the minimal basis set on the hydrogen atoms in the methyl group. In the figures the first label representing the basis set for the coupled fluorine atoms was dropped for the sake of readability. In Table 2 the best basis set for each molecule is given.

Table 2. The best basis sets for the molecules included in this study

Molecule	Basis[a]	Number
(**1**) Difluoroethyne	apTJ/apTJ	184
(**2**) *trans*-1,2-difluoroethene	apTJ/apTJ/apTJ	224
(**3**) *trans*-1,2-difluoropropene	apTJ/apTJ/[apTJ/pD]/m	238
(**4**) *cis*-1,2-difluoroethene	apTJ/apTJ/apTJ	224
(**5**) *cis*-1,2-difluoropropene	apTJ/pT/[pT/m]/m	186
(**6**) *antiperiplanar*-1,2-difluoroethane	apTJ/apTJ/pT	240
(**7**) *antiperiplanar*-1,2-difluoropropane	apTJ/apTJ/[apTJ/pD]/m	248
(**8**) *synperiplanar*-1,2-difluoroethane	apTJ/apTJ/pT	240
(**9**) *synperiplanar*-1,2-difluoropropane	apTJ/apTJ/[apTJ/pD]/m	248

[a] See Section 3 for nomenclature used.

4. RESULTS

The results of the LDBS study are presented graphically in Figs 1–10. The figures show the deviation of the results for the total vicinal F–F couplings as well as the OP, SD and FC contributions obtained with the given LDBS from the corresponding result obtained with the largest basis set as given in Table 2. The OD contribution is not included in the figures, because the changes in OD term are for most basis sets smaller than 0.01 Hz and the largest change is only 0.02 Hz. The label representing the basis set for the coupled fluorine atoms is not included in the figures.

The whole set of values for $^3J_{\text{F–F}}$ in the studied compounds are available on request.

4.1. Difluoroethyne

From Table 3 we can see that the negative OP contribution is the most important term in the vicinal F–F coupling in difluoroethyne (**1**). The SD and FC terms are

Table 3. $^3J_{^{19}\text{F}-^{19}\text{F}}$ coupling constants and their four contributions (in Hz) calculated with the best set (see Table 2) at the SOPPA level at MP2/cc-pVTZ geometry

	J^{OD}	J^{OP}	J^{SD}	J^{FC}	J	Exp.
(**1**)	−1.82	−54.64	28.39	6.55	−21.52	2.1[a]
(**2**)	−1.77	−143.27	22.69	−11.28	−133.62	−132.7[b]
(**3**)	−1.70	−134.90	18.44	−12.02	−130.18	
(**4**)	−0.42	−38.44	24.21	0.58	−14.06	−18.7[c]
(**5**)	−0.21	−29.50	22.31	0.96	−6.43	
(**6**)	−1.55	−39.18	14.34	−10.54	−36.93	−30.0[d]
(**7**)	−1.50	−29.23	15.13	−12.22	−27.82	
(**8**)	0.19	−12.60	8.94	35.80	32.32	
(**9**)	0.35	−18.73	7.37	40.25	29.24	

[a] Ref. [71].
[b] Ref. [72].
[c] Ref. [73].
[d] Estimated [74].
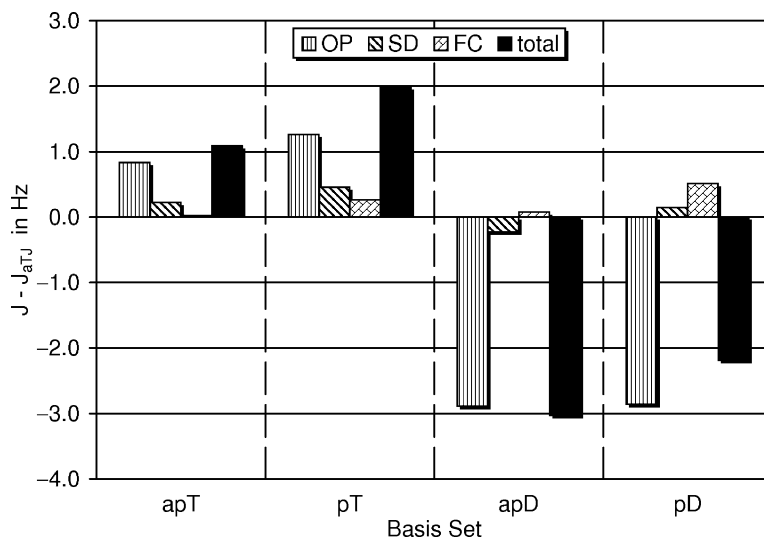
Fig. 1. Dependence of the vicinal F–F coupling constant in difluoroethyne on the basis set used for the carbon atoms: Deviation (in Hz) of the locally dense basis set result from the calculation with the apTJ/apTJ basis set. Only the basis sets on the non-coupled atoms are used as labels on the basis set axis. The apTJ basis set was used for fluorine in all calculations.

positive in this molecule and amount to only about 50 and 10% of the OP term, respectively.

In Fig. 1, the results of the LDBS study are shown. Usage of standard basis sets of valence triple and double ζ quality on the carbon atoms changes the vicinal F–F couplings by at most 3 Hz while the basis set can be reduced by 64 functions or 35%. The changes are a lot more important for the OP term than for the FC and SD terms. It is interesting to note that employing the apT or pT basis sets on carbon increases the OP term by $\sim$1 Hz whereas the apD and pD basis sets reduce it by $\sim$3 Hz. The additional diffuse functions in the apT and apD basis sets on the carbon atoms seem to be of no importance for the vicinal F–F couplings in difluoroethyne. The LDBS apTJ/pT (aug-cc-pVTZ-J on fluorine and cc-pVTZ on carbon) reproduces each term quite well with respect to the calculation with the most complete basis set. As pointed out in our previous paper on long-range F–F couplings [39] there is a large difference between our SOPPA result and the only available experimental result. Earlier semi-empirical calculations [75] predict -85.4 Hz, which is further away from the experimental value. The reason for this disagreement should be investigated further.

4.2. *trans*-1,2-difluoroethene and *trans*-1,2-difluoropropene

Analyzing the four contributions to the vicinal F–F couplings in *trans*-1,2-difluoroalkanes, (**2**) and (**3**), in Table 3 one sees that the large and negative OP term is the all dominating contribution, whereas the SD and FC term amount to

only about 16 and 8% of the OP term. The FC term is negative as for all *trans* or *app* vicinal couplings.

Despite the dominance of the OP term it is primarily the FC term which is influenced by the choice of the basis set on the non-coupled atoms in *trans*-1,2-difluoroethene (**2**). Only when we reduce the basis set on the carbon atoms to the cc-pVDZ level (LDBS apTJ/pD/pD), the change in the OP term (1.9 Hz) becomes larger than the change in the FC term (1.8 Hz) and the error in the total coupling exceeds 4 Hz. Similarly we observe larger changes in the OP and SD term when the basis set on the hydrogen atoms is reduced to the minimal basis set (LDBS apTJ/pT/m). However, the errors in the OP and SD term cancel nearly, so that the change in the total coupling is almost identical in the apTJ/pT/pD and apTJ/pT/m basis sets and is still < 1 Hz.

Using the aug-cc-pVTZ-J basis set for fluorine, cc-pVTZ for carbon and cc-pVDZ for hydrogen (LDBS apTJ/pT/pD) it is possible to reproduce each contribution to the vicinal F–F coupling from the most complete basis set apTJ/apTJ/apTJ without considerable loss of accuracy (<1 Hz) while reducing the size of the basis set by 62 functions or 28%.

Turning our attention now to *trans*-1,2-difluoropropene (**3**) we can see that the methyl group induces only minor changes in the vicinal *trans*-F–F coupling constant. The absolute values of the OP and SD terms are reduced while the FC becomes numerically larger. Comparing the individual terms we can set that the changes increase in the order FC < total < SD < OP.

With the LDBS study on *trans*-1,2-difluoropropene, Fig. 3, we wanted to investigate primarily the effect of the basis sets for the carbon atom in the methyl group. Therefore, we used the minimal basis set for the methyl hydrogens in all

Fig. 2. Dependence of the vicinal *trans* F–F coupling constant in *trans*-1,2-difluoroethene on the basis set used for the carbon atoms and hydrogen atoms: Deviation (in Hz) of the locally dense basis set result from the calculation with the apTJ/apTJ/apTJ basis set. Only the basis sets on the non-coupled atoms are used as labels on the basis set axis. The apTJ basis set was used for fluorine in all calculations.
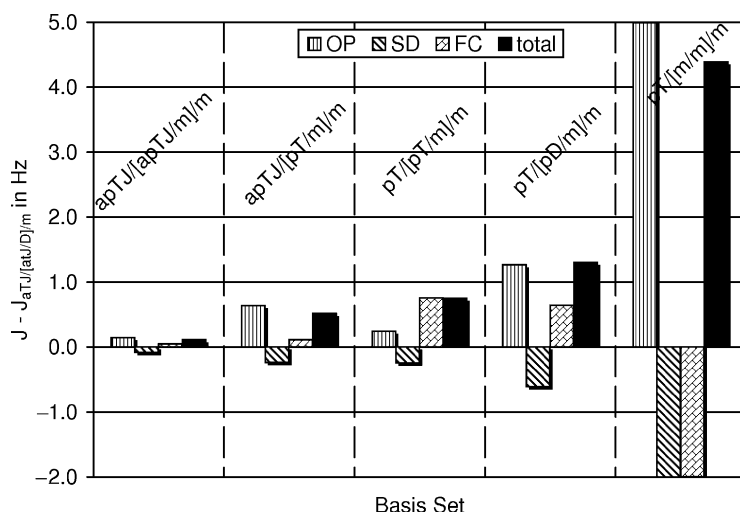
Fig. 3. Dependence of the vicinal *trans* F–F coupling constant in *trans*-1,2-difluoropropene calculated at the SOPPA level on the basis set used for the carbon atoms and hydrogen atoms: Deviation (in Hz) of the locally dense basis set result from the calculation with the apTJ/apTJ/[apTJ/pD]/m basis set. Only the basis sets on the non-coupled atoms are used as labels on the basis set axis. The apTJ basis set was used for fluorine in all calculations.

calculations shown in Fig. 3. Reducing the basis set for the vinyl hydrogen from cc-pVDZ to the minimal basis set introduces only insignificant changes in the order of 0.1 Hz and this basis set was thus used in all the other calculations for this molecule. Similarly the changes in the total coupling constant introduced by reducing the basis set for the two doubly bonded carbon atoms to the cc-pVTZ level are small. However, using the minimal basis for the carbon of the methyl group produces important changes in the OP, SD and FC contributions (LDBS apTJ/pT/[m/m]/m) and a total error of ∼ 4 Hz, whereas the basis set cc-pVDZ (LDBS apTJ/pT/[pD/m]/m) gives good results for each term and a total error of only 1.3 Hz while reducing the size of the basis set by 68 functions or 29% with respect to the apTJ/apTJ/[apTJ/pD]/m basis set.

4.3. *cis*-1,2-difluoroethene and *cis*-1,2-difluoropropene

The OD and OP contributions and the total value of the vicinal F–F coupling constants in *cis*-1,2-difluoroethene (**4**) and *cis*-1,2-difluoropropene (**5**) are all negative, whereas the SD and FC terms are positive, as can be seen from Table 3. The OP and SD terms are of the same order of magnitude whereas the FC terms are close to zero.

The basis set study for *cis*-1,2-difluoroethene (**4**), Fig. 4, shows that the hydrogens are well described with the cc-pVDZ basis set (e.g., LDBS apTJ/apTJ/pD, apTJ/apT/pD or apTJ/pT/pD), whereas with the minimal basis set the changes in the OP term and thus the total vicinal F–F coupling become about −3 Hz (e.g., LDBS apTJ/apTJ/m, apTJ/apT/m or apTJ/pT/m). It is interesting to note that
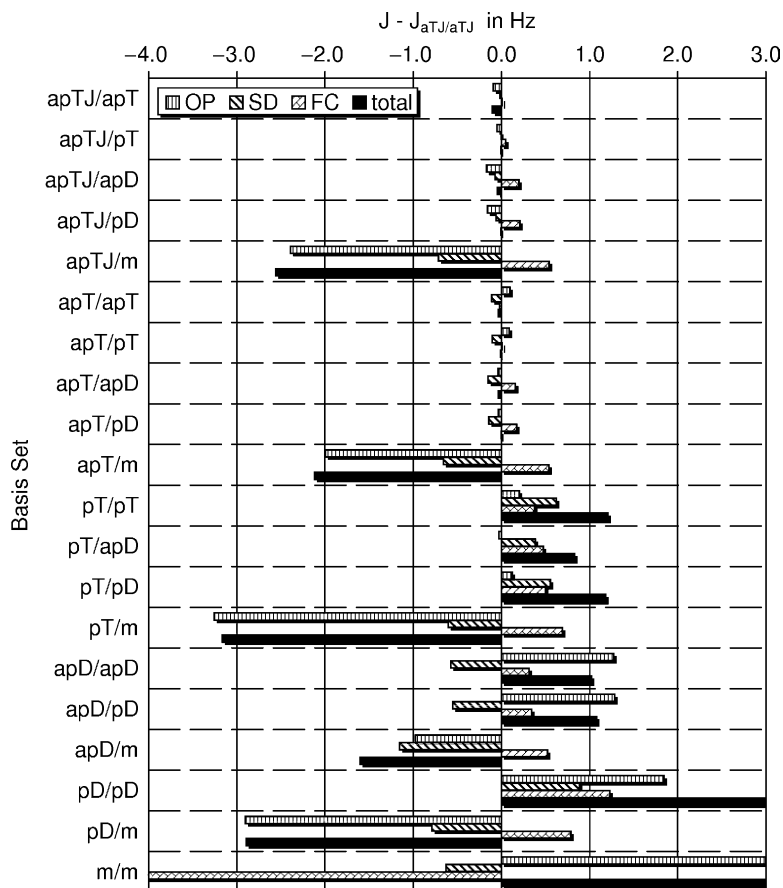
Fig. 4. Dependence of the vicinal *cis* F–F coupling constant in *cis*-1,2-difluoroethene calculated at the SOPPA level on the basis set used for the carbon atoms and hydrogen atoms: Deviation (in Hz) of the locally dense basis set result from the calculation with the apTJ/apTJ/apTJ basis set. Only the basis sets on the non-coupled atoms are used as labels on the basis set axis. The apTJ basis set was used for fluorine in all calculations.

all the calculations with the minimal basis for hydrogen give larger errors in the total F–F couplings in the *cis*-isomers than it was the case for the *trans*-isomers.

   Comparing the LDBS calculations with the cc-pVTZ and aug-cc-pVDZ basis set on the carbon atoms shows that in the former case the changes are mainly in the SD and FC term, whereas in the latter case there are large changes in the OP term, which are partially reduced by a now negative change in the SD term. The errors in the FC term are actually slightly smaller in the aug-cc-pVDZ basis set. The changes in the total vicinal F–F coupling constants are comparable in both basis sets (~ 1 Hz). Nevertheless, the cc-pVTZ basis should be preferred for carbon (LDBS apTJ/pT/pD) due to the smaller changes in the individual contributions.

   Calculations of the vicinal F–F coupling constant for *cis*-1,2-difluoropropene (**5**) suffer from triplet instabilities, when the aug-cc-pVTZ-J basis set is used

Fig. 5. Dependence of the vicinal *cis* F–F coupling constant in *cis*-1,2-difluoropropene on the basis set used for the carbon and hydrogen atoms: Deviation (in Hz) of the locally dense basis set result from the calculation with the apTJ/pT/[pT/m]/m basis set. Only the basis sets on the non-coupled atoms are used as labels on the basis set axis. The apTJ basis set was used for fluorine in all calculations.

for the doubly bonded carbon atoms (LDBS apTJ/apTJ/[apTJ/pD]/m, apTJ/apTJ/ [apTJ/m]/m, apTJ/apTJ/[pT/m]/m). We choose therefore the apTJ/pT/[pT/m]/m basis set as reference. From Table 3 one can see that the methyl group induces only minor changes in the vicinal *cis* F–F coupling constant. The absolute values of the OP and SD terms are reduced while the FC becomes larger. However, the changes in the FC and SD are rather small and of opposite sign such that the change in the total coupling is dominated by the OP term.

Figure 5 shows that the best overall description of the coupling constants is obtained with the combination of cc-pVTZ on the doubly bonded carbon atoms, cc-pVDZ on the methyl carbon atom and the minimal basis set on all hydrogens (LDBS apTJ/pT/[pD/m]/m) – the same basis set as for the *trans*-isomer.

4.4. *app*-1,2-difluoroethane and *app*-1,2-difluoropropane

There are several similarities between the vicinal F–F coupling constants in *antiperiplanar* conformers of 1,2-difluoroalkanes, (**6**) and (**7**), and the corresponding *trans*-1,2-difluoroalkenes, (**2**) and (**3**). The sign of the four contributions is the same, the SD is positive and all other contributions as well as the total coupling constant are negative. Furthermore, the FC terms are almost identical and thus do not depend on the character of the C–C bond in the coupling pathway. The SD and OP contributions on the other hand are smaller in the *app*-1,2-difluoroalkanes, the SD term is only about 2/3 and the OP roughly 1/4 of the values in the *trans*-1,2-difluoroalkenes. Furthermore, the FC and SD contributions are very similar but of different sign and the total coupling constant becomes
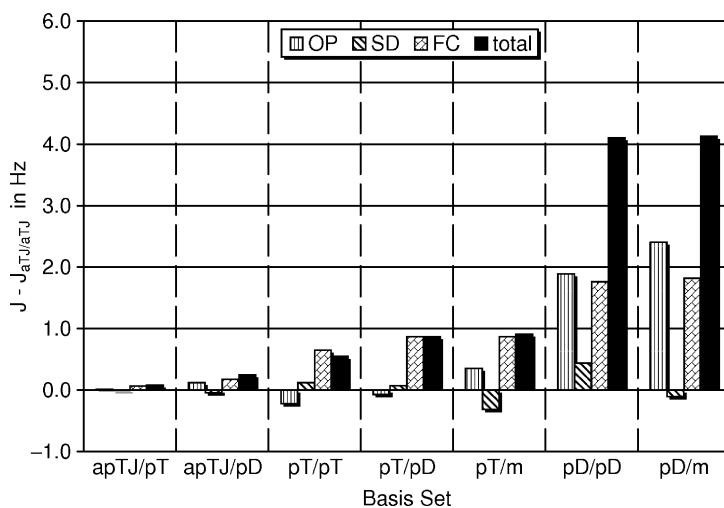
Fig. 6. Dependence of the vicinal *app* F–F coupling constant in *antiperiplanar*-1,2-difluoroethane on the basis set used for the carbon and hydrogen atoms: Deviation (in Hz) of the locally dense basis set result from the calculation with the apTJ/apTJ/pT basis set. Only the basis sets on the non-coupled atoms are used as labels on the basis set axis. The apTJ basis set was used for fluorine in all calculations.

therefore very close in value to the OP contribution. The introduction of the methyl group in *app*-1,2-difluoropropane (**7**) leads again to a reduction of the absolute value of the OP and a much smaller increase in the absolute value of the FC and SD term.

From Fig. 6 for *app*-1,2-difluoroethane (**6**) it can be seen that it is enough to describe each hydrogen with the cc-pVDZ basis set (LDBS apTJ/pT/pD), whereas with the minimal basis set on the hydrogen atoms the FC term change by more than 1 Hz (LDBS apTJ/pT/m). Nevertheless, the changes in the total coupling constant is still much less than 1 Hz due to a cancellation of errors. The carbon atoms are also well described by the cc-pVTZ basis set (LDBS apTJ/pT/pD). With this LDBS it is possible to reduce the size of the basis set by 68 functions (28%) without considerable loss of accuracy (<1 Hz). Using a smaller carbon basis sets, (LDBS apTJ/pD/pD) leads to larger errors in the FC term and the total coupling constant (~ 2 Hz). The extra diffuse functions in the augmented basis sets are again not necessary for describing the electronic densities around the carbon atoms in this molecule.

In the case of the *antiperiplanar* conformer of 1,2-difluoropropane (**7**) we studied again the influence of the basis for the carbon atom in the methyl group. For all hydrogen atoms we used the minimal basis set apart from the reference calculation where the cc-pVDZ basis set was employed on hydrogens '5H', '6H' and '7H'. The result, shown in Fig. 7, is the same as for *trans*-1,2-difluoropropene (**3**). The electron density around the methyl carbon, although it is out of the F–F bonding path, is not properly described with the minimal basis set. The OP, SD and FC terms are all not well reproduced by this calculation

Fig. 7. Dependence of the vicinal *app* F–F coupling constant in *antiperiplanar*-1,2-difluoropropane on the basis set used for the carbon and hydrogen atoms: Deviation (in Hz) of the locally dense basis set result from the calculation with the apTJ/apTJ/[apTJ/pD]/m basis set. Only the basis sets on the non-coupled atoms are used as labels on the basis set axis. The apTJ basis set was used for fluorine in all calculations.

(LDBS apTJ/pT/[m/m]/m). Nevertheless, due to a cancellation of the errors, the change in the total coupling constant is only -1.3 Hz. With the cc-pVDZ basis set on the carbon in the methyl group, on the other hand, all terms are correctly reproduced (LDBS apTJ/pT/[pD/m]/m), which allows to reduce the basis set by 76 functions (31%) with respect to the more complete calculation.

A comparison of Figs 2 and 6 or 3 and 7 shows that the changes in the FC and often also in the OP term due to the smaller basis sets are generally smaller in the alkanes than in the alkenes.

4.5. *spp*-1,2-difluoroethane and *spp*-1,2-difluoropropane

Contrary to all the other molecules studied here, the FC term is the largest contribution to the vicinal F–F coupling constants in the *synperiplanar* conformers of the 1,2-difluoroalkanes (**8**) and (**9**). This is quite remarkable, because it is a factor of 40–50 larger than in the corresponding difluoroalkenes, (**4**) and (**5**), and because there is no significant difference between the *trans*-difluoroalkenes, (**2**) and (**3**), and the *app*-difluoroalkanes, (**6**) and (**7**). The second largest contribution is the negative OP term. However, the total F–F coupling constants are quite similar to the FC term, because the OP and SD terms are of the same order of magnitude but have opposite signs.

It can be seen from Fig. 8 that the minimal basis set on the hydrogen atoms produces larger errors in the OP term and FC term of 1,2-difluoroethane in the *synperiplanar* conformation (**8**) than in the *antiperiplanar* conformation (**6**). The same difference was also observed between the *trans* and *cis* couplings in the
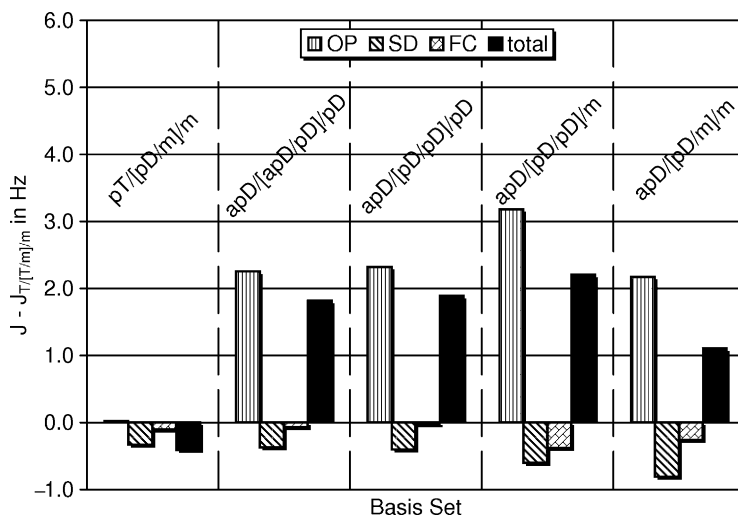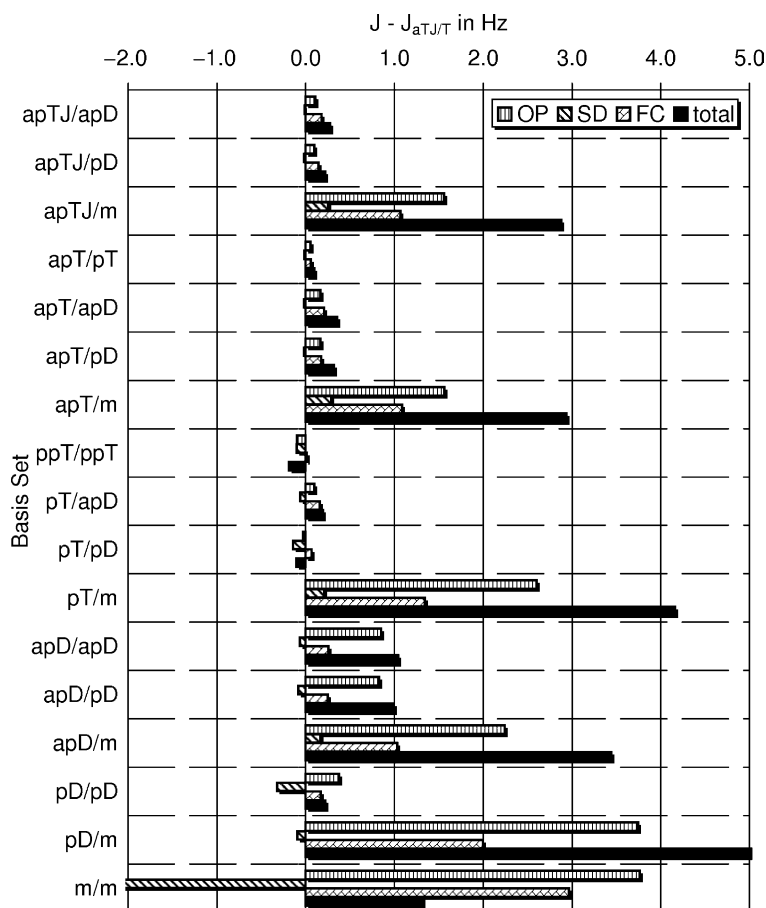
Fig. 8. Dependence of the vicinal *spp* F–F coupling constant in *synperiplanar*-1,2-difluoroethane on the basis set used for the carbon and hydrogen atoms: Deviation (in Hz) of the locally dense basis set result from the calculation with the apTJ/apTJ/pT basis set. Only the basis sets on the non-coupled atoms are used as labels for the basis set axis. The apTJ basis set was used for fluorine in all calculations.

difluoroalkanes, (**2**) and (**4**), and indicates a difference in the coupling pathway. But with the cc-pVDZ basis set for the hydrogen atoms one obtains good results (LDBS apTJ/apTJ/pD, apTJ/pT/pD, apTJ/apD/pD).

The carbon atoms are well described by the cc-pVTZ basis set. The F–F coupling is almost identical to the large basis set value. However, the size of the basis set can further be reduced by using the aug-ccpVDZ basis sets for the carbon atoms. Although the error in the OP term increases in this case, the change in the total coupling constants is still about 1 Hz only (LDBS apTJ/apD/pD).

Reducing the basis set for the non-methyl hydrogens to the minimal basis set gives also in *spp*-1,2-difluoropropane (**9**) a larger error as shown in Fig. 9. We have therefore carried out two series of basis set studies – one with the cc-pVDZ
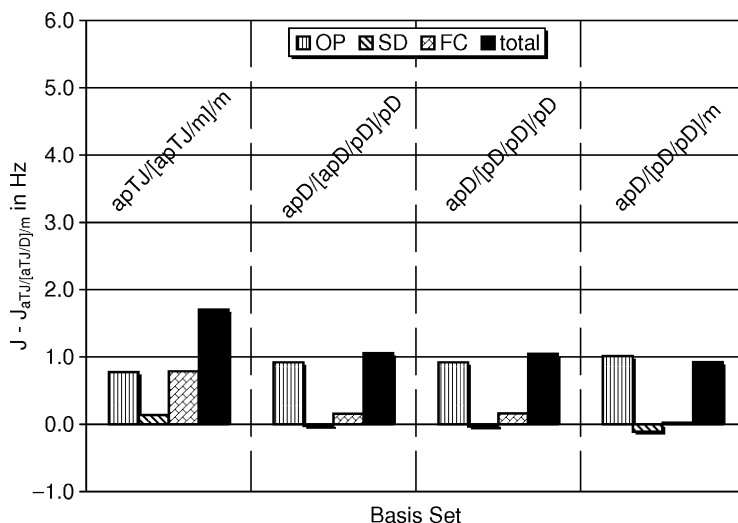
Fig. 9. Dependence of the vicinal *spp* F–F coupling constant in *synperiplanar*-1,2-difluoropropane on the basis set used for the carbon and hydrogen atoms: Deviation (in Hz) of the locally dense basis set result from the calculation with the apTJ/apTJ/ [apTJ/pD]/m basis set. Only the basis sets on the non-coupled atoms are used as labels for the basis set axis. The apTJ basis set was used for fluorine in all calculations.
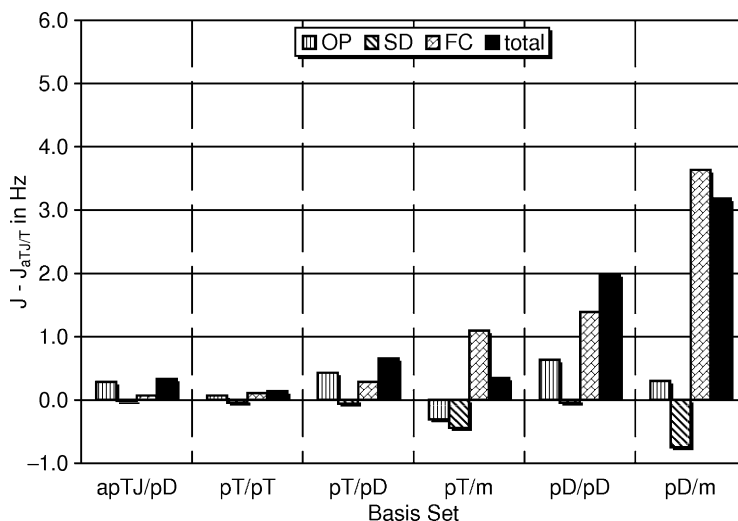

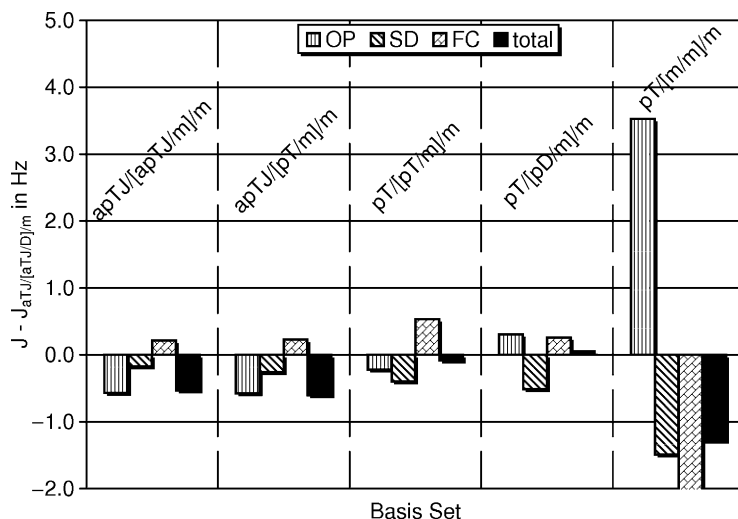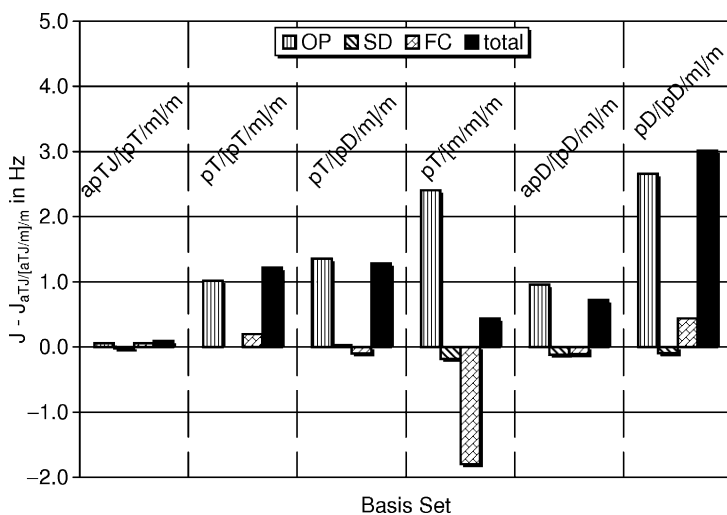**Fig. 10.** Dependence of the vicinal *spp* F–F coupling constant in *synperiplanar*-1,2-difluoropropane on the basis set used for the carbon and hydrogen atoms: Deviation (in Hz) of the locally dense basis set result from the calculation with the apTJ/apTJ/[pT/m]/m basis set. Only the basis sets on the non-coupled atoms are used as labels on the basis set axis. The apTJ basis set was used for fluorine in all calculations.

basis set on these hydrogen atoms (remaining columns in Fig. 9) and the second with only the minimal basis set. In the latter case, **10**, we choose then LDBS apTJ/apTJ/[apTJ/m]/m as the reference basis set. In this way, we can study the influence of the carbon basis sets. The conclusion is that the cc-pVDZ basis set is good enough to describe the carbon atoms of the methyl group, whereas the minimal basis set gives again larger changes in the OP and FC term, which however partly cancel out (Fig. 10). Secondly, reducing the basis set for the methyl hydrogens to the minimal basis set has not significant effect (see Fig. 9).

4.6. Physical implications

From an analysis of the LDBSs developed in the previous sections one can also gain insight on which parts of the electronic structure of the molecules are relevant or irrelevant for the transmission of the indirect nuclear spin coupling through the molecule.

For *trans*-1,2-difluoroethene, (**2**), and the *antiperiplanar* conformation of 1,2-difluoroethane, (**6**), a good LDBS consists of the aug-cc-pVTZ-J basis set for fluorine, cc-pVTZ for carbon and cc-pVDZ or a minimal basis set for the hydrogen atoms (LDBS apTJ/pT/pD or apTJ/pT/m). These basis sets lead to an error smaller than 1 Hz (see Table 4). They ensure an adequate treatment of the cusp of the wavefunction at the site of F nuclei [26] as well as a good description of the valence orbitals of the coupled fluorine atoms, even far away from the nuclei, due to the presence of four very tight *s*-functions and large number of diffuse and polarization functions in the aug-cc-pVTZ-J basis set. A good description of the valence orbitals of the carbon atoms is also ensured by the use of the cc-pVTZ basis set; however, this basis set does not contain tight or extra diffuse functions. The hydrogens can be described adequately by the cc-pVDZ basis set or even by a single *s*-function.

This analysis shows that in order to get a quantitative reproduction of the *trans*-vicinal F–F coupling it is necessary to describe properly the core orbitals of the coupled fluorine atoms as well as the valence orbitals of the whole system

Table 4. Errors in the vicinal F–F coupling constants and reduction in the number of basis functions for various locally dense basis sets in comparison with the apTJ/apTJ/apTJ basis set for difluoroethyne (**1**) and the 1,2-difluoroalkanes, (**2**) and (**4**), and the apTJ/apTJ/pT basis set for the 1,2-difluoroalkanes, (**6**) and (**8**). All calculations were carried out using SOPPA

	apTJ/pT/pD		apTJ/pT/m		apTJ/pD/pD		apTJ/pD/m	
	Hz	%	Hz	%	Hz	%	Hz	%
(**1**)	2.0	17			2.2	35		
(**2**)	0.9	28	0.9	31	4.1	42	4.1	46
(**4**)	1.2	28	−3.2	31	4.0	42	−2.9	46
(**6**)	0.7	28	0.4	35	2.0	42	3.2	48
(**8**)	−0.1	28	4.2	35	0.2	42	5.7	48

Table 5. Errors in the vicinal F–F coupling constants and reduction in the number of basis functions for various locally dense basis sets in comparison with the apTJ/apTJ/[apTJ/pD]/m basis set for *trans*-1,2-difluoropropene (**3**) and *app*-1,2-difluoropropane (**7**). All calculations were carried out using SOPPA

	apTJ/pT/[pD/m]/m		apTJ/pT[m/m]/m	
	Hz	%	Hz	%
(**3**)	1.3	29	4.4	32
(**7**)	0.1	31	−1.3	34

F–C–C–F of F–C=C–F. This suggest that the *J* coupling is transmitted, in both systems, mainly via the core and valence electrons of coupled fluorine atoms and the valence electrons of intermediate atoms. The orbitals of the hydrogen atoms, which are located in the region of the backloops of the C–F single bonds, on the other hand, play a minor role in the quantitative reproduction of the *trans*-vicinal F–F coupling. These results are in accord with previous findings based on different grounds (Ref. [32]).

By a similar analysis of the results for the *trans*-1,2-difluoropropene, (**3**), and the *antiperiplanar* conformation of 1,2-difluoropropane, (**7**), (see also Table 5) one can see that the previous findings are still valid when the LDBS scheme is apTJ/pT/[pD/m]/m. However, it can be seen in Figs 3 and 7 that for quantitative reproduction of the vicinal F–F coupling it is necessary to describe the carbon atom of the CH_3 substituent with a larger than a minimal basis set. In both cases, the cc-pVDZ basis set was used.

On the other hand, a quantitative reproduction of the vicinal F–F couplings in *cis*-1,2-difluoroethene (**4**) and the *synperiplanar* conformation of 1,2-difluoroethane (**8**) is only obtained when the basis set on the hydrogens is at least of valence double ζ quality (see Table 4 and Figs 4 and 8). This LDBS scheme shows the necessity to describe properly not only both the core and valence orbitals of the coupled fluorine atoms with the aug-cc-pVTZ-J basis and the valence orbitals of the carbon atoms with a cc-pVTZ basis set, but also the hydrogenic orbitals which are in the region of the backloops of the fluorine–carbon single bonds. This suggest that the main transmission mechanism of the coupling is slightly shifted to a side, closer to the hydrogens and away from the main F–C–C–F and F–C=C–F structure.

5. CONCLUSIONS

In this work, results of high level *ab initio* SOPPA calculations of vicinal fluorine–fluorine indirect nuclear spin couplings are presented for 1,2-difluoroethene, -propene, -ethane and -propane. The four contributions (OD, OP, SD, FC) and the total value of the coupling constant are analyzed.

We find that the OP is the most important term and the absolute values of the four contributions follow the order $|OP|>|SD|>|FC|>|OD|$ for all the molecules studied here with the exception of the *synperiplanar* conformations of 1,2-difluoroethane and 1,2-difluoropropane, where the FC term is the most important

one. In all multiply bonded systems, the FC term amounts to only 16% or less of the OP term. The SD term is generally of the same order of magnitude than the OP term with the exception of the *trans* couplings in the difluoroalkenes. The smallest non-contact terms are found for the *spp* F–F couplings in 1,2-difluoroalkanes. For the same molecules we find also the largest FC terms. Furthermore, we found that the OP terms are generally larger by a factor between 1.5 and 4.5 in the *trans* or *app* couplings than in the corresponding *cis* or *spp* couplings. The OP terms are also larger in the difluoroalkenes than in the difluoroalkanes and particularly large values of the OP term are found for the *trans* F–F couplings in the difluoro-alkenes. The SD term is smaller in the *trans* than in the *cis* couplings, but larger in the *app* couplings than in the *spp* couplings. On the other hand, it is always larger across the C–C double bond than across the single bond.

With respect to the sign of the four contributions or the total coupling constants we can see that the FC term is positive in difluoroethyne and for all *cis* or *spp* couplings and negative for the *trans* or *app* couplings. An earlier natural *J*-coupling analysis at the DFT level showed that the latter is mainly due to the fluorine lone pairs [76]. The SD term, on the other hand, is positive for all the molecules, whereas the OP term is negative. The total F–F coupling is consequently negative with the exception of the *synperiplanar* conformations of the 1,2-difluoroalkanes.

The main purpose of this study, however, was the development of LDBSs which will closely reproduce the results of large basis set for spin–spin coupling constant calculations with a much reduced number of basis functions. We find that the best choice of basis set for each atom belonging to the studied model compounds depends on its location with respect to those nuclei whose coupling are being calculated and depends also on the conformation of the latter atoms. The carbon atoms located out of the bonding path which connects the coupled nuclei may be described with smaller basis sets (cc-pVDZ) than those located in the coupling pathway (cc-pVTZ), although a good basis set on the latter atoms is more important for the structures in *trans* F–F conformation than for those in *cis* F–F conformation. A decent basis on the hydrogen atoms directly bound to the coupling pathway is more important for molecules with *cis* or *spp* F–F conformation (cc-pVDZ) than for molecules with *trans* or *app* F–F conformation. Hydrogen atoms not directly connected to the coupling pathway can safely be described by a minimal basis set.

We recommend therefore the following LDBS scheme for compounds and couplings equivalent to the ones studied in this paper:

- aug-cc-pVTZ-J for the coupled atoms, here fluorine
- cc-pVTZ for all atoms in the coupling pathway, here carbon
- cc-pVDZ for carbon and hydrogen atoms (only for *cis*- or *spp*-couplings) directly bonded to the coupling pathway
- a minimal basis set for hydrogens not directly connect to the coupling path and for the directly connected hydrogens in the case of *trans*- or *app*-couplings.

Our recommendation should not be applied without further tests to a phenyl group attached to the coupling pathway.

ACKNOWLEDGEMENTS

REFERENCES

[1] L. Zidek, R. Stefl and V. Sklenar, *Curr. Opin. Struct. Biol.*, 2001, **11**, 275.
[2] J. Oddershede, P. Jørgensen and N. H. F. Beebe, *J. Chem. Phys.*, 1975, **63**, 2996.
[3] J. Oddershede, P. Jørgensen and N. H. F. Beebe, *Chem. Phys.*, 1977, **25**, 451.
[4] J. Geertsen and J. Oddershede, *Chem. Phys.*, 1984, **90**, 301.
[5] J. Geertsen and J. Oddershede, *Chem. Phys.*, 1986, **104**, 67.
[6] J. Geertsen, J. Oddershede and G. E. Scuseria, *J. Chem. Phys.*, 1987, **87**, 2138.
[7] J. Geertsen, J. Oddershede and G. E. Scuseria, *Int. J. Quantum Chem. Symp.*, 1987, **21**, 475.
[8] J. Oddershede, J. Geertsen and G. E. Scuseria, *J. Phys. Chem.*, 1988, **92**, 3056.
[9] G. E. Scuseria, J. Geertsen and J. Oddershede, *J. Chem. Phys.*, 1989, **90**, 2338.
[10] J. Geertsen, J. Oddershede, W. T. Raynes and G. E. Scuseria, *J. Magn. Reson.*, 1991, **93**, 458.
[11] G. A. Aucar and J. Oddershede, *Int. J. Quantum Chem.*, 1993, **47**, 425.
[12] J. Geertsen, J. Oddershede and W. T. Raynes, *Magn. Reson. Chem.*, 1993, **31**, 722.
[13] W. T. Raynes, J. Geertsen and J. Oddershede, *Int. J. Quantum Chem.*, 1994, **52**, 153.
[14] J. Geertsen, J. Oddershede, W. T. Raynes and T. L. Marvin, *Mol. Phys.*, 1994, **82**, 29.
[15] S. Kirpekar, H. J. Aa. Jensen and J. Oddershede, *Chem. Phys.*, 1994, **188**, 171.
[16] S. Kirpekar, H. J. Aa. Jensen and J. Oddershede, *Theor. Chim. Acta*, 1997, **95**, 35.
[17] S. Kirpekar, T. Enevoldsen, J. Oddershede and W. T. Raynes, *Mol. Phys.*, 1997, **91**, 897.
[18] R. D. Wigglesworth, W. T. Raynes, S. P. A. Sauer and J. Oddershede, *Mol. Phys.*, 1997, **92**, 77.
[19] R. D. Wigglesworth, W. T. Raynes, S. P. A. Sauer and J. Oddershede, *Mol. Phys.*, 1998, **94**, 851.
[20] T. Enevoldsen, J. Oddershede and S. P. A. Sauer, *Theor. Chem. Acc.*, 1998, **100**, 275.
[21] T. Enevoldsen, L. Visscher, T. Saue, H. J. Aa. Jensen and J. Oddershede, *J. Chem. Phys.*, 2000, **112**, 3493.
[22] R. D. Wigglesworth, W. T. Raynes, S. Kirpekar, J. Oddershede and S. P. A. Sauer, *J. Chem. Phys.*, 2000, **112**, 3735.
[23] T. Helgaker, M. Jaszuński, K. Ruud and A. Górska, *Theor. Chem. Acc.*, 1998, **99**, 175.
[24] J. Guilleme and J. San Fabián, *J. Chem. Phys.*, 1998, **109**, 8168.
[25] P. F. Provasi, G. A. Aucar and S. P. A. Sauer, *J. Chem. Phys.*, 2000, **112**, 6201.
[26] P. F. Provasi, G. A. Aucar and S. P. A. Sauer, *J. Chem. Phys.*, 2001, **115**, 1324.
[27] J. E. Peralta, G. E. Scuseria, J. R. Cheeseman and M. J. Frish, *Chem. Phys. Lett.*, 2003, **375**, 452.
[28] D. B. Chesnut and K. D. Moore, *J. Comput. Chem.*, 1989, **10**, 648.
[29] D. B. Chesnut, B. E. Rusiloski, K. D. Moore and D. A. Egolf, *J. Comput. Chem.*, 1993, **14**, 1364.
[30] L. B. Krivdin, S. P. A. Sauer, J. E. Peralta and R. H. Contreras, *Magn. Reson. Chem.*, 2002, **40**, 187–194.
[31] P. F. Provasi, G. A. Aucar and S. P. A. Sauer, *Int. J. Mol. Sci.*, 2003, **4**, 231.
[32] V. Barone, P. F. Provasi, J. E. Peralta, J. P. Snyder, S. P. A. Sauer and R. H. Contreras, *J. Phys. Chem. A*, 2003, **107**, 4748.
[33] L. B. Krivdin, *Magn. Reson. Chem.*, 2003, **41**, 91.
[34] L. B. Krivdin, *Magn. Reson. Chem.*, 2003, **41**, 157.
[35] L. B. Krivdin, *Magn. Reson. Chem.*, 2003, **41**, 417.
[36] L. B. Krivdin, *Magn. Reson. Chem.*, 2003, **41**, 885.
[37] L. B. Krivdin, *Magn. Reson. Chem.*, 2004, **42**, 1.

[38] L. B. Krivdin, *Magn. Reson. Chem.*, 2004, **42**, 500.

[39] P. F. Provasi, G. A. Aucar and S. P. A. Sauer, *J. Chem. Phys. A*, 2004, **108**, 5393.

[40] S. P. A. Sauer and L. B. Krivdin, *Magn. Reson. Chem.*, 2004, **42**, 671.

[41] M. Tei, Y. Mizuno, Y. Manmoto, R. Sawae and K. Takarabe, *Int. J. Quantum Chem.*, 2003, **95**, 554.

[42] B. Bilgiçer, A. Fichera and K. Kumar, *J. Am. Chem. Soc.*, 2001, **123**, 4393.

[43] B. Bilgiçer, X. Xing and K. Kumar, *J. Am. Chem. Soc.*, 2001, **123**, 11815.

[44] H. S. Duewel, E. Daub, V. Robinson and J. F. Honek, *Biochemistry*, 2001, **40**, 13167.

[45] J. Feeney, J. E. McCormick, C. J. Dauer, B. Birdsall, C. M. Moody, B. A. Starkmann, D. W. Young, P. Francis, R. H. Havlin, W. D. Arnold and E. J. Oldfield, *J. Am. Chem. Soc.*, 1996, **118**, 8700.

[46] B. K. Park, N. R. Kitteringham and P. M. O'Neill, Metabolism of fluorine-containing drugs. *Annu. Rev. Pharmacol. Toxicol.*, 2001, **41**, 443.

[47] L. U. Colmenares, X. Zou, J. Liu and A. E. Asato, *J. Am. Chem. Soc.*, 1999, **121**, 5803.

[48] H. W. Kim, P. Rossi, R. K. Schoemaker and S. G. DiMagno, *J. Am. Chem. Soc.*, 1998, **120**, 9082.

[49] I. Ojima, J. R. McCarthy and J. T. Welch (eds.) *Biomedical Frontiers of Fluorine Chemistry. Number 639 in ACS Symposium Series*, Washington, DC.

[50] P. Bachert, *Prog. Nucl. Magn. Reson. Spectrosc.*, 1998, **33**, 1.

[51] J. Oddershede, P. Jørgensen and N. H. F. Beebe, *Int. J. Quantum Chem.*, 1977, **12**, 655.

[52] E. S. Nielsen, P. Jørgensen and J. Oddershede, *J. Chem. Phys.*, 1980, **73**, 6238.

[53] G. H. F. Diercksen, N. E. Grüner and J. Oddershede, *Comput. Phys. Commun.*, 1983, **30**, 349.

[54] J. Oddershede, P. Jørgensen and D. L. Yeager, *Comput. Phys. Rep.*, 1984, **2**, 33.

[55] M. J. Packer, E. K. Dalskov, T. Enevoldsen, Aa. H. J. Jensen and J. Oddershede, *J. Chem. Phys.*, 1996, **105**, 5886.

[56] K. L. Bak, H. Koch, J. Oddershede, O. Christiansen and S. P. A. Sauer, *J. Chem. Phys.*, 2000, **112**, 4173.

[57] N. F. Ramsey, *Phys. Rev.*, 1953, **91**, 303.

[58] I. Mills, T. Cvitaš, K. Homann, N. Kallay and K. Kuchitsu, *Quantities, Units and Symbols in Physical Chemistry*, 2nd edn, Blackwell Scientific Publications, Oxford, 1993.

[59] S. P. A. Sauer, *J. Chem. Phys.*, 1993, **98**, 9220.

[60] J. Linderberg and Y. Öhrn, *Propagator in Quantum Chemistry*, Academic Press, New York, 1973.

[61] D. J. Rowe, *Rev. Mod. Phys.*, 1968, **40**, 153.

[62] A. D. McLahlan and M. A. Ball, *Rev. Mod. Phys.*, 1964, **36**, 844.

[63] C. Møller and M. S. Plesset, *Phys. Rev.*, 1934, **46**, 618.

[64] J. A. Pople, J. S. Binkley and R. Seeger, *Int. J. Quantum Chem. Symp.*, 1976, **10**, 1.

[65] M. J. Frisch, G. W. Trucks, H. B. Schlegel, G. E. Scuseria, M. A. Robb, J. R. Cheeseman, V. G. Zakrzewski, J. A. Montgomery, Jr., R. E. Stratmann, J. C. Burant, S. Dapprich, J. M. Millam, A. D. Daniels, K. N. Kudin, M. C. Strain, O. Farkas, J. Tomasi, V. Barone, M. Cossi, R. Cammi, B. Mennucci, C. Pomelli, C. Adamo, S. Clifford, J. Ochterski, G. A. Petersson, P. Y. Ayala, K. Cui, Q. Morokuma, N. Rega, P. Salvador, J. J. Dannenberg, D. K. Malick, A. D. Rabuck, K. Raghavachari, J. B. Foresman, J. Cioslowski, J. V. Ortiz, A. G. Baboul, B. B. Stefanov, G. Liu, A. Liashenko, P. Piskorz, I. Komaromi, R. Gomperts, R. L. Martin, T. Fox, D. J. Keith, M. A. Al-Laham, C. Y. Peng, A. Nanayakkara, M. Challacombe, P. M. W. Gill, B. Johnson, W. Chen, M. W. Wong, J. L. Andres, C. Gonzalez, M. Head-Gordon, E. S. Replogle and J. A. Pople, *Gaussian98, Revision A.11.2*, Gaussian, Inc., Pittsburgh, PA, 2001.

[66] T. Helgaker, H. J. Aa. Jensen, P. Jørgensen, J. Olsen, K. Ruud, H. Ågren, A. A. Auer, K. L. Bak, V. Bakken, O. Christiansen, S. Coriani, P. Dahle, E. K. Dalskov, T. Enevoldsen, B. Fernandez, C. Heattig, K. Hald, A. Halkier, H. Heiberg, H. Hettema, D. Jonsson, S. Kirpekar, R. Kobayashi, H. Koch, K. V. Mikkelsen, P. Norman, M. J. Packer, T. Saue, S. P. A. Sauer, P. R. Taylor and O. Vahtras. *DALTON, an Electronic Structure Program, Release 1.2*. http://www.kjemi.uio.no/software/dalton/dalton.html, 2001.

[67] T. H. Dunning Jr., *J. Chem. Phys.*, 1989, **90**, 1007.

[68] R. A. Kendall, T. H. Dunning Jr. and R. J. Harrison, *J. Chem. Phys.*, 1992, **96**, 6796.

[69] D. E. Woon and T. H. Dunning Jr., *J. Chem. Phys.*, 1993, **98**, 1358.

[70] The aug-cc-pVTZ-J basis set can be found at http://fyskem.ki.ku.dk/sauer/basissets
[71] H. Bürger and S. Sommer, *Chem. Soc. Chem. Commun.*, 1991, **7**, 456.
[72] Y. Kanazawa, J. D. Baldeschwieler and N. C. Craig, *J. Mol. Spectrosc.*, 1965, **16**, 325.
[73] G. W. Flynn, N. C. Craig, M. Matsushima and J. D. Baldeschwieler, *J. Chem. Phys.*, 1963, **38**, 2995.
[74] R. J. Abraham and R. H. Kemp, *J. Chem. Soc. B*, 1971, 1240.
[75] K. Hirao, H. Nakatsuji, H. Kato and T. Yonezawa, *J. Am. Chem. Soc.*, 1972, **94**, 4078.
[76] S. Kurtkaya, V. Barone, J. E. Peralta, R. H. Contreras and J. P. Snyder, *J. Am. Chem. Soc.*, 2002, **9702**, 124.

Calculations of Dipole and Quadrupole Polarizability Radial Functions for LiH and HF: A Comparison of Different Linear Response Methods

Ivana Paidarová[1] and Stephan P. A. Sauer[2]

[1]*J. Heyrovský Institute of Physical Chemistry, Academy of Sciences of the Czech Republic, Dolejškova 3, Prague 8, 182 23 Czech Republic*
[2]*Department of Chemistry, University of Copenhagen Universitetsparken 5, DK-2100 København Ø, Denmark*

Abstract

Multiconfigurational self-consistent field (MCSCF) calculations of dipole and quadrupole polarizability tensors of LiH and HF are reported for a wide range of internuclear distance up to the dissociation limit. From the polarizability radial functions we have calculated state-specific polarizabilities for all the vibrational states of the electronic ground state. Furthermore, we compare the MCSCF polarizability radial functions around the equilibrium geometry with corresponding functions obtained by coupled cluster linear response calculations and calculations at the level of the second-order polarization propagator approximation (SOPPA) and the second-order polarization propagator approximation with coupled cluster singles and doubles amplitudes – SOPPA(CCSD).

Contents

1. INTRODUCTION

The calculation of polarizabilities is one of the research topics Jens Oddershede is working on since the beginning of his career [1–21]. Already in one of his first papers he discussed the dipole polarizability of HF [1] and returned to it several times later [3,6,13,14,18]. Therefore, we decided to contribute to this special issue with a study of static dipole and quadrupole polarizabilities which are still one of the most studied electromagnetic properties.

New experiments increase constantly the requirements on the quality and range of calculated electromagnetic properties. State-of-the-art quantum chemical methods can meet the experimental demands and there are numerous articles treating the electric polarizability at the highest level of accuracy. Nevertheless, also only a few of them treat the dependence of the tensor components of the polarizability on the internuclear distance far from the molecular equilibrium geometry. However, there are several good reasons for such studies.

- Molecular electric properties exhibit an appreciable dependence on nuclear geometry and knowledge of corresponding property radial functions is essential for the understanding of the role of vibrational and rotational contributions to these properties (see Ref. [22] and references therein).
- Using property radial functions calculated over the appropriate range of internuclear distances one can determine the dependence of the respective properties on the vibrational and rotational quantum numbers. Although most molecules are in their ground vibrational states at room temperature, the excited vibrational states become interesting, when dealing, e.g., with laser-induced fluorescence experiments or the spectra of cosmic objects [22]. Calculations of molecular properties in excited vibrational states, however, require knowledge of the property radial function also for distances far from the equilibrium geometry.
- Molecular dynamic studies used in the interpretation of experiments, such as collision processes, require reliable potential energy surfaces (PES) of polyatomic molecules. *Ab initio* calculations are often not able to provide such PES, at least not for the whole range of nuclear configurations. On the other hand, these surfaces can be constructed to sufficiently good accuracy with semi-empirical models built from carefully chosen diatomic quantities. The electric dipole polarizability tensor is one of the crucial parameters for the construction of such potential energy curves (PEC) or surfaces [23–25]. The dependence of static dipole properties on the internuclear distance in diatomic molecules can be predicted from semi-empirical models [25,26]. However, the results of *ab initio* calculations for selected values of the internuclear distance are still needed in order to test and justify the reliability of the models. Actually, this work was initiated by F. Pirani, who pointed out the need for *ab initio* curves of the static dipole polarizability of diatomic molecules for a wide range of internuclear distances.

Studies of the internuclear distance dependence of multipole polarizabilities are not new. They appeared, e.g., in the papers by Maroulis *et al.* [27] and references

therein. However, in the majority of these studies the polarizabilities were investigated in the vicinity of the equilibrium internuclear distance, where correlation method based on a single reference wavefunction, such as Møller–Plesset second-order perturbation theory (MP2) [28,29] or the coupled cluster singles and doubles with perturbative triples model (CCSD(T)) [30], normally give reliable results [31]. For calculations at larger distances, a multireference method has to be used.

In this study we examine, therefore, the possibility to use linear response theory for a multiconfigurational self-consistent field wavefunction (MCSCF) [32] in calculations of polarizabilities at large internuclear distances. The application of MCSCF linear response theory is not as straightforward as the use of single configuration linear response methods such as the second-order polarization propagator approximation (SOPPA) [5,33–35], the second-order polarization propagator approximation with coupled cluster singles and doubles amplitudes – SOPPA(CCSD) [36] or coupled cluster linear response theory (CCSD) [37] due to the difficulties in choosing a proper set of configuration state functions. We employ the complete active space (CAS) [38] and restricted active space (RAS) [39] versions of MCSCF as implemented in the Dalton program package [40] for this purpose. The selection of the active spaces for calculations over a wide range of internuclear distances is a demanding task and needs careful verification. In this comparative study we aim to investigate, whether and how, the static electric polarizabilities of diatomic molecules can be calculated as functions of the internuclear distance using MCSCF linear response theory. The MCSCF results will be compared with results from the above-mentioned 'black box' methods [41].

The role of quadrupole polarizabilities is less pronounced. Jens Oddershede, e.g., has studied the quadrupole polarizability of N_2 [10]. Furthermore, there are studies which point out the need for calculations of quadrupole polarizabilities, e.g., for the interpretation of spectra obtained by surface-enhanced Raman spectroscopy [42,43]. Generally the interest in multipole polarizabilities increases due to new experimental data. We decided, therefore, to also study how different linear response theory methods perform in the calculation of quadrupole polarizabilities.

The article is organized as follows. The main features of the linear response theory methods at different levels of correlation are presented in Section 2. Section 3 describes the calculation of the dipole and quadrupole polarizabilities of two small diatomic molecules LiH and HF. Different computational aspects are discussed for each of them. The LiH molecule permits very accurate MCSCF studies employing large basis sets and CASs. This gives us the opportunity to benchmark the results from the other linear response methods with respect to both the shape of the polarizability radial functions and their values in the vibrational ground states. The second molecule, HF, is undoubtedly one of the most studied molecules. We use it here in order to examine the dependence of the dipole and quadrupole polarizabilities on the size of the active space in the CAS and RASSCF approaches. The conclusions of this study will be important for our future studies of dipole and quadrupole polarizabilities of heavier diatomic molecules.

2. THEORY

All the methods used in this study are response methods. They describe the response of an observable such as an electric dipole moment $\vec{\mu}$ or quadrupole moment Θ to an external or internal perturbation, e.g., an electric field or field gradient. Response functions originated in various disciplines in physics. In statistical physics, they were used as time-correlation functions in the form of Green's functions [44,45]. Linderberg and Öhrn first showed the usefulness of this idea for quantum chemistry [46]. Since then response functions have been derived for many types of electronic wavefunctions. Four of these methods are employed here.

In the response function terminology [47] the i, j component of the frequency-dependent dipole polarizability tensor $\alpha_{i,j}(-\omega; \omega)$ (or the ij, kl component of the traceless quadrupole polarizability tensor $C_{ij,kl}(-\omega; \omega)$) is defined through an expansion of a Cartesian component of the time-dependent electronic dipole moment, $\mu_i(t)$ (or quadrupole moment $\Theta_{ij}(t)$), in the presence of an periodic electric field of strength E_j^ω (or a periodic electric field gradient of strength ∇E_{kl}^ω)

$$\mu_i(t) = \mu_i(0) + \int_{-\infty}^{\infty} \mathrm{d}\omega \, \alpha_{ij}(-\omega; \omega) E_j^\omega \, \mathrm{e}^{(-\mathrm{i}\omega + \varepsilon)t} + \cdots \tag{1}$$

$$\Theta_{ij}(t) = \Theta_{ij}(0) + \int_{-\infty}^{\infty} \mathrm{d}\omega \, C_{ij,kl}(-\omega; \omega) \nabla E_{kl}^\omega \, \mathrm{e}^{(-\mathrm{i}\omega + \varepsilon)t} + \cdots \tag{2}$$

where $\mu_i(0)$ and $\Theta_{ij}(0)$ are Cartesian components of the permanent electronic dipole and the traceless quadrupole moments. The static polarizabilities, which are concerned within this study, are the values of the frequency-dependent polarizabilities for zero frequency, $\omega = 0$.

In order to obtain computational expressions for the polarizabilities, the time-dependent moments are evaluated as time-dependent expectation values of the dipole $\hat{\mu}_i$ and quadrupole operators $\hat{\Theta}_{ij}$

$$\mu_i(t) = \langle \Psi_0^{(0)}(t) | \hat{\mu}_i | \Psi_0^{(0)}(t) \rangle \tag{3}$$

$$\Theta_{ij}(t) = \langle \Psi_0^{(0)}(t) | \hat{\Theta}_{ij} | \Psi_0^{(0)}(t) \rangle \tag{4}$$

An ansatz is then made for the time-dependent wavefunction $|\Psi_0^{(0)}(t)\rangle$ depending on time-dependent coefficients which are expanded in the orders of the perturbations E_j^ω or ∇E_{kl}^ω. The wavefunction coefficients in each order of the perturbation have to be determined from the time-dependent Schrödinger equation or an equivalent time-dependent variation principle. Expressions

for the polarizabilities are finally found by comparison with equations (1) and (2).

In MCSCF linear response theory [32] and the SOPPA and SOPPA(CCSD) [5,33,36] this leads to the following expression for the static dipole polarizability, e.g.,

$$\alpha_{ij} = \langle \Psi_0^{(0)} | [\hat{\mu}_i, \tilde{\mathbf{h}}] | \Psi_0^{(0)} \rangle \langle \Psi_0^{(0)} | [\mathbf{h}^\dagger, [\hat{H}, \tilde{\mathbf{h}}]] | \Psi_0^{(0)} \rangle^{-1} \langle \Psi_0^{(0)} | [\mathbf{h}^\dagger, \hat{\mu}_j] | \Psi_0^{(0)} \rangle \quad (5)$$

where $\hat{H}^{(0)}$ is the unperturbed Hamiltonian of the system and $\{h_n\}$ denotes a complete set of excitation and de-excitation operators, arranged as column vector $\mathbf{h}$ or as row vector $\tilde{\mathbf{h}}$. Completeness of the set of operators $\{h_n\}$ means that all possible excited states $|\Psi_n^{(0)}\rangle$ of the system must be generated by operating on $|\Psi_0^{(0)}\rangle$, i.e., $h_n|\Psi_0^{(0)}\rangle = |\Psi_n^{(0)}\rangle$.

In SOPPA [5] a Møller–Plesset perturbation theory expansion of the wave function [28,48] is employed:

$$|\Psi_0^{(0)}\rangle \approx N(|\Phi_{\mathrm{SCF}}\rangle + |\Phi^{(1)}\rangle + |\Phi^{(2)}\rangle + \cdots)$$

$$= N\left(|\Phi_{\mathrm{SCF}}\rangle \frac{1}{4} \sum_{\substack{ai \\ bj}} {}^{(1)}\kappa_{ij}^{ab} |\Phi_{ij}^{ab}\rangle + \sum_{ai} {}^{(2)}\kappa_i^a |\Phi_i^a\rangle + \cdots\right) \quad (6)$$

where $|\Phi_i^a\rangle$ and $|\Phi_{ij}^{ab}\rangle$ are Slater determinants obtained by replacing the occupied orbitals i and j in the Hartree–Fock determinant $|\Phi_{\mathrm{SCF}}\rangle$ by the virtual orbitals a and b; ${}^{(1)}\kappa_{ij}^{ab}$, ${}^{(2)}\kappa_i^a$, are the so-called Møller–Plesset correlation coefficients and N is a normalization constant. The set of operators $\{h_n\}$ consists of single and double excitation and de-excitation operators. All matrix elements involving single (de-)excitation operators in equation (5) are then evaluated to second order in the fluctuation potential, which is the difference between the instantaneous interaction of the electrons and the averaged interaction as used in the Hartree–Fock approximation. Matrix elements with single and double (de-)excitation operators are evaluated to first order and pure double (de-)excitation matrix elements only to zeroth order. With this definition of SOPPA only the single excited terms in the second-order correction to the wavefunction are needed. The SOPPA method gives excitation energies and transition moments correct to second order [49–51], whereas response functions like the frequency-dependent polarizability are correct through second order [5], meaning that in addition to all second-order terms also some higher order terms are included. The SOPPA response function, however, is not the response of a second-order wavefunction [13].

In the SOPPA(CCSD) method [36] the Møller–Plesset correlation coefficients ${}^{(1)}\kappa_{ij}^{ab}$ and ${}^{(2)}\kappa_i^a$ are replaced in all SOPPA matrix elements by the corresponding coupled cluster singles and doubles amplitudes τ_{ij}^{ab} and τ_i^a, whereas in the earlier CCSDPPA method [52,53] only some of the Møller–Plesset correlation coefficients were replaced. Although SOPPA(CCSD) is based on a CCSD wavefunction, it is still only correct through second order and not the linear

response of a CCSD wavefunction [37]. Since the MP2 correlation coefficients are the result of the first iteration for the CCSD amplitudes, the CCSD amplitudes give a more accurate description of the connected doubles contribution to electron correlation. Thus it may be expected that SOPPA(CCSD) gives a better description of electron correlation than SOPPA.

In MCSCF response theory [32] the reference state is approximated by a MCSCF wavefunction

$$|\Psi_0^{(0)}\rangle \approx |\Phi_{\text{MCSCF}}\rangle = \sum_i |\Phi_i\rangle C_{i0} \tag{7}$$

where $\{|\Phi_i\rangle\}$ are configuration state functions. The set of operators $\{h_n\}$ contains in addition to the non-redundant single excitation and de-excitation operators, i.e., the so-called orbital rotation operators [54], state transfer operators $\{R^\dagger, R\}$, which are defined as

$$R_n^\dagger = |\Phi_n\rangle\langle\Phi_{\text{MCSCF}}| \tag{8}$$

where $|\Phi_n\rangle = \sum_i |\Phi_i\rangle C_{in}$ are the orthogonal complement states of the MCSCF state. In this study we have used CAS [38] as well as RAS [39] wavefunctions in the MCSCF linear response calculations. Throughout the paper we use for the description of an active space the notation [55] $(n_{A1}, n_{B2}, n_{B1}, n_{A2})$, where n_Γ is the number of orbitals in the irreducible representation Γ of the C_{2v} point group. Furthermore, we will denote a CASSCF calculation by $^{\text{inactive}}\text{CAS}^{\text{active}}$ and a RASSCF calculation by $^{\text{inactive}}_{\text{RAS1}}\text{RAS}^{\text{RAS2}}_{\text{RAS3}}$.

The last method used in this study is CCSD linear response theory [37]. The frequency-dependent polarizabilities are again identified from the time evolution of the corresponding moments. However, in CCSD response theory the moments are calculated as transition expectation values between the coupled cluster state $|\Phi_{\text{CC}}^{(0)}(t)\rangle$ and a dual state $\langle\Phi_\Lambda^{(0)}(t)|$

$$\mu_i(t) = \langle\Phi_\Lambda^{(0)}(t)|\hat{\mu}_i|\Phi_{\text{CC}}^{(0)}(t)\rangle \tag{9}$$

$$\Theta_{ij}(t) = \langle\Phi_\Lambda^{(0)}(t)|\hat{\Theta}_{ij}|\Phi_{\text{CC}}^{(0)}(t)\rangle \tag{10}$$

Again, the coefficients describing the time dependence of the approximate coupled cluster wavefunctions $|\Phi_{\text{CC}}^{(0)}(t)\rangle$ and $\langle\Phi_\Lambda^{(0)}(t)|$ are expanded in the perturbation and are determined from the coupled cluster time-dependent Schrödinger equation. The frequency-dependent polarizability is then obtained from the linear term in the perturbation in the expansion of equation (10).

The isotropic dipole polarizability α, the dipole polarizability anisotropy $\Delta\alpha$ and the isotropic traceless quadrupole polarizability C are defined as

$$\alpha = \frac{1}{3}(\alpha_{xx} + \alpha_{yy} + \alpha_{zz}) \tag{11}$$

$$\Delta\alpha = \frac{1}{2}\sqrt{(\alpha_{xx} - \alpha_{yy})^2 + (\alpha_{yy} - \alpha_{zz})^2 + (\alpha_{zz} - \alpha_{xx})^2} \qquad (12)$$

$$C = \frac{1}{10}(8C_{xx,xx} + 8C_{xz,xz} + C_{zz,zz}) \qquad (13)$$

The methods described above are all based on the Born–Oppenheimer approximation. Therefore, they can be used to calculate polarizabilities of diatomic molecules for a given internuclear distance R. However, if one is interested in values of the polarizability tensors, α^v and C^v, for a particular vibrational state $|\Theta_{v,J}(R)\rangle$, one has to average the polarizability radial functions $\alpha(R)$ and $C(R)$ with the vibrational wavefunction $|\Theta_{v,J}(R)\rangle$, i.e., one has to calculate the following expectation value [56]

$$\alpha_{ij}^v = \langle\Theta_{v,J}|\alpha_{ij}(R)|\Theta_{v,J}\rangle \qquad (14)$$

For the vibrational ground state with quantum number $v=0$ the averaged polarizabilities are often expressed as the sum of the polarizability at an equilibrium geometry, R_e, and a zero-point-vibrational correction (ZPVC)

$$\alpha_{ij}^{v=0} = \alpha_{ij}(R_e) + \Delta\alpha_{ij}^{ZPVC} \qquad (15)$$

For diatomic molecules the vibrational wavefunctions can be obtained numerically as solution of the one-dimensional Schrödinger equation

$$\left\{-\frac{\hbar^2}{2\mu}\left(\frac{d^2}{dR^2} + \frac{J(J+1)}{R^2}\right) + \frac{e^2}{4\pi\varepsilon_0}\frac{Z_K Z_L}{R} + E_0(R)\right\}|\Theta_{v,J}\rangle = E_{v,J}|\Theta_{v,J}\rangle \qquad (16)$$

where J is the rotational quantum number and $E_0(R)$ is the electronic energy. The vibrational averaging in equation (14) can then be carried out numerically, if one calculates the polarizability pointwise as a function of the internuclear distance R.

3. RESULTS AND DISCUSSION

3.1. LiH

3.1.1. MCSCF radial functions

The dipole and quadrupole polarizability tensor components of LiH were calculated by MCSCF linear response theory with the basis set of Roos and Sadlej [57] which consists of 13s-, 8p-, 6d-, and 2f-type sets of uncontracted Gaussian functions on Li and 12s-, 8p-, and 5d-type sets of uncontracted Gaussians on H. Due to the small size of the molecule we could perform MCSCF calculations over the whole range of internuclear distances with a very large CAS ^{0000}CAS^{20,10,10,4}. In Fig. 1, we present the tensor components, isotropic, and anisotropic values of the dipole polarizability tensor α as function
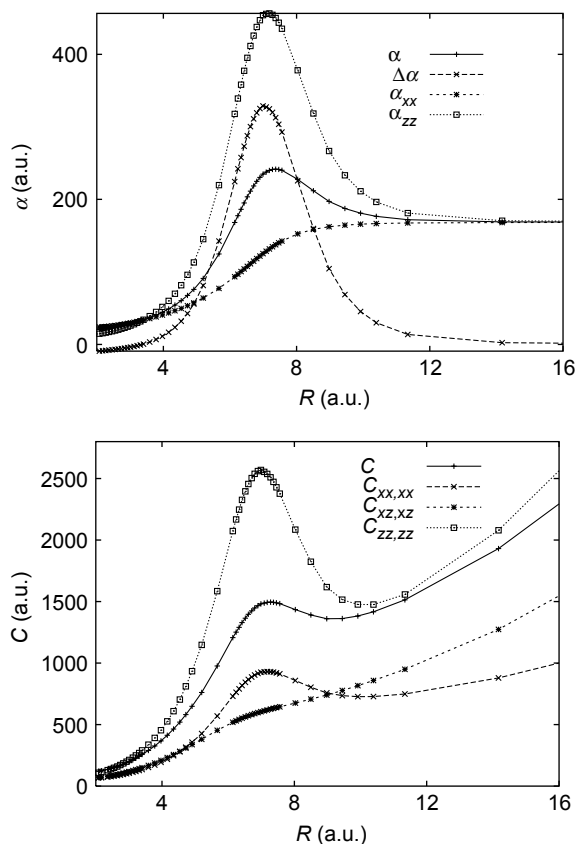
Fig. 1. LiH: dipole and quadrupole polarizability tensor radial function (in atomic units) calculated with a $^{0000}CAS^{20,10,10,4}$ wavefunction.

of the internuclear distance R. The components and the isotropic value of quadrupole polarizibility tensor C are also shown in Fig. 1. The corresponding numerical data are available on request from the authors.

The dipole polarizability curves are in excellent agreement with recently published values of Mérawa *et al.* [58] which were obtained with the time-dependent gauge invariant method and at the CCSD[T] level. Our values at the equilibrium internuclear distance $R_e = 3.014$ a.u., $\alpha_{xx} = 28.94$ a.u. and $\alpha_{zz} = 24.52$ a.u. are also in good agreement with R12-CCSD(T) results by Tunega and Noga [59] at $R_e = 3.015$ a.u.: $\alpha_{xx} = 29.57$ a.u. and $\alpha_{zz} = 25.79$ a.u. The results for the traceless quadrupole polarizability tensor calculated at the equilibrium internuclear distance, $C_{xx,xx} = 105.6$ a.u., $C_{xz,xz} = 118.3$ a.u. and $C_{zz,zz} = 212.6$ a.u., are similarly in good agreement with the earlier values of Bishop and Lam [60] obtained by a point charge technique at the MCSCF level using a smaller basis set: $C_{xx,xx} = 94$ a.u., $C_{xz,xz} = 118$ a.u., and $C_{zz,zz} = 222$ a.u.

Table 1. LiH: calculated values of the dipole and quadrupole polarizability (in atomic units) in the vibrational state v

v	α_{xx}^{v}	α_{zz}^{v}	α^{v}	$\Delta\alpha^{v}$	$C_{xx,xx}^{v}$	$C_{xz,xz}^{v}$	$C_{zz,zz}^{v}$	C^{v}
0	30.240	27.212	29.231	3.029	110.12	123.07	224.70	209.02
1	31.391	29.867	30.883	1.524	119.38	132.70	250.08	226.67
2	32.628	32.906	32.721	-0.278	129.62	143.01	278.52	245.96
3	33.962	36.418	34.781	-2.456	141.04	154.09	310.54	267.15
4	35.407	40.512	37.109	-5.105	153.82	165.99	346.68	290.51
5	36.975	45.285	39.745	-8.310	168.07	178.68	387.47	316.14
6	38.687	50.897	42.757	-12.210	184.04	192.25	433.70	344.40
7	40.572	57.576	46.240	-17.004	202.08	206.77	486.40	375.72
8	42.652	65.542	50.282	-22.890	222.46	222.24	546.50	410.41
9	44.966	75.116	55.016	-30.149	245.61	238.72	615.31	449.00
10	47.558	86.666	60.594	-39.109	271.96	256.26	694.26	492.01
11	50.484	100.632	67.200	-50.149	302.02	274.90	784.82	540.02
12	53.818	117.454	75.030	-63.636	336.16	294.69	888.12	593.49
13	57.643	137.586	84.291	-79.944	374.77	315.62	1004.96	652.81
14	62.084	161.545	95.238	-99.461	418.42	337.90	1136.24	718.68
15	67.285	189.312	107.961	-122.027	466.84	361.65	1279.62	790.75
16	73.449	220.069	122.322	-146.620	518.75	387.21	1429.17	867.69
17	80.814	252.139	137.922	-171.324	572.40	415.24	1575.66	947.67
18	89.731	281.911	153.791	-192.180	624.03	446.89	1701.28	1026.87
19	100.436	302.831	167.901	-202.395	667.36	483.75	1779.98	1098.89
20	113.437	308.296	178.390	-194.859	697.95	530.54	1790.18	1161.81
21	129.479	289.805	182.921	-160.326	711.16	598.61	1708.54	1218.67
22	147.875	241.192	178.981	-93.317	713.52	720.00	1569.54	1303.77

Calculated from the ^{0000}CAS^{20,10,10,4} polarizability radial functions and the ^{0000}CAS^{20,10,10,4} potential energy curve.

3.1.2. MCSCF vibrational averaging

In Table 1 the predicted dipole and quadrupole polarizability tensor components α_{ij}^{v} and $C_{ij,kl}^{v}$ for the vibrational states with quantum number v are given. They were calculated for all vibrational states supported by the potential energy function as expectation values of the polarizability radial functions $\alpha(R)$ and $C(R)$ over the vibrational wavefunction $|\Theta_{v,J}(R)\rangle$ (equation (14)). The latter were obtained from the one-dimensional Schrödinger equation for nuclear motion, equation (16) using the Cooley-Numeral technique [61]. The dependence of the vibrationally averaged polarizability tensors, α^{v} and C^{v}, on the vibrational quantum number v is illustrated in Fig. 2. It is interesting to note that the parallel components of the polarizabilities exhibit a maximum in the vibrational state $v=20$ which reflects the maximum in the radial functions in Fig. 1.

3.1.3. Comparison of linear response methods

The results of our very large MCSCF calculations can be used to benchmark the performance of other methods in the calculation of ZPVCs. Single configuration
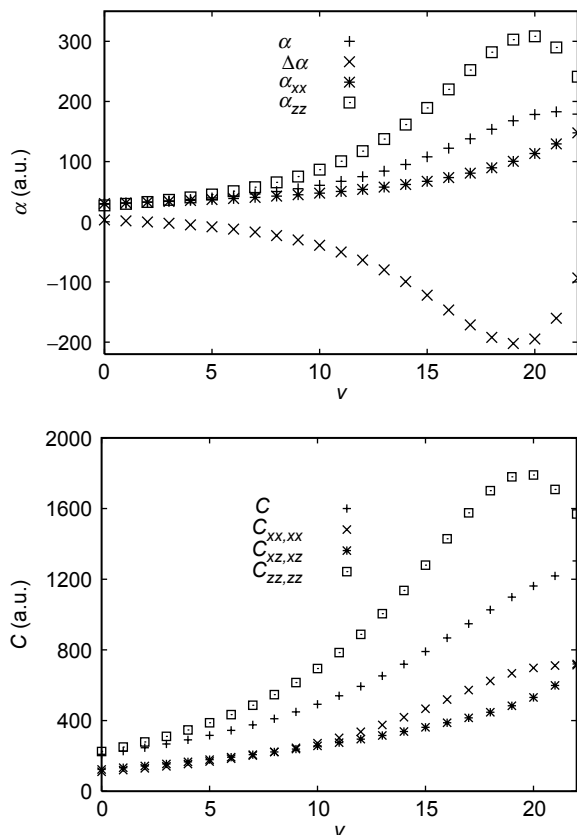
Fig. 2. LiH: dependence of the dipole and quadrupole polarizability tensor (in atomic units) on the vibrational quantum number v. Calculated from the ^{0000}CAS^{20,10,10,4} polarizability radial function and the ^{0000}CAS^{20,10,10,4} potential energy curve.

based methods as SOPPA, SOPPA(CCSD) and CCSD although not suitable for calculations at large internuclear distances, should perform well in the vicinity of the equilibrium internuclear distance. Furthermore, we can investigate the dependence of the ZPVCs on the methods employed for the calculation of the polarizability radial functions and for the PEC used in the solution of the nuclear Schrödinger equation (16). We have, therefore, performed two sets of vibrational averaging calculations where we used

(a) the vibrational wavefunction obtained from the ^{0000}CAS^{20,10,10,4} PEC together with polarizability radial functions obtained not only in ^{0000}CAS^{20,10,10,4} linear response, but also SOPPA, SOPPA(CCSD) and CCSD calculations. The results of these calculations are denoted with a superscript 'MCSCF' or as MCSCF/SOPPA, MCSCF/SOPPA(CCSD) and MCSCF/CCSD in the following.
(b) vibrational wavefunctions obtained from PEC calculated with the same (or associated) methods as the polarizability radial functions. For SOPPA, we

used thus the MP2 PEC and for SOPPA(CCSD) and CCSD the CCSD PEC. In the following these results are identified with the superscript 'own'.

In Table 2 we have collected values for the different equilibrium geometries, for the vibrational ground state and the corresponding ZPVCs obtained in this way. Several important conclusions can be drawn from these results.

There is almost no difference between the ZPVCs obtained with the CCSD and with the $^{0000}CAS^{20,10,10,4}$ PEC, nor between $P(R_e^{own})$ and $P(R_e^{MCSCF})$ for the SOPPA(CCSD) and CCSD polarizabilities. This shows that the CCSD and $^{0000}CAS^{20,10,10,4}$ PEC are very similar in the vicinity of the equilibrium geometry and that the respective equilibrium internuclear distances are almost

Table 2. LiH: dipole and quadrupole polarizability (in atomic units) for the vibrational ground state $v=0$ calculated with different response theory methods. $P(R_e)$ is the value at the minimum of the potential energy curve, $P_{0,0}$ is the value in the vibrational ground state and $\text{ZPVC} = P_{0,0} - P(R_e)$ is the corresponding zero-point-vibrational correction

	$P(R_e^{own})$	$P(R_e^{MCSCF})$	$P_{0,0}^{own}$	$P_{0,0}^{MCSCF}$	ZPVC^{own}	ZPVC^{MCSCF}
SOPPA						
α_{xx}	27.263	27.351	27.697	27.804	0.434	0.453
α_{zz}	23.513	23.685	24.463	24.678	0.950	0.993
$C_{xx,xx}$	98.928	99.619	102.854	103.728	3.926	4.109
$C_{xz,xz}$	113.510	114.340	117.997	119.026	4.487	4.686
$C_{zz,zz}$	203.330	205.210	214.453	216.862	11.123	11.652
SOPPA(CCSD)						
α_{xx}	27.484	27.483	27.955	27.955	0.471	0.472
α_{zz}	23.968	23.966	24.994	24.994	1.026	1.028
$C_{xx,xx}$	100.790	100.790	104.871	104.870	4.081	4.080
$C_{xz,xz}$	114.160	114.150	118.705	118.704	4.545	4.554
$C_{zz,zz}$	204.190	204.180	215.422	215.418	11.232	11.238
CCSD						
α_{xx}	29.642	29.641	30.190	30.190	0.548	0.549
α_{zz}	25.941	25.940	27.155	27.155	1.214	1.215
$C_{xx,xx}$	105.680	105.680	110.026	110.025	4.346	4.345
$C_{xz,xz}$	118.380	118.380	122.987	122.985	4.607	4.605
$C_{zz,zz}$	212.820	212.810	224.628	224.624	11.808	11.814
$^{0000}\mathbf{CAS^{20,10,10,4}}$						
α_{xx}	29.690		30.240		0.550	
α_{zz}	25.991		27.212		1.221	
$C_{xx,xx}$	105.770		110.118		4.348	
$C_{xz,xz}$	118.460		123.067		4.607	
$C_{zz,zz}$	212.900		224.000		11.100	

$P(R_e^{own})$, $P_{0,0}^{own}$, and $\text{ZPVC}^{own} = P_{0,0}^{own} - P(R_e^{own})$ were obtained from the polarizability radial functions and PEC calculated with the same method, whereas for $P(R_e^{MCSCF})$, $P_{0,0}^{MCSCF}$, and $\text{ZPVC}^{MCSCF} = P_{0,0}^{MCSCF} - P(R_e^{MCSCF})$ the $^{0000}CAS^{20,10,10,4}$ potential energy curve was used.

identical. On the other hand, there are larger differences between ZPVC^{MP2} and ZPVC^{MCSCF} and between $P(R_e^{MP2})$ and $P(R_e^{MCSCF})$ obtained at the SOPPA level. Furthermore, the MP2/SOPPA results deviate from the ^{0000}CAS^{20,10,10,4} ZPVC by about 3–22% with the exception of $C_{zz,zz}$. The agreement is slightly improved in the MCSCF/SOPPA averaging calculation with a deviation of 2–19%. Altogether this indicates that the MP2 PEC is not good enough even in the vicinity of the equilibrium geometry.

The ZPVC obtained from the CCSD and ^{0000}CAS^{20,10,10,4} polarizability radial functions are almost identical with the exception of the ZPVC for $C_{zz,zz}$. This shows that not only the CCSD PEC around the equilibrium geometry, but also the CCSD polarizability curves are very similar to the ^{0000}CAS^{20,10,10,4} curves.

The SOPPA(CCSD) results, obtained with the CCSD or the ^{0000}CAS^{20,10,10,4} PEC, are in general in better agreement with the ^{0000}CAS^{20,10,10,4} results than the pure SOPPA results. This applies to the equilibrium geometry results as well as to the vibrational averaged results. This shows that SOPPA(CCSD) performs better in the calculation of polarizabilities for LiH than SOPPA as might have been expected [36,41].

3.2. HF

3.2.1. Choice of one-electron basis set

An extensive study of the basis set effects on static dipole polarizabilities of the diatomic molecules N_2, CO, HF, HCl, and Cl_2, at the equilibrium nuclear geometry was recently published by Pecul and Rizzo [62]. They employed the CCSD linear response method. Basis set effects were previously also discussed by Christiansen *et al.* [63] and Dalskov [41]. We have extended the previous analysis of the basis set effects on the dipole and quadrupole polarizabilities to cover also larger internuclear distances $2R_e$ and $4R_e$ in addition to the equilibrium internuclear distance R_e. The dipole and quadrupole polarizabilities were calculated at these three internuclear distances using MCSCF linear response theory with different active spaces (see the next paragraph) and the series of correlation consistent basis sets [64–66] increasing from the daug-cc-pVDZ to the aug-cc-pV5Z basis set. Representative results obtained with the ^{1000}CAS^{8441} wave function are summarized in Table 3. We can see that in general the doubly augmented basis sets give larger values of the polarizabilities and that the gap between the augmented and doubly augmented basis sets decreases going from triple ζ to quadruple ζ. Furthermore, there are only small differences between the daug-cc-pVTZ and daug-cc-pVQZ results. We conclude thus that the daug-cc-pVQZ basis set is well converged and we use it, therefore, in all the following calculations.

3.2.2. Choice of active space

The choice of the active spaces for the MCSCF calculations on HF was based on the natural orbital occupancy numbers obtained in MP2 calculations

Table 3. HF: dependence of the polarizability tensors (in atomic units) on the basis sets used in the ^{1000}CAS^{8441} calculations for three internuclear distances

R	Basis set	α_x	α_z	C_{xx}	C_{xz}	C_{zz}
1.7328 a.u.	aug-cc-pVTZ	4.928	6.292	24.228	35.697	58.960
(R_e)	aug-cc-pVQZ	5.123	6.332	26.860	38.735	62.435
	aug-cc-pV5Z	5.186	6.340	28.338	39.704	63.616
	daug-cc-pVDZ	5.479	6.157	13.332	10.493	22.396
	daug-cc-pVTZ	5.269	6.336	28.861	40.227	64.110
	daug-cc-pVQZ	5.237	6.345	30.440	40.571	64.556
3.5 a.u.	aug-cc-pVTZ	7.229	25.194	109.65	133.21	386.91
($2R_e$)	aug-cc-pVQZ	7.446	25.533	142.67	116.78	405.03
	aug-cc-pV5Z	7.500	25.658	119.93	146.12	409.63
	daug-cc-pVDZ	7.626	25.774	109.62	146.67	402.06
	daug-cc-pVTZ	7.620	25.332	120.38	150.53	406.23
	daug-cc-pVQZ	7.575	25.584	123.74	150.31	413.80
7.0 a.u.	aug-cc-pVTZ	8.139	8.063	173.55	5065.6	645.27
($4R_e$)	aug-cc-pVQZ	8.286	8.278	188.05	5227.8	690.57
	aug-cc-pV5Z	8.307	8.264	190.74	5124.6	691.63
	daug-cc-pVDZ	8.266	8.260	174.65	5546.9	676.44
	daug-cc-pVTZ	8.423	8.337	196.13	5248.3	703.55
	daug-cc-pVQZ	8.336	8.299	196.26	5331.6	700.62

[67,68] at the experimental equilibrium internuclear distance $R_e = 1.7328$ a.u. and at $2R_e$. Calculations were performed with the daug-cc-pVTZ, aug-cc-pVQZ, and daug-cc-pVQZ basis sets in order to check the above conclusions with other MCSCF wavefunctions. The 1σ orbital was kept frozen in all calculations. The MP2 occupancy numbers suggested for all the basis sets considered that the active space should contain the (7,3,3,1), (8,4,4,1) or (9,5,5,2) orbitals. Static polarizabilities calculated with these active spaces, ^{1000}CAS^{7331}, ^{1000}CAS^{8441} and ^{1000}CAS^{9552}, and the daug-cc-pVQZ basis set at three internuclear distances are compared in Table 4. We can see that there are much larger differences between the ^{1000}CAS^{7331} and ^{1000}CAS^{8441} results than between the ^{1000}CAS^{8441} and ^{1000}CAS^{9552} polarizabilities, where the largest difference is only 1.4%. Therefore, we consider the ^{1000}CAS^{9552} to cover most of the correlation effects and estimate the remaining correlation error to be not larger than about 1.5%.

Our best results for the dipole and quadrupole polarizability tensor radial functions of HF, obtained with the daug-cc-pVQZ and the ^{1000}CAS^{9552} wavefunction, are presented in Fig. 3.

Although large CAS calculations are possible for HF, they will not be feasible for the heavier molecules which we want to study in the future. For these molecules one has to resort to the RAS method [39]. One possible approach is to divide the active space of the ^{1000}CAS^{9552} calculation into the orbitals doubly occupied in the Hartree–Fock wavefunction (2,1,1,0) and the remaining unoccupied orbitals (7,4,4,1). The doubly occupied orbitals will then span the RAS2 space whereas the unoccupied orbitals are included in a RAS3 space.

Table 4. HF: dependence of the polarizability tensors (in atomic units) on the number of active orbitals employed in the ^{1000}CAS$^{\text{active}}$-MCSCF calculations using the daug-cc-pVQZ basis set at three internuclear distances

CAS	R	α_x	α_z	$C_{xx,zz}$	$C_{xz,xz}$	$C_{zz,zz}$
^{1000}CAS^{7331}	1.733	5.0310	6.155	29.685	39.689	21.127
^{1000}CAS^{8441}		5.2371	6.345	10.147	13.524	21.519
^{1000}CAS^{9552}		5.2320	6.285	10.088	13.546	21.372
^{1000}CAS^{7331}	3.000	6.8278	21.809	31.230	37.326	99.742
^{1000}CAS^{8441}		7.0577	20.167	30.506	38.542	95.945
^{1000}CAS^{9552}		7.0062	19.977	30.229	38.026	95.139
^{1000}CAS^{7331}	7.000	8.2296	8.380	66.780	1789.108	239.345
^{1000}CAS^{8441}		8.3362	8.299	65.419	1777.327	233.541
^{1000}CAS^{9552}		8.3127	8.320	65.732	1777.306	234.928
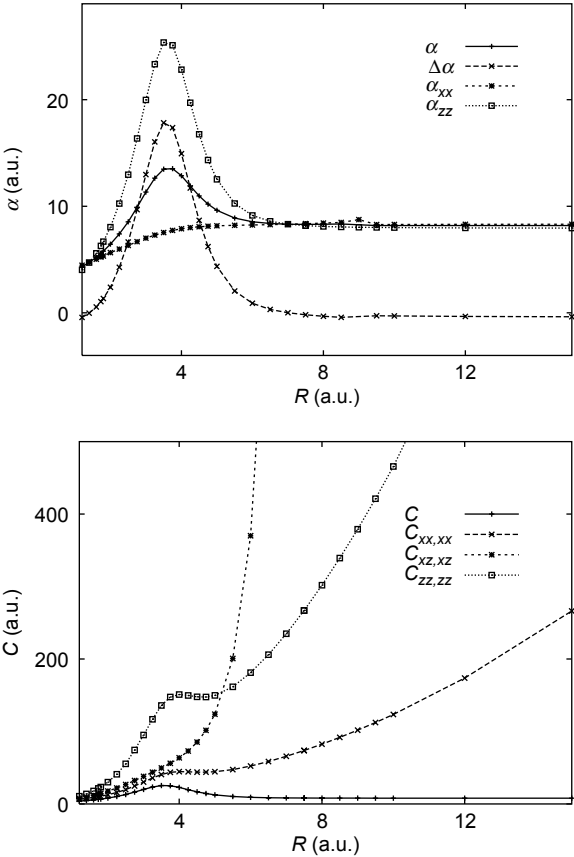
Fig. 3. HF: dipole and quadrupole polarizability tensors (in atomic units) calculated at the ^{1000}CAS^{9552} level with the daug-cc-pVQZ basis set.

The issue to be investigated is now how many electrons should be allowed to be excited from RAS2 to RAS3 in order to reproduce the results of the $^{1000}CAS^{9552}$ calculation with the $^{1000}RAS^{2110}_{7442}$ wavefunction. The results of such a study using the daug-cc-pVQZ basis set are shown in Table 5 and Fig. 4. The calculations with single and double excitations from RAS2 to RAS3 differ substantially from the CAS results, especially for the C tensor, however, the calculations with singles, doubles, and triples excitations to RAS3 give radial functions which are already very close to the $^{1000}CAS^{9552}$ results. Finally, the calculations with up to four electrons distributed over the orbitals in RAS3 give polarizability curves which are practically identical to the results of the $^{1000}CAS^{9552}$ calculations.

From the results presented in Figs 3 and 4 and unpublished results we can conclude, that for sufficiently large one-electron basis set, i.e., at least of aug-cc-pVQZ quality, and active spaces such as $^{1000}CAS^{8441}$ or $^{1000}RAS^{2110}_{7442}-SDT$ the general shape of the polarizability curves is reproduced. The different radial functions for the α components and for $C_{xx,xx}$ and $C_{zz,zz}$ are very close to each other over the whole interval of internuclear instances, whereas for $C_{xz,xz}$ this is only the case for distances up to $R=6$ a.u., after which the results obtained with the various models differ substantially. We expect that the findings of this comparative study will be useful for the calculation of property curves for heavier diatomic molecules, where the RAS approach is the only feasible one.

At this point we should mention that we encountered instability problems in the linear response calculations for some of the MCSCF wavefunctions at internuclear distances larger than $R=8$ a.u. We believe those instabilities to be artifacts of the calculations because their existence or position depends on the choice of basis set, active space or number of electrons allowed in the RAS3 space. This implies that even though it might not be possible to generate

Table 5. HF: dependence of the $^{1000}RAS^{2110}_{7442}$ results (in atomic units) on the number of electrons allowed in RAS3

RAS3 electrons	R	α_x	α_z	$C_{xx,xx}$	$C_{xz,xz}$	$C_{zz,zz}$
2	1.733	5.0484	6.138	9.779	13.150	20.874
3		5.1929	6.255	10.022	13.447	21.262
4		5.2240	6.278	10.074	13.527	21.349
8, i.e., CAS^{9552}		5.2320	6.285	10.088	13.546	21.372
2	3.50	7.3386	26.274	44.182	48.952	150.230
3		7.4404	25.663	40.526	48.721	135.730
4		7.5185	25.353	40.696	49.507	136.035
8, i.e., CAS^{9552}		7.5358	25.369	40.671	49.664	135.887
2	6.00	8.3289	27.390	105.040	391.009	151.387
3		8.1559	9.062	51.421	366.882	178.045
4		8.2163	9.128	52.041	356.483	180.282
8, i.e., CAS^{9552}		8.2444	9.141	52.276	370.040	181.129

Comparison is made at three internuclear distances using the daug-cc-pVQZ basis set.
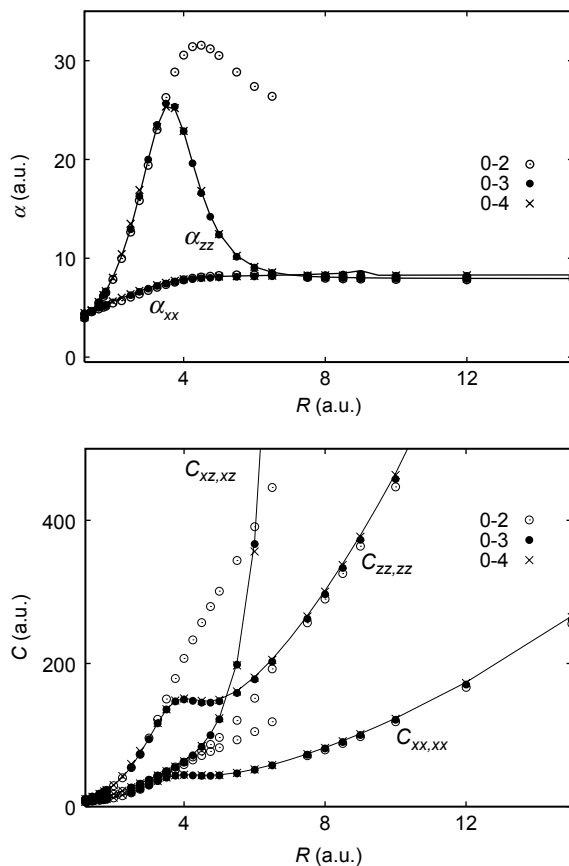
Fig. 4. HF: dipole and quadrupole polarizability tensors (in atomic units) calculated with a $^{1000}RAS^{2110}_{7442}$ wavefunction with 0–2, 0–3, and 0–4 electrons in RAS3 in comparison with the $^{1000}CAS^{9552}$ results (solid line). The daug-cc-pVQP basis set is used.

a smooth polarizability radial function for large internuclear distances from a single combination of basis set and active space, it is possible to do it piecewise. Despite this problem, we believe that the goal of our calculations at very large distances – to justify the results of semi-empirical models [69] – can be achieved.

3.2.3. Radial function and vibrational averaging

We have vibrationally averaged the $^{1000}CAS^{9552}$/daug-cc-pVQZ dipole and quadrupole polarizability tensor radial functions (equation (14)) with two different sets of vibrational wavefunctions $|\Theta_{v,J}(R)\rangle$. One was obtained by solving the one-dimensional Schrödinger equation for nuclear motion (equation (16)) with the $^{1000}CAS^{9552}$/daug-cc-pVQZ PEC and the other with an experimental RKR curve [70]. Both potentials provide identical vibrational
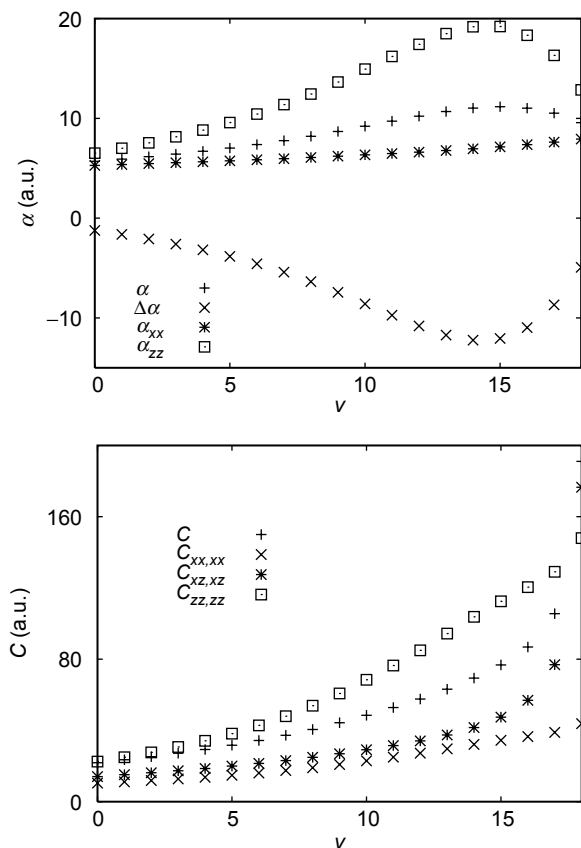
Fig. 5. HF: dependence of the dipole and quadrupole polarizability tensor (in atomic units) on the vibrational quantum number v. Calculated from the $^{1000}\text{CAS}^{9552}$ polarizability radial function and the $^{1000}\text{CAS}^{9552}$ potential energy curve.

wavefunctions for $v=0$–15. The components of the vibrationally averaged dipole and quadrupole polarizability tensors, α^v and C^v, are shown in Fig. 5 and in Table 6 as functions of the vibrational quantum number v. Similarly to LiH the zz component of the dipole polarizability goes through a maximum, whereas the xx component of the dipole polarizability and the three components of the quadrupole polarizability monotonically increase with the vibrational quantum number v.

3.2.4. Comparison of linear response methods

Very accurate values of the dipole and quadrupole polarizability for the equilibrium internuclear distance of HF can be found in a review article by Maroulis [71], calculated with finite-field Møller–Plesset perturbation theory at various orders and coupled cluster theory using a carefully selected basis set.

Table 6. HF: calculated values of the dipole and quadrupole polarizability (in atomic units) in the vibrational state v

v	α_{xx}^v	α_{zz}^v	α^v	$\Delta\alpha^v$	$C_{xx,xx}^v$	$C_{xz,xz}^v$	$C_{zz,zz}^v$	C^v
0	5.283	6.517	5.694	−1.234	10.433	14.085	22.541	21.869
1	5.376	7.002	5.918	−1.626	11.140	15.148	24.967	23.527
2	5.463	7.550	6.159	−2.087	11.910	16.233	27.667	25.281
3	5.552	8.157	6.420	−2.605	12.768	17.388	30.714	27.196
4	5.645	8.824	6.705	−3.179	13.731	18.640	34.173	29.314
5	5.745	9.581	7.024	−3.835	14.839	20.011	38.201	31.700
6	5.850	10.432	7.378	−4.582	16.097	21.493	42.823	34.354
7	5.961	11.377	7.766	−5.417	17.492	23.099	48.004	37.273
8	6.079	12.442	8.200	−6.363	19.069	24.888	53.902	40.555
9	6.208	13.646	8.687	−7.438	20.888	26.913	60.751	44.316
10	6.343	14.940	9.209	−8.597	22.917	29.146	68.447	48.495
11	6.476	16.210	9.720	−9.735	25.015	31.493	76.462	52.853
12	6.615	17.418	10.216	−10.803	27.242	34.150	84.994	57.613
13	6.774	18.496	10.682	−11.722	29.697	37.456	94.401	63.162
14	6.948	19.177	11.025	−12.229	32.147	41.634	103.769	69.402
15	7.144	19.204	11.164	−12.060	34.450	47.481	112.493	76.794
16	7.366	18.332	11.021	−10.967	36.578	56.931	120.446	86.852
17	7.621	16.312	10.518	−8.691	38.897	76.926	129.079	105.566
18	7.925	12.856	9.569	−4.931	43.808	176.524	147.990	191.065

Calculated from the ^{1000}CAS^{9552} polarizability radial functions and the ^{1000}CAS^{9552} potential energy curve.

He also investigated the dependence of the properties on the internuclear distance in the vicinity of the equilibrium internuclear separation R_e. However, our goal was not to look for the most accurate values or to compare with them, but to study the performance of various linear response methods. In particular we wanted to find out which level of correlation is necessary in order to reproduce the correct dependence on the internuclear distance for a wider range of R. In Fig. 6, it can be seen that the CCSD dipole polarizability curve is sufficiently close to the results of the ^{1000}CAS^{9552} calculations. The SOPPA dipole polarizability curves, on the other hand, are in general too high, whereas the SOPPA(CCSD) curves are between the pure SOPPA and the CCSD curves, as one would hope for. The same can be said about the quadrupole polarizability tensor in Fig. 7.

In Table 7 we compare the ZPVCs for the dipole and quadrupole polarizabilities of HF. In the same way as for LiH, we have calculated the vibrational averages for each method with two different wavefunctions – one obtained from the PEC of the same or related method as used in the calculation of the property curve and the other obtained from the ^{1000}CAS^{9552} PEC. Compared with the equivalent results for LiH we observe significant differences between the calculations on the two molecules. First of all the vibrational corrections are smaller than in LiH but roughly in the same ratio as the polarizabilities. The influence of the PEC is larger than in LiH.
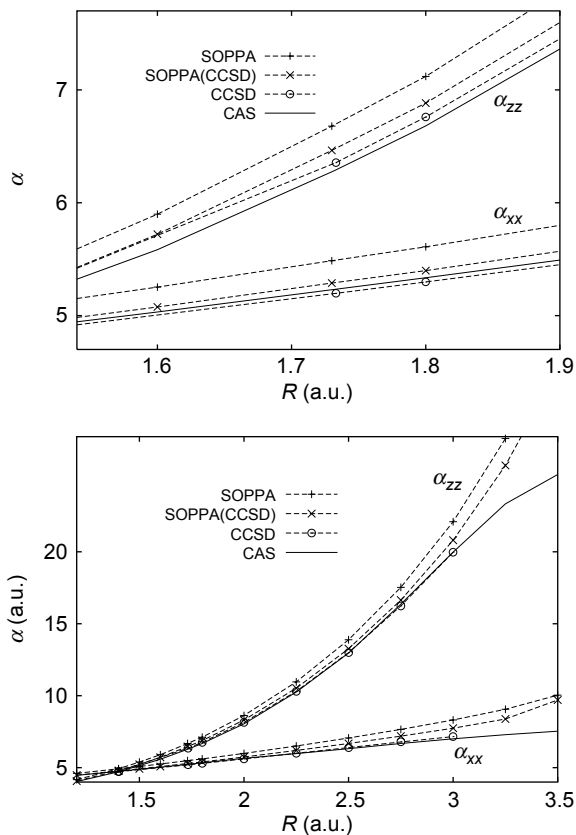
Fig. 6. HF: dipole polarizability tensors (in atomic units) calculated by different linear response methods in comparison with MCSCF method.

The MCSCF/CCSD ZPVC results, e.g., are in very close agreement with the MCSCF results. The maximum deviation in the ZPVC is about 4%, whereas, already the results of the pure CCSD calculations differ by more than 15%. Similar changes due to the change of the PEC are also observed for the SOPPA(CCSD) and SOPPA calculations. We can see the same effect also in the CCSD and SOPPA(CCSD) polarizability values for the minimum of the CCSD and MCSCF PEC. This indicates that the MCSCF and CCSD PEC are more different in the vicinity of the equilibrium geometry than it was the case for LiH. In general we note that the differences in the polarizability ZPVCs obtained with the same linear response method but with a different PEC are larger than the differences between two linear response methods but using the same PES. Furthermore, we find that the SOPPA(CCSD) results for the equilibrium geometry as well as vibrational state specific polarizabilities are again in better agreement with the MCSCF or CCSD values than the pure SOPPA results, as it was found for LiH.
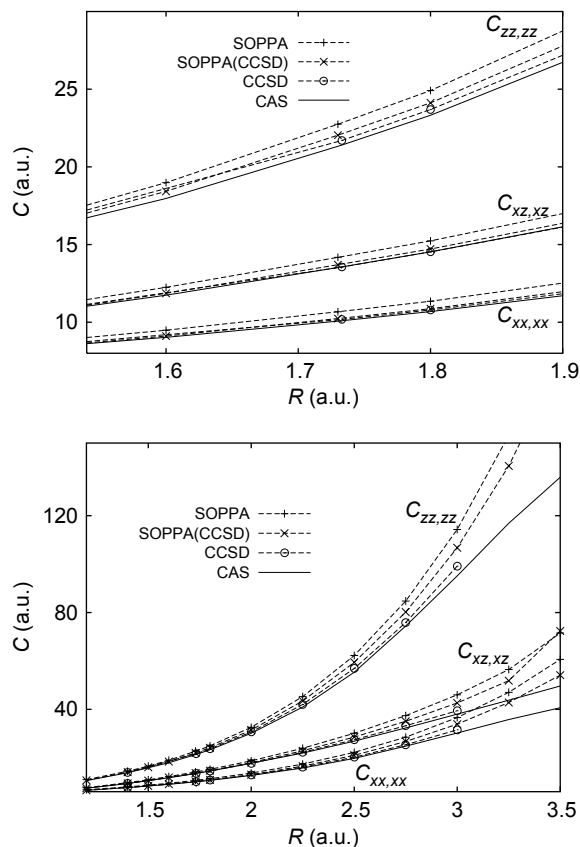
Fig. 7. HF: quadrupole polarizability tensor (in atomic units) calculated by different linear response methods in comparison with MCSCF method.

4. CONCLUSIONS

We report MCSCF calculations of the dipole and quadrupole polarizability tensor radial functions of LiH and HF for internuclear distance reaching from almost the unified atom to the dissociation limit. Large one-electron basis sets and MCSCF wavefunctions of the CAS type with large active spaces were employed in the calculations.

We have investigated the dependence of the polarizability radial functions on the one-electron basis set and the size of the CAS. We find that it is necessary to use basis sets of at least daug-cc-pVQZ quality for these properties. With respect to the size of the active space we observe very large differences between the results obtained with a (7331) and (8441) active space, but only small changes on increasing the active space to (9552). We conclude, therefore, that we recover the important correlation contributions with a $^{1000}\text{CAS}^{9552}$ wavefunction. Furthermore, we found that the results of the $^{1000}\text{CAS}^{9552}$ calculations can be reproduced with the much smaller $^{1000}\text{RAS}^{2110}_{7442}$ if one allows up to four electrons in RAS3.

Table 7. HF: dipole and quadrupole polarizability (in atomic units) for the vibrational ground state $v=0$ calculated with different response theory methods

	$P(R_e^{own})$	$P(R_e^{MCSCF})$	$P_{0,0}^{own}$	$P_{0,0}^{MCSCF}$	ZPVC^{own}	ZPVC^{MCSCF}
SOPPA						
α_{xx}	5.489	5.561	5.488	5.548	0.072	0.060
α_{zz}	6.688	6.978	6.686	6.935	0.290	0.250
$C_{xx,xx}$	10.717	10.713	11.145	11.079	0.428	0.366
$C_{xz,xz}$	14.240	14.234	14.879	14.774	0.639	0.540
$C_{zz,zz}$	22.881	22.869	24.296	24.086	1.415	1.217
SOPPA(CCSD)						
α_{xx}	5.279	5.344	5.290	5.343	0.065	0.053
α_{zz}	6.430	6.707	6.470	6.708	0.277	0.237
$C_{xx,xx}$	10.209	10.269	10.611	10.612	0.402	0.343
$C_{xz,xz}$	13.662	13.758	14.269	14.266	0.607	0.508
$C_{zz,zz}$	21.963	22.158	23.316	23.320	1.353	1.162
CCSD						
α_{xx}	5.193	5.250	5.203	5.249	0.056	0.046
α_{zz}	6.340	6.602	6.378	6.602	0.262	0.225
$C_{xx,xx}$	10.156	10.212	10.548	10.548	0.392	0.336
$C_{xz,xz}$	13.516	13.607	14.115	14.113	0.599	0.506
$C_{zz,zz}$	21.625	21.807	22.946	22.950	1.321	1.143
^{1000}CAS^{9552}						
α_{xx}	5.232		5.280		0.048	
α_{zz}	6.285		6.507		0.222	
$C_{xx,xx}$	10.097		10.433		0.336	
$C_{xz,xz}$	13.561		14.085		0.524	
$C_{zz,zz}$	21.401		22.541		1.140	

$P(R_e)$ is the value at the minimum of the potential energy curve, $P_{0,0}$ is the value in the vibrational ground state and ZPVC $= P_{0,0} - P(R_e)$ is the corresponding zero-point-vibrational correction. $P(R_e^{own})$, $P_{0,0}^{own}$, and ZPVC$^{own} = P_{0,0}^{own} - P(R_e^{own})$ were obtained from the polarizability radial functions and potential energy curves calculated with the same method, whereas for $P(R_e^{MCSCF})$, $P_{0,0}^{MCSCF}$, and ZPVC$^{MCSCF} = P_{0,0}^{MCSCF} - P(R_e^{MCSCF})$ the ^{1000}CAS^{9552} potential energy curve was used.

The calculated polarizability radial functions and corresponding MCSCF PEC were used to predict vibrational state specific dipole and quadrupole polarizability tensors for all vibrational states supported by the calculated PEC.

We have compared our MCSCF results for the vibrational ground state with CCSD, SOPPA, and SOPPA(CCSD) calculations. In particular we have investigated the importance of the PEC on the ZPVCs and find that there are significant differences between LiH and HF. In LiH the CCSD results for the ZPVC are very close to the MCSCF results independent on whether the CCSD or MCSCF PEC was employed. Similarly, the differences between SOPPA(CCSD) calculations with either the CCSD or the MCSCF energy surface are very small. In HF, on the other hand somewhat larger differences are found if the CCSD polarizabilities are averaged over the CCSD PEC and the difference between

SOPPA(CCSD) calculations with the CCSD or MCSCF PEC are also larger. In general the differences in the ZPVC are larger between the different PEC than between the different linear response methods. The SOPPA(CCSD) results for the equilibrium geometry as well as the vibrationally averaged polarizabilities are in both molecules in better agreement with the MCSCF results than the pure SOPPA values.

The polarizability radial functions obtained in this work can be used for the construction of semi-empirical PES necessary for molecular dynamics studies.

ACKNOWLEDGEMENTS

REFERENCES

[1] J. Oddershede, P. Jørgensen and N. H. F. Beebe, *J. Chem. Phys.*, 1975, **63**, 2996.
[2] P. Jørgensen, J. Oddershede and N. H. F. Beebe, *J. Chem. Phys.*, 1978, **68**, 2527.
[3] P. Jørgensen, J. Oddershede, P. Albertsen and N. H. F. Beebe, *J. Chem. Phys.*, 1978, **68**, 2533.
[4] E. N. Svendsen and J. Oddershede, *J. Chem. Phys.*, 1979, **71**, 3000.
[5] E. S. Nielsen, P. Jørgensen and J. Oddershede, *J. Chem. Phys.*, 1980, **73**, 6238.
[6] J. Oddershede and E. N. Svendsen, *Chem. Phys.*, 1982, **64**, 359.
[7] A. Jäpelt, E. N. Svendsen and J. Oddershede, in *Geometrical Derivatives of Energy Surfaces and Molecular Properties* (eds P. Jørgensen and J. Simons), Reidel, Dordrecht, 1986, p. 279.
[8] S. Canuto, W. Duch, J. Geertsen, F. Müller-Plathe, J. Oddershede and G. E. Scuseria, *Chem. Phys. Lett.*, 1988, **147**, 435.
[9] G. H. F. Diercksen, J. Oddershede, I. Paidarová and J. R. Sabin, *Int. J. Quantum Chem.*, 1991, **39**, 755.
[10] J. Geertsen, J. Oddershede and J. R. Sabin, *Mol. Phys.*, 1991, **72**, 1267.
[11] S. P. A. Sauer, G. H. F. Diercksen and J. Oddershede, *Int. J. Quantum Chem.*, 1991, **39**, 667.
[12] M. Feyereisen, J. Nichols, J. Oddershede and J. Simons, *J. Chem. Phys.*, 1992, **96**, 2978.
[13] J. Fagerström and J. Oddershede, *J. Chem. Phys.*, 1994, **101**, 10775.
[14] S. P. A. Sauer and J. Oddershede, *Int. J. Quantum Chem.*, 1994, **50**, 317.
[15] M. J. Packer, S. P. A. Sauer and J. Oddershede, *J. Chem. Phys.*, 1994, **100**, 8969.
[16] M. J. Packer, E. K. Dalskov, S. P. A. Sauer and J. Oddershede, *Theor. Chim. Acta*, 1994, **89**, 323.
[17] S. Kirpekar, J. Oddershede and H. J. Aa. Jensen, *J. Chem. Phys.*, 1995, **103**, 2983.
[18] E. K. Dalskov, H. J. Aa. Jensen and J. Oddershede, *Mol. Phys.*, 1997, **90**, 3.
[19] L. Visscher, T. Saue and J. Oddershede, *Chem. Phys. Lett.*, 1997, **274**, 181.
[20] E. K. Dalskov, J. Oddershede and D. M. Bishop, *J. Chem. Phys.*, 1998, **108**, 2152.
[21] S. P. Apell, J. R. Sabin, S. B. Trickey and J. Oddershede, *Int. J. Quantum Chem.*, 2002, **86**, 35.
[22] P. Piecuch, V. Špirko, A. E. Kondo and J. Paldus, *Mol. Phys.*, 1998, **94**, 55.
[23] S. P. J. Rodriques and A. J. C. Varandas, *Phys. Chem. Chem. Phys.*, 2000, **2**, 435.
[24] R. Cambi, D. Cappelletti, G. Liuti and F. Pirani, *J. Chem. Phys.*, 1991, **95**, 1952.
[25] A. Aquilanti, D. Cappelletti and F. Pirani, *Chem. Phys.*, 1996, **209**, 299.
[26] A. J. C. Varandas and S. P. J. Rodriques, *Chem. Phys. Lett.*, 1995, **245**, 66.
[27] G. Maroulis, *J. Chem. Phys.*, 2003, **118**, 2673.
[28] C. Møller and M. S. Plesset, *Phys. Rev.*, 1934, **46**, 618.

[29] J. A. Pople, J. S. Binkley and R. Seeger, *Int. J. Quantum Chem. Symp.*, 1976, **10**, 1.
[30] K. Raghavachari, G. W. Trucks, J. A. Pople and M. Head-Gordon, *Chem. Phys. Lett.*, 1989, **157**, 479.
[31] T. Helgaker, T. A. Ruden, P. Jørgensen, J. Olsen and W. Klopper, *J. Phys. Org. Chem.*, 2004, **17**, 913.
[32] J. Olsen and P. Jørgensen, *J. Chem. Phys.*, 1985, **82**, 3235.
[33] J. Oddershede, P. Jørgensen and D. L. Yeager, *Comput. Phys. Rep.*, 1984, **2**, 33.
[34] M. J. Packer, E. K. Dalskov, T. Enevoldsen, H. J. Aa. Jensen and J. Oddershede, *J. Chem. Phys.*, 1996, **105**, 5886.
[35] K. L. Bak, H. Koch, J. Oddershede, O. Christiansen and S. P. A. Sauer, *J. Chem. Phys.*, 2000, **112**, 4173.
[36] S. P. A. Sauer, *J. Phys. B: At. Mol. Opt. Phys.*, 1997, **30**, 3773.
[37] H. Koch and P. Jørgensen, *J. Chem. Phys.*, 1990, **93**, 3333.
[38] B. O. Roos, in *Ab Initio Methods in Quantum Chemistry – II. Advances in Chemical Physics* (ed. K. P. Lawley), Wiley, Chichester, 1987, p. 399.
[39] J. Olsen, B. O. Roos, P. Jørgensen and H. J. Aa. Jensen, *J. Chem. Phys.*, 1988, **89**, 2185.
[40] T. Helgaker, H. J. Aa. Jensen, P. Jørgensen, J. Olsen, K. Ruud, H. Ågren, A. A. Auer, K. L. Bak, V. Bakken, O. Christiansen, S. Coriani, P. Dahle, E. K. Dalskov, T. Enevoldsen, B. Fernandez, C. Hättig, A. Hald, K. Halkier, H. Heiberg, H. Hettema, D. Jonsson, S. Kirpekar, R. Kobayashi, H. Koch, K. V. Mikkelsen, P. Norman, M. J. Packer, T. B. Pedersen, T. A. Ruden, A. Sanchez, T. Saue, S. P. A. Sauer, B. Schimmelpfennig, K. O. Sylvester-Hvid, P. R. Taylor and O. Vahtras, DALTON, an electronic structure program, Release 1.2. http://www.kjemi.uio.no/software/dalton/dalton.html, 2001.
[41] E. K. Dalskov and S. P. A. Sauer, *J. Phys. Chem. A*, 1998, **102**, 5269.
[42] U. Hohm, *Vacuum*, 2000, **58**, 117.
[43] G. S. Kedziora and G. C. Schatz, *Spectrochim. Acta Part A*, 1999, **55**, 625.
[44] D. N. Zubarev, *Sov. Phys. Usp.*, 1960, **3**, 320.
[45] D. N. Zubarev, *Nonequilibrium Statistical Thermodynamics*, Consultants Bureau, New York, 1974.
[46] J. Linderberg and Y. Öhrn, *Propagators in Quantum Chemistry*, Academic Press, London, 1973.
[47] J. Oddershede, in *Methods in Computational Molecular Physics* (eds S. Wilson and G. H. F. Diercksen), Plenum Press, New York, 1992, p. 303.
[48] J. A. Pople, J. S. Binkley and R. Seeger, *Int. J. Quantum Chem. Symp.*, 1976, **10**, 1.
[49] J. Oddershede and P. Jørgensen, *J. Chem. Phys.*, 1977, **66**, 1541.
[50] J. Oddershede, P. Jørgensen and N. H. F. Beebe, *Int. J. Quantum Chem.*, 1977, **12**, 655.
[51] J. Oddershede, P. Jørgensen and N. H. F. Beebe, *J. Phys. B.*, 1978, **11**, 1.
[52] J. Geertsen and J. Oddershede, *J. Chem. Phys.*, 1986, **85**, 2112.
[53] J. Geertsen, S. Eriksen and J. Oddershede, *Adv. Quantum Chem.*, 1991, **22**, 167.
[54] T. Helgaker, P. Jørgensen and J. Olsen, *Molecular Electronic Structure Theory*, Wiley, Chichester, 2000.
[55] A. Rizzo, T. Helgaker, K. Ruud, A. Barszczewicz, M. Jaszuński and P. Jørgensen, *J. Chem. Phys.*, 1995, **102**, 8953.
[56] S. P. A. Sauer and M. J. Packer, in *Computational Molecular Spectroscopy* (eds P. R. Bunker and P. Jensen), Wiley, London, 2000, p. 221, Chapter 7.
[57] B. J. Roos and A. J. Sadlej, *Chem. Phys.*, 1985, **94**, 43.
[58] M. Mérawa, D. Bégué and A. Dargelos, *J. Phys. Chem. A*, 2003, **107**, 9628.
[59] D. Tunega and J. Noga, *Theor. Chem. Acc.*, 1998, **100**, 78.
[60] D. M. Bishop and B. Lam, *Chem. Phys. Lett.*, 1985, **120**, 69.
[61] J. W. Cooley, *Math. Comput.*, 1961, **15**, 363.
[62] M. Pecul and A. Rizzo, *J. Chem. Phys.*, 2001, **116**, 1259.
[63] O. Christiansen, C. Hättig and J. Gauss, *J. Chem. Phys.*, 1998, **109**, 4745.
[64] T. H. Dunning Jr., *J. Chem. Phys.*, 1989, **90**, 1007.
[65] R. A. Kendall, T. H. Dunning and R. J. Harrison, *J. Chem. Phys.*, 1992, **96**, 6796.
[66] D. E. Woon and T. H. Dunning Jr., *J. Chem. Phys.*, 1994, **100**, 2975.
[67] H. J. Aa. Jensen, P. Jørgensen, H. Ågren and J. Olsen, *J. Chem. Phys.*, 1988, **88**, 3834.

[68] H. J. Aa. Jensen, P. Jørgensen, H. Ågren and J. Olsen, *J. Chem. Phys.*, 1988, **89**, 5354.
[69] D. Bassi, S. Falcinelli, F. Pirani, B. Rapaccini, P. Tossi, F. Vecchiocattivi and M. Vecchiocattivi, *Int. J. Mass Spectrom.*, 2003, **223–224**, 327.
[70] G. Di Lonardo and A. E. Douglas, *Can. J. Phys.*, 1973, **51**, 434.
[71] G. Maroulis, *J. Mol. Struct. (THEOCHEM)*, 2003, **633**, 177.

Rotation–Vibration Motion of Pyramidal XY_3 Molecules Described in the Eckart Frame: The Calculation of Intensities with Application to NH_3

Sergei N. Yurchenko,[1] Walter Thiel,[1] Miguel Carvajal,[2] Hai Lin[3] and Per Jensen[4]

[1]*Max-Planck-Institut für Kohlenforschung, Kaiser-Wilhelm-Platz 1, D-45470 Mülheim an der Ruhr, Germany*
[2]*Departamento de Fisica Aplicada, Facultad de Ciencias Experimentales, Avda. de las FF.AA. s/n, Universidad de Huelva, 21071, Huelva, Spain*
[3]*Department of Chemistry, University of Minnesota, 207 Pleasant Street SE, Minneapolis, MN 55455, USA*
[4]*FB C – Theoretische Chemie, Bergische Universität, D-42097 Wuppertal, Germany*

Abstract

We present a theoretical model, with accompanying computer program, for simulating rotation–vibration absorption spectra of XY_3 pyramidal molecules in isolated electronic states. The theoretical approach is based on a recent computational scheme for solving the rotation–vibration Schrödinger equation of such molecules variationally [S. N. Yurchenko, M. Carvajal, P. Jensen, H. Lin, J. Zheng, and W. Thiel, *Mol. Phys.*, 2005, **103**, 359], and it makes use of dipole moment surfaces calculated *ab initio*. We apply the theory to $^{14}NH_3$ and demonstrate that the theoretical results show good agreement with experimental findings.

Contents

1. INTRODUCTION

In a very recent publication [1], we have presented a new model for the rotation–vibration motion of pyramidal XY_3 molecules, based on the Hougen–Bunker–Johns (henceforth: HBJ) approach [2] (see also Chapter 15, in particular Section 15.2, of Ref. [3]). In this model, inversion is treated as a large-amplitude motion in the HBJ sense, while the other vibrations are assumed to be of small amplitude; they are described by linearized stretching and bending coordinates. The rotation–vibration Schrödinger equation is solved variationally to determine rotation–vibration energies. The reader is referred to Ref. [1] for a complete description of the theoretical and computational details.

We have already made several applications of the new model. Prior to Yurchenko *et al.* [1], we reported high-level *ab initio* potential energy surfaces for the NH_3 electronic ground state together with variational calculations of the associated vibrational energies [4]. Analogous nuclear-motion calculations for PH_3 [5] were based on the *ab initio* potential energy surface of Wang *et al.* [6], which was refined [5] in a simultaneous least-squares fitting to *ab initio* data and experimentally derived vibrational term values. In Ref. [1] we extended the theoretical treatment of Refs. [4,5] to include rotation and described some technical improvements to the original model for the vibrational motion. The resulting model for rotation and vibration was tested in calculations for $^{14}NH_3$ using an analytical potential function derived from high-level *ab initio* calculations [1]. These test calculations produced the $J=0$ vibrational energies up to 6100 cm^{-1}, the $J \leq 2$ energies for the vibrational ground state and the ν_2, ν_4, and $2\nu_2$ excited vibrational states, and the $J \leq 7$ energies for the $4\nu_2^+$ vibrational state. The computed energies were found to be in very satisfactory agreement with the corresponding experimentally derived values, and superior in this regard to the results of other recent theoretical calculations [7,8].

The new model has also been applied to the calculation of thermally averaged probability density functions for the out-of-plane inversion motion of the CH_3^+ and H_3O^+ ions [9]. Such probability densities can be obtained experimentally by means of Coulomb Explosion Imaging (CEI) techniques (see, for example, Refs. [10,11]), and the results in Ref. [9] will be useful in the interpretation of the resulting images, just as analogous calculations of the bending probability distribution for the CH_2^+ ion were instrumental in the interpretation of its CEI images (see Refs. [9,12] and references therein).

Another application is concerned with highly excited rotational levels of the PH_3 molecule [13,14]. The calculations show that these rotational levels form near-degenerate six-fold energy clusters analogous to the four-fold clusters formed in triatomic dihydrides H_2X (see, for example, Refs. [3,15,16] and references therein).

One of the most important aims of our theoretical work is to assist in the interpretation and understanding of high-resolution molecular spectroscopy experiments. We have already been able [1] to provide assistance of this kind in that, with our calculated values for the rotational energies in the $4\nu_2^+$ vibrational state of $^{14}NH_3$, we could verify (and, for a few transitions, refute) the tentative assignment to the $4\nu_2^+$ band [17] of 55 weak transitions observed in an

experimental study of the ν_1, ν_3, and $2\nu_4$ bands of ^{14}NH$_3$. To provide theoretical support for high-resolution molecular spectroscopy experiments it is not sufficient, however, to calculate only molecular rotation–vibration energies. It is highly desirable to predict also theoretical intensities so that spectra can be simulated. As discussed in Ref. [1], our approach to the computation of molecular rotation–vibration energies and wavefunctions can be applied to rotation–vibration states with high J values (e.g., up to $J \leq 80$ for PH$_3$ [14]) where alternative variational treatments (see, for example, Refs. [7,8]), which make use of a nuclear kinetic energy operator exact within the Born–Oppenheimer approximation, are no longer feasible. This advantage arises from the maximum separation of rotation and vibration inherently built into the HBJ theory that we employ. We can calculate the energies and wavefunctions for states with J values sufficiently high that realistic spectra can be simulated. In the present work, we describe the extension of our model to the computation of the *line strengths* that determine the intensities of electric dipole transitions within the electronic state under consideration. The derivation is guided by Jensen and Špirko [18,19] and by Chapter 14 of Ref. [3]. The line strengths are obtained from the rovibronic wavefunctions that we generate as described in Ref. [1], and from *ab initio* molecular dipole moment surfaces. With the computed line strengths we can simulate absorption spectra of XY$_3$ molecules if we assume that the absorbing molecules are in thermal equilibrium at a known absolute temperature. We can also simulate emission spectra if we know the non-thermal population distribution of the emitting molecules.

2. THEORETICAL INTENSITIES AND SELECTION RULES

2.1. Line strengths

The intensity of an electric dipole transition in absorption or emission depends, on one hand, on factors particular to the experiment measuring the intensity, e.g., the number density of molecules in the initial state of the transition and, for absorption experiments, the absorption path length and the intensity of the incident light. On the other hand, the intensity involves a factor independent of the experimental parameters. This factor, *the line strength* $S(f \leftarrow i)$, determines the probability that a molecule in the initial state i of the transition f $\leftarrow$ i will end up in the final state f within unit time.

If we assume that the initial state i and the final state f are both non-degenerate, then the line strength of the electric dipole transition between them [3] is given by

$$S(f \leftarrow i) = \sum_{A=X,Y,Z} |\langle \Phi_f | \mu_A | \Phi_i \rangle|^2. \tag{1}$$

As in Ref. [1], we describe the molecule in a space-fixed (or laboratory-fixed) axis system XYZ, and μ_A is the component of the molecular dipole moment along the axis $A = X$, Y, or Z. The complete internal wavefunctions of the initial and final states are written as $|\Phi_i\rangle$ and $|\Phi_f\rangle$, respectively. In the present work, we take the

complete internal wavefunctions to be given as

$$|\Phi_{\mathrm{w}}\rangle = |\Phi_{\mathrm{ns}}^{(\mathrm{w})}\rangle|\Phi_{\mathrm{elec}}^{(\mathrm{w})}\rangle|\Phi_{\mathrm{rv}}^{(\mathrm{w})}\rangle, \tag{2}$$

where w = i or f. We can separate out the nuclear spin wavefunction $|\Phi_{\mathrm{ns}}^{(\mathrm{w})}\rangle$ [3] because we assume the molecular energies to be independent of nuclear spin (i.e., we neglect *hyperfine structure*). The remaining factorization into a product of an electronic wavefunction $|\Phi_{\mathrm{elec}}^{(\mathrm{w})}\rangle$ and a rotation–vibration wavefunction $|\Phi_{\mathrm{rv}}^{(\mathrm{w})}\rangle$ follows from the Born–Oppenheimer approximation (see, for example, Ref. [3]) which we assume to be valid.

Inserting the wavefunction from equation (2) in the matrix element square of equation (1), we obtain

$$|\langle\Phi_{\mathrm{f}}|\mu_A|\Phi_{\mathrm{i}}\rangle|^2 = |\langle\Phi_{\mathrm{ns}}^{(\mathrm{f})}|\Phi_{\mathrm{ns}}^{(\mathrm{i})}\rangle|^2|\langle\Phi_{\mathrm{rv}}^{(\mathrm{f})}\Phi_{\mathrm{elec}}^{(\mathrm{f})}|\mu_A|\Phi_{\mathrm{elec}}^{(\mathrm{i})}\Phi_{\mathrm{rv}}^{(\mathrm{i})}\rangle|^2 \tag{3}$$

where we have made use of the fact that the dipole moment component μ_A does not depend on the nuclear spin. The nuclear spin functions are orthogonal and normalized. Consequently, the integral on the left-hand side of equation (3) vanishes unless $|\Phi_{\mathrm{ns}}^{(\mathrm{f})}\rangle = |\Phi_{\mathrm{ns}}^{(\mathrm{i})}\rangle$ so that $|\langle\Phi_{\mathrm{ns}}^{(\mathrm{f})}|\Phi_{\mathrm{ns}}^{(\mathrm{i})}\rangle|^2 = 1$.

As mentioned above, we assume that the molecular energy does not depend on the nuclear spin state $|\Phi_{\mathrm{ns}}^{(\mathrm{w})}\rangle$. For the initial rovibronic state $|\Phi_{\mathrm{elec}}^{(\mathrm{i})}\rangle|\Phi_{\mathrm{rv}}^{(\mathrm{i})}\rangle$, we have g_{ns} nuclear spin functions $|\Phi_{\mathrm{ns}}^{(\mathrm{i})}\rangle$ available, for which the product function $|\Phi_{\mathrm{i}}\rangle$ in equation (2) is an allowed complete internal state for the molecule in question, because it obeys Fermi–Dirac statistics by permutations of identical fermion nuclei, and Bose–Einstein statistics by permutations of identical boson nuclei (see Chapter 8 in Ref. [3]). By necessity [3], the same g_{ns} nuclear spin functions can be combined with the final rovibronic state $|\Phi_{\mathrm{elec}}^{(\mathrm{f})}\rangle|\Phi_{\mathrm{rv}}^{(\mathrm{f})}\rangle$ to form allowed complete internal states $|\Phi_{\mathrm{f}}\rangle$. The quantity g_{ns} is referred to as the *nuclear spin statistical weight factor*.

In our approximation, the upper and lower states of the transition f ← i are both g_{ns}-fold degenerate owing to the availability of the g_{ns} 'allowed' nuclear spin functions. Furthermore, they have *m-degeneracy* since for a molecule in field-free space, the energy does not depend on m, the projection of the total angular momentum on the Z axis. We denote the m value of the initial state as m_{i} and that of the final state as m_{f}. In the calculation of the line strength, we account for the nuclear spin degeneracy and the m-degeneracy by generalizing equation (1) to

$$S(\mathrm{f} \leftarrow \mathrm{i}) = g_{\mathrm{ns}} \sum_{m_{\mathrm{f}}, m_{\mathrm{i}}} \sum_{A=X,Y,Z} |\langle\Phi_{\mathrm{rv}}^{(\mathrm{f})}\Phi_{\mathrm{elec}}^{(\mathrm{f})}|\mu_A|\Phi_{\mathrm{elec}}^{(\mathrm{i})}\Phi_{\mathrm{rv}}^{(\mathrm{i})}\rangle|^2 \tag{4}$$

where we have made use of equation (3) with $|\langle\Phi_{\mathrm{ns}}^{(\mathrm{f})}|\Phi_{\mathrm{ns}}^{(\mathrm{i})}\rangle|^2 = 1$.

2.2. Intensities

If, in an absorption experiment, a parallel beam of light at wavenumber $\tilde{\nu}$ with intensity $I_0(\tilde{\nu})$ passes through a length l of gas at a concentration of c_{g}, the intensity of the transmitted light $I_{\mathrm{tr}}(\tilde{\nu})$ is given by the Lambert–Beer law

$$I_{tr}(\tilde{\nu}) = I_0(\tilde{\nu}) \exp[-lc_g\varepsilon(\tilde{\nu})] \qquad (5)$$

where $\varepsilon(\tilde{\nu})$ is the absorption coefficient. By integrating the absorption coefficient over an absorption line one obtains the expression

$$I(\mathrm{f} \leftarrow \mathrm{i}) = \int_{\mathrm{Line}} \varepsilon(\tilde{\nu})\, d\tilde{\nu} = \frac{8\pi^3 N_A \tilde{\nu}_{if}}{(4\pi\varepsilon_0)3hc} \frac{e^{-E_i/kT}}{Q}[1 - \exp(-hc\tilde{\nu}_{if}/kT)]S(\mathrm{f} \leftarrow \mathrm{i}) \quad (6)$$

for the intensity of the absorption line for the transition from the state i with energy E_i, in thermal equilibrium at the temperature T, to the state f with energy E_f, where $hc\tilde{\nu}_{if} = E_f - E_i$, N_A is the Avogadro constant, h is Planck's constant, c is the speed of light in vacuum, k is the Boltzmann constant, ε_0 is the permittivity of free space, $S(\mathrm{f} \leftarrow \mathrm{i})$ is the line strength defined in equation (4), and, finally, Q is the partition function defined as

$$Q = \sum_j g_j\, e^{-E_j/kT}, \qquad (7)$$

where g_j is the total degeneracy of the state with energy E_j and the sum runs over all energy levels of the molecule.

The 'molecule-intrinsic' factor in the intensities of emission spectra can be obtained from the well-known Einstein coefficients (see, for example, Refs. [20, 21]). For the two states i and f considered above, whose energies are E_i and E_f, respectively, with $E_i < E_f$, we define B_{if} as the Einstein coefficient for absorption, B_{fi} as the Einstein coefficient for stimulated emission, and A_{fi} as the Einstein coefficient for spontaneous emission. We denote by N_i and N_f the number of molecules with energies E_i and E_f, respectively, and the Einstein coefficients are defined such that, for example, the change in N_f caused by electric dipole transitions to and from i is given by

$$\frac{dN_f}{dt} = \rho(\nu)[N_i B_{if} - N_f B_{fi}] - N_f A_{fi}. \qquad (8)$$

The energy density function $\rho(\nu)$ is defined so that $dE = \rho(\nu)d\nu$ is the amount of available radiation energy per unit volume originating in radiation with *frequency* in the infinitesimal interval $[\nu, \nu + d\nu]$. Thus, $\rho(\nu)$ is expressed in the SI units $J/(m^3\ Hz) = J\,s/m^3$, so that B_{fi} and B_{fi} have the SI units $m^3/(J\,s^2)$. A_{fi} is expressed in s^{-1}. The Einstein coefficients defined in this manner are related to the line strength by

$$g_i B_{if} = g_f B_{fi} = \frac{8\pi^3}{3h^2(4\pi\varepsilon_0)}S(\mathrm{f} \leftarrow \mathrm{i}) \qquad (9)$$

and

$$g_f A_{fi} = \frac{64\pi^4}{3h(4\pi\varepsilon_0)}\tilde{\nu}_{if}^3 S(\mathrm{f} \leftarrow \mathrm{i}), \qquad (10)$$

where g_i and g_f are the total degeneracies of the states i and f, respectively.

Sometimes an alternative definition of the Einstein coefficients is employed. With this definition, equation (8) is replaced by

$$\frac{dN_f}{dt} = \tilde{\rho}(\tilde{\nu})[N_i \tilde{B}_{if} - N_f \tilde{B}_{fi}] - N_f \tilde{A}_{fi}. \tag{11}$$

where $\tilde{\rho}(\tilde{\nu})$ is defined so that $dE = \tilde{\rho}(\tilde{\nu})d\tilde{\nu}$ is the amount of available radiation energy per unit volume originating in radiation with *wavenumber* in the infinitesimal interval $[\tilde{\nu}, \tilde{\nu} + d\tilde{\nu}]$. We have $\tilde{\rho}(\tilde{\nu}) = c\rho(\tilde{\nu}c) = c\rho(\nu)$ together with $\tilde{B}_{if} = B_{if}/c$, $\tilde{B}_{fi} = B_{fi}/c$, and $\tilde{A}_{fi} = A_{fi}$. The SI units for $\tilde{\rho}(\tilde{\nu})$ are $J/(m^3\ m^{-1}) = J/m^2$, and those of $\tilde{B}_{if}$ and $\tilde{B}_{fi}$ are $m^2/(J\ s)$.

2.3. A detailed expression for the line strength

In the present section, we obtain an expression for the line strength in equation (4) in a form suitable for numerical calculation. This derivation closely follows the theory developed in Refs. [18,19] and in Chapter 14 of Ref. [3], and so we give only an outline here.

As discussed in Ref. [1], we describe the rotation of the molecule by means of a molecule-fixed axis system *xyz* defined in terms of Eckart and Sayvetz conditions (see Ref. [1] and references therein). The orientation of the *xyz* axis system relative to the *XYZ* system is defined by the three standard Euler angles (θ, ϕ, χ) [1]. To simplify equation (4), we must first express the space-fixed dipole moment components (μ_X, μ_Y, μ_Z) in this equation in terms of the components (μ_x, μ_y, μ_z) along the molecule-fixed axes. This transformation is most easily done by rewriting the dipole moment components in terms of so-called irreducible spherical tensor operators. In the notation in Ref. [3], the space-fixed irreducible tensor operators are

$$\mu_s^{(1,\pm1)} = \frac{1}{\sqrt{2}}(\mp\mu_X - i\mu_Y) \quad \text{and} \quad \mu_s^{(1,0)} = \mu_Z \tag{12}$$

with analogous expressions for the molecule-fixed operators

$$\mu_m^{(1,\pm1)} = \frac{1}{\sqrt{2}}(\mp\mu_x - i\mu_y) \quad \text{and} \quad \mu_m^{(1,0)} = \mu_z. \tag{13}$$

It can be shown that the space-fixed components are given in terms of the molecule-fixed components by equations (14) and (15) of Ref. [3]:

$$\mu_s^{(1,\sigma)} = \sum_{\sigma'=-1}^{1} [D_{\sigma\sigma'}^{(1)}(\phi, \theta, \chi)]^* \mu_m^{(1,\sigma')} \tag{14}$$

where $D_{\sigma\sigma'}^{(1)}(\phi, \theta, \chi)$ is an element of the standard rotation matrices given, for example, by Zare [22].

By inverting equation (12) to obtain (μ_X, μ_Y, μ_Z) and inserting the result in equation (4), we find that

$$S(\mathrm{f} \leftarrow \mathrm{i}) = g_{\mathrm{ns}} \sum_{m_{\mathrm{f}}, m_{\mathrm{i}}} \sum_{\sigma=-1}^{1} |\langle \Phi_{\mathrm{rv}}^{(\mathrm{f})} \Phi_{\mathrm{elec}}^{(\mathrm{f})} | \mu_{\mathrm{s}}^{(1,\sigma)} | \Phi_{\mathrm{elec}}^{(\mathrm{i})} \Phi_{\mathrm{rv}}^{(\mathrm{i})} \rangle|^2 \tag{15}$$

and we can now insert equation (14) in this expression. Simultaneously, we insert the expressions for the initial and final rotation–vibration wavefunctions $|\Phi_{\mathrm{rv}}^{(\mathrm{w})}\rangle$ from equation (67) of Ref. [1]:

$$|\Phi_{\mathrm{rv}}^{(\mathrm{i})}\rangle = \sum_{V'' K'' \tau_{\mathrm{rot}}''} C_{V'' K'' \tau_{\mathrm{rot}}''} |V''\rangle |J'' K'' m_{\mathrm{i}} \tau_{\mathrm{rot}}''\rangle; \quad K'' \geq 0 \tag{16}$$

$$|\Phi_{\mathrm{rv}}^{(\mathrm{f})}\rangle = \sum_{V' K' \tau_{\mathrm{rot}}'} C_{V' K' \tau_{\mathrm{rot}}'} |V'\rangle |J' K' m_{\mathrm{f}} \tau_{\mathrm{rot}}'\rangle; \quad K' \geq 0 \tag{17}$$

where $C_{V'' K'' \tau_{\mathrm{rot}}''}$ and $C_{V' K' \tau_{\mathrm{rot}}'}$ are the expansion coefficients obtained as eigenvector components in the diagonalization of the Hamiltonian matrix [1], and the vibrational basis functions $|V\rangle$ are

$$|V\rangle = |n_1\rangle |n_2\rangle |n_3\rangle |n_{\mathrm{b}}, l_{\mathrm{b}}, \tau_{\mathrm{bend}}\rangle |n_{\mathrm{i}}, J, K, \tau_{\mathrm{inv}}\rangle; \tag{18}$$

V is used as a shorthand notation for all the quantum numbers and symmetry labels n_1, n_2, n_3, n_{b}, l_{b}, τ_{bend}, n_{i}, and τ_{inv} that label the vibrational basis functions. All the functions $|JKm\tau_{\mathrm{rot}}\rangle$, $|n_1\rangle$, $|n_2\rangle$, $|n_3\rangle$, $|n_{\mathrm{b}}, l_{\mathrm{b}}, \tau_{\mathrm{bend}}\rangle$, and $|n_{\mathrm{i}}, J, K, \tau_{\mathrm{inv}}\rangle$ occurring in equations (16)–(18), and the quantum numbers labelling them, are defined in detail in Ref. [1]: $|JKm\tau_{\mathrm{rot}}\rangle$ is a symmetrized rotational wavefunction defined in equations (68) and (69) of Ref. [1], $|n_1\rangle$, $|n_2\rangle$, and $|n_3\rangle$ are one-dimensional Morse oscillator eigenfunctions describing the stretching motion of the XY$_3$ molecule, $|n_{\mathrm{b}}, l_{\mathrm{b}}, \tau_{\mathrm{bend}}\rangle$ is a symmetrized eigenfunction of the two-dimensional harmonic oscillator modelling the small-amplitude bending motion, and $|n_{\mathrm{i}}, J, K, \tau_{\mathrm{inv}}\rangle$ is a symmetrized inversion basis function obtained by numerical solution of a zero-order inversion Schrödinger equation. Concerning the quantum numbers, it suffices to say here that each of the three quantum numbers τ_{rot}, τ_{bend}, and τ_{inv} assumes the values 0 or 1 in such a way that the parity (see below) of $|JKm\tau_{\mathrm{rot}}\rangle$ is $(-1)^{\tau_{\mathrm{rot}}}$, the parity of $|n_{\mathrm{b}}, l_{\mathrm{b}}, \tau_{\mathrm{bend}}\rangle$ is $(-1)^{\tau_{\mathrm{bend}}}$, and the parity of $|n_{\mathrm{i}}, J, K, \tau_{\mathrm{inv}}\rangle$ is $(-1)^{\tau_{\mathrm{inv}}}$.

Insertion of equations (14), (16), and (17) in equation (15) produces

$$\begin{aligned}
S(\mathrm{f} \leftarrow \mathrm{i}) = g_{\mathrm{ns}} \sum_{m_{\mathrm{i}}, m_{\mathrm{f}}} \sum_{\sigma=-1}^{1} \Bigg| &\sum_{V' K' \tau_{\mathrm{rot}}'} \sum_{V'' K'' \tau_{\mathrm{rot}}''} C_{V' K' \tau_{\mathrm{rot}}'}^* C_{V'' K'' \tau_{\mathrm{rot}}''} \\
&\times \sum_{\sigma'=-1}^{1} \langle V' | \langle \Phi_{\mathrm{elec}}^{(\mathrm{f})} | \mu_{\mathrm{m}}^{(1,\sigma')} | \Phi_{\mathrm{elec}}^{(\mathrm{i})} \rangle | V'' \rangle \\
&\times \langle J' K' m_{\mathrm{f}} \tau_{\mathrm{rot}}' | [D_{\sigma\sigma'}^{(1)}(\phi, \theta, \chi)]^* | J'' K'' m_{\mathrm{i}} \tau_{\mathrm{rot}}'' \rangle \Bigg|^2.
\end{aligned} \tag{19}$$

We have factorized the matrix element in equation (19) by making use of the fact that the vibrational basis functions $|V''\rangle$ and $|V'\rangle$, the electronic wavefunctions $|\Phi_{\mathrm{elec}}^{(\mathrm{i})}\rangle$ and $|\Phi_{\mathrm{elec}}^{(\mathrm{f})}\rangle$, and the molecule-fixed dipole moment operator $\mu_{\mathrm{m}}^{(1,\sigma')}$ depend

on the vibrational and electronic coordinates only (these coordinates are defined in Ref. [1]), whereas the functions $|J'K'm_f\tau'_{rot}\rangle$, $|J''K''m_i\tau''_{rot}\rangle$, and $[D^{(1)}_{\sigma\sigma'}(\phi,\theta,\chi)]^*$ depend solely on the Euler angles (θ,ϕ,χ).

In the present work, we are only concerned with transitions within one electronic state so we have $|\Phi^{(f)}_{elec}\rangle = \Phi^{(i)}_{elec}\rangle$. We define the electronically averaged dipole moment operators

$$\bar{\mu}^{(1,\sigma')}_m = \langle \Phi^{(i)}_{elec}|\mu^{(1,\sigma')}_m|\Phi^{(i)}_{elec}\rangle_{el}; \tag{20}$$

the subscript 'el' signifies that in the matrix element, integration is over the electronic coordinates only so that $\bar{\mu}^{(1,\sigma')}_m$ is a function of the vibrational coordinates. We intend to obtain the $\bar{\mu}^{(1,\sigma')}_m$ functions from *ab initio* calculations as described in Section 3. By inserting equation (20) in equation (19); using equations (68) and (69) from Ref. [1] in conjunction with equation (14–23) from Ref. [3] to obtain analytical expressions for the integral involving $|J'K'm_f\tau'_{rot}\rangle$, $|J''K''m_i\tau''_{rot}\rangle$, and $[D^{(1)}_{\sigma\sigma'}(\phi,\theta,\chi)]^*$; and carrying out a significant amount of tedious algebra (using the results in Chapter 14 of Ref. [3]), we obtain the following expression for the line strength:

$$
\begin{aligned}
S(f \leftarrow i) = g_{ns}(2J'+1)(2J''+1)\Bigg| \sum_{V'K'\tau'_{rot}} \sum_{V''K''\tau''_{rot}} C^*_{V'K'\tau'_{rot}} C_{V''K''\tau''_{rot}} (i)^{\tau''_{rot}-\tau'_{rot}} \\
\times \Bigg\{ \delta_{K'K''}\frac{1}{2}(-1)^{\sigma'_{rot}+\sigma''_{rot}+K'}(1+(-1)^{\tau'_{rot}+\tau''_{rot}+1}) \\
\times \begin{pmatrix} J'' & 1 & J' \\ K'' & 0 & -K' \end{pmatrix} \langle V'|\bar{\mu}^{(1,0)}_m|V''\rangle + [(\sqrt{2}-1)\delta_{K''0}+1] \\
\times \delta_{K',K''+1}\frac{1}{2}(-1)^{\sigma'_{rot}+\sigma''_{rot}+K'} \begin{pmatrix} J'' & 1 & J' \\ K'' & 1 & -K' \end{pmatrix} \\
\times [\langle V'|\bar{\mu}^{(1,+1)}_m|V''\rangle + (-1)^{\tau'_{rot}+\tau''_{rot}}\langle V'|\bar{\mu}^{(1,-1)}_m|V''\rangle] \\
+ [(\sqrt{2}-1)\delta_{K'0}+1]\delta_{K',K''-1}\frac{1}{2}(-1)^{\sigma'_{rot}+\sigma''_{rot}+K'} \\
\times \begin{pmatrix} J'' & 1 & J' \\ K'' & -1 & -K' \end{pmatrix} [\langle V'|\bar{\mu}^{(1,-1)}_m|V''\rangle \\
+ (-1)^{\tau'_{rot}+\tau''_{rot}}\langle V'|\bar{\mu}^{(1,+1)}_m|V''\rangle] \Bigg\} \Bigg|^2
\end{aligned}
\tag{21}
$$

where quantities such as

$$\begin{pmatrix} J'' & 1 & J' \\ K'' & -1 & -K' \end{pmatrix}$$

are standard 3*j*-symbols [3,22] and σ_{rot} is defined as

$$\sigma_{\text{rot}} = \begin{cases} K \bmod 3 & \text{for } \tau_{\text{rot}} = 1 \\ 0 & \text{for } \tau_{\text{rot}} = 0. \end{cases} \tag{22}$$

With the phase choices made for the basis functions in the present work, we obtain the real, positive line strength in equation (21) in the form $|is|^2$, where s is real, that is, as the module square of a purely imaginary number.

The *ab initio* calculations provide us with the Cartesian components of the dipole moment in the molecule-fixed axis system:

$$\bar{\mu}_\alpha = \langle \Phi^{(i)}_{\text{elec}} | \mu_\alpha | \Phi^{(i)}_{\text{elec}} \rangle_{\text{el}}, \quad \alpha = x, y, \text{ or } z, \tag{23}$$

and we obtain the vibrational matrix elements required in equation (21) from

$$\langle V' | \bar{\mu}^{(1,0)}_{\text{m}} | V'' \rangle = \langle V' | \bar{\mu}_z | V'' \rangle \tag{24}$$

together with

$$\langle V' | \bar{\mu}^{(1,+1)}_{\text{m}} | V'' \rangle + (-1)^{\tau'_{\text{rot}} + \tau''_{\text{rot}}} \langle V' | \bar{\mu}^{(1,-1)}_{\text{m}} | V'' \rangle$$

$$= -\frac{1}{\sqrt{2}} ([1 - (-1)^{\Delta\tau_{\text{rot}}}] \langle V' | \bar{\mu}_x | V'' \rangle + i[1 + (-1)^{\Delta\tau_{\text{rot}}}] \langle V' | \bar{\mu}_y | V'' \rangle), \tag{25}$$

where $\Delta\tau_{\text{rot}} = \tau'_{\text{rot}} - \tau''_{\text{rot}}$, and

$$\langle V' | \bar{\mu}^{(1,-1)}_{\text{m}} | V'' \rangle + (-1)^{\tau'_{\text{rot}} + \tau''_{\text{rot}}} \langle V' | \bar{\mu}^{(1,+1)}_{\text{m}} | V'' \rangle$$

$$= \frac{1}{\sqrt{2}} ([1 - (-1)^{\Delta\tau_{\text{rot}}}] \langle V' | \bar{\mu}_x | V'' \rangle - i[1 + (-1)^{\Delta\tau_{\text{rot}}}] \langle V' | \bar{\mu}_y | V'' \rangle). \tag{26}$$

We note that on the right-hand side of equations (25) and (26), the terms involving $\langle V' | \bar{\mu}_x | V'' \rangle$ and $\langle V' | \bar{\mu}_y | V'' \rangle$ are never simultaneously non-vanishing.

2.4. Symmetry and selection rules

For the XY$_3$ molecules considered here, we employ the Molecular Symmetry Group (MS group) D_{3h}(M) [3], given as the direct product [3],

$$D_{3h}(\text{M}) = C_{3v}(\text{M}) \otimes \{E, E^*\} \tag{27}$$

where E is the identity operation, E^* is the inversion operation which inverts all particles in the molecular centre of mass [3], and the group

$$C_{3v}(\text{M}) = \{E, (123), (132), (12)^*, (13)^*, (23)^*\}. \tag{28}$$

Here, (123) and (132) are cyclic permutations of the three Y nuclei (labelled 1, 2, 3) in XY$_3$ and each of the permutation-inversion operations $(12)^*$, $(13)^*$, and $(23)^*$ involves the interchange of two of the Y nuclei and the inversion operation E^* [3]. The character table of D_{3h}(M) is given in Table 1. The Complete Nuclear

Table 1. The character table of the MS group D_{3h}(M) [3]

	E	(123)	(23)	E^*	$(123)^*$	$(23)^*$	
	1	2	3	1	2	3	
A'_1	1	1	1	1	1	1	$(r_1 + r_2 + r_3)/\sqrt{3}$, $1/\sqrt{3}(\alpha_1 + \alpha_2 + \alpha_3)$, $\sin\rho$, Γ_{B}^+
A''_1	1	1	1	-1	-1	-1	Γ^*, Γ_{B}^-
A'_2	1	1	-1	1	1	-1	$\hat{J}_z$, Γ_{F}^+
A''_2	1	1	-1	-1	-1	1	$\cos\rho$, $\hat{J}_\rho$, $\bar{\mu}_z$, Γ_{F}^-
E'	2	-1	0	2	-1	0	$([\,2r_1 - r_2 - r_3]/\sqrt{6},$ $[r_2 - r_3]/\sqrt{2})$, $([\,2\alpha_1 - \alpha_2 - \alpha_3]/\sqrt{6},$ $[\alpha_2 - \alpha_3]/\sqrt{2}), (\bar{\mu}_x, \bar{\mu}_y)$
E''	2	-1	0	-2	1	0	$(\hat{J}_x, \hat{J}_y)$

Permutation Inversion (CNPI) Group [3], which contains all possible permutation-inversion operations [3] for a given molecule, has 24 elements for the XY_3 molecule, and the 12-member group D_{3h}(M) is obtained by deleting from the CNPI group the 12 *unfeasible* [3] symmetry operations that, when applied to an initial molecular geometry, take the molecule into a new geometry that can only be reached from the initial one by the breaking and reformation of bonds. We assume that the breaking and reformation of bonds are associated with energy barriers so large that this type of motion does not take place on the typical timescale of the spectroscopy experiments whose results we simulate.

The MS group D_{3h}(M) is obviously appropriate for planar XY_3 molecules such as CH_3^+ and for 'floppy' molecules like NH_3 with a pyramidal, non-planar equilibrium configuration but a barrier to planarity so low that tunnelling through the barrier is facile already at room temperature. For pyramidal molecules with a high barrier to planarity, such as PH_3, the appropriate MS group is C_{3v}(M) in equation (28).

In Table 1, we give for each class of D_{3h}(M) a representative element and the number of elements in the class. Also, we indicate the D_{3h}(M) symmetries of some quantities of interest: ρ is the HBJ inversion coordinate [1] (see also Fig. 1) and $\hat{J}_\rho$ is its conjugate momentum, $(\hat{J}_x, \hat{J}_y, \hat{J}_z)$ are the components of the total angular momentum along the molecule-fixed xyz axes, $(\bar{\mu}_x, \bar{\mu}_y, \bar{\mu}_z)$ are the electronically averaged dipole moment components along the molecule-fixed axes (see below), (r_1, r_2, r_3) are the instantaneous values of the bond lengths of the XY_3 molecule, while $\alpha_1 = \angle(Y_2XY_3)$, $\alpha_2 = \angle(Y_1XY_3)$, and $\alpha_3 = \angle(Y_1XY_2)$ are the three bond angles (Y_i is the Y nucleus labelled $i = 1,2,3$). The irreducible representation $\Gamma^* = A''_1$ is the so-called *electric dipole representation*; it has character $+1$ under each of the permutation operations in D_{3h}(M) and character -1 under each of the permutation-inversion operations. It is required for determining the symmetry selection rules for electric dipole transitions. Finally, the two irreducible representations $\Gamma_{\mathrm{F}}^+ = A'_2$ and $\Gamma_{\mathrm{F}}^- = A''_2$ are the Pauli-allowed symmetries for NH_3
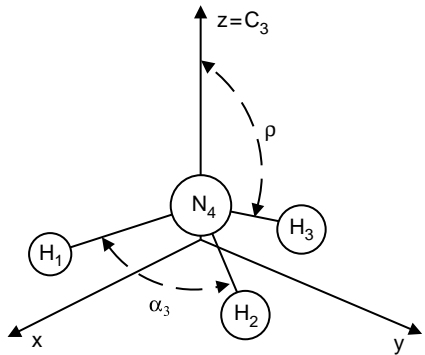
Fig. 1. The geometrically defined coordinates and the labelling of the nuclei chosen for NH^3.

(or for a general XY$_3$ molecule whose Y nuclei are fermions): Owing to Fermi–Dirac statistics, the complete internal wavefunctions of NH$_3$ must transform as A_2' or A_2'' in D_{3h}(M). Complete internal wavefunctions of NH$_3$ with A_2' symmetry have $+$ *parity* in that they have a character of $+1$ under the inversion operation E^*; those with A_2'' symmetry have $-$ *parity*, i.e., a character of -1 under E^*. The irreducible representations $\Gamma_{\mathrm{B}}^+ = A_1'$ and $\Gamma_{\mathrm{B}}^- = A_1''$ are the symmetries with $+$ and $-$ parity, respectively, that are allowed by Bose–Einstein statistics for an XY$_3$ molecule, ND$_3$ say, whose Y nuclei are bosons.

The nuclear spin statistical weight factors g_{ns} for ^{14}NH$_3$ are determined in Section 8.4.1 of Ref. [3] and we do not repeat the derivation here. The results are summarized in Table 2. The 24 nuclear spin functions (see Chapter 8 in Ref. [3]) of ^{14}NH$_3$ span the representation

$$\Gamma_{\mathrm{nspin}}^{\mathrm{tot}} = 12A_1' \oplus 6E' \tag{29}$$

of D_{3h}(M). In Table 2, Γ_{rve} is the MS group symmetry of the rovibronic wavefunction $|\Phi_{\mathrm{elec}}^{(\mathrm{w})}\rangle|\Phi_{\mathrm{rv}}^{(\mathrm{w})}\rangle$, and for each possible Γ_{rve} we give under the heading 'Γ_{ns}' the number of spin functions available for forming complete internal wavefunctions of symmetry $\Gamma_{\mathrm{int}} = \Gamma_{\mathrm{F}}^+ = A_2'$ and $\Gamma_{\mathrm{int}} = \Gamma_{\mathrm{F}}^- = A_2''$, respectively, the total number of such spin functions equals the nuclear spin statistical weight

Table 2. Determination of statistical weight of the rovibronic states of ^{14}NH$_3$ in the MS group D_{3h}(M) [3]

Γ_{rve}	Γ_{ns}	Γ_{int}	g_{ns}
A_1'	$-;\ -$	$A_2';\ A_2''$	0
A_1''	$-;\ -$	$A_2';\ A_2''$	0
A_2'	$12A_1';\ -$	$A_2';\ A_2''$	12
A_2''	$-;\ 12A_1'$	$A_2';\ A_2''$	12
E'	$6E';\ -$	$A_2';\ A_2''$	6
E''	$-;\ 6E'$	$A_1';\ A_2''$	6

factor g_{ns}. We note that for $\Gamma_{rve} = A_1'$ or A_1'', $g_{ns} = 0$, so that the corresponding energy levels are *missing*. They do not exist because their rovibronic wavefunctions cannot be combined with nuclear spin functions in such a way as to obey Fermi–Dirac statistics.

We have [3]

$$\Gamma_{rve} = \Gamma_{elec} \otimes \Gamma_{rv}, \tag{30}$$

where Γ_{elec} is the symmetry of $|\Phi_{elec}^{(w)}\rangle$ and Γ_{rv} is the symmetry of $|\Phi_{rv}^{(w)}\rangle$. We are concerned with the electronic ground state of NH_3 for which $\Gamma_{elec} = A_1'$ so that for the rovibronic states of interest $\Gamma_{rve} = \Gamma_{rv}$. If $|\Phi_{rv}^{(i)}\rangle(|\Phi_{rv}^{(f)}\rangle)$ has the MS group symmetry $\Gamma_{rv}''(\Gamma_{rv}')$ then the line strength $S(f \leftarrow i)$ can only be non-vanishing [3] if

$$\Gamma_{rv}'' \otimes \Gamma_{rv}' \supset \Gamma^* = A_1''. \tag{31}$$

In consequence, the symmetry selection rules on Γ_{rv} (with the corresponding g_{ns} values) are

$$A_2' \leftrightarrow A_2''; \quad g_{ns} = 12 \tag{32}$$

$$E' \leftrightarrow E''; \quad g_{ns} = 6. \tag{33}$$

These selection rules, in conjunction with the general rotational selection rules

$$\Delta J = J' - J'' = 0, \pm 1 \quad (J'' + J' \geq 1) \tag{34}$$

determine the allowed electric dipole transitions of $^{14}NH_3$.

3. THE DIPOLE MOMENT FUNCTIONS

3.1. The *ab initio* calculation of the dipole moment

The NH_3 dipole moment surface used in the present study is obtained from two sets of *ab initio* data. As reported previously [4], the *ab initio* calculations were done at the CCSD(T)/aug-cc-pVTZ level of theory (i.e., coupled cluster theory with all single and double substitutions [23] and a perturbative treatment of connected triple excitations [24,25] with the augmented correlation-consistent triple-zeta basis [26,27]). The frozen-core approximation was applied. Dipole moments were computed by using a numerical finite-difference procedure with an added external dipole field of 0.005 a.u. The calculations employed the MOLPRO2000 [28,29] package. The convergence thresholds were 10^{-10} for density and 10^{-7} a.u. for energy in Hartree–Fock (HF) calculations, and 10^{-10} a.u. for energy and 10^{-10} for coefficients in CCSD(T) computations.

The first set of data was obtained on a two-dimensional grid (the 2D grid in Ref. [4]) consisting of 420 geometries of C_{3v} or D_{3h} symmetry, with bond distances R_{NH} between 0.60 and 1.65 Å, and angles α_{HNH} between 70 and 120°. The data points were more dense in the vicinity of the equilibrium geometry and the saddle point. The second set of data was determined on a six-dimensional

grid (the 6D-1 grid in Ref. [4]) consisting of 14,400 unique geometries that form a regular grid in the range $0.85 \text{ Å} \leq r_1 \leq r_2 \leq r_3 \leq 1.20 \text{ Å}$ and $80° \leq \alpha_1 \leq \alpha_2 \leq \alpha_3 \leq 120°$.

The *ab initio* calculations give the components of the molecular dipole moment in a right-handed Cartesian axis system $x'y'z'$ with origin in the nitrogen nucleus. The H_1 nucleus lies on the z' axis with a positive value of the z' coordinate, and the plane defined by the nitrogen nucleus and the protons H_1 and H_2 is the $y'z'$ plane. Thus, in the $x'y'z'$ axis system, N has the coordinates $(0,0,0)$, H_1 has the coordinates $(0,0,z_1')$ with $z_1' > 0$, H_2 has the coordinates $(0,y_2',z_2')$, and H_3 has the coordinates (x_3', y_3', z_3'). In general, all the coordinates y_2', z_2', x_3', y_3', and z_3' are different from zero.

3.2. The analytical representation of the dipole moment

The *ab initio* calculations produce values of $(\bar{\mu}_{x'}, \bar{\mu}_{y'}, \bar{\mu}_{z'})$, i.e., the components of the electronically averaged dipole moment along the $x'y'z'$ axes defined above. In order to calculate molecular line strengths, however, we must determine, as functions of the vibrational coordinates, the dipole moment components $(\bar{\mu}_x, \bar{\mu}_y, \bar{\mu}_z)$ along the molecule-fixed axes xyz (see equation (23)) defined by Eckart and Sayvetz conditions [1].

An *ab initio* calculation generally gives the components of the electronically averaged dipole moment in a *body-fixed* axis system such as the $x'y'z'$ system. For a body-fixed axis system, the orientation of the axes is determined directly from the instantaneous positions of the nuclei. So, for the $x'y'z'$ axis system, the z' axis lies along the NH_1 bond, and the $y'z'$ plane is the NH_1H_2 plane. The definition of the molecule-fixed axis system xyz is more complicated since it rests on the Eckart–Sayvetz conditions. The values of the Euler angles θ, ϕ, χ, which determine the orientation of the xyz axis system in space, are determined, together with the inversion coordinate ρ and the three centre-of-mass coordinates, by the solution of a system of seven coupled equations [1]. Consequently, in line strength calculations, we are required to transform the dipole moment from the body-fixed axis system $x'y'z'$, as used in the *ab initio* calculation, to the xyz axis system. In the present section, we discuss strategies for carrying out this transformation, and we discuss suitable analytical functions for representing the molecule-fixed components of the dipole moment.

In the papers on intensity calculations for triatomic molecules [18,19], which guide the present work, the body-fixed dipole moment components $(\bar{\mu}_{x'}, \bar{\mu}_{y'}, \bar{\mu}_{z'})$ are represented by parameterized analytical functions of geometrically defined coordinates (i.e., bond lengths and bond angles). The values of the parameters in these functions are determined by least-squares fittings to the *ab initio* points. The analytical functions $(\bar{\mu}_{x'}, \bar{\mu}_{y'}, \bar{\mu}_{z'})$ are then subjected to two transformations: One transforms from the $x'y'z'$ body-fixed system (called the xpq axis system in Ref. [19]) to the xyz molecule-fixed system, and the other transforms the dipole moment components from depending on the geometrically defined coordinates to depending on the coordinates that we have chosen to describe the vibrational motion. In our HBJ-inspired models for molecular rotation and vibration, these

coordinates are not geometrically defined. In Refs. [18,19] these two transformations are made, by a combination of analytical and numerical techniques, as part of the intensity calculation.

In the present work, we must carry out transformations of the dipole moment functions analogous to those described for triatomic molecules in Refs. [18,19]. Our approach to this problem is completely different from that made in Refs. [18,19]. We do not transform analytical expressions for the body-fixed dipole moment components $(\bar{\mu}_{x'}, \bar{\mu}_{y'}, \bar{\mu}_{z'})$. Instead we obtain, at each calculated *ab initio* point, discrete values of the dipole moment components $(\bar{\mu}_x, \bar{\mu}_y, \bar{\mu}_z)$ in the *xyz* axis system, and we fit parameterized, analytical functions of our chosen vibrational coordinates (see below) through these values. This approach has the disadvantage that we must carry out a separate fitting for each isotopomer of a molecule: Different isotopomers with the same geometrical structure have different *xyz* axis systems (because the Eckart and Sayvetz conditions depend on the nuclear masses) and therefore different dipole moment components $(\bar{\mu}_x, \bar{\mu}_y, \bar{\mu}_z)$. We resort to the approach of transforming the dipole moment at each *ab initio* point because the direct transformation of analytical expressions for the body-fixed dipole moment components $(\bar{\mu}_{x'}, \bar{\mu}_{y'}, \bar{\mu}_{z'})$ is not practicable for a four-atomic molecule. The fact that the four-atomic molecule has six vibrational coordinates causes a huge increase in the complexity of the transformations relative to that encountered for the triatomic molecules (with three vibrational coordinates) treated in Refs. [18,19].

By carrying out the transformation $(\bar{\mu}_{x'}, \bar{\mu}_{y'}, \bar{\mu}_{z'}) \rightarrow (\bar{\mu}_x, \bar{\mu}_y, \bar{\mu}_z)$ at each *ab initio* point separately and then fitting the resulting values of $(\bar{\mu}_x, \bar{\mu}_y, \bar{\mu}_z)$, we obtain a representation of the dipole moment tailor-made for computing the matrix elements $\langle V'|\bar{\mu}_{\mathrm{m}}^{(1,\sigma)}|V''\rangle$ ($\sigma = 0, \pm 1$) entering into equation (21) in terms of the vibrational wavefunctions $|V\rangle$ employed in our model for the rotation and vibration of XY_3 molecules [1]. We would like, however, to make our NH_3 dipole moment surfaces generally available in a form independent of our particular choice of the molecule-fixed axis system *xyz*. We describe such a 'universal' representation of the electronically averaged dipole moment vector $\bar{\mu}$, the so-called *Molecular Bond (MB) representation*, in Section 3.2.1. From the MB expression for the dipole moment vector [equation (35)], the dipole moment components for *any* choice of the molecule-fixed axis system can be determined in terms of general, geometrically defined coordinates. In the sections following Section 3.2.1, we then return to the problem of calculating line strengths from equation (21), i.e., with our Eckart–Sayvetz choice of the molecule-fixed axis system *xyz*.

3.2.1. The molecular bond (MB) representation

We write $\bar{\mu}$ in the form given in Refs. [30,31]:

$$\bar{\mu} = \bar{\mu}_1^{\text{Bond}}\mathbf{e}_1 + \bar{\mu}_2^{\text{Bond}}\mathbf{e}_2 + \bar{\mu}_3^{\text{Bond}}\mathbf{e}_3 \qquad (35)$$

where the three functions $\bar{\mu}_i^{\text{Bond}}$, $i = 1, 2, 3$, depend on the vibrational coordinates, and $\mathbf{e}_i$ is the unit vector along the N–H$_i$ bond,

$$\mathbf{e}_i = \frac{\mathbf{r}_i - \mathbf{r}_4}{|\mathbf{r}_i - \mathbf{r}_4|} \tag{36}$$

with $\mathbf{r}_i$ as the position vector of nucleus i (the protons are labelled 1, 2, 3, and the nitrogen nucleus is labelled 4, see Fig. 1) in the xyz axis system. We see that the representation of the dipole moment in equation (35) is universal in the sense discussed above: The unit vectors $\mathbf{e}_i$ are defined in terms of the instantaneous positions of the nuclei and do not depend on a particular choice of the molecule-fixed axis system.

We have found that we can obtain a particularly accurate representation of the *ab initio* dipole moment values by introducing the projections

$$\bar{\mu}_i = \bar{\mu} \cdot \mathbf{e}_i, \quad i = 1, 2, 3. \tag{37}$$

Inserting equation (35) in equation (37), we derive

$$\bar{\mu}_i = \bar{\mu} \cdot \mathbf{e}_i = \sum_{j=1}^{3} \bar{\mu}_j^{\text{Bond}}(\mathbf{e}_j \cdot \mathbf{e}_i) = \sum_{j=1}^{3} A_{ij} \bar{\mu}_j^{\text{Bond}}, \tag{38}$$

where $A_{ij} = \mathbf{e}_j \cdot \mathbf{e}_i$ is an element of the non-orthogonal 3×3 matrix

$$\mathbf{A} = \begin{pmatrix} 1 & \cos \alpha_3 & \cos \alpha_2 \\ \cos \alpha_3 & 1 & \cos \alpha_1 \\ \cos \alpha_2 & \cos \alpha_1 & 1 \end{pmatrix}. \tag{39}$$

When the determinant $|\mathbf{A}| \neq 0$ we can invert $\mathbf{A}$ analytically and compute

$$\begin{pmatrix} \bar{\mu}_1^{\text{Bond}} \\ \bar{\mu}_2^{\text{Bond}} \\ \bar{\mu}_3^{\text{Bond}} \end{pmatrix} = \mathbf{A}^{-1} \begin{pmatrix} \bar{\mu}_1 \\ \bar{\mu}_2 \\ \bar{\mu}_3 \end{pmatrix}. \tag{40}$$

When the molecule is planar, i.e., when $\alpha_1 + \alpha_2 + \alpha_3 = 2\pi$, the determinant $|\mathbf{A}| = 0$ and $\mathbf{A}$ cannot be inverted. This is because in this particular situation, $\mathbf{e}_1$, $\mathbf{e}_2$, and $\mathbf{e}_3$ are linearly dependent and there are infinitely many possible values of $(\bar{\mu}_1^{\text{Bond}}, \bar{\mu}_2^{\text{Bond}}, \bar{\mu}_3^{\text{Bond}})$. In this case, we can express $\bar{\mu}$ in terms of $\mathbf{e}_1$ and $\mathbf{e}_2$ only [in that we set $\bar{\mu}_3^{\text{Bond}} = 0$ in equation (35)], and we can determine $\bar{\mu}_1^{\text{Bond}}$ and $\bar{\mu}_2^{\text{Bond}}$ in terms of $\bar{\mu}_1$ and $\bar{\mu}_2$.

The inversion operation E^* [3] in D_{3h}(M) has the effect of reversing the directions of $\bar{\mu}$ and each of the $\mathbf{e}_i$: $E^* \bar{\mu} = -\bar{\mu}$ and $E^* \mathbf{e}_i = -\mathbf{e}_i, i = 1, 2, 3$. Therefore,

$$E^* \bar{\mu}_i = (-\bar{\mu}) \cdot (-\mathbf{e}_i) = \bar{\mu}_i, \quad i = 1, 2, 3, \tag{41}$$

from equation (37). That is, $\bar{\mu}_i$ is invariant under E^* and we can write it in terms of the geometrically defined coordinates r_1, r_2, r_3, α_1, α_2, and α_3; these coordinates are all invariant under E^*. We define a new function $\bar{\mu}_0$ so that

$$\bar{\mu}_1 = \bar{\mu}_0(r_1, r_2, r_3, \alpha_1, \alpha_2, \alpha_3). \tag{42}$$

By making use of the fact that the permutation operations (123), (132), (12), (13), and (23) in $D_{3h}(M)$ leave $\bar{\mu}$ unchanged [3], we derive the symmetry relations

$$\bar{\mu}_1 = \bar{\mu}_0(r_1, r_2, r_3, \alpha_1, \alpha_2, \alpha_3) = \bar{\mu}_0(r_1, r_3, r_2, \alpha_1, \alpha_3, \alpha_2), \tag{43}$$

$$\bar{\mu}_2 = \bar{\mu}_0(r_2, r_3, r_1, \alpha_2, \alpha_3, \alpha_1) = \bar{\mu}_0(r_2, r_1, r_3, \alpha_2, \alpha_1, \alpha_3), \tag{44}$$

$$\bar{\mu}_3 = \bar{\mu}_0(r_3, r_1, r_2, \alpha_3, \alpha_1, \alpha_2) = \bar{\mu}_0(r_3, r_2, r_1, \alpha_3, \alpha_2, \alpha_1). \tag{45}$$

Obviously all three functions $\bar{\mu}_1$, $\bar{\mu}_2$, and $\bar{\mu}_3$ are given in terms of $\bar{\mu}_0$, and we express this function as an expansion

$$\bar{\mu}_0 = \mu_0^{(0)} + \sum_k \mu_k^{(0)}\xi_k + \sum_{k,l} \mu_{k,l}^{(0)}\xi_k\xi_l + \sum_{k,l,m} \mu_{k,l,m}^{(0)}\xi_k\xi_l\xi_m$$

$$+ \sum_{k,l,m,n} \mu_{k,l,m,n}^{(0)}\xi_k\xi_l\xi_m\xi_n + \cdots, \tag{46}$$

where

$$\xi_k = r_k \exp\left(-\beta^2 r_k^2\right), \quad k = 1, 2, 3, \tag{47}$$

$$\xi_l = \cos(\alpha_{l-3}) - \cos\left(\frac{2\pi}{3}\right) = \frac{1}{2} + \cos(\alpha_{l-3}), \quad l = 4, 5, 6. \tag{48}$$

The expansion function is chosen such that $\bar{\mu}_0 = 0$ for ($r_1 = r_2 = r_3 = 0$, $\alpha_1 = \alpha_2 = \alpha_3 = 2\pi/3$). The factor $\exp(-\beta^2 r_k^2)$ is required to keep the expansion in equation (46) from attaining unreasonably large values at large r_i [31].

In the axis system $x'y'z'$ employed in the *ab initio* calculations, the N nucleus has the coordinates (0,0,0), and H_1 has the coordinates $(0,0,z_1')$ with $z_1' > 0$. It follows from equation (36) that the unit vector $\mathbf{e}_1$ has the coordinates (0,0,1) in the $x'y'z'$ axis system and so

$$\bar{\mu}_1 = \bar{\mu}_0 = \bar{\mu} \cdot \mathbf{e}_1 = \bar{\mu}_{z'} \tag{49}$$

where $\bar{\mu}_{z'}$ is obtained directly from the *ab initio* calculation. Therefore, in principle, it should be possible to obtain the values of the parameters defining the function $\bar{\mu}_0(r_1, r_2, r_3, \alpha_1, \alpha_2, \alpha_3)$ by fitting equation (46) through the computed values of $\bar{\mu}_{z'}$ only. However, we have made *ab initio* calculations at geometries for which $r_1 \leq r_2 \leq r_3$ always. If we simply fit the available, computed values of $\bar{\mu}_{z'}$, we are always fitting the projection of the dipole moment onto the *shortest* bond. This introduces an asymmetry which degrades the accuracy of our fitting. We could circumvent this problem by generating, for each *ab initio* point, the $\bar{\mu}_{z'}$ values at the 11 symmetrically equivalent points, to which the initial point is connected by operations $R \neq E$ in $D_{3h}(M)$, and then fit all the resulting $\bar{\mu}_{z'}$ values. Another, equivalent way of circumventing the problem is to fit simultaneously the calculated values of $\bar{\mu}_1$, $\bar{\mu}_2$, and $\bar{\mu}_3$ at the original set of *ab initio* geometries with $r_1 \leq r_2 \leq r_3$. We have chosen the latter approach.

We fit equation (46) through the computed values of $\bar{\mu}_1$, $\bar{\mu}_2$, and $\bar{\mu}_3$ given by equations (43)–(45). It should be noted that the parameters in equation (46) are subject to constraints resulting from the fact that $\bar{\mu}_0(r_1, r_2, r_3, \alpha_1, \alpha_2, \alpha_3)$ is invariant to the simultaneous interchange of r_2 and r_3 and of α_2 and α_3 [equation (43)].

The expansion in equation (46), taken to fourth order, was fitted through the $3 \times 14{,}440$ *ab initio* dipole moment projections calculated for NH$_3$ at the CCSD(T)/aug-cc-pVTZ level of theory. In the fitting, we could usefully vary 91 parameters, and the root-mean-square (rms) deviation attained was 0.0006 D.[1] This is a remarkable fitting accuracy, compared to the 0.084 D attained in Ref. [31], where a much larger range of geometries was used. At the ATZfc *ab initio* equilibrium geometry [4] of $r_1 = r_2 = r_3 = r_e = 1.0149$ Å and $\alpha_1 = \alpha_2 = \alpha_3 = \alpha_e = 106.40°$, we calculate the 'equilibrium' dipole moment $\mu_e = 1.5198$ D. The experimental value is (1.561 ± 0.005) D [32].

We have also checked the effect on the rms deviation of including higher order terms in equation (46). Extending the expansion in equation (46) to sixth order, we obtain an rms deviation of 0.00006 D in the fitting to the $3 \times 14{,}440$ *ab initio* dipole moment values. However, the number of parameters required is about 400, substantially more than with the fourth-order expansion. These results demonstrate the very high internal consistency (i.e., smoothness) of the *ab initio* dipole moment surface.

In spite of the fact that we have introduced the factor of $\exp(-\beta^2 r_i^2)$ in equation (47), our analytical expression for the dipole moment does not have a qualitatively correct asymptotic behaviour for the bond lengths $r_i \rightarrow \infty$. The function does not converge to the dipole moment of the NH$_2$ fragment if we 'remove' a hydrogen atom. However, neither does it diverge: The calculated dipole moment values at large r_i are around 2–3 D depending on which dissociation path we use. Obviously, the asymptotic behaviour of the dipole moment is of no importance for the simulations carried out in the present work; we are only concerned with molecular states well below dissociation.

3.2.2. The representation in the xyz axis system

In order that we can compute the matrix elements $\langle V'|\bar{\mu}_{\mathrm{m}}^{(1,\sigma)}|V''\rangle$ ($\sigma = 0, \pm 1$), that enter into the expression for the line strength in equation (21), in terms of the vibrational basis functions $|V\rangle$ employed in our model for the rotation and vibration of XY$_3$ molecules [1], we must necessarily represent the electronically averaged dipole moment vector as

$$\bar{\boldsymbol{\mu}} = \bar{\mu}_x \mathbf{e}_x + \bar{\mu}_y \mathbf{e}_y + \bar{\mu}_z \mathbf{e}_z, \tag{50}$$

where $\mathbf{e}_x$, $\mathbf{e}_y$, $\mathbf{e}_z$ are unit vectors defining the orientations of the x, y, and z axes, respectively. These unit vectors are defined by the Eckart and Sayvetz conditions [1,3]. In the present section, we discuss how to obtain parameterized, analytical

---

[1] The fitted parameter values are available from the authors on request.

expressions for $(\bar{\mu}_x, \bar{\mu}_y, \bar{\mu}_z)$, given in terms of the vibrational coordinates that the vibrational wavefunctions $|V\rangle$ depend on.

3.2.2.1. *The transformation of the ab initio dipole moment*
values to the xyz axis system

If we know the components of the electronically averaged dipole moment $(\bar{\mu}_X, \bar{\mu}_Y, \bar{\mu}_Z)$ in the space-fixed axis system XYZ, and we know the values of the Euler angles (θ, ϕ, χ) that define the orientation of the xyz axes relative to the XYZ axes (see, for example, Ref. [3]), we can compute the xyz components $(\bar{\mu}_x, \bar{\mu}_y, \bar{\mu}_z)$ of the dipole moment from the relations

$$\bar{\mu}_\alpha = \sum_{A=X,Y,Z} S_{\alpha,A}(\theta, \phi, \chi)\bar{\mu}_A, \quad \alpha = x, y, z, \tag{51}$$

where the $S_{\alpha,A}(\theta,\phi,\chi)$ are the elements of an orthogonal, 3×3 transformation matrix $\mathbf{S}$ (see, for example, Refs. [3,33]). We determine the values of (θ, ϕ, χ) from the equation expressing the coordinate transformation from the xyz to the XYZ axis system [1]:

$$R_{i,A} = R_A^{CM} + \sum_{\alpha=x,y,z} (\mathbf{S}^{-1})_{A,\alpha}(\theta, \phi, \chi)\left[a_{i,\alpha}(\rho) + \sum_{\lambda=1,2,3,4a,4b} A_{i\alpha,\lambda}(\rho)S_\lambda^\ell\right], \tag{52}$$

In equation (52), $R_{i,A}$ $(A = X, Y, Z)$ is the A-coordinate of the position vector for nucleus i, and R_A^{CM} is the A-coordinate of the nuclear centre of mass. $(\mathbf{S}^{-1})_{A,\alpha}(\theta, \phi, \chi)$ is an element of $\mathbf{S}^{-1}$, the elements of the ρ-dependent matrix $A_{i\alpha}(\rho)$ are defined in Ref. [1], whereas the α-coordinate $a_{i\alpha}(\rho)$ $(\alpha = x, y, z)$ of nucleus i in the HBJ reference configuration [1] is given in Ref. [34]. The HBJ inversion coordinate ρ is defined in Ref. [1]. When the molecule is in the reference configuration, which has C_{3v} or D_{3h} geometrical symmetry (i.e., it has $r_1 = r_2 = r_3 = r_e$ and $\alpha_1 = \alpha_2 = \alpha_3$), ρ is the angle between the C_3 rotational symmetry axis and any one of the N–H bonds. That is, $0 \le \rho \le \pi$ (see Ref. [1] and Fig. 1). Finally, in equation (52), the S_λ^ℓ are the linearized coordinates defined in Ref. [1]; these coordinates measure the displacement of the molecule from the reference configuration. For $\lambda = 1, 2, 3$ we have $S_\lambda^\ell = r_\lambda^\ell - r_e$, where $r_\lambda^\ell \approx r_\lambda$ when the molecule is near the reference configuration. Further,

$$S_{4a}^\ell = \frac{1}{\sqrt{6}}(2\alpha_1^\ell - \alpha_2^\ell - \alpha_3^\ell), \tag{53}$$

$$S_{4b}^\ell = \frac{1}{\sqrt{2}}(\alpha_2^\ell - \alpha_3^\ell). \tag{54}$$

where $\alpha_i^\ell \approx \alpha_i$ when the molecule is near the reference configuration.

At each calculated *ab initio* point we set the space-fixed XYZ axis system equal to the $x'y'z'$ axis system employed in the *ab initio* calculations. That is, we set $(R_{i,X}, R_{i,Y}, R_{i,Z}) = (x_i', y_i', z_i')$ for $i = 1, 2, 3, 4$. We then use least-squares methods to determine from equation (52) a set of 12 coordinates $\rho, R_X^{CM}, R_Y^{CM}, R_Z^{CM}, \theta, \phi, \chi, S_1^\ell, S_2^\ell, S_3^\ell, S_{4a}^\ell, S_{4b}^\ell$ (to any desired accuracy). These coordinate values

will, by necessity, satisfy the Eckart and Sayvetz conditions [1]; this is ensured by the form of the matrix elements $A_{i\alpha,\lambda}(\rho)$ [1]. With the computed values of θ, ϕ, χ, and the known *ab initio* values of $(\bar{\mu}_X, \bar{\mu}_Y, \bar{\mu}_Z) = (\bar{\mu}_{x'}, \bar{\mu}_{y'}, \bar{\mu}_{z'})$, we can then compute $(\bar{\mu}_x, \bar{\mu}_y, \bar{\mu}_z)$ from equation (51).

3.2.2.2. The analytical representations of $(\bar{\mu}_x, \bar{\mu}_y, \bar{\mu}_z)$
We fit analytical functions of ρ, S_1^ℓ, S_2^ℓ, S_3^ℓ, S_{4a}^ℓ, and S_{4b}^ℓ through the values of $(\bar{\mu}_x, \bar{\mu}_y, \bar{\mu}_z)$ resulting from the transformation described above. The analytical representation of $\bar{\mu}_\alpha$ ($\alpha = x, y, z$) is chosen as

$$\bar{\mu}_\alpha(\xi_1^\ell, \xi_2^\ell, \xi_3^\ell, \xi_{4a}^\ell, \xi_{4b}^\ell; \rho) = \mu_0^\alpha(\rho) + \sum_k \mu_k^\alpha(\rho)\xi_k^\ell + \sum_{k \leq l} \mu_{kl}^\alpha(\rho)\xi_k^\ell\xi_l^\ell$$
$$+ \sum_{k \leq l \leq m} \mu_{klm}^\alpha(\rho)\xi_k^\ell\xi_l^\ell\xi_m^\ell + \sum_{k \leq l \leq m \leq n} \mu_{klmn}^\alpha(\rho)\xi_k^\ell\xi_l^\ell\xi_m^\ell\xi_n^\ell \dots$$

(55)

by analogy with the Type B representation of the potential energy surface defined in Ref. [1]. In equation (55) we have introduced the linearized variables

$$\xi_k^\ell = 1 - \exp(-aS_k^\ell), \quad k = 1, 2, 3, \tag{56}$$

$\xi_{4a}^\ell = S_{4a}^\ell$, $\xi_{4b}^\ell = S_{4b}^\ell$, and the range parameter a occurring in the analytical representation for the potential energy function [1]. The quantities ξ_1^ℓ, ξ_2^ℓ, ξ_3^ℓ, ξ_{4a}^ℓ, and ξ_{4b}^ℓ are discussed further in Ref. [1].

The ρ-dependent functions $\mu_{kl\dots}^\alpha(\rho)$ ($\alpha = x$ or y) in equation (55) are chosen as

$$\mu_{kl\dots}^\alpha(\rho) = \sum_{s \geq 0} \mu_{kl\dots}^{\alpha(s)}(\sin \rho_0 - \sin \rho)^s, \quad 0 \leq \rho \leq \pi, \tag{57}$$

where we take $\rho_0 = \pi/2$, corresponding to the planar configuration. The dipole moment components $(\bar{\mu}_x, \bar{\mu}_y)$ have E' symmetry in $D_{3h}(M)$ and therefore ($\alpha = x$ or y)

$$E^* \mu_{kl\dots}^\alpha(\rho) = \mu_{kl\dots}^\alpha(\rho) \tag{58}$$

or, equivalently,

$$\mu_{kl\dots}^\alpha(\pi - \rho) = \mu_{kl\dots}^\alpha(\rho) \tag{59}$$

since $E^*\rho = \pi - \rho$. The function $\mu_{kl\dots}^\alpha(\rho)$ given in equation (57) satisfies this requirement.

The dipole moment component $\bar{\mu}_z$ has A_2'' symmetry in $D_{3h}(M)$ so that

$$\mu_{kl\dots}^z(\pi - \rho) = -\mu_{kl\dots}^z(\rho). \tag{60}$$

We choose ($\rho_0 = \pi/2$)

$$\mu_{kl\dots}^z(\rho) = \sum_{s > 0} \mu_{kl\dots}^{z(s)}(\cos \rho_0 - \cos \rho)^s \quad \text{for} \quad \frac{\pi}{2} \leq \rho \leq \pi, \tag{61}$$

and

$$\mu_{kl\ldots}^z(\rho) = -\mu_{kl\ldots}^z(\pi - \rho) \quad \text{for } 0 \le \rho < \frac{\pi}{2}. \tag{62}$$

Since, with the definition in equation (61), $\mu_{kl\ldots}^z(\pi/2) = 0$, no inconsistency arises because of equation (62). If we allowed only odd powers s in the sum of equation (61), we could let this equation define $\mu_{kl\ldots}^z(\rho)$ in the entire interval $0 \le \rho \le \pi$. However, we have found that a better fit to the *ab initio* dipole moment values can be obtained when we include both odd and even s in equation (61) and extend the definition by equation (62).

Equations (59) and (62) ensure that the analytical representations of $(\bar{\mu}_x, \bar{\mu}_y, \bar{\mu}_z)$ have the correct transformation properties under the inversion operation E^*. Since the appropriate symmetry group for NH$_3$, D_{3h}(M), can be written as the direct product given in equation (27), we must now ascertain that $(\bar{\mu}_x, \bar{\mu}_y, \bar{\mu}_z)$ also transform appropriately under the operations in C_{3v}(M). If this is the case, they will have correct transformation properties under all operations in D_{3h}(M).

Correlation from D_{3h}(M) to C_{3v}(M) shows that $(\bar{\mu}_x, \bar{\mu}_y)$ have E symmetry in C_{3v}(M) and $\bar{\mu}_z$ has A_1 symmetry. We investigate the transformation properties of $(\bar{\mu}_x, \bar{\mu}_y, \bar{\mu}_z)$ in C_{3v}(M) by means of a newly developed MAPLE VI [35] routine.[2] By definition [3], the effect of a symmetry operation R in C_{3v}(M) on the dipole moment component $\bar{\mu}_\alpha(\xi_k^\ell)$ is given by

$$R\bar{\mu}_\alpha(\xi_k^\ell) = \bar{\mu}_\alpha(R\xi_k^\ell), \tag{63}$$

where ξ_k^ℓ is a shorthand notation for all the variables $\xi_1^\ell, \xi_2^\ell, \xi_3^\ell, \xi_{4a}^\ell, \xi_{4b}^\ell$, and we omit the coordinate ρ which is invariant under the operations in C_{3v}(M). For example, since $\bar{\mu}_z$ has A_1 symmetry in C_{3v}(M), it is left unchanged by the operation $(23)^*$:

$$(23)^* \bar{\mu}_z(\xi_1^\ell, \xi_2^\ell, \xi_3^\ell, \xi_{4a}^\ell, \xi_{4b}^\ell) = \bar{\mu}_z(\xi_1^\ell, \xi_2^\ell, \xi_3^\ell, \xi_{4a}^\ell, \xi_{4b}^\ell). \tag{64}$$

On other hand, it is straightforward to determine the effect of $(23)^*$ on the variables $\xi_1^\ell, \xi_2^\ell, \xi_3^\ell, \xi_{4a}^\ell, \xi_{4b}^\ell$:

$$(23)^* \bar{\mu}_z(\xi_1^\ell, \xi_2^\ell, \xi_3^\ell, \xi_{4a}^\ell, \xi_{4b}^\ell) = \bar{\mu}_z(\xi_1^\ell, \xi_3^\ell, \xi_2^\ell, \xi_{4a}^\ell, -\xi_{4b}^\ell). \tag{65}$$

Comparison of equations (64) and (65) produces

$$\bar{\mu}_z(\xi_1^\ell, \xi_2^\ell, \xi_3^\ell, \xi_{4a}^\ell, \xi_{4b}^\ell) = \bar{\mu}_z(\xi_1^\ell, \xi_3^\ell, \xi_2^\ell, \xi_{4a}^\ell, -\xi_{4b}^\ell). \tag{66}$$

When we now insert the expansion from equation (55) on both sides of equation (66), relations between the expansion coefficients in equation (55) ensue. For example, from equation (66) the first-order expansion coefficients in the expression for $\bar{\mu}_z$ must satisfy

$$\mu_2^{z(s)} = \mu_3^{z(s)} \tag{67}$$

---

[2] This routine is available from the authors on request.

$$\mu_{4a}^{z(s)} = -\mu_{4a}^{z(s)} \tag{68}$$

so that $\mu_{4a}^{z(s)} = 0$. By combining these relations with the results of applying other $C_{3v}(M)$ operations, we obtain that to first order

$$\bar{\mu}_z = \mu_0^z(\rho) + \mu_1^z(\rho)(\xi_1^\ell + \xi_2^\ell + \xi_3^\ell). \tag{69}$$

Relations for the higher order parameters $\mu_{klmn\ldots}^\alpha$ (up to sixth order) are derived analytically using the MAPLE command 'solve', which arbitrarily chooses a minimum set of independent parameters and expresses the other parameters in terms of them. The derived relations are then converted to FORTRAN and become part of the intensity program. Analogous MAPLE procedures have also been applied for the dipole moment function in the MB representation and for the potential function expansions [1].

3.2.2.3. The least-squares fitting of $(\bar{\mu}_x, \bar{\mu}_y, \bar{\mu}_z)$

Having derived the symmetry relations between the expansion parameters in equation (55), we can proceed to fit the expansions through the *ab initio* dipole moment values. The expansion parameters in the expressions for $\bar{\mu}_x$ and $\bar{\mu}_y$ are connected by symmetry relations since these two quantities have E' symmetry in $D_{3h}(M)$, and so $\bar{\mu}_x$ and $\bar{\mu}_y$ must be fitted together. The component $\bar{\mu}_z$, with A_2'' symmetry, can be fitted separately. The variables ξ_k^ℓ, ρ in equation (55) are chosen to reflect the properties of the potential surface, rather than those of the dipole moment surfaces. Therefore, the fittings of $(\bar{\mu}_x, \bar{\mu}_y, \bar{\mu}_z)$ require more parameters than the fittings of the MB dipole moment representations. We fitted the 14,400 *ab initio* data points using 77 parameters for the $\bar{\mu}_z$ component and 141 parameters for $\bar{\mu}_x$, $\bar{\mu}_y$. The rms deviations attained were 0.00016 and 0.0003 D, respectively.

The parameterized, analytical representations of $(\bar{\mu}_x, \bar{\mu}_y, \bar{\mu}_z)$ determined in the fitting are in a form suitable for the calculation of the vibronic transition moments $\langle V'|\bar{\mu}_m^{(1,\sigma)}|V''\rangle$ ($\sigma = 0, \pm 1$), that enter into the expression for the line strength in equation (21). These matrix elements are computed in a manner analogous to that employed for the matrix elements of the potential energy function in Ref. [1].

4. APPLICATIONS

4.1. Transition moments

In this section, we report calculated values of the vibrational transition moments for vibrational transitions $v_2'\nu_2^\mp \leftarrow v_2''\nu_2^\pm$ of ^{14}NH$_3$, where ν_2 is the inversion mode,[3] $\nu_2'' \leq 4$ and $\nu_2' \leq 4$. These transition moments are matrix elements of $\bar{\mu}_z$; they are essentially determined by the dependence of $\bar{\mu}_z$ on the inversion coordinate ρ.

---

[3] In the labelling of the vibrational states, a superscript $+$ indicates the lower (symmetric) inversion component; the upper (antisymmetric) component is indicated by a superscript $-$.

The transition moments are calculated from the *ab initio* dipole moment surface, represented in the *xyz* axis system as described above. They are defined as

$$\mu_{\mathrm{fi}} = \sqrt{\sum_{\alpha=x,y,z} |\langle \Phi_{\mathrm{rv}}^{(\mathrm{f})} | \bar{\mu}_\alpha | \Phi_{\mathrm{rv}}^{(\mathrm{i})} \rangle|^2}, \tag{70}$$

where $\bar{\mu}_\alpha$ is given in equation (55), while $|\Phi_{\mathrm{rv}}^{(\mathrm{i})}\rangle$ and $|\Phi_{\mathrm{rv}}^{(\mathrm{f})}\rangle$ are the $J=0$ rotation–vibration functions computed variationally as described in Ref. [1]. As mentioned above, for the vibrational transitions that we consider here, only matrix elements of $\bar{\mu}_z$ are non-vanishing in equation (70). The wavefunctions $|\Phi_{\mathrm{rv}}^{(\mathrm{i})}\rangle$ and $|\Phi_{\mathrm{rv}}^{(\mathrm{f})}\rangle$ are obtained from the *ab initio* potential energy surface CBS**-5 [36]. This surface is determined as follows: ATZfc electronic energies were computed at 51,816 nuclear geometries using the CCSD(T) method (coupled cluster theory with all single and double substitutions [23] and a perturbative treatment of connected triple excitations [24,25]) with the augmented correlation-consistent triple-zeta basis aug-cc-pVTZ [26,27]. At 3814 selected geometries, more accurate CBS+ energies were determined by extrapolating the CCSD(T) results to the complete basis set limit and including corrections for relativistic effects and core–valence correlation [4]. The differences between the ATZfc and CBS+ energies were fitted by a sixth-order polynomial in geometrically defined, internal coordinates, and the corrections were added to the ATZfc energies at all 51,816 grid points to generate the CBS**-5 surface (which is close to CBS+ quality). An analytical representation of this surface was obtained by fitting the sixth-order expansion given in equation (7) of Ref. [4] through all CBS**-5 data points. The resulting 181 potential parameter values will be given elsewhere [36] and are also available from the authors on request.

In the variational calculations, the expansions of the kinetic energy factors $G_{\alpha\beta}$ and the pseudo-potential U [1] are taken to fourth order, and, as mentioned above, the potential energy V is expanded through sixth order. In the numerical integration of the inversion Schrödinger equation a grid of 1000 points is used. The basis set [1] is truncated so that

$$P = 2(v_1 + v_2 + v_3) + v_{\mathrm{inv}} + v_4 \leq 14. \tag{71}$$

With $P \leq 14$, the $J=0$ matrix blocks corresponding to A_1 and E symmetry in the group $C_{3v}(\mathrm{M})$ have the dimensions $N(A_1)=1455$ and $N(E)=2571$, respectively. The matrices are diagonalized with routines from the LAPACK library [37].

The calculated transition moments are listed in Table 3, where they are compared with the available experimental data [38–44] and also with the values calculated by Marquardt *et al.* [31] and Pracna *et al.* [45]. Our results are in good agreement with both the experimental and the theoretical data.

There is a qualitative change in the dependence of the $\Delta v_2 = 1$ transition moments on the inversion state at the top of the barrier to planarity, which is about $1800\,\mathrm{cm}^{-1}$ [4,46–50]. Below the inversion barrier, the matrix elements $\langle (v_2 - 1)^+ | \bar{\mu}_z | v_2^- \rangle$ and $\langle (v_2 - 1)^- | \bar{\mu}_z | v_2^+ \rangle$ are approximately equal. Above the barrier

Table 3. Transition moments (in D) for vibrational transitions $v_2' \nu_2^{\mp} \leftarrow v_2'' \nu_2^{\pm}$ of ^{14}NH$_3$

$(v_2'')^{\pm}$	$(v_2')^{\pm}$	Obs.	References[a]	Reference [45]	Reference [31]	Present work
0^+	1^-	0.236	[38]	0.237	0.208	0.235
0^-	1^+	0.248	[38]	0.247	0.218	0.245
1^+	2^-	0.285	[39]	0.287	0.270	0.286
1^-	2^+			0.525	0.508	0.514
2^+	3^-			0.111	0.083	0.112
2^-	3^+	1.05	[40]	0.901	0.943	0.888
3^+	4^-					0.034
3^-	4^+					0.993
0^+	0^-	1.4719	[41]	1.471	1.574	1.456
1^+	1^-	1.2448	[42]	1.248	1.355	1.238
2^+	2^-	1.02	[40]	0.948	1.047	0.938
3^+	3^-			0.981	1.039	0.967
4^+	4^-			1.043	1.072	1.020
0^+	2^-	0.0033	[43]	0.000	0.026	0.003
0^-	2^+	0.0204	[43]	0.019	0.009	0.020
0^+	3^-	0.0037	[44][b]	0.005	0.016	0.003
0^-	3^+	0.0060	[44][b]	0.008	0.026	0.005
0^+	4^-					0.001
0^-	4^+					0.002

[a] Reference for the observed value given under the heading 'Obs.'
[b] Benedict *et al.* [44] as cited in Ref. [45].

(i.e., for $v_2 > 2$) the $\langle (v_2 - 1)^+ | \bar{\mu}_z | v_2^- \rangle$ transition moment is much smaller than $\langle (v_2 - 1)^- | \bar{\mu}_z | v_2^+ \rangle$. We explain this behaviour by means of wavefunction analysis.

First we note that, as shown in Fig. 2, $|\bar{\mu}_z|$ is zero at planar configurations and increases with inversion displacement. Consequently, a large value of
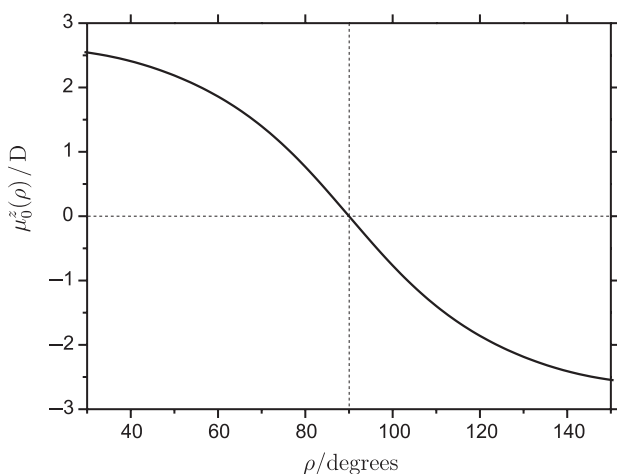
Fig. 2. The function $\mu_0^z(\rho)$ for ^{14}NH$_3$. Note that $\mu_0^z(\pi - \rho) = -\mu_0^z(\rho)$.

the transition moment $\langle (v_2'')^\pm | \bar{\mu}_z | (v_2')^\mp \rangle$ requires that the two wavefunctions $|(v_2'')^\pm \rangle$ and $|(v_2')^\mp \rangle$ have a significant overlap at distorted geometries with ρ near 0 or ρ near π. To investigate how the wavefunctions overlap, we plot in Fig. 3 the inversion angle probability distribution, obtained by integrating the square of the vibrational wavefunction over the stretching and small-amplitude bending coordinates S_1^ℓ, S_2^ℓ, S_3^ℓ, S_{4a}^ℓ, and S_{4b}^ℓ, for states $v_2 v_2^\pm$ with $v_2 \leq 4$. The normalized inversion-coordinate probability density function $f(\rho)$ is given by

$$f(\rho) = \int dV |\psi_{\rm vib}|^2, \tag{72}$$

where dV is the volume element for the stretching and small-amplitude bending coordinates S_1^ℓ, S_2^ℓ, S_3^ℓ, S_{4a}^ℓ, and S_{4b}^ℓ.

In Fig. 3, the states $v_2 v_2^\pm$ are combined in pairs $[(v_2 - 1)^\pm, v_2^\mp]$ corresponding to the vibrational transitions in Table 3. At $v_2 \leq 2$ (i.e., below the inversion barrier), the figure shows that for each of the two wavefunction pairs $[(v_2 - 1)^-, v_2^+]$ and $[(v_2 - 1)^+, v_2^-]$, the pair members overlap in a similar manner and have significant comparable overlaps for ρ near 0 or ρ near π. At higher v_2 values, the members of the $[(v_2 - 1)^-, v_2^+]$ pair overlap only at very distorted geometries with ρ near 0 or ρ near π. The corresponding transition moments are therefore large. The members of the $[(v_2 - 1)^+, v_2^-]$ pair overlap near planarity ($\rho \approx \pi/2$), where $|\bar{\mu}_z|$ is small, and so the corresponding transition moments are small. These wavefunctions are dephased for ρ near 0 or ρ near π. Thus, the qualitative variation of $[(v_2 - 1)^-, v_2^+]$ and $[(v_2 - 1)^+, v_2^-]$ with excitation of the inversion mode is connected with the fact that the amplitude of the inversion wavefunctions is shifted away from the planar configuration, i.e., it is shifted towards $\rho = 0$ or $\rho = \pi$, in higher excited inversion states.

4.2. Simulations of rotation–vibration spectra

As detailed in Section 2, we have derived and programmed the expression for line strengths of individual rotation–vibration transitions of XY_3 molecules; the line strengths depend on the vibronic transition moments entering into equation (70). With the theory of Section 2, we can simulate rotation–vibration absorption spectra of XY_3 molecules. In computing the transition wavenumbers, line strengths, and intensities we use rovibronic wavefunctions generated as described in Ref. [1].

In the present section, we give examples of simulated vibrational bands of $^{14}NH_3$. These bands start in the lowest inversion states $0^\pm$ and end in the states $v_2 v_2^\mp$ with $v_2 \leq 4$. The rovibrational wavefunctions with $J \leq 18$ are calculated variationally as described in Ref. [1]. To make these variational calculations feasible the size of the vibrational basis set is reduced relative to that employed for the calculations of vibrational transition moments in Section 4.1. We now require that

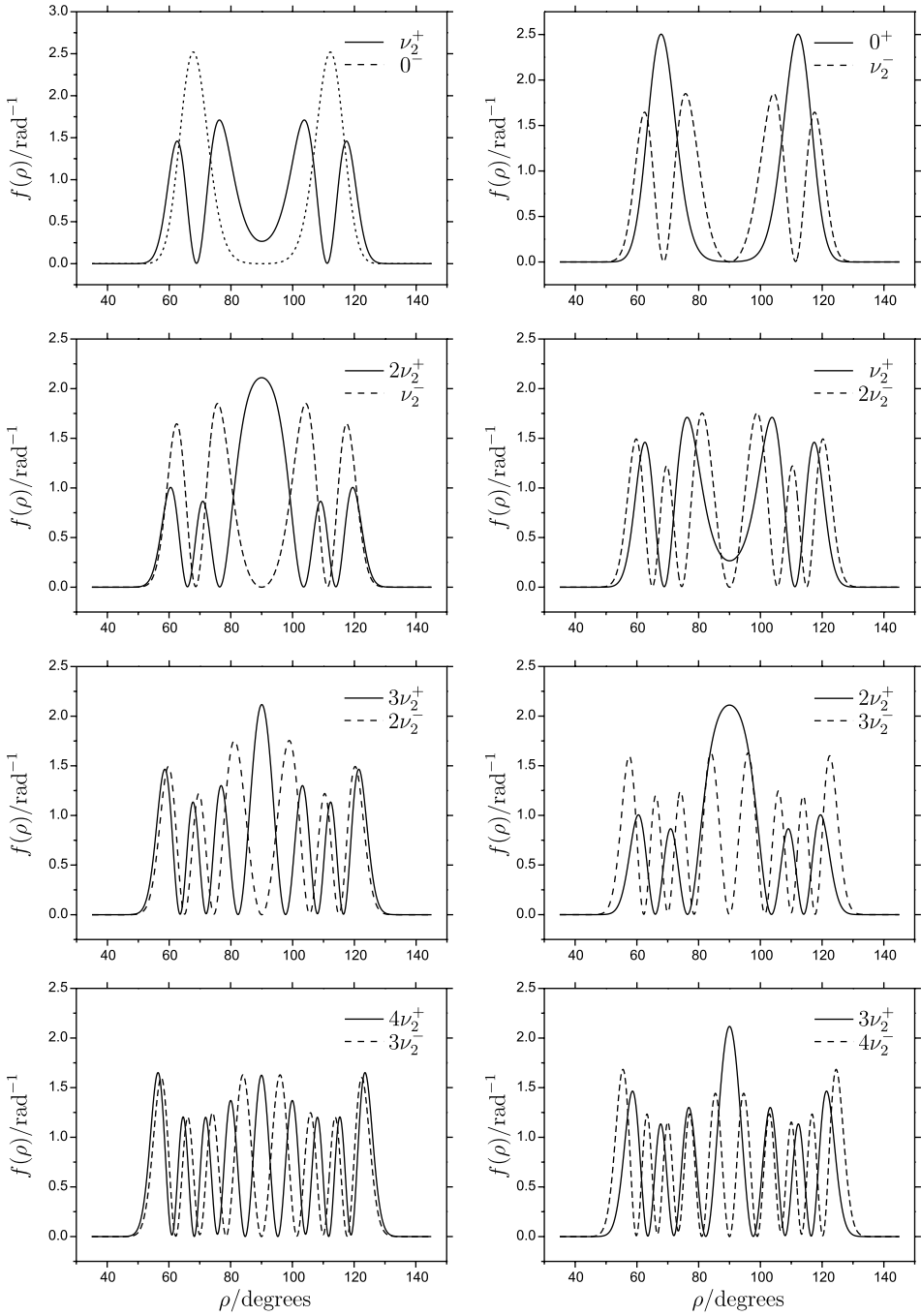$$P = 2(v_1 + v_2 + v_3) + v_{\rm inv} + v_4 \leq 8. \tag{73}$$

Fig. 3. Inversion probability density functions for the ^{14}NH$_3$ inversion states $v_2\nu_2^{\pm}$ with $v_2 \leq 4$.

The largest matrix blocks obtained with this basis set are the E symmetry blocks at $J = 18$; they have the dimension $N(E) = 9150$.

In Fig. 4, we show simulations of the vibrational absorption bands $v_2' v_2'^{\pm} \leftarrow 0^{\pm} (v_2' \leq 4)$ for $^{14}NH_3$. The simulated spectra are drawn as stick diagrams where the height of the stick representing a line is the integrated absorption coefficient from equation (6), calculated from the line strengths given by equation (21) at the absolute temperature $T = 295$ K. In these calculations, we use the partition function value $Q = 1713.33$, which is obtained from the $J \leq 18$ term

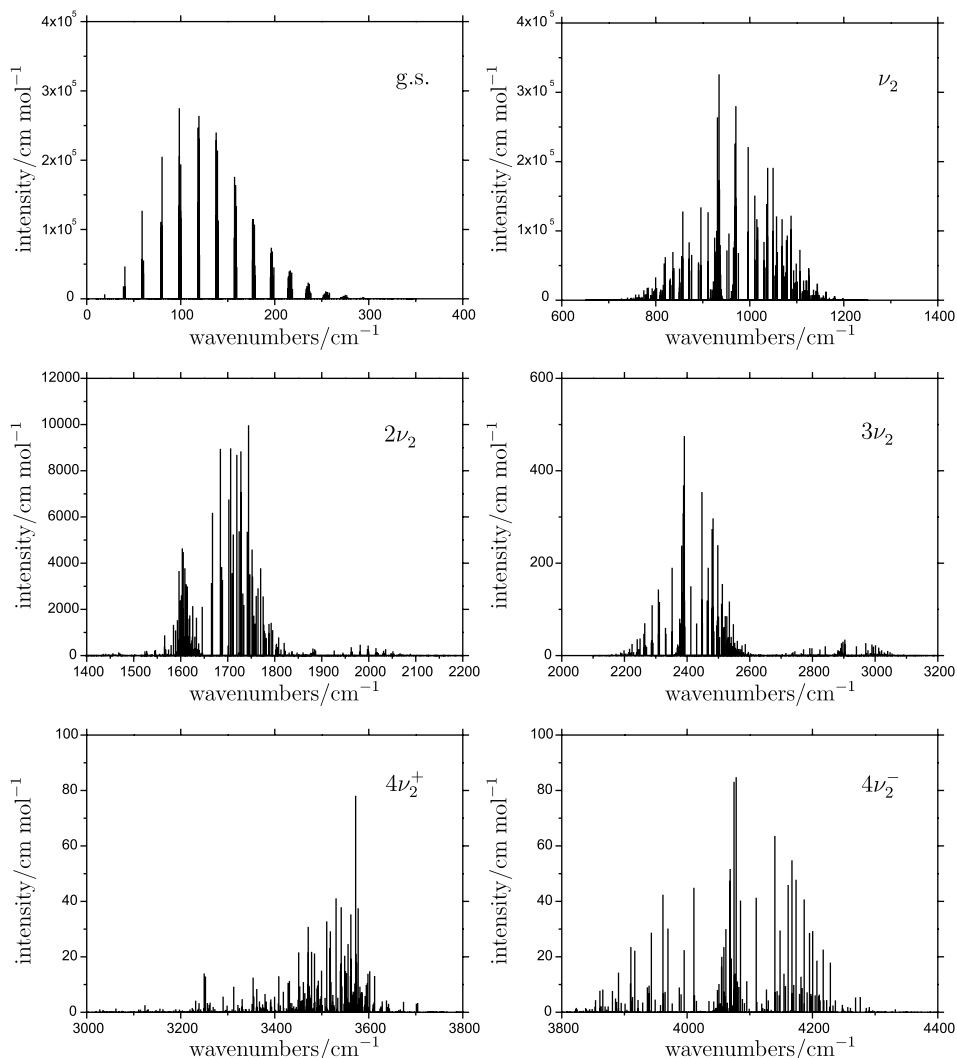**Fig. 4.** Simulations of the vibrational absorption bands $v_2' v_2'^{\mp} \leftarrow 0^{\pm} (v_2' \leq 4)$ for $^{14}NH_3$ at the absolute temperature $T = 295$ K. The plots for ν_2, $2\nu_2$, and $3\nu_2$ comprise the two components $v_2' v_2'^{+} \leftarrow 0^{-}$ and $v_2' v_2'^{-} \leftarrow 0^{+}$.
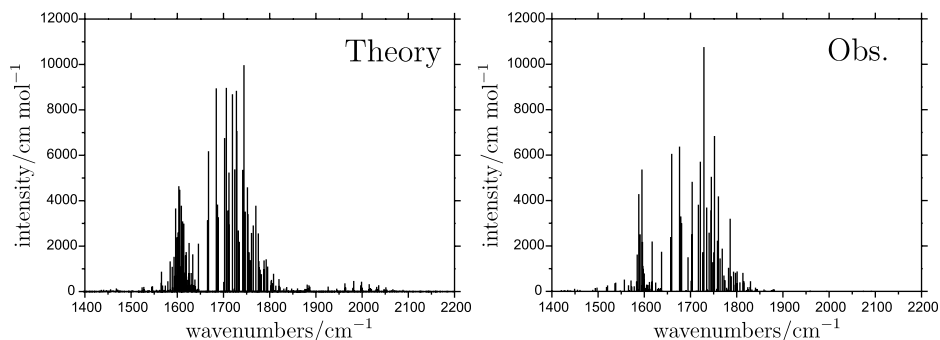
Fig. 5. Simulations of the $2\nu_2$ and ν_4 bands of ^{14}NH$_3$ at $T=295$ K compared to experimental data from Ref. [43].

values calculated variationally below 6000 cm^{-1} and the spin statistical weight factors for ^{14}NH$_3$ from Table 2. This value of Q can be compared to the value of 574.16 from Ref. [51], obtained at $T=295$ K with spin statistical weight factors which, in an obvious notation, can be written as $g_{ns}(A_1)=0$, $g_{ns}(A_2)=4$, and $g_{ns}(E)=2$. That is, the spin statistical weights employed in Ref. [51] are three times smaller than those given in Table 2. The reason is that Urban *et al.* [51] ignore the factor of 3 which the ^{14}N nucleus (with spin $I=1$) contributes to each nuclear spin statistical weight factor. This difference does not matter for the calculation of the integrated absorption coefficient $I(f\leftarrow i)$ from equation (6) since the line strength factor $S(f\leftarrow i)$ in this equation contains a factor of g_{ns} [equation (21)], while all terms in the partition function Q also contain g_{ns}-factors. Multiplying all g_{ns}-values by a constant factor thus does not change $I(f\leftarrow i)$. In the present work, we follow Bunker and Jensen [3] in defining g_{ns} as the actual nuclear-spin degeneracy of each rotation–vibration level, and this leads to the g_{ns}-values in Table 2. When we multiply the Q value from Ref. [51] by 3, we get $Q=1722.48$, in satisfactory agreement with the value of 1713.33 from the present work.

In the simulated band $4\nu_2^\pm \leftarrow 0^\pm$ in Fig. 4, both components ($+\leftarrow-$ and $-\leftarrow+$) have comparable intensities, whereas in the bands $2\nu_2^\pm \leftarrow 0^\pm$ and $3\nu_2^\pm \leftarrow 0^\pm$ the $+\leftarrow-$ component dominates as suggested by the transition moments in Table 3.

To assess the quality of the simulated spectra, we compare in Fig. 5 the simulated $2\nu_2$ and ν_4 bands of ^{14}NH$_3$ with stick spectra drawn with the experimental data given in appendix of Ref. [43]. That is, the 'experimental' spectrum shows only the transitions *assigned* in Ref. [43], which explains why the experimental spectrum contains less lines than the simulated one. In the simulated and the 'experimentally derived' stick spectra, the intensities are given as integrated absorption coefficients in cm mol^{-1}. The experimental values, originally [43] given in cm^{-2} atm^{-1}, were converted to cm mol^{-1} at $T=295$ K. We see that there is significant similarity between the simulated and 'experimentally derived' stick spectra: The agreement with experiment is rather good.

5. CONCLUSIONS

In the present paper, we have described a complex, but powerful 'tool' for simulating spectra of NH_3. The simulated spectra are directly comparable with experimentally observed spectra. The tool consists of

- a variationally based model, with accompanying computer program, for accurate calculations of rovibrational energies and wavefunctions of XY_3 pyramidal molecules [1],
- an accurate *ab initio* potential energy function for NH_3 [36],
- a computational procedure for intensity simulations based on the results of the variational calculations [Section 2.3, in particular equation (21)], and
- high quality *ab initio* dipole moment surfaces for NH_3.

The accuracy of the dipole moment surfaces is documented by the calculated transition moments in Table 3.

In Fig. 5, the agreement of the calculated absolute intensity values with the corresponding experimental values is an indication of the high quality of the *ab initio* dipole moment surfaces employed in the calculation. The qualitatively correct appearance of the bands indicates that our solution of the rotation–vibration Schrödinger equation and the potential energy surface employed are satisfactory. It should be emphasized that the *ab initio* potential energy and dipole moment surfaces have not been adjusted to fit experiment.

ACKNOWLEDGEMENTS

REFERENCES

[1] S. N. Yurchenko, M. Carvajal, P. Jensen, H. Lin, J. Zheng and W. Thiel, *Mol. Phys.*, 2005, **103**, 359.
[2] J. T. Hougen, P. R. Bunker and J. W. C. Johns, *J. Mol. Spectrosc.*, 1970, **34**, 136.
[3] P. R. Bunker and P. Jensen, *Molecular Symmetry and Spectroscopy*, 2nd edn., NRC Research Press, Ottawa, 1998.
[4] H. Lin, W. Thiel, S. N. Yurchenko, M. Carvajal and P. Jensen, *J. Chem. Phys.*, 2002, **117**, 11265.
[5] S. N. Yurchenko, M. Carvajal, P. Jensen, F. Herregodts and T. R. Huet, *Chem. Phys.*, 2003, **290**, 59.
[6] D. Wang, Q. Shi and Q.-S. Zhu, *J. Chem. Phys.*, 2000, **112**, 9624.

[7] C. Léonard, N. C. Handy, S. Carter and J. M. Bowman, *Spectrochim. Acta A*, 2002, **58**, 825.

[8] S. M. Colwell, S. Carter and N. C. Handy, *Mol. Phys.*, 2003, **101**, 523.

[9] S. N. Yurchenko, P. R. Bunker and P. Jensen, *J. Mol. Struct.*, 2005, **742**, 43.

[10] L. Lammich, H. Buhr, H. Kreckel, S. Krohn, M. Lange, D. Schwalm, R. Wester, A. Wolf, D. Strasser, D. Zajfman, Z. Vager, I. Abril, S. Heredia-Avalos and R. Garcia-Molina, *Phys. Rev. A*, 2004, **69**, 062904.

[11] F. Légaré, K. F. Lee, I. V. Litvinyuk, P. W. Dooley, S. S. Wesolowski, P. R. Bunker, P. Dombi, F. Krausz, A. D. Bandrauk, D. M. Villeneuve and P. Corkum, *Phys. Rev. A*, 2005, **71**, 013415.

[12] P. Jensen, T. E. Odaka, W. P. Kraemer, T. Hirano and P. R. Bunker, *Spectrochim. Acta A*, 2002, **58**, 763.

[13] S. N. Yurchenko, W. Thiel, S. Patchkovskii and P. Jensen, Contributed Lecture M3, 18th International Conference on High Resolution Molecular Spectroscopy, Prague, Czech Republic, September 8–12, 2004.

[14] S. N. Yurchenko, W. Thiel, S. Patchkovskii and P. Jensen, *Phys. Chem. Chem. Phys.* 2005, **7**, 573.

[15] P. Jensen, G. Osmann and I. N. Kozin, in *Vibration–Rotational Spectroscopy and Molecular Dynamics* (ed. D. Papoušek), World Scientific, Singapore, 1997.

[16] P. Jensen, *Mol. Phys.*, 2000, **98**, 1253.

[17] I. Kleiner, L. R. Brown, G. Tarrago, Q.-L. Kou, N. Picqué, G. Guelachvili, V. Dana and J.-Y. Mandin, *J. Mol. Spectrosc.*, 1999, **193**, 46.

[18] P. Jensen and V. Špirko, *J. Mol. Spectrosc.*, 1986, **118**, 208.

[19] P. Jensen, *J. Mol. Spectrosc.*, 1988, **132**, 429.

[20] S. S. Penner, *Quantitative Molecular Spectroscopy and Gas Emissivities*, Addison-Wesley, Reading, MA, 1959.

[21] G. K. Woodgate, *Elementary Atomic Structure*, McGraw-Hill, Maidenhead, 1970.

[22] R. N. Zare, *Angular Momentum*, Wiley, New York, 1988.

[23] G. D. Purvis and R. J. Bartlett, *J. Chem. Phys.*, 1982, **76**, 1910.

[24] M. Urban, J. Noga, S. J. Cole and R. J. Bartlett, *J. Chem. Phys.*, 1985, **83**, 4041.

[25] K. Raghavachari, G. W. Trucks, J. A. Pople and M. Head-Gordon, *Chem. Phys. Lett.*, 1989, **157**, 479.

[26] T. H. Dunning, *J. Chem. Phys.*, 1989, **90**, 1007.

[27] D. E. Woon and T. H. Dunning, *J. Chem. Phys.*, 1993, **98**, 1358.

[28] MOLPRO2000 is a package of *ab initio* programs written by H.-J. Werner and P. J. Knowles, with contributions from R. D. Amos, A. Bernhardsson, A. Berning, P. Celani, D. L. Cooper, M. J. O. Deegan, A. J. Dobbyn, F. Eckert, C. Hampel, G. Hetzer, T. Korona, R. Lindh, A. W. Lloyd, S. J. McNicholas, F. R. Manby, W. Meyer, M. E. Mura, A. Nicklass, P. Palmieri, R. Pitzer, G. Rauhut, M. Schütz, H. Stoll, A. J. Stone, R. Tarroni and T. Thorsteinsson.

[29] C. Hampel, K. Peterson and H.-J. Werner, *Chem. Phys. Lett.*, 1992, **190**, 1 and references therein. The program to compute the perturbative triples corrections has been developed by M. J. O. Deegan and P. J. Knowles, *Chem. Phys. Lett.*, 1994, **227**, 321.

[30] S.-G. He, J.-J. Zheng, S.-M. Hu, H. Lin, Y. Ding, X.-H. Wang and Q.-S. Zhu, *J. Chem. Phys.*, 2001, **114**, 7018.

[31] R. Marquardt, M. Quack, I. Thanopulos and D. Luckhaus, *J. Chem. Phys.*, 2003, **119**, 10724.

[32] M. D. Marshall, K. C. lzgi and J. S. Muenter, *J. Chem. Phys.*, 1997, **107**, 1037.

[33] D. Papoušek and M. R. Aliev, *Molecular Vibrational–Rotational Spectra*, Elsevier, Amsterdam, 1982.

[34] D. Papoušek, J. M. R. Stone and V. Špirko, *J. Mol. Spectrosc.*, 1973, **48**, 17.

[35] M. B. Monagan, K. O. Geddes, K. M. Heal, G. Labahn, S. M. Vorkoetter and J. McCarron, Maple 6 Programming Guide, Waterloo Maple, Toronto, 2000.

[36] H. Lin, J. J. Zheng, S. N. Yurchenko, P. Jensen and W. Thiel, to be published.

[37] E. Anderson, Z. Bai, C. Bischof, S. Blackford, J. Demmel, J. Dongarra, J. Du Croz, A. Greenbaum, S. Hammarling, A. McKenney and D. Sorensen, LAPACK Users' Guide, http://www.netlib.org/lapack/, 3rd edn., 1999.

[38] T. Nakanaga, S. Kondo and S. Saëki, *J. Mol. Spectrosc.*, 1985, **112**, 39.

[39] P. H. Beckwith, D. J. Danagher and J. Reid, *J. Mol. Spectrosc.*, 1987, **121**, 209.

[40] M. Takami, H. Jones and T. Oka, *J. Chem. Phys.*, 1979, **70**, 3557.

[41] K. Tanaka, H. Ito and T. Tanaka, *J. Chem. Phys.*, 1987, **87**, 1557.

[42] Y. Ueda and J. Iwahori, *J. Mol. Spectrosc.*, 1986, **116**, 191.

[43] C. Cottaz, I. Kleiner, G. Tarrago, L. R. Brown, J. S. Margolis, R. L. Poynter, H. M. Pickett, T. Fouchet, P. Drossart and E. Lellouch, *J. Mol. Spectrosc.*, 2000, **203**, 285.

[44] W. S. Benedict, E. K. Plyler and E. D. Tidwell, *J. Chem. Phys.*, 1958, **29**, 829.

[45] P. Pracna, V. Špirko and W. P. Kraemer, *J. Mol. Spectrosc.*, 1989, **136**, 317.

[46] T. Rajamäki, A. Miani and L. Halonen, *J. Chem. Phys.*, 2003, **118**, 10929.

[47] J. Pesonen, A. Miani and L. Halonen, *J. Chem. Phys.*, 2001, **115**, 1243.

[48] C. Léonard, S. Carter and N. C. Handy, *Chem. Phys. Lett.*, 2003, **370**, 360.

[49] A. G. Császár, W. D. Allen and H. F. Schaefer III., *J. Chem. Phys.*, 1998, **108**, 9751.

[50] W. Klopper, C. C. M. Samson, G. Tarczay and A. G. Császár, *J. Comput. Chem.*, 2001, **22**, 1306.

[51] Š Urban, D. Papoušek, V. M. Devi, B. Fridovich, R. D'Cunha and K. N. Rao, *J. Mol. Spectrosc.*, 1984, **106**, 38.

Dissociative Low-Energy Electron Attachment to the C–S Bond of H₃CSCH₃ Influenced by Coulomb Stabilization

Monika Sobczyk,[1,2] Piotr Skurski[1,2] and Jack Simons[1]

[1]*Chemistry Department, Henry Eyring Center for Theoretical Chemistry, University of Utah, Salt Lake City, UT 84112, USA*
[2]*Department of Chemistry, University of Gdansk, 80-952 Gdansk, Poland*

Abstract

In earlier works by our group, it was suggested that the presence of stabilizing Coulomb potentials can allow low-energy electrons (i.e., with kinetic energies <1 eV) to attach to σ* orbitals of certain bonds and to thus cleave those bonds. In these earlier efforts, we focused on S–S bond cleavage and in breaking a variety of bonds that occur in typical peptides and proteins. In the present effort, we focus primarily on the stabilizing effects of nearby positive charges on the electron attachment process to dimethyl sulfide (DMS) to break one of the C–S bonds. *Ab initio* electronic structure calculations have been used to explore the influence of Coulomb potentials on the ability of low-energy electrons to directly attach to the σ* orbital of the C–S bond and to effect bond cleavage, as well as to examine σ* anion energy evolution as a function of C–S bond length.

Contents

1. INTRODUCTION

There exist a variety of experimental mass spectrometric methods for effecting fragmentation of gas-phase charged samples of a wide range of organic and inorganic systems. Because of their ability to cause very specific and limited bond cleavages, electron capture dissociation (ECD) [1–4] experiments, where very low-energy electrons are attached to the gaseous sample after which specific bonds break, have shown great promise.

Recent studies carried out by our group show [5] that low-energy electrons can directly attach to and subsequently fragment S–S σ bonds in disulfide-linked dimers of Ac-Cys-Ala$_n$-Lys (with $n = 10$, 15, and 20) that are protonated at their two Lys sites. An example of such a species is shown in Fig. 1 where the alanine

Fig. 1. Structure of an $(AcCA_{15}K+H)_2^{2+}$ disulfide-linked dimer [6]. The disulfide linkage is at the center and the two protonated sites are at the left and right ends.

helices are marked red, the cystine linkage containing the S–S bond appears in the center, and the two Lys sites are at the termini.

According to the mechanism treated in Ref. [5], an excess electron enters the S–S antibonding σ^* orbital to form a metastable anion that can either undergo electron auto-detachment at a rate $> 10^{14}\,s^{-1}$ or fragment (promptly because of the repulsive nature of the σ^* anion's energy surface) to form an R–S radical and an $^-$S–R$'$ anion. The yield of bond cleavage per attached electron is governed by competition between fragmentation on the σ^* surface and the auto-detachment process. The *ab initio* calculations of Ref. [5] were carried out on a very simple model of the disulfide shown in Fig. 1, the H_3C–S–S–CH_3 molecule. The R–S–S–R$'$ neutral and corresponding anion potential energy curves for dimethyl disulfide as functions of the S–S distance are depicted in Fig. 2.

The data shown in Fig. 2 suggest that the near vertical attachment of an electron into the S–S σ^* orbital of MeS–SMe would require an electron with kinetic energy of *ca.* 0.9 eV and would generate the σ^* anion on a reasonably repulsive part of its energy surface. This results in the well-known dissociative electron attachment (DEA) process [7,8] which has been well studied experimentally for MeS–SMe. Figure 2 also suggests that lower-energy electrons can attach to the σ^* S–S orbital
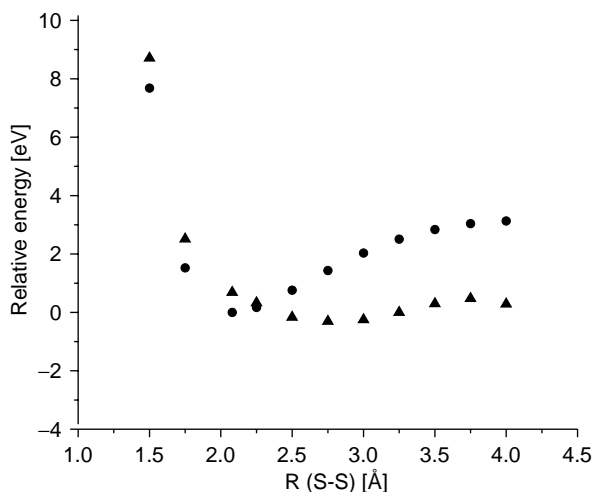

Fig. 2. Energies of the dimethyl disulfide neutral (circles) and σ^* anion (triangles) as functions of the S–S bond length (Å) with all other geometrical degrees of freedom relaxed to minimize the energy.

but only if the S–S bond is stretched to near 2.25 Å, which would require *ca.* 0.5 eV of vibrational excitation. Of course, except at considerably elevated temperatures, such high vibrational excitation is extremely improbable. So, the most likely means by which electrons can enter the S–S σ* orbital of a room-temperature sample is to have *ca.* 0.9 eV of kinetic energy and to do so in a near vertical manner.

The effects that proximal positively charged groups can have on the DEA process were the primary focus in Ref. [5]. Specifically, we considered the Coulomb stabilization that one or more nearby positive groups (e.g., simulating the protonated Lys sites in the molecule shown in Fig. 1) can have on the nascent σ* anion. As an example of the effects of Coulomb interactions, in Fig. 3 we show the MeS–SMe neutral and MeS–SMe⁻ σ* anion potentials as in Fig. 2 but calculated in the presence of two +1 charges each 30 or 10 Å from the midpoint
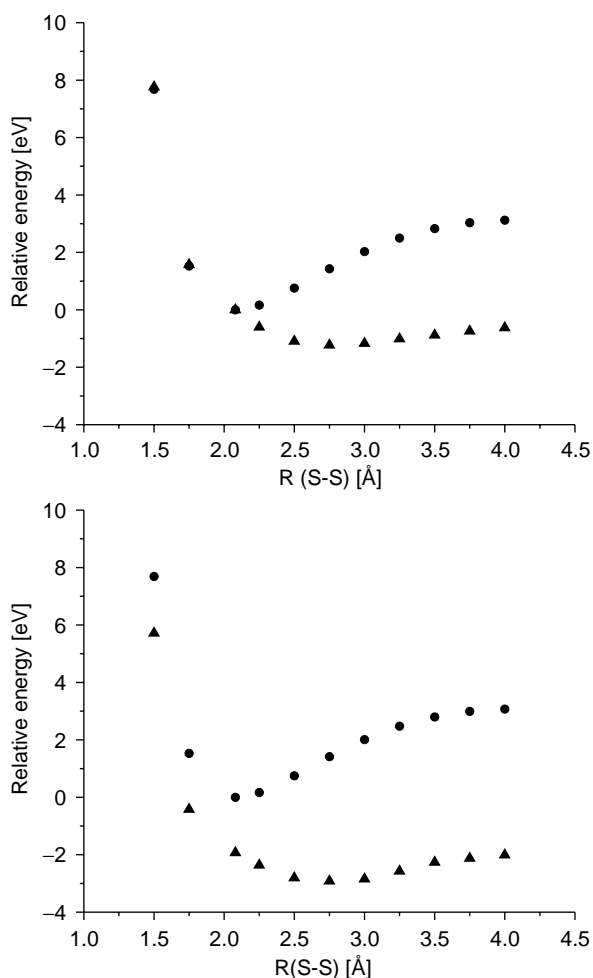

Fig. 3. Neutral (circles) and σ* anion (triangles) curves of MeS–SMe in the presence of two +1 charges 30 Å (top) and 10 Å (bottom) from the midpoint of the S–S bond.

of the S–S bond (i.e., one $+1$ charge on one side of the bond and the other $+1$ charge in the opposite direction). Clearly, in comparison with Fig. 2, the σ* anion curves in Fig. 3 are lowered in energy by a substantial amount relative to the energy of the neutral. This causes the anion curve to intersect the neutral at smaller S–S separations (e.g., at bond lengths that may be accessed in the zero-point vibration of the S–S bond) and at much lower energy.

We have observed that the energy lowering of the σ* anion curve can, in fact, be estimated in terms of the Coulomb potential produced by the two $+1$ charges. For example, when the two charges are 30 Å distant, the Coulomb energy at the midpoint of the S–S bond is 2(14.4 eV Å/30 Å)=0.96 eV; when the two charges are 10 Å away, the Coulomb stabilization energy is 2.88 eV. The rigidity of the compounds shown in Fig. 1 caused by their helical subunits allowed us to accurately know the distances between the S–S bond and the two $+1$ sites, so these species provided excellent support for postulate that our model MeS–SMe compounds were designed to probe.

Based upon the results of such studies, we suggested in Ref. [5] that Coulomb potentials produced by nearby positive charges could stabilize the σ* metastable anion states to an extent that might render them electronically stable. Under such circumstances, the endothermic DEA process illustrated in Fig. 2 might be made exothermic or thermo-neutral and thus able to effect bond breakage at a much higher yield. The data of Fig. 3 suggest that S–S σ bonds, which require electrons of *ca.* 0.9 eV to induce DEA in the absence of positive charges, can attach essentially zero-energy electrons to produce S–S bond cleavage if two $+1$ charges are within 30 Å (or, equivalently, if one $+1$ charge were within 15 Å).

Our suggestion that proximal positively charged groups can substantially alter the energy requirements and efficiencies of DEA processes can be of great significance to workers who study electron-induced bond fragmentation propensities in, for example, gas-phase mass spectrometric (including ion-cyclotron resonance) experiments on charge peptides and proteins. In particular, the use of ECD [1–4] methods for fragmenting such bio-molecules gives rise to very specific bond-cleavage patterns but the mechanisms involved are not yet fully understood. In fact, an unusual outcome [6] in ECD experiments on the kind of molecule shown in Fig. 1 is what motivated us to examine the effects of Coulomb stabilization in the first place.

To extend our previous studies of such processes, we decided to examine in the present effort the anion that results from attaching an electron to the C–S σ* orbital of Me–S–Me shown in Fig. 4 as well as the neutral and anion energy surfaces associated with cleaving the C–S bond in the absence and presence of two positive $+1$ charges at 10, 20, and 30 Å.

2. METHODS

Prior to stretching C–S bond, we optimized the geometry of the anionic Me–S–Me$^-$ molecule and parent neutral molecule at the unrestricted second-order Møller–Plesset (UMP2) perturbation level of theory (in order to take into account the effect of electron correlation) with aug-cc-pVDZ basis sets [9]. We also
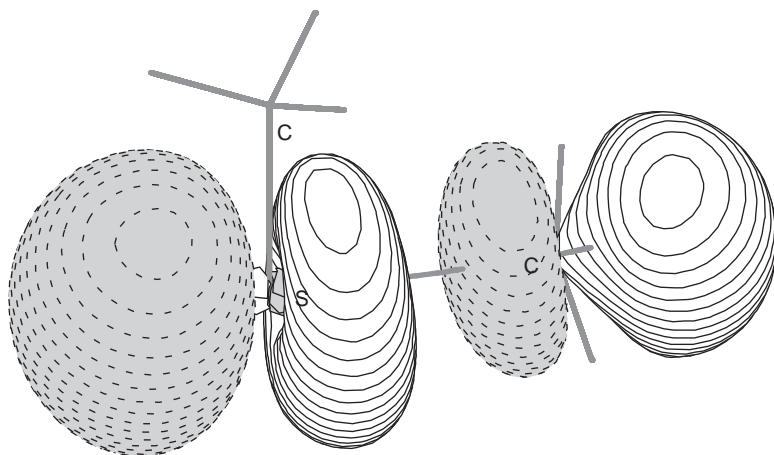
Fig. 4. The singly occupied σ* molecular orbital of the C–S bond (at $R_{CS} = 2.5$ Å) that holds the excess electron of the Me–S–Me$^-$ anion.

calculated all vibrational frequencies of the neutral and anionic species to make sure the structures thus found were indeed minima on the energy surface.

In addition, to generate the neutral molecule and anion energies as functions of the C–S bond length (R), we performed such UMP2 calculations at a range of R-values using partial geometry optimization, with only the C–S bond distance frozen and all other geometrical degrees of freedom relaxed to minimize the energy. In all calculations, the values of $\langle S^2 \rangle$ never exceeded 0.7780 (after annihilation) for the doublet states, so we are confident that spin-contamination effects do not have significant influence on our results.

The anion calculations are especially problematic at R-values, where the anion's energy lies above that of the neutral (i.e., when the anion is metastable). In such cases, great care must be taken to avoid having the anion's wave function undergoing variational collapse (i.e., to describe an electron distant from the neutral molecule and having little kinetic energy). When stretching the C–S bond, we had to be careful to monitor the anion's orbital occupancy to guarantee that the σ* orbital was indeed the singly occupied molecular orbital. At large R-values, this is rather straightforward because, at such distances, the anion is electronically stable. However, at R-values where the C–S σ* anion's energy lies above that of the neutral molecule, we had to employ special techniques for such an electronically metastable state.

In the method we used to overcome these problems for metastable anions, we increased the nuclear charges on the two atoms (e.g., C and S, when stretching the C–S bond) involved in the bond cleavage by an amount δq and carried out the anion and neutral calculations. These increased nuclear charges cause the C–S σ* anion state to be differentially lowered in energy and to thus become electronically stable relative to the neutral molecule. In this way, we were able to make sure that the anion energy and orbital occupancy we obtained in our UMP2 calculations corresponded to the proper σ* anion. By employing this δq
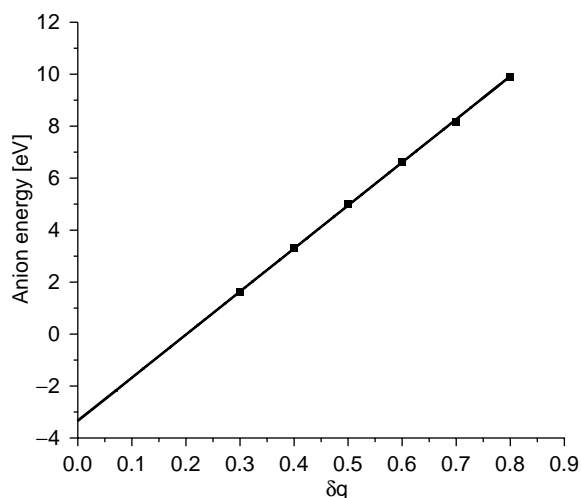
Fig. 5. Plot of the energy of the anion relative to that of the neutral in which an electron is in a C–S σ* orbital *vs.* the stabilizing partial charge δq added to the C and S atoms.

charge-increase technique for a range of δq values (e.g., δq=0.1–1.0 was typical) within which the σ* anion is electronically stable, we could then plot the stable energies E (δq) of the σ* anion *vs.* δq and extrapolate to δq=0 to evaluate the metastable σ* anion's energy. An example of such an extrapolation is shown in Fig. 5.

As a result of such a treatment, we were able to compute the electronic energy of the neutral Me–S–Me molecule as a function of the C–S bond length as well as the electronic energy of the anion state of interest at all *R*-values. In particular, we were able to evaluate the anion's energy both at geometries where it is electronically stable and where it is metastable, the latter being especially important for estimating the vertical electron attachment energies that relate to DEA processes.

In addition to carrying out such calculations in the absence of any stabilizing Coulomb potentials, we repeated each calculation with Coulomb potentials present. In all such calculations, we placed two +1 charges at 10, 20, or 30 Å from the midpoint of the C–S bond, and repeated the evaluation of the neutral and anion energies.

Because we find that the presence of a +1 charge stabilizes the anion curves in a highly predictable manner (i.e., by lowering the σ* curve by 14.4 eV/*R*, where *R* is the distance in Å to each +1 charge), we can predict the energy and shape of the σ* anion curve for arbitrary values of the local Coulomb potential. This, in turn, allows us to utilize our findings to predict the effects, for example, of protonated adjacent groups whose distance to a given bond may even fluctuate as the molecule undergoes thermal motions. So, even though we carry out calculations for only certain strengths of the Coulomb potential, we suggest that our data can be used to predict under what Coulomb potentials a given bond will or will not be susceptible to exothermic DEA.

In the absence of additional positive stabilizing charges, the electronic instability of the Me–S–Me$^-$ anion does not occur for C–S bond lengths larger than 2.37 Å, where the excess electron is localized on the Me–S fragment. It is known [10] that Me–S possesses a positive electron affinity of *ca.* 1.87 eV which is 1.79 eV larger than the electron affinity of the methyl radical. This difference in the values of the electron affinities directly influences the localization of the excess electron on the Me–S–Me$^-$ anion during fragmentation. When two positive $+1$ charges are present, the anionic energy curve is shifted down to lower energies where it remains 'below' the corresponding neutral energy curve for C–S bond lengths larger than 1.95 Å. This is because the anion with the singly occupied σ^* orbital shown in Fig. 4 is stabilized by the electrostatic Coulomb potential of the positive point charges added.

All of our calculations were performed with the Gaussian98 suite [11] of codes on AMD Athlon 2000+ 1.6 GHz and Pentium IV 1.7 GHz computers, as well as on SGI Origin2000 and Compaq Sierra systems. The three-dimensional plots of molecular orbitals were generated with the MOLDEN program [12].

3. RESULTS

Before discussing the significance of our data, we wish to point out that the C–S bond is a reasonably strong σ bond. As a result, the σ^* anion curve lies high above the neutral curve near the equilibrium bond length of the neutral parent molecule. Therefore, the σ^* anion state has a high energy and a correspondingly very short lifetime (*ca.* 10^{-14} s or shorter). The short lifetime produces a very broad Heisenberg width and thus makes the determination of the center of the DEA cross-section difficult to determine. Moreover, the short lifetime causes detachment to overwhelm dissociation of the σ^* anion, thus making the bond-cleavage yield of the DEA process very low. All of these issues conspire to make DEA data on the bond we are studying very scarce but still existent.

In Fig. 6 we show how the electronic energies of the neutral and anionic systems vary along the C–S bond length with all other internal geometry parameters relaxed to minimize the neutral or anion energy, respectively. These plots allow us to examine where the anion's energy surface lies relative to that of the neutral, which obviously, is directly germane to attachment of a free electron to the σ^* orbital of the C–S bond.

Examining the data used to create Fig. 6 in comparison with known experimental values, we conclude that:

(i) The dissociation energy for Me–S–Me $\rightarrow$ MeS + Me is 3.28 eV. The experimental estimate of this energy derived from the laser photodissociation and photoionization of DMS is 3.25 ± 0.06 eV [13].

(ii) The electron affinity of MeS is estimated to be 1.81 eV. This value is also in reasonable agreement with the experimental value [10] of 1.87 eV. So, we believe that our calculations provide satisfactory results in this case.
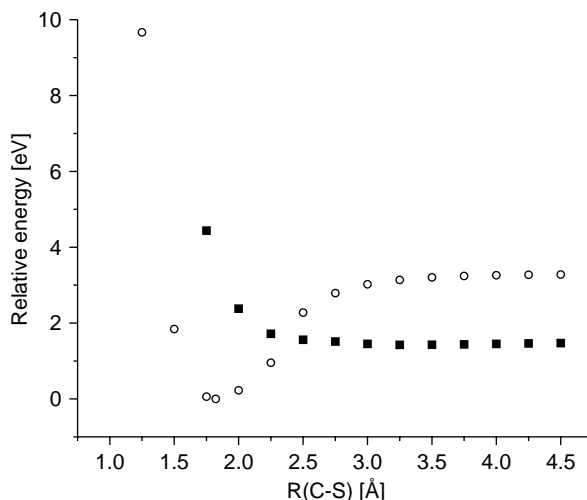
Fig. 6. Neutral (circles) and σ* anion (squares) energies as functions of the C–S bond length in the absence of stabilizing charges.

We note that the σ* anion lies 3.80 eV above the minimum of the neutral species in our calculations, which is somewhat higher than the experimentally determined 3.25 eV value in the DEA yield spectrum [7] (although this peak is 0.5 eV broad). We also note that the anion and neutral curves cross *ca.* 1.63 eV above the neutral's minimum. This amount of energy seems to be too high for vibrational excitation of the C–S bond to access at room temperature and thus accessing this crossing point remains unrealizable except at considerably elevated temperatures.

In Fig. 7 we show the corresponding neutral and anion curves (n.b., computed at the unrestricted MP2 level) associated with cleaving of the C–S bond when two $+1$ charges are located 10 Å from the midpoint of the bond being cleaved. The positive charges are used to represent the Coulomb potential presented by two protonated amine sites as, for example, in the dication in Fig. 1.

We see that in Fig. 7 the anion is electronically stable for values of C–S bond larger than 1.95 Å. The anion and neutral curves cross *ca.* 0.16 eV above the neutral's minimum. The amount of energy needed to access the crossing here is 10 times smaller than in Fig. 6 and thus can be thermally attainable at room temperature. Note that the energy of the anion relative to the neutral at $R = 1.82$ Å (the neutral's R_e) moves from 3.80 eV in Fig. 6 to 1.08 eV in Fig. 7. This means that direct vertical attachment would require an electron to have *ca.* 1 eV of kinetic energy in this case. The 2.72 eV of Coulomb stabilization observed in this case is very close to that predicted by the equation for two positive charges at 10 Å: $2(14.4/(10 + R_e/2))$ eV $= 2.64$ eV. This success of such simple Coulomb stabilization model may be surprising, but we remind the reader that this same kind of model has proven highly successful when used to predict electronic stabilities of anions in the past [14].
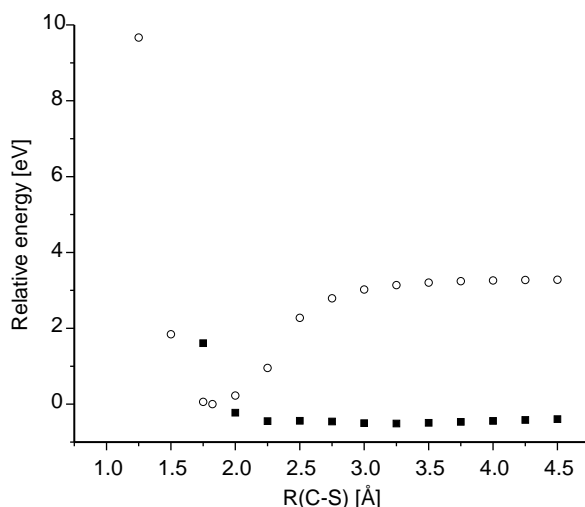
Fig. 7. Neutral (circles) and σ* anion (squares) energies as functions of the C–S bond length when two positive $+1$ charges are located 10 Å from the midpoint of the bond.

Before examining the results obtained with the two $+1$ positive charges placed 20 or 30 Å from the midpoint of C–S bond, let us see what the Coulomb model predicts in those two cases. Specifically, it predicts the anion to be located relative to the minimum of the neutral at the following energies:

$3.80 - 2(14.4/20.91) = 2.42$ eV with the two $+1$ charges 20 Å away
$3.80 - 2(14.4/30.91) = 2.87$ eV with the two $+1$ charges 30 Å away

In Figs 8 and 9 we show the neutral and σ* anion curves when two $+1$ charges are 20 or 30 Å from the C–S bond midpoint, and we note that these estimates are indeed quite good.

So, in the two latter cases we expect the C–S bond to be able to attach an excess electron, but only if the electron has 2.4–2.9 eV of kinetic energy or if the C–S bond is vibrationally excited by 0.7–1.0 eV.

Clearly, even when the two positive sites are only 10 Å away, the σ* Me–S–Me anion is not electronically stable with respect to the neutral very near the equilibrium bond length of the neutral. Nevertheless, because the anion–neutral crossing occurs at low energy (i.e., 0.16 eV), direct electron attachment to the C–S bond to effect fragmentation seems to be possible when two positive sites are present and as distant as 10 Å and the C–S bond is elongated by vibrational motion. These findings and the Coulomb model that seems to be consistent with them suggest that when the two protonated sites are closer than *ca.* 6.67 Å, the σ^*_{CS} anion will be vertically stable [15] relative to the neutral, so direct electron attachment of zero-energy electrons would then not require any energy input (e.g., vibrational excitation to access the surface crossing).
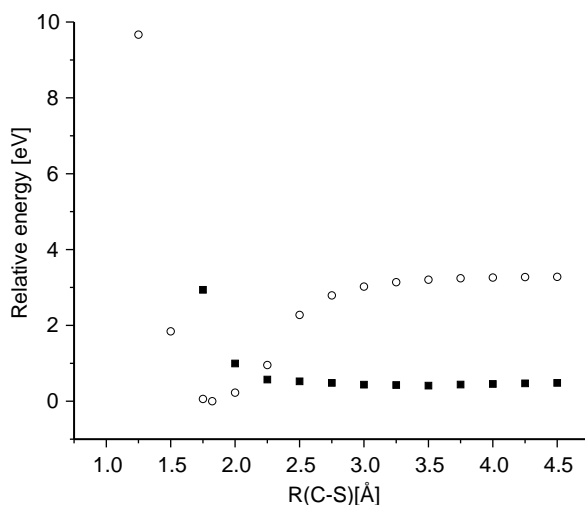
Fig. 8. Neutral (circles) and σ* anion (squares) energies as functions of the C–S bond length when two +1 charges are located 20 Å from the midpoint of the bond.

Because the Coulomb potential plays a central role in the model outlined above, it seems important to examine the full electrostatic potential experienced by an electron as it approaches the C–S bond region. In Fig. 10 we show the electrostatic potential for Me–S–Me molecule in the absence of any positive charges, with blue denoting attractive regions and red labeling repulsive regions.
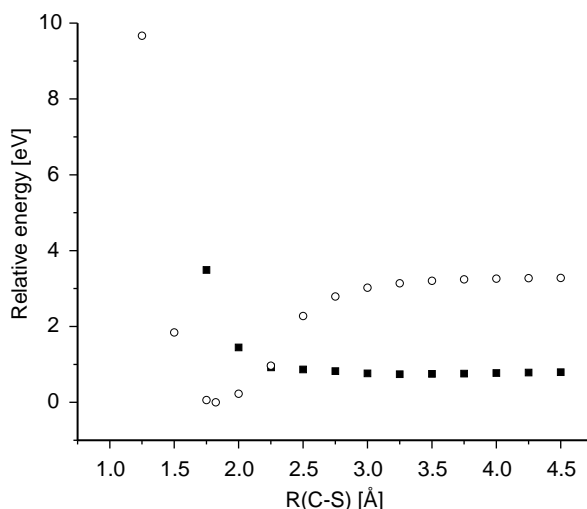
Fig. 9. Neutral (circles) and σ* anion (squares) energies as functions of the C–S bond length when two +1 charges are located 30 Å from the midpoint of the bond.
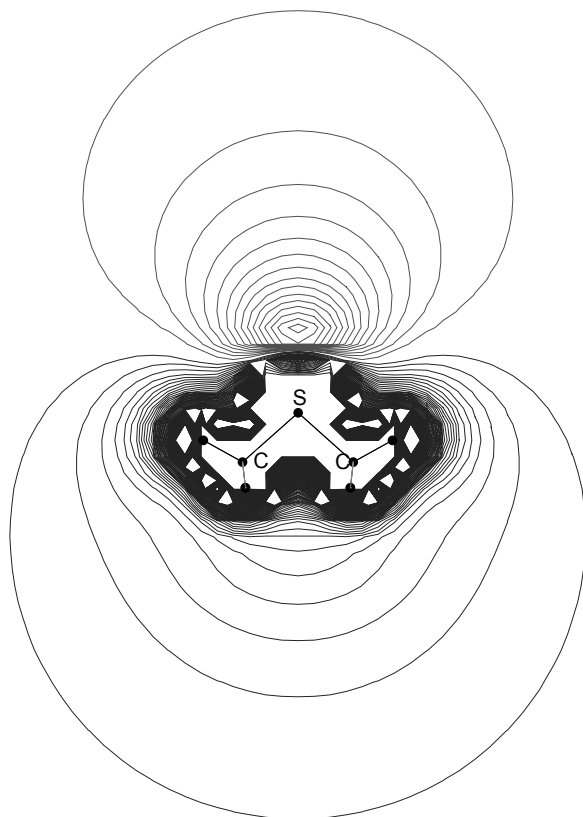
Fig. 10. The electrostatic potential of Me–S–Me molecule. Red regions are repulsive to an electron, blue are attractive.

The region where the lone pair orbitals of the sulfur atom reside is repulsive while the rest of DMS molecule is characterized by attractive potentials. There is no clearly attractive region near the C–S bond that would tend to guide an incident electron toward the σ^*_{CS} orbital because this figure corresponds to the equilibrium C–S bond length and the CS σ^* orbital lies high in energy. However, in cases where the two $+1$ positive charges are present at 10, 20, or 30 Å, an electron is most strongly attracted to regions near these positively charges sites where deep potential wells clearly exist, but our findings suggest that the region of the σ^*_{CS} orbital can also be attractive to such electron, especially when the C–S bond is elongated.

4. SUMMARY

Direct attachment of an electron to the σ^* orbital of the C–S bond of Me–S–Me shown in Fig. 4 has been examined using *ab initio* electronic structure methods.

Particular care has been devoted to establishing a qualitatively correct description of the metastable anion state that arises.

For the situations in which a C–S bond is cleaved, so Me and MeS radicals are formed, the corresponding Me–S$^-$ anion has a 1.81 eV positive electron binding energy.

The vertical attachment of an electron to the σ* orbital of this bond is highly endothermic in the absence of Coulomb stabilization and requires the electron to have a kinetic energy of *ca.* 3.80 eV (experiments probing the position of the σ* shape resonance give somewhat lower values). Even when Coulomb stabilization of 2.88 eV is present (i.e., equivalent to two +1 charges 10 Å distant or one +1 charge 5 Å away), the σ* anion curve lies vertically 1.08 eV above the neutral and intersects the neutral at a distance of 1.95 Å and 0.16 eV above the neutral's minimum. It therefore seems unlikely that such strong σ bond will be susceptible to cleavage by a direct low-energy (<3 eV) DEA mechanism when positive charges are absent. To effect exothermic vertical attachment to such a σ bond lying >3.80 eV above the neutral, one would have to have, for example, a protonated amine site within 6.67 Å. Of course, one can imagine multiply protonated species for which the total Coulomb stabilization at the σ bond site could move that site's σ* anion below the corresponding neutral, but such cases are probably not common. The species shown in Fig. 1 represents such an unusual case in which two +1 charges as distant as 30 Å are able to allow direct DEA to occur. It is the weakness of the S–S bond (which causes the energy of the σ* orbital to be low lying) and the magnitude (*ca.* 1.8 eV) of the EA of the S–R' radical formed upon bond cleavage that make this case special.

For the very strong C–S σ bond whose data are summarized in Figs 6–9, the bond strengths and radical EAs do not combine to permit efficient direct DEA when low-energy (i.e., <3 eV) electrons are involved. We therefore expect that Coulomb-assisted C–S bond DEA will not be effective in gaseous peptide samples except for bonds that happen to be very near two or more protonation sites. That is, our data suggest that direct low-energy electron attachment to and subsequent cleavage of the C–S σ bond is not likely except for highly positively charged samples. So, the results presented here seem to offer good insight into one aspect of the ECD process and they provide a means by which one can estimate (based on a simple Coulomb energy formula) which bonds may be susceptible to cleavage by low-energy electron attachment.

REFERENCES

[1] R. A. Zubarev, N. Kruger, E. K. Fridriksson, M. A. Lewis, D. M. Horn, B. K. Carpenter and F. W. McLafferty, *J. Am. Chem. Soc.*, 1999, **121**, 2857.

[2] R. A. Zubarev, D. M. Horn, E. K. Fridriksson, N. L. Kelleher, N. A. Kruger, M. A. Lewis, B. K. Carpenter and F. W. McLafferty, *Anal. Chem.*, 2000, **72**, 563.

[3] E. A. Syrstad and F. Turecek, *J. Phys. Chem. A*, 2001, **105**, 11144.

[4] F. Turecek and E. A. Syrstad, *J. Am. Chem. Soc.*, 2003, **125**, 3353.

[5] A. Sawicka, P. Skurski, R. R. Hudgins and J. Simons, *J. Phys. Chem. B*, 2003, **107**, 13505.

[6] R. R. Hudgins, K. Håkansson, J. P. Quinn, C. L. Hendrickson and A. G. Marshall (unpublished but in preparation). Although yet unpublished, these results have been presented in public at: R. R. Hudgins, K. Håkansson, J. P. Quinn, C. L. Hendrickson and A. G. Marshall, *Proceedings of the 50th ASMS Conference on Mass Spectrometry and Allied Topics*, Orlando, FL, June 2–6, 2002.

[7] C. Dezarnaud-Dandine, F. Bournel, M. Tronc, D. Jones and A. Modelli, *J. Phys. B: At. Mol. Opt. Phys.*, 1998, **31**, L497.

[8] A. Modelli, D. Jones, G. Distefano and M. Tronc, *Chem. Phys. Lett.*, 1991, **181**, 361.

[9] R. A. Kendall, T. H. Dunning Jr. and R. J. Harrison, *J. Chem. Phys.*, 1992, **96**, 6796.

[10] J. C. Riensta-Kiracofe, G. S. Tschumper, H. F. Schaefer III., S. Nandi and G. B. Ellison, *Chem. Rev.*, 2002, **102**, 231.

[11] M. J. Frisch, G. W. Trucks, H. B. Schlegel, G. E. Scuseria, M. A. Robb, J. R. Cheeseman, J. A. Montgomery, Jr., T. Vreven, K. N. Kudin, J. C. Burant, J. M. Millam, S. S. Iyengar, J. Tomasi, V. Barone, B. Mennucci, M. Cossi, G. Scalmani, N. Rega, G. A. Petersson, H. Nakatsuji, M. Hada, M. Ehara, K. Toyota, R. Fukuda, J. Hasegawa, M. Ishida, T. Nakajima, Y. Honda, O. Kitao, H. Nakai, M. Klene, X. Li, J. E. Knox, H. P. Hratchian, J. B. Cross, C. Adamo, J. Jaramillo, R. Gomperts, R. E. Stratmann, O. Yazyev, A. J. Austin, R. Cammi, C. Pomelli, J. W. Ochterski, P. Y. Ayala, K. Morokuma, G. A. Voth, P. Salvador, J. J. Dannenberg, V. G. Zakrzewski, S. Dapprich, A. D. Daniels, M. C. Strain, O. Farkas, D. K. Malick, A. D. Rabuck, K. Raghavachari, J. B. Foresman, J. V. Ortiz, Q. Cui, A. G. Baboul, S. Clifford, J. Cioslowski, B. B. Stefanov, G. Liu, A. Liashenko, P. Piskorz, I. Komaromi, R. L. Martin, D. J. Fox, T. Keith, M. A. Al-Laham, C. Y. Peng, A. Nanayakkara, M. Challacombe, P. M. V. Gill, B. Johnson, W. Chen, M. W. Wong, C. Gonzalez and J. A. Pople, Gaussian 03, Revision A.1, Gaussian, Inc., Pittsburgh, PA, 2003.

[12] G. Schaftenaar and J. H. Noordik, Molden: a pre- and post-processing program for molecular and electronic structures. *J. Comput.-Aided Mol. Des.*, 2000, **14**, 123.

[13] S. Nourbakhsh, K. Norwood, H.-M. Yin, C.-L. Liao and C. Y. Ng, *J. Chem. Phys.*, 1991, **95**, 5014.

[14] J. Simons, P. Skurski and R. Barrios, *J. Am. Chem. Soc.*, 2000, **122**, 11893.

[15] This estimate is obtained by equating the intrinsic instability of the anion (3.80 eV) to the Coulomb model's prediction of stabilization $2(14.4/(R + 1.82/2))$ in eV.

Dunham's Formalism Applied in Reduction of Spectral Data of Diatomic Molecules and the Development of Computational Spectrometry

J. F. Ogilvie[1] and J. Oddershede[2]

[1]*Escuela de Quimica, Universidad de Costa Rica, San Pedro de Montes de Oca, San Jose 2060, Costa Rica*
[2]*Syddansk Universitet, Campusvej 55, DK-5230 Odense M, Denmark*

Abstract

We examine the derivation of information about molecular structure and properties from analysis of pure rotational and vibration-rotational spectral data of diatomic molecular species on the basis of Dunham's algebraic formalism, making comparison with results from alternative approaches. According to an implementation of computational spectrometry, wave-mechanical calculations of molecular electronic structure and properties have already played an important role in spectral reduction through interaction of quantum chemistry and spectral analysis.

Contents

1. INTRODUCTION

During the brief span 1904–1933 of his life, James Lawrence Dunham published only five technical papers [1–5], but they continue to exert a significant impact on approaches to analysis of spectra of diatomic molecules. For instance, in 1950

Herzberg cited Dunham's work at more than eight points in his monograph [6] on spectra of diatomic molecules; of at least 1940 total citations of those five papers, about 29 appeared during year 2003 [7], and in other papers of unknown number published each year authors allude to Dunham's work through his name without citing his publications. Because Dunham's work might in recent years be more frequently cited than its significance be understood, the centennial anniversary of his birth seems a fitting occasion to review why his work maintains a strong influence on this narrow but both pedagogically and practically momentous sector of optical spectroscopy: this field of spectra of diatomic molecules is important pedagogically because their properties illustrate fundamental principles of quantum effects typically explained in terms of an oscillator in one dimension, and practically because many diatomic molecules that are crucial to a comprehensive treatment of atmospheric chemical phenomena are detected through their spectra in absorption, emission or Raman scattering; in either case Dunham's formalism is not merely applicable but prominent. After the discovery of deuterium through observation of a visible spectral line [8] that intensified investigation of isotopic effects, in 1936 van Vleck [9] extended Dunham's formalism to encompass deficiencies that Dunham partly recognised [5], and their collective results and subsequent extension enable a quantitative description of essentially all effects of nuclear mass in band spectra, requiring in addition only effects of nuclear volume to complete treatment of frequency data and effects of vibration-rotational interaction for intensity data. Over the ensuing decades other workers have contributed to details of this treatment through their experimental and theoretical analyses, making an approach to spectral analysis based on this formalism comprehensive and thoroughly practicable. Our present task is to assess this approach, from both experimental and theoretical points of view, in the light of the current status of spectral measurements on diatomic molecules.

For the first time in application to details of spectral analysis, we recognise also the role of wave-mechanical computations that herald the emergence of computational spectrometry as a partner with experimental and theoretical spectrometry in revealing information about molecular structure and properties: in relating frequencies and strengths of spectral lines to molecular properties, the work of Dunham and of van Vleck, for instance, constitutes theoretical spectrometry, whereas the measurement of those frequencies and strengths, with concomitant assignment to transitions between quantum states and fitting of spectral data to theoretical quantities, is the practice of experimental spectrometry. The concern of computational spectrometry is a quantum-chemical calculation, through methods applicable to molecular electronic structure, of some or all factors that affect the frequency and strength of a spectral line with an accuracy comparable with that of typical contemporary research measurements. As a consequence of subsequent evolution, the effective hamiltonian underpinning the results of Dunham and van Vleck is directly appropriate for the practice of computational spectrometry.

In an analysis of a molecular spectrum, the primary task is, for purpose of characterisation, to assign each narrow spectral feature to a transition between two molecular states specified with rotational, vibrational and electronic quantum numbers or other indices. Nearly as important as the former, another task is to

represent archetypal properties of each spectral line – the frequency at maximum intensity and its total intensity – by means of formulae that reproduce those features, within the accuracy of their measurement, with parameters fewer than the number of features represented. The latter process constitutes data reduction; apart from compactness in relation to storage and retrieval of data, an advantage of such a reduced representation in an appropriately selected form is a possibility of modest extrapolation of data so as to allow prediction of further features beyond a range of measurements included in reduced data. Even though gross extrapolation, in absence of both exact data and an exact theoretical model, be a practice statistically unreliable and hence universally deprecated, a limited extent serves as a legitimate basis for tentative further investigation and for verification of the correctness of a theoretical formulation. For atomic spectra a seminal instance of such data reduction was Balmer's success in reproducing, within the accuracy of their measurement, the wave lengths of four lines emitted by atomic H by means of a formula containing only one parameter and one integer variable [10]; subsequent discovery of lines in other series led to modification of that formula so as to apply to all series with only two integer variables. In this particular case, the parameter – actually, or proportional to, the Rydberg constant – has direct physical significance in relation to the energy of ionisation of a hydrogen atom. For molecular spectra an observation of Deslandres, almost concurrent with Balmer's discovery, that the separation of wave numbers of many lines in a band system of CN in emission increases nearly linearly [11] enabled fitting of a formula containing only three parameters [6, p. 42]. In this case, and typically for subsequent analyses of infrared and Raman spectral data pertaining to gaseous diatomic samples, parameters are merely artefacts of a particular formulation or model, inaccessible to direct physical measurement. This distinction concerning the observable nature of parameters is important in subsequent discussion.

2. BASIS OF ANALYSIS TO THE EXTENT OF DUNHAM'S THEORY

Although Dunham's first three papers [1, Intensities in the harmonic band of hydrogen chloride; 2, Intensities of vibration-rotation bands with special reference to those of HCl; 3, The isotope effect on band spectrum intensities] treated spectral intensities, two most commonly cited papers [4, The Wentzel-Brillouin-Kramers method of solving the wave equation; 5, The energy levels of a rotating vibrator] pertain to energies of molecular states in relation to frequencies of spectral lines observable such as through measurements of infrared absorption and emission or Raman scattering by diatomic molecular substances in gaseous samples at small total densities; band spectra involving also transitions between electronic states might be another source of such data. As the inverse of wave length, wave number $\tilde{\nu}$ is proportional to frequency, but was measurable more precisely than the knowledge of the speed c of light in vacuo, before the value of that fundamental constant became eventually fixed. We work strictly with wave number of a narrow spectral line of a particular isotopic species as a difference

between values of spectral terms [6] of combining states according to Bohr's relation:

$$\tilde{\nu} = E^i_{v'J'} - E^i_{v''J''} \tag{1}$$

here a term value $E^i_{v'J'}$, pertaining to a state of discrete energy characterised with quantum numbers principally vibrational v' and rotational J' (and others), implies greater energy than another term value $E^i_{v''J''}$ specified with quantum numbers v'' and J'' that take generally integer values, for these two states that combine in a transition $|v',J'\rangle \leftarrow |v'',J''\rangle$ in absorption, in accordance with standard practice [6]. Before Dunham's last publication, these term values pertaining to the same electronic state and to a particular isotopic species i were commonly represented implicitly or explicitly through a double sum involving vibrational v and rotational J quantum numbers in functionals to various powers in a form

$$E^i_{vJ} = \sum_{k=0} \sum_{l=0} A^i_{kl}(v + 1/2)^k [J(J+1)]^l \tag{2}$$

in which term coefficients A^i_{kl} are regarded as merely *phenomenological fitting parameters* [12], freely adjustable, of arbitrarily selectable subscripts and of minimal number, to obtain an optimal fit according to a selected criterion, such as a minimum sum of squares of residuals; $A_{0,0}=0$ for the electronic ground state. Earlier usages of just v as a simple integer variable pertaining to a vibrational motion and of $J+\frac{1}{2}$ as a functional pertaining to rotational motion were superseded when quantum mechanics became applied to spectra through analogies to a simple linear harmonic oscillator and a rigid rotor [6]; as no real molecule is a rigid rotor – nor an harmonic oscillator – in its nuclear motions within an electronic framework, there is no logical basis to prefer $J(J+1)$ to $(J+\frac{1}{2})^2$, for which the differences $(\frac{1}{4})^l A_{kl}$ are readily accommodated, but the former convention is tenaciously established. In such implicit usage for a particular isotopic variant, term coefficients were generally denoted unsystematically such as in the following correspondences, some of which involve compound symbols,

$$\begin{aligned}
A_{1,0} &= \omega_e, & A_{2,0} &= -\omega_e x_e, & A_{3,0} &= \omega_e y_e, \\
A_{0,1} &= B_e, & A_{1,1} &= -\alpha_e, & A_{2,1} &= \gamma_e, \\
A_{0,2} &= -D_e, & A_{1,2} &= -\beta_e, & A_{0,3} &= H_e,
\end{aligned} \tag{3}$$

in values of rotational terms for a particular vibrational state,

$$F_v(J) = B_v[J(J+1)] - D_v[J(J+1)]^2 + H_v[J(J+1)]^3 + \ldots \tag{4}$$

and of vibrational terms,

$$G(v) = \omega_e(v + 1/2) - \omega_e x_e(v + 1/2)^2 + \omega_e y_e(v + 1/2)^3 + \ldots \tag{5}$$

with subsidiary relations,

$$B_v = B_e - \alpha_e(v + 1/2) + \gamma_e(v + 1/2)^2 + \ldots \tag{6}$$

$$D_v = D_e + \beta_e(v + 1/2) + \ldots \tag{7}$$

and so forth, with some variability, depending on researcher, of inclusion ad hoc of minus signs to make selected parameters assume generally positive values. In an absence of net orbital, electronic and nuclear spin momenta that might couple with rotational angular momenta, a sum of these vibrational and rotational terms is simply the value of a spectral term, $E_{vJ}^{i} = G(v) + F_v(J)$, within a particular electronic state. The objective of fitting wave numbers of spectral lines in perceived sets to expressions involving quantum numbers v and J is to enable reproduction of those wave numbers of many lines with fewer parameters within formulae of simple form. Sufficient parameters of selected kind are employed to reproduce data satisfactorily. By means of coefficients either A_{kl}^{i} or their unsystematic equivalents, spectral reduction might be generally achieved such that these parameters number only about one quarter of the number of wave numbers of measured transitions.

In his last paper Dunham obtained a formula for values of spectral terms for a particular isotopic species i in a particular electronic state, which we suppose generally to be of symmetry class $^1\Sigma$ or 0 implying neither net electronic orbital nor net intrinsic electronic angular momentum;

$$E_{vJ}^{i} = \sum_{k=0}^{\infty} \sum_{l=0}^{\infty} Y_{kl}^{i} (v + 1/2)^k [J(J+1)]^l \qquad (8)$$

we likewise ignore intrinsic angular momenta of atomic nuclei. This expression appears similar to formula 2, but here $Y_{0,0} \neq 0$, even for an electronic ground state. Dunham actually wrote K instead of J with no explanation of that symbol, but during that era such a symbol to denote rotational angular momentum was common practice. Correspondences with unsystematic parameters are only approximate:

$$
\begin{array}{lll}
Y_{1,0} \cong \omega_e, & Y_{2,0} \cong -\omega_e x_e, & Y_{3,0} \cong \omega_e y_e, \\
Y_{0,1} \cong B_e, & Y_{1,1} \cong -\alpha_e, & Y_{2,1} \cong \gamma_e, \\
Y_{0,2} \cong -D_e, & Y_{1,2} \cong -\beta_e, & Y_{0,3} \cong H_e,
\end{array}
\qquad (9)
$$

An important distinction between term coefficients A_{kl}^{i} and Y_{kl}^{i} is that, whereas the former are regarded as freely adjustable, the latter are formally inter-related; for instance, although a relation

$$Y_{0,2} \approx -4Y_{0,1}^3 / Y_{1,0}^2 \qquad (10)$$

thus connecting D_e, B_e and ω_e, might be derivable directly from perturbation theory, other relations such as

$$Y_{0,3} \approx 8Y_{0,1}^3 (Y_{1,1}Y_{1,0} + 12Y_{0,1}^2)/(3Y_{1,0}^4) \qquad (11)$$

thus connecting H_e, α_e, B_e and ω_e, are less readily derived without an intermediate model. It is essentially a truism to state that the essence of Dunham's approach to analysis of molecular spectra involves the *primacy of Dunham coefficients Y_{kl},*

that differ from freely adjustable coefficients A_{kl} in being explicitly related to each other through algebraic formulae, such as that above, although many authors of papers involving reduction of spectral data have ignored this distinction.

Two further comments about formula 8 and its parameters are noteworthy. The number of terms with coefficients Y_{kl}^i in the double sum is formally doubly infinite so that formula 8 can represent spectral terms involving arbitrarily large values of v and J; with data of finite extent the sums become truncated in a systematic and consistent manner conforming to parameters of a minimum number required according to that intermediate model. Instead of exact equalities in formulae 10 and 11, the approximations arise because each term coefficient Y_{kl}^i constitutes a sum of contributions [5],

$$Y_{kl}^i = \sum_{m=0} Y_{kl}^{2m} \tag{12}$$

of which magnitudes of successive contributions $Y_{kl}^{(0)}$, $Y_{kl}^{(2)}$, $Y_{kl}^{(4)}$... for a particular isotopic species generally decrease rapidly with increasing value of m, hence assuring rapid convergence for not too large values of v and – particularly – J; a superscript, $2m$ with m integer, denoting order of contribution takes only even values by dint of their relation to a JBKW procedure [13], based on that developed concurrently by Brillouin [14,15], Kramers [16] and Wentzel [17], itself dependent on a mathematical method developed by Jeffreys [18], according to which Dunham originally derived expressions for these term coefficients [4]. The approximate relations 10 and 11 become exact equalities when only leading contributions $Y_{kl}^{(0)}$ are employed in those, and analogous, relations. The effect of atomic mass varies for these contributions; denoting by U_{kl} a factor independent of mass in $Y_{kl}^{(0)}$, we express this dependence on reduced mass μ of a particular isotopic species as

$$Y_{kl}^{(0)} \propto \mu^{-(k+2l)/2}, \quad Y_{kl}^{(0)} = U_{kl}\mu^{-(k+2l)/2} \tag{13}$$

in which the molecular reduced mass is defined as $\mu = M_a M_b/(M_a + M_b)$, with M_a and M_b being masses of separate neutral atoms into which a diatomic molecule AB, whether net electrically neutral or a molecular ion, dissociates. For further contributions $Y_{kl}^{(2)}$, $Y_{kl}^{(4)}$..., the corresponding factors incorporating reduced mass are respectively $\mu^{-(k+2l+2)/2}$, $\mu^{-(k+2l+4)/2}$ ...

Dunham achieved inter-relations between term coefficients Y_{kl}^i through use of an intermediate radial function $V(R)$ in an effective hamiltonian for motion of atomic nuclei of this form,

$$\mathcal{H}(R) = \hat{p}^2/(2\mu) + \hbar^2 J(J+1)/(2\mu R^2) + V(R) \tag{14}$$

that contains terms to represent kinetic energy parallel and perpendicular to an internuclear vector with the centre of mass as origin of coordinates, and potential energy $V(R)$, respectively; the second term hence corresponds to rotational motion about the centre of mass. Here $\hat{p}$ is a linear momentum conjugate to a vector to represent instantaneous internuclear separation R, and the next term involves

the square of an angular momentum that takes discrete values $\hbar[J(J+1)]^{1/2}$, with J a non-negative integer or half integer. Instead of direct use of this variable R, Dunham employed a reduced displacement x, thus dimensionless,

$$x = (R - R_e)/R_e, \quad R = R_e(1 + x) \tag{15}$$

in which R_e denotes an equilibrium internuclear distance, for a particular electronic state, at which the postulated internuclear potential energy $V(R)$ or $V(x)$ associated with nuclear motion along the internuclear vector is a minimum; $x=0$ at $R=R_e$. To avoid working with coefficients of which the units vary with the power of that variable, such a dimensionless variable is highly desirable. According to a formal separation of electronic and nuclear motions, the total electronic energy plus the coulombic repulsion between stationary nuclei becomes a potential energy for motion of those nuclei. Dunham actually employed, instead of x, a greek letter ξ, but in much subsequent work [13] the former symbol is adopted, as here; apart from ease of typewriting, relation to further symbols y and z for cognate variables is facilitated. Dunham adopted a function of potential energy having the form of a polynomial or truncated power series,

$$V(x) = V_0 + hca_0x^2\left(1 + \sum_{j=1} a_jx^j\right) \tag{16}$$

in which V_0 is the potential energy at the minimum; for the electronic ground state of a particular molecular species with a particular net electric charge $V_0 \equiv 0$, and the polynomial is truncated as limited by an extent of available spectral data. The leading term $a_0 x^2$ of this radial function, which remains if all $a_j=0$ for $j>0$, corresponds to potential energy of the canonical linear harmonic oscillator, for which classically the frequency is independent of vibrational amplitude and quantally the frequency of transitions between adjacent terms is constant; further terms $a_j x^j$ that make an oscillator anharmonic hence take into account how transitions of a real molecule differ from a limiting harmonic behaviour near $R = R_e$. In terms of these coefficients for potential energy, term coefficients such as

$$Y_{1,1}^{(0)} = 6B_e^2(1 + a_1)/\omega_e \tag{17}$$

and

$$Y_{0,3}^{(0)} = 16B_e^5(3 + a_1)/\omega_e^4 \tag{18}$$

thus become simply related to each other, as here through formula 11 for instance, on elimination of coefficients a_j for potential energy.

Dunham [5] derived these expressions $Y_{kl}^i(\omega_e, B_e, a_j)$, necessarily manually, through a JBKW procedure, which he claimed to make more general [4] than what had appeared in previous literature. Dunham reported expressions Y_{kl}^i containing coefficients a_j up to a_6, and Sandeman [19] and Woolley [20] extended manually these results according to a roughly analogous procedure. Kilpatrick [21] applied perturbation theory in successive orders to derive expressions for Y_{kl}^i, and Bouanich [22] applied Rayleigh-Ritz perturbation theory for solution of

Schrodinger's equation with a separate Fortran programme to calculate each numerical coefficient of a term in Y_{kl}^i comprising products of various a_j; Brukhanov and coworkers [23] also employed perturbation theory but produced with computer algebra many expressions for Y_{kl}^i. Bessis and coworkers conducted calculations of Y_{kl}^i of a complicated symbolic nature according to a method involving differential operators [24], at first manually, but invoked computer algebra to assist extension of this approach [25]. The JBKW method has been programmed, with an algorithm [26] similar to Dunham's, or more directly [27]. Uehara has reported explicit expressions for a few coefficients [28,29], also derived with this JBKW method and with symbolic computation. The most efficient algorithm to generate extensive expressions of Y_{kl} is based on hypervirial perturbation theory, or perturbation theory without wave functions [30]. Both matrix mechanics with perturbation theory [31] and classical mechanics [32,33,13] have been applied to the effective hamiltonian in formula 13 to yield expressions for term coefficients Y_{kl}^i. With unequally spaced Fourier components [33,13], according to even classical mechanics one would produce expressions for these term coefficients identical with those from all other approaches listed above.

Before 1977 many spectroscopists reduced their wave number data to phenomenological term coefficients A_{kl}^i for a particular isotopic species; despite imposing no inter-relations of types in expressions 10 and 11, they employed notation Y_{kl}^i, thus failing to recognise the profound significance of Dunham's work. This approach involves only linear regression, with readily obtainable uncertainties associated with those parameters A_{kl}^i, but many coefficients of correlation between those parameters inevitably assume magnitudes near unity. In other cases some workers selected a subset of these term coefficients, typically $Y_{k,0}$ and $Y_{k,1}$ taking as many values of k in each as required, from which to evaluate a few coefficients a_j for potential energy; non-linear fitting is required, best performed iteratively until convergence to self consistency. In 1978 the distinction between freely fitted coefficients A_{kl}^i and coefficients Y_{kl}^i was formally recognised [12]. Only in 1976 was undertaken [34] the first analysis of error associated with these parameters a_j. With spectral data comprising wave numbers of only moderate precision, discrepancies between freely fitted coefficients A_{kl}^i and coefficients Y_{kl}^i calculated from parameters for potential energy are generally not much greater than experimental error of evaluation of those quantities A_{kl}^i. In 1974 there had already been noticed significant discrepancies of this nature for CO in precise spectral measurements of multiple isotopic variants [35]; further empirical term coefficients $\Delta_{kl}^{a,b}$ associated with separate atomic centres A or B in diatomic molecular species AB were hence introduced and evaluated significantly. According to this formula proposed empirically,

$$E_{vJ}^i = \sum_{k=0}^{\infty} \sum_{l=0}^{\infty} U_{kl} \mu^{-(k+2l)/2}[1 + m_e(\Delta_{kl}^a/M_a + \Delta_{kl}^b/M_b)](v + 1/2)^k[J(J + 1)]^l \quad (19)$$

parameters $\Delta_{kl}^{a,b}$, like U_{kl} defined in formula 13, are formally independent of atomic mass within sets of isotopes of atoms A or B; for an electronic ground

state there exist neither $U_{0,0}$ nor $\Delta_{0,0}^{a,b}$. The latter parameters $\Delta_{kl}^{a,b}$ tend to accumulate a contribution from $Y_{kl}^{(2)}$ in formula 12. For parameters U_{kl} not inter-related through formulae similar to 11, thus lacking a defined relation to Dunham coefficients Y_{kl} according to formula 13 and becoming merely further phenomenological fitting parameters, analogous to A_{kl} but still independent of isotopic mass, we propose a distinguishing symbol B_{kl}.

Notwithstanding these developments, some spectroscopists continued to express their results in terms of only freely fitted coefficients A_{kl}^i, and obtained from an arbitrarily selected subset thereof divergent values of coefficients a_j for the same molecular species in isotopic variants. For HCl [36], derived values of a_6 in formula 16 for $^1H^{35}Cl$ and for $^1H^{37}Cl$ differed by ten times the stated standard errors of these quantities, but these disparate results proved no cause for concern because they reproduced successfully the wave numbers of transitions of each isotopic species through their insertion into expressions for coefficients Y_{kl}^i. For $^1H^{81}Br$, fitting spectral data directly to term coefficients A_{kl}^i in a linear fit resulted in a reduced standard deviation $\hat{\sigma} = 0.76$, indicating by its magnitude less than unity that estimates of uncertainties of measurements of wave numbers of spectral lines were somewhat conservative, whereas fitting the same spectral data directly to coefficients a_j through expressions for Y_{kl}^i resulted in a reduced standard deviation $\hat{\sigma} = 1.3$ [37]; that these values of $\hat{\sigma}$ appear to differ significantly might reflect the effect of "*l*-uncoupling" phenomena to which Dunham alluded [5], or other factors not taken into account [37].

Apart from the distance variable x that Dunham used in his function $V(x)$ for potential energy, other variables are amenable to production of term coefficients Y_{kl}^i in symbolic form as functions of the corresponding coefficients in a power series of exactly the same form as in formula 16. Through any method to derive algebraic expressions for Dunham coefficients Y_{kl}^i, the hamiltonian might have x as its distance variable, but after those expressions are produced they are convertible to contain coefficients of other variables possessing more convenient properties. To replace x, two defined variables are y [38],

$$y = (R - R_e)/R, \quad R = R_e/(1 - y) \tag{20}$$

for which the leading term $V(y) = b_0 \, y^2$ in an expansion for potential energy was the first function for interatomic potential energy, devised by Kratzer [39], and for which Fues made a subsequent wave-mechanical treatment [40], and z [41]:

$$z = 2(R - R_e)/(R + R_e), \quad R = R_e(2 + z)/(2 - z) \tag{21}$$

The latter variable eliminates a finite range [42] of convergence of series both of x at $2 R_e$, because of a pole due to internuclear coulombic repulsion as $R \rightarrow 0$, and of y at $\frac{1}{2} R_e$, for a similar phenomenon as $R \rightarrow \infty$. Expressions for Y_{kl}^i in terms of coefficients c_j in the latter series are available in a large consistent collection in Fortran coding [43] up to c_{10}; such expressions, readily calculated, through symbolic computation with efficient procedures [44], first in terms of coefficients a_j and thence converted to b_j or c_j as required, are further converted to Fortran or C code for numerical applications.

3. BASIS OF ANALYSIS BEYOND DUNHAM'S THEORY, BY VAN VLECK AND OTHERS

Dunham recognised that his theory was adequate only when motions of electrons are totally correlated to one or other nucleus during molecular vibration and rotation about the centre of mass, to which motions Dunham referred as mechanical effects [5]; especially with highly precise measurements of wave numbers of transitions through a large spectral range or range of vibrational quantum numbers, such an assumption is evidently untenable. The principal reason that Dunham's theory is inadequate is that the hamiltonian for nuclear motion lacks terms to take into account the true nature of a diatomic molecule – that it contains not two structureless atoms but two atomic nuclei, each of finite mass and size, and their associated electrons, and that these electrons fail to follow perfectly one or other nucleus in its rotational and vibrational motions with respect to the centre of molecular mass; in the light of Dunham's term, we describe these effects as extra-mechanical [13]. Considering nuclear mass subsequently, we devote attention first to effects of nuclear size.

A hamiltonian commonly applied to describe the electronic structure of a molecule includes a coulombic or electrostatic term arising from a point-like centre of charge for each nucleus. As is generally known by chemists but with implications still largely ignored, an atomic nucleus has extension in space, with a root-mean-square radius of order typically 2×10^{-15} m: the distribution of electronic charge and the electronic energy are accordingly perturbed by this extended distribution of nuclear charge, resulting in slight shifts of energy relative to an hypothetical unperturbed coulombic potential [45]. These shifts of energy lack direct spectral observation, but variations in shifts occur on isotopic substitution because the spatial distribution of nuclear charge varies from one nuclidic species of a particular chemical element to another. Discussing in 1922 an influence of nuclear volume on atomic spectra, Bohr [46] suggested that spectral shifts reflected a variation of internal nuclear structure between isotopic nuclei, producing a correspondingly varying field of force surrounding those nuclei [47]. Not only variation of nuclear volume but also variation of nuclear shape or of a distribution of nuclear charge produces a field shift [48]. Despite the latter complication, discussion of a field shift in regard to molecular spectra is couched conventionally in terms of mean squared nuclear radius $\langle r^2 \rangle_{a,b}$ of atomic centre A or B, by means of an extended relation

$$Y_{kl}^{(0)} + Z_{kl}^{f,a} + Z_{kl}^{f,b} = U_{kl}\mu^{-(2k+1)/2}(1 + V_{kl}^a\langle r^2\rangle_a + V_{kl}^b\langle r^2\rangle_b) \tag{22}$$

with term coefficients U_{kl} independent of mass and volume as defined in formula 13, and Z_{kl}^f collecting additional terms containing mean squared nuclear radii separately for both atomic centres A and B. Parameters $V_{kl}^{a,b}$ for the field shift are functions of electronic density $\rho_{el}^{a,b}(R)$ that varies with internuclear distance. Here follow simple expressions [49] for the leading coefficients for rotational,

$$V_{0,1}^{a,b} = Z_{a,b}e^2 d\rho_{el}^{a,b}(R)/dR|_{R_e}(3\varepsilon_0 k_e R_e) \tag{23}$$

and vibrational energies,

$$V_{1,0}^{a,b} = Z_{a,b}e^2(d^2\rho_{el}^{a,b}(R)/dR^2|_{Re} - 3a_1/R_e d\rho_{el}^{a,b}(R)/dR|_{Re})/(12\varepsilon_0 k_e) \qquad (24)$$

together with an analogous expression for electronic energy,

$$V_T^{a,b} = Z_{a,b}e^2/(6\varepsilon_0 h)\rho_{el}^{a,b}(R_e) \qquad (25)$$

in which appear protonic numbers $Z_{a,b}$ of each atomic centre, harmonic force coefficient k_e, fundamental constants e, h and ε_0, and coefficient a_1 in formula 16 for internuclear potential energy. According to empirical values of coefficients $V_{kl}^{a,b}$ from precise spectral measurements, one would be able to evaluate, from measurement of wave numbers of vibration-rotational spectra of a particular diatomic molecular species in its isotopic variants, the electronic density at one nucleus as a function of the separation of the other nucleus if absolute values of mean squared radii were available. Such values of nuclear radii are difficult to measure because an atomic nucleus contains mass and charge in a diffuse distribution, even if that distribution be much less diffuse than for electronic charge outside a particular nucleus; hence various experiments provide disparate measures of such mean squared radii [50]. Because only differences in effective mean squared radii of nuclear charge between isotopes of atomic nuclei with the same atomic number are known with reasonable accuracy, formula 22 became rewritten [49] as

$$Y_{kl}^{(0)} + Z_{kl}^{f,a} + Z_{kl}^{f,b} = U_{kl}\mu^{-(2k+1)/2}(1 + V_{kl}^a\delta\langle r^2\rangle_{aa'} + V_{kl}^b\delta\langle r^2\rangle_{bb'}) \qquad (26)$$

in which $\delta\langle r^2\rangle_{aa'}$ is a difference of mean squared radii between isotope A and a selected standard isotope A$'$ of that atomic type, and analogously for atomic type B. Compiled values [50] of $\delta\langle r^2\rangle_{aa'}$ are available from isotopic shifts of frequencies of optical transitions in atomic spectra, for which effects of mass and volume might be more readily disentangled than for molecular spectra into which an additional dependence on internuclear distance R enters; absolute values of nuclear radii are also available [51], subject to a qualification explained above. For hydrogen, the difference between wave numbers of Lyman α lines of ^{1}H and ^{2}H or D is 2237.955 ± 0.020 m^{-1} [52], due mostly to a difference of reduced mass; the field shift due to disparate nuclear volumes is only -0.020 m^{-1} for D relative to H, despite a formally large difference between root-mean-squared nuclear radii/ 10^{-15} m, 0.800 ± 0.020 for H and 2.096 ± 0.014 for D [53]. What matters for the extent of the field shift is clearly the mean squared radius of nuclear charge, rather than merely the cross section of nuclear volume. Evaluating the gradient of electronic density with internuclear distance at equilibrium separations for a few chalcogenide compounds of lead, and halide compounds of thallium, on the basis of measured rotational energies, Tiemann et alii [45] discovered an approximately linearly decreasing trend for this property. These authors mention [45] also that for a field shift to be significant as a contribution to the total isotopic effect requires a mass number of an atomic nucleus greater than 40, such as Ca with atomic number $Z=20$; the smallest mass numbers for which a field shift has been detected in diatomic molecules pertain to tin, $Z=50$, mass number $A\sim120$ [49]. For compounds of Pb and Tl the largest contribution to isotopic effects arises from

the variation of the volume or shape of nuclear centres on isotopic substitution, such that for those elements the effects of volume variation are several times the magnitude of expected effects of mass variation in the auxiliary coefficients Z_{kl} [49]. Because only relative shifts are observable, precise spectral data for at least three isotopes of a given element in a particular diatomic molecular species are required to yield information on these field shifts.

For molecules containing light atoms, we accordingly neglect this effect of finite nuclear volume or field shift, but other effects prevent exact application of isotopic ratios that one might expect on the basis of a proportionality with $Y_{kl}^{(0)}$ in formula 13 instead of total Y_{kl}. For this reason we supplement term coefficients Y_{kl}^{i} in formula 8 for a particular isotopic species i with auxiliary coefficients Z_{kl}^{i} [54],

$$E_{vJ}^{i} = \sum_{k=0}^{\infty} \sum_{l=0}^{\infty} (Y_{kl}^{i} + Z_{kl}^{i})(v + 1/2)^{k}[J(J + 1)]^{l} \tag{27}$$

separate from Z_{kl}^{f} above for the effect of finite nuclear volume. We moreover distinguish two contributions to these further auxiliary coefficients – those, Z_{kl}^{r}, that are required to obtain accurate applications of inter-relations, such as those in formulae 10 and 11, between term coefficients Y_{kl} of a single isotopic variant subject to restriction to leading terms $Y_{kl}^{(0)}$, and those, Z_{kl}^{v}, that become observable only on comparing parameters from spectra of isotopic species. These auxiliary coefficients furthermore become partitioned into contributions from each separate atomic type, A or B in diatomic molecule AB. With such an expansion and apart from the field shift or effect of finite nuclear volume, we rewrite the preceding formula as [55]

$$E_{vJ}^{i} = \sum_{k=0}^{\infty} \sum_{l=0}^{\infty} (Y_{kl} + Z_{kl}^{v,a} + Z_{kl}^{v,b} + Z_{kl}^{r,a} + Z_{kl}^{r,b})(v + 1/2)^{k}[J(J + 1)]^{l} \tag{28}$$

in which all term coefficients on the right side pertain implicitly to a particular isotopic variant. As an effective hamiltonian for nuclear motion in formula 14 suffices to yield term values according to Dunham's formula, 8, involving only coefficients Y_{kl}^{i}, we require further terms in another hamiltonian, which might be in the form of corrections because each component of Z_{kl}^{i}, and all components in total, are typically much smaller than corresponding Y_{kl}^{i}. We remedy this deficiency by including at least one correction for each term in an effective hamiltonian, formula 14,

$$\mathcal{H}(R) = \hat{p}(1 + g_{v}(R)m_{e}/m_{p})\hat{p}/(2\mu) + (1 + g_{r}(R)m_{e}/m_{p})\hbar^{2}J(J + 1)/(2\mu R^{2})$$

$$+ V(R) + V'(R) + V''(R) \tag{29}$$

in which g_{v} and g_{r} are called respectively vibrational and rotational g factors, and m_{e} and m_{p} are rest masses of electron and proton respectively; $V'(R)$ is an analogous correction to the internuclear potential energy $V(R)$. $V''(R)$ is a further correction of which we allude merely to its dependence on atomic mass.

The rotational g factor relates to the fact that a free molecule acquires a magnetic dipolar moment as a result of molecular rotation [56]. Of seven terms in this expanded effective hamiltonian, for only the rotational g factor can experimental information be derived separately from other effects: for instance, for a pure rotational transition of a diatomic molecule in electronic state $^1\Sigma$ from the rotationless state with $J=0$ to a state with $J=1$, one line in absence of a magnetic field becomes a triplet, with the two additional lines displaced in frequency symmetrically and proportional to the density B of magnetic flux; the essential factor of proportionality is the rotational g factor, specifically an expectation value, $\langle J=1|g_r(R)|J=1\rangle$, of a radial function $g_r(R)$ for that rotational state, which might have a positive or negative sign. From the influence of a magnetic field on transport properties of a gaseous substance – specifically the direction of transverse transport of thermal energy or momentum, the sign of g_r is derivable [57], which task is difficult through application of the Zeeman effect on spectra unless circularly polarized radiation be applied; results of these signs were reported for diatomic species N_2, CO, HD, O_2 and NO [58], for which the sign pertains to a value of g_r averaged over rotational states occupied at the temperature of measurements. Apart from other experiments described previously [56], even estimates of the magnitude of g_r as well as sign are obtainable from measurements of thermal conductivity and shear viscosity for a gaseous substance in absence and presence of a magnetic field, plus other information; this method has been implemented for N_2 and CO [59]. For the vibrational g factor there exists no magnetic effect of low order that might provide direct experimental measurement [60].

Theoretical calculation of any atomic or molecular property through application of computational methods based on quantum mechanics or other sophisticated approach is typically practicable through approximate methods. The internuclear potential energy $V(R)$ independent of mass is conventionally derived from the results of computations of molecular electronic structure according to a scheme of wave mechanics,

$$-\left\{(\hbar^2/2m_e)\sum_{j=1}^{N}\nabla_j^2 + (e^2/4\pi\varepsilon_0)\left(-\sum_{j=1}^{N}(Z_a/r_{a,j}+Z_b/r_{b,j}) + \sum_{j=1}^{N}\sum_{l>j}^{N}1/r_{i,j}+Z_aZ_b/R\right)\right\}$$
$$\times\Psi(r_j;R) = W(R)\Psi(r_j;R)$$

(30)

in which $r_{a,j}$ denotes a distance between atomic nucleus A and electron j, and $r_{b,j}$ analogously for nucleus B, $r_{i,j}$ is an interelectronic distance, and $\psi(r_j;R)$ is an assumed total wave function for motion of N electrons with a parametric dependence on fixed internuclear distance R; we neglect magnetic effects in this formula. The total energy $W(R)$ of a molecular system, including coulombic repulsion between atomic nuclei, with these nuclei fixed at a separation R thereby becomes a potential energy $V(R)$ for the relative motion of these nuclei, according to an effective hamiltonian approximately in formula 14 or accurately in formula 29. Such an ansatz based on a formal crude separation of electronic and nuclear motions was first described by Born and Oppenheimer [61] in1927, to

justify expressing a molecular energy as an approximate sum of separate contributions from rotational and vibrational motions of atomic nuclei and electronic motions. Expressing energies in such a sum had been practised implicitly for some years before this treatment appeared, and Born subsequently sought an improved derivation [62]; since that time many attempts to improve the analysis of molecular energies have been made, notably those by Longuet-Higgins through a variational principle [63] and by Fernandez [64] through application of perturbation theory, but a comprehensive analysis including both vibrational and rotational nuclear motions with electronic motions is still lacking.

Including explicitly both electronic and nuclear motions, Schrodinger's equation has never been solved exactly, even for an isolated hydrogen atom; approximate numerical solutions of an entire molecular system, involving integration over both electronic and nuclear coordinates, would yield all feasible energies of discrete and continuous states with no vestige of molecular structure in a traditional sense [65]. An intermediate approach, as incorporated in formula 29 above, involves treating atomic nuclei first as having infinite mass, thus denied kinetic energy, and solution of electronic energies on that basis. Relaxing that criterion to finite mass requires various corrections that affect, to a greater or lesser degree, energies accessible to a particular isotopic species, depending on those masses. A function $V'(R)$ constitutes a correction called adiabatic because it involves calculation with wave functions of only a particular electronic state of interest, hence yielding wave-mechanical expectation values of operators for nuclear momentum operating on electronic wave functions; after standard manipulation to eliminate a dependence on the position of the centre of nuclear mass [66], one expresses this correction in this general form as a radial function,

$$V'(R) = -1/2\hbar^2 \langle 0|\nabla_a^2/M_a + \nabla_b^2/M_b|0\rangle \tag{31}$$

in which ∇_a or ∇_b is a differential operator with respect to nuclear coordinates that operates on the electronic wave function. This formula includes approximations: 0 denotes an electronic wave function $\psi(r_j; R)$ for the electronic ground state that is a solution of equation 29 applicable to infinite masses, and atomic masses M_a and M_b appear instead of respective nuclear masses. For that adiabatic correction in $V'(R)$, the ratio of its magnitude to that of internuclear potential energy $V(R)$ is clearly of order a ratio m_e/M of electronic mass to mean atomic mass M [30], hence 5.5×10^{-4} at most for a typical molecular species. Because both rotational $g_r(R)$ and vibrational $g_v(R)$ factors that appear in formula 29 have as coefficient a ratio of electronic and protonic masses, with these g factors having magnitudes of order unity at most, these terms are likewise smaller than their addend unity by a factor $\sim 5 \times 10^{-4}$. The ratio of the magnitude of the most important parts of contributions $V''(R)$, described as nonadiabatic because they involve matrix elements of operators for linear and angular momentum between an electronic ground state of interest and electronically excited states, to $V(R)$ is of order a squared ratio [67] of electronic mass and mean atomic mass, $(m_e/M)^2$, hence 3×10^{-7} at most for a stable molecular species and negligible except in relation to spectral data having atypically great precision. These various corrections present in formula 29 beyond terms in formula 14 affect rotational

and vibrational contributions to molecular energies in disparate manners; within a context of that effective hamiltonian, the recognition and disentangling of these contributions during spectral analysis constitutes a major challenge.

Although Herzberg [6, page 230] illustrated pictorially how *L uncoupling* might affect the energies of rotational states, it is unclear how such an explanation might be directly applicable quantitatively to vibration-rotational spectra. The fact is that, in absence of further coefficients Z_{kl}, values, for $l > 1$, of Y_{kl} of a particular isotopic species derived from precise measurements of spectra in which appear no explicit multiplets implied in Herzberg's diagram deviate significantly from those expected on a basis of $Y_{k,0}$ and $Y_{k,1}$; these systematic deviations constitute a basis for distinction of Z_{kl}^r from Z_{kl}^v, such that for diatomic molecules with like nuclear charges, for which $Z_a = Z_b$, and for hydrides, for which the atomic number of the other atomic centre much exceeds unity, some values of Z_{kl}^r for $l > 1$ might be derived or estimated from spectra of only one isotopic species [55]. By definition, values of Z_{kl}^r with $l = 0$ vanish. Values of Z_{kl}^v are derivable experimentally through analysis of spectra of isotopic variants; for a reasonably significant evaluation of several values of both Z_{kl}^v and Z_{kl}^r, numerous spectral data for isotopic variants of both atomic types over the same range of energy as for a principal isotopic species are essential. A presence either of a ratio m_e/m_p as factor of radial functions for rotational and vibrational g factors or of a ratio of electronic to nuclear masses implicitly within adiabatic corrections $V'(R)$, as explained above, implies that auxiliary term coefficients Z_{kl} that have their source in such effects have magnitudes much smaller than those of dominant term coefficients $Y_{kl}^{(0)}$, and nonadiabatic corrections $V''(R)$ even smaller; typically $Z_{kl} \sim Y_{kl}^{(2)}$ and effects of $V''(R)$ would be $\sim Y_{kl}^{(4)}$. A further contribution Z_{kl}^f to total auxiliary term coefficient Z_{kl} that is due to an effect of nuclear volume or field shift, and proportional to $V_{kl}^a \delta \langle r^2 \rangle_{aa'}$, from formula 26, might have a magnitude comparable with contributions from mass effects for atoms of large atomic number, as mentioned above.

For a particular isotopic variant of a diatomic molecule with like charges on atomic centres, i.e. $Z_a = Z_b$, and for which we assume no net molecular electric dipolar moment at any internuclear distance, i.e. $p(R) = 0$ for all R, we hence express the coefficient of $(v + \frac{1}{2})^k [J(J+1)]^l$ in formula 27 as a sum,

$$Y_{kl} + Z_{kl}^v + Z_{kl}^r + Z_{kl}^f \tag{32}$$

The rotational and vibrational g factors have a dependence [66] on masses of atomic centres of forms

$$g_r(R) = m_p g_r^{irr}(R)[1/M_a + 1/M_b] = g_r^{irr}(R) m_p/\mu \tag{33}$$

$$g_v(R) = m_p g_v^{irr}(R)[1/M_a + 1/M_b] = g_v^{irr}(R) m_p/\mu \tag{34}$$

in which $g_r^{irr}(R)$ and $g_v^{irr}(R)$ contain electronic contributions regarded to pertain to irreducible nonadiabatic functions pertaining to rotational and vibrational motions [66], respectively. Simplified from formula 31, the adiabatic correction becomes

analogously expressed compactly as

$$V'(R) = -1/2\hbar^2 \langle 0|\nabla_a^2|0\rangle/\mu \tag{35}$$

because $\nabla_a^2 = \nabla_b^2$. Because field shifts between isotopic nuclei have their source in significant differences between distributions of nuclear charges in space, or nuclear volume, no comparable compacting of expression is practicable for this effect; formulae 22 and 26 remain applicable to a species with $Z_a = Z_b$ just as for $Z_a \neq Z_b$.

For a diatomic molecule with unlike charges on atomic centres, so $Z_a \neq Z_b$, we express the coefficient of $(v+\tfrac{1}{2})^k [J(J+1)]^l$ in formula 27 as a sum of seven addends,

$$Y_{kl} + Z_{kl}^{v,a} + Z_{kl}^{v,b} + Z_{kl}^{r,a} + Z_{kl}^{r,b} + Z_{kl}^{f,a} + Z_{kl}^{f,b} \tag{36}$$

The rotational and vibrational g factors of net electrically neutral molecule $^-AB^+$ with an indicated electric polarity show a dependence [66] on masses of atomic centres of forms

$$g_r(R) = [g_r^{irr}(R) - p(R)/(eR)]m_p/M_a + [g_r^{irr}(R) + p(R)/(eR)]m_p/M_b \tag{37}$$

$$g_v(R) = [g_v^{irr}(R) - (1/e)dp(R)/dR]m_p/M_a + [g_v^{irr}(R) + (1/e)dp(R)/dR]m_p/M_b \tag{38}$$

in which $p(R)$ denotes a radial function for electric dipolar moment, and $dp(R)/dR$ its first derivative with respect to internuclear distance. Formulae 37 and 38 exhibit a partition of total nuclear and electronic contributions to rotational and vibrational g factors into contributions of separate atomic centres [66] in a neutral molecule that is consistent with their expression in this more compact form,

$$g_r(R) = g_r^{irr}(R)m_p/\mu - m_p[1/M_a - 1/M_b]p(R)/(eR) \tag{39}$$

$$g_v(R) = g_v^{irr}(R)m_p/\mu - (m_p/e)[1/M_a - 1/M_b]dp(R)/dR \tag{40}$$

Electronic contributions to $g_r(R)$ and $g_v(R)$ relate to nonadiabatic rotational and vibrational effects, respectively, as electronic matrix elements [9], whereas a nuclear contribution, the same in each case,

$$g_r^{nuc} = g_v^{nuc} = m_p(Z_a M_b/M_a + Z_b M_a/M_b)/(M_a + M_b) \tag{41}$$

simply depends on atomic numbers and atomic masses, independent of internuclear distance [66]. Scrutiny of the applicable quantities reveals that this nuclear contribution can adopt only a positive value, whereas the total electronic contributions to both $g_r(R)$ and $g_v(R)$ have invariably negative values; the sign of the net value of $g_r(R)$ or $g_v(R)$ hence depends on the relative magnitudes of these negative and positive contributions. The total adiabatic corrections can assume both negative and positive values. For a diatomic molecule with $Z_a \neq Z_b$, the corresponding adiabatic correction is given simply in its general form, formula 31, and formula 26 is applicable to the relative field shift.

4. BASIS OF APPLICATION OF DUNHAM'S AND VAN VLECK'S THEORY TO ANALYSIS OF DIATOMIC SPECTRA

Bearing in mind that the primary objective of spectral analysis in its two stages combined is to evaluate parameters of minimal number that serve to reproduce archetypal characteristics of spectral lines in related sets, we consider how to apply formulae presented above for analysis of data of type wave number or frequency of spectral transitions. On a purely empirical basis for spectra of each separate isotopic species, one might simply apply formulae 2 and 3 in combination,

$$\tilde{\nu} = \sum_{k=0} \sum_{l=0} A_{kl}\{(v' + 1/2)^k [J'(J' + 1)]^l - (v'' + 1/2)^k [J''(J'' + 1)]^l\} \qquad (42)$$

For many values of wave number $\tilde{\nu}$ for diverse transitions within a particular range of quantum numbers v and J to yield a few values of phenomenological parameters A_{kl} for each separate isotopic variant, a standard statistical treatment to evaluate these over-determined parameters involves merely linear regression, best performed according to a criterion of least sum χ^2 of squares of residuals; a residual is a difference between a measured value of $\tilde{\nu}$ and the corresponding value calculated with A_{kl} in a given set. This treatment, like all succeeding improvements thereon, is naturally amenable to weighting of each measured wave number to take into account a variable ratio of signal to noise among spectral lines in a set, partial overlap of lines et cetera. For typical vibration-rotational data in a collection for a particular species, the most important parameters A_{kl} are those pertaining to vibrational energies, $A_{k,0}$, and those pertaining to rotational energies, $A_{k,1}$; additional parameters of type $A_{k,2}$, $A_{k,3}$ … related to centrifugal distortion are typically added empirically to a set under test until further addition of parameters yields no diminution of χ^2. As a rough guide to the extent of parameters of type $A_{k,0}$, for data extending over a typical range from $v = 0$ to v_{max} the corresponding maximum level of $A_{k,0}$ would have $k = v_{max}$; especially for diatomic species other than hydrides, such an extent of $A_{k,0}$ is unlikely to be required, and the maximum value of k might be only $\frac{1}{2} v_{max}$. The range of parameters of type $A_{k,1}$ is likely to require a maximum value of k the same as, or one unit less than, is required for parameters of type $A_{k,0}$, and several further $A_{k,2}$, $A_{k,3}$, $A_{k,4}$ … might be judiciously included for smaller k.

In an analogous manner, this approach is extensible to treat simultaneously data of multiple isotopic variants of a particular diatomic species; such a treatment might be based on application of differences of spectral terms according to formula 19, with empirical parameters B_{kl} and $\Delta_{kl}^{a,b}$ therein as explained at that point. In such a treatment there is convenience in distributing a factor reduced mass μ between vibrational and rotational quantum numbers, or rather their respective functionals, in the following form, known as *mass-reduced quantum numbers* [68],

$$(v + 1/2)/\mu^{1/2}, \quad [J(J + 1)]/\mu \qquad (43)$$

Hence these functionals of quantum numbers v and J become compounded with reduced mass μ; differences of these quantities to various powers k and l that serve

as regressors no longer retain integer values, respectively, for molecules in electronic state of class $^1\Sigma$ or 0.

As mentioned above, reduction of spectral data in terms of such empirical parameters A_{kl}, or B_{kl} and $\Delta_{kl}^{a,b}$, achieves an objective of this process, namely that those parameters number appreciably fewer than the number of fitted wave numbers $\tilde{\nu}$ of separate transitions. One obtains further reduction on applying constraints to freely adjustable parameters A_{kl}, or B_{kl}, to convert them to Dunham coefficients Y_{kl}, or U_{kl}, respectively. One might even retain linear regression in this process, implying that initial estimates of parameters are not required, according to an iterative approach that Tiemann developed [69]: in the first iteration, parameters A_{kl}, or B_{kl} and $\Delta_{kl}^{a,b}$, are freely adjustable within a selected set defined by subscripts k and l, and coefficients a_j for potential energy according to Dunham's formula 16, or some equivalent such as b_j or c_j coefficient of y or z respectively in formulae 20 and 21, are subsequently evaluated from $A_{k,0}$ and $A_{k,1}$. In the next iteration these values of coefficients for potential energy are substituted into expressions for Y_{kl} with $l > 1$, and the corresponding contributions $Y_{kl}^i(v + 1/2)^k[J(J+1)]^l$ with $l > 1$ to spectral terms E_{kl}^i are subtracted from those terms; the remaining parts of those terms are refitted to define further values of coefficients a_j for potential energy. This iterative process is continued until convergence, or self consistency, of values of coefficients for potential energy according to an appropriate criterion. One consequently obtains, with empirical parameters $\Delta_{kl}^{a,b}$, Dunham coefficients Y_{kl}^i, or their equivalent quantities U_{kl} formally independent of nuclear mass, in a set from $Y_{0,0}$ to $Y_{k,0}$ and $Y_{0,2k}$ consistent with coefficients a_j, or convenient alternative such as c_j, up to some maximum level of j. Further coefficients Y_{kl}^i are taken to be zero according to truncation of infinite sums in formula 8 necessitated by spectral data having finite number, whereas further coefficients a_j, or alternative, have values entirely indeterminate, but which are unlikely to be zero. By inserting published values of parameters a_j into known expressions of term coefficients Y_{kl}^i, one can satisfy oneself that this criterion of consistent truncation of sums in formula 8 has been practised such as in work on HBr [37] and HCl [36] since the commencement of efforts to employ Dunham's formulae for Y_{kl}^i in a consistent manner; although such a criterion is only implicit within Dunham's paper [5], it has nevertheless been essentially universally applied; insinuation of further primary quantities Y_{kl}^i with non-zero values other than those supported directly by the data set into a treatment of data in a particular set beyond that implied by subsidiary parameters such as a_j or c_j to a specific level is recognised to be incongruous.

On the basis of this criterion one might attempt to estimate some further subsidiary parameters, according to the following scheme [69]. If the fitted value of a_j of ultimate order j be even, with value m for instance, that condition implies a non-zero value of some Dunham coefficient $Y_{k,0}$ of largest value of k, such as n, and thereby other coefficients $Y_{n-1,2}$, $Y_{n-2,4}$ … with even l, and other coefficients $Y_{n-1,1}$, $Y_{n-2,3}$ … with odd l. One might then estimate a_{m+1} from a formula for $Y_{n,1} = 0$, or alternatively from $Y_{n-1,3} = 0$, or analogously for other Y_{kl} with lesser k but increasing odd values of l. This operation fails to yield consistent results because that estimate of a_{m+1} from $Y_{n,1} = 0$ likely differs significantly from the corresponding estimate from $Y_{n-1,3} = 0$. One might argue that one should prefer

the former value because it arises from an assumption that a principal Dunham coefficient $Y_{n,l}$ with $l=0$ or 1 has a zero value, but such an argument involves an arbitrary selection. In any case, further such application of this scheme, to yield an estimate of a_{m+2} from $Y_{k+1,0}$ and so forth, rapidly leads to divergent and unphysical magnitudes of these parameters a_j, such that this scheme becomes impracticable and unreliable [70], like any other contrivance to extrapolate in lack of both an exact model and exact data. Whether the above argument involves Y_{kl} or their equivalents U_{kl} independent of mass, which would be actually employed in reduction of spectral data of multiple isotopic variants, is immaterial: the same conclusion follows.

Although a traditional approach without Tiemann's extension [69] yields parameters a_j of minimum number, which hence imply primary coefficients Y_{kl} of minimum number in a consistent set, there remain empirical parameters $\Delta_{kl}^{a,b}$ that might have their number reducible through their expression to radial coefficients in functions for extra-mechanical effects – such as $g_r(R)$, $g_v(R)$ and $V'(R)$ introduced above. A few approximate relations such as [71]

$$\Delta_{0,2} \approx 3\Delta_{0,1} - 2\Delta_{1,0} \tag{44}$$

have been derived, but a more systematic approach in terms of those radial functions is clearly required. Although, on the basis of application of a JBKW approach [26], formulae were derived to relate quantities equivalent to $V'(R)$ and $g_r(R)$ in an effective hamiltonian, formula 29 apart from V'', without g_v, a full solution including $g_v(R)$ beyond a constant term awaited development of hypervirial perturbation theory and its application first to derivation of Dunham coefficients Y_{kl} [28], and subsequently to auxiliary term coefficients Z_{kl} [72]. Employing an effective hamiltonian [66] in an alternative form in formula 29 above that is equivalent to that applied in that derivation [72], and observing that, on a basis of formulae 34, 33 and 31, these extra-mechanical effects are expressible in terms of sums of contributions involving reciprocal masses M_a and M_b of separate neutral atoms [66], we postulate the following radial functions for vibrational and rotational g factors and adiabatic corrections, respectively, in terms of reduced displacement variable z defined in formula 21:

$$g_v(R) \rightarrow g_v(z) = m_p \left(\sum_{j=0} s_j^a z^j / M_a + \sum_{j=0} s_j^b z^j / M_b \right) \tag{45}$$

$$g_r(R) \rightarrow g_r(z) = m_p \left(\sum_{j=0} t_j^a z^j / M_a + \sum_{j=0} t_j^b z^j / M_b \right) \tag{46}$$

$$V'(R) \rightarrow V'(z) = hc m_e \left(\sum_{j=0} u_j^a z^j / M_a + \sum_{j=0} u_j^b z^j / M_b \right) \tag{47}$$

This formulation [72] includes terms only linear in a ratio m_e/M_a of electronic and atomic masses. Whereas coefficients c_j pertaining to potential energy, or their

counterparts a_j in Dunham's expressions [5], occur non-linearly in Dunham coefficients Y_{kl}, as exhibited in this instance,

$$Y_{2,1} = (B_e^3/\omega_e^2)(45c_1^3 + 27c_1^2 - 78c_1c_2 + 30c_3) + \ldots \tag{48}$$

in which B_e and ω_e are primary rotational and vibrational parameters appearing in formulae 6 and 5 respectively, coefficients $s_j^{a,b}$, $t_j^{a,b}$ and $u_j^{a,b}$ occur only linearly in auxiliary coefficients Z_{kl}^v or Z_{kl}^r for either atomic type in formula 28, as this instance demonstrates.

$$Z_{1,0}^{v,a} = 1/2\,\omega_e s_0^a m_p/M_a + 2(B_e/\omega_e)[u_1^a(1 - 3c_1/2) + u_2^a]m_e/M_a \tag{49}$$

Despite the linear occurrence of $s_j^{a,b}$, $t_j^{a,b}$ and $u_j^{a,b}$ among themselves, they occur in products with other parameters c_j, B_e and ω_e; the latter two quantities each separately contain, implicitly, reduced mass, as μ^{-1} in B_e and $\mu^{-1/2}$ in ω_e through these explicit formulae,

$$B_e \equiv h/(8\pi^2 c\mu R_e^2) \tag{50}$$

$$\omega_e \equiv (k_e/\mu)^{1/2}/(2\pi c) \tag{51}$$

consistent with formula 13. These two quantities constitute convenient forms to represent parameters R_e and c_0, which belong to $V(z)$ according to a definition of z in formula 21 and the following explicit formula,

$$V(R) \to V(z) = V_0 + hcc_0 z^2 \left(1 + \sum_{j=1} c_j z^j\right) \tag{52}$$

with

$$c_0 = a_0 \equiv \omega_e^2/(4B_e) = 1/2\,k_e R_e^2/hc \tag{53}$$

The right sides of both latter expressions evidently contain no dependence on mass, and formula 52 is analogous to formula 16. Consistent with use of reduced quantum numbers according to formulae 43, in practice $U_{1,0}$ replaces ω_e and $U_{0,1}$ replaces B_e during fitting of spectral data with mass-reduced quantum numbers. Inversion of spectral data to coefficients c_j, $s_j^{a,b}$, $t_j^{a,b}$ and $u_j^{a,b}$ and R_e in pertinent radial functions to represent in a compact form, according to an ultimate spectral reduction, Dunham coefficients Y_{kl} and auxiliary coefficients Z_{kl} in sets consistent with radial coefficients at particular levels clearly requires estimation of non-linear parameters in the form of those radial coefficients. The first algorithm to achieve this objective is embodied in a Fortran programme for weighted non-linear regression called Radiatom [55], in which a main routine serves to specify masses and to read data; its call also of a subroutine [73] initiates activity of an efficient fitting algorithm according to a method that Newton originated and that Levenberg, Marquardt, Choleski, Hammarling, Morrison, Osborne [73] and others developed subsequently. That subroutine in turn calls another subroutine

that calculates both the wave numbers of transitions, according to fixed values of regressors – masses of atoms constituting a particular isotopic variant and quantum numbers of lower and upper states of an assigned transition in a list in the data set – and adjusted or constrained values of parameters – radial coefficients or associated quantities as explained above, and the derivatives of residuals with respect to those parameters. The wave number of each transition is calculated directly through Dunham, Y_{kl}, and auxiliary coefficients, collectively Z_{kl}, as in

$$
\tilde{\nu} = \sum_{k=0} \sum_{l=0} (Y_{kl} + Z_{kl}^{v,a} + Z_{kl}^{v,b} + Z_{kl}^{r,a} + Z_{kl}^{r,b})\{(v' + 1/2)^k [J'(J' + 1)]^l
$$
$$
- (v'' + 1/2)^k [J''(J'' + 1)]^l\} \tag{54}
$$

These coefficients Y_{kl} and collectively Z_{kl} are employed precisely as the primary quantities according to the theory of Dunham [5] and van Vleck [9], calculated through their expressions in terms of radial parameters in other subroutines; those many expressions have simply the forms shown in formulae 48 and 49 above. Their radial coefficients serve to maintain a consistent level of Y_{kl} and each component of Z_{kl}. Further subroutines of Radiatom contain expressions for derivatives of these primary quantities with respect to radial coefficients. Symbolic expressions for derivatives of residuals with respect to radial parameters enable fitting more efficient than merely numerically calculated derivatives, through first or second finite differences; such symbolic derivatives in a fitting procedure facilitate convergence, and hence require initiate estimates of parameters less near the ultimately fitted values than for numerical derivatives. All these expressions in these subroutines were initially formed directly with symbolic processors Reduce and Maple, through automatic generation of Fortran code, and are evaluated with numerical precision of calculations set at 32 decimal digits. With increasing speed of computer hardware and increasing sophistication of software, generation of expressions for Y_{kl} and various Z_{kl} with Maple and subsequent utilisation of these expressions in a separate fitting procedure entirely within Maple that evaluates selected radial coefficients according to another procedure also based on work of Levenberg and Marquardt has become feasible; Radiatom II functions in this manner, with precision readily selectable but set typically at 24 decimal digits. Taking full advantage of use of software for computer algebra, a novel feature of the latter procedure is utilisation therein of symbolic differentiation of an algebraic procedure (M. B. Monagan and J. F. Ogilvie, in preparation) that builds a grand expression for E_{vJ}^i through a sum of Y_{kl} and all appropriate components of Z_{kl}. Operation of Radiatom II is practical for data in a set numbering less than 500; such a computation to converged parameters involves typically a duration up to 2000s, relative to as little as 90s for data and parameters in the same sets and the original Radiatom in Fortran with a powerful processor; the difference reflects that Fortran programmes are fully compiled, whereas Maple procedures employ compiled numerical subroutines but operate at the top level in an interpreted manner, hence slowly. Although estimated standard errors of parameters and coefficients of correlation between parameters are practically identical for analyses of the same data with Radiatom in these two versions, the converged values of parameters are not quite identical but

agree within the stated errors. Extensive vibration-rotational data in appropriate sets of which an analysis might involve effects of finite size of atomic nuclei are lacking; for neither Radiatom nor Radiatom II has there been made an attempt to encompass these effects. For both procedures typically 10–20 iterations are required to reach convergence according to a specified criterion.

For Radiatom, upon approach to convergence, that criterion involves a test that involves the sensitivity of parameters to adjustment; ample experience with Radiatom has demonstrated that this test fails if initial estimates of adjusted parameters, typically numbering 10–25, are near the finally converged values. This peculiarity has led to use of deliberately rough values of $U_{1,0}$ and $U_{0,1}$ with characteristic standard values of c_1 and c_2 as initial estimates [13, table 4.26]; initial estimates of all other values of adjustable parameters are entered as zero. For this reason the initial value, for both Radiatom and Radiatom II, of a sum of weighted residuals, χ^2, is typically of order 10^{15}, eventually decreasing to a value typically of order 10^4 at convergence; during this process values of parameters sample a large area of the hypersurface of χ^2, and local minima seem to be avoided in favour of an apparent global minimum, at least within a physically reasonable domain of parameter space. For this reason also a deliberate attempt to seek a local minimum of χ^2, or otherwise to influence the ultimate values of parameters, is impracticable; the process of evaluating parameters, within a particular set, thus becomes as objective as practicable within a limitation of necessarily providing initial estimates of parameters as dictated by the nature of non-linear regression. A further property of Radiatom is its inability to fit linearly dependent parameters; an error message "Parameter … is linearly dependent upon previous parameters" appears on initiating any attempt of this type, and execution terminates at that point, generally at the first iteration. Experience with Radiatom II is less extensive than with the original Radiatom, but similar behaviour seems to apply; this manner of performance might be a general feature of regression according to the algorithm of Levenberg and Marquardt when applied to many parameters.

5. APPLICATIONS OF DUNHAM'S FORMALISM TO SPECTRAL ANALYSIS

As an objective, spectral reduction involves evaluating parameters of minimal number that serve to reproduce wave numbers of transitions within, on average, their precision of measurement. According to an approach based on the formalism of Dunham and its extension by van Vleck, one seeks hence to evaluate term coefficients Y_{kl} and various Z_{kl} in sets that are both minimal and consistent, achieving the latter property through secondary parameters of some appropriate kind. Although Dunham's original derivation involved a function $V(x)$ and its parameters a_j, an alternative scheme has generated as its result exactly formula 2 above incorporating Y_{kl}^{GCA}; instead of potential energy and kindred radial functions this generator-coordinate approach [74,75] involves integral kernels prospectively obtained from calculations of molecular electronic structure and matrix elements of nuclear operators, hence directly transcending the crude

approximation resulting from formula 30. One can not emphasise too strongly that a radial function, such as V(R) for potential energy or p(R) for electric dipolar moment that according to conventional treatments is taken to govern wave numbers or strengths, respectively, of lines associated with typical transitions measured in infrared spectra, is an artefact of a formal separate treatment, which is approximate, of electronic and nuclear motions; notwithstanding this global truth, one includes further radial functions that serve as corrections, such as those in formula 29 beyond terms in formula 14, to improve reproduction of experimental data by transcending somewhat that approximation when such corrections are sufficiently small to be considered acceptable perturbations. There exists hence at least one fully theoretically justified alternative to use of radial functions that have as argument either directly internuclear distance R or a functional of R in combination with R_e. In sum, a radial function such as potential energy is an artefact of a theoretical ansatz – an artificial distinction between motions of subatomic particles unjustifiable according to rigorous quantum mechanics even though quantum-mechanical methods might serve to calculate applicable quantities in a semi-classical approach. A radial function is not an experimentally observable quantity, and is not even essential to the practice of Dunham's formalism in analysis of molecular spectra. Furthermore, since Dunham's time proof has existed [76,77] that inversion of spectral data involving only bound states fails to define uniquely a function for potential energy, with or without auxiliary functions for adiabatic corrections, vibrational and rotational g factors et cetera. A simple example of such lack of uniqueness exists for equal differences between adjacent vibrational energies: the number of corresponding functions for potential energy is uncountable [78,13]. To evaluate V(R) uniquely from data pertaining to only a particular angular momentum, one requires also knowledge of phase shifts of all continuum states [79], although scattering data at fixed energy enable recovery of potential energy [80]. The essential raison d'etre of a radial function is precisely to ensure that Dunham coefficients, Y_{kl} extended with various Z_{kl}, comprise a consistent set of minimal number, in accordance with the principle of parsimony or Occam's razor, thus allowing one to achieve maximal spectral reduction; the underlying evaluated radial parameters or prospective integral kernels incidentally also number minimally within a consistent set. These Dunham coefficients, independent of any model that inter-relates them such as a function for potential energy or integral kernels based on a generator coordinate, constitute a systematic representation, through formula 54 as extended to include effects of nuclear volume if necessary, of actual or feasible measurements of wave numbers of spectral lines within a range of quantum numbers v and J for which values of these coefficients are valid.

Notwithstanding the preceding fundamental verity, one discerns qualitative similarities between features of these radial functions and observable quantities from other than spectral experiments. For instance, a value of the hypothetical equilibrium internuclear distance R_e deduced from spectra of gaseous CO in its electronic ground state is similar to a value of interatomic distance derived from crystallographic data obtained in experiments with diffraction of xrays, and expected to be similar also for deductions from experiments with diffraction of electrons or neutrons, even though the latter three experiments might yield

significant variation of that parameter even for samples measured at the same temperature and state of aggregation. Moreover, one expects that radial functions derived from disparate methods of spectral reduction of data in a common set likely exhibit similar characteristics and trends, although there is no reason to envisage exact agreement.

How does one proceed to evaluate Dunham coefficients Y_{kl} and Z_{kl} from spectral data comprising transitions combining several vibrational and many rotational states of a particular diatomic molecular species in multiple isotopic variants? We here assume that assignments of all transitions in terms of v and J of combining states are already made, although in practice it is entirely feasible to undertake an analysis of spectra of a particular species involving making such assignments for a selected subset of measured lines and using tentative values of both Y_{kl} consistent with underlying parameters such as a_j or c_j to extend assignments. Such a procedure has been applied, for instance, in analysis of spectra of vapours of RbCl [81] and GeO [82] in absorption. If parameters be evaluated for individual bands of the most abundant isotopic species, one can generally be guided to the maximum necessary value of k in $Y_{k,0}$ by fitting the origins or centres of vibration-rotational bands to a polynomial in $v + \frac{1}{2}$ in formula 5 or equivalent, and the corresponding maximum necessary value of k in $Y_{k,1}$ through an analogous fit of B_v in formula 6; for a typical collection of spectral data including vibration-rotational bands, the value of k derived from thus fitting B_v is likely within one unit of the value of k derived from fitting band origins. Such fits of individual bands are useful also to provide estimated standard deviations of wave numbers that can serve as weights in the ensuing regression to evaluate radial and Dunham coefficients. In lack of such guidance, a direct fit of an entire set of spectral data, with weights estimated from other observations, can proceed with trial selection of ranges of radial coefficients, eventually to achieve convergence and monitored with values of statistical indicators of goodness of fit. Because radial coefficients a_j or c_j for potential energy occur in algebraic formulae of Y_{kl} in a highly non-linear manner, as shown in formula 48 for instance, it is mandatory to retain all those quantities as parameters up to a particular maximum value, even though an estimated standard error of an intermediate coefficient might indicate its nominal lack of significance. Moreover, successive radial coefficients become introduced into expressions for energies of vibration-rotational states through successive orders according to perturbation theory of Rayleigh and Schrodinger in hypervirial form [30] or otherwise [21]. The JBKW method with all quantum corrections yields the same series as standard quantal perturbation theory for an anharmonic oscillator [72,83,84]; hence the corresponding infinite series are identical, although each approach might generate terms in distinct manners: to have the terms identical order by order one must choose the same perturbation parameter and invert the BKW equation up to the same order chosen in quantal perturbation theory. For this reason also, it is illogical and improper to reject parameters such as a_j or c_j that occur first in a particular order of perturbation theory but to accept analogous parameters that become introduced according to this theory in a higher order. When this theory is applied in a consistent and systematic manner, the practical generation thereby of radial coefficients for potential energy in a minimal set from given frequency data,

and hence of consistent parameters Y_{kl}, generally suffers from no ambiguity of extent of polynomial.

In contrast, selection of radial coefficients for extra-mechanical effects poses significant difficulty: the reason is that, even ignoring the effect of nuclear volume and of further nonadiabatic effects in $V''(R)$, these effects number three for an atomic centre of each distinct atomic number, according to parameters in formulae 45, 46 and 47, whereas auxiliary coefficients of types Z_{kl}^v or Z_{kl}^r number only two. Moreover, although adiabatic effects contribute to only Z_{kl}^v and the rotational g factor to only Z_{kl}^r, parameters pertaining to the vibrational g factor appear in formulae for both Z_{kl}^v and Z_{kl}^r, but with no net contribution to $Z_{0,l}^v + Z_{0,l}^r$. Without either additional information from experiments with samples in applied electric and magnetic fields or equivalent information obtained through a practice of computational spectrometry, one must either make an – at least somewhat – arbitrary selection of parameters of types s_j, t_j and u_j, in formulae 45, 46 and 47 respectively, or construct modified parameters in various combinations for the purpose of fitting spectra [28,85]; in either case a numerical value of such a parameter might lose its nominal *physical* significance in regard to a particular term in a hamiltonian, although the overall objective of deriving values of coefficients Y_{kl} and Z_{kl} to reproduce spectral data is unaffected.

We examine a few particular radial coefficients in detail. Coefficients $u_0^{a,b}$ pertaining to adiabatic corrections in $V'(R)$ appear in only an expression for auxiliary coefficient $Z_{0,0}^v$, explicitly in this form [55]:

$$Z_{0,0}^v = m_e(u_0^a/M_a + u_0^b/M_b) \qquad (55)$$

Being the coefficient of $(v+\frac{1}{2})^0 [J(J+1)]^0$, this term $Z_{0,0}^v$ is merely a contribution to residual energy and is indeterminate from measurements of wave numbers of spectral transitions between bound vibration-rotational states within the same electronic state. For radiative dissociation of diatomic molecule AB into atomic ions A^- and B^+, one can measure the energy with considerable accuracy, equivalent to $\sim 100\ m^{-1}$ for such a diatomic molecular reactant [86]; application of this experiment to HCl and to DCl enabled measurement of a difference $(320 \pm 100)\ m^{-1}$ after other differences of dissociation energy and residual energy were taken into account [86]. A possibility exists that this difference might be attributed to u_0^H, which implies a value $(1.2 \pm 0.4) \times 10^6\ m^{-1}$ of this quantity: such a magnitude is comparable with values$/10^6\ m^{-1}$ for $u_1^H = -6.1233 \pm 0.0026$ and $u_2^H = 18.3836 \pm 0.0097$ deduced from analysis of infrared spectra of HCl [55], although the latter value is susceptible to contamination from coefficient s_0^H related to the vibrational g factor for reasons explained above; explicit calculation of adiabatic corrections for HCl would verify this point. Such calculations of $Z_{0,0}^v$ are reported for diatomic molecules H_2, HF, N_2 and F_2 [87], not HCl; a notable result of those calculations, unmentioned by the authors, is a finding that a ratio of $Z_{0,0}^v$ to total electronic energy tends to decrease with increasing atomic number or mass. Handy and Lee investigated the effects of adiabatic corrections on "bond length" and "vibrational frequencies" of diatomic molecules [87]; these effects also decrease with increasing atomic number or mass, but for some molecules nonadiabatic effects are more important than adiabatic corrections in this context [88]. In any case, because

coefficients $u_0^{a,b}$ in $V'(R)$ appear in only $Z_{0,0}^v$ that imposes no tangible effect on wave numbers of spectral transitions between bound states within a particular electronic state, we ignore them in further deliberations here.

Of leading radial coefficients of two other types in relation to extra-mechanical effects, $s_0^{a,b}$ pertain to the vibrational g factor, and $t_0^{a,b}$ pertain to the rotational g factor; in both cases these quantities also involve electric dipolar moment through its radial function p(R), or equivalently in terms of reduced displacements x or z in p(x) or p(z). We express the latter in an expansion,

$$p(R) \to p(z) = \sum_{j=0} p_j z^j \qquad (56)$$

according to these relations [66] applicable to a molecule of relative polarity $^-AB^+$,

$$s_0^a = \mu[g_v(R_e)/m_p - 2p_1/(eR_eM_b)] \qquad (57)$$

$$s_0^b = \mu[g_v(R_e)/m_p + 2p_1/(eR_eM_a)] \qquad (58)$$

$$t_0^a = \mu[g_r(R_e)/m_p - 2p_0/(eR_eM_b)] \qquad (59)$$

$$t_0^b = \mu[g_r(R_e)/m_p + 2p_0/(eR_eM_a)] \qquad (60)$$

which involve values of rotational and vibrational g factors, electric dipolar moment and its derivative all evaluated at R_e. If one could evaluate significantly these radial coefficients through reduction of pure rotational and vibration-rotational spectra measured for samples of a diatomic compound in the absence of applied electric or magnetic field, one might thus be able to estimate electric and magnetic properties of this molecule in the same electronic state, specifically one or other g factor and either the permanent electric dipolar moment p_0 or its gradient p_1 at the equilibrium internuclear distance [89]. Doubt has been expressed [90] about the feasibility of such a significant evaluation of t_0^a and t_0^b under those conditions, but this reservation arises from inadequate understanding of expressions for auxiliary coefficients Z_{kl}. If one consider only the total quantity $Z_{0,1}$ for an atomic centre of type A according to this relation,

$$Z_{0,1}^a = Z_{0,1}^{v,a} + Z_{0,1}^{r,a} = (B_e t_0^a + \gamma^2 u_1^a)m_e/M_a \qquad (61)$$

in which $\gamma \equiv 2 B_e/\omega_e$, and if one suppose that only the total quantity $Z_{0,1}^a$ be deducible from spectral data for a sample without applied field, radial coefficients t_0^a and u_1^a are perfectly correlated – because factors B_e and γ^2 have the same dependence on reduced mass μ – and can thus not be significantly evaluated, which is the basis of the purported argument [90]. Other relations, however, such as

$$Z_{0,2}^a = Z_{0,1}^{v,a} + Z_{0,1}^{r,a} = \{B_e[-2t_0^a + t_1^a] + \gamma^2[u_1^a(-3c_1/2 - 2) + u_2^a]\}\gamma^2 m_e/M_a \quad (62)$$

break that perfect correlation because therein t_0^a and u_1^a occur with other than unit numerical factors. If one take total auxiliary coefficients Z_{kl} up to $Z_{3,0}^a, Z_{2,2}^a, Z_{1,4}^a$

and $Z_{0,6}^a$ – or equivalently Δ_{kl}^a in formula 19 with subscripts in the same range – that number 15 in total, excluding $Z_{0,0}^a$, these imply radial coefficients in subsets, excluding u_0^a, up to s_4^a, t_5^a and u_6^a, hence numbering 17 variables. Unknown radial parameters thus outnumber auxiliary coefficients Z_{kl} through which the former might be evaluated in principle. For this reason not all those radial coefficients can be evaluated without supplementary information. In practice, a truncated subset would require arbitrarily discarding two selected coefficients, most reasonably two among the three, s_4^a, t_5^a and u_6^a, that derive from greatest orders of perturbation theory. Values of some remaining coefficients, at least those at the highest remaining levels, would thereby adopt a mixed character, and would accordingly lose their connection to a particular term in an effective hamiltonian and hence to a particular source of effect such as rotational or vibrational g factor. One expects reasonably, however, that values of radial coefficients at the least levels, such as s_0^a, t_0^a and u_1^a, would assume little or no mixed character and thus retain essentially their pure relation, apart from error of these parameters propagated from measurements of wave numbers of spectral lines, to particular terms in the effective hamiltonian, formula 29 with neglect of $V''(R)$. An objective to take these various parameters in combinations, optimal or otherwise, as fitting coefficients overcomes this indeterminacy [29,85], but at a loss of all or most correspondence between evaluated parameters and terms in that hamiltonian. To illustrate this problem we consider in detail one instance of significant evaluation of a rotational g factor, and two other instances in which this difficulty of evaluation is circumvented to some extent through application of information additional to wave numbers of spectral transitions, as a direct application of computational spectrometry.

6. GALLIUM HYDRIDE, GaH

Gallium hydride is an esoteric and obscure chemical compound, of no particular technical significance; through infrared spectra, its vapour nevertheless proves useful for elucidation of diatomic molecular properties in an exemplary manner. Although vibration-rotational spectra but no pure rotational spectra of gallium hydride have been measured, 1094 lines in this data set comprise an especially useful collection because spectra, from experiments entailing absorption [91,92] or emission [93] of radiation in the mid infrared region, of four isotopic variants – $^{69}Ga^1H$, $^{71}Ga^1H$, $^{69}Ga^2H$ and $^{71}Ga^2H$ – involve vibration-rotational energies over almost the same range, corresponding to $v = 5$ maximum for GaH and $v = 7$ maximum for GaD. Reduction of all data from emission spectra [93] with unduplicated data for GaH in absorption [91] according to the Dunham approach with Radiatom yields evaluated parameters according to results presented in Table 1.

Each stated uncertainty in this and other tables represents one estimated standard error, propagated to parameters from uncertainties of measurements of wave numbers; the uncertainties of the latter measurements were provided by authors of papers [91,93] reporting those data, and the weight of each datum in the non-linear regression was taken as the reciprocal square of those uncertainties. As the reduced standard deviation of the fit was 0.92, so less than unity, the authors

Table 1. Coefficients of radial functions and other molecular parameters of GaH X $^1\Sigma^+$

c_0/m^{-1}	10463962 ± 22	s_0^{Ga}	0.696 ± 0.066
c_1	-1.3474749 ± 0.0000078	t_0^{Ga}	-3.38 ± 0.33
c_2	1.038431 ± 0.000030	t_1^{Ga}	5.33 ± 0.65
c_3	-0.521864 ± 0.000111	t_0^{H}	-3.16990 ± 0.00060
c_4	0.04433 ± 0.00054	t_1^{H}	7.3384 ± 0.0167
c_5	-0.1159 ± 0.0026	t_2^{H}	-14.82 ± 0.26
c_6	0.2471 ± 0.0067	t_3^{H}	16.19 ± 0.42
c_7	-0.0182 ± 0.031	$u_1^{\text{H}}/10^6\ \text{m}^{-1}$	-10.80866 ± 0.00105
c_8	-1.688 ± 0.106	$u_3^{\text{H}}/10^6\ \text{m}^{-1}$	29.71 ± 0.86
		$u_4^{\text{H}}/10^6\ \text{m}^{-1}$	-66.4 ± 3.8
		$u_5^{\text{H}}/10^6\ \text{m}^{-1}$	127.6 ± 10.9
		$u_6^{\text{H}}/10^6\ \text{m}^{-1}$	-223 ± 27
$U_{0,1}/\text{m}^{-1}\ \text{u}$	611.64646 ± 0.00163		
$U_{1,0}/\text{m}^{-1}\ \text{u}^{1/2}$	159996.185 ± 0.044		
$R_{\text{e}}/10^{-10}\ \text{m}$	1.6601526 ± 0.0000022		
$k_{\text{e}}/\text{N}\ \text{m}^{-1}$	150.823636 ± 0.000084		

likely expressed those uncertainties slightly conservatively, but clearly an application of Dunham's formalism embedded in computer programme Radiatom provides a satisfactory reduction of these data. Parameters in the left column pertain to mechanical effects, according to Dunham's term [5], and in the right column to extra-mechanical effects. Only ten parameters in the left column are independent: those explicitly fitted include c_j with $1 \leq j \leq 8$, $U_{1,0}$ and $U_{0,1}$; parameters c_j are coefficients in $V(z)$ according to formulae 21 and 52, and two others are defined in terms of the corresponding Dunham coefficients through formulae 13. The leading coefficient c_0 for potential energy is defined as

$$c_0 = U_{1,0}^2/(4U_{0,1}) \tag{63}$$

thus maintaining its rigorous independence of atomic mass; the equilibrium force coefficient k_e, pertaining to Hooke's law in the limit of an harmonic oscillator, is related to $U_{1,0}$ through

$$k_e = (2\pi c U_{1,0})^2/(10^3 N_A) \tag{64}$$

whereas the equilibrium internuclear separation R_e is related to $U_{0,1}$ through

$$R_e[10^3 N_A h/(8\pi^2 c U_{0,1})]^{1/2} \tag{65}$$

A factor Avogadro's constant multiplied by 10^3 enters these expressions on condition that atomic and electronic masses be expressed, as is customary in spectral analyses, in unified atomic mass unit; both $U_{1,0}$ and $U_{0,1}$ contain mass in their units, despite their values being formally independent of atomic mass. The standard errors associated with values of k_e and R_e in Table 1 include contributions from errors of pertinent fundamental physical constants [94].

Of values in the right column of Table 1, the specified parameters are coefficients of z in formulae 45, 46 and 47, pertaining to vibrational and rotational g factors and adiabatic corrections respectively, with atomic centres B$=$Ga and A$=$H for this particular compound. Apart from the value of u_2^H that was constrained to zero in the ultimate fit because preliminary fits indicated that its standard error much exceeded its magnitude, values of other parameters beyond c_8, s_0^{Ga}, t_1^{Ga}, t_3^H and u_6^H in their respective series, and also all u_j^{Ga} and s_j^H, are not assumed to be zero, but are simply indeterminate from available spectral data within the chosen model, as explained above. Although it is absolutely inappropriate to constrain to zero the value of a particular parameter within a selected set of parameters c_j, even though an estimated standard error of that parameter considered for rejection be larger than its magnitude, it is appropriate, if warranted on an objective basis of statistical criteria, to constrain to zero value a particular parameter within a selected set s_j, t_j or u_j, as is practised with u_2^H in this case; a crucial distinction between these methods of handling parameters arises because c_j occur non-linearly in expressions both Y_{kl} and Z_{kl} – see formula 48 for instance, whereas the latter parameters for extra-mechanical effects occur only linearly in expressions for Z_{kl} – compare formula 49. In our original report [89], we employed parameters in not quite the same set; the set here takes account of the fact that adiabatic corrections, reflected by coefficients of type u_j, are expected

to be more important for a light species such as H than the effect of the vibrational g factor, reflected in coefficients of type s_j, and vice versa for a massive species such as Ga, on a basis of calculations of adiabatic corrections [87] discussed above and our accumulated experience with rotational and vibrational g factors. The latter supposition is subject to verification when calculations of adiabatic corrections for GaH become practicable. Parameters in a set selected for this fit thus reflect arbitrary selection to some extent; of parameters in all various sets that were tested, this set in Table 1 produced the smallest reduced standard deviation of fit. Although parameters in an alternative set might produce an even smaller standard deviation, if such a set were to include parameters that arise in higher orders of perturbation theory to the exclusion of parameters in lower orders, such a set would be clearly illegitimate.

Before drawing deductions about molecular properties from results in Table 1, we consider further statistical aspects. The program Radiatom produces not only estimated standard errors of parameters, such as those presented in Table 1, that derive from variances, but also their coefficients of correlation ρ_{jk} from a corresponding covariance matrix. For GaH and results appearing in Table 1, there are 22 adjustable parameters: hence a symmetric matrix of these coefficients contains 231 distinct entries; numerical magnitudes of only 19 exceed 0.9. Such a proportion of magnitudes greater than 0.9 is a typical occurrence in fits of real positive numbers to polynomials that are not orthogonal. Magnitudes of correlation coefficients near unity derived from the covariance matrix pose no problem for numerical stability in Radiatom because it operates with nominal precision 32 decimal digits. For GaH, 14 values with $|\rho| > 0.9$ occur between coefficients u_j^H, as expected because these coefficients have mostly no counterparts t_j^H that arise in the same orders of perturbation theory. Of other magnitudes near unity, between t_0^{Ga} and $U_{0,1}$ the value of ρ is -0.997, which is still not the largest magnitude off the diagonal of this correlation matrix; such a large magnitude is reasonable because the difference of reduced mass between $^{69}Ga^1H$ and $^{71}Ga^1H$ is minute. Likewise a value of ρ connecting s_0^{Ga} and $U_{1,0}$ is -0.95. In contrast only one moderate magnitude of ρ connects t_0^H with another parameter, specifically t_1^H; the value is -0.82, whereas for u_1^H the largest magnitude of ρ to another parameter is less that 0.28 – entirely innocent; these results reflect the large difference of reduced mass between Ga^1H and Ga^2H, and hence a large sensitivity of values of extra-mechanical parameters for H to moderately precise spectral data. A claim [90] that coefficients u_1^a and t_0^a are necessarily highly correlated is hereby refuted; such correlation is broken as explained above. To indicate a context for these values, the value of ρ between c_1 and c_2 is -0.87, not for only GaH but typically also for other molecular species, again characteristic of fits to non-orthogonal polynomials. On a basis of both standard errors and correlation coefficients, coefficients $t_0^H = -3.16990 \pm 0.00060$ and $u_1^H/10^6 \ m^{-1} = -10.80866 \pm 0.00105$ are hence clearly statistically well defined, whereas $t_0^{Ga} = -3.38 \pm 0.33$ and $s_0^{Ga} = 0.696 \pm 0.066$ are poorly defined despite ratios of their magnitudes to respective standard errors exceeding 10.

Production of an acceptable value of reduced standard deviation of a fit required multiple parameters u_j^H, up to $j=6$. Values of these parameters with $j>2$ likely reflect not only adiabatic corrections; their association with a particular term in

the effective hamiltonian is hence questionable. From both a point of view of partition of effects among parameters s_j, t_j and u_j in an incomplete subset for a particular range of Z_{kl}, as discussed above, and from particular statistical considerations, however, parameters t_0^H and u_1^H can be confidently attributed to pertain practically exclusively to the rotational g factor and to adiabatic corrections, respectively.

On this basis we proceed to deduce, from pertinent radial coefficients in table 1, values of molecular properties, within a quasi-physical model consistent with an effective hamiltonian of form in formula 29. The equilibrium internuclear distance is purportedly a measure of the length of the chemical bond between atomic centres Ga and H; for this highly precise value of R_e in table 1 the relative error is about one part per million, and the absolute error is about one tenth of a typical nuclear radius. Evidently just as precisely evaluated, the equilibrium force coefficient k_e has a value about a quarter of that typical of hydrides such as CH and NH with 'single' chemical bonds, consistent with GaH having a thermochemical dissociation energy smaller than that of these other specified hydrides [95] and with a general decrease of such force coefficients with atomic centres involving chemical elements beyond the row in the periodic chart containing Li and Ne. The radial function $V(z)$ for potential energy has a maximum range of validity $1.3 \leq R/10^{-10}$ m ≤ 2.4, consistent with the classical turning points for vibrational state $v = 5$ of GaH. Coefficients c_j up to $j = 8$ imply expressions Y_{kl}^i up to $Y_{5,0}$, $Y_{4,2}, \ldots, Y_{0,10}$, in total 36 applicable to each isotopic variant, hence 144 numerical values of coefficients in formula 27 that, with corresponding numerical values for Z_{kl}^i derived from other radial coefficients in the right column of table 1, not only reproduce the measured wave numbers of 1094 spectral lines within their precision, on average, but also predict accurately the wave numbers of unmeasured transitions within the same range of v and J; less accurate prediction moderately beyond that range is likely also practicable. The radial functions pertaining to extra-mechanical effects have smaller ranges of validity because they are evaluated to lesser degrees of polynomials in z and because they likely contain mixed effects of $g_v(z)$, $g_r(z)$ and $V'(z)$, apart from contamination from $V''(z)$ that is unlikely to be significant.

Upon inverting formulae 59 and 60, we obtain these relations [89],

$$p_0 = 1/2 \, eR_e(t_0^{Ga} - t_0^H) \tag{66}$$

$$g_r(R_e) = m_p(t_0^H/M_H + t_0^{Ga}/M_{Ga}) \tag{67}$$

by means of which we estimate values of electric dipolar moment and rotational g factor of ^{69}Ga^{1}H at R_e. From formula 66, the value $(2.8 \pm 4.4) \times 10^{-30}$ C m is clearly insignificant, indicating neither magnitude nor sign of p_0 relative to the molecular axis, because, according to table 1, even the nominal error of t_0^{Ga} is larger than the difference between t_0^{Ga} and t_0^H. In contrast, through formula 67 the rotational g factor of ^{69}Ga^{1}H at R_e is highly significantly evaluated, -3.1188 ± 0.0049, because t_0^{Ga} and its error are divided by a large atomic mass. Apart from a negative sign, the latter value has a large magnitude, relative to those of HI, HBr

HCl and HF [56] with increasing values in a range [0.10, 0.45] respectively; a negative sign and large magnitudes are common to other hydrides of group 13, for which calculations yield values -8.207 for $^{11}B^1H$ [96] and -3.370 for $^{27}Al^1H$ [97]. Calculations [98] of $g_r(R_e)$ for $^{69}Ga^1H$ yield values in a range $[-2.9457, -3.4440]$ depending on a level of sophistication of computations of molecular electronic structure. Upon inverting formulae 58 and 59, we obtain relations [66] analogous to those above,

$$p_1 = 1/2 \, eR_e(s_0^{Ga} - s_0^H) \tag{68}$$

$$g_v(R_e) = m_p(s_0^H/M_H + s_0^{Ga}/M_{Ga}) \tag{69}$$

but these are inapplicable in the present circumstances to deduce a value of the vibrational g factor for GaH because we lack an estimate of s_0^H. By means of further relations [66],

$$p_1 - p_0 = 1/2 \, eR_e(t_1^{Ga} - t_1^H) \tag{70}$$

$$dg_r(z)/dz_{|R_e} = m_p(t_1^H/M_H + t_1^{Ga}/M_{Ga}) \tag{71}$$

we might apply the latter to estimate the derivative of rotational g factor of $^{69}Ga^1H$ at R_e to be 7.412 ± 0.019, but the former relation can yield only a rough estimate $(-2.67 \pm 0.86) \times 10^{-29}$ C m of a difference between coefficients p_1 and p_0 in a radial function, formula 56, for electric dipolar moment because p_0 is indeterminate from present spectral data of GaH. We might nevertheless infer that the permanent electric dipolar moment of GaH is likely to be small, but its derivative at R_e likely large; these conditions are reminiscent of similar characteristics of CO [99] and NO [100], for which a small permanent electric dipolar moment occurs and for which the polarity of the radial function alters near the equilibrium distance. Because these differences between radial coefficients s_j and t_j occur in formulae such as 66, 68 and 70, we concur with a suggestion [90] that electric dipolar moments obtained from spectra of samples in absence of electric or magnetic field might be difficult to evaluate or unreliable from only moderately precise spectral data, but the situation is clearly different for at least the rotational g factor of GaH.

We compare results of the present treatment of GaH with those published elsewhere. From measurements of absorption spectra of $^{69}Ga^1H$ and $^{71}Ga^1H$ [91], parameters of type A_{kl} were evaluated for separate isotopic variants. After further measurements of also $^{69}Ga^2H$ and $^{71}Ga^2H$, parameters of type A_{kl} for the latter species and of types B_{kl} and Δ_{kl} common to all four variants were reported [92]. Our first analysis [101] of spectra of GaH was based on only absorption spectra, 208 lines reported in two papers [91,92]; although it resulted in evaluation of parameters of essentially empirical radial functions, similar to V(z), V'(z) and $g_r(z)$ in formula 29, the treatment was hampered by both paucity of data and incompletely developed theory. After publication of data from emission spectra [93], a subsequent reanalysis [89] demonstrated the possibility of evaluation of

molecular electric and magnetic properties from analysis of vibration-rotational spectral data of samples measured without applied fields, but again the treatment suffered from lack of a theoretical basis that became available subsequently [66]. Comparison of our present results with those from only emission spectra [93] sheds light on several aspects of the present discussion. From spectra that included 1045 lines (omitting previously reported lines [91,92]) in sequences with $\Delta v = 1$ up to $v = 4$ for GaH and $v = 7$ for GaD, a fit of these data yielded freely adjustable parameters A_{kl} in formula 2 for each of four isotopic variants; these parameters numbered 70 in total. Combining data for all four species yielded first 19 unconstrained parameters B_{kl}, defined above in relation to formula 19, with 11 further parameters $\Delta_{kl}^{Ga,H}$; in a further stage, ten constrained parameters $U_{k,0}$ and $U_{k,1}$ were evaluated that imply a further 25 parameters U_{kl} with $l > 1$, also with 11 further parameters $\Delta_{kl}^{Ga,H}$. The final stage of data reduction involved numerical solution of Schrodinger's equation, 1045 times per iteration for several iterations, in which a radial function for potential energy is based on that of Morse [102] but with a polynomial in argument $\frac{1}{2}z$ in the exponent, accompanying expansions in displacement $(R - R_e)$ corresponding roughly to $V'(R)$ and $g_r(R)m_e/m_p$ in formula 29. (That numerical approach is incapable of handling directly another radial function $g_v(R)$ in formula 29.) In contrast, according to Dunham's symbolic approach, to obtain the general exact algebraic expressions one solves Schrodinger's equation once [30], or equally well applies matrix mechanics [31] or other methods [26], because those expressions are independent of a correct method of their production; only simple substitution at arbitrarily selected precision is required thereafter to evaluate Dunham coefficients Y_{kl} during fits of data, and therefrom the wave numbers of transitions according to formula 54. That reduction [93] resulted in values of R_e and 27 coefficients, each presented with 16 decimal digits, of radial functions – $10\beta_j$ in the exponent, four coefficients for Ga and eight for H in functions corresponding to those in formula 47 but with displacement as argument, and five coefficients for only H in an expansion resembling one of those in formula 46, also in terms of displacement; hence these authors used disparate variables related to distance within the same fit. Although their expansions of fourth and ninth orders similar to formula 47 clearly pertain primarily to adiabatic corrections, Campbell et alii [93] attribute these to "Born-Oppenheimer breakdown and homogeneous nonadiabatic mixing"; the latter, actually associated with the vibrational g factor, enters also into values of their parameters for their other radial functions with argument displacement, as described above. Whereas to fit 1094 data in table 1 we evaluate five parameters of type u_j^H, that alternative approach [93] required a polynomial of ninth order to fit 1045 data over a smaller range of wave number $\tilde{\nu}$, or vibrational quantum number v, for GaH.

Even for potential energy the other approach [93] required one parameter additional to ours, apart from $\mathcal{D}_e$; the latter quantity, equilibrium binding energy, is stated to be based on "thermochemical" data, but the cited source [95] indicates a value of dissociation energy $\mathcal{D}_0$ "< 2.84 eV" to arise from spectral analysis. Such an upper limit must be understood to provide an asymptotic limit for $V(R)$ at large R in a formula of Morse type because an attempted evaluation of $\mathcal{D}_e$ from only infrared spectral data is unreliable. The stated reason for the choice

of such a fitting form is to generate "a reliable internuclear potential-energy function…to obtain information on the high-lying v, J levels" [93]. If "a reliable…function" be supposed to imply accurately predictable wave numbers of transitions involving such states, how reliable such information might be is questionable at best because the value of $\mathcal{D}_e$ is specified [93] as "2.29×10^4 cm^{-1}", without acknowledging that it is an upper limit, with precision implied to be 8100 m^{-1} at best; as the best precision of measured wave numbers of GaH is ~ 0.02 m^{-1} [93], the ratio of these values is ~ 400000. In any case there exists an atomic isotopic effect such that the energy of separate Ga and H atoms differs from that of separate Ga and D atoms, reflected in distinct values of $\mathcal{D}_e$, by ~ 300 m^{-1}, likewise much greater than the precision of measured infrared spectral lines. The known vibrational states occupy only the lowest third of that range of potential energy below the maximum value of the supposed dissociation limit; the error implied by an uncertainty in $\mathcal{D}_e$ would be comparable with the vibrational spacing of GaD at a moderate value of quantum number v, much less than a value $v_D \sim 40$ expected just below the dissociation limit. That function for potential energy of modified Morse form [93] might appear superficially to possess a qualitatively appropriate shape, although it is obviously not correct because limiting behaviour at large R must conform to an inverse power of R rather than an exponential approach to an asymptotic limit; as a possibility of a maximum in that function or other effect of significant interaction with electronically excited states can not be excluded, the selected form is entirely speculative. Any justification of a radial function for potential energy of that chosen form is clearly spurious. The polynomial of ninth degree for extra-mechanical effects diverges rapidly on either side of the defined range, further contributing to massive deterioration of accuracy of predictions of wave numbers of transitions even modestly beyond the range of vibrational states included in that analysis [93], even if the function for potential energy might be reliable beyond that range. From a statistical point of view, in lack of an exact theoretical model – which exists for neither potential energy nor auxiliary radial functions, an objective of predicting accurately the wave numbers of transitions involving vibration-rotational states with large values of quantum numbers v and J is unattainable, because gross extrapolation, based on increasingly inaccurate data as v increases to 4 for GaH or 7 for GaD, would be required, even with an exactly defined asymptotic limiting value of V(R) at large R. Although the nature of reduced displacement variable z allows limiting conditions [103] to be applied to V(z) at both $R = 0$ for the united atom and $R \to \infty$ for the separate atoms, unlike Dunham's function V(x), these conditions have never been applied systematically because consideration of the underlying physical implications signifies that such application would not be sensible.

Parameter R_e is no physical observable, merely a fitting parameter like any other, even though it represents a special point on a curve of V(R) that is likewise no physical observable. Jones and coworkers reported no value of R_e; their value (611.6337 ± 0.0045) m^{-1} u [92] of "$U_{0,1}$" (actually $B_{0,1}$) implies $R_e/10^{-10}$ m $= 1.6601699 \pm 0.0000061$, which differs inappreciably from a corresponding value in table 1. Because we take into account practically all factors that influence the value of R_e, the latter value is highly accurate, within its stated uncertainty, not merely precise and prone to systematic error. That tabulated value of R_e is larger

than that reported by Bernath and coworkers [93] by ~ 47 of their standard errors, which take no account of uncertainty of fundamental physical constants; the reason for their value being smaller is clearly the failure to include in their fit any parameter related to the rotational g factor, which consequently causes that systematic deviation. The results present in table 1 differ little from those published [89] after appearance of data from emission spectra [93], but for these data of GaH even the latter results [89] demonstrate unequivocally the superiority of the application of a method of reduction of diatomic molecular spectra of GaH based systematically on Dunham's algebraic approach over an approach based on purely numerical procedures [93]: more numerous data are reproduced accurately with fewer parameters, and at least one such parameter t_0^H embodies physical significance beyond an arbitrarily selected approximate model because it predicts accurately the result [98] of a prospective experiment based on the Zeeman effect [56].

The quality and consistency of 1094 data for GaH in a set of which reduction with computer programme Radiatom yields parameters present in table 1 invite a more general numerical test of Dunham's theory. A question might arise about an ability to represent rotational effects based on vibrational information. For instance, coefficient a_6 in V(x), formula 16, or c_6 in V(z), formula 52, occurs first in Dunham coefficients $Y_{4,0}$ for pure vibrational effects and $Y_{0,8}$ for pure rotational effects, apart from $Y_{3,2}$, $Y_{2,4}$ and $Y_{1,6}$ for vibration-rotational effects. As parameters c_j, $1 \le j \le 6$, in table 1 are well defined statistically, one clearly expects both $Y_{4,0}$ and $Y_{0,8}$ to be correspondingly well defined, despite the disparity in their magnitudes: for ^{69}Ga^{1}H, $Y_{4,0} = -0.6111704$ m^{-1} and $Y_{0,8} = -8.447813 \times 10^{-28}$ m^{-1}. Even when the latter quantity be multiplied by $[J(J+1)]^8$ for $J = 29$ – the largest value in measured spectra [91,93], the product is only -2.8×10^{-4} m^{-1}, much smaller than the precision, ≥ 0.06 m^{-1}, of measurement of wave numbers of transitions. A fit of spectral data to fitting coefficients A_{kl} is thus unlikely to yield directly a significant value of $A_{0,8}$, but a value of $Y_{0,8}$ derived consistently, even though indirectly from the same spectral data through other parameters such as a_j or c_j, is attained with great significance. We tested the sensitivity of rotational contributions to vibrational data by greatly diminishing the weight of the wave number of each transition in the data set with $J > 5$; although such transitions remain within the data set so that calculated and measured wave numbers become directly compared in the output from a fit, that fit becomes entirely insensitive to corresponding measured wave numbers of these transitions. With parameters in the same set as in table 1, the results of this fit demonstrate only a slightly degraded quality of fit, reflecting the effectively decreased number of fitted data, and calculated wave numbers of transitions with altered weights differ almost negligibly from those in other fits with standard weights. Hence Dunham's approach that involves taking into account rotational effects through expansion of $B_e/(1+x)^2$ in the effective potential energy [5] is entirely justified. Provided that additional terms in an effective hamiltonian for non-mechanical effects – those in formula 29, except V$''(R)$, beyond those in formula 14 – are properly taken into account, Dunham's theory provides a sufficient and complete description of regular molecular spectra – those free of

heterogeneous perturbations, as is typically the case for diatomic molecular species within their electronic ground states.

7. DIHYDROGEN, H_2

A diatomic molecule for which atomic numbers of both atomic centres are the same – $Z_a = Z_b$ – but for which masses M_a and M_b of separate atoms A and B might differ poses advantages for testing theories. For instance instead of parameters for extra-mechanical effects in two sets when $Z_a \neq Z_b$ – one for each of two atomic types, there is only one set, and a molecular reduced mass is applicable instead of individual atomic masses of separate atoms; compare formulae 33, 34 and 35 with their counterparts 37, 38 and 31, for instance. Precisely measured spectra of such elemental molecular species are rare: of chemically stable and gaseous diatomic species near 300 K, only H_2, N_2, O_2 and three dihalogen species are readily available; many other diatomic elemental species formed at elevated temperatures above solid elements have electronic ground states for which spin and orbital angular momentum complicate the spectra. Of those six, F_2, which is highly reactive in any case, lacks any practical isotopic variants, and O_2 has an electronic ground state X $^3\Sigma_g^-$ with accompanying complications from net electronic angular momentum and its coupling with rotational angular momentum; some application of Dunham theory has nevertheless been made to O_2 [104]. Although for N_2 there are fairly precise measurements of coherent Raman spectra [105], the extra-mechanical effects are small and poorly defined. For all six specified gaseous homonuclear species plus I_2, electronic spectra have been measured with attendant vibrational and rotational structures, but the precision of those measurements is generally much smaller than for typical contemporary vibration-rotational spectra of heteronuclear molecules in infrared absorption or emission, and a direct involvement of excited electronic states within a particular spectral analysis introduces correlations between parameters for these combining states. The problem arises from the fact that infrared spectra of homonuclear diatomic molecules in the gaseous phase corresponding to vibration-rotational transitions in absorption or emission are extremely weak, relying on magnetic dipolar or electric quadrupolar transition moments for their observed intensity; an alternative technique, Raman scattering, applied to transitions other than pure rotational and fundamental vibration-rotational bands yields only exceedingly weak signals.

Hydrogen is the most abundant chemical element in the universe, and in its various atomic and molecular forms furnishes a sensitive test of all of experimental, theoretical and computational methods. Vibration-rotational spectra of dihydrogen in six isotopic variants constituting all binary combinations of H, D and T have nevertheless been recorded in Raman scattering, in either spontaneous or coherent processes, and spectra of HD have been recorded in absorption. Despite the widely variable precision of these measurements, the quality of some data for small values of vibrational quantum number is still superior to that of data from electronic spectra [106], almost necessarily measured in the ultraviolet region with its concomitant large widths of spectral lines. After collecting 420

measurements of wave numbers of lines reported in 32 papers originating in 16 laboratories, we analysed [107,108] these spectral data with Radiatom and Radiatom II; we rejected 30 data that are severely discordant with remaining data, reflecting poor calibration or blunder of measurement. To avoid arbitrary exclusion of some data in favour of other, we retained among accepted data duplicate measurements of some transitions from separate laboratories, but all data were carefully weighted to reflect their varied precision. In view of data of such questionable quality, one can clearly not contemplate attempting to evaluate directly molecular parameters related to extra-mechanical effects without additional information. As a dihydrogen molecule contains only two electrons, calculations of molecular electronic structure and properties based on that structure are eminently practicable. Kolos and Wolniewicz calculated adiabatic corrections [110,111], and according to methods [56] developed for other diatomic and triatomic molecular species such as those already cited [96,97,98] we made new calculations of the rotational and vibrational g factors as a function of internuclear distance over a large range.

Fitting calculated results of $g_r(R)$ to a polynomial in z, we imposed coefficients t_j thereof as constraints in a separate fit of 390 accepted spectral data to evaluate R_e and coefficients c_j, s_j and u_j. Those values of coefficients t_j appear within brackets in a column headed 'fit T' in table 2 with standard errors of that fit to a polynomial; standard errors of other parameters in that column reflect results of the fit with Radiatom. On a basis of this fit we were able to predict a value $g_v(R_e) = 0.3136 \pm 0.0046$ of the vibrational g factor for $^1H_2$. Although this value differs from a value $g_v(R_e) = 0.2325$ from subsequent calculations [107], the experimental estimate is still much smaller than a similarly calculated rotational g factor, $g_r(R_e) = 0.8908$ [56], that agrees almost exactly with direct experimental measurement [112]. To confirm the stability of our approach to fitting spectra, we undertook a separate fit, in this case employing adiabatic corrections as constraints, to evaluate R_e and radial coefficients c_j, s_j and t_j. In the results in table 2, column 'fit U', the values of u_j fitted in a polynomial in z to computational data for adiabatic corrections [110,111] appear within brackets, with other radial coefficients and their standard errors from a fit of the same 390 spectral data. We consequently derive another estimate of the vibrational g factor, $g_v(R_e) = 0.2800 \pm 0.0086$ for $^1H_2$, which is smaller than the other value deduced from spectra but still larger than the calculated value. Fitted values of t_0 and t_1 in column 'fit U' are near the corresponding calculated values in column 'fit T'; conversely, fitted values of u_1 and u_2 in column 'fit U' are near the corresponding calculated values in column 'fit T'. Further fitted parameters s_j, t_j and u_j for extra-mechanical effects reflect the rough data, indicated by the reduced standard deviation of either fit being $\hat{\sigma} = 1.46$, significantly greater than unity; inconsistencies among 390 retained data from diverse sources, apart from gross discordance that required 30 other data to be rejected, are responsible for this condition, and emphasize the need for a thorough experimental remeasurement of spectra for pure rotational and vibration-rotational transitions of H_2 in its several isotopic variants, preferably extending the range of vibrational and rotational states sampled in transitions. Other parameters pertaining to potential energy $V(z)$ have comparable values between the two fits, as they are less sensitive to

Table 2. Coefficients of radial functions and other molecular parameters of H_2 X $^1\Sigma_g^+$ or $^1\Sigma^+$

	Fit T	Fit U
c_0/m^{-1}	7970836.8 ± 79	7970784.5 ± 77
c_1	-0.604167 ± 0.000118	-0.603753 ± 0.000135
c_2	0.21030 ± 0.00024	0.20973 ± 0.00033
c_3	-0.14441 ± 0.00187	-0.14889 ± 0.00186
c_4	0.01276 ± 0.0025	0.02164 ± 0.0026
c_5	-0.1404 ± 0.0085	-0.1308 ± 0.0086
c_6	0.1973 ± 0.0102	0.1737 ± 0.0100
c_7	-0.0524 ± 0.0106	-0.0614 ± 0.0109
c_8	-0.0737 ± 0.0178	-0.0459 ± 0.0173
c_9	0.0880 ± 0.0092	0.0694 ± 0.0082
c_{10}	-0.1074 ± 0.0172	-0.1055 ± 0.0169
s_0	0.1569 ± 0.0023	0.1301 ± 0.0043
s_1	$[0]$	-0.528 ± 0.026
s_2	$[0]$	$[0]$
s_3	6.69 ± 0.69	9.59 ± 0.83
t_0	$[0.44562 \pm 0.00044]$	0.4523 ± 0.0030
t_1	$[-0.09858 \pm 0.0025]$	-0.0836 ± 0.0174
t_2	$[-0.09558 \pm 0.0066]$	-0.603 ± 0.108
t_3	$[-0.09219 \pm 0.021]$	$\ldots$
t_4	$[-0.1354 \pm 0.0140]$	$\ldots$
t_5	$[-0.0468 \pm 0.043]$	$\ldots$
t_6	$[0.4275 \pm 0.027]$	$\ldots$
$u_0/10^6\ m^{-1}$	$\ldots$	$[10.52472 \pm 0.00072]$
$u_1/10^6\ m^{-1}$	-4.025 ± 0.024	$[-4.0384 \pm 0.0049]$
$u_2/10^6\ m^{-1}$	2.007 ± 0.061	$[2.1451 \pm 0.0197]$
$u_3/10^6\ m^{-1}$	$[0]$	$[1.728 \pm 0.033]$
$u_4/10^6\ m^{-1}$	2.75 ± 0.23	$[1.384 \pm 0.086]$
$u_5/10^6\ m^{-1}$	$\ldots$	$[0.353 \pm 0.053]$
$u_6/10^6\ m^{-1}$	$\ldots$	$[-0.727 \pm 0.109]$
$U_{0,1}/m^{-1}\ u$	3066.7339 ± 0.0110	3066.7074 ± 0.0124
$U_{1,0}/m^{-1}\ u^{1/2}$	312694.3 ± 2.1	312691.95 ± 2.15
$R_e/10^{-10}\ m$	$0.74141301 \pm 0.00000133$	$0.74141620 \pm 0.00000150$
$k_e/N\ m^{-1}$	576.0898 ± 0.0078	576.0810 ± 0.0079

irregularities in the data. From table 2, the mean value of equilibrium internuclear distance, $R_e/10^{-10}$ m$=0.7414146 \pm 0.0000020$, from experiment agrees satisfactorily with, but is likely more accurate than, the calculated value 0.74143×10^{-10} m [110] (with a current value of Bohr radius [94]), if these quantities be accorded their conventional meanings. Our experimental value formally takes into account all extra-mechanical terms in formula 29, except those in $V''(z)$, that might affect the value of R_e at a level of order 10^{-16} m, which is comparable with experimental error 2×10^{-16} m of this quantity propagated from measurements of wave numbers of transitions; in contrast the effect of the rotational g factor on the value of R_e occurs at a level of order 5×10^{-14} m.

Each radial function – $V(z)$, $g_v(z)$, $g_r(z)$ and $V'(z)$ – of which coefficients of z are evaluated from spectral data has a maximum range of validity, depending on the quality and quantity of spectral data for isotopic variants, and expressible in terms of a range of quantum numbers of vibration-rotational states, or spectral term E_{vJ}, or range of internuclear distance. For $V'(z)$ and $g_r(z)$ the latter range of $R/10^{-10}$ m is [0.53, 1.05], corresponding to classical turning points of $V(R)$ for $v \sim 2$ for $^1H_2$; although spectral data for isotopic species are available for greater energies, their quality precludes reliability over a greater range. Because acceptable data for H_2 are available up to $v = 5$ and for HD to $v = 6$, or $E \sim 2.1 \times 10^6$ m^{-1} in either case, for $V(z)$ the corresponding range of $R/10^{-10}$ m is larger, [0.47, 2.05]. For $g_v(z)$, because of the disparity of results between fits T and U, from experiment a mean value $g_v \sim 0.3$ would be applicable near R_e; further coefficients s_1 and s_3 from either fit lack other than nominal numerical significance for reasons mentioned above. Plots of curves of any radial function derived from experiment are impracticable without an assumption that further, and unevaluated, radial coefficients have explicit numerical values, zero or otherwise, which is unwarranted according to application of Dunham's formalism to spectral analysis. From computations of molecular electronic structure, values of g_r and g_v as a function of internuclear distance over a broad range, and discussion of their features, are presented elsewhere [107].

There exists no significant comprehensive fit of spectral data of H_2 with which we might here make comparison. Our discussion above demonstrates that, as for GaH above, application of an algorithm based on Dunham's algebraic approach to analysis of vibration-rotational spectral data of H_2, especially through implementation of hypervirial perturbation theory [30,72] that allows the term for the vibrational g factor in the hamiltonian in formula 29 to be treated directly in that form, proves extremely powerful to derive values of fitting parameters that not only have intrinsic value in reproducing experimental data of wave numbers of transitions but also relate to other theoretical and experimental quantities.

8. LITHIUM HYDRIDE, LIH

The only other diatomic molecular species for which calculations of the radial dependence of adiabatic corrections, rotational and vibrational g factors are available is LiH. Although at 300 K this compound is a crystalline solid substance with a structure of KCl type, at temperatures above its standard melting point 951 K the vapour contains polar diatomic molecules of stoichiometry according to its formula, as well as dimers and molecular clusters in variable proportions; spectral measurements on this vapour in absorption or emission have hence yielded data on not only wave numbers of pure rotational and vibration-rotational transitions, among others, of these diatomic molecules but also information on their electric and magnetic properties through applications of Zeeman and Stark effects respectively in appropriate experiments. Like H_2, lithium hydride is amenable to practice of calculations of molecular electronic structure for internuclear distance over a broad range because a molecule contains only two light atomic nuclei and four electrons; relativistic effects, which accurate calculations

must take into account but which do not directly enter analysis of experimental data, on differences of molecular energies are therefore negligible, like radiative effects [113], at a level pertinent to typical spectra at moderately great resolution, although they both become important for calculations on LiH at a level of spectral resolution at which effects of $V''(z)$ must be considered. Ignoring effects of nuclear volume or field shifts, we require seven radial functions, with their corresponding parameters, for direct fitting of spectra of LiH – potential energy, and contributions to adiabatic corrections, rotational and vibrational g factors for atomic centres of each type, according to formulae 52, 47, 45 and 46 respectively. We expect contributions to total $Y_{kl} + Z_{kl}$ from each of the latter three effects to have comparable magnitudes, but smaller than a dominant contribution from potential energy by a factor a ratio of electronic and protonic rest masses, m_e/m_p, or less.

This species LiH was the first for which, by way of interactive computational spectrometry, we combined experimental data and results of calculations of molecular electronic structure to make a global fit [114] of wave numbers of transitions from available infrared and microwave spectra. The basis of that procedure was that, in principle, measurements of the rotational g factor for vibration-rotational states with v and J over a large range would allow one to calculate the radial function $g_r(R)$; as measurements of g_r of $^7Li^1H$ and $^7Li^2H$ are available for only $v = 0$ and $J = 1$ [115], with the rotational dependence of g_r roughly estimated [116], we simulated prospective results from further such experiments through those computations. Repeating this strategy with improved calculations [107,109], we fitted available spectra to obtain results presented in table 3; as for H_2 in table 2 and fit T, 17 values of $t_j^{Li,H}$, reported within brackets with their standard errors, result from fitting computed results for $g_r(R)$ and $p(R)$ to a polynomial in z for each value of internuclear distance, based on use of formulae 59 and 60 with R instead of R_e. Although 14 values of $t_j^{Li,H}$, $0 \leq j \leq 6$, are imposed as constraints in fitting experimental data, likely only eight of these have any impact on the fit, in the sense that parameters beyond those eight – t_j^{Li}, $0 \leq j \leq 2$, and t_j^H, $0 \leq j \leq 4$ – define the rotational g factor in ranges of R to which available spectral data are insensitive. Values of another 20 independently adjusted parameters – $U_{1,0}$, $U_{0,1}$, c_j with $1 \leq j \leq 9$, $s_0^{Li,H}$, s_1^H, $u_1^{Li,H}$, $u_2^{Li,H}$, u_3^H and u_4^H – obtained from fitting wave numbers of 1000 data selected from various sources [117–121] are presented in table 3; as before, values of c_0, R_e and k_e are derived from values of $U_{1,0}$ and $U_{0,1}$, but values of $u_0^{Li,H}$ are evaluated from published data for adiabatic corrections [122].

According to application of Dunham's formalism to analysis of molecular spectra, as for GaH and H_2, these radial coefficients of seven types represent many Dunham coefficients Y_{kl} and their auxiliary coefficients Z_{kl} of various types that collectively allow wave numbers of observed transitions to be reproduced almost within their uncertainty of measurement through formula 54. Mostly because of inconsistency between reported values of frequencies of pure rotational transitions [118,119], the reduced standard deviation of the fit reported in table 3 is 1.25, slightly greater than unity that would be applicable with consistent data for which uncertainty of each measurement were carefully assigned.

In the present context of generation of consistent term coefficients Y_{kl} and Z_{kl} through coefficients in selected radial functions, the major points of interest in

Table 3. Coefficients of radial functions and other molecular parameters of LiH X $^1\Sigma^+$

c_0/m^{-1}	6572379.3 ± 5.6	s_0^{Li}	0.9126 ± 0.0181
c_1	-0.8970678 ± 0.0000057		
c_2	0.348233 ± 0.000040	s_0^{H}	-0.2612 ± 0.0029
c_3	-0.093085 ± 0.000196	s_1^{H}	-0.3733 ± 0.0195
c_4	-0.044426 ± 0.00087		
c_5	0.0765 ± 0.0027	$u_0^{\mathrm{Li}}/10^6\,\mathrm{m}^{-1}$	$[168.411 \pm 0.002]$
c_6	-0.1143 ± 0.0078	$u_1^{\mathrm{Li}}/10^6\,\mathrm{m}^{-1}$	-5.53900 ± 0.0082
c_7	-0.2078 ± 0.024	$u_2^{\mathrm{Li}}/10^6\,\mathrm{m}^{-1}$	6.357 ± 0.134
c_8	0.6024 ± 0.049	$u_0^{\mathrm{H}}/10^6\,\mathrm{m}^{-1}$	$[12.829 \pm 0.002]$
c_9	-0.7538 ± 0.115	$u_1^{\mathrm{H}}/10^6\,\mathrm{m}^{-1}$	-5.15624 ± 0.00096
$U_{0,1}/\mathrm{m}^{-1}\,\mathrm{u}$	662.708918 ± 0.000082	$u_2^{\mathrm{H}}/10^6\,\mathrm{m}^{-1}$	4.923 ± 0.021
$U_{1,0}/\mathrm{m}^{-1}\,\mathrm{u}^{1/2}$	131993.551 ± 0.064	$u_3^{\mathrm{H}}/10^6\,\mathrm{m}^{-1}$	-3.340 ± 0.051
$R_{\mathrm{e}}/10^{-10}\,\mathrm{m}$	$1.59491242 \pm 0.00000020$	$u_4^{\mathrm{H}}/10^6\,\mathrm{m}^{-1}$	4.828 ± 0.158
$k_{\mathrm{e}}/\mathrm{N}\,\mathrm{m}^{-1}$	102.649202 ± 0.000100		
t_0^{Li}	$[0.749508 \pm 0.000142]$	t_0^{H}	$[-0.772779 \pm 0.000051]$
t_1^{Li}	$[0.60714 \pm 0.00115]$	t_1^{H}	$[1.28086 \pm 0.00047]$
t_2^{Li}	$[-1.2181 \pm 0.0022]$	t_2^{H}	$[-1.7927 \pm 0.00191]$
t_3^{Li}	$[1.077 \pm 0.022]$	t_3^{H}	$[2.0040 \pm 0.0088]$
t_4^{Li}	$[-1.710 \pm 0.106]$	t_4^{H}	$[-1.6797 \pm 0.0198]$
t_5^{Li}	$[3.546 \pm 0.160]$	t_5^{H}	$[2.375 \pm 0.033]$
t_6^{Li}	$[-2.586 \pm 0.34]$	t_6^{H}	$[-0.5685 \pm 0.079]$
t_7^{Li}	$[-6.825 \pm 0.65]$	t_7^{H}	$[-0.8264 \pm 0.042]$
$t_8^{\mathrm{Li}}t_8^{\mathrm{Li}}$	$[6.37 \pm 0.31]$		

these results are comparisons of experimental and calculated values of extra-mechanical effects within the same context; alternative theoretical and computational approaches to evaluation of molecular energies and properties of $^7Li^1H$ impose no such radial functions in that generation [123,124]. From values of coefficients $s_j^{Li,H}$ we derive this formula for the vibrational g factor,

$$g_v = (-0.1291 \pm 0.0039) + (-0.3733 \pm 0.0195)z \qquad (72)$$

valid within a range $R/10^{-10}$ m$=[1.17, 2.25]$ for comparison with a formula from fitted data from computations,

$$
\begin{aligned}
g_v = &(-0.136553 \pm 0.000056) + (-0.69064 \pm 0.00073)z \\
&+ (0.6381 \pm 0.0038)z^2 + (0.0435 \pm 0.027)z^3 - (0.388 \pm 0.056)z^4 \\
&- (0.155 \pm 0.29)z^5 + (1.402 \pm 0.35)z^6 - (6.285 \pm 0.93)z^7 \\
&- (17.96 \pm 1.14)z^8
\end{aligned}
\qquad (73)
$$

valid in a much larger range, $R/10^{-10}$ m$=[1.05, 3.0]$. Agreement of the constant terms is satisfactory, but the single further coefficient from experiment implies a slope only half that calculated theoretically, doubtless reflecting the truncation at a linear term. For adiabatic corrections we can compare not only the total function but also contributions of individual atomic centres. From fitted values of u_1^{Li} and u_2^{Li} in table 2 plus u_0^{Li} derived from published calculations [122], we produce the following formula to represent a radial function for adiabatic corrections associated with the lithium atomic centre independent of atomic mass,

$$V'Li(z)/(hc)/u\ m^{-1} = [92385.19] + (-3086.8 \pm 8.2)z + (3597 \pm 73)z^2 \qquad (74)$$

compared with an exact polynomial representation of calculated points [122] that yields this formula:

$$
\begin{aligned}
&V'Li(z)/(hc)/u\ m^{-1} \\
&= 92385.19 - 3169.90z + 4896.87z^2 + 1987.27z^3 - 11905.13z^4 \\
&\quad - 37933.27z^5 + 71718.27z^6 + 74959.08z^7
\end{aligned}
\qquad (75)
$$

Coefficients of z to various powers in these formulae differ from values of u_j in table 3 because the latter reflect a presence of a factor m_e in formula 47; all values of constant terms are derived from calculation [122], not from fits to frequency data. Coefficients of corresponding linear and quadratic terms in formulae 74 and 75 have comparable signs and magnitudes. From fitted values of u_j^H, $1 \leq j \leq 4$, in table 3 we derive analogously a corresponding formula to represent a radial

function for adiabatic corrections associated with the hydrogen atomic centre,

$$V'^H(z)/(hc)/u\ m^{-1}$$

$$= [7035.2] + (-2828.48 \pm 0.52)z + (2688.2 \pm 11.5)z^2$$

$$+ (-1405 \pm 59)z^3 + (1331 \pm 187)z^4 \qquad (76)$$

The corresponding exact fit to calculated points [122] is

$$V'^H(z)/(hc)/u\ m^{-1}$$

$$= 7035.2 - 3160.75z + 5584.07z^2 + 13854.46z^3 - 100067.32z^4$$

$$+ 13622.76z^5 + 502328.20z^6 - 523003.44z^7 \qquad (77)$$

The sign and magnitude of the linear term in formula 76 concur moderately satisfactorily with those properties of a corresponding term in formula 77, but agreement between other corresponding terms is lacking. We compare the total adiabatic corrections for $^6Li^1H$ from a sum of corrections of separate atomic centres in formulae 74 and 76 divided by their masses,

$$V'(z) = V'^{Li}(z)/M_{Li} + V'^H(z)/M_H \qquad (78)$$

which yields this formula,

$$V'(z)/(hc)/u\ m^{-1} = [22342.6] - 3311.8z + 3259.4z^2 - 1818.0z^3$$

$$+ 2628.0z^4 \qquad (79)$$

with a formula interpolated from points for the corresponding total calculated adiabatic corrections [122] for $^6Li^1H$,

$$V'(z)/(hc)/u\ m^{-1} = 22342.6 - 3722.1z + 6709.4z^2 + 16517z^3 - 115968z^4$$

$$+ 7699.5z^5 + 585535z^6 - 587860z^7 \qquad (80)$$

Like formulae for contributions to total adiabatic corrections from individual atomic centres above, the corresponding coefficients for the linear term have the same sign and comparable magnitude, but for subsequent coefficients agreement is lacking. The maximum region of validity of the experimental functions is the same as for the vibrational g factor, specified above, whereas the region for which the calculated points define the contributions and total adiabatic correction [122] is $R/10^{-10}\ m = [1,3]$.

For comparison with our results in table 3, which presents values of 20 adjusted parameters with 15 parameters constrained to define the rotational g factor, Dulick et alii [115] required also 20 adjusted parameters, with a constrained parameter $\mathcal{D}_e$ for the equilibrium binding energy for a function of potential energy having a modified Morse form. The latter parameter is specified as

$\mathcal{D}_e = 2028600$ m^{-1} but this value varies ~ 300 m^{-1} among various isotopic molecular species composed of ^{6}Li, ^{7}Li, ^{1}H and ^{2}H because each has a distinct value of $\mathcal{D}_e$ within that range. Although in this case the experimental curve of potential energy [115] conforms superficially to points from computations of molecular electronic structure [125] on the scale of that plot, with no discernible maximum or other anomaly, extrapolation to predict vibration-rotational transitions much beyond the range of $v=6$ for ^{7}Li^{1}H, or $\sim 8.2 \times 10^5$ m^{-1}, must be subject to progressive propagation of error from measured transitions, apart from the variability of $\mathcal{D}_e$ that affects such a prediction increasingly on approach to the dissociation limit. The measured transitions define the lower two fifths of the range of energy to the dissociation limit. As for GaH [93], representations of empirical functions for LiH [115] to take into account extra-mechanical effects have the form of truncated polynomials in displacement, $R-R_e$; their claimed maximum range of validity is $R/10^{-10}$ m$=[1.16, 2.48]$. Beyond that range such polynomials, of degree sixth and cubic, tend to diverge rapidly, much more rapidly than a polynomial in z, as published plots clearly demonstrate [115]. This behaviour confirms the superiority of properties of variable z; for instance an increment from $R/10^{-10}$ m from 3 to 4 is four times as large as the corresponding increment in z for LiH from 0.61 to 0.86. The accuracy of prediction of wave numbers of transitions involving states with terms greater than $\sim 8.5 \times 10^5$ m^{-1} becomes thereby progressively and severely diminished. A ratio of error due to uncertainty in $\mathcal{D}_e$ to the best claimed accuracy of actual measurements for LiH, 0.05 m^{-1} [115], is ~ 6000, but the absolute and relative accuracy of predictions for even moderate v due to invalidity of radial functions for extra-mechanical effects expressed as polynomials in displacement is much worse. Despite the apparent quality of the function for potential energy of modified Morse type [115], which still possesses an incorrect limiting dependence on R toward the dissociation limit, the quality of predictions beyond the range of measured transitions is hence highly doubtful. Apparent agreement between this modified Morse curve and computationally derived points [125], themselves subject to error, must be regarded as fortuitous: over much of the illustrated range before an avoided crossing at $R_x = 3.857 \times 10^{-10}$ m with a curve for potential energy of state A $^1\Sigma^+$ [126], there is a strong contribution to molecular binding from coulombic attraction between essentially atomic ions, for which the potential energy varies according to R^{-1} and for which an exponential representation is consequently poor. For $R_e < R < R_x$, the curve for potential energy thus has such an inverse dependence on internuclear distance heading toward an asymptote corresponding to a limit of dissociation into ions Li$^+$ and H$^-$, whereas after that point the adiabatic curve of potential energy for the electronic ground state proceeds toward an asymptotic limit of dissociation at smaller energy into neutral atoms Li and H [127]. A postulated advantage of accurate prediction of wave numbers of transitions far above the measured range through representing potential energy in a modified Morse form is plainly illusory.

For vibration-rotational data of LiH in a smaller set, an approach of optimal fitting parameters for extra-mechanical effects has also been applied [85]; as for other fits described above, 20 selected parameters were adjusted to reproduce satisfactorily the data, numbering 583 rather than 1000 for which results appear

in table 3. As these data sets differ markedly, comparison of parameters is impracticable.

9. CARBON OXIDE, CO

Here we consider mainly intensities of vibration-rotational spectra in absorption; as a function for potential energy is a prerequisite for calculations involving intensities, we necessarily include this aspect. In contrast with measurements of wave numbers of reasonably spectral lines in an infrared spectrum of a diatomic molecule, for which relative precision $\sim 10^{-6}$ is routinely achievable, for measurement of a strength of a particular spectral line to attain a relative precision superior to one per cent is exceptional; through the smoothing effect of multiple data contributing to this quantity, the corresponding strength of a band might thus attain a relative precision 0.1 per cent at best. The relative precision of a strength of a line in a Raman spectrum is generally worse. Expectation values of quantities from Stark and Zeeman effects might be measured with precision of order 0.1 per cent at best; in such cases few measurements are practicable, hence precluding significant improvement in derived quantities through a smoothing effect. There thus exists almost no need of refined treatment of intensities in the manner of van Vleck's extension of Dunham's theory for data of frequency type. Dunham's approach in his first two publications indeed survives in an almost similar form for analysis of intensities of infrared spectral lines of the best contemporary quality.

Dunham's consideration of available spectra of HCl in 1930 [1,2] resulted in production of a radial function for electric dipolar moment that we express in a contemporary form, similar to that in formula 56 but in terms of variable x, defined in formula 15, instead of z, defined in formula 21:

$$\text{p}(x)/10^{-30}\ \text{C m} = p_0 + 3.54x + \{0.177\ \text{or}\ 7.61\}x^2 \tag{81}$$

At that time the permanent electric dipolar moment p_0 of HCl had already been estimated to be $\sim 3.59 \times 10^{-30}$ C m [128], but Dunham made no use of this value; hence we leave p_0 in symbolic form. One or other value of coefficient p_2 depends on a ratio $\langle 1/\text{p}(x)|0\rangle/\langle 2|\text{p}(x)|0\rangle$ of pure vibrational matrix elements of electric dipolar moment between the vibrational ground state and vibrationally excited state $v = 1$ or 2. We compare these data with an extended radial function derived from 33 expectation values and matrix elements in a comprehensive statistical treatment [129],

$$\begin{aligned}
\text{p}(x)/10^{-30}\ \text{C m} = {} & (3.64587 \pm 0.00025) + (4.12334 \pm 0.00147)x \\
& + (0.00688 \pm 0.0177)x^2 + (-5.110 \pm 0.044)x^3 \\
& + (-3.065 \pm 0.088)x^4 + (-1.174 \pm 0.142)x^5 \\
& + (-1.46 \pm 0.24)x^6 + (1.17 \pm 0.69)x^7
\end{aligned} \tag{82}$$

Apart from the greatly increased precision of coefficients reflecting improved spectral resolution over 70 years between generation of these functions, one

discerns that early values of p_0 and p_1 are roughly correct and that one possible value that Dunham [2] proposed for p_2 has a magnitude comparable with the current value.

The quandary that Dunham confronted in proposing an alternative value of p_2 was solved through the work of Herman and Wallis [130] in the spirit of Dunham's symbolic approach. A major problem affecting the derivation of radial functions from data of intensity type is that the strength of a spectral line or band is proportional to a square of a matrix element, making its sign directly indeterminate. Explicitly, for a gaseous sample of a diatomic molecular species in electronic state X $^1\Sigma^+$ in absorption at temperature T, the strength S_l of a line due to a spectral transition from a state $|0, J''\rangle$ to another state $|v', J'\rangle$ in a vibration-rotational spectrum is expressed according to this formula [13],

$$S_l = (8\pi^3/3hc)[\exp(-hcE_{0J}/k_BT)/4\pi\varepsilon_0 Q]\tilde{\nu}_l[1 - \exp(-hc\tilde{\nu}_1/k_BT)]$$
$$\times |\iota|\langle v'J'|\mathrm{p}(x)|0, J''\rangle|^2 \tag{83}$$

in which appear fundamental physical constants h, c, k_B and ε_0, total partition function Q, value of spectral term $E_{0,J}$ of an initial state $|0, J'\rangle$ of a transition relative to the minimum term $E_{0,0}$, and wave number $\tilde{\nu}_l$ of a spectral line representing that transition; $\iota \equiv \frac{1}{2}[J'(J'+1) - J''(J''+1)]$ is a running number of value $J''+1$ for a line in branch R or $-J''$ for a line in branch P. In $|\langle v'J'|\mathrm{p}(x)|0, J''\rangle|^2$ that is the square of an experimental matrix element for a transition between specified vibration-rotational states, $\mathrm{p}(x)$ is a radial function for electric dipolar moment of an absorbing molecular species in terms of reduced displacement x, as in formula 82 and equivalent to formula 56 for $\mathrm{p}(z)$. The rotational dependence is supposed factorable according to a formula [130,13]

$$|\langle v'J'|\mathrm{p}(x)|0, J''\rangle|^2 = |\langle v'|\mathrm{p}(x)|0\rangle|^2(1 + C_0^{v'}\iota + D_0^{v'}\iota^2 + \ldots) \tag{84}$$

in which $|\langle v'|\mathrm{p}(x)|0\rangle|^2$ is the square of the pure vibrational matrix element of electric dipolar moment; the latter quantity is coefficient to a Herman-Wallis factor containing, in a representation as a truncated polynomial up to a quadratic term, Herman-Wallis coefficients $C_0^{v'}$ and $D_0^{v'}$. In the latter quantities that are composite functions [13] containing parameters for potential energy in V(x) or V(z) and for dipolar moment $\mathrm{p}(x)$ or $\mathrm{p}(z)$ in the numerator and with matrix element $\langle v'|\mathrm{p}(x)|0\rangle$ in the denominator, Herman and Wallis demonstrated that vibration-rotational interaction causes strengths of lines to vary linearly with coefficients p_j. Fitting squared vibration-rotational matrix elements $|\langle v'J'|\mathrm{p}(x)|0, J''\rangle|^2$ as a function of ι, according to formula 84, hence yields essentially the squared vibrational matrix element $|\langle v'|\mathrm{p}(x)|0\rangle|^2$ as a constant term and parameters $C_0^{v'}$ and $D_0^{v'}$ as coefficients of ι and ι^2; comparison of calculated values of the latter quantities as functions of coefficients p_j and $\langle v'|\mathrm{p}(x)|0\rangle$ – a signed quantity – with the corresponding experimental values then yields the latter quantities according to the best match [13], as we illustrate below.

To complete the set of formulae required in analysis of intensities of spectral lines in absorption, an experimental measure of a band strength S_b is a sum of

measured strengths S_l of all lines in that band,

$$S_b = \sum S_l \tag{85}$$

whereas a theoretical measure relates to the pure vibrational matrix element of electric dipolar moment,

$$S_b = 8\pi^3 \tilde{v}_o |\langle v'|p(x)|0\rangle|^2 /(3hc4\pi\varepsilon_0) \tag{86}$$

in which $\tilde{v}_o$ is the wave number characterising the origin of the band. A line strength is derived from integrated absorbance of a particular spectral line, a known number density N of molecules per unit volume in a gaseous sample at temperature T and the effective length ℓ of optical path:

$$S_l = (1/N\ell) \int \ln[I_0(\tilde{v})/I(\tilde{v})]d\tilde{v} \tag{87}$$

On the basis of these formulae one can convert measurements of area, which equals the integral in the latter formula, under spectral lines into values of coefficients in a selected radial function for electric dipolar moment for a polar diatomic molecular species. Just such an exercise resulted in the formula for that radial function [129] of HCl in formula 82, combining in this case other data for expectation values $\langle 0,J|p(x)|0,J\rangle$ from measurements of the Stark effect as mentioned above. For applications involving these vibration-rotational matrix elements in emission spectra, the Einstein coefficients for spontaneous emission conform to this relation,

$$A_{nm} = 16\pi^3 \tilde{v}^3 |\langle n|p(x)|m\rangle|^2 |\iota|/[3h\varepsilon_0(2J'+1)] \tag{88}$$

in which n and m denote collectively the vibrational and rotational quantum numbers in sets specifying states combining in a transition from n to m.

A radial function for electric dipolar moment for a hydrogen halide appears to have a single extremum, near the equilibrium internuclear distance R_e, such that, for $^1H^{35}Cl$ for instance in formula 82, $p(x)=0$ for both the united atom ^{36}Ar at $R=0$ or $x=-1$ and the separate atoms ^1H and ^{35}Cl as R or $x\to\infty$, but not elsewhere. The behaviour of this function on approaching these limits is known [13]: as $R\to 0$ for all neutral diatomic molecules, $p(R)\propto R^3$, whereas as $R\to\infty$, $p(R)\propto R^{-7}$ if states of both separate atoms have total electronic angular momentum $<\hbar$ or $p(R)\propto R^{-4}$ otherwise; for instance the former condition is applicable to LiH, whereas the latter condition is applicable to hydrogen halides, CO, NO and many other species. For HF, HCl and HBr, the extremum in $p(x)$ occurs at $R>R_e$ [13]; accordingly p_1 or the slope of $p(x)$ at R_e is positive. In contrast, for HI the extremum in $p(x)$ occurs at $R<R_e$, with a small negative slope near R_e, confirmed by both precise calculations of molecular electronic structure and experimental data [131]; as in the calculations relativistic effects were included to obtain that result, one might consider the qualitatively different slope to be a relativistic effect.

Some data for spectral intensities of HCl for $v>3$ have questionable quality, whereas recent measurements of intensities of CO are generally superior; for this

reason we consider the latter molecule in some detail. Carbon oxide CO plays an important role in combustion of carbonaceous fuels and terrestrial processes in the atmosphere, and has been detected through its spectral lines for pure rotational transitions in many extra-terrestrial environments. Accordingly, a knowledge of radiative properties of CO is extremely important in relation to both investigation of dynamics of combustion processes and modeling of radiative properties of the terrestrial atmosphere. Like a commercially and technologically important laser based on carbon dioxide CO_2, a laser with working substance CO oscillates on vibration-rotational transitions. Most known vibration-rotational transitions [132] of diatomic molecules that exhibit stimulated emission occur in the fundamental band, $v' = 1 \rightarrow v'' = 0$, or in sequences with $\Delta v = 1$. Most transitions for which laser action is reported involve lines in P branches because these lines are favoured both by non-equilibrium conditions of extensive vibrational excitation but by small rotational excitation and a less stringent condition on rotational degeneracies: g_n as $2J' + 1$ can be $2J - 1$ for a P branch rather than $2J + 3$ for an R branch; laser emission in a P branch serves simultaneously to decrease vibrational excitation and to increase rotational energy, facilitating an approach to thermal equilibrium [13]. For $^{12}C^{16}O$ about 700 transitions have been measured in bands $1 \rightarrow 0$ up to $37 \rightarrow 36$, covering discontinuously a range $1.2 \le \tilde{\nu}/10^5 \text{ m}^{-1} \le 2.0$, and even some laser lines with $\Delta v = 2$ have been observed [133]; more than 100 laser transitions of CO in other isotopic species are also reported [132]. A device that provided those sequences with $\Delta v = 1$ in laser action also produced emission of CO in seven isotopic variants with sequences $\Delta v = 1$, $\Delta v = 2$ and $\Delta v = 3$ up to $v' = 41$ [134]; although parameters calculated from several thousand transitions were described [134] as Dunham coefficients, implying Y_{kl} according to formula 8, because constraints between these parameters were not applied, they actually correspond to coefficients A_{kl} in formula 2.

The fundamental vibration-rotational band of CO in the mid infrared region was the first spectral feature of a gaseous sample of a diatomic molecular substance to be measured in this region [135]; subsequent measurements exploited progressively increasing spectral resolution and accuracy of the wave number scale. Overtone spectra of CO exhibit progressively decreasing strengths of bands [99], such that, whereas the first overtone at a conventional boundary of the mid infrared region is readily measurable, the second overtone in the near infrared requires an extended optical path; the third overtone approaches the limits of detectability with an optical path 100 m and a gaseous sample at approximately atmospheric pressure, and with conventional methods for absorption spectra. Attempting to detect the fourth overtone with product of length of absorbing path and pressure equal to 3000 m bar, Herzberg and Rao [136] searched unsuccessfully, like our subsequent attempt [99]: 1 bar = 10^5 N m^{-2}. Eventual success [137] in detecting band $v' = 5 - v'' = 0$ was attained through adapting a *cavity-ringdown* spectral technique [138] to the near infrared region; intensities of only lines in branch P of this band were measurable, but estimates of the strength of each line in a series $P_3–P_{18}$ from fitting its profile to a lorentzian shape enabled deduction of a pure vibrational matrix element $\langle 5|p(x)|0 \rangle$ consistent with Herman-Wallis coefficient C_0^5 and a strength of the entire

Table 4. Band origin, pure vibrational matrix element and strength of vibration-rotational bands of $^{12}C^{16}O$

Band	$\tilde{\nu}_0/m^{-1}$	$\langle v'|p(x)|0\rangle/C\,m$	S_b/m
0 – 0		3.6632×10^{-31}	
1 – 0	214327.11	-3.53×10^{-31}	1.00×10^{-19}
2 – 0	426006.22	2.22×10^{-32}	7.83×10^{-22}
3 – 0	635043.91	-1.36×10^{-33}	4.42×10^{-24}
4 – 0	841446.93	6.95×10^{-35}	1.53×10^{-26}
5 – 0	1045222.22	3.62×10^{-36}	6.13×10^{-29}

vibration-rotational band. Results of such measurements for all vibration-rotational bands originating in the vibrational ground state [99,137], with a further expectation value for that ground state from experiments on a molecular beam [139], are collected in table 4.

To convert these data into radial functions, one might apply algebraic expressions for vibrational matrix elements of x to various powers, of form such as

$$\langle 1|x|0\rangle = \gamma/\sqrt{2} + \sqrt{2}\gamma^{3/2}(11a_1^2/32 - 3a_2/8) + \dots \qquad (89)$$

in which appear coefficients a_j for potential energy according to Dunham's function in formula 16 and γ as defined in relation to formula 61. We evaluated values of corresponding coefficients c_j up to c_{12} from a fit of 16947 data up to $v=41$ and $J\sim115$, including some duplication of vibration-rotational and pure rotational transitions, for CO in isotopic variants with $^{12,13,14}C$ and $^{16,17,18}O$ in various combinations to parameters in radial functions for potential energy, adiabatic corrections and vibrational g factors, constraining parameters $t_j^{C,O}$ related to the rotational g factor to values consistent with computations of molecular electronic structure [99]. Likely because procedure Radiatom lacks full contributions to some Dunham coefficients Y_{kl} that require calculation according to hypervirial perturbation theory up to order 26 (and consequently that severely tax available computational resources), slight systematic discrepancies [99] exist between calculated and measured wave numbers of transitions involving $v>39$, but remain within 3.5 times their nominal uncertainties σ; the overall reduced standard deviation of the fit to 20 adjustable and 10 constrained parameters was still acceptable. This data set would benefit from thorough reappraisal, but original data for many vibration-rotational transitions are unavailable and secondary sources contain slightly disparate values of both wave numbers and their uncertainties – hence the duplication. Nevertheless for calculations involving vibrational states up to $v=5$, the derived values of parameters c_j up to $j=8$ are sufficient and reliable, and thus serve for calculations involving matrix elements of electric dipolar moment with expressions of the type in formula 89. These expressions are readily generated to any desired extent of v or x^l [44] to sufficient precision involving terms with γ to increasing exponents; as for all known stable neutral diatomic molecular

species γ has values less than 0.026 – for instance, $\gamma = 0.0070838$ for $^{12}C^{16}O$ – convergence within a desired precision is generally rapid. A theoretical expression for a pure vibrational matrix element of electric dipolar moment $p(x)$ expressed as a polynomial in terms of these matrix elements of x^l is simply

$$\langle v'|p(x)|0\rangle = \sum_{j=0} p_j \langle v'|x^l|0\rangle \tag{90}$$

including as many terms in the sum as necessary, generally $v' + 1$ in total. On the basis of these experimental numerical values of vibrational matrix elements and algebraic expressions for $\langle v'|x^l|0\rangle$ into which numerical values of coefficients a_j and γ are inserted, one solves a system of simultaneous linear equations to evaluate coefficients p_j. As these parameters are not overdetermined, direct statistical methods are inapplicable to yield required uncertainties of evaluated parameters; in such a case a Monte-Carlo method [140] of analysis of error propagated from values of pure vibrational matrix elements to coefficients p_j is suitable. In general, signs of $\langle v'|p(x)|0\rangle$ are unknown because experiments yield their magnitudes or squares, according to formula 84 for instance. One then applies these derived values of coefficients p_j in sets depending on a chosen sign of each value of $\langle v'|p(x)|0\rangle$, relative to a particular sign chosen typically for p_0 or $\langle 0|p(x)|0\rangle$, to calculate coefficients $C_0^{v'}$ and $D_0^{v'}$ according to algebraic expressions [13,44] in terms of coefficients a_j pertaining to potential energy and γ, coefficients p_j for electric dipolar moment and values of $\langle v'|p(x)|0\rangle$ with one or other sign. Signs of $\langle v'|p(x)|0\rangle$ in a particular set that yield best agreement between thus calculated values of $C_0^{v'}$ and $D_0^{v'}$ and their experimental counterparts from formula 84 are hence preferable, thereby evaluating elegantly the radial function $p(x)$ for electric dipolar moment. Instead of coefficients a_j and p_j of x to various powers, one can naturally work with coefficients c_j and p_j (according to formula 56) of z to various powers, as the corresponding algebraic expressions for vibrational matrix elements and Herman-Wallis coefficients are just as readily generated [44] in terms of these quantities.

As an illustration of this approach to solution of a radial function $p(x)$ for $^{12}C^{16}O$, we present in table 5 experimental [99] and calculated values of Herman-Wallis coefficients $C_0^{v'}$ and $D_0^{v'}$, calculated on the basis of this radial

Table 5. Experimental and calculated values of Herman-Wallis coefficients $C_0^{v'}$ and $D_0^{v'}$ for $^{12}C^{16}O$

band $v' - 0$	$C_0^{v'}/10^{-2}$		$D_0^{v'}/10^{-4}$	
	exp'l	calc'd	exp'l	calc'd
0 – 0	—			−2.05
1 – 0	0.024 ± 0.021	0.0196	—	0.067
2 – 0	0.533 ± 0.014	0.496	0.44 ± 0.10	0.35
3 – 0	1.153 ± 0.025	1.210	1.03 ± 0.18	0.99
4 – 0	3.370 ± 0.033	3.284	4.27 ± 0.34	4.3
5 – 0	~ -10	−9.33	—	17.6

function p(x) derived from experiment [135];

$$p(x)/10^{-30} \text{ C m} = 0.407871 - 11.8634x + 1.3060x^2 + 13.378x^3$$
$$- 2.740x^4 - 0.17x^5 \tag{91}$$

this function has a range $R/10^{-10}$ m of validity [0.99, 1.33]. A value of C_0^5 was indicated only roughly from preliminary experiment [137]; experimental values of D_0^0, D_0^1 and D_0^5 are unavailable.

Changing the sign of $\langle 5|p(x)|0\rangle$ from positive to negative correspondingly alters the sign of p_5, the value calculated for C_0^5 from -0.093 to $+0.093$ and the value calculated for D_0^4 from 0.00043 to 0.00037, but affects other calculated values negligibly. As the latter calculated value is almost inconsistent with an experimental value of D_0^4 specified in table 5, the negative value of C_0^5 is clearly preferable, even though indicated only roughly in the reported experiment [137]. Chackerian and Tipping [141] predicted $\langle 5|p(x)|0\rangle = 6.588 \times 10^{-36}$ C m, $C_0^5 = -0.0529$ and $D_0^5 = 0.00040$; because the former value is only about twice the experimental value $(3.62 \pm 0.3) \times 10^{-36}$ C m, we might expect their predictions $\langle 6|p(x)|0\rangle = -3.66 \times 10^{-36}$ C m, $C_0^6 = -0.014$ and $D_0^5 = -0.00014$ for band $6 - 0$ to have comparable reliability. The ratios of strengths between successive vibration-rotational bands from experiment are thus 128, 177, 289, 250. On a basis of a predicted strength 6.25×10^{-29} m for band $6 - 0$ [141], the fifth overtone is remarkably predicted to have almost the same intensity as the fourth overtone. We contrast these ratios of strengths of vibration-rotational bands of $^{12}\text{C}^{16}\text{O}$ with those of $^{14}\text{N}^{16}\text{O} - 61.2, 48.5, 23.3, 13.4, 8.6$ [142] – which thus decrease regularly in the same order of increasing vibrational quantum number v. The radial functions for electric dipolar moment of NO and CO share common features of two extrema, with a reversal of polarity between these two extrema and small magnitudes of permanent electric moment $p(R_e)$. In each case the polarities, $^-\text{NO}^+$ and $^-\text{CO}^+$, at that condition contradict expectations from crude consideration of conventional electronegativities.

As an alternative procedure to predict coefficients of a radial function p(x) for electric dipolar moment, one might attempt to convert the latter function from polynomial form, as in formula 91, which has unreliable properties beyond its range of validity from experimental data, into a rational function [13] that conforms to properties of electric dipolar moment as a function of internuclear distance R towards limits of united and separate atoms. When such a rational function is constrained to yield the values of its derivatives the same as coefficients p_j in a polynomial representation, that rational function becomes a Padé approximant. For CO an appropriate formula that conforms to properties described above would be

$$p(x) = p_0(1 + x)^3 / \left(1 + \sum_{j=1} q_j x^j + C_\infty x^7 \right) \tag{92}$$

in which in the sum in the denominator as many terms are taken as necessary; the numerator bestows a property p(x) $\rightarrow 0$ proportional to R^3 as $R \rightarrow 0$, whereas

the last term in the denominator ensures that $p(x) \to 0$ as R becomes large, in practice greater than $\sim 10R_e$. Coefficient C_∞ might be accorded a value based on some knowledge of the behaviour of this radial function at large R, such as a value of p from calculations of molecular electronic structure; such a value has no effect on recalculated values of p_j or $\langle j|p(x)|0\rangle$ for $j < 7$. Application of this formula for CO yields a function that suffers severely from a pole within a region of interest, which makes it unusable. An alternative form that might be applicable to a radial function for electric dipolar moment that possesses two extrema in a region defined by experiment, with a reversal of polarity between distances of these extrema at x_0, is

$$p(x) = p_0(1 + x)^3(x - x_0)/\left(-x_0 + \sum_{j=1} q_j x^j + C_\infty x^8 \right) \qquad (93)$$

but this formula applied to CO also suffers from poles dictated by roots in the denominator within the region of interest. Under these conditions one might be forgiven for neglecting the behaviour of $p(x)$ as $x \to -1$ or $R \to 0$ because this region lacks chemical interest; a rational function that still qualifies as a Padé approximant and retains the correct limiting behaviour as x or $R \to \infty$, which is of chemical interest, has this form for CO that has a reversal of polarity at $x = x_0$:

$$p(x) = p_0(x + 1)(x/x_0 - 1)/\left(1 + \sum_{j=1} q_j x^j + C_\infty x^6 \right) \qquad (94)$$

Although transformation of coefficients p_j into coefficients q_j is readily practicable, the resulting values for CO adopt unwieldy magnitudes. Chackerian and Tipping [141] fitted a function of the latter form from experimental and theoretical (computations of molecular electronic structure) information in judicious combination, according to which they calculated vibration-rotational matrix elements for transitions in bands $5 - 0$ and $6 - 0$; fitting the latter values with formula 84 yielded the values of quantities presented above. Rational functions, such as those in formulae $92 - 94$ or others, transcend the spirit of Dunham's approach because their construction incorporates physical knowledge of a quantity that is superfluous for invocation of a mere truncated polynomial.

10. DISCUSSION

When Dunham [4,5] presented formula 8 for vibration-rotational terms, he derived a functional $v + \frac{1}{2}$ explicitly because in his JBKW formulation the addend $\frac{1}{2}$ results from exact solution of an integral. In contrast, Dunham assumed a functional $K(K + 1)$, equivalent to $J(J + 1)$ in contemporary notation, to contain a quantum number K, now J, for rotational angular momentum. To generate an effective potential energy comprising both internuclear potential

energy V(R) and kinetic energy $\hbar^2 J(J + 1)/2\mu R^2$), Dunham expressed R in the latter denominator as $R_e(1 + x)$ and then expanded the resulting denominator about $x = 0$ as follows:

$$R_e^{-2}/(1 + x)^2 \approx R_e^{-2}(1 - 2x + 3x^2 - 4x^3 + \ldots) \qquad (95)$$

Dunham then combined these terms with corresponding terms in V(x) through rotationally dependent coefficients $a_j(J)$ for potential energy to produce his general expressions for term coefficients Y_{kl}. Each expression for a further such coefficient Y_{kl} in a sequence $Y_{k,l}$, $Y_{k,l+1}$, $Y_{k,l+2}\ldots$ contains a factor γ^2 that, with $\gamma \ll 1$, ensures rapid convergence; under these conditions inclusion of a set of Y_{kl} down to $Y_{0,2k}$ assures that any error due to the approximation in formula 95 is negligible in comparison with experimental error due to measurement of frequency data; a particular test appears in discussion of spectral data of GaH above. In an alternative procedure for analysis of vibration-rotational spectral data called *deformationally self-consistent*, Molski employed algebraic expressions for term coefficients $Y_{k,0}$ but employed a numerical scheme to generate the rotational dependence of spectral terms [143] that essentially circumvents the approximation implied in an expansion in formula 95. Comparison of results for NaCl under controlled conditions [143] demonstrates no advantage for this approach; a slight disadvantage arises from an algorithm for estimation of non-linear parameters. Molski's approach has produced questionable results in several cases [144] and appears unreliable for its intended purpose.

Although authors [74,75] have claimed that a generator-coordinate theory yields an expression for spectral terms exactly of Dunham's form, as in formula 8, in which however term coefficients Y_{kl}^{GCA} encompass intrinsically effects of at least adiabatic corrections, it is unclear from those papers how the functionals of v and J in their expression for E_{vJ}^i arise. As mentioned above, Dunham [4,5] derived the addend ½ of v but assumed the form $K(K + 1)$ instead of deriving it; authors of the generator-coordinate theory [74,75] appear to have assumed the forms of both functionals $(v + ½)$ and $J(J + 1)$. In lack of explicit expressions for any coefficient Y_{kl}^{GCA} that differs from results from application of classical mechanics one can not identify justification for these details.

The effective hamiltonian in formula 29 incorporates approximations that we here consider. Apart from a term $V''(R)$ that originates in nonadiabatic effects [67] beyond those taken into account through the rotational and vibrational g factors, other contributions arise that become amalgamated into that term. Replacement of nuclear masses by atomic masses within factors in terms for kinetic energy for motion both along and perpendicular to the internuclear axis yields a term of this form for the atomic reduced mass,

$$\mu^{-1} = [(m_a + Z_a m_e) + (m_b + Z_b m_e)]/[(m_a + Z_a m_e) + (m_b + Z_b m_e)] \qquad (96)$$

in which m_a and m_b are nuclear masses of atomic centres A and B respectively. The relation of this term to the nuclear reduced mass μ_n is [66]

$$\mu^{-1} \cong [1 - m_e(Z_a m_b/m_a + Z_b m_a/m_b)/(m_a + m_b)]/\mu_n \qquad (97)$$

As the subtrahend in this numerator has clearly the form of a ratio of electronic and nuclear masses, its effect can become absorbed within $V''(R)$ that contains contributions of like ratio of electronic and nuclear mass. Use of atomic rather than nuclear masses in the adiabatic correction $V'(R)$ in formula 31 yields an analogous correction that becomes likewise absorbed within $V''(R)$, and eventually neglected at present. Practical application of an effective hamiltonian for atoms with atomic number over a large range requires that one employ atomic rather than nuclear masses because atomic mass is accurately measured directly in experiment and because derivation of nuclear mass from such a quantity would involve not only subtracting electronic mass but also taking into account the binding energy of each electron. The latter quantity might have an associated error much larger than the imprecision of known atomic masses [145]; the relative precision of an atomic mass, 1.0×10^{-11}, is best for ^{16}O, and has typically a value $\sim 10^{-8}$ for other stable nuclides. For comparison the best measurements [146] of frequencies associated with vibration-rotational transitions have a relative precision $\sim 2 \times 10^{-10}$, although a relative precision for superior vibration-rotational transitions is typically $\sim 10^{-7}$, and approaches $\sim 10^{-8}$ for superior measurements of pure rotational [147] and vibration-rotational [148] transitions. As these relative precisions of measurements of mass and of frequency or wave number have clearly comparable ranges, the numerical significance of parameters independent of isotopic mass that are intended to reproduce accurate experimental measurements of wave number demonstrably depends critically on the values of atomic and electronic masses employed in deriving those parameters. Incorporation of precise further data into a set previously subjected to analysis typically requires for their reproduction parameters of increased number and of various types. For instance, for 17 pure rotational and 1223 vibration-rotational transitions of $^{23}Na^{35}Cl$ and $^{23}Na^{37}Cl$ within ranges $v \leq 8$ and $J \leq 120$, six independent fitted parameters, specifically R_e, k_e and $c_1 - c_4$, with two constrained parameters – $t_0^{Na,Cl}$ estimated from electric dipolar moment and a rotational g factor nearly zero, suffice to reproduce the wave numbers for which the best relative precision is 3×10^{-7} [81]. Addition of 189 pure rotational lines of these isotopic species [149], within ranges $v \leq 4$ and $J \leq 76$ but with relative precision up to 3×10^{-8}, requires further parameters; not only c_5 and c_6 for potential energy, reflecting enhanced sensitivity of the entire set of data to effects of centrifugal distortion, but also a parameter t_1^{Cl} related to the rotational g factor and a parameter u_1^{Cl} associated with adiabatic corrections, reflecting enhanced sensitivity of additional data to isotopic effects associated with Cl, become evaluated. These four additional parameters are essential even though all these further transitions involve vibrational and rotational states well within the previously existing range; there is no indication that further nonadiabatic effects, present in $V''(R)$, are required to be taken into account in this fit, consistent with $(m_e/\mu)^2 \sim 10^{-9}$ for NaCl being smaller than the best precision. Values of these parameters obtained from fits of data with Radiatom I, with the corresponding reduced standard deviations of the respective fits are presented in table 6; all parameters therein convey the same significance as in preceding tables $1 - 3$. Comparison of values of the same parameters in the separate fits indicates that only small changes occur; hence for corresponding parameters these fits are reasonably stable. Because the

Table 6. Coefficients of radial functions and other molecular parameters of NaCl X $^1\Sigma^+$, depending on extent of data set and constrained parameters

Parameter	1223 data, $[t_0^{\text{Na}}, t_0^{\text{Cl}}]$	1412 data, $[t_0^{\text{Na}}, t_0^{\text{Cl}}]$	1412 data, $[t_0^{\text{Na}}]$
c_0/m^{-1}	15247257 ± 18	15247401 ± 22	15247425 ± 24
c_1	-2.076785 ± 0.000037	-2.0768284 ± 0.0000095	-2.0768239 ± 0.0000095
c_2	2.54160 ± 0.00027	2.53836 ± 0.00048	2.53836 ± 0.00048
c_3	-1.8567 ± 0.0020	-1.84459 ± 0.00162	-1.84459 ± 0.00162
c_4	-0.2888 ± 0.0176	0.0198 ± 0.042	0.0195 ± 0.042
c_5	...	1.97 ± 0.29	1.975 ± 0.29
c_6	...	-2.21 ± 0.41	-2.22 ± 0.41
s_0^{Cl}	...	...	-0.238 ± 0.032
t_0^{Na}	$[0.81]$	$[0.81]$	$[0.727]$
t_0^{Cl}	$[-0.77]$	$[-0.77]$	-0.8527 ± 0.0082
t_1^{Cl}	...	-1.685 ± 0.067	...
$u_1^{\text{Cl}}/10^6\text{m}^{-1}$	...	-1.240 ± 0.126	...
$U_{0,1}/\text{m}^{-1}\,\text{u}$	302.465982 ± 0.000047	302.466455 ± 0.000039	302.467076 ± 0.000039
$U_{1,0}/\text{m}^{-1}\,\text{u}^{1/2}$	135820.124 ± 0.091	135820.873 ± 0.106	135821.120 ± 0.115
$R_\text{e}/10^{-10}\,\text{m}$	$2.36080425 \pm 0.00000058$	$2.36080240 \pm 0.00000057$	$2.36079998 \pm 0.00000057$
$k_\text{e}/\text{N m}^{-1}$	108.687209 ± 0.000147	108.688406 ± 0.000171	108.688801 ± 0.000184
$\hat{\sigma}$	0.921	0.880	0.881

additional pure rotational data [149] are so precise, we avoided constraining a value of t_0^{Cl} in a further fit. With a known precise value of p_0 of $^{23}\text{Na}^{35}\text{Cl}$ [143] and fitted value of t_0^{Cl} in formulae 66 and 67, we calculate $g_{\text{r}}(R_{\text{e}}) = 0.00741 \pm 0.00060$ and t_0^{Na}; the latter value was included as a constraint in the fitting until convergence was attained. This value of g_{r} for $^{23}\text{Na}^{35}\text{Cl}$ is a genuine prediction as no value is known from other experiment or calculation, but its reliability rests on the assumption of negligible adiabatic corrections as explained above for GeS.

In contrast, the precision of measurement of intensity of spectral lines has increased little in the past half century; most of that minor increase reflects improved spectral resolution in the frequency domain, in many cases through either a Fourier transform of interferometric measurements in a distance domain with continuous sources of radiation or use of infrared lasers; in either case a spectral feature associated with a particular transition between discrete vibration-rotational states might be optimally isolated and well defined, with minimal distortion of shape and area due to a measuring device. Even the best strengths of individual isolated lines, measured essentially as an area under a spectral curve, are likely to have a relative precision worse than 10^{-3}; in cases of weak lines for which merely increasing the concentration or length of absorbing path is impracticable, or of difficult samples such as transient species, one might have reluctantly to accept a relative precision even $\sim 10^{-1}$. Under these conditions one has clearly to accept that only the principal factor affecting intensity, such as a matrix element for electric dipolar moment for a typical band in absorption or emission or electric dipolar polarizability for a typical band observed through Raman scattering, is a significant influence, and further contributions related to adiabatic or nonadiabatic effects – or even magnetic dipolar or electric quadrupolar contributions – must perforce be neglected during reduction of experimental data. Measurements of frequency shifts on application of external electric or magnetic field, relying on a Stark or Zeeman effect, might attain greater precision, likely $\sim 10^{-4}$ at best; as these measurements generally imply a difference between two expectation values for the involved states, they might be less sensitive to a desired property than a matrix element directly proportional to that property. In such cases there prevails consequently little or no need for a refined treatment of experimental data to encompass extra-mechanical effects or theoretical quantities representing other than a smallest order of approximation.

That effective hamiltonian according to formula 29, with neglect of $V''(R)$, appears to be the most comprehensive and practical currently available for spectral reduction when one seeks to take into account all three principal extra-mechanical terms, namely radial functions for rotational and vibrational g factors and adiabatic corrections. The form of this effective hamiltonian differs slightly from that used by van Vleck [9], who failed to recognise a connection between the electronic contribution to the rotational g factor and rotational nonadiabatic terms [150,56]. There exists nevertheless a clear evolution from the advance in van Vleck's [9] elaboration of Dunham's [5] innovative derivation of vibration-rotational energies into the present effective hamiltonian in formula 29 through the work of Herman [60,66]. The notation g for two radial functions pertaining to extra-mechanical effects in formula 29 alludes to that connection between

nonadiabatic rotational effects and the magnetogyric ratio [56] that applies directly to the rotational g factor; the vibrational g factor in a product with linear momentum squared shares a similar designation [60] despite the lack of known magnetic effect. If a need arise to include effects of $V''(R)$ in formula 29, there appears also to be a direct mechanism to extend its applicability in the following way: for all contributions to $V''(R)$ that have as factor the same dependence, relative to $V(R)$, on a ratio $(m_e/m)^2$ of electronic and nuclear mass of individual atomic centres, the algebraic form of contributions to $Z_{kl}^{v,a}$ and $Z_{kl}^{v,b}$ would have exactly the same form as those from $V'(R)$, through truncated polynomials analogous to those in formula 47. (Further contributions within $V''(R)$ with dependence on m_e/m to greater than second power would naturally continue to be negligible.) Any values of fitted coefficients in such polynomials would inevitably contain, besides the additional nonadiabatic effects formally in $V''(R)$, contributions propagated from approximations involving use of atomic mass rather than nuclear mass in relation to $g_r(R)$, $g_v(R)$ and $V'(R)$; the relative magnitudes of these contributions and of $V''(R)$ therein are difficult to predict. If concern about a relation between fitted parameters and particular terms within an effective hamiltonian be lacking, an alternative formulation [151] is likely practical. This hamiltonian is based on Watson's effective hamiltonian [152], in which, in a derivation towards its ultimate form, a term related to the rotational g factor at R_e is set to zero; a use [90] of such a formulation as a basis to argue that one can not deduce reliable estimates of electric dipolar moment and rotational g factor from spectra without further information from either application of external fields or theoretically calculated data is questionable. As the existence of the rotational g factor through both experiment and a theoretical basis [56] was appreciated long before Watson's derivation [152], its neglect in that derivation is a serious deficiency and an impediment to realistic application of that hamiltonian. A justification of setting equal to zero that term related to $g_r(R_e)$ is spurious, as such a criterion is both arbitrary and avoidable, as demonstrated in an alternative derivation for the same objective [72]. With the ready availability of both many experimental and calculated data for the rotational g factor [56] and computer programs to undertake such a calculation, use of Watson's hamiltonian should be avoided if one seeks to deduce from spectra a value of R_e maximally independent of atomic mass. Application of Watson's postulate [152] of a reduced mass for a diatomic molecular ion that is inconsistent in having a mass of an atomic ion in the denominator but masses of only neutral atoms in the numerator should likewise be eschewed [66]; the g factors, vibrational and rotational, properly encompass such effects for ions. Either the hamiltonian in formula 29 or an approximate variant [66] are preferable for practical application in reduction of diatomic spectral data.

In our account here we neglect a third aspect of a spectral line, specifically its shape, beyond its characteristic frequency and strength. A natural line shape is almost impracticable to observe and would yield on analysis little or no additional information about intrinsic molecular properties. Another shape merely reflects components of molecular velocities in a direction parallel to the direction of propagation. Apart from these effects, further broadening of spectral lines due to finite durations, between collisions, of molecules in particular quantum states is attributed to interactions between colliding molecules rather than directly to

intrinsic molecular properties of an absorbing or emitting molecule of interest. Analysis of such effects involving multiple oscillators is not only much more complicated than a treatment of a single anharmonic oscillator from a theoretical point of view that lends itself to definition of characteristic parameters useful in fitting spectra, but has also received much less attention from a theoretical or computational point of view. A relation between terms in an effective hamiltonian for a system of only two diatomic molecules interacting during a collision and observable effects of broadening of spectral lines and modification of the shape of those lines is indirect, involving averages over several angular variables and over time. Discussion of general aspects of these collisional effects appears elsewhere [13].

A notable development since at least 1994 in relation to an application of Dunham's formalism in practical spectral analysis is a significant interplay between quantum chemistry, in a form of sophisticated calculations of molecular electronic structure and properties, and spectral reduction. In a few cases it has proved practicable to deduce information about electric and magnetic properties of diatomic molecules directly from spectral analysis through application of Dunham's formalism and its extensions, such as a significant estimate of the rotational *g* factor of GaH [89] already mentioned. In another instance, estimates of electric dipolar moment and rotational *g* factor of GeS relied upon an assumption, justified above, that adiabatic corrections are less important than nonadiabatic effects in relation to moderately massive atomic centres [153]. In these cases no assistance to spectral analysis from quantum-chemical calculations arose. In other cases [13] and likely a more typical situation, results for the radial dependence of the rotational *g* factor and adiabatic corrections have been incorporated within the reduction of spectral data of frequency type, enabling evaluation of spectral parameters of maximal quasi-physical significance – within a context of a traditional notion of molecular structure and its attendant hamiltonian; both LiH, the first application [112] of this approach, and H_2, as discussed above, are significant examples of successful derivation of information about adiabatic corrections and the vibrational *g* factor following an imposition of information about the rotational *g* factor during fitting of frequency data. For H_2 also, an imposition of information involving adiabatic corrections enabled recovery of information from experiments without externally applied electric or magnetic field about the rotational *g* factor. Although calculation of adiabatic corrections was accomplished many years ago, for instance by Kolos and Wolniewicz [108] for H_2 in 1964 through calculations of a nature specific for that molecular target, a general approach to calculation of the rotational *g* factor required further decades before suitable methods became developed; the first calculation involved direct sums of electronic matrix elements over electronic states [154], but a refined method, more practical for molecules containing many electrons, involving a polarization propagator [155], ensued a few years subsequently. A practical algorithm for calculation of the vibrational *g* factor has subsequently been devised [107,108]. With an incorporation of computer code required for all three extra-mechanical properties into computer program *Dalton* [156] for general calculations of molecular electronic structure and properties, it will have become practical to supplement point-wise calculations of a radial

function for potential energy, with basis sets of great quality and taking into account electronic correlation, with these auxiliary influences on vibration-rotational energies; one can hence calculate the wave number of such a transition almost within the accuracy of typical superior measurements. Likewise one can calculate influences on intensities of transitions, such as not only the principal factors of electric dipolar moment or electric dipolar polarizability but also magnetic dipolar and electric quadrupolar moments; this information can much assist the search for further transitions for known carriers of a vibration-rotational spectrum or new transitions of uncommon species.

The result of this interaction between quantum chemistry, through methods to calculate molecular electronic structure, of not merely gross determinants of spectral features but even intimate details marks the emergence of an approach to conduct of scientific research properly termed *computational spectrometry*. Although calculations of electric dipolar moments of molecules have been practised essentially since the earliest years after the evolution of quantum mechanics in forms of wave mechanics and matrix mechanics, typical results pertained to only a single internuclear distance, generally at or near a known R_e, so equivalent to p_0; such a value pertains to the intensity of the pure rotational band but not to vibration-rotational bands that are generally more readily measurable. Early solutions for prototypical systems, including an anharmonic oscillator by Heisenberg in his original treatment [157] that became matrix mechanics and a rigid rotor by Dennison whose treatment according to matrix mechanics [158] during work in Bohr's institute in Copenhagen preceded Schrodinger's treatment of a rotating harmonic oscillator according to wave mechanics [159], continue indeed to serve, with Bohr's [160] and Schrodinger's [161] treatments of the H atom, as standard simple models for the interpretation of gross features of atomic and molecular spectra. Even though radial functions for potential energy were also calculated early, with typically only qualitatively correct results, practical methods of calculating minor but significant contributions to discrete energies of molecular states have been developed much more recently. The principal factor governing the intensity of vibration-rotational transitions observed in Raman scattering is the electric dipolar polarizability; unlike the static polarizability, for which some early calculations were made, the dynamic polarizability [162,163], which is dependent on the frequency of excitation of the Raman scattering and which is consequently required to produce an accurate comparison with or prediction for experiment, was a more recent target of accurate calculations. As remarked above, measurement of intensities of typical vibration-rotational and pure rotational spectra in absorption and emission and in Raman scattering, whether by spontaneous or coherent mechanisms [13], yields only modest accuracy, and hence requires only the dominant factors of electric dipolar moment and polarizability quantities to be calculated, nevertheless accurately, as a function of internuclear distance for an adequate theoretical description or computational prediction of these spectral properties. In contrast the great accuracy of measurement of wave number of radiation, or energy of photons, corresponding to differences between spectral terms, or energies, of vibration-rotational states, requires not only sophisticated calculation of radial functions for potential energy but also for rotational and vibrational g factors

and adiabatic corrections. With the accomplishment of the latter capabilities in standard software one can consider computational spectrometry to have attained a mature state. As a basis of application of Dunham's algebraic formulation, the effective hamiltonian in formula 29 is clearly well suited to the practice of computational spectrometry because a direct relation exists between terms in this hamiltonian and quantities readily subject to theoretical calculation [66]. In principle, even the generator-coordinate approach [74,75] constitutes a mechanism for computational spectrometry still conforming to the Dunham formulation because it is expected to be able to encompass intrinsically [164] what are regarded as supplementary adiabatic and nonadiabatic corrections to molecular energies according to a traditional separation of electronic and nuclear motions. The rotational g factor seems to have been ignored in the development of that generator-coordinate approach, despite a well founded connection of g_r to both experimental and theoretical quantities; because g_r is just as much an experimentally observable quantity, through the Zeeman effect, as a wave number of a spectral line, this property warrants attention if the generator-coordinate approach is to be considered a serious means to interpret molecular spectra.

11. CONCLUSION

Dunham's expression in formula 8 for vibration-rotational terms is a double expansion in vibrational and rotational quantum numbers based on the minimum vibration-rotational energy in a particular electronic state; likewise his radial function for internuclear potential energy $V(x)$, in formula 16, which serves as a basis to relate Dunham coefficients Y_{kl}, is an expansion about the minimum potential energy of that electronic state, which occurs at the equilibrium internuclear separation R_e: both expansions thus possess the disadvantages from which all such truncated power series suffer. This property of a limited range of convergence hence bestows emphasis on vibrational states with small values of quantum number v – those states that with their associated rotational states typically pertain to almost all measurements of infrared and Raman spectra of gaseous substances containing diatomic molecular species, and even to many electronic spectra of such samples in absorption. An alternative general formula for vibration-rotational terms encompassing all states within a manifold up to a dissociation limit has never been devised [13]. The exponentially increasing extent of expressions for coefficients Y_{kl}, despite a powerful implementation of symbolic software to their elucidation [44], with increasing terms or parameters in $V(x)$, and associated functions, remains a formal impediment to enhanced application according to a theory based on an algebraic approach of Dunham and his successors, although in practice a limiting condition has seldom if ever arisen.

An important fact underlying this approach to analysis of molecular spectra based on a formalism arising from pioneering work of Dunham and van Vleck, and advances contributed by their successors, or any other approach, is that not merely coefficients A_{kl}^i, $V_{kl}^{a,b}$, $\Delta_{kl}^{a,b}$, B_{kl} or their equivalents but also Y_{kl}^i, various Z_{kl}^i, U_{kl}, radial coefficients a_j, c_j, p_j, s_j, t_j, u_j or their equivalent, and even R_e and k_e, or fitted values that nominally represent prospective integral kernels in

expressions for Y_{kl}^{GCA} according to the generator-coordinate theory [74,75], are, first and foremost, merely *fitting parameters*; their particular numerical values adopted according to a given fitting procedure reflect both the quality and quantity of fitted data through extents both of ranges of vibrational and rotational quantum numbers and of isotopic variants, as exemplified through results for NaCl described above. Apart from representatives of integral kernels, the coefficients $a_j \ldots u_j$ listed above pertain to radial functions that are artifacts of a method of separate treatment of electronic and nuclear motions; those radial functions, such as of potential energy or electric dipolar moment, are not experimentally observable, even though they might be susceptible to calculation according to some ansatz. Some fitting parameters of one or other type might be more suitable to use for moderate extrapolation beyond those extents of data than parameters of other types if a theoretically justified fitting model be chosen, but any such extrapolation is fundamentally statistically unreliable and susceptible to propagation of error associated with the original experimental measurements, even if limiting forms or conditions be imposed on the fitting formula; the reliability or accuracy invariably decreases with an increasing extent of extrapolation beyond characterised states of molecular energies. Although some parameters of selected type according to a selected model might be amenable to comparison with quantities calculated theoretically, the latter calculations involve both approximate models and approximations in implementation that proscribe an exact comparison, because any diatomic molecule must involve interaction of at least three elementary particles for which the problem of *many bodies* fundamentally lacks an exact solution. Nevertheless, a nominally theoretical – actually still *semi-empirical* in practice – calculation of pertinent quantities can beneficially guide experimental measurements; conversely, experimental measurements can guide development of theories, as has occurred repeatedly since the first measurements of optical spectra. Of course any ansatz of purported calculation from first principles or *ab initio* reflects, implicitly, prior experimental information and influence. The development of molecular spectrometry represents a prime confluence of theory, experiment and computation – the latter through methods of quantum chemistry, and has afforded many implications for our understanding of myriad chemical and physical phenomena. An approach to a quantitative description of spectra of diatomic molecular species through Dunham's systematic algebraic formalism, based naturally on Dunham coefficients Y_{kl}, has served as a model for an area of science much broader than the number of atomic centres in a molecule of a size that attracted his attention might indicate.

ACKNOWLEDGEMENTS

REFERENCES

[1] J. L. Dunham, *Phys. Rev.*, 1929, **34**, 438.

[2] J. L. Dunham, *Phys. Rev.*, 1930, **35**, 1347.

[3] J. L. Dunham, *Phys. Rev.*, 1930, **36**, 1553.

[4] J. L. Dunham, *Phys. Rev.*, 1932, **41**, 713.

[5] J. L. Dunham, *Phys. Rev.*, 1932, **41**, 721.

[6] G. Herzberg, *Molecular Spectra and Molecular Structure. I. Spectra of Diatomic Molecules*, 2nd edn, van Nostrand, New York, 1950.

[7] Science Citation Index, 2004.

[8] H. C. Urey, G. M. Murphy and F. G. Brickwedde, *Phys. Rev.*, 1932, **40**, 1.

[9] J. H. van Vleck, *J. Chem. Phys.*, 1936, **4**, 327.

[10] J. J. Balmer, *Ann. Phys. Chem.*, 1885, **25**, 80.

[11] H. Deslandres, *Comptes Rendus Acad. Sci. Paris*, 1886, **103**, 972.

[12] M. M. Hessel and C. R. Vidal, *J. Chem. Phys.*, 1979, **70**, 4439.

[13] J. F. Ogilvie, *The Vibrational and Rotational Spectrometry of Diatomic Molecules*, Academic Press, London, 1998, and references therein.

[14] L. Brillouin, *Comptes Rendus Acad. Sci. Paris*, 1926, **183**, 24, and 270.

[15] L. Brillouin, *J. Phys. Radium*, 1926, **7**, 136, and 353.

[16] H. A. Kramers, *Z. Phys.*, 1926, **39**, 828.

[17] G. Wentzel, *Z. Phys.*, 1926, **38**, 518.

[18] H. Jeffreys, *Proc. London Math. Soc.*, 1925, **23**, 428.

[19] I. Sandeman, *Proc. R. Soc. Edinburgh*, 1940, **60**, 210.

[20] (a) H. W. Woolley, *J. Chem. Phys.*, 1962, **37**, 1307; (b) H. W. Woolley, *J. Chem. Phys.*, 1972, **56**, 1792.

[21] J. E. Kilpatrick, *J. Chem. Phys.*, 1959, **30**, 801.

[22] J. P. Bouanich, *J. Quant. Spectrosc. Radiat. Transfer*, 1978, **19**, 381.

[23] V. N. Brukhanov, V. Y. Galin, V. E. Zuev, Y. S. Makushkin and V. G. Tyuterev, *Opt. Spectrosc.*, 1982, **52**, 33.

[24] N. Bessis, G. Hadinger and Y. S. Tergiman, *J. Mol. Spectrosc.*, 1984, **107**, 343.

[25] G. Hadinger, Y. S. Tergiman and G. J. Hadinger, *J. Chem. Phys.*, 1987, **87**, 2143.

[26] J. F. Ogilvie and R. H. Tipping, *Int. Rev. Phys. Chem.*, 1983, **3**, 3.

[27] J. F. Ogilvie and M. B. Monagan, *MapleTech*, 1997, **4**, 100.

[28] H. Uehara, *J. Mol. Spectrosc.*, 1998, **188**, 215.

[29] H. Uehara, K. Horiai and K. Akiyama, *Bull. Chem. Soc. Jpn*, 2004, **77**, xxx–xxx.

[30] F. M. Fernandez and J. F. Ogilvie, *Phys. Rev. A*, 1990, **42**, 4001.

[31] M. B. Monagan and J. F. Ogilvie, *Math. Comput. Simulat.*, 1999, **49**, 221.

[32] R. H. Tipping, *J. Mol. Spectrosc.*, 1972, **43**, 31.

[33] R. H. Tipping and J. F. Ogilvie, *Chin. J. Phys.*, 1990, **28**, 237.

[34] J. F. Ogilvie and D. Koo, *J. Mol. Spectrosc.*, 1976, **61**, 332.

[35] A. H. M. Ross, R. S. Eng and H. Kildal, *Opt. Commun.*, 1974, **12**, 433.

[36] C. M. Clayton, D. W. Merdes, J. Pliva, T. K. McCubbin and R. H. Tipping, *J. Mol. Spectrosc.*, 1983, **98**, 168.

[37] P. Niay, P. Bernage, C. Coquant and A. Fayt, *Can. J. Phys.*, 1977, **55**, 1829.

[38] G. Simons, R. G. Parr and J. M. Finlan, *J. Chem. Phys.*, 1973, **59**, 3229.

[39] A. Kratzer, *Z. Phys.*, 1920, **3**, 289.

[40] E. Fues, *Ann. Phys.*, 1926, **80**, 367.

[41] (a) J. F. Ogilvie, *Proc. R. Soc. London*, 1981, **A378**, 287; (b) J. F. Ogilvie, *Proc. R. Soc. London*, 1982, **A381**, 479, and references therein.

[42] C. L. Beckel, *J. Chem. Phys.*, 1976, **65**, 4319.

[43] J. F. Ogilvie, *Comput. Phys. Commun.*, 1983, **30**, 101.

[44] F. M. Fernandez and J. F. Ogilvie, *MapleTech*, 1998, **5**, 42.

[45] E. Tiemann, H. Knockel and J. Schlembach, *Ber. Bunsenges. Phys. Chem.*, 1982, **86**, 821.

[46] N. Bohr, *Nature*, 1922, **109**, 746.

[47] W. H. King, *Isotope Shifts in Atomic Spectra*, Plenum Press, London, 1984.

[48] P. Brix and H. Kopfermann, *Z. Phys.*, 1949, **126**, 344.

[49] J. Schlembach and E. Tiemann, *Chem. Phys.*, 1982, **68**, 21.

[50] P. Aufmuth, K. Heilig and A. Steudel, *At. Data Nucl. Data Tables*, 1987, **37**, 455.

[51] G. Fricke, C. Bernhardt, K. Heilig, L. A. Schaller, L. Schellenberg, E. B. Shera and C. W. de Jager, *At. Data Nucl. Data Tables*, 1995, **60**, 177.

[52] C. Wieman and T. W. Hansch, *Phys. Rev. A*, 1980, **22**, 192.

[53] G. W. Erickson, *J. Phys. Chem. Ref. Data*, 1977, **6**, 831.

[54] (a) R. M. Herman and S. Short, *J. Chem. Phys.*, 1968, **48**, 1266; (b) R. M. Herman and S. Short, *J. Chem. Phys.*, 1970, **50**, 572.

[55] J. F. Ogilvie, *J. Phys. At. Mol. Opt. Phys. B*, 1994, **27**, 47.

[56] J. F. Ogilvie, J. Oddershede and S. P. A. Sauer, *Adv. Chem. Phys.*, 2000, **111**, 475, and references therein.

[57] J. Korving, H. Hulsman, L. J. F. Hermans, J. J. de Groot, H. F. P. Knapp and J. J. M. Beenakker, *J. Mol. Spectrosc.*, 1966, **20**, 294.

[58] L. J. F. Hermans, A. Schutte, H. F. P. Knapp and J. J. M. Beenakker, *Physica*, 1970, **46**, 491.

[59] H. Moraal and F. R. McCourt, *Phys. Rev. A*, 1971, **4**, 511.

[60] R. M. Herman and A. Asgharian, *J. Mol. Spectrosc.*, 1966, **19**, 305.

[61] M. Born and J. R. Oppenheimer, *Ann. Phys. Leipzig*, 1927, **84**, 457.

[62] M. Born and K. Huang, *Dynamical Theory of Crystal Lattices*, Clarendon Press, Oxford, 1954.

[63] H. C. Longuet-Higgins, *Adv. Spectrosc.*, 1961, **2**, 263.

[64] F. M. Fernandez, *Phys. Rev.*, 1994, **50**, 2953.

[65] R. G. Woolley, *Adv. Phys.*, 1976, **25**, 27.

[66] R. M. Herman and J. F. Ogilvie, *Adv. Chem. Phys.*, 1998, **103**, 187.

[67] P. R. Bunker and R. E. Moss, *Mol. Phys.*, 1977, **33**, 417.

[68] W. C. Stwalley, *J. Chem. Phys.*, 1975, **63**, 3062.

[69] E. Tiemann and J. F. Ogilvie, *J. Mol. Spectrosc.*, 1994, **165**, 377.

[70] J. F. Ogilvie, *J. Mol. Spectrosc.*, 1996, **180**, 193.

[71] J. F. Ogilvie, *Spectrosc. Lett.*, 1989, **22**, 477.

[72] F. M. Fernandez and J. F. Ogilvie, *Chin. J. Phys.*, 1992, **30**, 177, and 599.

[73] M. R. Osborne, *J. Aust. Math. Soc. B*, 1976, **19**, 343.

[74] L. Lathouwers and P. van Leuven, *Adv. Chem. Phys.*, 1982, **49**, 115.

[75] L. Lathouwers, P. van Leuven, E. Deumens and Y. Ohrn, *J. Chem. Phys.*, 1987, **86**, 6352.

[76] G. Poeschl and E. Teller, *Z. Phys.*, 1933, **83**, 143.

[77] R. Engelke, *Am. J. Phys.*, 1989, **57**, 339.

[78] M. M. Nieto, *Phys. Rev. D*, 1981, **24**, 1030.

[79] I. M. Gelfand and B. M. Levitan, *Izv. Akad. Nauk USSR, Math. Ser.*, 1951, **15**, 309.

[80] (a) A. G. Ramm, *Inv. Prob.*, 1988, **4**, 877; (b) A. G. Ramm, *Inv. Prob.*, 1988, **5**, 255.

[81] J. F. Ogilvie, H. Uehara and K. Horiai, *Bull. Chem. Soc. Jpn*, 2000, **73**, 321.

[82] J. F. Ogilvie, H. Uehara and K. Horiai, *Can. J. Anal. Sci. Spectrosc.*, 1999, **44**, 141.

[83] F. M. Fernandez and J. F. Ogilvie, *J. Math. Chem.*, 1994, **15**, 131.

[84] F. M. Fernandez, *J. Math. Phys.*, 1995, **36**, 3922, and references therein.

[85] H. Uehara and J. F. Ogilvie, *J. Mol. Spectrosc.*, 2001, **207**, 143.

[86] Q. J. Hu, T. C. Melville and J. W. Hepburn, *J. Chem. Phys.*, 2003, **119**, 8938.

[87] N. C. Handy and A. M. Lee, *Chem. Phys. Lett.*, 1996, **252**, 425.

[88] J. F. Ogilvie, *Chem. Phys. Lett.*, 1997, **267**, 590.

[89] J. F. Ogilvie and S. C. Liao, *Chem. Phys. Lett.*, 1994, **226**, 281.

[90] J. K. G. Watson, *J. Mol. Spectrosc.*, 2003, **217**, 157.

[91] R. D. Urban, H. Birk, P. Polomsky and H. Jones, *Chem. Phys. Lett.*, 1989, **154**, 135.

[92] R. D. Urban, H. Birk, P. Polomsky and H. Jones, *J. Chem. Phys.*, 1991, **94**, 2523.

[93] J. M. Campbell, M. Dulick, D. Klapstein, J. B. White and P. F. Bernath, *J. Chem. Phys.*, 1993, **99**, 8379.

[94] P. J. Mohr and B. N. Taylor, *Rev. Mod. Phys.*, 2005, **77**, 1.

[95] K. P. Huber and G. Herzberg, *Constants of Diatomic Molecules*, van Nostrand-Reinhold, New York, 1979.

[96] S. P. A. Sauer, J. Oddershede and J. Geertsen, *Mol. Phys.*, 1992, **76**, 445.

[97] S. P. A. Sauer and J. F. Ogilvie, *J. Phys. Chem.*, 1994, **98**, 8617.

[98] S. P. A. Sauer, *Chem. Phys. Lett.*, 1996, **260**, 271.

[99] J. F. Ogilvie, S.-L. Cheah, Y.-P. Lee and S. P. A. Sauer, *Theor. Chem. Acc.*, 2002, **108**, 85.

[100] S. R. Langhoff, C. W. Baushlicher and H. Partridge, *Chem. Phys. Lett.*, 1994, **223**, 416.

[101] J. F. Ogilvie, *Chem. Phys. Lett.*, 1992, **191**, 592.

[102] P. M. Morse, *Phys. Rev.*, 1929, **34**, 57.

[103] J. F. Ogilvie, *J. Chem. Phys.*, 1988, **88**, 2804.

[104] J. F. Ogilvie, *Can. J. Spectrosc.*, 1988, **33**, 72.

[105] M. L. Orlov, J. F. Ogilvie and J. W. Nibler, *J. Mol. Spectrosc.*, 1997, **185**, 128.

[106] I. Dabrowski, *Can. J. Phys.*, 1984, **62**, 1639.

[107] K. L. Bak, S. P. A. Sauer, J. Oddershede and J. F. Ogilvie, *Ohio State Univ. Int. Symp. Mol. Spectrosc.*, 2003, **58**, Abstract FD02.

[108] K. L. Bak, S. P. A. Sauer, J. Oddershede and J. F. Ogilvie, *Phys. Chem. Chem. Phys.*, 2005, **7**, 1747.

[109] S.P.A. Sauer, J. Oddershede, J.F. Ogilvie, Evaluation of parameters in radial functions from rotational and vibration–rotational spectra and calculation of rotational and vibrational g factors for LiH $X^1\Sigma^+$, in preparation.

[110] W. Kolos and L. Wolniewicz, *J. Chem. Phys.*, 1964, **41**, 3663.

[111] L. Wolniewicz, *J. Chem. Phys.*, 1993, **99**, 1851.

[112] R. G. Barnes, P. J. Bray and N. F. Ramsey, *Phys. Rev.*, 1954, **94**, 893.

[113] J. D. Garcia, *Phys. Rev.*, 1966, **147**, 66.

[114] J. F. Ogilvie, J. Oddershede and S. P. A. Sauer, *Chem. Phys. Lett.*, 1994, **228**, 183.

[115] R. R. Freeman, A. R. Jacobson, D. W. Johnson and N. F. Ramsey, *J. Chem. Phys.*, 1975, **63**, 2597.

[116] T. R. Lawrence, C. H. Anderson and N. F. Ramsey, *Phys. Rev.*, 1963, **130**, 1865.

[117] M. Dulick, K.-Q. Zhang, B. Guo and P. F. Bernath, *J. Mol. Spectrosc.*, 1998, **188**, 14.

[118] E. F. Pearson and W. Gordy, *Phys. Rev.*, 1969, **177**, 59.

[119] G. M. Plummer, E. Herbst and F. C. de Lucia, *J. Chem. Phys.*, 1984, **81**, 4893.

[120] F. Matsushima, H. Odashima, D. B. Wang, S. Tsunekawa and K. Takagi, *Jpn. J. Appl. Phys.*, 1994, **33**, 315.

[121] M. Bellini, P. de Natale, M. Inguscio, T. D. Varberg and J. M. Brown, *Phys. Rev. A*, 1995, **52**, 1954.

[122] D. M. Bishop and L. M. Cheung, *J. Chem. Phys.*, 1983, **78**, 1396.

[123] C. E. Scheu, D. B. Kinghom and L. Adamowicz, *J. Chem. Phys.*, 2001, **114**, 3393.

[124] M. Cafiero, S. Bubin and L. Adamowicz, *Phys. Chem. Chem. Phys.*, 2003, **5**, 1491.

[125] H. Partridge and S. R. Langhoff, *J. Chem. Phys.*, 1981, **74**, 2361.

[126] W. C. Stwalley and W. T. Zemke, *J. Phys. Chem. Ref. Data*, 1993, **22**, 87.

[127] J. F. Ogilvie, *Cryst. Eng.*, 2004, **6**, 255.

[128] C. P. Smyth, *Philos. Mag.*, 1923, **45**, 849.

[129] J. F. Ogilvie and Y. P. Lee, *Chem. Phys. Lett.*, 1989, **159**, 239.

[130] R. Herman and R. F. Wallis, *J. Chem. Phys.*, 1955, **23**, 637.

[131] J. N. P. van Stralen, L. Visscher and J. F. Ogilvie, *Chem. Phys. Phys. Chem.*, 2004, **6**, 3779.

[132] R. Beck, W. Englisch and K. Gurs, *Table of Laser Lines in Gases and Vapours*, 3rd edn, Springer, Berlin, 1980.

[133] M. Gromoll-Bohle, W. Bohle and W. Urban, *Opt. Commun.*, 1989, **69**, 409.

[134] G. Guelachvili, D. de Villeneuve, R. Farrenq, W. Urban and J. Verges, *J. Mol. Spectrosc.*, 1983, **98**, 64.

[135] K. Angstrom, *Ofvers. Kongl. Vet. Akad. Forh. Stockholm*, 1889, **46**, 203.

[136] G. Herzberg and K. N. Rao, *J. Chem. Phys.*, 1949, **17**, 1099.

[137] C.-Y. Chung, Y.-P. Lee, J. F. Ogilvie, to be published, 2005.

[138] A. O'Keefe and D. A. G. Deacon, *Rev. Sci. Instrum.*, 1988, **59**, 2544.

[139] J. S. Muenter, *J. Mol. Spectrosc.*, 1975, **55**, 490.

[140] J. F. Ogilvie, *Chem. Comput.*, 1984, **8**, 205.

[141] C. Chackerian and R. H. Tipping, *J. Mol. Spectrosc.*, 1983, **99**, 431.

[142] Y.-P. Lee, S.-L. Cheah and J. F. Ogilvie, *Infrared Phys. Tech.*, 2005, **46**, in press.

[143] J. F. Ogilvie and M. Molski, *Spectrochim. Acta A*, 1999, **55**, 1427, and references therein.

[144] J. F. Ogilvie, *Chem. Phys. Lett.*, 2001, **348**, 447, and references therein.

[145] G. Audi, A. H. Wapstra and C. Thibault, *Nucl. Phys. A*, 2003, **729**, 337.

[146] S. Saupe, B. Meyer, M. H. Wappelhorst, W. Urban and A. G. Maki, *J. Mol. Spectrosc.*, 1996, **179**, 13.

[147] F. Lewen, S. Brunken, G. Winnewisser, M. Simeckova and S. Urban, *J. Mol. Spectrosc.*, 2004, **226**, 113.

[148] S. Klee and J. F. Ogilvie, *Spectrochim. Acta A*, 1993, **49**, 345.

[149] M. Caris, F. Lewen and G. Winnewisser, *Z. Naturforsch*, 2002, **57a**, 663.

[150] B. Rosenblum, A. H. Nethercot and C. H. Townes, *Phys. Rev.*, 1958, **109**, 400.

[151] H. Uehara, K. Horiai and K. Akiyama, *Bull. Chem. Soc. Jpn*, 2004, **77**, 1821.

[152] J. K. G. Watson, *J. Mol. Spectrosc.*, 1980, **80**, 411.

[153] J. F. Ogilvie, *Mol. Phys.*, 1996, **88**, 1055.

[154] D. M. Bishop and L. M. Cheung, *J. Chem. Phys.*, 1981, **74**, 1817.

[155] J. Oddershede and J. R. Sabin, *Chem. Phys.*, 1988, **122**, 291.

[156] Dalton, a molecular–electronic–structure program, release 2.0 (2004), written by T. Helgaker, H. J.Aa. Jensen, P. Joergensen, J. Olsen, K. Ruud, H. Aagren, A. A. Auer, K. L. Bak, V. Bakken, O. Christiansen, S. Coriani, P. Dahle, E. K. Dalskov, T. Enevoldsen, B. Fernandez, C. Hattig, K. Hald, A. Halkier, H. Heiberg, H. Hettema, D. Jonsson, S. Kirpekar, R. Kobayashi, H. Koch, K. V. Mikkelsen, P. Norman, M. J. Packer, T. B. Pedersen, T. A. Ruden, A. Sanchez, T. Saue, S. P. A. Sauer, B. Schimmelpfennig, K. O. Sylvester-Hvid, P. R. Taylor, O. Vahtras; on Internet, http://www.kjemi.uio.no/software/dalton/dalton.html

[157] W. Heisenberg, *Z. Phys.*, 1925, **33**, 879.

[158] D. M. Dennison, *Phys. Rev.*, 1926, **28**, 318.

[159] E. Schrodinger, *Ann. Phys. Leipzig*, 1926, **79**, 489.

[160] N. Bohr, *Philos. Mag.*, 1913, **26**, 1.

[161] E. Schrodinger, *Ann. Phys. Leipzig*, 1926, **79**, 361.

[162] J. Oddershede, P. Joergensen and N. H. F. Beebe, *J. Chem. Phys.*, 1975, **63**, 2996.

[163] J. Oddershede and E. N. Svendsen, *Chem. Phys.*, 1982, **64**, 359.

[164] L. Lathouwers and P. van Leuven, *Chem. Phys. Lett.*, 1980, **70** , 410.

Quantum-Chemical Calculations of Radial Functions for Rotational and Vibrational *g* Factors, Electric Dipolar Moment and Adiabatic Corrections to the Potential Energy for Analysis of Spectra of HeH$^+$

Stephan P. A. Sauer,[1] Hans Jørgen Aa. Jensen[2] and John F. Ogilvie[3]

[1]Department of Chemistry, University of Copenhagen, Universitetsparken 5, DK-2100 København Ø, Denmark
[2]Department of Chemistry, University of Southern Denmark, Campusvej 55, DK-5230 Odense M, Denmark
[3]Escuela de Quimica, Universidad de Costa Rica, San Pedro de Montes de Oca, San Jose 2060, Costa Rica

Abstract

Computational spectrometry, which implies an interaction between quantum chemistry and analysis of molecular spectra to derive accurate information about molecular properties, is needed for the analysis of the pure rotational and vibration–rotational spectra of HeH$^+$ in four isotopic variants to obtain precise values of equilibrium internuclear distance and force coefficient. For this purpose, we have calculated the electronic energy, rotational and vibrational *g* factors, the electric dipolar moment, and adiabatic corrections for both He and H atomic centres for internuclear distances over a large range 10^{-10}m [0.3, 10]. Based on these results we have generated radial functions for atomic contributions for g_r, g_v, and adiabatic corrections, involving the coefficients s_j^{He}, s_j^{H}, t_j^{He}, t_j^{H}, u_j^{He}, and u_j^{H} of z^j for ^{4}He^{1}H$^+$ for further spectral analysis.

Contents

1. INTRODUCTION

Computational spectrometry [1] implies an interaction between quantum chemistry, in a practice of calculations of molecular electronic structure, and analysis of spectra of small free molecules so as to derive, from the latter, information of maximal physical and statistical significance. The best relative accuracy of measurement of spectral frequencies is about two parts in 10^{10} [2]; to obtain a comparable accuracy in differences of quantum-mechanical energies still exceeds the capabilities of algorithms and computer hardware, but the calculation of other pertinent quantities can play a valuable role in the analysis of spectra. For instance, an accurate knowledge of the dynamic electric dipolar polarisability [3–7] of a particular molecular species facilitates the observation of that compound through Raman scattering; likewise accurate data for the molecular rotational g_r factor [8–14] and electric dipolar moment [15] enable extraction of information about the vibrational g_v factor and adiabatic effects from frequency data for pure rotational and vibration–rotational transitions [16–18] as well as an accurate function for the internuclear potential energy, within a conventional treatment involving separation of electronic and nuclear motions. Our work on LiH [17] was undertaken before a comprehensive theoretical treatment relating the vibrational g_v factor and spectral parameters became available [19]. Afterward we developed and implemented an algorithm for the calculation of the vibrational g_v factor [18]. With a new implementation of the coding of adiabatic corrections in an established suite of Fortran routines for quantum-chemical calculations in Dalton [23], we are able to calculate to satisfactory accuracy the principal auxiliary terms in an effective Hamiltonian for vibrational and rotational motion of atomic centres in a diatomic molecule. Because these auxiliary terms have only a small, but significant, effect on energies of molecular vibration–rotational states, there is no necessity to attain an accuracy comparable with that of electronic energy.

Here we apply this quantum-chemical capability to provide quantitative knowledge about these auxiliary quantities to assist the extraction of information about equilibrium properties of helium hydride diatomic molecular cation, HeH^+. By its ionic nature, this compound is highly reactive under laboratory conditions and hence only a transient species in experiments in the gaseous phase, but measurements of spectra have yielded moderately precise frequencies of pure rotational and vibration–rotational transitions throughout energies in a range from the ground state up to the dissociation limit – even beyond that limit for further states quasi-bound within the centrifugal barrier – for both $^4He^1H^+$ and $^4He^2H^+$, as well as less abundant data for two analogous species containing ^3He. Because the curve for the internuclear potential energy of this molecule in the ground electronic state possesses both a broad and a shallow minimum, a radial function to represent that potential energy encompasses internuclear distances over a large range. To cover satisfactorily a corresponding range of energies and ancillary molecular properties would require radial functions involving as parameters some 70 or 80 coefficients of a distance variable to various powers, which would require fitting from known frequencies of only some 200 measured transitions within the electronic ground state. In contrast, wave numbers of about 5500 transitions of GeO are satisfactorily reproduced with only six fitted parameters [24], but these

many transitions sample energy for only a small fraction of states below the dissociation limit. Moreover, the small masses of both nuclei in HeH$^+$ cause intervals of energy between adjacent states in vibrational manifolds to be relatively large, and likewise for rotational manifolds, such that below the dissociation limit this curve for the potential energy supports only a few vibrational states, with their associated rotational manifolds. For these reasons the simultaneous reduction of all these spectral data of HeH$^+$ is challenging to an extent far beyond that associated with other and less elusive diatomic molecular species existing in the gaseous phase. In contrast, the calculation of molecular electronic structure and properties is greatly facilitated by the facts that there are only two electrons associated with two atomic nuclei and that the symmetry class of the electronic ground state of HeH$^+$ is $^1\Sigma^+$, implying that no important magnetic effects need be included in the computation of those properties. In summary, one can readily appreciate that this molecular species is an excellent candidate for the application of the practice of computational spectrometry, so that analysis of molecular spectra thus assisted can yield information about equilibrium and other properties to serve both for characterization of this molecular species and as reference for future calculations.

2. THEORY

As a point of departure we assume, within a conventional separation of nuclear and electronic motions, an effective Hamiltonian for the motion of two atomic nuclei and their associated electrons both along and perpendicular to the internuclear vector, directly applicable to a molecule of symmetry class $^1\Sigma^+$ for which magnetic effects are absent or negligible [25]:

$$
\hat{H}(R) = \frac{1}{2\mu}\ \hat{P}\left(1 + \frac{m_e}{m_p}g_v(R)\right)\hat{P} + \left(1 + \frac{m_e}{m_p}g_r(R)\right)\frac{\hbar^2 J(J+1)}{2\mu R^2}
$$
$$
+ V(R) + V'(R) \tag{1}
$$

here $\hat{P}$ is an operator for linear momentum conjugate to internuclear distance R; $\mu = M_a M_b/(M_a + M_b)$ is the atomic reduced mass for atomic centres A and B and their respective masses M_a and M_b; $g_v(R)$ and $g_r(R)$ are, respectively, radial functions for the vibrational and rotational g factors; J is a quantum number for angular momentum of the molecule about the molecular centre of mass; $V(R)$ denotes internuclear potential energy independent of nuclear mass (including relativistic corrections); and $V'(R)$ denotes adiabatic corrections to take into account a small dependence on nuclear mass that $V(R)$ would otherwise exhibit. Both rotational and vibrational g factors have an electronic contribution, which is regarded to pertain to rotational and vibrational non-adiabatic effects, as discussed below. An additional contribution to both the g factors, which is normally called the nuclear contribution, arises on the transition from nuclear masses to atomic masses in the effective Hamiltonian [18,19]. Energy values of this effective

Hamiltonian are expressed in this form [25]

$$E_{v,J} = \sum_k \sum_l (Y_{k,l} + Z_{k,l}) \left(v + \frac{1}{2} \right)^k [J(J+1)]^l \tag{2}$$

in which Dunham coefficients $Y_{k,l}$ result from the principal terms in the effective Hamiltonian, equation (1), and $Z_{k,l}$ reflect the presence therein of auxiliary terms – the rotational and vibrational g factors and adiabatic corrections.

2.1. The g_r and g_v factors

The electronic contributions to the g factors arise in second-order perturbation theory from the perturbation of the electronic motion by the vibrational or rotational motion of the nuclei [19,26]. This non-adiabatic coupling of nuclear and electronic motion, which exemplifies a breakdown of the Born–Oppenheimer approximation, leads to a mixing of the electronic ground state with excited electronic states of appropriate symmetry. The electronic contribution to the vibrational g factor of a diatomic molecule is then given as a sum-over-excited-states expression

$$g_v^{\mathrm{el}}(R) = \frac{m_{\mathrm{p}}}{m_{\mathrm{e}}} \frac{2\hbar}{\mu} \sum_{n \neq 0} \frac{|\langle \Psi_0(\{\vec{r}_i\}, R)| \{ \frac{\partial}{\partial R} | \Psi_n(\{\vec{r}_i\}, R) \rangle \}|^2}{E_0^{\mathrm{BO}}(R) - E_n^{\mathrm{BO}}(R)} \tag{3}$$

whereas the electronic contribution to the rotational g factor of a diatomic molecule consists of two contributions

$$g_r^{\mathrm{el}}(R) = g_r^{\mathrm{para}}(R) + g_r^{\mathrm{dia}}(R) \tag{4}$$

The 'paramagnetic' contribution again involves excited states

$$g_r^{\mathrm{para}}(R) = \frac{m_{\mathrm{p}}}{m_{\mathrm{e}}} \frac{1}{\mu R^2} \left\{ \sum_{n \neq 0} \left(\frac{\langle \Psi_0 | \sum_i l_{i,x}(\vec{R}_0) | \Psi_n \rangle \langle \Psi_n | \sum_i l_{i,x}(\vec{R}_{\mathrm{CM}}) | \Psi_0 \rangle}{E_0^{\mathrm{BO}}(R) - E_n^{\mathrm{BO}}(R)} \right. \right.$$
$$\left. \left. + \frac{\langle \Psi_0 | \sum_i l_{i,y}(\vec{R}_{\mathrm{CM}}) | \Psi_n \rangle \langle \Psi_n | \sum_i l_{i,y}(\vec{R}_0) | \Psi_0 \rangle}{E_0^{\mathrm{BO}}(R) - E_n^{\mathrm{BO}}(R)} \right) \right\} \tag{5}$$

in which for brevity $\Psi_{0|n}(\{\vec{r}_i\}, R)$ is abbreviated in this equation as $\Psi_{0|n}$, whereas the 'diamagnetic' contribution is a simple average value over the electronic

ground state:

$$g_r^{\text{dia}}(R) = -\frac{m_p}{\mu R^2} \left\{ \frac{1}{2} \left(\langle \Psi_0(\{\vec{r}_i\}, R) | \sum_i (r_{i,x} - R_{\text{CM},x})(R_{\text{o},x} - R_{\text{CM},x}) | \Psi_0(\{\vec{r}_i\}, R) \rangle \right. \right.$$

$$\left. + \langle \Psi_0(\{\vec{r}_i\}, R) | \sum_i (r_{i,y} - R_{\text{CM},y})(R_{\text{o},y} - R_{\text{CM},y}) | \Psi_0(\{\vec{r}_i\}, R) \rangle \right)$$

$$\left. + \langle \Psi_0(\{\vec{r}_i\}, R) | \sum_i (r_{i,z} - R_{\text{CM},z})(R_{\text{o},z} - R_{\text{CM},z}) | \Psi_0(\{\vec{r}_i\}, R) \rangle \right\} \tag{6}$$

The nuclear contribution to the rotational or vibrational g factor becomes for a diatomic molecule AB containing nucleus A of protonic number Z_a along the z-axis at $z_a = |\vec{R}_a - \vec{R}_{\text{CM}}|$, and nucleus B with protonic number Z_b at $z_b = |\vec{R}_b - \vec{R}_{\text{CM}}|$

$$g^n = \frac{m_p}{I}(Z_a z_a^2 + Z_b z_b^2) = m_p \frac{Z_a M_b^2 + Z_b M_a^2}{M_a M_b (M_a + M_b)} \tag{7}$$

in which the moment of inertia is

$$I = \mu R^2 = \frac{M_a M_b}{M_a + M_b}(\vec{R}_a - \vec{R}_b)^2. \tag{8}$$

The second form of g_r^n shows that the nuclear contribution, being independent of internuclear distance, is constant for a particular molecular species in all its electronic states.

Calculation of rotational and vibrational g factors by linear response methods using multiconfigurational self-consistent-field wave functions is described in detail elsewhere [18,27].

According to convention we suppose that the g factors of a neutral diatomic molecule can be partitioned into a term depending on the electric dipolar moment $\vec{d}$ or its derivative dd_z/dR and an 'irreducible' non-adiabatic contribution $g_{r/v}^{\text{irr}}$ [19,28]

$$g_r(R) = g_r^{\text{irr}}(R) - \frac{m_p}{eR} d_z(\vec{R}_{\text{CM}}, R)\left(\frac{1}{M_a} - \frac{1}{M_b}\right) \tag{9}$$

$$g_r(R) = g_v^{\text{irr}}(R) - \frac{m_p}{e}\frac{dd_z(\vec{R}_{\text{CM}}, R)}{\partial R}\left(\frac{1}{M_a} - \frac{1}{M_b}\right) \tag{10}$$

in which the sign of the dipolar moment is chosen to be $d_z < 0$ for a molecule of polarity $+AB-$ and with the z-axis pointing from A to B. A detailed expression for this irreducible non-adiabatic contribution to the rotational g factor has been derived [29]

$$g_r^{\text{irr}}(R) = \frac{1}{2}\left(g_r^A(R) + g_r^B(R)\right) \tag{11}$$

in which

$$
g_r^{A|B}(R) = \frac{m_p}{\mu} Z_{b|a} + \frac{m_p}{m_e} \frac{1}{\mu R^2} \left\{ \sum_{n \neq 0} \left(\frac{|\langle \Psi_0(\{\vec{r}_i\}, R)| \sum_i l_{i,x}(\vec{R}_{a|b})|\Psi_n(\{\vec{r}_i\}, R)\rangle|^2}{E_0^{BO}(R) - E_n^{BO}(R)} \right. \right.
$$
$$
\left. \left. + \frac{|\langle \Psi_0(\{\vec{r}_i\}, R)| \sum_i l_{i,y}(\vec{R}_{a|b})|\Psi_n(\{\vec{r}_i\}, R)\rangle|^2}{E_0^{BO}(R) - E_n^{BO}(R)} \right) \right\} \tag{12}
$$

A related function called $R_{b|a}^{(n)} = (\mu/m_p)g_r^{A|B}$ was previously introduced [30].

For a molecular ion with charge number Q a transformation between isotopic variants becomes complicated in that the g factors are related directly to the electric dipolar moment and irreducible quantities for only one particular isotopic variant taken as standard; for this species these factors become partitioned into contributions for atomic centres A and B separately. For another isotopic variant the same parameters independent of mass are still applicable, but an extra term must be taken into account to obtain the g factor and electric dipolar moment of that variant [19]. The effective atomic mass of each isotopic variant other than that taken as standard includes another term [19]. In this way the relations between rotational and vibrational g factors and d_z and its derivative, equations (9) and (10), are maintained as for neutral molecules. Apart from the qualification mentioned below, each of these formulae applies individually to each particular isotopic variant, but, because the electric dipolar moment, referred to the centre of molecular mass of each variant, varies from one cationic variant to another because the dipolar moment depends upon the origin of coordinates, the coefficients in the radial function apply rigorously to only the standard isotopic species; for any isotopic variant the extra term is required to yield the correct value of either g factor from the value for that standard species [19].

Although the relation between the vibrational g factor and the derivative of electric dipolar moment, equation (10), is formally equivalent to the relation between the rotational g factor and this dipolar moment, equation (9), there arises an important distinction. The derivative of the electrical dipolar moment involves the linear response of the ground-state wave function and thus a non-adiabatic expression for a sum over excited states similar to electronic contributions to the g factors. The vibrational g factor can hence not be partitioned in the same as was the rotational g factor into a contribution that depends only on the ground-state wave function and 'irreducible non-adiabatic' contribution. Nevertheless $g_v^{irr}(R)$ is treated as such. A detailed expression for $g_v^{irr}(R)$ in terms of quantum-mechanical operators and a sum over excited states, similar to equations (11) and (12), is not yet reported.

2.2. The adiabatic correction

The adiabatic correction to the Born–Oppenheimer potential energy for a diatomic molecule A–B is simply given by the sum of the expectation values of the nuclear

kinetic energy operators [20,21]:

$$V'(R) = \frac{1}{M_A} \Delta U^A(R) + \frac{1}{M_B} \Delta U^B(R) \tag{13}$$

in which ($K=A$ or $K=B$)

$$\frac{1}{M_K} \Delta U^K(R) = \langle \Psi_0(\{\vec{r}_i\}, R)| - \frac{1}{2M_K} \Delta_K |\Psi_0(\{\vec{r}_i\}, R)\rangle. \tag{14}$$

By calculating $\Delta U^A(R)$ and $\Delta U^B(R)$ separately, we can straightforwardly calculate the total adiabatic correction $V'(R)$ for any isotopes of A and B. The adiabatic corrections are calculated by numerical differentiation of the multi-configurational self-consistent field (MCSCF) wave functions calculated with Dalton [23]. The numerical differentiation was performed with the Westa program developed 1986 by Ågren, Flores-Riveros and Jensen [22].

3. COMPUTATIONAL DETAILS

Both the electronic energy and the electronic contributions to the rotational and vibrational g factors, dipolar moment and derivative of the dipolar moment were calculated with full CI wave functions using the aug-cc-pVTZ basis set of Dunning and co-workers [31,32]. In the calculation of the rotational g factor we used rotational London orbitals [27,33]. In the calculation of the adiabatic correction to the potential energy surface we used an MCSCF wavefunction [34] of the complete-active-space type (CASSCF) [35] with two electrons in nine orbitals (5σ and 2π orbitals) included in the active space and using the aug-cc-pVQZ basis set. This model was verified for the iso-electronic H_2 molecule, for which we found that the differences to the reference values by Kołos and Wolniewicz [36] were up to the order of 0.5 cm^{-1}. It was also verified that the reported digits do not include any errors because of the numerical differentiation. All calculations were performed with local development versions of Dalton [23] and Westa [22]. In Table 1 and Figs 1 and 2 we present calculated values of the total electronic energy E_0^{BO} and of rotational and vibrational g factors as a function of internuclear distance R from nearly a putative united atom to barely interacting He and H atoms far apart. Each g factor comprises two contributions, one from nuclei, equation (7), that depends on only atomic numbers and masses and that has hence for ^{4}He^{1}H$^+$ the same value 0.8997 at all internuclear distances, and another from electrons that is related formally to non-adiabatic effects of either type. For g_v the total value at a particular R is just the sum of an electronic contribution, equation (3), that is invariably negative, and the positive nuclear contribution; the net result is either positive or negative depending on the relative magnitudes. For g_r, equation (4), the same positive nuclear contribution sums with a diamagnetic term, equation (6), that is invariably positive, and a paramagnetic term, equation (5), that is

Table 1. Calculated properties of ^{4}He^{1}H$^+$ in its electronic ground state $X\,^1\Sigma^+$ as a function of internuclear distance R – electronic energy, vibrational g factor, diamagnetic and paramagnetic electronic contributions to rotational g factor, and total molecular rotational g factor

$R\,10^{-10}$ m	Energy/hartree	g_v	g_r^{dia}	g_r^{para}	g_r
0.3	-2.2315269416	0.6255	0.0023	-0.0328	0.8692
0.4	-2.6867512113	0.6489	0.0001	-0.0321	0.8676
0.5	-2.8713081448	0.6687	0.0002	-0.0336	0.8663
0.6	-2.9456497493	0.6814	0.0005	-0.0371	0.8630
0.7	-2.9713464311	0.6869	0.0008	-0.0416	0.8588
0.77438	-2.9753915000	0.6867	0.0010	-0.0451	0.8556
0.8	-2.9750955024	0.6858	0.0011	-0.0462	0.8545
0.9	-2.9692499440	0.6792	0.0011	-0.0506	0.8501
1.0	-2.9597610664	0.6683	0.0010	-0.0549	0.8458
1.1	-2.9495466617	0.6552	0.0009	-0.0590	0.8415
1.2	-2.9399959858	0.6431	0.0008	-0.0630	0.8375
1.3	-2.9316980164	0.6357	0.0009	-0.0669	0.8336
1.4	-2.9248160702	0.6354	0.0009	-0.0707	0.8298
1.5	-2.9192916304	0.6429	0.0009	-0.0743	0.8263
1.6	-2.9149610967	0.6568	0.0009	-0.0777	0.8229
1.7	-2.9116242596	0.6746	0.0009	-0.0807	0.8198
1.8	-2.9090833625	0.6938	0.0008	-0.0835	0.8170
1.9	-2.9071628083	0.7123	0.0007	-0.0859	0.8144
2.0	-2.9057163342	0.7288	0.0006	-0.0880	0.8123
2.25	-2.9034704823	0.7590	0.0004	-0.0919	0.8081
2.5	-2.9023290253	0.7758	0.0003	-0.0945	0.8054
3.0	-2.9013546908	0.7894	0.0002	-0.0975	0.8024
4.0	-2.9008220843	0.7958	0.0002	-0.0998	0.8001
5.0	-2.9006867790	0.7976	0.0002	-0.1006	0.7993
10.0	-2.9006033488	0.7991	0.0001	-0.1013	0.7985

invariably negative. For ^{4}He^{1}H$^+$ net values of g_r are invariably positive, but another molecular species might have a negative or positive value.

Equations (9) and (11) indicate how the auxiliary radial function for the rotational factor g_r becomes separable into contributions from atomic centres of types A and B. An analogous separation is practicable for both the vibrational g factor and the total adiabatic corrections; for the latter quantity this separation is effected in the original quantum-chemical calculations. Accordingly we express these calculated values of rotational and vibrational g factors, presented in Table 1, and adiabatic corrections, presented in Table 3, of ^{4}He^{1}H$^+$ to generate coefficients of radial functions for atomic centres of either type, He or H. The most useful variable for these functions is z, defined in terms of instantaneous R and equilibrium R_e internuclear distances as

$$z = 2\frac{R - R_e}{R + R_e} \tag{15}$$
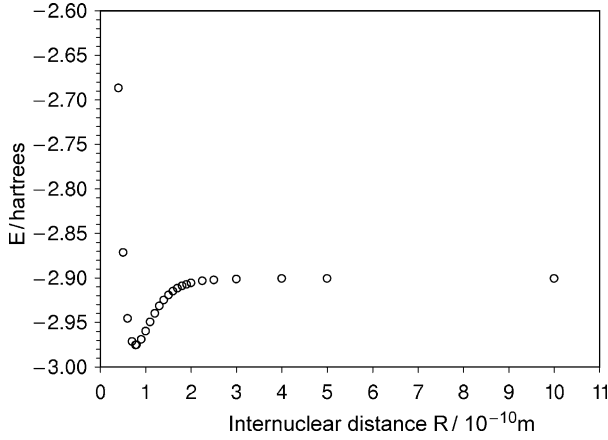
Fig. 1. Energy of ^{4}He^{1}H$^+$ as a function of internuclear distance R; circles denote points from quantum-chemical calculations.

We have for adiabatic effects [26]

$$\frac{U_{ad}(R)}{hc} \rightarrow \frac{V'(z)}{hc} = m_e \left(\frac{1}{M_{He}} \sum_{j=1} u_j^{He} z^j + \frac{1}{M_H} \sum_{j=1} u_j^H z^j \right) \qquad (16)$$

for non-adiabatic rotational effects [26]

$$\frac{m_e}{m_p} g_r(R) \rightarrow \frac{m_e}{m_p} g_r(z) = m_e \left(\frac{1}{M_{He}} \sum_{j=0} t_j^{He} z^j + \frac{1}{M_H} \sum_{j=0} t_j^H z^j \right) \qquad (17)$$
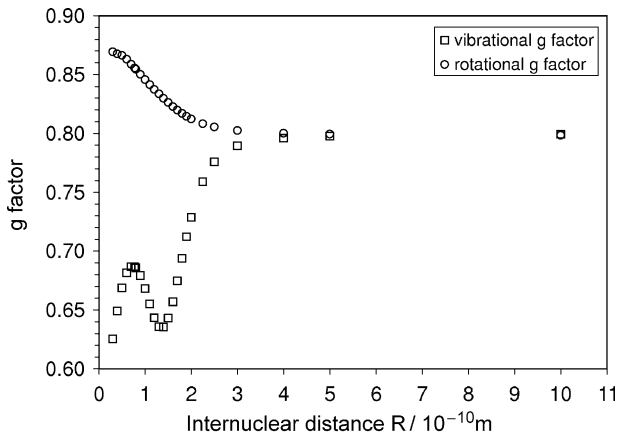
Fig. 2. Rotational and vibrational g factors of ^{4}He^{1}H$^+$ in electronic ground state $X\,^1\Sigma^+$ as a function of internuclear distance R; points from quantum-chemical calculations ($\circ$ for $g_r(R)$ and $\square$ for $g_v(R)$).

Table 2. Calculated electric dipolar moment d_z and derivative of dipolar moment $\mathrm{d}d_z/\mathrm{d}R$, both in atomic units, of $^4\mathrm{He}^1\mathrm{H}^+$ in electronic ground state $X\,^1\Sigma^+$ as a function of internuclear distance R. The origin of the coordinate system is located at the centre of atomic mass.

$R\ 10^{-10}$ m	d_z a.u.	$\mathrm{d}d_z/\mathrm{d}R$ a.u. 10^{10} m^{-1}
0.3	0.135301	0.722545
0.4	0.217406	0.918361
0.5	0.318590	1.102836
0.6	0.437390	1.269955
0.7	0.571942	1.418063
0.77438	0.681154	1.517001
0.8	0.720432	1.548979
0.9	0.881192	1.663442
1.0	1.052533	1.760218
1.1	1.232545	1.836251
1.2	1.418970	1.887935
1.3	1.609252	1.913332
1.4	1.800798	1.913702
1.5	1.991305	1.893508
1.6	2.179027	1.859144
1.7	2.362884	1.817262
1.8	2.542417	1.773467
1.9	2.717648	1.731718
2.0	2.888907	1.694312
2.25	3.303014	1.624030
2.5	3.703300	1.582100
3.0	4.483148	1.543951
4.0	6.013826	1.522514
5.0	7.532529	1.515933
10.0	15.092297	1.510389

and for non-adiabatic vibrational effects [26]

$$\frac{m_\mathrm{e}}{m_\mathrm{p}}g_v(R) \rightarrow \frac{m_\mathrm{e}}{m_\mathrm{p}}g_v(z) = m_\mathrm{e}\left(\frac{1}{M_\mathrm{He}}\sum_{j=0}s_j^\mathrm{He}z^j + \frac{1}{M_\mathrm{H}}\sum_{j=0}s_j^\mathrm{H}z^j\right) \qquad (18)$$

The coefficients of z^j, s_j^He and s_j^H for the vibrational factor g_v, t_j^He and t_j^H for the rotational factor g_r, and u_j^He and u_j^H for adiabatic corrections, are obtained from fitting corresponding data in Tables 1–3. The resulting values of coefficients are presented in Table 4, and they reproduce satisfactorily the computational results within the likely precision for internuclear distances over the entire specified range.

4. RESULTS AND DISCUSSION

4.1. Electronic structure calculations

The most striking features of the radial function for the vibrational g factor, $g_v(R)$, are a minimum at an internuclear distance of about 1.4×10^{-10} m and a maximum

Table 3. Calculated adiabatic corrections for He and H, and total adiabatic correction for ^{4}He^{1}H$^+$ according to equation (19)

R 10^{-10} m	ΔU^{He} 10^2 u m^{-1}	ΔU^{H} 10^2 u m^{-1}	$V'(R)$ 10^2 m^{-1}
0.3	357.53	58.81	147.68
0.4	345.30	43.68	129.61
0.5	338.95	32.73	117.16
0.6	336.66	24.88	108.80
0.7	337.04	19.17	103.23
0.77438	338.43	15.89	100.32
0.8	339.06	14.91	99.51
0.9	342.08	11.66	97.04
1.0	345.65	9.15	95.43
1.1	349.40	7.18	94.42
1.2	353.07	5.63	93.79
1.3	356.42	4.39	93.40
1.4	359.33	3.39	93.14
1.5	361.74	2.60	92.95
1.6	363.64	1.96	92.79
1.7	365.11	1.45	92.66
1.8	366.22	1.06	92.54
1.9	367.04	0.76	92.46
2.0	367.65	0.54	92.39
2.25	368.58	0.23	92.31
2.5	369.03	0.09	92.29
3.0	369.41	0.02	92.31
4.0	369.61	0.00	92.35
5.0	369.67	0.00	92.36
10.0	369.70	0.00	92.36

at an internuclear distance of about 0.7×10^{-10} m (Fig. 2). We note, furthermore, that the derivative of the electric dipolar moment, dd_z/dR, has a maximum at about the same internuclear distance as that minimum in the vibrational g factor (Fig. 3). From equation (10) we discern that this condition implies that the maximum in the vibrational g factor at about 0.7×10^{-10} m is due to g_v^{irr} whereas the minimum at about 1.4×10^{-10} m must have a common origin with a maximum in the dipolar gradient at the same internuclear distance.

We learn about the origin of these extrema through an expression for the sum over excited states for the electronic contribution to the vibrational g factor in equation (3). For that purpose we calculate the excitation energies, $E_n^{\text{BO}}(R) - E_0^{\text{BO}}(R)$, of excited states of least energy but the same symmetry as the ground state and the corresponding transition moments

$$\langle \Psi_0(\{\vec{r}_i\}, R) | \left\{ \frac{\partial}{\partial R} | \Psi_n(\{\vec{r}_i\}, R) \rangle \right\}.$$

Excitation energies are readily obtained as poles of a polarization propagator [37–40], whereas the transition moments are known as first-order non-adiabatic

Table 4. Fitted coefficients of z^j in the radial functions for vibrational (s_j) and rotational (t_j) g factors and adiabatic corrections (u_j) of $^4\mathrm{He}^1\mathrm{H}^+$ in its electronic ground state $X^1\Sigma^+$

j	s_j^{He}	s_r^{H}	t_j^{He}	t_j^{H}	$u_j^{\mathrm{He}}\ 10^6\,\mathrm{m}^{-1}$	$u_j^{\mathrm{H}}\ 10^6\,\mathrm{m}^{-1}$
0	0.10804	0.82887	-0.06000	0.87112	61.69249	2.89692
1	-1.00630	0.21951	-0.56414	0.10765	3.20200	-5.61943
2	-1.00294	0.23343	-0.14567	0.02173	7.72925	3.19362
3	-1.07478	0.26823	-0.04424	0.01772	1.29965	-0.24166
4	0.28861	-0.06439	-0.11731	-0.00518	-1.81693	-0.23783
5	1.79498	-0.42044	0.40975	-0.10477	-16.78919	-2.60926
6	-5.31950	1.23250	0.47226	-0.02612	4.92581	3.98440
7	-1.36709	0.32900	-0.61852	0.14400	19.19119	2.29043
8	12.15919	-2.82900	-0.21459	0.03022	-15.70526	-7.17792
9	-6.49368	1.52457	0.38251	-0.08647	3.49290	4.42733
10	-6.77346	1.58536	-0.10033	0.02491	0	-0.87705
11	7.42127	-1.75617	0	0	0	0
12	-1.94495	0.46452	0	0	0	0

coupling matrix elements (NACME) of which the calculation is also implemented in the Dalton program [41].

In Fig. 4 we present the energies and matrix elements for the first three excited states and in Fig. 5 we show the contributions of the five lowest excited states to the electronic contribution of the vibrational g factor, equation (3). The terms with $n = 1, 2, 3$ in equation (3) are displayed with hollow symbols, whereas the solid symbols and lines are the result of summation over n from 1 to 2, from 1 to 3, from 1 to 5 and all n in equation (3). According to Fig. 4 the energy of the first three excited states exhibits no atypical behaviour, but that the NACME to the first
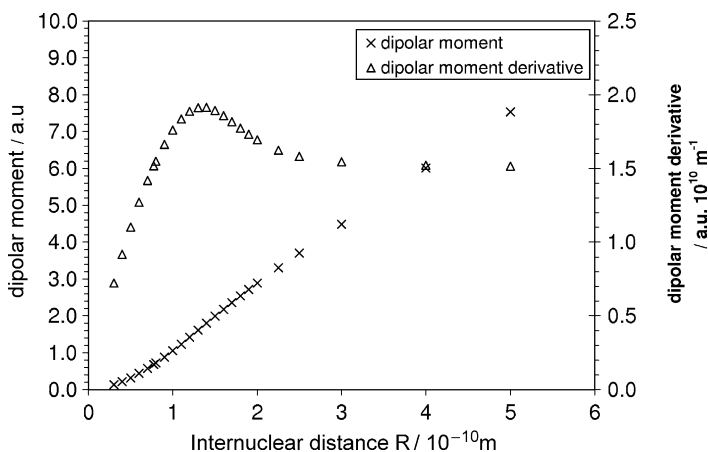
Fig. 3. Electric dipolar moment d_z and derivative of dipolar moment $\mathrm{d}d_z/\mathrm{d}R$ of $^4\mathrm{He}^1\mathrm{H}^+$ in electronic ground state $X^1\Sigma^+$ as a function of internuclear distance R; points from quantum-chemical calculations ($\times$ for d_z and $\triangle$ for $\mathrm{d}d_z/\mathrm{d}R$). The origin of the coordinate system is located at the centre of atomic mass.
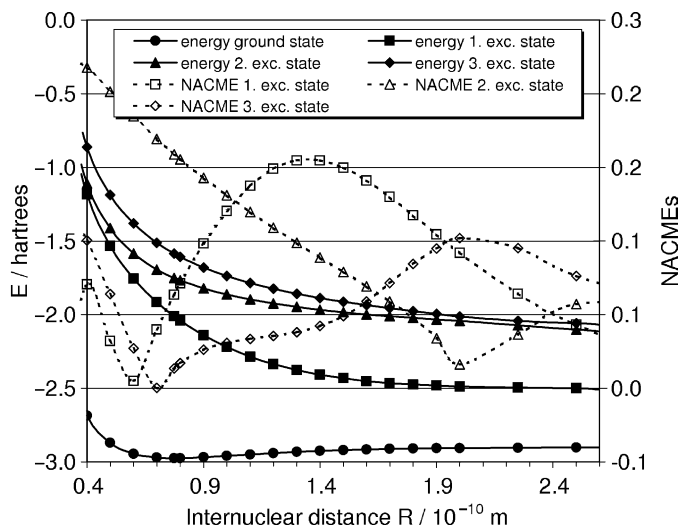
Fig. 4. Calculated energies (solid lines with filled symbols) and first-order non-adiabatic coupling matrix elements (NACME) (dotted lines with empty symbols) of the first three excited states in ^{4}He^{1}H$^+$ as a function of internuclear distance R.

excited state has a clear maximum at an internuclear distance of 1.4×10^{-10} m and a minimum at about 0.6×10^{-10} m. The NACME to the second and third excited states show disparate behaviour: the first falls steeply and goes through a minimum at about 2.0×10^{-10} m, whereas the latter has a minimum at about 0.7×10^{-10} m, increases to a maximum at 2.0×10^{-10} m and then decays slowly.
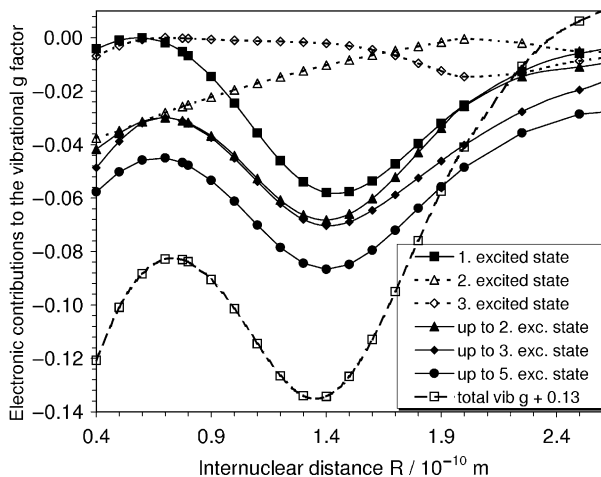
Fig. 5. Contributions from the lowest five excited states to the electronic contribution to the vibrational g factor, equation (3), of ^{4}He^{1}H$^+$ as a function of internuclear distance R. Dotted lines and empty symbols are contributions from a particular excited state whereas solid lines and symbols are the sum of the contributions up to and including the given excited state. The total electronic contribution (dashed line with □) is shifted by 1.3.

According to Fig. 5 the maximum and minimum in the NACME to the first excited state produce a minimum and maximum in the corresponding contribution to the electronic contribution to the vibrational g factor. The extrema are at the same internuclear distances and have positions near the extrema in the total electronic contribution to $g_v(R)$, but are not as steep. The contributions from the second, third, and up to the fifth excited states modify slightly the position and the form of the extrema but introduce no fundamental modification. We, therefore, conclude that the extrema in the vibrational g factor reflect extrema in the first-order NACME to the first excited state, and not in the energy of the excited state. The exact position of the minimum in the vibrational g factor is, however, influenced by more highly excited states.

Figure 2 shows directly that both rotational and vibrational g factors of $^4\mathrm{He}^1\mathrm{H}^+$ approach a common value of 0.8 as R becomes large. This behaviour is characteristic of $^4\mathrm{He}^1\mathrm{H}^+$, as for both neutral diatomic molecular species $^1\mathrm{H}_2$ [18] or $^7\mathrm{Li}^1\mathrm{H}$ for which we have undertaken analogous calculations the asymptotic value of both g_r and g_v is zero. For $^3\mathrm{He}^2\mathrm{H}^+$ the corresponding value of g_r at $R = 10^{-9}$ m is 0.3.

The adiabatic corrections for the individual atomic centres He and H, listed as a function of R in Table 3, are combined in the final column of that table into a total correction according to this formula

$$\frac{V'(R)}{hc} = m_{\mathrm{e}} \left(\frac{\Delta U^{\mathrm{He}}(R)}{M_{\mathrm{He}}} + \frac{\Delta U^{\mathrm{H}}(R)}{M_{\mathrm{H}}} \right) \tag{19}$$

in which m_{e} is the electronic rest mass. The total adiabatic correction for $^4\mathrm{He}^1\mathrm{H}^+$ approaches the value for the helium atom that reflects a difference in electronic energy calculated with the reduced mass of that atom in terms of nucleus and electrons and with the centre of coordinates at the position of the nucleus, because HeH^+ in its electronic ground state $X\,^1\Sigma^+$ dissociates into a neutral helium atom and an ionized hydrogen atom or bare proton.

4.2. Preliminary analysis of spectral data

As an application of this implementation of computational spectrometry, we present preliminary results of analysis of frequencies of pure rotational and vibration–rotational transitions, from the literature, of HeH^+ in four isotopic variants formed from $^4\mathrm{He}$, $^3\mathrm{He}$, $^1\mathrm{H}$ and $^2\mathrm{H}$ in appropriate combinations. With the values of $s_j^{\mathrm{He}|\mathrm{H}}$, $t_j^{\mathrm{He}|\mathrm{H}}$ and $u_j^{\mathrm{He}|\mathrm{H}}$ in Table 4, we evaluated the auxiliary coefficients $Z_{k,l}$ in equation (2) and fitted available spectral data to obtain values of the Dunham coefficients $Y_{k,l}$. From $Y_{0,1}$ and $Y_{1,0}$, respectively, in equation (2) or equivalent quantities independent of nuclear mass, the equilibrium internuclear distance independent of nuclear mass has a value $R_e\ 10^{-10}$ m $= 0.7743424 \pm 0.0000020$, and the force coefficient has a value k_e N m$^{-1} = 491.536 \pm 0.022$. For comparison, corresponding values for H_2 from spectral analysis [18] are 0.7414144 ± 0.0000020 and 576.0854 ± 0.0090, respectively. The equilibrium distances for these two molecular species in which the binding involves in each

case only two electrons are hence almost identical, whereas the smaller force coefficient for HeH$^+$ likely reflects that its equilibrium binding energy is less than half that of H$_2$. From interpolation of the three, or five, points of least energy in Table 1 the corresponding value of R_e 10^{-10} m is 0.77843, or 0.77595, but these quantum-chemical computations are not intended for this purpose. Results from quantum-chemical calculations in Tables 1 and 2 will be applied in further analysis of spectra of HeH$^+$.

5. FINAL REMARKS AND CONCLUSIONS

Computational spectrometry can serve as a powerful adjunct in analysis of molecular spectra, especially in a challenging case such as HeH$^+$. Even for less esoteric diatomic molecules such as H$_2$ and LiH, the results of this approach are essential to allow an analyst to disentangle the effects of auxiliary terms in the effective Hamiltonian, equation (1), because of three auxiliary terms – rotational and vibrational g factors and adiabatic corrections – coefficients in only two such radial functions can, in general, be evaluated from data of only spectral frequencies of pure rotational and vibration–rotational transitions for samples without applied electric or magnetic field. In such circumstances these quantum-chemical calculations serve as a substitute for information from experiments involving applied fields, but they are able to generate satisfactorily accurate data for internuclear distance over a range much greater than has ever been derived from such experiments.

ACKNOWLEDGEMENTS

REFERENCES

[1] J. F. Ogilvie and J. Oddershede, *Adv. Quantum Chem.*, 2005, **48**, 253.
[2] S. Saupe, B. Meyer, M. H. Wappelhorst, W. Urban and A. G. Maki, *J. Mol. Spectrosc.*, 1996, **179**, 13.
[3] J. Oddershede, P. Jørgensen and N. H. F. Beebe, *J. Chem. Phys.*, 1975, **63**, 2996.
[4] J. Oddershede and E. N. Svendsen, *Chem. Phys.*, 1982, **64**, 359.
[5] S. P. A. Sauer, G. H. F. Diercksen and J. Oddershede, *Int. J. Quantum Chem.*, 1991, **39**, 667.
[6] M. J. Packer, S. P. A. Sauer and J. Oddershede, *J. Chem. Phys.*, 1994, **100**, 8969.
[7] E. K. Dalskov and S. P. A. Sauer, *J. Phys. Chem. A.*, 1998, **102**, 5269.
[8] J. Oddershede and J. R. Sabin, *Chem. Phys.*, 1988, **122**, 291.
[9] S. P. A. Sauer, V. Špirko and J. Oddershede, *Chem. Phys.*, 1991, **153**, 189.
[10] S. P. A. Sauer, J. Oddershede and J. Geertsen, *Mol. Phys.*, 1992, **76**, 445.

[11] S. P. A. Sauer, V. Špirko, I. Paidarová and J. Oddershede, *Chem. Phys.*, 1994, **184**, 1.

[12] S. P. A. Sauer, *Chem. Phys. Lett.*, 1996, **260**, 271.

[13] T. Enevoldsen, T. Rasmussen and S. P. A. Sauer, *J. Chem. Phys.*, 2001, **114**, 84.

[14] S. P. A. Sauer, *Adv. Quantum Chem.*, 2005, **48**, 469.

[15] J. F. Ogilvie, S.-L. Cheah, Y.-P. Lee and S. P. A. Sauer, *Theor. Chem. Acc.*, 2002, **108**, 85.

[16] S. P. A. Sauer and J. F. Ogilvie, *J. Phys. Chem.*, 1994, **98**, 8617.

[17] J. F. Ogilvie, J. Oddershede and S. P. A. Sauer, *Chem. Phys. Lett.*, 1994, **228**, 183.

[18] K. L. Bak, S. P. A. Sauer, J. Oddershede and J. F. Ogilvie, *Phys. Chem. Chem. Phys.*, DOI.10.1039/B500992H.

[19] R. M. Herman and J. F. Ogilvie, *Adv. Chem. Phys.*, 1998, **103**, 187.

[20] N. C. Handy and A. M. Lee, *Chem. Phys. Lett.*, 1996, **252**, 425.

[21] W. Kutzelnigg, *Mol. Phys.*, 1997, **90**, 909.

[22] H. Ågren, A. Flores-Riveros and H. J. Aa. Jensen, *Phys. Rev. A*, 1986, **34**, 4606.

[23] T. Helgaker, H. J. Aa. Jensen, P. Jørgensen, J. Olsen, K. Ruud, H. Ågren, A. A. Auer, K. L. Bak, V. Bakken, O. Christiansen, S. Coriani, P. Dahle, E. K. Dalskov, T. Enevoldsen, B. Fernandez, C. Hättig, A. Hald, K. Halkier, H. Heiberg, H. Hettema, D. Jonsson, S. Kirpekar, R. Kobayashi, H. Koch, K. V. Mikkelsen, P. Norman, M. J. Packer, T. B. Pedersen, T. A. Ruden, A. Sanchez, T. Saue, S. P. A. Sauer, B. Schimmelpfennig, K. O. Sylvester-Hvid, P. R. Taylor and O. Vahtras. DALTON, an electronic structure program, Release 1.2. http://www.kjemi.uio.no/software/dalton/dalton.html, 2001.

[24] J. F. Ogilvie, H. Uehara and K. Horiai, *Canad. J. Anal. Sci. Spectrosc.*, 1999, **44**, 141.

[25] J. F. Ogilvie, *The Vibrational and Rotational Spectrometry of Diatomic Molecules*, Academic Press, London, 1998.

[26] J. F. Ogilvie, J. Oddershede and S. P. A. Sauer, *Adv. Chem. Phys.*, 2000, **111**, 475.

[27] J. Gauss, K. Ruud and T. Helgaker, *J. Chem. Phys.*, 1996, **105**, 2804.

[28] E. Tiemann and J. F. Ogilvie, *J. Mol. Spectrosc.*, 1994, **165**, 377.

[29] S. P. A. Sauer, *Chem. Phys. Lett.*, 1998, **297**, 475.

[30] J. K. G. Watson, *J. Mol. Spectrosc.*, 1980, **80**, 411.

[31] T. H. Dunning Jr., *J. Chem. Phys.*, 1989, **90**, 1007.

[32] D. E. Woon and T. H. Dunning Jr., *J. Chem. Phys.*, 1993, **98**, 1358.

[33] T. Helgaker and P. Jørgensen, *J. Chem. Phys.*, 1991, **95**, 2595.

[34] T. Helgaker, P. Jørgensen and J. Olsen, *Molecular Electronic Structure Theory*, Wiley, Chichester, 2000.

[35] B. O. Roos, *Ab Initio* Methods in Quantum Chemistry – II, in *Advances in Chemical Physics* (ed. K. P. Lawley), Wiley, Chichester, 1987, pp. 399.

[36] W. Kołos and L. Wolniewicz, *J. Chem. Phys.*, 1964, **41**, 3663.

[37] J. Linderberg and Y. Öhrn, *Propagators in Quantum Chemistry*, Academic Press, London, 1973.

[38] P. Jørgensen and J. Simons, *Second Quantization-Based Methods in Quantum Chemistry*, Academic Press, New York, 1981.

[39] J. Olsen and P. Jørgensen, *J. Chem. Phys.*, 1985, **82**, 3235.

[40] J. Oddershede, P. Jørgensen and D. L. Yeager, *Comput. Phys. Rep.*, 1984, **2**, 33.

[41] K. L. Bak, P. Jørgensen, H. J. Aa. Jensen, J. Olsen and T. Helgaker, *J. Chem. Phys.*, 1992, **97**, 7573.

From the Orbital Implementation of the Kinetic Theory to the Polarization Propagator Method in the Study of Energy Deposition Problems

R. Cabrera-Trujillo,[1] S. A. Cruz[2] and J. Soullard[3]

[1]*Department of Physics, University of Florida, Gainesville, FL, 32611-8435, USA*
[2]*Departamento de Fisica, Universidad Autonoma Metropolitana, Iztapalapa, Apdo. Postal 55-534, 09340, Mexico, D. F., Mexico*
[3]*Instituto de Fisica, UNAM, Apdo. Postal 20-364, 01000, Mexico, D. F., Mexico*

Abstract

The energy deposited by swift atomic-ion projectiles when colliding with a given target material has been a topic of special scientific interest for the last century due to the variety of applications of ion beams in modern materials technology as well as in medical physics. In this work, we summarize our contributions in this field as a consequence of fruitful discussions and enlightening ideas put forward by one of the main protagonists in stopping power theory during the last three decades: Jens Oddershede. Our review, mainly motivated by Jens' work, evolves from the extension of the orbital implementation of the kinetic theory of stopping through the orbital local plasma approximation, its use in studies of orbital and total mean excitation energies for the study of atomic and molecular stopping until the advances on generalized oscillator strength and sum rules in the study of stopping cross sections. Finally, as a tribute to Jens' work on the orbital implementation of the kinetic theory of stopping, in this work we present new results on the use of the Thomas–Fermi–Dirac–Weizsäcker density functional for the calculation of orbital and total atomic mean excitation energies. The results are applied to free-atoms and and extension is done to confined atoms – taking Si as an example – whereby target pressure effects on stopping are derived. Hence, evidence of the far-yield of Jens' ideas is given.

Contents

1. FOREWORD

It is a pleasure and honor for us, who are friends, colleagues, and collaborators of Jens Oddershede, to offer this contribution in his honor on the occasion of his 60th birthday. One of Jens' major interests has been the study of energy deposition to a material target by swift projectiles. Particularly the applications of the response theory, the use of the kinetic theory of stopping to the description of the stopping cross section, and the study of the Bethe and Thomas–Reiche–Khun sum rules. Applications to molecular targets required the introduction of a simplified view of the system, thus the introduction of cores and bonds in the treatment of energy deposition was required. In this overview, we summarize our contributions motivated by Jens' work. Mostly, we are happy to take this opportunity to thank Jens for his help, inspiration, and friendship for all over these years.

2. INTRODUCTION

Few people have the ability to influence the field of their research, and Jens Oddershede is one of them. As a quantum chemist, he began in the 1970s to tackle fundamental problems within the response theory that later allowed him to implement it in the field of energy deposition. It will take a big part of this article to summarize all his contributions. It is our intention to celebrate his 60th birthday with a review of the consequences of his ideas in a concise way. *Tillykke med fødselsdagen*, Jens

3. THE ORBITAL IMPLEMENTATION OF THE KINETIC THEORY OF STOPPING AND ITS CONSEQUENCES

Stopping power theory has been developed during nearly nine decades after the pioneering work of outstanding scientists who – among others – contributed prominently also to the foundations of modern physics, to wit, Sir Ernest Rutherford and his work on alpha-particle scattering experiments [1], Niels Bohr and his fundamental contributions to the problem of charged particle penetration in matter [2–4] and Hans Bethe with his first quantum approach to the problem [5,6]. The problem, being of such a complex many-body nature, attracted – since then – the interest of other bright physicists like Felix Bloch [7], Ugo Fano [8],

Enrico Fermi [9], Jens Lindhard [10–12] and Oleg B. Firsov [13], all of whom contributed with different views and approaches to a better understanding on the mechanisms through which an ion loses energy while traversing matter. On the other hand, the advent of ion-beam accelerators made it possible to develop controlled experiments whereby the fundamental feedback between theory and experiment was enhanced. In general, three well-defined regions were recognized experimentally in the behavior of the electronic stopping cross section (S_e) as a function of projectile energy: the low, intermediate and high-energy regions. Before 1982 the theoretical treatment of stopping was largely focused to two main energy regions: the low-energy region, which considered the stopping process as a drag-force effect explained either as the collective response of the medium through its dielectric function (Lindhard–Scharff theory [10–12]) or as that due to a momentum exchange between projectile and target electrons (Firsov theory [13]). On the other hand, stopping in the high-energy region has been attributed to ionization processes ruled by the Bethe–Bloch theory, which properly accounts for the main contribution to the electronic stopping cross section (S_e) in that region. In the intermediate energy region more complex energy loss processes such as excitation, charge exchange and ionization compete and although some refinements were introduced to the low and intermediate region by Barkas to account for Z^3 effects [14], before 1982 there was not a satisfactory theory to properly account for all these processes which only recently have been tackled through sophisticated approaches [15–18].

As is usually the case, experimental evidence has been a guiding means to improve the theoretical approach to a particular problem and – as more refined stopping experiments were developed – the details of more subtle effects started appearing in the behavior of the energy loss of ions traversing matter. One of the first observed effects at low energies is the oscillation of the electronic stopping cross section of different ions (Z_1) traversing different target materials (Z_2) – the Z_1, Z_2 oscillation effect – which was definitely related with the electronic shell structure of both projectile and target within different implementations of low-energy stopping theory [19]. Another important effect on S_e evidenced by experiment – mainly at intermediate energies – is that due to chemical binding and physical-phase state of the target material [20–25]. With two different approaches: one for high and another for low-energy stopping, the challenge to theory was monumental and new ideas had to be put forward to explain the observed effects. It was first necessary to yield a theory which could establish a reasonable bridge between low and high-energy stopping.

In 1982, Peter Sigmund developed the kinetic theory of stopping (KT) [26], based on the binary encounter approximation, whereby the energy loss problem is treated through individual scattering events between projectile and target electrons. The KT accounts for the velocity distribution of scatterers in the target material (electrons), which is an important aspect to consider, so that when the projectile velocity becomes large enough the scatterers may be considered at rest and the Bethe stopping cross section is recovered. Otherwise the momentum distribution of target scatterers will noticeably affect the stopping dynamics. The development of the KT established a reasonable framework to bridge between the low and high-energy stopping regions, since it incorporates in an *ad hoc* manner

the characteristics of momentum transfer at low-energies and ionization processes at high-energies through the Bethe term. Although the KT lacks of a formal quantum basis to account for charge-exchange and excitation mechanisms, it may be considered as a physically appealing interpolating theory.

In dealing with the electronic stopping cross section of atoms and molecules for the simplest projectiles (protons), Jens Oddershede together with Jack Sabin recognized the important role of shell-wise contributions to stopping. Oddershede and Sabin proved that the KT accounts very well for atomic stopping, provided it is implemented on an orbital by orbital basis [27–31]. Within this scheme, the total electronic stopping cross section is expressed as

$$S_e(v) = \sum_k^{\text{shells}} S_{e,k}(v) \tag{1}$$

with $S_{e,k}(v)$ the orbital contribution to $S_e(v)$ for a projectile moving with velocity v, i.e.

$$S_{e,k}(v) = \frac{4\pi e^4 Z_1^2 Z_2}{mv^2} L_k(v) \tag{2}$$

with

$$L_k(v) = \pi \int_0^\infty \rho_k(v_2) v_2 \, dv_2 \int_{|v-v_2|}^{v+v_2} \frac{\omega_k}{Z_2} \ln\left(\frac{2mv'^2}{I_k}\right)\left[1 + \frac{v^2}{v'^2} - \frac{v_2^2}{v'^2}\right] dv' \tag{3}$$

the orbital stopping number. Z_1 and Z_2 are the projectile and target atomic numbers, respectively, and $\rho_k(v_2)$ is the target electron velocity distribution in orbital k such that

$$4\pi \int_0^\infty \rho_k(v_2) v_2^2 \, dv_2 = 1 \tag{4}$$

The orbital mean excitation energies, I_k, given in equation (3) are defined by requiring that the total mean excitation energy is written as

$$\ln I = \frac{1}{Z_2} \sum_k \omega_k \ln I_k \tag{5}$$

with ω_k the orbital weights

$$\omega_k = (n_k + n_k f_k)/2 \tag{6}$$

given in terms of the orbital occupation numbers n_k and total oscillator strengths $n_k f_k$ of all optical transitions from level k into the unoccupied states (both discrete and in the continuum) [27].

Equations (1)–(6) constitute a remarkable contribution by Oddershede–Sabin to the improvement of the KT in the analysis of atomic and molecular stopping. The partitioning in the stopping contributions from different atomic/molecular orbitals requires the fundamental assumption implied by equation (5) whereby

the total mean excitation energy is decomposed into orbital mean excitation energies I_k with the orbital weight factors ω_k derived from corresponding Hartree–Fock orbital oscillator strengths. Formally, the calculation of f_k requires an *ab initio* treatment of atomic/molecular orbitals which, even for small systems becomes intricate.

3.1. Atomic stopping

In the case of atomic stopping, the orbital implementation of the KT brought as a natural consequence the ability to calculate shell correction terms as [27,32]

$$C_k(v) = \omega_k \ln\left(\frac{2mv^2}{I_k}\right) - Z_2 L_k(v) \tag{7}$$

with the orbital stopping number and weight factors given by equations (3) and (6), respectively. Oddershede and Sabin made a thorough study for proton stopping in a wide range of target elements ($Z_2 \leq 36$) [33] yielding in general excellent predictions – relative to experiments in gaseous target materials – for the qualitative and quantitative behavior of proton stopping cross sections and shell corrections for the whole range of non-relativistic velocities. Their treatment was done on the basis of Hartree–Fock wavefunctions to generate the momentum distribution profiles of target electrons and using the orbital oscillator strengths f_k calculated by Inokuti *et al.* [34–36] to obtain the orbital weight factors ω_k necessary for the computation of orbital and total mean excitation energies according to equation (5). The relevance of this contribution stems on their use of a purely theoretical input – free of arbitrary parameters – using accurate atomic wavefunctions and oscillator strengths, hence constituting an important reference to calibrate alternative implementations of the KT.

3.1.1. Birth of the orbital local plasma approximation

One of the first consequences of the above ideas was the development of the Orbital Local Plasma Approximation (OLPA) by Meltzer *et al.* [37–39]. The main ingredients in the OLPA consist in approximating the orbital weight factors by the orbital occupation numbers and adapting the Lindhard–Scharff Local Plasma Approximation (LPA) [10–12] to an orbital scheme whereby the orbital mean excitation energy was originally defined as [37,38]

$$\ln I_k = \frac{1}{n_k} \int \rho_k(\mathbf{r})\ln\left[\gamma_k\left(\frac{4\pi e^2 \rho_k(\mathbf{r})}{m}\right)^{1/2}\right]d^3\mathbf{r} \tag{8}$$

where $\rho_k(\mathbf{r})$ is the local electronic density of orbital k and γ_k the corresponding scaling parameter as proposed in the LPA to account for polarization effects. In a more recent analysis on density decomposition options in the OLPA, Meltzer *et al.* [39] have refined their original OLPA treatment making a physically

more consistent evaluation of the plasma frequency as determined by the total electron density at the point of consideration. Accordingly, instead of equation (8), the recommended expression for the OLPA treatment of I_k is

$$\ln I_k = \frac{1}{n_k} \int \rho_k(\mathbf{r}) \ln \left[\gamma_k \left(\frac{4\pi e^2 \rho(r)}{m} \right)^{1/2} \right] d^3\mathbf{r} \qquad (9)$$

where $\rho(r)$ is the local total electron density obtained after taking the angular average of each orbital charge density. Without going too much into the details [25,37–39] we note here that equations (5) and (9) constitute the backbone of the OLPA for the computation of orbital and total mean excitation energies which, together with equations (1)–(4) render the stopping cross section. Noteworthy, the OLPA brings the stopping cross section expression as a functional of the density. This idea was certainly exploited by Meltzer *et al.* by constructing the orbital densities through the local-spin-density approximation to density functional theory (LSDA-DFT) with the aim to treat mean excitation energies for either atoms or extended systems, the latter being in the domain of DFT treatments. Using Kohn–Sham orbitals, the results for atomic systems [37,38] rendered very good agreement with tabulated results by Oddershede and Sabin [33]. Also, an important extension was done for the treatment of condensed matter targets, like ultra-thin solid films [40] with encouraging results to distinguish differences in proton stopping between bulk and first surface layers in the material. Indeed, differences in proton stopping between gas-phase and condensed-phase target materials may be deemed with this approach, as originally suggested by Oddershede and Sabin [33,41]. This set of studies clearly demonstrates the far-yield of the orbital implementation of the KT by Oddershede and Sabin, which is flexible enough to allow for alternative adaptations as is the case of the OLPA.

3.2. Molecular stopping

A major advantage of the orbital decomposition scheme of the KT is its ability to deal with orbital contributions to S_e from molecular targets. This virtue has been particularly useful to theoretically analyze [25,33,40,41] the origin of the experimentally observed chemical binding effects and physical phase-state effects in the stopping power of light ions in compounds in the gas or in the condensed phase [20–24].

The orbital calculation of the atomic stopping cross section (equation (1)) was generalized by Oddershede and Sabin [29,30] to the case of the molecular stopping cross section as

$$S_e^{\text{molecule}}(v) = \sum_i^{\text{cores}} S_i^{\text{cores}}(v) + \sum_j^{\text{bonds}} S_j^{\text{bonds}}(v) \qquad (10)$$

where explicit consideration is given now to the contributions from core and bond (CAB) orbitals. Accordingly, the total mean excitation energy I corresponding

to equation (5) was cast in terms of CAB contributions, i.e.,

$$\ln I = \frac{1}{N} \left[\sum_i^{\text{cores}} \omega_i \ln I_i^{\text{cores}} + \sum_j^{\text{bonds}} \omega_j \ln I_j^{\text{bonds}} \right] \tag{11}$$

where N is the total number of electrons and ω_i the corresponding orbital weight factors which satisfy the sum rule:

$$\sum_i^{\text{cores+bonds}} \omega_i = N \tag{12}$$

With these assumptions, Jens Oddershede and Jack Sabin brought to land the first firm theoretical basis for the treatment of CAB contributions to stopping from molecular targets. Indeed, equation (10) is the equivalent to a Bragg-like sum of molecular orbital contributions, as clearly discussed in one of their seminal papers [29]. The key aspect here is the consistency required in the calculation by introducing the appropriate molecular wavefunctions – obtained from an *ab initio* procedure – which properly describe the isotropic Compton profiles for molecular valence electrons (bonds) and the corresponding mean excitation energy calculated according to equation (11). The task was not simple, since it is not always possible to extract this information, except for small molecular systems, and recourse to experimental information was necessary. In spite of this, the ideas put forward on this aspect by Oddershede and Sabin once again paved the way for further developments.

3.2.1. Development of the OLPA/FSGO treatment of molecular stopping

The appealing results obtained by the above mentioned studies motivated us [25,42] to use simpler analytical representations for the molecular orbitals, which would allow to explore the predicting capability of the theory for other systems. To this end, we used localized molecular orbitals based on floating spherical gaussians (FSGO) proposed by Frost [43] in his *ab initio* studies of closed-shell molecules. The advantage in using the FSGO rests on the possibility to identify each core, bond and lone-pair doubly occupied orbital with a very simple minimal representation:

$$\Psi_i(\mathbf{r}, \mathbf{R}_i) = \left(\frac{2\alpha_i}{\pi} \right)^{3/4} e^{-\alpha_i(\mathbf{r}-\mathbf{R}_i)^2}, \tag{13}$$

where α_i is the square of the inverse of the orbital radius and $\mathbf{R}_i$ is the position vector of the orbital center. The value of these parameters were optimized through a self-consistent energy minimization procedure described by Frost [43]. We note at this stage that the FSGO are generated through a purely *ab initio* process and hence no *ad hoc* quantities are introduced.

A further simplification was introduced in Ref. [42] by performing the calculations equivalent to equations (2) and (3) in the frame of reference moving with

the projectile whereby S_e was cast as

$$S_e(v_1) = -\int f(\mathbf{v}_1 - \mathbf{v}') \frac{\mathbf{v}_1 \cdot \mathbf{v}'}{v_1 v'} S_0(v') \mathrm{d}^3 \mathbf{v}' \tag{14}$$

where $\mathbf{v}'$ is the velocity of target electrons relative to the projectile, $f(\mathbf{v}_1 - \mathbf{v}')$ is the target electron velocity distribution *in the laboratory frame* and $S_0(v')$ is the value for S_e when the scatterers are at rest, i.e., the Bethe term

$$S_0(v') = \frac{4\pi Z_1^2 Z_2 e^4}{mv'^2} \ln\left(\frac{2mv'^2}{I}\right) \tag{15}$$

Using equation (14) and assuming isotropic orbital velocity distributions $f_k(\mathbf{v}_1 - \mathbf{v}')$ the corresponding expression to equation (2) for the orbital contribution to the molecular stopping was obtained as

$$S_{e,k}(v_1) = \frac{4\pi^2 e^4 Z_1^2 \omega_k}{m} \int_{\beta_k}^{\infty} \ln\left[\frac{2mv'^2}{I_k}\right] \mathrm{d}v'$$
$$\times \int_0^{\pi} f_k\left(\sqrt{v_1^2 + v'^2 - 2v_1 v' \cos\theta}\right) \mathrm{d}(\sin^2\theta) \tag{16}$$

where I_k is the orbital mean excitation energy, ω_k the orbital population and $\beta_k = \sqrt{I_k/2m}$. The function $f_k(|\mathbf{v}_1 - \mathbf{v}'|)$ in equation (16) corresponds to the Fourier transform of the FSGO (equation (13)) and the total stopping being given by equation (1).

In these first studies, resort was done to the OLPA scheme to estimate I_k for the CAB contributions to the molecular mean ionization energy. By combining equations (8), (11), and (13) I_k was obtained using the scaling parameter $\gamma_k = 1$ yielding the following simple expression in terms of the orbital parameters [42]:

$$I_k = 2^{11/4} \pi^{-1/4} (e^2/2a_0) \omega_k^{1/2} e^{-3/4} \alpha_k^{3/4} \tag{17}$$

Equations (16) and (17) were then used to calculate the molecular orbital contributions to S_e and – just as Oddershede and Sabin did in their more accurate calculations – a table for the velocity-dependence of core, bond, and lone-pair contributions to S_e for protons was constructed [25,42]. These results together with equation (10) lead to the calculation of the proton stopping cross section in compound materials with chemical binding effects incorporated.

Using the so-obtained values for the various CAB contributions to S_e for protons [42] – as a sample calculation of the above procedure – we choose oxygen, for which Oddershede and Sabin do not report the O=O contribution. Figure 1 displays the velocity dependence of S_e for protons on atomic oxygen (continuous line) (one half of the stopping cross section of the O_2 molecule) as compared with the fit to a database of corresponding experimental results compiled by Berger (dashed line) [44,45]. General qualitative and quantitative agreement is observed between theory and experiment, with the theoretical values slightly greater ($\sim 15\%$) than the experimental ones. This behavior is consistent with the same
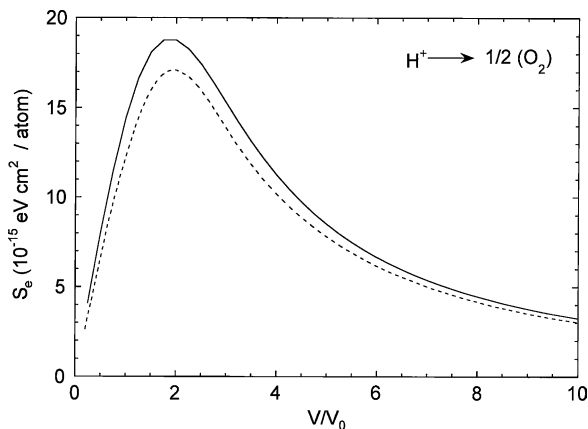
Fig. 1. Velocity dependence of the electronic stopping cross section for protons in atomic oxygen. (—) prediction by the OLPA-FSGO treatment [42]. (- - -) best fit curve to experimental data from Refs. [44,45].

type of calculations reported before for other systems [42]. Note, however, that Barkas and Bloch terms have not been accounted for in these and the following calculations, hence, care must be taken in making proper comparison with experiment in the velocity region below and around the maximum of the stopping curve.

As a further example, using the OLPA-FSGO orbital contributions (Table 3 in Ref. [42]) and those originally obtained by Oddershede and Sabin (OS) (Table 2 in Ref. [29]), we have calculated the corresponding curves for protons in propane. Figure 2 shows the results of this calculation for the OLPA-FSGO treatment (continuous line) as compared with the original OS treatment (dotted line).
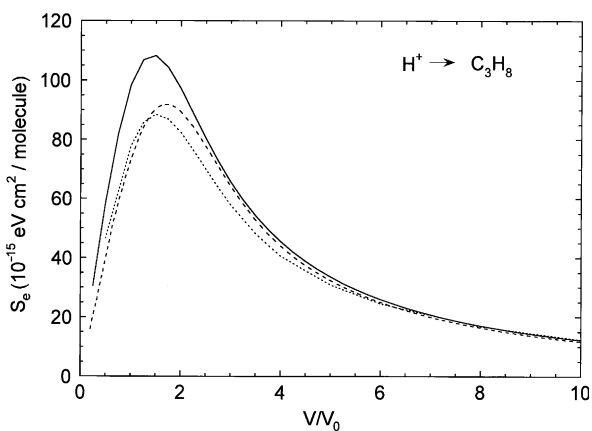
Fig. 2. Velocity dependence of the electronic stopping cross section for protons in propane. (—) prediction by the OLPA-FSGO treatment [42]. (· · ·) Oddershede and Sabin calculations [29]. (- - -) best fit curve to experimental data from Refs. [44,45].

The dashed curve in this figure corresponds to Berger's fit to experimental data [44,45]. As may be gathered from this figure, the OS results show a better agreement with experiment than the OLPA-FSGO ones, the latter being $\sim 20\%$ too high relative to experiment in the low and intermediate-energy region.

It is interesting to observe from this and the previous studies, that – although a fair qualitative agreement is observed between the OLPA-FSGO and the OS calculations – in general the former curves lie systematically above ($\sim 25\%$) those from OS in the low and intermediate-energy regions. This may be further recognized from Fig. 3, where we have plotted the velocity dependence of S_e for protons incident on propane and its derivates (propylene: C_3H_6 and allene: C_3H_4) as predicted by the OS and OLPA-FSGO treatments. The different description of the input wavefunctions and computation of total and orbital mean excitation energies (equation (8)) may be the cause for the quantitative differences between both types of calculations. In this connection, it has been recently shown [25] that the alternative choice given by equation (9) for the estimate of the orbital mean excitation energies yields OLPA-FSGO S_e values closer to those by OS, as indicated in Fig. 4 for the case of protons in methane. In this case, however, equation (9) cannot be reduced to a simple expression as equation (17) and must be done numerically since the angularly averaged total local electron density entering the argument of the logarithm in equation (9) now becomes

$$\rho(r) = 2\Big\langle \sum_{j,k} \Psi_j^*(\mathbf{r}, \mathbf{R}_j)\Psi_k(\mathbf{r}, \mathbf{R}_k)T_{jk} \Big\rangle_{\varOmega} \qquad (18)$$

with ψ_ν given by equation (13) and T_{jk} the elements of the inverse overlap matrix [25].

Since the formal settlement of the CAB approach was advanced by Sabin and Oddershede on firm theoretical grounds using the kinetic theory of stopping, its adequacy has been shown in reproducing with reasonable success the
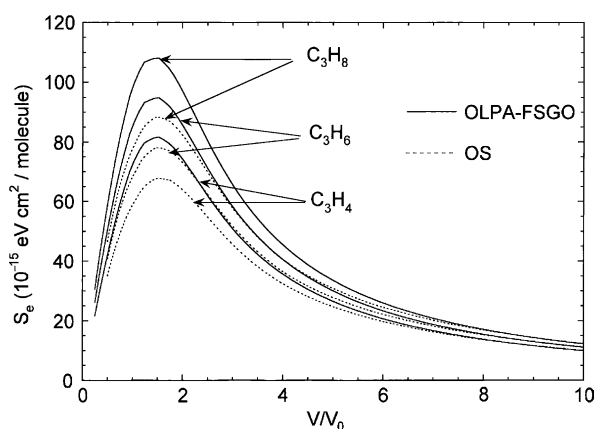
Fig. 3. Comparison between OLPA-FSGO and OS predictions for the velocity dependence of the electronic stopping cross section for protons in propane (C_3H_8), propylene (C_3H_6), and allene (C_3H_4).
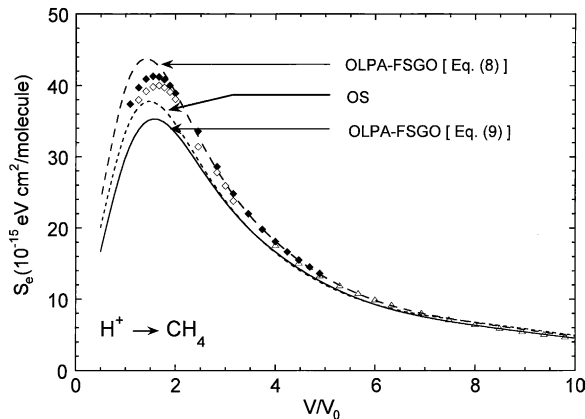
Fig. 4. Comparison of theoretical predictions for the electronic stopping cross section of protons in methane using the OLPA-FSGO treatment with I_k given by equation (8) (- - -) and using equation (9) (—). The dotted line corresponds to reference calculations by Oddershede and Sabin [29]. Symbols represent experimental values from Ref. [46] ($\blacklozenge$); Ref. [47] ($\Diamond$) and Ref. [48] ($\triangle$).

experimentally observed proton electronic stopping curves for various molecular targets in the gaseous phase. Furthermore, it has been shown that the use of approximate molecular wavefunctions such as the FSGO, together with the OLPA, provide a useful means to extend the predictions of the CAB approach-based theory to other molecular systems.

4. EXPLORING THE ORBITAL DECOMPOSITION OF THE KINETIC THEORY WITH STATISTICAL ATOMIC MODELS

The OLPA implementation to the KT follows closely the original ideas by Oddershede and Sabin and represents an important simplification to the various ingredients required in the original theory without significant loss of the relevant qualitative and quantitative predictions for proton stopping cross sections. In this section we use basic DFT through the Thomas–Fermi–Dirac–Weizsäcker (TFDW) energy-density functional [49–52] using known properties of the atomic orbital electron densities, originally put forward by Wang and Parr [49,50]; further extended by Hernández and Gázquez [51] and recently advanced for the study of free and confined many-electron atoms [52]. Our aim here is to show that even with a lower-level self-consistent DFT approach – as compared to the Kohn–Sham treatments – the OLPA predictions for proton stopping cross sections in atomic targets show good agreement with those obtained by Oddershede and Sabin [33] and Meltzer *et al.* [37–39] discussed before. Moreover, the TFDW treatment of confined many-electron atoms allows for the study of target pressure effects on S_e in the case of atomic targets, as a counterpart of what has been done for the molecular case using FSGO [25]. Here we shall concentrate mainly on proton stopping by free-atoms and some advances will be given for stopping by

atoms under pressure. In all cases, the orbital decomposition of the KT proposed by Oddershede and Sabin will play the central role in the evaluation of S_e, thus highlighting the importance of their contribution. For completeness, let us briefly summarize below the main aspects concerning the generation of orbital densities through the TFDW-DFT.

4.1. Generation of orbital densities for free and confined atoms through the TFDW-DFT

Let us assume a many-electron atom enclosed within an infinitely hard spherical cavity of radius R and develop the method and calculations so that we may recover the free-atom case when $R \to \infty$. This procedure also allows to look at the evolution of its ground state energy as the cage volume shrinks as has been done elsewhere [25,53]. The TFDW energy-density functional for an atom enclosed within a spherical cavity of radius R is written as

$$E[\rho, R] = T[\rho, R] + V_{en}[\rho, R] + V_{ee}[\rho, R] \tag{19}$$

where $T[\rho, R]$ is the kinetic energy given here as the well-known first two terms of its gradient expansion [49–51,54]

$$T[\rho, R] = T_0[\rho, R] + \lambda T_W[\rho, R] \tag{20}$$

with

$$T_0[\rho, R] = \frac{3}{10}(3\pi^2)^{2/3} \int_\Gamma \rho^{5/3} \, d\tau \tag{21}$$

the free-electron gas kinetic energy [55,56], and

$$T_W[\rho, R] = \frac{1}{8} \int_\Gamma \frac{\nabla\rho \cdot \nabla\rho}{\rho} \, d\tau \tag{22}$$

the inhomogeneity correction introduced by Weizsäcker [57]. Γ indicates the domain of integration within the cavity volume. The factor λ in equation (20) has been established formally as $\lambda = 1/9$ arising from the second-order correction to the gradient expansion of the Thomas–Fermi kinetic energy [58]. However, other values for λ have been proposed empirically when equation (19) is optimized to yield energies close to their Hartree–Fock value [54,59]. In the present calculations we shall use $\lambda = 1/8$ which has been shown to yield optimum overall energy values [52]. For this reason, the functional described here will be referred to as TFD(1/8)W.

The electron–nuclear attraction energy $V_{en}[\rho, R]$ and electron–electron repulsion energy $V_{ee}[\rho, R]$ in equation (19) are given, respectively, as

$$V_{en}[\rho, R] = -Z \int_\Gamma \frac{\rho}{r} \, d\tau \tag{23}$$

with Z the nuclear charge and

$$V_{\text{ee}}[\rho, R] = \frac{1}{2} \int_\Gamma \rho\phi \, \mathrm{d}\tau + X[\rho, R] \tag{24}$$

where the first term is the classical Coulomb repulsion, with ϕ the electrostatic potential due to charge density ρ and the second term is the Dirac exchange-only energy [60] given as

$$X[\rho, R] = -\frac{3}{4}(3/\pi)^{1/3} \int_\Gamma \rho^{4/3} \, \mathrm{d}\tau \tag{25}$$

According to Wang and Parr, a variational optimization procedure for the energy functional given by equation (19) may be defined by an appropriate ansatz representation for the electron density $\rho(\xi_1, \ldots, \xi_n : r, R)$ where ξ_i are variational parameters such that

$$\frac{\partial E}{\partial \xi_i} = 0, \quad i = 1, \ldots, n \tag{26}$$

with the constriction

$$\int_\Gamma \rho \, \mathrm{d}\tau = N, \tag{27}$$

where N is the total number of electrons. In our case we shall deal only with neutral atoms ($N = Z$).

For the atomic density of the confined system we use

$$\rho(r, R) = \sum_k \rho_k(r, R, \xi_k) \tag{28}$$

where ρ_k is the density of orbital k given as

$$\rho_k(r, R, \xi_k) = N_k r^{2\nu_k - 2} e^{-2\xi_k r}(1 - r/R) \tag{29}$$

where ν_k the principal quantum number associated to orbital k, ξ_k a variational parameter and N_k the normalization factor such that

$$\int_0^R \rho_k(r, R, \xi_k)\mathrm{d}\tau = n_k \tag{30}$$

The multiplying factor in equation (29) is chosen so that the Dirichlet boundary condition is satisfied for each orbital density, i.e., $\rho_k(r = R) = 0$.

Given a confinement radius, R, the orbital density parameters ξ_k are allowed to evolve freely until the total energy given by equation (19) becomes a minimum subject to the normalization constraint indicated in equations (27) and (30). An auxiliary condition for the free-case ($R \to \infty$) is the fulfillment of the Virial

theorem [49,50]. The interested reader is kindly addressed to Ref. [52] for a detailed analysis.

4.2. The case of free atoms

We have applied the above procedure to a selected number of free atoms with $Z \leq 36$ not reported in Ref. [52]. Table 1 displays the optimized orbital parameters and total ground state energies as compared to corresponding Hartree–Fock estimates [61]. Note that for most of the systems, the TFD(1/8)W energies are systematically below the HF values by about 0.1% difference indicating a possible best value for the λ parameter close to $\lambda = 1/8$.

4.2.1. Calculation of OLPA-TFD(1/8)W orbital and total mean excitation energies

Using the obtained values of the orbital parameters contained in Table 1 and those reported in Ref. [52] for all atoms with $2 \leq Z_2 \leq 36$ we have calculated the corresponding orbital and total mean excitation energies using equations (5), (9), (28), and (29). Table 2 shows the results calculated here (TFDW) as compared to those by Oddershede and Sabin (OS) and Meltzer, Sabin, and Trickey (MST). In general, the 1s, 2s, 3s, and 3p orbital mean excitation energies obtained through the TFDW method are closer to the OS values as compared to the MST estimates. Major differences are observed for the 2p, 3d, 4s, and 4p orbitals, with the MST values closer to those by OS except for the 4s orbital for atoms from Zn to Kr.

For purposes of comparison with the other calculations, the set of calculated orbital mean excitation energies shown in Table 1 were grouped in shell-like contributions as suggested by Chen *et al.* [62], i.e.,

$$\ln I_s = \frac{1}{Z_S} \sum_i \omega_{iS} \ln I_{iS} \tag{31}$$

where S stands for shell K, L, M; Z_S is the number of electrons in shell-S and the sum is done over orbitals composing that shell with corresponding orbital population ω_S and mean orbital excitation energy I_{iS}.

Figure 5 shows the mean excitation energies of the K, L, and M shells as a function of atomic number obtained in this work (TFD(1/8)W) (solid circles) as compared to calculations by Oddershede and Sabin (OS) [33] (open squares) and the original OLPA method developed by MST [37,38] based on the LSDA-DFT (open diamonds). It seems clear from this figure that the predictions of the TFD-(1/8)W-based OLPA method for the shell (and orbital) mean excitation energies are in reasonable agreement with the other – more elaborate – calculations. We note that all the OLPA-based calculations use $\gamma_i = 1$.

Interestingly, the K-shell predictions of this work are overall in better agreement with the calculations by OS. This may be related with the adequate description of the TFD(1/8)W cusp density at the origin for the 1s orbital [52]. Yet, some quantitative discrepancy between this work and the others in the case

Table 1. Best orbital parameters ξ_k and total energies $E_{\text{TFD}(1/8)\text{W}}$ for the ground state of selected free atoms obtained through the TFD(1/8)W energy density functional

Atom	ξ_{1s}	ξ_{2s}	ξ_{2p}	ξ_{3s}	ξ_{3p}	ξ_{4s}	ξ_{3d}	ξ_{4p}	$-E_{\text{TFD}(1/8)\text{W}}$	$-E_{\text{HF}}$
C	5.57071	2.70341	1.23256						37.68	37.689
O	7.61733	4.06832	1.66998						75.28	74.809
F	8.6437	4.7712	1.86817						99.83	99.409
Na	10.7118	6.15307	2.47578	1.07516					161.67	161.858
Al	12.8044	7.46971	3.32896	1.57429	1.57831				241.79	241.877
P	14.9065	8.78573	4.18635	2.44164	1.71034				340.99	340.719
S	15.9625	9.4184	4.62600	2.93838	1.84711				398.09	397.505
Cl	17.0184	10.0609	5.06203	3.41489	2.00982				460.34	459.482
Sc	21.2703	12.5746	6.89391	2.12451	4.12047	1.69448	2.18517		763.98	759.736
Ti	22.3332	13.2109	7.34191	5.15813	3.73474	2.27649	1.34953		853.90	848.406
Cr	24.4656	14.4582	8.27156	3.58654	5.17946	1.29270	2.07146		1051.58	1043.355
Mn	25.5337	15.0478	8.75252	4.38297	5.42326	1.59037	2.33871		1159.40	1149.866
Co	27.6706	16.3119	9.68135	5.23572	6.12408	1.49034	2.61877		1393.58	1381.414
Ni	28.7401	16.9366	10.1505	5.83133	6.42687	1.46584	2.74813		1520.07	1506.871
Ga	31.9502	18.8269	11.5519	7.33281	7.42716	1.65382	3.27974	1.65448	1938.28	1923.260
As	34.0943	20.0710	12.5011	8.17960	8.11828	2.30744	3.82669	1.84567	2250.38	2234.238
Se	35.1671	20.6919	12.9777	8.58089	8.46897	2.73512	4.09702	1.95180	2416.57	2399.866
Br	36.2406	21.3169	13.4547	8.79710	8.87983	3.16591	4.36472	2.08233	2589.62	2572.441

The corresponding Hartree–Fock energies E_{HF} are shown from Ref. [61]. All quantities are given in atomic units.

Table 2. Orbital (I_k) and total (I) mean excitation energies (in eV) for atoms with $2 \leq Z \leq 36$ obtained in this work (TDFW) as compared with calculations from Ref. [33] (OS) and Refs. [37,38] (MST)

Atom	Source	I_{1s}	I_{2s}	I_{2p}	I_{3s}	I_{3p}	I_{4s}	I_{3d}	I_{4p}	I
He	TFDW	38.36								38.36
	OS	38.83								38.83
	MST	33.66								33.66
Li	TFDW	74.36	7.40							34.50
	OS	109.32	3.29							34.00
	MST	69.73	3.17							24.90
Be	TFDW	127.77	15.43							44.40
	OS	203.78	7.32							38.62
	MST	113.91	7.81							29.80
B	TFDW	171.12	17.08	37.72						50.30
	OS	320.21	16.33	11.55						50.22
	MST	164.39	12.14	8.07						31.70
C	TFDW	257.76	50.90	14.33						57.30
	OS	451.34	27.57	20.97						61.95
	MST	220.78	19.93	17.19						40.00
N	TFDW	336.32	74.73	21.20						66.90
	OS	590.00	41.24	32.68						76.79
	MST	283.07	21.82	27.59						50.20
O	TFDW	422.19	102.18	28.87						77.40
	OS	729.41	56.86	46.64						93.28
	MST	349.72	27.33	40.82						63.20
F	TFDW	514.78	132.91	37.28						88.60
	OS	861.33	74.04	62.86						111.31
	MST	421.58	32.80	54.78						76.90
Ne	TFDW	613.56	166.58	46.24						100.30
	OS	982.68	92.22	81.37						130.94
	MST	497.75	38.35	70.81						92.50

Na	TFDW	720.60	204.51	63.31	5.30			97.30
	OS	1110.36	119.24	124.41	2.46			123.14
	MST	577.82	47.12	93.51	2.98			84.00
Mg	TFDW	833.89	244.72	82.56	9.86			102.10
	OS	1243.15	151.05	169.86	4.45			120.74
	MST	661.87	56.77	118.75	6.08			85.20
Al	TFDW	953.13	287.09	104.06	15.02	15.10		109.70
	OS	1373.04	187.14	221.15	9.01	4.85		123.67
	MST	749.74	66.87	145.18	8.40	4.48		81.90
Si	TFDW	1078.10	331.50	127.69	25.30	16.10		117.20
	OS	1497.54	226.08	278.63	14.56	8.87		131.04
	MST	841.22	77.39	172.81	10.75	9.06		85.20
P	TFDW	1208.67	378.79	152.72	37.58	19.27		124.50
	OS	1618.33	266.84	342.50	21.30	13.71		140.34
	MST	936.24	88.56	201.65	13.15	14.24		90.70
S	TFDW	1344.30	427.11	180.57	52.85	23.26		132.80
	OS	1733.73	308.23	412.71	29.40	19.37		151.26
	MST	1034.70	100.29	231.89	15.57	20.06		97.40
Cl	TFDW	1485.02	477.82	209.83	69.46	28.34		141.80
	OS	1844.43	349.09	489.36	38.91	25.76		162.87
	MST	1136.50	112.49	263.31	17.99	26.46		105.00
Ar	TFDW	1629.91	530.26	240.19	87.62	33.92		151.10
	OS	1948.72	388.29	572.56	49.93	32.95		175.35
	MST	1241.21	125.13	295.87	20.53	33.17		113.00
K	TFDW	1781.80	585.20	274.80	103.30	45.70	5.30	150.60
	OS	2055.32	429.39	662.36	60.43	48.78	1.60	168.20
	MST	1349.55	138.35	329.70	23.95	42.14	2.27	106.40
Ca	TFDW	1937.50	641.30	310.80	118.30	58.90	9.30	155.70
	OS	2161.01	472.33	759.01	72.49	64.83	2.70	163.52
	MST	1460.60	151.92	364.80	27.67	50.69	4.35	105.40

Table 2. (*continued*)

Atom	Source	I_{1s}	I_{2s}	I_{2p}	I_{3s}	I_{3p}	I_{4s}	I_{3d}	I_{4p}	I
Sc	TFDW	2098.20	698.40	350.10	32.80	102.40	11.80	34.50		161.50
	OS	2262.31	519.23	847.49	82.66	77.32	3.15	42.69		171.63
	MST	1574.70	165.93	401.10	30.84	57.64	4.91	13.04		105.60
Ti	TFDW	2262.60	758.40	388.30	148.10	89.90	22.70	12.75		168.60
	OS	2433.00	582.70	933.14	91.65	90.43	3.51	56.31		182.05
	MST	1691.70	180.34	438.50	33.67	62.95	3.52	19.25		103.50
V	TFDW	2431.90	819.20	429.60	161.90	107.20	14.50	28.80		176.90
	OS	2539.60	625.00	1012.46	102.22	103.49	3.79	69.43		191.70
	MST	1811.50	195.11	476.86	36.84	69.68	3.76	27.39		108.60
Cr	TFDW	2605.50	883.30	472.30	87.00	154.90	5.97	32.80		180.30
	OS	2652.59	692.84	1081.66	109.28	112.68	3.23	65.38		211.19
	MST	1934.10	210.25	516.23	40.06	76.49	4.00	36.22		125.90
Mn	TFDW	2782.90	945.90	517.50	122.30	169.80	10.70	41.60		187.70
	OS	2811.39	746.73	1159.55	12.96	129.90	4.57	99.38		215.75
	MST	2059.20	225.75	556.50	43.62	84.67	6.49	52.52		130.40
Fe	TFDW	2965.30	1015.90	561.50	120.70	195.60	9.50	48.90		193.60
	OS	2881.38	792.34	1224.75	138.00	140.53	4.92	113.89		226.42
	MST	2187.10	241.68	598.30	46.77	91.18	5.83	58.95		139.60
Co	TFDW	3151.00	1081.90	610.00	166.80	210.10	9.10	53.20		200.60
	OS	3023.68	875.16	1263.85	148.13	153.46	5.17	132.33		239.56
	MST	2317.60	258.17	641.12	49.97	97.49	4.76	65.99		151.20
Ni	TFDW	3341.00	1151.80	658.70	199.10	229.00	8.70	59.30		208.00
	OS	3227.87	906.75	1315.15	158.33	163.22	5.50	149.45		251.64
	MST	2450.80	274.81	684.71	53.29	104.37	4.62	75.09		160.80

Cu	TFDW	3534.50	1224.00	708.00	240.40	245.80	4.70	61.50		221.90
	OS	3382.26	1010.46	1336.95	165.20	165.69	5.52	144.29		268.50
	MST	2586.00	291.90	729.22	56.43	111.18	4.50	90.75		173.60
Zn	TFDW	3732.20	1297.60	759.60	263.90	270.50	8.20	72.70		224.50
	OS	3449.96	1089.16	1372.04	179.44	181.11	6.19	188.44		278.84
	MST	2723.80	309.15	774.23	60.54	120.25	7.79	105.64		174.40
Ga	TFDW	3933.70	1372.60	812.80	290.10	295.20	12.10	84.90	12.10	229.90
	OS	3642.55	1100.06	1416.84	206.97	199.95	9.67	240.33	4.84	283.42
	MST	2864.10	326.78	819.73	64.66	129.53	9.33	125.28	4.74	172.20
Ge	TFDW	4138.90	1449.20	867.30	312.30	322.30	18.30	97.90	14.40	236.70
	OS	3650.25	1185.35	1434.24	214.33	225.58	13.91	295.59	8.13	290.81
	MST	3006.50	344.69	866.93	68.85	139.49	10.89	147.10	8.77	175.80
As	TFDW	4421.70	1680.50	919.50	348.20	344.70	26.90	111.90	16.50	244.90
	OS	3852.74	1202.15	1484.64	237.50	249.84	18.60	353.88	11.79	300.39
	MST	3151.30	362.88	914.58	73.57	149.93	12.52	163.94	13.10	179.30
Se	TFDW	4559.90	1605.70	980.90	378.60	372.00	38.30	126.60	19.10	250.80
	OS	4022.64	1286.55	1541.54	264.87	277.32	24.07	415.85	15.21	310.38
	MST	3298.40	381.43	963.06	78.24	160.83	14.14	183.80	17.43	184.40
Br	TFDW	4775.93	1686.50	1039.40	397.80	402.80	51.30	142.00	22.40	258.50
	OS	4150.43	1282.35	1545.54	277.06	315.34	30.77	477.69	19.72	319.73
	MST	3447.60	400.28	1012.40	83.12	172.06	15.72	203.67	22.10	190.20
Kr	TFDW	4995.30	1768.40	1099.40	428.20	431.00	66.30	158.00	27.20	268.60
	OS	4229.23	1353.15	1588.54	290.12	344.29	38.22	564.77	23.81	329.59
	MST	3599.10	419.46	1062.50	88.12	183.57	17.27	224.99	27.07	196.70
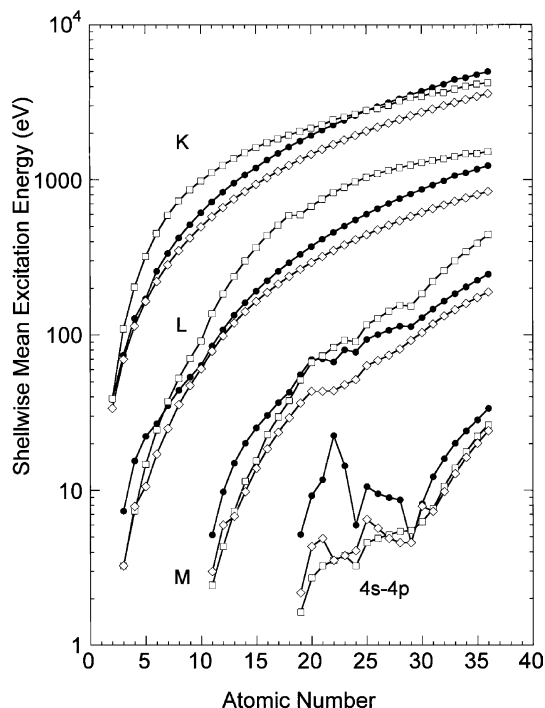
Fig. 5. Mean excitation energy (eV) of the K, L, M shells and 4s–4p orbitals for He through Kr obtained through equation (31) and I_k values from Table 2. (●) this work; (□) Oddershede and Sabin [33]; (◇): Meltzer *et al.* [37,38].

of the L-shell for Li, Be, and B and in general for the M-shell and the 4s–4p contributions remains still to be explained. In spite of this, the total mean excitation energies obtained through equation (5) show the right qualitative behavior and an improved quantitative trend over other OLPA-based methods as may be verified from Table 2 and Fig. 6, where we have plotted the corresponding values by OS and those by MST. Hence, we may deem the TFD(1/8)W method as promising means to treat, with some confidence, the orbital and total mean excitation energies.

4.2.2. Calculation of proton electronic stopping within the OLPA-TFD(1/8)W scheme

Using the orbital implementation of the kinetic theory together with the derived TFDW mean excitation energies obtained in the previous section, we have calculated the proton stopping as a function of projectile velocity for a selected number of elemental target materials in the gas phase (O, Ar, and Br) and in the condensed phase (Si, Ni, and Ga), as an example. Figures 7 and 8 show the results of this calculation (continuous curves) as compared with the predictions by OS [33] (solid circles) and with the corresponding empirical fit to experimental values
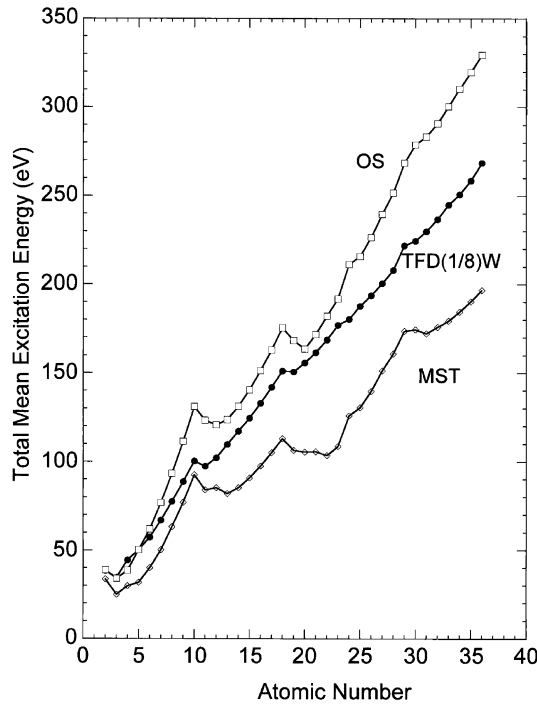
Fig. 6. Total mean excitation energies (eV) for first and second-row atoms obtained through equation (5) and the I_k values from Table 2. (●) This work; (□) Oddershede and Sabin [33]; (◇) Meltzer *et al.* [37,38].

obtained from the code SRIM-03 by Ziegler and Biersack [63] (chain curves). For the purposes of discussion, in what follows we shall refer to the SRIM values as 'experiment', considering that these values represent the average over a wide database of experimental results for a given target material [64].

From Fig. 7(a)–(c) we note that for the gaseous targets a reasonable general qualitative and quantitative agreement between the OLPA-TFD(1/8)W and OS calculations as compared with experiment. Major differences between theory and experiment are observed in the region around the maximum of the stopping curve. This is expected, since important correction terms for this region – such as the Barkas effect [33,65] – have not been incorporated in the theory. Note, however, that the OLPA-TFD(1/8)W calculations tend to overestimate the stopping values relative to those by OS – particularly for heavier target gas atoms – while keeping slightly overall better agreement with experiment.

On the other hand, for targets in the condensed phase, such as Si, Ni and Ga (Fig. 8(a)–(c)), the OS values show good agreement with experiment for projectile velocities $v/v_0 > 5$, with marked differences in the low and intermediate-velocity region. A similar behavior is observed for the OLPA-TFD(1/8)W values, with a more rapid rise in the stopping values as the projectile velocity is reduced and with a better correspondence with the position of the experimental stopping maximum. Note however that – as in the OS calculation – also in this case the predicted
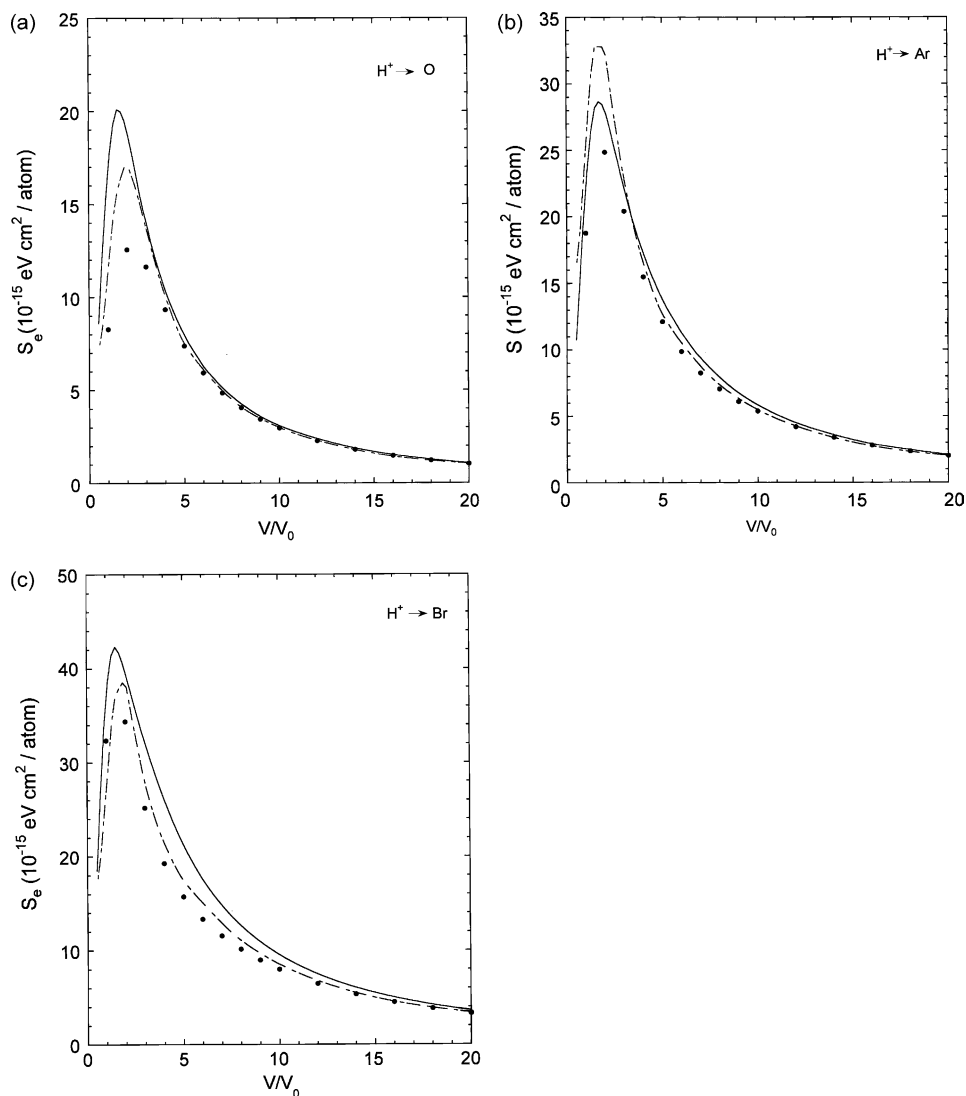
Fig. 7. Proton stopping cross section in atomic gaseous targets: (a) Oxygen, (b) Argon, (c) Bromine as a function of projectile velocity (atomic units). (—) OLPA-TFD(1/8)W calculation. (- – -) SRIM03 empirical fit to experimental data [64]. (•) Theoretical calculation from Oddershede and Sabin [33].

values for the stopping cross section in the low and intermediate-velocity region differ substantially from experiment. As pointed out by Oddershede and Sabin [33,65], this is not surprising, since for targets in the condensed phase the atomistic description of valence electrons (which render the most important contribution to stopping in this velocity region) is no longer the most adequate one to estimate I_k and other criteria – within the same level of theory – must be used to account for this *phase-effect* [40].
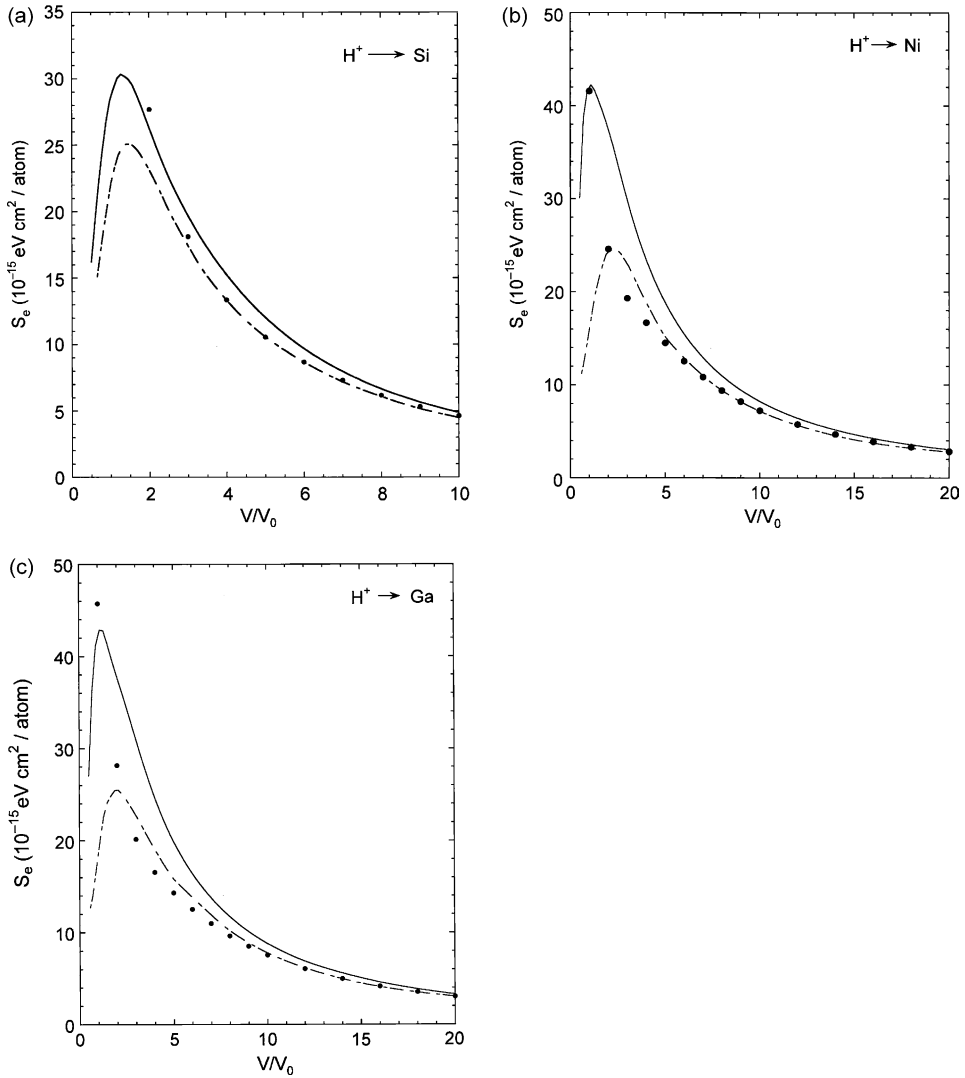
Fig. 8. Proton shopping cross section in solid targets: (a) silicon, (b) nickel and (c) gallium as a function of projectile velocity. Lines and symbols have the same meaning as in Fig. 7.

This aspect, in addition to the neglect of the Barkas effect, may explain the differences observed with experiment in Fig. 8(a)–(c). The corresponding differences between the OS and OLPA-TFD(1/8)W stopping curves may be explained by recognizing that the outer-shell (valence) orbitals contribute dominantly to stopping in the low and intermediate projectile velocity range [37,38]. Inspection of Table 2 indicates that the OLPA mean excitation energies obtained in this work (TFDW) for the outermost orbitals in Si, Ni, and Ga show marked differences with those by Oddershede and Sabin (OS) and Meltzer,

Sabin and Trickey (MST). This behavior is also expected mainly for elements with $19 < Z_2 < 30$, as may be gathered from Fig. 5.

4.3. The approach to pressure effects on stopping

So far we have given evidence for the flexibility and adequacy of the orbital implementation of the KT by Oddershede and Sabin to study atomic and molecular stopping through different approaches. A major breakthrough based on this theory is the OLPA put forward by Meltzer *et al.*, since it incorporates the simplicity – yet physically sound basis – of the LPA for the calculation of mean excitation energies.

In this section, we shall briefly discuss recent developments on the application of the OLPA-TFD(1/8)W approach for the study of proton stopping in elemental targets under pressure. The relevance of this class of studies is not only academic, but may be of importance in defining the role of pressure on fission-fragment track registration lengths in materials exhumed from deep boreholes in the earth crust for purposes of geological dating [66,67]. Also, the role of pressure on stopping cross sections may be of interest in astrophysical problems dealing with acceleration mechanisms of charged particles in dense stellar atmospheres.

Pressure effects on stopping cross sections have been recently addressed within the OLPA-FSGO scheme for molecular targets [25] and preliminary calculations have been reported for stopping and total path ranges of He^+ and Li^+ ions in compressed solid water and methane [68], where total path ranges were found to be predominantly decreased in comparison with those at normal pressure.

As discussed before, a major advantage of the OLPA is the representation of orbital and total mean excitation energies in terms of the electronic density. Accordingly, changes in the electronic density in matter under high pressures may render changes in the mean excitation energy and consequently in S_e. Here we study these changes by resorting to the OLPA-TFD(1/8)W approach and the model of atomic confinement briefly introduced in Section 4.1 whereby energy and electron density are self-consistently obtained for a given confinement radius R.

The effect of pressure on the ground-state electronic and structural properties of atoms and molecules have been widely studied through quantum confinement models [53,69,70] whereby an atom (molecule) is enclosed within, e.g., a spherical cage of radius R with infinitely hard walls. In this class of models, the ground-state energy evolution as a function of confinement radius renders the pressure exerted by the electronic density on the wall as $P = -\partial E/\partial V$. For atoms confined within hard walls, as in this case, pressure may also be obtained through the Virial theorem [69]:

$$P(R) = \frac{E(R) + K(R)}{3V} \tag{32}$$

with R the cage radius, V its volume and $E(R)$, $K(R)$ the corresponding total ground-state electronic and kinetic energy, respectively, which are self-consistently obtained for each cage radius, as described in Section 4.1.

According to equation (26), given a confinement radius R, energy optimization implies a change in the orbital parameters ξ_i and consequently a change in the electron density as pressure increases. Hence, the OLPA as given by equations (5) and (9) will reflect corresponding changes in the orbital and total mean excitation energies. Thus, by virtue of equations (1), (16), and (32), the electronic stopping cross section becomes explicitly pressure-dependent.

As a sample calculation, we have applied the OLPA-TFD(1/8)W approach – as described above – to a Si target at $P=11.6$ GPa ($R=6$ a.u.) and 160 GPa ($R=4$ a.u.). For completeness, we give in Table 3 the corresponding orbital and total mean excitation energies as well as those calculated for the free-atom [71]. Note that as the confinement radius decreases (increasing pressure) a monotonic increase in the orbital mean excitation energies is expected. However, for $R=6$ (11.3 GPa), the 3s orbital shows a slight decrease relative to the free-atom value and then increases for $R=4$ a.u. (160 GPa). While this behavior may be attributed to the non-orthogonal and nodeless character of the orbitals used to construct the ansatz density given by equation (29) [52], this behavior may be related to the so-called 'orbital collapse' discussed by Connerade *et al.* [70] whereby the filling order of shells is strongly influenced by confinement. It is deemed that the source of this phenomenon is the energy-level crossing induced by confinement where – for instance – a 3d state corresponds to a lower energy than a 4s state. Therefore, a regular behavior of mean excitation energies should not be expected for confined systems as the one discussed here.

Figure 9 shows the OLPA-TFD(1/8)W predictions for proton stopping in compressed a-Si at $P=11.3$ (dashed curve) and 160 GPa (dotted curve) as compared to the pressure-free target (continuous curve). The major differences between the free-system and the compressed ones $\sim 25\%$ for 11.3 GPa and 50% for 106 GPa appear in the low and intermediate projectile velocity regime together with a shift of the maximum of the stopping curves towards higher projectile velocities. Since the rate of energy loss (stopping power) of an ion traversing a medium with atomic number density is related to the electronic stopping cross section through the well-known relation

$$\frac{\mathrm{d}E}{\mathrm{d}x} = -nS_e \tag{33}$$

the pressure-induced differences in S_e compete with corresponding pressure-induced changes in bulk density n, so that the resulting rate of energy loss (stopping power) no longer remains the same for any pressure. For instance, in the case of a-Si under high pressures, *ab initio* simulations of pressure-induced amorphous–amorphous phase transitions [72] indicate bulk density changes from $\rho=2.69$ g/cm^2 at normal pressure up to $\rho=3.02$ g/cm^2 at 11.3 GPa. Thus for, e.g., $P=11.3$ GPa the relative *increase* in bulk density becomes of the order of 12% while the corresponding reduction in S_e is of the order of 25%. Accordingly, ion ranges in compressed target materials should not necessarily remain the same as for the same target material at normal pressures [68].

Thus far, an account of developments based on the Oddershede–Sabin orbital implementation of the KT for stopping has been briefly reviewed. Although the

Table 3. Optimized orbital exponents (ξ_k), orbital (I_k), and total (I) mean excitation energies of Si for confinement radii R (a.u.)$=4, 6$, and ∞

R (a.u.)	ξ_{1s}	ξ_{2s}	ξ_{2p}	ξ_{3s}	ξ_{3p}	$\langle I \rangle$ (eV)	$E_{\mathrm{TFD(1/8)W}}$ (eV)	P (GPa)
∞	13.86020	8.12421	3.76604	2.00485	1.60051			
						117.20	-7858.95 $(-7856.83)^{\mathrm{a}}$	0
I_k (eV)	1078.10	331.50	127.70	25.30	16.10			
6	13.7765	8.03791	3.67982	1.80613	1.80652			
						123.30	-7852.91	11.30
I_k (eV)	1078.40	332.10	129.50	23.60	23.60			
4	13.7353	8.00241	3.63377	2.02159	2.02164			
						136.00	-7826.31	160
I_k (eV)	1079.30	334.00	133.80	31.50	31.50			

The corresponding total energies ($E_{\mathrm{TFD(1/8)W}}$) and pressure (P) are shown. Values are taken from Ref. [71].
[a] Hartree–Fock value [61].
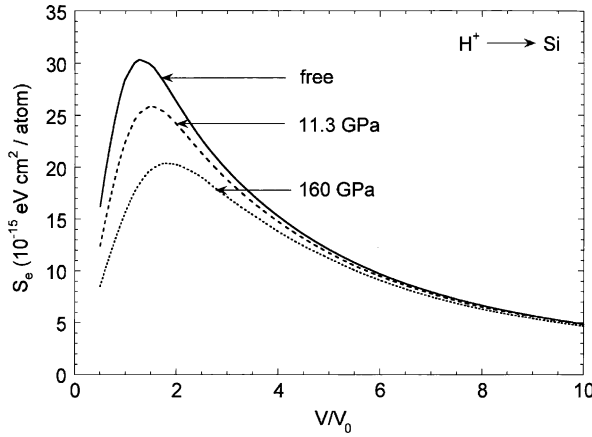
Fig. 9. Pressure dependence of the proton stopping cross section in Si as obtained in this work.

KT has a strong basis on classical mechanics, Oddershede and Sabin had the insight to incorporate into this theory the necessary quantum ingredients to account for the contribution from the internal degrees of freedom of the target scattering components. Clearly, the mean excitation energy is the relevant quantity to consider in the mechanisms of energy loss and its proper evaluation requires of a formal quantum treatment, which currently involves consideration of the Generalized Oscillator Strength (GOS) Distribution. In the following section, we shall briefly summarize some of the relevant contributions by Jens, Jack and one of the present authors (RCT) on this aspect.

5. THE BETHE SUM RULE IN THE RPA

In the Bethe theory of stopping, the GOS characterize the excitation spectrum of a target for a given momentum transfer $\mathbf{q}$ and they are given by

$$F_{0n}(\mathbf{q}) = \frac{2(E_n - E_0)}{\hbar q^2} \left| \left\langle 0 \left| \sum_{j=1}^{N} e^{-i\mathbf{q}\cdot\mathbf{r}_j} \right| n \right\rangle \right|^2 \tag{34}$$

The sum is over all the target electrons N with coordinates $\mathbf{r}_j$. Of particular interest is the fact that the GOS satisfy the Bethe sum rule, i.e.,

$$\sum_{n=0} F_{0n}(\mathbf{q}) = N \tag{35}$$

for all the momentum transfer $\mathbf{q}$, and in the optical approximation (small momentum transfer) ($e^{-i\mathbf{q}\cdot\mathbf{r}_j} \approx 1 - i\mathbf{q}\cdot\mathbf{r}_j$) reduces to the well-known

Thomas–Reiche–Kuhn (TRK) sum rule

$$\sum_{n=0} f_{0n} = N \tag{36}$$

with f_{0n} the dipole oscillator strength. Both of these sum rules state that for a *complete basis* the oscillator strength for the system sum to the number of electrons. However, complete basis sets are hard to come by in practical calculations. Thus, one is required to truncate basis sets, thus introducing inaccuracies into the problem. Nevertheless, the TRK sum rule has been used as a necessary condition to test basis set completeness in the random phase approximation (RPA) [73–75]. However, the fulfillment involving finite momentum transfer in the RPA was not warrant. In 1999, one of us, Oddershede and Sabin [76] proved that also the Bethe sum rule is satisfied in a complete basis set in the RPA. The idea is based on that – in the RPA – the transition amplitude from state $|0\rangle$ to $|l\rangle$ for any one electron operator O is written as

$$\langle 0|O|l\rangle = \sum_{h,p} \left[\langle p|O|h\rangle^* X_{h,p}^l + \langle h|O|p\rangle^* Y_{h,p}^l \right] \tag{37}$$

where $|h\rangle$ and $|p\rangle$ are the complete sets of occupied and unoccupied orbitals which are solutions to the Hartree–Fock equation

$$[h_{\mathrm{o}} + J - K]|i\rangle = \varepsilon_i |i\rangle \tag{38}$$

with h_{o} the kinetic energy and nuclear attraction operator while J and K are the Coulomb and exchange operators, respectively. The coefficients $X_{h,p}^l$ and $Y_{h,p}^l$ are solutions of the RPA for the lth transition with excitation energy ω_l and are written as

$$\omega_l X_{h,p}^l = (\varepsilon_p - \varepsilon_h) X_{h,p}^l + \sum_{h',p'} \left[\langle ph'||hp'\rangle X_{h',p'}^l + \langle pp'||hh'\rangle Y_{h',p'}^l \right] \tag{39}$$

$$-\omega_l Y_{h,p}^l = (\varepsilon_p - \varepsilon_h) Y_{h,p}^l + \sum_{h',p'} \left[\langle hp'||ph'\rangle Y_{h',p'}^l + \langle hh'||pp'\rangle X_{h',p'}^l \right] \tag{40}$$

Thus, in this representation, the energy weighted sum of the transition matrix element can be written as [76]

$$2 \sum_{l>0} \omega_l |\langle 0|O|l\rangle|^2 = \langle C^*, \tilde{C}^* | O, -\tilde{O} \rangle \tag{41}$$

where $C = [h_{\mathrm{o}}, O]$ and ω_l the excitation energy for the lth transition in the RPA. It can be verified that for $O = \mathbf{r}$ and $O = \mathrm{e}^{-i\mathbf{q}\cdot\mathbf{r}_j}$, the TRK and the Bethe sum rule are fulfilled.

6. SUM RULES WITH AN EXTERNAL ELECTROMAGNETIC FIELD

One of the questions that arose during the investigation of the fulfillment of the Bethe sum rule, is its validity when the target system in question (atom or

molecule) is under a static, external, electromagnetic field. In 1998, one of us (RCT), Sabin, Ohrn, and Oddershede [77] demonstrated that in fact the Bethe and TRK sum rules are not affected by the electromagnetic field.

The idea behind this conclusion was obtained as follows. The non-relativistic Hamiltonian for a system under an external electromagnetic field is given by

$$H = \sum_i \frac{1}{2m}(\mathbf{p}_i + e\mathbf{A}_i)^2 + V - e\varphi \tag{42}$$

where $\mathbf{A}$ and ϕ are the vector and scalar potential, respectively, and V is the electronic potential.

The Schrödinger equation for the system in the presence of the electromagnetic field is

$$H|n\rangle = E_n|n\rangle \tag{43}$$

where $|n\rangle$ is the complete set of solutions $\sum_n |n\rangle \langle n| = 1$. Applying this last two properties to the Bethe sum rule (equation (35)), one obtains

$$\sum_n F_{0n}(\mathbf{q}) = \frac{2m}{\hbar^2 q^2} \left\langle 0 \left| \sum_j e^{-i\mathbf{q}\cdot\mathbf{r}_j} \left[H, \sum_k e^{-i\mathbf{q}\cdot\mathbf{r}_j} \right] \right| 0 \right\rangle \tag{44}$$

By performing the calculation of the commutator, and using the current density for the Hamiltonian of equation (42), one obtains

$$\sum_n F_{0n}(\mathbf{q}) = N + \frac{2m\mathbf{q}}{e\hbar q^2} \cdot \sum_{j\neq k} \int d\tau\, e^{i\mathbf{q}\cdot(\mathbf{r}_j - \mathbf{r}_k)} \mathbf{J}_k^0 \tag{45}$$

The superscript in the current density denotes that it is defined for the ground state, and can be shown then that $\mathbf{J}_k^0 = 0$. Thus, the Bethe sum rule in the presence of a constant electromagnetic field is fulfilled [77].

7. POLARIZATION PROPAGATOR METHOD

In order to calculate the GOS, one requires the excitation energies and the generalized transition moments. Oddershede and Sabin had already started in 1992 the investigation of the GOS and the stopping cross section in the first Born approximation by means of the polarization propagator method [78].

The energy representation of the propagator method is

$$\langle\langle A; B \rangle\rangle = \sum_{n\neq 0} \left\{ \frac{\langle 0|A|n\rangle \langle n|B|0\rangle}{E - (E_n - E_0)} - \frac{\langle 0|B|n\rangle \langle n|A|0\rangle}{E + (E_n - E_0)} \right\} \tag{46}$$

where A and B are two property operators. The polarization propagator describes the linear response of the time-dependent average value of A when the system is under a perturbation described by the operator B. For the operators A and B, we see that the first order poles and the corresponding residues of the polarization

propagator are the excitation energies and the generalized transition moments. Thus, when $A = e^{-i\mathbf{q}\cdot\mathbf{r}}$ and $B = A^{\dagger}$, one is able to calculate $F_{n0}(\mathbf{q})$.

However, the assumption on the idea behind the use of the polarization propagator is based on the use of a complete basis set. In practical terms that is not possible and one has to resort to truncated basis set. The question that arises then is how large is the angular momentum required in the basis set to satisfy the Bethe sum rule within the polarization propagator in the RPA approximation?

In 1998, as a consequence of the RPA study, one of us (RCT), Sabin, Oddershede, and Sauer [76], set out to study the criteria for a basis set choice in the study of the Bethe sum rule and in the stopping cross section.

The main result is that if we consider a calculation where the orbitals are expanded in a basis

$$|\chi_j\rangle = \sum_k c_{jk}|\varphi_k\rangle \tag{47}$$

of Cartesian Gaussian functions of the form

$$\varphi_k = N_k x^{l_k} y^{m_k} z^{n_k} e^{-\alpha_k r^2} \tag{48}$$

then the integrals we need to evaluate can be written in terms of primitive integrals over basis functions

$$\langle p|e^{-i\mathbf{q}\cdot\mathbf{r}}|h\rangle = \sum_{j,k} c_{jp}^* c_{kh} \langle j|e^{-i\mathbf{q}\cdot\mathbf{r}}|k\rangle \tag{49}$$

For simplicity, if we restrict the momentum transfer to the z-axis, then one can prove

$$|\langle j|e^{-i\mathbf{q}\cdot\mathbf{r}}|k\rangle|^2 \sim G_w\left(\frac{q_z}{2a}\right) = e^{-q_z^2/2a} H_w^2\left(\frac{q_z}{2a}\right) \tag{50}$$

with $a = \sqrt{\alpha_j + \alpha_k}$ and $w = n_j + n_k$. One immediately can notice that the function $G_w(Q)$ is an oscillating function that decays exponentially for large Q values. However, one can find relations that depend on the orbital exponents and the angular momentum of the basis such that there is a constructive summation of the maxima of the $G_w(Q)$ function when it is added [See Ref. [76] for a detailed explanation].

The problem has not been easy to solve and even today is an open field of research, particularly for time-dependent processes where truncated basis sets are in use.

8. CONCLUSIONS

Jens Oddershede's ideas on stopping power theory and their impact and consequences have been briefly reviewed. We have centered our analysis on the relevance of the orbital implementation of the kinetic theory (KT) of stopping and the Bethe and Thomas–Reiche–Khun sum rules, since they have influenced profoundly the development of our research along these lines.

The orbital implementation of the KT has established a firm theoretical basis for the CAB formalism whereby chemical binding effects on proton stopping cross sections may be estimated. Furthermore, we have given evidence on the flexibility of this theory to allow for the incorporation of alternative descriptions of orbital and total mean excitation energies – such as the OLPA scheme – which may be adapted for the study of energy-loss problems in matter under different conditions (i.e., gases, solids, and matter under high pressure).

For gas targets (atomic and molecular) the theory yields quite reasonable predictions of proton stopping cross sections as compared with experiment. Moreover, since chemical binding effects are naturally incorporated in the theory, the construction of tables of the velocity-dependence of CAB contributions to S_e for different compounds allows – once and for all – the estimate of S_e for protons in materials with similar CAB components without resource to Bragg's additivity rule.

For materials in the condensed phase, the orbital implementation of the KT – when based on an atomistic description – overestimates in general the values of S_e relative to experiment in the low and intermediate projectile velocity region. Since the KT is based on the binary encounter approach, this result is expected since the electronic states in a solid are mainly of a collective character and cannot be fully described by local atomic properties. However, the orbital implementation of the KT may be adapted for solid targets by introducing band states instead of atomic states.

In the case of matter under high pressure, although its description corresponds more closely to the condensed phase, an atomistic view based on the orbital implementation of the KT renders useful information on the effects of pressure on stopping. We have shown here that this theory together with the TFDW density-functional method adapted to atomic confinement models allows for the estimate of pressure effects on stopping, as well as for stopping due to free-atoms.

Finally – and equally important – Jens' contribution to the formal treatment of GOS based on the polarization propagator method and Bethe sum rules has been shown to provide a correct quantum description of the excitation spectra and momentum transfer in the study of the stopping cross section within the Bethe–Bloch theory. Of particular interest is the correct description of the mean excitation energy within the polarization propagator for atomic and molecular compounds. This motivated the study of the GOS in the RPA approximation and in the presence of a static electromagnetic field to ensure the validity of the sum rules.

To conclude, the great benefit that Jens' ideas have brought to the advance in fundamental aspects of atomic collision processes makes this a special occasion to celebrate his 60th birthday.

REFERENCES

[1] E. Rutherford, *Phil. Mag.*, 1911, **21**, 669.
[2] N. Bohr, *K. Dan Vidensk. Selsk. Mat. Fys. Medd.*, 1948, **18**, 8.
[3] N. Bohr, *Phil. Mag.*, 1913, **25**, 10.
[4] N. Bohr, *Phil. Mag.*, 1915, **30**, 581.

[5] H. Bethe, *Ann. Phys. (Leipzig)*, 1930, **5**, 325.
[6] H. Bethe, *Z. Physik*, 1932, **76**, 293.
[7] F. Bloch, *Ann. Phys. (Leipzig)*, 1933, **16**, 285.
[8] U. Fano, *Annu. Rev. Nucl. Sci.*, 1963, **13**, 1.
[9] E. Fermi and E. Teller, *Phys. Rev.*, 1947, **72**, 399.
[10] J. Lindhard and M. Scharff, *K. Dan Videnskab. Selsk. Mat-Fys. Medd.*, 1953, **27**, 15.
[11] J. Lindhard, *K. Dan Videnskab. Selsk. Mat-Fys. Medd.*, 1954, **28**, 8.
[12] J. Lindhard and M. Scharff, *Phys. Rev.*, 1961, **124**, 128.
[13] O. B. Firsov, *ZH. Eksp. Teor. Fiz.*, 1959, **36**, 1517, (*Sov. Phys. JETP*, 1959, **9**, 1076).
[14] W. H. Barkas, W. Birnbaum and F. M. Smith, *Phys. Rev.*, 1956, **101**, 778.
[15] G. Schiwietz and P. Grande, *Nucl. Instrum. Methods B*, 1994, **90**, 10.
[16] P. Grande and G. Schiwietz, *Adv. Quantum Chem.*, 2004, **45**, 7.
[17] M. Bergsmann, W. Raab, G. Schrenk, F. Kastner, R. Diez Muiño, A. Arnau, A. Salin, P. Bauer and P. M. Echenique, *Phys. Rev. B*, 2000, **6**, 3153.
[18] R. Cabrera-Trujillo, J. R. Sabin, E. Deumens and Y. Ohrn, *Adv. Quantum Chem.*, 2004, **45**, 99.
[19] S. A. Cruz, *Radiat. Effects*, 1986, **88**, 159.
[20] D. I. Thwaites, *Nucl. Instrum. Methods B*, 1992, **69**, 53.
[21] D. I. Thwaites, *Nucl. Instrum. Methods B*, 1987, **27**, 293.
[22] D. I. Thwaites, *Nucl. Instrum. Methods B*, 1985, **12**, 84.
[23] D. I. Thwaites, *Radiat. Res.*, 1983, **95**, 495.
[24] P. Bauer and D. Semrad, *Adv. Quantum Chem.*, 2004, **46**, 153.
[25] S. A. Cruz and J. Soullard, *Adv. Quantum Chem.*, 2004, **46**, 195.
[26] P. Sigmund, *Phys. Rev. A*, 1982, **26**, 2497.
[27] J. R. Sabin and J. Oddershede, *Phys. Rev. A*, 1982, **26**, 3209.
[28] J. R. Sabin and J. Oddershede, *Phys. Rev. A*, 1984, **29**, 1757.
[29] J. Oddershede and J. R. Sabin, *Nucl. Instrum. Methods B*, 1989, **42**, 7.
[30] J. R. Sabin and J. Oddershede, *Nucl. Instrum. Methods B*, 1987, **27**, 280.
[31] J. Oddershede and J. R. Sabin, *Int. J. Quantum Chem.: Quant. Chem. Symp.*, 1989, **23**, 557.
[32] J. R. Sabin and J. Oddershede, *Nucl. Instrum. Methods B*, 1990, **44**, 253.
[33] J. Oddershede and J. R. Sabin, *At. Data Nucl. Data Tables*, 1984, **31**, 275.
[34] M. Inokuti, J. Dehmer, T. Baer and J. D. Hanson, *Phys. Rev. A*, 1981, **23**, 95.
[35] M. Inokuti, T. Baer and J. L. Dehmer, *Phys. Rev. A*, 1978, **17**, 1229.
[36] J. L. Dehmer, M. Inokuti and R. P. Saxon, *Phys. Rev. A*, 1975, **12**, 102.
[37] D. E. Meltzer, J. R. Sabin and S. B. Trickey, *Phys. Rev. A*, 1990, **41**, 220.
[38] D. E. Meltzer, J. R. Sabin and S. B. Trickey, *Phys. Rev. A*, 1990, **42**, 666(E).
[39] D. E. Meltzer, J. R. Sabin, S. B. Trickey and J. Z. Wu, *Nucl. Instrum. Methods B*, 1993, **82**, 493.
[40] J. Z. Wu, S. B. Trickey, J. R. Sabin and D. E. Meltzer, *Nucl. Instrum. Methods B*, 1991, **56/57**, 340.
[41] J. R. Sabin and J. Oddershede, *Nucl. Instrum Methods B*, 1989, **36**, 249.
[42] R. Cabrera-Trujillo, S. A. Cruz and J. Soullard, *Nucl. Instrum. Methods B*, 1994, **93**, 166.
[43] A. A. Frost, *Theor. Chim. Acta*, 1970, **18**, 156.
[44] M. J. Berger, Technical Report No. ICRU Report 49, Internal Commission on Radiation Units and Measurements, Bethesda, MD 20814, USA, unpublished.
[45] M. J. Berger, Technical Report No. 4992, Report NISTIR, unpublished.
[46] H. K. Reynolds, D. N. F. Dunbar, W. A. Wentzel and W. Whaling, *Phys. Rev.*, 1953, **92**, 742.
[47] J. T. Park and E. J. Zimmerman, *Phys. Rev.*, 1963, **131**, 1611.
[48] H. Bichsel and L. E. Porter, *Phys. Rev. A*, 1982, **25**, 2499.
[49] W. P. Wang and R. G. Parr, *Phys. Rev. A*, 1977, **16**, 891.
[50] W. P. Wang, *Phys. Rev. A*, 1982, **25**, 2901.
[51] E. Hernández and J. L. Gázquez, *Phys. Rev. A*, 1982, **25**, 107.
[52] S. A. Cruz, C. Díaz-García and G. Covarrubias, *Int. J. Quantum Chem.*, 2005, **102**, 897.
[53] S. A. Cruz and J. Soullard, *Chem. Phys. Lett.*, 2004, **391**, 138.
[54] W. Yang, *Phys. Rev. A*, 1986, **34**, 4575.
[55] L. H. Thomas, *Proc. Camb. Phil. Soc.*, 1926, **23**, 542.
[56] E. Fermi, *Rend. Lincei*, 1927, **6** (6), 602.
[57] C. F. Weizsäcker, *Z. Phys.*, 1935, **96**, 431.

[58] D. A. Kirshnits, *Zh. Eksp. Teor. Fiz.*, 1957, **32**, 115, (Sov. Phys. JETP, 1957, **5**, 64).
[59] Y. Tomishima and K. Yonei, *J. Phys. Soc. Jpn*, 1966, **20**, 142.
[60] P. A. M. Dirac, *Proc. R. Soc. London A*, 1926, **112**, 661.
[61] E. Clementi and C. Roetti, *At. Data Nucl. Data Tables*, 1974, **14**, 177.
[62] Y. Chen, C. M. Kwei and C. J. Tung, *J. Phys. B: At. Mol. Opt. Phys.*, 1993, **26**, 1071.
[63] J. F. Ziegler and J. P. Biersack, SRIM, Version. 2003.26. Obtained from <http://www.SRIM.org>.
[64] H. Paul and A. Schinner, *Nucl. Instrum. Methods B*, 2003, **209**, 252.
[65] J. R. Sabin, J. Oddershede and P. Sigmind, *Nucl. Instrum. Methods B*, 1985, **12**, 80.
[66] A. Wendt, O. Vidal and L. Chadderton, *Radiat. Meas.*, 2003, **36**, 339.
[67] O. Vidal, A. S. Wendt and L. T. Chadderton, *Earth Planet Sci. Lett.*, 2003, **215**, 307.
[68] S. A. Cruz, *Nucl. Instrum. Methods B*, 2004, **222**, 411.
[69] E. V. Ludeña, *J. Chem. Phys.*, 1978, **69**, 1770.
[70] J. Connerade, V. Dolmatov and P. Lakshmi, *J. Phys. B: At. Mol. Opt. Phys.*, 2000, **33**, 251.
[71] A. P. Pathak, S. A. Cruz and J. Soullard, Radiat. Eff. Defect. S. (in press).
[72] M. Duranduru and D. A. Deabold, *Phys. Rev. B*, 2001, **64**, 014101.
[73] R. A. Harris, *J. Chem. Phys.*, 1969, **50**, 3947.
[74] P. Jørgensen and J. Linderberg, *Int. J. Quantum Chem.*, 1970, **4**, 587.
[75] P. Jørgensen and J. Oddershede, *J. Chem. Phys.*, 1983, **78**, 1898.
[76] R. Cabrera-Trujillo, J. R. Sabin, J. Oddershede and S. P. A. Sauer, *Adv. Quantum Chem.*, 1999, **35**, 175.
[77] R. Cabrera-Trujillo, J. R. Sabin, Y. Ohrn and J. Oddershede, *Phys. Rev. A*, 1998, **57**, 3115.
[78] E. H. Mortensen, J. Oddershede and J. R. Sabin, *Nucl. Instrum. Methods*, 1992, **B69**, 24.

Magnetic Balance and Explicit Diamagnetic Expressions for Nuclear Magnetic Resonance Shielding Tensors

Lucas Visscher

Theoretical Chemistry Section, Faculty of Sciences, Vrije Universiteit Amsterdam, 1081 HV Amsterdam, The Netherlands

This paper is dedicated to professor Jens Oddershede on the occasion of his 60th birthday.

Abstract

Two recently proposed formally exact theories for the relativistic calculation of nuclear shielding tensors are numerically evaluated for the xenon atom and the hydrogen fluoride and hydrogen iodide molecules. Both theories are shown to yield significantly different shieldings and partitionings into diamagnetic and paramagnetic contributions. A short analysis is given and directions for further research are indicated.

Contents

1. INTRODUCTION

Recently, there has been discussion about the validity of the Sternheim [1] approximation in the relativistic calculation of NMR shielding constants. This approximation is invoked to avoid the use of extended small component basis sets that are necessary for an accurate solution of the linear response equations based on the Dirac Hamiltonian. The *magnetic balance* functions increase the cost of the calculations and may also lead to numerical instabilities due to the near-linear dependencies with the kinetic balance functions. The generalized Sternheim formalism was initially presented in the calculation of NMR indirect spin–spin coupling constants by Aucar *et al.* [2] where it gave results in good agreement with the full linear response formalism. It was later incorporated as a standard procedure in the 2000 version of the DIRAC program [3]. The formalism was then

also applied to compute relativistic effects on the shielding constants by Visscher *et al.* [4]. In these calculations, the results of the relativistic calculation with the generalized Sternheim approximation were found to lie close to the values that were obtained by an perturbative approach with the relativistic correction operators proposed by Fukui *et al.* [5]. The full response formalism suffered from basis set incompleteness problems, however. It thus appeared reasonable to invoke the Sternheim approximation also as a method to improve both the efficiency and the accuracy of relativistic NMR shielding calculations. A few years later Vaara and Pyykko [6] used the linear response formalism with larger basis sets to establish an absolute shielding scale for the noble gas elements. In these calculations, with a nearly complete basis set, they found a large difference between the Sternheim approximated result and the full response approach, especially for the heavier elements. The same picture appeared in the later calculations of Manninen *et al.* [7] on the shielding tensors of the hydrogen halides and water analogues. On the basis of these results, Manninen *et al.* concluded that the good agreement between the Sternheim approximation and the results obtained on the basis of perturbation theory was coincidental and that the full linear response approach is to be preferred. This conclusion is supported by the recent calculations by Fukui *et al.* [8] on the basis of an infinite order Foldy–Wouthuysen transformed Hamiltonian [9] and by Melo *et al.* [10,11], who used perturbation theory, that also give shieldings considerably below the Sternheim approximated values. The widely varying range of results asks, however, for a more detailed study of the effect of the generalized Sternheim and related approximations in order to establish a preferred method. Experimental data is unfortunately of little help in this discussion because the differential effects on the shielding are likely to be cancelled in the measured chemical shifts. It is even so that the computed diamagnetic term will affect the 'experimental' absolute shielding scale, since the extraction of absolute shielding constants from experimental nuclear spin-rotation constants is usually done by the method of Flygare [12,13] that needs as input an accurately calculated diamagnetic value.

Another aspect is the interpretation of the diamagnetic contribution in relativistic theory. Kutzelnigg [14] proposed an alternative derivation based on the minimization of the coupling of large and small components through the magnetic field in the Dirac Hamiltonian. The resulting transformed Hamiltonian includes a term that is quadratic in the vector potential and can be readily interpreted as the 'missing' diamagnetic operator in the Dirac theory. This transformed Hamiltonian is given in terms of a nonterminating series in powers of the magnetic field strength so that higher derivatives (e.g., hypermagnetizabilities) are difficult to obtain and molecules in very strong magnetic fields cannot be treated. For the calculation of second order properties, like shieldings, the Kutzelnigg formalism has the advantage that the perturbative operators closely resemble those used in nonrelativistic theory, which facilitates implementation and analysis.

In the present paper, these formalisms for the relativistic calculation of shielding tensors are discussed and numerically evaluated by calculation of the heavy element shielding tensors of HF, HI and Xe.

2. THEORY

All equations are written in the atomic unit systems in which the mass of the electron and Planck's constant are equal to one. The speed of light, c is approximately 137 in this unit system. We consider magnetic fields that can be represented by a vector potential $\mathbf{A}$ that is the sum of the vector potential $\mathbf{A}^{ext}$ for the homogenous external magnetic field $\mathbf{B}^{ext}$

$$\mathbf{A}^{ext} = \frac{1}{2}\mathbf{B} \times \mathbf{r}_O \tag{1}$$

and the vector potential $\mathbf{A}^{int}$ for the internal magnetic fields caused by the nuclei

$$\mathbf{A}^{int} = \sum_K^{nuclei} \frac{\gamma_K}{c^2} \frac{\mathbf{I}_K \times \mathbf{r}_K}{r_K^3} \tag{2}$$

where $\mathbf{I}_K$ is the spin and γ_K the gyromagnetic ratio for nucleus K, and $\mathbf{r}_O$ and $\mathbf{r}_K$ are the position of the electron relative to the gauge origin O and the nucleus K, respectively. By applying the principle of minimal coupling [15,16] $\mathbf{p} \rightarrow \mathbf{p} + e\mathbf{A}$ to the nonrelativistic Hamiltonian

$$H^{(0)} = \frac{(\sigma \cdot \mathbf{p})^2}{2} + V \tag{3}$$

one obtains a new Hamiltonian $H = H^{(0)} + H^{(1)} + H^{(2)}$ that has a term linear in the vector potential

$$H^{(1)} = (\mathbf{A} \cdot \mathbf{p} + \sigma \cdot \mathbf{B}) \tag{4}$$

and a term that is quadratic in the vector potential

$$H^{(2)} = \frac{1}{2}A^2. \tag{5}$$

The diamagnetic contribution to the shielding tensors can be defined as the derivative of this Hamiltonian with respect to the magnetic moment $\mu_K = \gamma_K \mathbf{I}_K$ of nucleus K and the external magnetic field $\mathbf{B}^{ext}$

$$\sigma_{K,tu}^d = \left\langle 0 \left| \frac{\partial^2 H}{\partial \mu_t \partial B_u} \right| 0 \right\rangle \tag{6}$$

$$= \left\langle 0 \left| \frac{\partial^2 H^{(2)}}{\partial \mu_t \partial B_u} \right| 0 \right\rangle \tag{7}$$

$$= \frac{1}{2c^2} \left\langle 0 \left| \frac{\mathbf{r}_O \cdot \mathbf{r}_K \delta_{tu} - r_{O,t} r_{K,u}}{r_K^3} \right| 0 \right\rangle. \tag{8}$$

The paramagnetic contribution can be defined as the linear response function or polarization propagator [17]

$$\sigma_{K,tu}^{p} = \left\langle\!\left\langle \frac{\partial H^{(1)}}{\partial \mu_t} ; \frac{\partial H^{(1)}}{\partial B_u} \right\rangle\!\right\rangle = \left\langle\!\left\langle \frac{\partial h^{PSO}}{\partial \mu_t} ; \frac{\partial h^{OZ}}{\partial B_u} \right\rangle\!\right\rangle. \tag{9}$$

The definitions of the paramagnetic spin orbit (PSO) h^{PSO} and the orbital Zeeman (OZ) h^{OZ} operators are given in Appendix A. This response function is nowadays usually computed using gauge-including atomic orbitals to remove the dependence on the gauge origin of the external magnetic field. In order not to complicate the discussion we will use the position of the heaviest nucleus as the common gauge origin in the present work, however.

In relativistic theory, we apply the minimal coupling recipe to the Dirac Hamiltonian

$$D^{(0)} = \beta mc^2 + c(\alpha \cdot \mathbf{p}) + V. \tag{10}$$

and obtain a Hamiltonian $D = D^{(0)} + D^{(1)}$ that depends only linearly on the vector potential

$$D^{(1)} = c(\alpha \cdot \mathbf{A}), \ \ D^{(2)} = 0. \tag{11}$$

The definitions given above would thus imply that the diamagnetic contribution is absent and that all contributions to the shielding tensor are to be classified as paramagnetic. This makes the comparison of nonrelativistic and relativistic theory rather awkward. One may, for instance, consider closed shell atoms for which nonrelativistic theory contributes all shielding to the diamagnetic term. In relativistic theory, there is no diamagnetic term which makes the whole shielding paramagnetic. This is an extreme case of the so-called 'picture change' [18] that needs to be applied in the analysis of molecular properties when going from four-component to one- or two-component theories. The two pictures may be reconciled by approximating the relativistic paramagnetic contribution. It was shown by Sternheim [1] that a diamagnetic operator can be derived from $D^{(1)}$ in a second order perturbation expansion if negative energy states are included in the sum-over-states expression for the second order energy. This diamagnetic term has the same form as the nonrelativistic expression (5), the generalization needed to apply it to four-component wave functions is to multiply the scalar operator by the four-component unit matrix. The use of this Sternheim operator in many-electron calculations was recently criticized by Kutzelnigg [14] who pointed out that its derivation via the summation over negative energy states is unphysical since a proper theory for an electron should not depend on such states. Summations over the negative energy states do occur in the framework of quantum electrodynamics (QED), but then the energy difference between the ground state and states with a positron–electron pair is of the order of $+2mc^2$ and not $-2mc^2$ as in the case of a simple application of perturbation theory along the lines of Sternheim. The root of the problem lies in the fact that the Dirac theory for the electron is a single particle theory that cannot be straightforwardly generalized to many-electron systems. In order to do so one must carefully take into account

the underlying theory, QED, and make sure that no unphysical steps are taken. In his criticism Kutzelnigg does also refer to the paper by Aucar *et al.* [2] that was mentioned in Section 1. In this paper, the Sternheim derivation was, however, only reviewed for the one-electron case after which it was demonstrated that the same formula can be derived in the many-electron case using response theory. In the latter derivation one keeps the no-pair approximation that neglects electron–positron pair creation processes but allows for the dependence of the second quantized QED Hamiltonian on the external electric and magnetic fields through the electron creation operators. If one takes the relaxation of the these operators into account and approximates the response function

$$\sigma_{K,tu}^{r} = \left\langle\!\!\left\langle \frac{\partial D^{(1)}}{\partial \mu_t} ; \frac{\partial D^{(1)}}{\partial B_u} \right\rangle\!\!\right\rangle \tag{12}$$

one may also obtain the Sternheim operator in a theoretically sound manner. This is a justification for the use of the Sternheim formula in many-electron calculations: it can be considered as a well-defined simplification of the exact linear response formalism. The first step in the series of approximations that leads to the Sternheim expression is a decoupling of the positive–positive (pp) and positive–negative (pn) energy orbital rotation parameters in the Hessian

$$\sigma_{K,tu}^{r} \approx \sigma_{K,tu}^{p1} + \sigma_{K,tu}^{d1} \tag{13}$$

$$\sigma_{K,tu}^{p1} = \left\langle\!\!\left\langle \frac{\partial D^{(1)}}{\partial \mu_t} ; \frac{\partial D^{(1)}}{\partial B_u} \right\rangle\!\!\right\rangle^{(pp)} \tag{14}$$

$$\sigma_{K,tu}^{d1} = \left\langle\!\!\left\langle \frac{\partial D^{(1)}}{\partial \mu_t} ; \frac{\partial D^{(1)}}{\partial B_u} \right\rangle\!\!\right\rangle^{(pn)}. \tag{15}$$

After this step one may already identify the paramagnetic and diamagnetic terms as arising from the pp and pn first order orbital corrections to the zeroth order wave function. The σ^{d1} contribution is then further approximated by neglecting all off-diagonal terms in the pn–pn part of the Hessian

$$\sigma_{K,tu}^{d1} \approx \frac{\partial^2}{\partial \mu_t \partial B_u} \sum_{i}^{occ.orbitals} \sum_{s}^{n.e.orbitals} \frac{\langle i|\alpha \cdot \mathbf{A}|s\rangle\langle s|\alpha \cdot \mathbf{A}|i\rangle}{\varepsilon_i - \varepsilon_s}. \tag{16}$$

The resulting equation is identical to the expression from which Sternheim started. We may thus proceed by approximating the energy differences between positive and negative orbital energies by the constant value $-2c^2$. This step gives an overestimation of contributions from highly localized negative energy orbitals (that have energies ε_s much lower than $-2c^2$) and gives an explanation for the observed discrepancies between the unapproximated response formalism and the Sternheim result. The final approximation is

$$\sigma_{K}^{d1} \approx \frac{\partial^2}{\partial \mu_t \partial B_u} \sum_{i}^{occ.orbitals} \frac{\langle i|A^2|i\rangle}{2}. \tag{17}$$

in which the incomplete sum over negative energy orbitals is replaced by a complete sum to make closure possible. This step corrects for basis set truncation errors in the original sum but introduces a spurious contribution of order c^{-2} due to the summation over positive energy orbitals. I will numerically analyze the consequences of these steps in Section 4.

Although the formal objections against the use of the Sternheim operator may thus be overcome it is still true that the approximations made in its derivation introduce significant errors. An efficient alternative for the evaluation of the diamagnetic term is therefore welcome and the new approach of Kutzelnigg, that was presented in Ref. [14], looks quite promising. He suggests to solve the problem of the 'missing' diamagnetic term in relativistic theory by first performing a unitary transformation of the full Dirac Hamiltonian D that reduces the order to which the vector potential couples the large and the small components of the wave functions

$$\tilde{D} = \exp\left(\frac{\beta\alpha\cdot\mathbf{A}}{2c}\right) D \exp\left(-\frac{\beta\alpha\cdot\mathbf{A}}{2c}\right) = D^{(0)} + \tilde{D}^{(1)} + \tilde{D}^{(1)} + \mathrm{O}(A^3). \tag{18}$$

The terms linear in $\mathbf{A}$ appear now on the diagonal positions of the transformed Hamiltonian $\tilde{D}$

$$\tilde{D}^{(1)} = \beta H^{(1)} \tag{19}$$

while quadratic terms are found both at the diagonal and at the off-diagonal positions

$$\tilde{D}^{(2)} = \beta H^{(2)} - \frac{1}{4c}[H^{(1)}, \alpha\cdot\mathbf{A}]_+. \tag{20}$$

The paramagnetic contribution can again be defined as a response function involving the terms linear in $\mathbf{A}$. We write it as a sum of six terms

$$\sigma_{\mathrm{K,tu}}^{\mathrm{p2}} = \left\langle\!\!\left\langle \frac{\partial\tilde{D}^{(1)}}{\partial\mu_{\mathrm{t}}} ; \frac{\partial\tilde{D}^{(1)}}{\partial B_{\mathrm{u}}} \right\rangle\!\!\right\rangle \tag{21}$$

$$= \left\langle\!\!\left\langle \beta\frac{\partial(h_{\mathrm{t}}^{\mathrm{PSO}} + h_{\mathrm{t}}^{\mathrm{FC}} + h_{\mathrm{t}}^{\mathrm{SD}})}{\partial\mu_{\mathrm{t}}} ; \beta\frac{\partial(h_{\mathrm{u}}^{\mathrm{OZ}} + h_{\mathrm{u}}^{\mathrm{SZ}})}{\partial B_{\mathrm{u}}} \right\rangle\!\!\right\rangle \tag{22}$$

$$= \sigma_{\mathrm{K,tu}}^{\mathrm{PSO\text{–}OZ}} + \sigma_{\mathrm{K},\alpha\beta}^{\mathrm{SD\text{–}OZ}} + \sigma_{\mathrm{K,tu}}^{\mathrm{FC\text{–}OZ}} \tag{23}$$

$$+ \sigma_{\mathrm{K,tu}}^{\mathrm{PSO\text{–}SZ}} + \sigma_{\mathrm{K,tu}}^{\mathrm{SD\text{–}SZ}} + \sigma_{\mathrm{K,tu}}^{\mathrm{FC\text{–}SZ}} \tag{24}$$

to indicate the close resemblance to nonrelativistic theory. The superscripts indicate the partitioning of $H^{(1)}$ in terms of the magnetic perturbation operators defined in Appendix A. The difference with nonrelativistic theory is that all operators are multiplied by the four-component matrix β. If the small component part of the wave function plays a minor role and the large component resembles

the nonrelativistic wave function, as is the case in light elements, results will be close to those obtained using nonrelativistic theory. For light systems, the contribution $\sigma_{K,\alpha\beta}^{p,\text{PSO–OZ}}$ will dominate because this is the only term that survives in the nonrelativistic limit. For heavier elements the other terms may be important as well.

The diamagnetic contribution to the shielding tensor consists of two terms

$$\sigma_{K,tu}^{DSO} = \left\langle 0 \left| \frac{\partial^2 \tilde{D}^{(2)}}{\partial \mu_t \partial B_u} \right| 0 \right\rangle = \sigma_{K,tu}^{DSO1} + \sigma_{K,tu}^{DSO2} \tag{25}$$

$$\sigma_{K,tu}^{DSO1} = \left\langle 0 \left| \beta \frac{\partial^2 h^{DSO}}{\partial \mu_t \partial B_u} \right| 0 \right\rangle \tag{26}$$

$$\sigma_{K,tu}^{DSO2} = -\frac{1}{4c} \left\langle 0 \left| \frac{\partial^2 [H^{(1)}, \alpha \cdot \mathbf{A}]_+}{\partial \mu_t \partial B_u} \right| 0 \right\rangle. \tag{27}$$

The diagonal term σ^{DSO1} resembles the Sternheim formula but instead of by the identity matrix the nonrelativistic operator is now multiplied by the β matrix. This is important for heavy elements for which the small component density becomes substantial. The off-diagonal term σ^{DSO2} has no counterpart in nonrelativistic theory.

2.1. Evaluation of the contributions in the Kutzelnigg formalism

Most of the necessary integrals for the terms in the Kutzelnigg formalism could be evaluated using the Hermit integral evaluator that is contained in DIRAC04 electronic structure program [19]. The appearance of the beta matrix instead of the unity matrix in $\tilde{D}^{(1)}$ required a trivial generalization of the input section for the molecular property module. In the calculation of the response functions (21) we considered only pp orbital rotations because inclusion of pn rotations, although possible in practice, would lead to a mixing of the order to which the couplings between large and small components through the magnetic perturbations are taken into account. The first part of the diamagnetic contribution is trivial, but the integrals needed to evaluate σ^{DSO2} were not available yet. We implemented these in our local version of HERMIT as follows. The anticommutator in the second term in equation (25) reduces to

$$[H^{(1)}, \alpha \cdot \mathbf{A}]_+ = (\alpha \cdot \mathbf{A})(\mathbf{A} \cdot \mathbf{p}) + (\mathbf{p} \cdot \mathbf{A})(\alpha \cdot \mathbf{A}) \tag{28}$$

since

$$[\sigma \cdot \mathbf{B}, \sigma \cdot \mathbf{A}]_+ = 2(\mathbf{A} \cdot \mathbf{B}) = 0, \tag{29}$$

and we may employ the Coulomb gauge $\nabla \cdot \mathbf{A} = 0$. We define the vectors

$$\mathbf{P}_t = \frac{\mathbf{r}_O l_{K,t}}{r_K^3} \tag{30}$$

$$\mathbf{Q}_u = \frac{\mathbf{r}_K l_{O,u}}{r_K^3} \tag{31}$$

so that we can write the expectation value as

$$\sigma_{K,tu}^{DSO2} = \frac{1}{2c} \langle 0 | (\alpha \times \mathbf{P}_t)_u + (\alpha \times \mathbf{Q}_u)_t | 0 \rangle \tag{32}$$

Routines to take the expectation value of such a four-component vector products were already available in the DIRAC program, and the evaluation of the $\mathbf{P}$ and $\mathbf{Q}$ primitive integrals was done by modifying an existing HERMIT routine for the evaluation of shielding tensor integrals with London atomic orbitals in which the same scalar integrals are combined into a different vector.

3. COMPUTATIONAL DETAILS

All calculations were performed with a local version of the Dirac04 electronic structure program [19] that included the modifications outlined above, running on a single processor of a 1.8 GHz Macintosh G5 computer. Basis sets and structures for HF and HI were taken from our earlier work [4], whereas the basis set from Xe is the Dyall valence triple zeta set [20], used in uncontracted form. The speed of light was set to the value of 137.0359895 a.u., instead of the more recent 2002 value of CODATA [21] to remain consistent with earlier work. Both the Hartree–Fock (HF) and the response equations were solved without applying any approximations in the evaluation of the integrals over small component functions. In the calculations where we explicitly include pn-rotations we employed the unrestricted kinetic balance scheme to provide approximate magnetically balanced small component functions. In all other calculations we employed the restricted kinetic balance scheme. The Gaussian finite nuclear model [22] was used in the generation of the zeroth order wave function, whereas the point dipole model was used to represent the nuclear magnetic field.

4. RESULTS AND DISCUSSION

Isotropic shielding constants for the heavy elements are listed in Table 1 and show a consistent picture. In all cases we find that relativity reinforces the shielding,

Table 1. Isotropic shielding constants (ppm) for F, I and Xe calculated with different response formalisms (see text)

Formalism	HF	HI	Xe
Nonrelativistic	414.3	4541.3	5642.3
Kutzelnigg	414.9	5436.6	5939.1
Sternheim	423.3	6768.4	7976.5
Full response	418.5	5855.3	7011.6

which can be qualitatively related to the relativistic contraction of the core orbitals. The Sternheim approximation gives a much larger relativistic effect than the full response formalisms, whereas the Kutzelnigg formulation gives a smaller relativistic effect. For Xe the full response results can be compared to the results of Vaara and Pyykko [6] who used the same formalism with restricted kinetic balance for the small component and a larger basis with more high exponent high-ℓ functions. They report a value of 6938 ± 21 ppm that should be converged with respect to basis set extensions. This value is in reasonable agreement with our value. One may observe the large influence of completeness of the small component basis set: with the Dyall basis and the restricted kinetic balance approach a value of only 6451.6 ppm is obtained. This large difference relative to the two other response calculations may be attributed to the magnetically balanced functions that the unrestricted kinetic balance procedure provides in this case. If the gauge origin of the external field coincides with the center of a large component basis function all functions that are generated by magnetic balance

$$\chi^{S,MB}(\mathbf{r}_O) = \sigma \cdot \mathbf{A}^{ext} \chi^L(\mathbf{r}_O) = -\frac{1}{2} \mathbf{B}^{ext} \cdot (\sigma \times \mathbf{r}_O) \chi^L(\mathbf{r}_O) \tag{33}$$

can also be represented by a linear combination of the three functions that are generated by unrestricted kinetic balance on a Gaussian type function

$$\chi^{S,UKB}(\mathbf{r}_O) = \nabla \chi^L(\mathbf{r}_O). \tag{34}$$

This is not the case for the restricted kinetic balance scheme

$$\chi^{S,RKB}(\mathbf{r}_O) = \sigma \cdot \nabla \chi^L(\mathbf{r}_O), \tag{35}$$

in which only a fixed linear combination of the three functions is included in the small component basis. This means that the restricted balance scheme requires larger basis sets to reach convergence in the computed shieldings. The particular advantage of the unrestricted kinetic balance scheme does, however, only hold for atomic or nearly atomic systems like the hydrogen halides.

The Sternheim approximated result may be further analyzed by considering the steps taken in the derivation of equation (17). Decoupling the blocks of the Hessian that connect the pp and pn orbital rotations, equation (13), does hardly influence the computed shielding parameters. The same is true for the subsequent approximation (16) in which only diagonal elements of the pn–pn part of the Hessian are retained. This observation may be valuable in practical calculations because equation (16) makes evaluation of the pn response function an inexpensive one-step procedure that does not involve the construction of the perturbed Fock operator. This procedure may thus replace the Sternheim approach that indeed leads to large errors as is seen in the last rows of Table 2. Both the replacement of the actual orbital energy differences by the common denominator $-2c^2$ as well as the subsequent resolution of identity approximation give errors of the order of a few hundred ppm in the computed iodine and xenon shielding parameters.

Table 2. Contributions to the isotropic shielding constants (ppm) for F, I and Xe calculated with the generalized Sternheim series of approximations (see text)

	HF	HI	Xe
Total shielding			
Full response formalism, equation (12)	418.5	5855.3	7011.6
Decoupled response functions, equation (13)	418.5	5855.9	7012.6
Diagonal approximation	418.5	5858.2	7015.0
Common denominator approximation	420.7	6190.4	7370.5
Resolution of identity	423.3	6765.7	7973.0
Paramagnetic contribution			
Decoupled response function, equation (14)	−59.7	966.8	2019.8
Diamagnetic contribution			
Decoupled response function, equation (15)	478.2	4889.1	4992.8
Diagonal approximation, equation (16)	478.2	4891.4	4995.2
Common denominator approximation	480.4	5223.6	5350.8
Resolution of identity, equation (17)	483.0	5799.0	5953.2

We now turn to further analysis of the results obtained with the Kutzelnigg formalism. This approach gives contributions from six individual response functions (although the FC and SD part will usually be combined for computational efficiency) and two expectation values. In Table 3, we see that for the lightest element, fluorine, only the relativistic effect due to the FC terms makes an appreciable contribution and increases the shielding slightly relative to the nonrelativistic value. The same small relativistic effect is seen for Xe where the Kutzelnigg formalism gives a much smaller relativistic effect than the other approaches. For the heavier elements the FC terms become larger in magnitude than the PSO–OZ contribution indicating the importance of relativity in calculation of heavy atom shieldings. The difference in diamagnetic contribution when compared to the Sternheim formula is caused by the small component contribution that counteracts the dominant large component contribution in the Kutzelnigg formalism while enlarging the shielding in the Sternheim formalism. The main reason for the observed difference between the two response formulas appears to be the larger relativistic effect on the paramagnetic contribution in the unmodified Dirac formalism. It would be interesting to compare the individual terms in the Kutzelnigg approach to the outcome of the perturbative quadratic response approaches by Manninen *et al.* [7] and Melo *et al.* [10,11], since these approaches give an identification of passive or active spin–orbit and scalar

Table 3. Contributions to the isotropic shielding constants (ppm) for F, I, and Xe calculated within the nonrelativistic and Kutzelnigg formalisms (see text)

	HF	HI	Xe
Nonrelativistic			
PSO–OZ	-67.86	-966.4	–
DSO	482.18	5505.4	5642.3
Kutzelnigg paramagnetic terms			
PSO–OZ	-68.11	-1464.7	-214.8
SD–OZ	0.05	-233.4	-236.3
FC–OZ	6.40	3359.9	2836.5
PSO–SZ	0.02	275.1	340.5
SD–SZ	-0.03	304.7	393.7
FC–SZ	-5.68	-2410.7	-2928.5
Total paramagnetic	-60.88	-169.2	191.1
Kutzelnigg diamagnetic terms			
DSO1	482.24	5558.5	5696.8
DSO2	0.04	47.3	51.2
Total diamagnetic	482.28	5605.8	5748.0

relativistic corrections on the FC, SD and PSO terms. Such an analysis requires, however, a more detailed study of the similarities and differences between the various response functions for the four-component wave functions and the perturbative relativistic operators, than was intended in this pilot application of the Kutzelnigg formalism. One will thereby, e.g., need to assess the effect of the nuclear model that is used to generate the zeroth order wave function. We employed a finite, Gaussian, nuclear model, while in most perturbative approaches one does assume a point charge model that may enhance relativistic effects. Basis set incompleteness effects due to lack of tight high-ℓ functions in the Dyall can also play a role. It is unlikely, however, that such effects will fully explain the observed differences between the outcomes of the various approaches.

5. FINAL REMARKS AND CONCLUSIONS

The situation with respect to establishing a reliable absolute shielding scale for heavy elements remains somewhat unclear. Two methods that are both in principle exact give significantly different results, whereas more approximate methods give yet another result. As the quantity of interest is difficult to measure experimentally, it will be necessary to analyze the causes for the discrepancy in more detail, both theoretically and numerically. Another interesting study could be the analysis of the effects that the differences between the Kutzelnigg and unmodified Dirac response formalisms will have on chemical shifts. In that case, one could use experimental data to decide upon a preferred formalism.

APPENDIX A

The definitions of the first and second order magnetic perturbation operators are given below. In the nonrelativistic formalism these operators are two-component operators, in the Kutzelnigg formalism all operators are to be multiplied by the four-component β matrix. All operators are given in the atomic unit system and we do not apply QED corrections so that the free electron g-factor g_e is precisely equal to 2.

The Orbital-Zeeman operator

$$h^{OZ} = \frac{1}{2}\mathbf{B}^{ext} \cdot \boldsymbol{\ell}_O \tag{A.1}$$

The Spin-Zeeman operator

$$h^{SZ} = \frac{1}{2}\mathbf{B}^{ext} \cdot \sigma \tag{A.2}$$

The Paramagnetic Spin-Orbit operator

$$h_K^{PSO} = \frac{\gamma_K}{2c^2}\frac{\mathbf{I}_K \cdot \boldsymbol{\ell}_K}{r_K^3} \tag{A.3}$$

The Fermi Contact operator

$$h_K^{FC} = \frac{\gamma_K}{c^2}\frac{4\pi}{3}(\mathbf{I}_K \cdot \sigma)\delta(\mathbf{r}_K) \tag{A.4}$$

The Spin Dipolar operator

$$h_K^{SD} = \frac{\gamma_K}{2c^2}\frac{3(\mathbf{I}_K \cdot \mathbf{r}_K)(\sigma \cdot \mathbf{r}_K) - (\mathbf{I}_K \cdot \sigma)r_K^2}{r_K^5} \tag{A.5}$$

The Diamagnetic Spin-Orbit operator

$$h_K^{DSO} = \frac{\gamma_K}{2c^2}\frac{(\mathbf{I}_K \cdot \mathbf{B}^{ext})(\mathbf{r}_K \cdot \mathbf{r}_O) - (\mathbf{I}_K \cdot \mathbf{r}_K)(\mathbf{r}_O \cdot \mathbf{B}^{ext})}{r_K^3} \tag{A.6}$$

REFERENCES

[1] M. M. Sternheim, *Phys. Rev.*, 1962, **128**, 676.
[2] G. A. Aucar, T. Saue, L. Visscher and H. J. Aa. Jensen, *J. Chem. Phys.*, 1999, **110**, 6208–6218.
[3] T. Saue, V. Bakken, T. Enevoldsen, T. Helgaker, H. J. Aa. Jensen, J. K. Laerdahl, K. Ruud, J. Thyssen and L. Visscher, Dirac, a relativistic ab initio electronic structure program, Release 3.2, 2000.
[4] L. Visscher, T. Enevoldsen, T. Saue, H. J. Aa. Jensen and J. Oddershede, *J. Comput. Chem.*, 1999, **20**, 1262.
[5] H. Fukui, T. Baba and H. Inomata, *J. Chem. Phys.*, 1996, **105**, 3175, Erratum: *J. Chem. Phys.*, 1997, **106**, 2987.

[6] J. Vaara and P. Pyykko, *J. Chem. Phys.*, 2003, **118**, 2973–2976.
[7] P. Manninen, P. Lantto, J. Vaara and K. Ruud, *J. Chem. Phys.*, 2003, **119**, 2623–2637.
[8] H. Fukui, T. Baba, Y. Shiraishi, S. Imanishi, K. Kudo, K. Mori and M. Shimoji, *Mol. Phys.*, 2004, **102**, 641–648.
[9] M. Barysz, A. J. Sadlej and J. G. Snijders, *Int. J. Quantum Chem.*, 1997, **65**, 225–239.
[10] J. I. Melo, M. C. R. de Azua, C. G. Giribet, G. A. Aucar and R. H. Romero, *J. Chem. Phys.*, 2003, **118**, 471–486.
[11] J. I. Melo, M. C. R. de Azua, C. G. Giribet, G. A. Aucar and P. F. Provasi, *J. Chem. Phys.*, 2004, **121**, 6798–6808.
[12] W. H. Flygare, *J. Chem. Phys.*, 1964, **41**, 793–800.
[13] D. L. Bryce and R. E. Wasylishen, *Acc. Chem. Res.*, 2003, **36**, 327–334.
[14] W. Kutzelnigg, *Phys. Rev. A*, 2003, **67**, 032109.
[15] M. Gell-Mann, *Nuovo Cimento Suppl.*, 1956, **4**, 848.
[16] T. Saue, in *Relativistic Electronic Structure Theory. Part I. Fundamentals* (ed. P. Schwerdtfeger), Elsevier, Amsterdam, 2002, p. 356.
[17] J. Oddershede, P. Jrgensen and D. L. Yeager, *Comput. Phys. Rep.*, 1984, **2**, 33.
[18] E. J. Baerends, W. H. E. Schwarz, P. Schwerdtfeger and J. G. Snijders, *J. Phys. B*, 1990, **23**, 3225–3240.
[19] H. J. Aa. Jensen, T. Saue, and L. Visscher with contributions from V. Bakken, E. Eliav, T. Enevoldsen, T. Fleig, O. Fossgaard, T. Helgaker, J. Laerdahl, C. V. Larsen, P. Norman, J. Olsen, M. Pernpointner, J. K. Pedersen, K. Ruud, P. Salek, J. N. P. van Stralen, J. Thyssen, O. Visser and T. Winther, Dirac, a relativistic ab initio electronic structure program, Release DIRAC04.0, 2004 (http://dirac.chem.sdu.dk).
[20] K. G. Dyall, *Theor. Chem. Acc.*, 2002, **108**, 335.
[21] Values for the physical constants are taken from the CODATA list at http://physics.nist.gov/cuu/Constants/international.html
[22] L. Visscher and K. G. Dyall, *Atom. Data Nucl. Data Tables*, 1997, **67**, 207.

Spin-Interactions and the Non-relativistic Limit of Electrodynamics

Trond Saue

*UMR 7751 CNRS/Université Louis Pasteur, Laboratoire de Chimie Quantique
et de Modélisation Moléculaire, 4 rue Blaise Pascal,
67000 Strasbourg, France*

Abstract

This chapter discusses how to extinguish spin–orbit interactions and/or scalar relativistic effects from four-component relativistic molecular calculations in order to assess their importance on molecular properties. It is pointed out that standard non-relativistic calculations use the non-relativistic free-particle Hamiltonian $\hat{H}_p$, but the *relativistic* Hamiltonian $\hat{H}_{int}$ which describes the interaction between particles and fields. In the strict non-relativistic limit, electrodynamics reduce to electrostatics, that is there are no effects of retardation and no magnetic interactions. It is, however, perfectly reasonable from a pragmatic point of view to introduce both scalar and vector potentials in a non-relativistic framework. Non-relativistic theory can perfectly well accommodate magnetic sources, including spin, but does not provide a mechanism for generating them. We demonstrate that the pragmatic approach leads to some inconsistencies in that non-relativistic theory cannot describe spin–same orbit interactions, but spin–other orbit interactions. We also emphasize that the distinction between spin–orbit interactions and other spin interactions is somewhat artificial and highly dependent on the chosen reference frame.

In a previous paper [L. Visscher and T. Saue, *J. Chem. Phys.*, 2000, **113**, 3996] we demonstrated how to eliminate spin–orbit interaction from four-component relativistic calculations of spectroscopic constants by deleting the quaternion imaginary parts of matrix representations of the modified Dirac equation. In this chapter, we discuss the extension of this approach to second-order electric and magnetic properties. We will demonstrate the elimination of poles corresponding to spin-forbidden transitions from the dispersion of the dipole polarizability of the mercury atom. More care is needed when considering second-order magnetic properties in that the elimination of quaternion imaginary parts will extinguish *all* spin interactions. A procedure is developed which allows us to demonstrate important spin–orbit effects on the NMR shielding polarizabilities of the xenon atom. It is also possible to extinguish all spin interactions in relativistic calculations, but only within the framework of the Sternheim approximation, that is when calculating the diamagnetic contribution as an expectation value.

Contents

1. INTRODUCTION

With the exception of recent extensions to electroweak theory [1] chemistry deals exclusively with electromagnetic interactions. The starting point for a quantum theory to describe these interactions is the Lagrangian formalism since it allows the correct identification of conjugated momenta appearing in the Hamiltonian [2]. Full-fledged quantum electrodynamics (QED) is based on a Lagrangian of the form

$$L = L_{\mathrm{p}} + L_{\mathrm{int}} + L_{\mathrm{f}} \tag{1}$$

where L_{p} and L_{f} describe particles and fields separately and L_{int} their interaction. More approximate theories can be discerned that retain only the degrees of freedom associated either with fields or particles. Maxwell's equations allow the determination of electric and magnetic fields generated by specified sources (particles). In quantum mechanics, on the other hand, it is the external fields that are fixed and Hamiltonians can be derived from only a knowledge of $L_{\mathrm{p}} + L_{\mathrm{int}}$. The overwhelming majority of quantum chemical calculations are carried out using non-relativistic theory. However, we shall see that what is normally called non-relativistic theory is based on the *non-relativistic* Lagrangian L_{p} for the particles combined with the *relativistic* interaction term L_{int}.

Relativity and the lanthanide contraction [3] are the major factors explaining the deviations of trends in the lower part of the periodic table. Relativistic effects can be defined [4] as the differences between our world with a finite speed of light $c = 137.0359998$ a.u. [5] and a theoretical world for which $c \rightarrow \infty$. Relativistic effects can be divided into scalar relativistic and spin–orbit effects. Scalar relativistic effects are due to the relativistic mass increase and change in kinematics of electrons. In hydrogen-like atoms, the average speed of the 1s electron is Z a.u. The Lorentz factor can thereby be expressed as $\gamma = (1 - Z^2/c^2)^{-1/2}$ which shows that relativity rapidly becomes important as the nuclear charge Z increases. The dominant scalar relativistic effects can be included in standard non-relativistic quantum chemical codes at almost no extra cost through the use of relativistic pseudopotentials [6] or scalar relativistic (spinfree) versions of approximate relativistic Hamiltonians such as the second-order Douglas–Kroll–Hess Hamiltonian [7–9] or the zeroth-order regular approximation (ZORA) [10,11]. The spin–orbit interaction, on the other hand, leads to the introduction of complex algebra, couples the spin and spatial degrees of freedom, thus breaking non-relativistic symmetry, and therefore generally requires dedicated code.

Four-component relativistic molecular calculations are based directly on the Dirac equation. They include both scalar relativistic effects and spin–orbit

coupling and provide benchmarks for more approximate methods. However, there are situations where one would like to eliminate spin–orbit coupling from calculations. The comparison of calculations with and without spin–orbit coupling allows the assessment of its importance. Furthermore, in situations where the effect of spin–orbit coupling is small, one would like to eliminate it in order to reduce computational cost. Computational savings are also possible by including spin–orbit coupling only at the correlated level.

In this chapter, we therefore consider whether it is possible to eliminate spin–orbit coupling from four-component relativistic calculations. This is a situation quite different from that of more approximate relativistic methods where a considerable effort is required for the inclusion of spin–orbit coupling. We have previously shown that it is indeed possible to eliminate spin–orbit coupling from the calculation of spectroscopic constants [12,13]. In this chapter, we consider the extension of the previous result to the calculation of second-order electric and magnetic properties, i.e., linear response functions. Although the central question of this article may seem somewhat technical, it will be seen that its consideration throws considerable light on the fundamental interactions in molecular systems. We will even claim that four-component relativistic theory is the optimal framework for the understanding of such interactions since they are inherently relativistic.

This chapter is outlined as follows: in Section 2.1, we discuss the basic mechanism of the spin–orbit interaction. We then, in Section 2.2, consider the proper non-relativistic limit of electrodynamics. This is an important result in itself and is a key to a deeper understanding of the interactions in chemistry. In Section 2.3, we review the relativistic Hamiltonian and the interactions it describes. In Section 2.4, we show how a non-unitary transformation of the Dirac equation leads to the so-called modified Dirac equation from which the spin–orbit interaction can be eliminated. We then, in Section 2.5, apply this theory to the calculation of second-order electric and magnetic properties. We will demonstrate the elimination of poles corresponding to spin-forbidden transitions from the dispersion of the dipole polarizability of the mercury atom. On the other hand, in the consideration of magnetic properties we encounter a fundamental difficulty and enlightenment: all spin interactions can be considered as spin–orbit interactions. We are, however, able to develop a procedure that allows us to demonstrate important spin–orbit effects on the shielding polarizabilities of the xenon atom. Final remarks and conclusions are given in Section 3. Throughout this chapter we will employ SI-based atomic units [14,15] and implicit summation over repeated Greek indices.

2. THEORY

2.1. The physics of the spin–orbit interaction

In this section, we will review basic features of spin–orbit interaction. Most of what follows is standard textbook material, but will be reviewed for notation, clarification and self-consistency, as well as to prepare the ground for the ensuing

discussion. Excellent reviews of spin–orbit coupling in molecular systems have been given by Marian and co-workers [16,17].

It is often stated that the phenomenon of spin–orbit interaction arises from the coupling between the spin and the orbital angular momentum of an electron (see, e.g., Ref. [18]). However, this is not a very satisfying explanation since it completely neglects the dependence on the presence of other charges moving relative to the electron under consideration. In the Breit–Pauli Hamiltonian [19], one usually distinguishes three forms of spin–orbit interaction: the one-electron spin–orbit (SO) term

$$\hat{h}(i)^{\text{SO}} = \frac{1}{4m^2c^2}\,\boldsymbol{\sigma}_i\cdot(\mathbf{E}_i\times\mathbf{p}_i) \quad \phi = \sum_A \frac{Z_A}{r_{iA}} \quad \sum_A \frac{Z_A}{4m^2c^2r_{iA}^3}\,\boldsymbol{\sigma}_i\cdot(\mathbf{r}_{iA}\times\mathbf{p}_i), \quad (2)$$

due to the presence of the nuclear framework, and the spin–same (SSO) and spin–other (SOO) orbit terms

$$\hat{h}^{\text{SSO}}(i,j) = -\frac{1}{4m^2c^2r_{ij}^3}\,\boldsymbol{\sigma}_i\cdot(\mathbf{r}_{ij}\times\mathbf{p}_i); \quad \hat{h}^{\text{SOO}}(i,j) = \frac{1}{2m^2c^2r_{ij}^3}\,\boldsymbol{\sigma}_i\cdot(\mathbf{r}_{ij}\times\mathbf{p}_j), \quad (3)$$

due to the presence of other electrons.

The basic mechanism of spin–orbit coupling is magnetic induction. It is therefore a truly relativistic effect, as will be discussed shortly. The potentials of a moving charge can be found from Maxwell's equations, as direct solutions or from Lorentz transformations of potentials of a static charge to a moving frame. Maxwell's equations can be divided into the homogeneous pair

$$\boldsymbol{\nabla}\cdot\mathbf{B} = 0; \quad \boldsymbol{\nabla}\times\mathbf{E} + \frac{\partial\mathbf{B}}{\partial t} = 0 \tag{4}$$

and the inhomogeneous pair

$$\boldsymbol{\nabla}\cdot\mathbf{E} = 4\pi\rho; \quad \boldsymbol{\nabla}\times\mathbf{B} - \frac{1}{c^2}\frac{\partial\mathbf{E}}{\partial t} = \frac{4\pi}{c^2}\mathbf{j}, \tag{5}$$

containing the sources, that is the charge density ρ and the current density $\mathbf{j}$. With the introduction of potentials

$$\mathbf{E} = -\boldsymbol{\nabla}\phi - \frac{\partial\mathbf{A}}{\partial t}; \quad \mathbf{B} = \boldsymbol{\nabla}\times\mathbf{A} \tag{6}$$

the homogeneous pair (4) is automatically solved and the inhomogeneous pair (5) becomes

$$\begin{aligned} &\boldsymbol{\nabla}^2\phi - \frac{\partial}{\partial t}(\boldsymbol{\nabla}\cdot\mathbf{A}) = -4\pi\rho, \\ &\left[\boldsymbol{\nabla}^2 - \frac{1}{c^2}\frac{\partial^2}{\partial t^2}\right]\mathbf{A} - \boldsymbol{\nabla}\left[(\boldsymbol{\nabla}\cdot\mathbf{A}) + \frac{1}{c^2}\frac{\partial\phi}{\partial t}\right] = -\frac{4\pi}{c^2}\mathbf{j} \end{aligned} \tag{7}$$

The solution of these equations can be simplified with the proper choice of gauge [20]. In Coulomb gauge, $\mathbf{\nabla}\cdot\mathbf{A}=0$, one obtains the Poisson equation for the scalar potential ϕ

$$\mathbf{\nabla}^2\phi = -4\pi\rho \Rightarrow \phi(\mathbf{r}_1,t) = \int \frac{\rho(\mathbf{r}_2,t)}{r_{12}}\,d\tau_2 \tag{8}$$

whereas all the complicated effects of magnetic interactions and retardation are buried in the equation for the vector potential $\mathbf{A}$. In Lorentz gauge

$$\partial_\mu A_\mu = (\mathbf{\nabla}\cdot\mathbf{A}) + \frac{1}{c^2}\frac{\partial\phi}{\partial t} = 0 \tag{9}$$

Maxwell's equations reduce to the very compact form

$$\Box^2 A_\mu = -\frac{4\pi}{c^2}j_\mu \tag{10}$$

where $\Box^2 = \mathbf{\nabla}^2 - (1/c^2)(\partial^2/\partial t^2)$ is the d'Alembertian. These four-dimensional Poisson equations have general solutions

$$\phi(\mathbf{r}_1,t) = \int \frac{\rho(\mathbf{r}_2,t_r)}{r_{12}}\,d\tau_2; \quad \mathbf{A}(\mathbf{r}_1,t) = \int \frac{\mathbf{j}(\mathbf{r}_2,t_r)}{c^2 r_{12}}\,d\tau_2 \tag{11}$$

where $t_r = t - r_{12}/c$ is retarded time, that is the time of emission of the signal. In the case of a moving point charge in some frame K the solutions reduce to the Liénard–Wiechert potentials

$$\phi(\mathbf{r}_1,t) = \frac{q}{r_{12} - (\mathbf{v}_2\cdot\mathbf{r}_{12})/c}\bigg|_{t_r}; \quad \mathbf{A}(\mathbf{r}_1,t) = \frac{\phi\mathbf{v}_2}{c^2}\bigg|_{t_r} \tag{12}$$

where position $\mathbf{r}_2$ and velocity $\mathbf{v}_2$ of the charge are to be evaluated at retarded time. In the rest frame K' of the particle the vector potential is zero and the scalar potential reduces to a standard Coulomb potential

$$\phi'(\mathbf{r}_1',t') = \frac{q}{r_{12}'}; \quad \mathbf{A}'(\mathbf{r}_1',t') = 0 \tag{13}$$

This magnetic induction is the mechanism behind the spin–orbit interaction: in the rest frame of a nucleus only a static electric field is observed, whereas an electron in relative motion will experience a magnetic field with which it can interact through its spin.

The Liénard–Wiechert potentials (12) can also be derived from a rotation-free Lorentz transformation (boost) of the four potential of a static charge (13) to the moving frame at retarded time. For a charge moving at constant velocity the potentials can also be expressed in terms of the current position giving [21]

$$\phi(\mathbf{r}_1,t) = \gamma\frac{q}{\sqrt{r_{12} + (\mathbf{v}_2\cdot\mathbf{r}_{12})^2\gamma^2/c^2}}; \quad \mathbf{A}(\mathbf{r}_1,t) = \frac{\mathbf{v}_2}{c^2}\phi(\mathbf{r}_1,t) \tag{14}$$

Subsequent expansion in terms of v/c and transformation to Coulomb gauge gives

$$\phi(\mathbf{r}_1, t) = \frac{q}{r_{12}}; \quad \mathbf{A}(\mathbf{r}_1, t) = \left\{ \frac{q\mathbf{v}_2}{2c^2 r_{12}} + \frac{q\mathbf{r}_{12}(\mathbf{r}_{12} \cdot \mathbf{v}_2)}{2c^2 r_{12}^3} + O\left[\left(\frac{v}{c}\right)^4\right] \right\} \tag{15}$$

These expressions are quite useful in that the effects of acceleration does not enter to this low order, as first shown by Darwin [22], yet the straightforward calculation of the magnetic field and subsequent spin–orbit interaction from the above potentials led to fine structure splittings that were a factor two larger than experiment. The missing factor two was explained by Thomas as a kinematic factor due to the accelerated motion of the charges [23,24]. The accelerated motion of the charge due to the presence of other charges has to be treated by a succession of Lorentz transformations, thus introducing rotations and the Thomas precession [25,26]. A number of simple approximate derivations of the Thomas precession have been given in the literature [27–30], whereas the exact derivation of the product of two boost takes considerable more work (see Ref. [31]). A particularly elegant exact derivation has been given by Baylis and Jones [32] using Pauli algebra.

2.2. The non-relativistic limit of electrodynamics

Although the null result of the Michelson–Morley ether-drift experiment is often cited as an important motivator for the development of the special theory of relativity, Einstein himself seems to have been hardly aware of it in 1905 and was more puzzled by the appearance of seemingly different forces, electric or magnetic, depending on the choice of reference frame [33]. The theory of special relativity lead to significant modifications of non-relativistic Newtonian mechanics, but left classical electrodynamics almost unscathed, being already a full-fledged relativistic theory. It is perhaps for this reason that the non-relativistic limit of electrodynamics is rarely considered [15,34–36], yet it is important for the formulation of a rigorous and consistent non-relativistic theory of particles and fields and will be the subject of this section.

Maxwell's equations, as well as the Lorentz force, can be derived from the Lagrangian density

$$\mathcal{L} = \mathcal{L}_{\text{int}} + \mathcal{L}_{\text{f}}; \quad \mathcal{L}_{\text{int}} = j_\alpha A_\alpha; \quad \mathcal{L}_{\text{f}} = -\frac{c^2}{16\pi} F_{\alpha\beta} F_{\alpha\beta}$$

in which appears the electromagnetic field tensor $F_{\alpha\beta} = \partial_\alpha A_\beta - \partial_\beta A_\alpha$. The interaction part of the Lagrangian, first suggested by Schwarzschild [37],

$$L = \int \mathcal{L}_{\text{int}} d\tau = \int (\mathbf{j} \cdot \mathbf{A} - \rho\phi)\, d\tau \tag{16}$$

may furthermore be combined with the Lagrangian for a free particle to give the Hamiltonian of a charge q in the presence of specified fields. It is found that the resulting Hamiltonian can be obtained from its free-particle counterpart by the substitutions

$$p_\mu \to p_\mu - qA_\mu \to \begin{cases} \mathbf{p} & \to & \mathbf{p} - q\mathbf{A} \\ E & \to & E - q\phi \end{cases} \tag{17}$$

called the principle of minimal electromagnetic coupling [38]. The same substitutions are obtained whether one starts from a relativistic or a non-relativistic free-particle Lagrangian. However, the interaction Lagrangian itself was obtained in a relativistic framework and is Lorentz covariant. Its introduction in a non-relativistic framework is therefore inconsistent, albeit perfectly reasonable from a pragmatic point of view.

In order to develop a fully consistent non-relativistic theory for particles and fields we must first determine the non-relativistic limit of Maxwell's equations. This is to some extent hampered by the fact that the equations, and in particular the occurrence of the speed of light c, change according to the unit system chosen, a situation that has been analyzed by Jackson [25] and Kutzelnigg [15,35]. In SI-based atomic units, the non-relativistic limit is obtained directly as the limit $c \to \infty$ and leads to the equations

$$\begin{aligned} \boldsymbol{\nabla}\cdot\mathbf{B} = 0; \quad &\boldsymbol{\nabla}\times\mathbf{E} + \frac{\partial\mathbf{B}}{\partial t} = 0 \\ \boldsymbol{\nabla}\cdot\mathbf{E} = 4\pi\rho; \quad &\boldsymbol{\nabla}\times\mathbf{B} = 0 \end{aligned} \tag{18}$$

The same conclusion was reached by Lévy-Leblond [34] and Kutzelnigg [15,35], but these authors do not seem to appreciate the full implications of the result. Maxwell's equations constitute a set of coupled first-order differential equations and boundary conditions are therefore necessary to ensure the unique determination of electric and magnetic fields for given sources. For finite systems the boundary condition is that the electric and magnetic fields should go to zero at infinite distance from the sources; the uniqueness of the solutions is then guaranteed by the Helmholtz theorem. In the case of the non-relativistic Maxwell's equations, the Helmholtz theorem leads us to conclude unequivocally that the magnetic field $\mathbf{B}$ is zero everywhere in space. A strong argument in favor of this rather drastic conclusion is that the Liénard–Wiechert vector potential (12) is at least a factor c smaller than the corresponding scalar potential in any unit system. In the non-relativistic limit, electrodynamics is thereby seen to reduce to electrostatics. There are no effects of retardation or any magnetic interaction. Electric fields are purely longitudinal and vector potentials as well as the concept of gauge becomes superfluous.

2.3. The relativistic Hamiltonian

In this section, we review the relativistic Hamiltonian with special emphasis on how interactions are introduced. Within the Born–Oppenheimer approximation the electronic Hamiltonian, relativistic or not, has the generic form

$$\hat{H} = \sum_i \hat{h}(i) + \frac{1}{2}\sum_{i \neq j} \hat{g}(i,j) + V_{\mathrm{NN}}; \quad V_{\mathrm{NN}} = \frac{1}{2}\sum_{K \neq L} \frac{Z_K Z_L}{R_{KL}}$$

where V_{NN} is the classical repulsion of nuclei. Four-component relativistic theory starts from the free-particle Dirac operator

$$\hat{h}_0^R(i) = \beta' mc^2 + c(\boldsymbol{\alpha} \cdot \mathbf{p}) \tag{19}$$

where the Dirac β matrix is replaced by the matrix $\beta' = \beta - mc^2$ to align relativistic and non-relativistic energy scales. As it is well known this operator includes spin. It does not commute with orbital angular momentum $\mathbf{l}$ alone

$$[\mathbf{l}, \hat{h}_0^R] = i(c\boldsymbol{\alpha} \times \mathbf{p}) = -\frac{1}{2}[\boldsymbol{\Sigma}, \hat{h}_0^R], \tag{20}$$

rather with total angular momentum $\mathbf{j} = \mathbf{l} + (1/2)\boldsymbol{\Sigma}$. In contrast, the non-relativistic free-particle operator commutes separately with orbital angular momentum and spin

$$[\mathbf{l}, \hat{h}_0^{NR}] = i\left(\frac{\mathbf{p}}{m} \times \mathbf{p}\right) = 0 = [\boldsymbol{\sigma}, \hat{h}_0^{NR}] \tag{21}$$

The commutators of the relativistic and non-relativistic free-particle operators with orbital angular momentum look rather different, but can be recast in the same mathematical form using the velocity operators of respective domains

$$\mathbf{v}^R = -i[\mathbf{r}, \hat{h}^R] = c\boldsymbol{\alpha}; \quad \mathbf{v}^{NR} = -i[\mathbf{r}, \hat{h}^{NR}] = \frac{\mathbf{p}}{m} \tag{22}$$

obtained from Heisenberg's equation of motion.

External fields are introduced in the relativistic free-particle operator by the minimal substitutions (17). One should at this point carefully note that the principle of minimal electromagnetic coupling requires the specification of particle charge. This becomes particularly important for the Dirac equation which describes not only the electron, but also its antiparticle, the positron. We are interested in electrons and therefore choose $q = -1$ in atomic units which gives the Hamiltonian

$$\hat{h}^R = \beta' mc^2 + c(\boldsymbol{\alpha} \cdot \mathbf{p}) + c(\boldsymbol{\alpha} \cdot \mathbf{A}) - \phi \tag{23}$$

All solutions of this Hamiltonian are thereby electronic, whether they are of positive or negative energy and contrary to what is often stated in the literature. Positronic solutions are obtained by charge conjugation. From the expectation value of the Dirac Hamiltonian (23) and from consideration of the interaction Lagrangian (16) relativistic charge and current density are readily identified as

$$\rho = \frac{\delta E}{\delta \phi} = -\psi^\dagger I_4 \psi; \quad \mathbf{j} = -\frac{\delta E}{\delta \mathbf{A}} = -\psi^\dagger c\boldsymbol{\alpha}\psi \tag{24}$$

In the non-relativistic domain the Coulomb term is chosen as the two-electron operator $\hat{g}(i,j)$, which is fully consistent with the non-relativistic limit of electrodynamics discussed in the previous section. In the relativistic domain the two-electron interaction is considerably more complicated since it contains all effects of retardation and magnetic interactions. It can therefore not be written on

closed form. In Coulomb gauge it is written as a perturbation expansion in terms of c^{-2} with the Coulomb term

$$\hat{g}_{ij}^{\text{Coul}} = \frac{I_4 I_4}{r_{ij}}$$

as the zeroth-order term. The first-order term is the Breit term [39]

$$\hat{g}_{ij}^{\text{Breit}} = -\left\{ \frac{(c\boldsymbol{\alpha}_i)\cdot(c\boldsymbol{\alpha}_j)}{2c^2 r_{ij}} + \frac{(c\boldsymbol{\alpha}_i\cdot\mathbf{r}_{ij})(c\boldsymbol{\alpha}_j\cdot\mathbf{r}_{ij})}{2c^2 r_{ij}^3} \right\}$$

It can also be rearranged and expressed as the sum of the Gaunt term

$$\hat{g}_{ij}^{\text{Gaunt}} = -\frac{(c\boldsymbol{\alpha}_i)\cdot(c\boldsymbol{\alpha}_j)}{c^2 r_{ij}}$$

and the so-called gauge-dependent term

$$\hat{g}_{ij}^{\text{gauge}} = -\frac{(c\boldsymbol{\alpha}_i\cdot\boldsymbol{\nabla}_i)(c\boldsymbol{\alpha}_j\cdot\boldsymbol{\nabla}_j)r_{ij}}{2c^2}$$

The Breit term can be derived from QED, but can also be obtained in a simpler and heuristic manner by inserting the relativistic velocity operator $c\boldsymbol{\alpha}$ (22) into the vector potential (15) and then introduce the resulting potential into the Dirac operator, which is indeed how Breit obtained the first-order correction to the non-relativistic two-electron interaction. Comparison with the relativistic charge and current density, equation (24), shows that the Coulomb and Gaunt term has the form of charge–charge and current–current interactions, respectively. By a Foldy–Wouthuysen transformation the spin–same orbit $\hat{h}^{\text{SSO}}$ and spin–other orbit $\hat{h}^{\text{SOO}}$ operators of the Breit–Pauli Hamiltonian can be extracted from the Coulomb and Gaunt terms, respectively [39–41]. An immediate conclusion is that the spin–orbit coupling $\hat{h}^{\text{SO}}$ arising from the nuclear framework is of the spin–same orbit type and that spin–other orbit type interactions can be envisaged beyond the Born–Oppenheimer approximation.

2.4. Eliminating relativistic effects

We now consider how to eliminate either all relativistic effects or exclusively the spin–orbit interaction from the relativistic Hamiltonian. We start from the Dirac equation in the molecular field

$$\begin{bmatrix} V & c(\boldsymbol{\sigma}\cdot\mathbf{p}) \\ c(\boldsymbol{\sigma}\cdot\mathbf{p}) & V - 2mc^2 \end{bmatrix} \begin{bmatrix} \psi^{\text{L}} \\ \psi^{\text{S}} \end{bmatrix} = \begin{bmatrix} \psi^{\text{L}} \\ \psi^{\text{S}} \end{bmatrix} E \tag{25}$$

where

$$V(1) = -\sum_A Z_A \int \frac{\rho_A(r_2)}{r_{12}}\, d\tau_2 \tag{26}$$

and ρ_A is the normalized charge distribution of nucleus A. We start from this equation and not the more general form with arbitrary electric and magnetic fields since we will later consider the calculation of electric and magnetic properties in the framework of perturbation theory. It is not possible to obtain its proper non-relativistic limit by simply setting $c \rightarrow \infty$ since the speed of light appears linearly and even quadratically in the operator. Instead, a non-unitary transformation is introduced

$$\begin{bmatrix} \psi^L \\ \psi^S \end{bmatrix} = \begin{bmatrix} I_2 & 0_2 \\ 0_2 & c^{-1}I_2 \end{bmatrix} \begin{bmatrix} \psi^L \\ \chi^S \end{bmatrix} \tag{27}$$

giving the equation

$$\begin{bmatrix} V & (\boldsymbol{\sigma} \cdot \mathbf{p}) \\ (\boldsymbol{\sigma} \cdot \mathbf{p}) & Vc^{-2} - 2m \end{bmatrix} \begin{bmatrix} \psi^L \\ \chi^S \end{bmatrix} = E \begin{bmatrix} I_2 & 0_2 \\ 0_2 & c^{-2}I_2 \end{bmatrix} \begin{bmatrix} \psi^L \\ \chi^S \end{bmatrix} \tag{28}$$

The limit $c \rightarrow \infty$ can now be taken provided that (1) V is everywhere non-singular, which is true for finite nuclei [42] but not point nuclei, and that (2) $|E| \ll c^2$ which is true for the (shifted) positive-energy solutions only. With this procedure all relativistic effects are eliminated and one obtains the four-component non-relativistic Lévy-Leblond equation [34,43]

$$\begin{bmatrix} V & (\boldsymbol{\sigma} \cdot \mathbf{p}) \\ (\boldsymbol{\sigma} \cdot \mathbf{p}) & -2m \end{bmatrix} \begin{bmatrix} \psi^L \\ \chi^S \end{bmatrix} = E \begin{bmatrix} I_2 & 0_2 \\ 0_2 & 0_2 \end{bmatrix} \begin{bmatrix} \psi^L \\ \chi^S \end{bmatrix} \tag{29}$$

which can be shown to be equivalent to the Schrödinger equation.

We now consider how to eliminate the spin–orbit interaction, but not scalar relativistic effects, from the Dirac equation (25). The straightforward elimination of spin-dependent terms, taken to be terms involving the Pauli spin matrices, certainly does not work as it eliminates all kinetic energy as well. A minimum requirement for a correct procedure for the elimination of spin–orbit interaction is that the remaining operator should go to the correct non-relativistic limit. However, this check does not guarantee that some scalar relativistic effects are eliminated as well, as pointed out by Visscher and van Lenthe [44]. Dyall [12] suggested the elimination of the spin–orbit interaction by the non-unitary transformation

$$\begin{bmatrix} \psi^L \\ \psi^S \end{bmatrix} = \begin{bmatrix} I_2 & 0 \\ 0 & \dfrac{1}{2mc}(\boldsymbol{\sigma} \cdot \mathbf{p}) \end{bmatrix} = \begin{bmatrix} \psi^L \\ \phi^S \end{bmatrix} \tag{30}$$

leading to the so-called modified Dirac equation

$$\begin{bmatrix} V & \hat{T} \\ \hat{T} & \dfrac{1}{4m^2c^2}(\boldsymbol{\sigma} \cdot \mathbf{p})V(\boldsymbol{\sigma} \cdot \mathbf{p}) - \hat{T} \end{bmatrix} \begin{bmatrix} \psi^L \\ \phi^S \end{bmatrix} = \begin{bmatrix} 1 & 0 \\ 0 & \dfrac{\hat{T}}{2mc^2} \end{bmatrix} \begin{bmatrix} \psi^L \\ \phi^S \end{bmatrix} E \tag{31}$$

where $\hat{T}$ is the non-relativistic operator of kinetic energy. Further manipulation of the spin-dependent term using the Dirac identity gives

$$\frac{1}{4m^2c^2}(\boldsymbol{\sigma}\cdot\mathbf{p})V(\boldsymbol{\sigma}\cdot\mathbf{p}) = \frac{1}{4m^2c^2}\mathbf{p}V\cdot\mathbf{p} + \frac{i}{4m^2c^2}\boldsymbol{\sigma}\cdot(\mathbf{p}V\times\mathbf{p}). \tag{32}$$

The second term on the right-hand side of the equation gives for point nuclei directly the one-electron spin–orbit operator (2) of the Breit–Pauli Hamiltonian and can be eliminated to give a spin-free equation that becomes equivalent to the Schrödinger equation in the non-relativistic limit. In a quaternion formulation of the Dirac equation the elimination becomes particularly simple. The algebra of the quaternion units is that of the Pauli spin matrices

$$\check{\mathbf{i}} \longleftrightarrow i\sigma_z, \quad \check{\mathbf{j}} \longleftrightarrow i\sigma_y, \quad \check{\mathbf{k}} \longleftrightarrow i\sigma_x \tag{33}$$

In the quaternion modified Dirac equation the spin-free equation is thereby obtained simply by deleting the quaternion imaginary parts. For further details, the reader is referred to Ref. [13].

2.5. On the elimination of the spin–orbit interaction from electric and magnetic properties

2.5.1. General considerations

On matrix form the non-unitary transformations (27) and (30) of the previous section are easily extended to the complete Hamiltonian and have therefore allowed relativistic and non-relativistic spin-free calculations of spectroscopic constants and first-order properties at the four-component level (see, for instance, Refs. [45–47]). In this section, we consider the elimination of spin–orbit interaction in four-component calculations of second-order electric and magnetic properties. Formulas are restricted to the Hartree–Fock [48] or Kohn–Sham [49] level of theory, but are straightforwardly generalized.

Second-order molecular properties can be defined as second derivatives of the (time-averaged) quasienergy Q with respect to frequency-dependent perturbation strengths $\varepsilon_B(\omega_b)$ at zero perturbation ($\boldsymbol{\varepsilon}=\mathbf{0}$)

$$\frac{\mathrm{d}^2 Q}{\mathrm{d}\varepsilon_A(\omega_a)\mathrm{d}\varepsilon_B(\omega_b)}\bigg|_{\boldsymbol{\varepsilon}=\mathbf{0}} = \langle\langle\hat{H}_A;\hat{H}_B\rangle\rangle_{\omega_b}\delta(\omega_a+\omega_b). \tag{34}$$

They reduce to regular energy derivatives in the static limit [48,50]. The linear response function

$$\langle\langle\hat{H}_A;\hat{H}_B\rangle\rangle_\omega = -\mathbf{E}_A^{[1]\dagger}(E_0^{[2]} - \omega S^{[2]})^{-1}\mathbf{E}_B^{[1]} \tag{35}$$

corresponds to the polarization propagator in the energy representation at the RPA level [51,52] and is constructed from property gradients $\mathbf{E}_A^{[1]}$ and $\mathbf{E}_B^{[1]}$ as well as the perturbation-independent resolvent $(E_0^{[2]} - \omega S^{[2]})^{-1}$ which contains the electronic Hessian $E_0^{[2]}$ and the generalized metric $S^{[2]}$. The linear response

function is generally constructed by a two-step procedure. In the first step, the response equation

$$(E_0^{[2]} - \omega S^{[2]})\mathbf{X}_B(\omega) = -\mathbf{E}_B^{[1]} \tag{36}$$

is solved by expanding the solution vector $\mathbf{X}_B(\omega)$ in trial vectors. The computer-intensive part of the calculation is the construction of the σ-vector, that is the contraction of the Hessian $E_0^{[2]}$ with a trial vector $\mathbf{b}_i$. This operation may be expressed as the sum of a one-index transformed regular Fock-matrix $\mathbf{F}^{\{1\}}$ and a two-electron Fock matrix $\mathbf{G}$ generated from the first-order perturbed density

$$\sigma_{pq} = \sum_{rs} E_{0;pq,rs}^{[2]} b_{rs} = -(\mathbf{F}_{pq}^{\{1\}} + \mathbf{G}_{pq}). \tag{37}$$

In the second step, the solution vector $\mathbf{X}_B(\omega)$, corresponding to the first-order response of the wave function, is contracted with property gradient $\mathbf{E}_A^{[1]}$ to form the linear response function. For further details the reader is referred to Refs. [48,49].

A variety of properties can be defined and calculated; I will restrict attention to the operators involved in the calculation of dipole polarizabilities and NMR parameters, corresponding to the introduction of a uniform electric field $\mathbf{E}$ represented by the scalar potential

$$\phi(\mathbf{r}_i) = -\mathbf{r}_i \cdot \mathbf{E}, \tag{38}$$

a uniform magnetic field $\mathbf{B}$ represented by the vector potential

$$\mathbf{A}(\mathbf{r}_i) = \frac{1}{2}(\mathbf{B} \times \mathbf{r}_{iO}); \quad \mathbf{r}_{iO} = \mathbf{r}_i - \mathbf{r}_O, \tag{39}$$

where $\mathbf{r}_O$ is the chosen gauge origin, and the magnetic dipole moment $\mathbf{M}_K = \gamma_K \mathbf{I}_K$ of nucleus K represented by the vector potential

$$\mathbf{A}_K(\mathbf{r}_i) = \frac{\mathbf{M}_K \times \mathbf{r}_{iK}}{c^2 r_{iK}^3} \tag{40}$$

All potentials satisfy Coulomb gauge. The corresponding potentials are introduced into the relativistic Hamiltonian, and the perturbation operators are obtained as

$$\hat{H}_A = \frac{\mathrm{d}h(i)}{\mathrm{d}\varepsilon_A}\bigg|_{\varepsilon=0}. \tag{41}$$

The resulting property operators at the four-component relativistic level are listed in Table 1. From the property operators associated with uniform electric and magnetic fields one may directly read off the relativistic operators of electric dipole moment $\mu_i = -\mathbf{r}_i$ and magnetic dipole moment $\mathbf{m}_i = -\frac{1}{2}c(\mathbf{r}_{iO} \times \boldsymbol{\alpha}_i)$, respectively [36].

These operators may be contrasted with the property operators obtained at the non-relativistic level. The Lévy-Leblond equation given in (29) is consistent with the rigorous non-relativistic limit in that only scalar potentials are included. We now follow the standard, pragmatic approach and consider the operator form

Table 1. First-order *relativistic* one-electron perturbation operators $\hat{H}_A = \frac{dh(i)}{d\varepsilon_A}\big|_{\varepsilon=0}$ from the introduction of a uniform electric field **E**, a uniform magnetic field **B** and a nuclear magnetic dipole moment $\mathbf{M}_K$

ε_A	
E	$\mathbf{r}_i$
B	$\frac{1}{2}c(\mathbf{r}_O \times \boldsymbol{\alpha}_i)$
$\mathbf{M}_K$	$\frac{1}{cr_{iK}^3}(\mathbf{r}_{iK} \times \boldsymbol{\alpha}_i)$

when both scalar and vector potentials are included. The equivalence of the Lévy-Leblond and Schrödinger equations is based on the identity $p^2 = (\boldsymbol{\sigma}\cdot\mathbf{p})(\boldsymbol{\sigma}\cdot\mathbf{p})$. Using the right-hand side of the identity for minimal substitution (17) gives the Hamiltonian

$$\hat{h}^{\text{NR}} = \frac{p^2}{2m} - \phi + \frac{1}{m}(\mathbf{A}\cdot\mathbf{p}) + \frac{A^2}{2m} + \frac{1}{2m}(\boldsymbol{\sigma}\cdot\mathbf{B}) \tag{42}$$

assuming Coulomb gauge. If the left-hand side of the identity is used, the final term of spin-Zeeman type in the Hamiltonian disappears. This term has the electronic g_e factor of two from Dirac theory; in non-relativistic quantum chemistry codes the experimental $g_e = 2.0023193044$ is often used instead. First-order property operators derived from the total operator is given in Table 2. The electric dipole operator is identical to its relativistic counterpart, which is not surprising since there is nothing inherently relativistic about electrostatics. Magnetic operators are on the other hand quite different, although the connection is made more clear by identification of the velocity operators (22) of respective domains. The orbital Zeeman term $\hat{h}_B^{\text{orb}}$ is proportional to the electronic magnetic dipole moment induced by molecular rotation such that in closed-shell molecules the electronic contribution to the spin-rotation tensor is proportional to the paramagnetic part of the NMR shielding tensor

Table 2. First-order *non-relativistic* one-electron perturbation operators $\hat{H}_A = \frac{dh(i)}{d\varepsilon_A}\big|_{\varepsilon=0}$ from the introduction of a uniform electric field **E**, a uniform magnetic field **B** and a nuclear magnetic dipole moment $\mathbf{M}_K$

ε_A	
E	$-\hat{h}_E^{\text{dip}} = \mathbf{r}_i$
B	$\hat{h}_B^{\text{orb}} = \left(\frac{1}{2m}\right)(\mathbf{r}_{iO} \times \mathbf{p}_i)$
	$\hat{h}_B^{\text{spn}} = \left(\frac{1}{2m}\right)\boldsymbol{\sigma}_i$
$\mathbf{M}_K$	$\hat{h}_K^{\text{pso}} = \left(\frac{1}{mc^2 r_{iK}^3}\right)(\mathbf{r}_{iK} \times \mathbf{p}_i)$
	$\hat{h}_K^{\text{sd}} = -\left(\frac{1}{2mc^2}\right)\frac{\boldsymbol{\sigma}_i r_{iK}^2 - 3(\boldsymbol{\sigma}_i \cdot \mathbf{r}_{iK})\mathbf{r}_{iK}}{r_{iK}^5}$
	$\hat{h}_K^{\text{fc}} = \left(\frac{4\pi}{3c^2}\right)\delta(\mathbf{r}_{iK})\boldsymbol{\sigma}_i$

$$M_{ij}^K = 2\gamma_K \sigma_{ij}^{K;\mathrm{p}}/I_{jj}. \tag{43}$$

Likewise the electronic contribution to the rotational g tensor is proportional to the paramagnetic part of the magnetizability

$$g_{ij} = 4m_\mathrm{p}\xi_{ij}^\mathrm{p}/I_{jj}. \tag{44}$$

The above equations assume that the gauge origin is chosen as the molecular center-of-mass and are defined in the principal axis system of the moment of inertia tensor I. In a linear molecule, the parallel component of paramagnetic shielding and magnetizability is zero so that the perpendicular components can be determined from experimental measurements of the spin-rotation constant and the rotational g factor, respectively [53]. However, in relativistic systems there is no longer proportionality between the electronic magnetic dipole moment and angular momentum and so the parallel component of shielding and magnetizability is generally non-zero and not accessible by such measurements [54,55]. Also the explicit relativistic operator for the rotationally induced magnetic moment may need further clarification [56].

The presence of the diamagnetic term gives rise to second-order operators as well, of which some examples are listed in Table 3. In relativistic theory, the diamagnetic contribution is formally absent, but can be associated with rotations between occupied positive-energy and virtual negative-energy orbitals upon the response of the wave function to a magnetic perturbation [57]. It can be introduced explicitly by a Gordon decomposition [58,59] or by a unitary transformation of Foldy–Wouthuysen type, as suggested by Kutzelnigg [60].

The Hamiltonian in equation (42) contains magnetic interactions, but no spin–orbit interaction. This shows that magnetic fields can be introduced in non-relativistic theory, but there is no mechanism to generate them; magnetic induction is absent. As shown by Lévy-Leblond [43,61], spin can be accommodated by the non-relativistic Galilean group. Still, it appears more reasonable to classify the magnetic moment of the electron as a relativistic effect along with other magnetic interactions, even though the mechanism of spin remains a mystery.

The distinction in standard non-relativistic theory between spin–orbit interaction as relativistic on the one hand and other spin interactions as non-relativistic on the other hand does lead to some inconsistencies. Consider, for instance, a hydrogen-like atom where the coordinate system is shifted from the

Table 3. Second-order *non-relativistic* one-electron perturbation operators $\hat{H}_{AB} = \frac{\mathrm{d}^2 h(i)}{\mathrm{d}\varepsilon_A \mathrm{d}\varepsilon_B}\big|_{\boldsymbol{\varepsilon}=\mathbf{0}}$ from the introduction of a uniform magnetic field $\mathbf{B}$ and a nuclear magnetic dipole moment $\mathbf{M}_K$

ε_A	ε_B	
$\mathbf{B}$	$\mathbf{B}$	$\hat{h}_{BB}^{\mathrm{dia}} = \frac{1}{8m}[I_3 r_i^2 - \mathbf{r}_i \cdot \mathbf{r}_i^\mathrm{T}]$
$\mathbf{B}$	$\mathbf{M}_K$	$\hat{h}_{BK}^{\mathrm{dia}} = \frac{1}{2mc^2}\left[\frac{I_3(\mathbf{r}_i \cdot \mathbf{r}_{iK}) - \mathbf{r}_i \mathbf{r}_{iK}^\mathrm{T}}{r_{iK}^3}\right]$
$\mathbf{M}_K$	$\mathbf{M}_L$	$\hat{h}_{KL}^{\mathrm{dso}} = \left(\frac{1}{mc^4}\right)\left[\frac{I_3(\mathbf{r}_{iK} \cdot \mathbf{r}_{iL}) - \mathbf{r}_{iK}\mathbf{r}_{iL}^\mathrm{T}}{r_{iK}^3 r_{iL}^3}\right]$

nucleus to the electron. Then, inserting the potentials (15) and replacing the velocity of the nucleus by the negative of the non-relativistic electron velocity operator (22), a spin–orbit interaction term appears in the non-relativistic Hamiltonian. One might argue that the change of frame has been accompanied by a Lorentz transformation of potentials and that the vector potential goes to zero in the non-relativistic limit due to its c^{-2} dependence. However, the same c^{-2} dependence is found in the vector potential of the dipole magnetic moment of nuclear spin (40), yet the corresponding property operator is widely used in non-relativistic calculations. A uniform magnetic field, equation (39), is generated by moving charges and the spin-Zeeman interaction would therefore have been regarded as a spin–orbit interaction if the coordinate system had been placed on the moving charges. These are clearly awkward choices of reference frames, but inconsistencies remain even if one stays within a coordinate system fixed on the nuclear framework. Consider the introduction of a second electron. In the molecule-fixed frame its potentials are given by equation (15). Insertion into the non-relativistic Hamiltonian now gives the complete spin–other orbit interaction $\hat{h}^{SOO}$ (3), but no spin–same orbit interaction $\hat{h}^{SSO}$. The spin–other orbit interaction $\hat{h}^{SOO}$ also appears if one inserts the vector potential associated with the magnetic dipole moment of the electron, obtained from the substitution $\mathbf{M}_K \rightarrow -\frac{1}{2}\boldsymbol{\sigma}$ in equation (40), into the orbital paramagnetic term $\frac{1}{m}(\mathbf{A}\cdot\mathbf{p})$ of the non-relativistic Hamiltonian (42). This contribution can, however, be eliminated as redundant since it is just another way of viewing the first interaction. The vector potential of the second electron appears in the nuclear frame to the same order in c^{-2} as the vector potential associated with nuclear spin (40) and gives rise to exactly the same kind of interaction. It is therefore hard to justify that it is normally neglected from the standard non-relativistic Hamiltonian.

2.5.2. Sample calculations

The somewhat artificial separation between spin–orbit interaction and other spin interactions leads to difficulties when one tries to eliminate the former interaction in four-component calculations of magnetic properties by the procedure outlined in Section 2.4, that is by eliminating the quaternion imaginary parts of matrix representations of the modified Dirac equation. This can be illustrated by a simple test calculation. Unless otherwise stated, the calculations reported in this chapter have been carried out using a development version of the DIRAC code [62]. We will, however, first show the elimination of the spin–orbit interaction from calculations of electric properties. Figure 1 shows the frequency-dependent dipole polarizability of the mercury atom calculated at the four-component relativistic DFT level using the BLYP functional [63,64] and the basis uncDZ* of Ref. [49], derived from the relativistic finite nucleus Gaussian basis sets developed by Dyall [65]. The full calculation (SR+SO) gives a static dipole polarizability of 33.60 a.u., to be compared with the value 33.92 a.u. from experiment [66]. When all spin–orbit interaction is eliminated, the calculated value is modified only slightly to 33.57 a.u. On the other hand, the full calculation shows two poles corresponding to excitations $^1S_0 \rightarrow {}^3P_1$ and $^1S_0 \rightarrow {}^1P_1$ (experimental values are
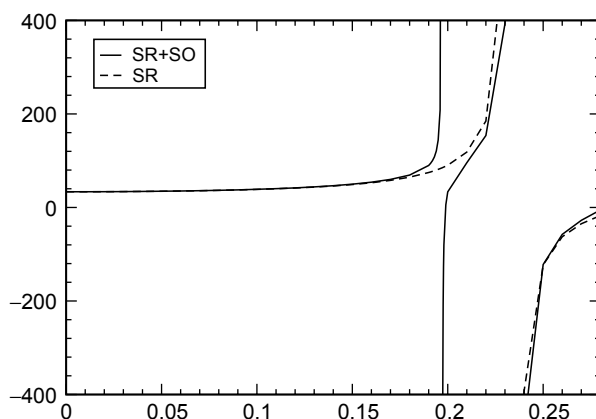
Fig. 1. BLYP/uncDZ* mean dipole polarizability of the mercury atom as a function of frequency. All values in atomic units. SR + SO refers to calculations based on the Dirac–Coulomb Hamiltonians, whereas SR refers to calculations in which all spin–orbit interaction has been eliminated.

0.1796 and 0.2464 a.u., respectively [67]), whereas the first, spin-forbidden transition is absent in the spin-free calculation.

The difficulties encountered in the calculation of magnetic properties are illustrated by a series of Hartree–Fock calculations of the indirect spin–spin coupling constant of the $^{11}B^1H$ molecule at the experimental geometry 1.232425 Å using the cc-pVDZ [68] basis set in uncontracted form. The results are given in Table 4. For reference, we have given the result obtained by the non-relativistic DALTON code [69]. The paramagnetic contribution to the coupling may be split into a Fermi-contact (FC) contribution, a spin-dipole (SD) contribution and a paramagnetic spin–orbit (PSO) contribution, the former two contributions being spin dependent. In these latter two contribution, we have used $g_e = 2$ for direct comparison with Dirac theory. Four different calculations have then been carried out using the DIRAC code, a point nucleus and the Lévy-Leblond Hamiltonian with the diamagnetic contribution calculated as an expectation value. In the first (LLI) calculation, the quaternion imaginary parts have been eliminated from the regular Fock matrix prior to the one-index transformation in the construction of the σ-vector (37) in the solution of the response equation (36). The results are then in perfect agreement with the results obtained with the DALTON code. However, when quaternion imaginary parts are deleted from the property gradients $\mathbf{E}_{A/B}^{[1]}$ as well (LL3) *all* spin-dependent contributions are deleted, and the paramagnetic contribution reduces to the PSO contribution. The result can be readily understood by application of the transformation (30) for the modified Dirac equation to a general relativistic magnetic operator

$$\begin{bmatrix} 0 & c(\boldsymbol{\sigma}\cdot\mathbf{A}) \\ c(\boldsymbol{\sigma}\cdot\mathbf{A}) & 0 \end{bmatrix} \rightarrow \begin{bmatrix} 0 & \dfrac{1}{2m}(\boldsymbol{\sigma}\cdot\mathbf{A})(\boldsymbol{\sigma}\cdot\mathbf{p}) \\ \dfrac{1}{2m}(\boldsymbol{\sigma}\cdot\mathbf{p})(\boldsymbol{\sigma}\cdot\mathbf{A}) & 0 \end{bmatrix} \qquad (45)$$

Table 4. The isotropic indirect spin–spin coupling constant of ^{11}B^{1}H calculated at various levels of theory. 'LL' refers to the Lévy-Leblond Hamiltonian. 'std' refers to a full relativistic calculation using restricted (RKB) or unrestricted (UKB) kinetic balance. 'spf' refers to calculations based on a spin-free relativistic Hamiltonian. Columns F, G and $\mathbf{E}_{A/B}^{[1]}$ refer to whether quaternion imaginary parts are deleted (0) or not (1) from the regular Fock matrix F prior to one-index transformation, from the two-electron Fock matrix G constructed from the first-order perturbed density or from the property gradients $\mathbf{E}_{A/B}^{[1]}$

DALTON	Total	Paramagnetic	Diamagnetic	FC	SD	PSO
$g_e = 2$	52.6562	53.1201	-0.4639	52.9694	1.0485	-0.8977
DIRAC	Total	Paramagnetic	Diamagnetic	F	G	$\mathbf{E}_{A/B}^{[1]}$
LL1	52.6549	53.1188	-0.4639	0	1	1
LL2	19.0402	19.5041	-0.4639	0	0	1
LL3	-1.3616	-0.8977	-0.4639	0	1	0
LL4	-1.3616	-0.8977	-0.4639	0	0	0
DIRAC	Total	'Paramagnetic'	'Diamagnetic'	F	G	$\mathbf{E}_{A/B}^{[1]}$
std (RKB)	52.4885	53.0398	-0.5520	1	1	1
std (UKB)	52.6047	53.0398	-0.4351	1	1	1
spf1	52.5586	53.1098	-0.5512	0	1	1
spf2	18.9620	19.5145	-0.5526	0	0	1
spf3	-1.0149	-0.9019	-0.1130	0	1	0
spf4	-1.0149	-0.9019	-0.1130	0	0	0

Using the Dirac identity then gives

$$\frac{1}{2m}(\boldsymbol{\sigma}\cdot\mathbf{p})(\boldsymbol{\sigma}\cdot\mathbf{A}) = \frac{1}{2m}\mathbf{p}\cdot\mathbf{A} + i\boldsymbol{\sigma}\times(\mathbf{p}\times\mathbf{A}) \tag{46}$$

and comparison with equation (42) shows that the contributions of spin-Zeeman type have been eliminated. The procedure outlined in Section 2.4 for the elimination of the spin–orbit interaction is therefore incapable of distinguishing this interaction from other spin interactions and perhaps justly so, since they can all be considered spin–orbit interactions. If the quaternion imaginary parts are retained in the property gradients, but eliminated from the G matrix of the σ-vector (LL2), a non-sense result is obtained. This is because the wave function is not allowed to respond properly to the spin interactions described by the property operators. If these spin interactions are already eliminated from the property gradient (LL4) a result identical to that of calculation LL3 is obtained, since no response to spin interactions is required. We have also carried out a series of four-component relativistic calculations. The division between paramagnetic and diamagnetic contributions is now based on the contribution to the final response functions from rotations (++) between occupied and virtual positive-energy orbitals on the one hand and the contributions from rotations ($+-$) between occupied positive-energy and virtual negative-energy orbitals on the other hand, in agreement with the conclusions of Ref. [57]. We have carried out full four-component relativistic calculations using restricted (RKB) and unrestricted (UKB) kinetic balance. One may observe that whereas the 'paramagnetic' contributions are identical some discrepancy occurs in the 'diamagnetic'

contribution with the UKB result being closest to the non-relativistic result. This can be understood from the fact that the diamagnetic contribution is obtained from the $(+-)$ rotations in the non-relativistic limit from a resolution of identity

$$\text{Re}\left[\sum_i \langle\psi^L|(\boldsymbol{\sigma}\cdot\mathbf{A})|\psi_i^S\rangle\langle\psi_i^S|(\boldsymbol{\sigma}\cdot\mathbf{A})|\psi^L\rangle\right] = \langle\psi^L|A^2|\psi^L\rangle \tag{47}$$

which requires magnetic balance that is a coupling between the large and small components different from that of RKB [57]. UKB is as such more flexible and allows a better realization of magnetic balance. Unfortunately, our present implementation in DIRAC allows only the use of RKB in spin-free calculations. In Table 4 one may observe that the various flavors of spin-free calculations give results close to the corresponding Lévy-Leblond results. A significant difference, though, is that 'diamagnetic' contributions are significantly modified when quaternion imaginary parts are deleted from the property gradients. This can be understood from consideration of equation (47) which shows that the spin-free diamagnetic contribution, which contains no spin, is obtained from a resolution of identity involving quantities with spin dependence. Note, however, that it is now the magnetic operator (46) of the modified Dirac equation that should be employed.

From the above discussion it becomes clear that in order to eliminate the spin–orbit interaction in four-component relativistic calculations of magnetic properties one must delete the quaternion imaginary parts from the regular Fock matrix and not from other quantities appearing in the response function (35). It is also possible to delete all spin interactions from magnetic properties, but this requires the use of the Sternheim approximation [57,73], that is calculating the diamagnetic contribution as an expectation value.

We apply this technique to study the effect of the spin–orbit coupling on an NMR shielding tensor and the shielding polarizability of the xenon atom. The shielding polarizabilities are defined as the second derivatives of nuclear shielding constants with respect to an electric field $\mathbf{E}$

$$\sigma_{ijkl}^{K''} = \left.\frac{\partial^2\sigma_{ij}^K(\mathbf{E})}{\partial E_k\partial E_l}\right|_{\mathbf{E}=0} \tag{48}$$

In a previous publication [70], we calculated the shielding polarizabilities of all noble gases from helium to xenon at the Hartree–Fock level using a mixed analytic-numerical approach, that is calculating the shielding tensor as a linear response function and then performing numerical differentiation with respect to an applied uniform electric field along the x-axis. We found that relativistic effects on the shielding polarizabilities were quite sizable and larger than for the shielding tensor itself. Due to opposing trends in the parallel and perpendicular components, the relativistic effect on the mean shielding polarizability

$$B_{xx}^K = -\frac{1}{6}(\sigma_{xxxx}^{K''} + 2\sigma_{yyxx}^{K''}) \tag{49}$$

is somewhat quenched. The parallel shielding polarizability σ_{xxxx}'' forms a rather regular monotonically decreasing sequence with increasing noble gas nuclear

charge, but for the perpendicular component σ''_{yyxx} this trend is broken when going from krypton (-7944.8 ppm/(au field^2)) to xenon ($+3468.9$ ppm/(au field^2)). In order to investigate this irregularity, we subsequently calculated second- and third-order relativistic corrections to the shielding polarizability starting from the non-relativistic HF wave function and following the approach of Ref. [71], but the results were not entirely conclusive. In the present chapter, we show that the observed irregularity in the perpendicular shielding polarizability σ''_{yyxx} is a spin–orbit effect.

We have carried out a sequence of Hartree–Fock calculations of the shielding polarizability of the xenon atom using the methodology of Ref. [70]. We used the large uncontracted Gaussian basis set of Ref. [72], but supplemented with a diffuse s-exponent (0.01491595) to give a total large component 25s19p22d11f8g basis set. Results are given in Table 5. The extra diffuse s-exponent shifts the value of the shielding constant by $+93$ ppm from the value 6938.0 ppm in the original basis [72] and is needed for a proper description of the shielding polarizability. The SO effect on the shielding constant is quite small – 16.3 ppm – compared to a scalar relativistic effect of 1371.8 ppm and an order of magnitude smaller than the SO effect (303.51 ppm) given by Manninen *et al.* [71]. The effect of spin–orbit coupling on the shielding polarizability is on the other hand substantial, being -21110.6 ppm/(au field^2) and 29598.5 ppm/(au field^2) for the parallel and perpendicular components, respectively. Whereas SO effects completely dominate relativistic effects on the parallel shielding polarizability

Table 5. The NMR shielding constant and shielding polarizabilities of the xenon atom calculated at the Hartree–Fock level using the Dirac–Coulomb Hamiltonian (SR+SO), its spin-free version (SR) as well as the non-relativistic Lévy-Leblond Hamiltonian. The shielding constant is given in ppm and shielding polarizabilities in ppm/(au field2) (1 a.u. field$=5.14220642\times10^{11}$ V m^{-1})

	Total	'Paramagnetic'	'Diamagnetic'
SR+SO			
σ	7030.4	2031.4	4999.0
σ''_{xxxx}	$-21,395.2$	$-21,082.9$	-312.3
σ''_{yyxx}	2940.2	3260.6	-321.2
B_{xx}	2585.8	2427.0	159.1
SR			
σ	7014.1	2011.6	5002.6
σ''_{xxxx}	-284.6	16.2	-300.7
σ''_{yyxx}	$-26,670.9$	$-26,349.1$	-322.2
B_{xx}	8933.5	8776.2	157.5
Non-relativistic			
σ	5642.3	0.00	5642.3
σ''_{xxxx}	-293.8	0.00	-293.8
σ''_{yyxx}	$-12,218.4$	$-11,909.9$	-308.5
B_{xx}	4121.8	3970.0	151.8

σ''_{xxxx}, a large scalar relativistic effect of -14439.9 ppm/(au field^2), opposing the SO effect, is observed for the perpendicular component σ''_{yyxx}. Whereas large SO effects explain the irregularities observed for the perpendicular shielding polarizability of the noble gases, their elimination introduces irregularities for the parallel component, and a more extensive study is therefore required to fully untangle the various effects contributing to the calculated shielding polarizabilities.

3. FINAL REMARKS AND CONCLUSIONS

The electronic Hamiltonian within the Born–Oppenheimer approximation may be split into two parts

$$\hat{H} = \hat{H}_p + \hat{H}_{int}.$$

It is pointed out in this chapter that standard non-relativistic calculations use the *non-relativistic* free-particle operator $\hat{H}_p$ combined with the *relativistic* Hamiltonian $\hat{H}_{int}$ which describes the interaction between particles and fields. This observation prompted us to look for the rigorous non-relativistic electronic Hamiltonian. We find that in the non-relativistic limit of Maxwell's equations both the divergence and the curl of the magnetic field **B** is zero. From the boundary conditions on Maxwell's equations combined with the Helmholtz theorem we are then led to the conclusion that the magnetic field **B** is zero all over space, and that electrodynamics reduce to electrostatics in the non-relativistic limit. However, from a pragmatic point of view it is perfectly reasonable to introduce both scalar and vector potentials into the non-relativistic Hamiltonian, simply because it gives a better description of our physical world. However, this approach does lead to some inconsistencies. We show that the pragmatic approach is unable to describe spin–orbit interaction arising from the nuclear framework or the spin–same orbit interaction arising from the presence of other electrons, but can perfectly well describe the spin–other orbit interaction which is an interaction equivalent to the interaction with nuclear spins. We also point out that *all* spin interactions can be considered spin–orbit interactions depending on the reference frame chosen.

   We then turn to the question of how to eliminate the spin–orbit interaction in four-component relativistic calculations. This allows the assessment of spin–orbit effects on molecular properties within the framework of a single theory. In a previous publication [13], we have shown how the spin–orbit interaction can be eliminated in four-component relativistic calculations of spectroscopic properties by deleting the quaternion imaginary parts of matrix representations of the quaternion modified Dirac equation. We show in this chapter how the application of the same procedure to second-order electric properties takes out spin-forbidden transitions in the spectrum of the mercury atom. Second-order magnetic properties require more care since the straightforward application of the above procedure will extinguish *all* spin interactions. After careful analysis on how to proceed we

demonstrate the effect of spin–orbit coupling on the NMR shielding and shielding polarizability of the xenon atom. It is also possible to calculate magnetic properties with all spin interactions eliminated, but only within the framework of the Sternheim approximation [57,73], that is by calculating the diamagnetic contribution as an expectation value.

ACKNOWLEDGEMENTS

REFERENCES

[1] M. Quack, *Angew. Chem. Int. Ed.*, 2002, **41**, 4618.
[2] D. P. Craig and T. Thirunamachandran, *Molecular Quantum Electrodynamics*, Dover, New York, 1998.
[3] V. M. Goldschmidt, T. Barth and G. Lunde, *Norske Vidensk. Akad. Skrifter I Mat. Naturv. Kl.*, 1925, **7**, 1.
[4] P. Pyykkö, *Chem. Rev.*, 1988, **88**, 563.
[5] P. J. Mohr and B. N. Taylor, *Rev. Mod. Phys.*, 2000, **72**, 351.
[6] M. Dolg, in *Relativistic Electronic Structure Theory – Part 1. Fundamentals* (ed. P. Schwerdtfeger), Elsevier, Amsterdam, 2002, p. 523.
[7] M. Douglas and N. M. Kroll, *Ann. Phys.*, 1974, **82**, 89.
[8] B. A. Hess, *Phys. Rev. A*, 1985, **32**, 756.
[9] B. A. Hess, *Phys. Rev. A*, 1986, **33**, 3742.
[10] E. van Lenthe, E. J. Baerends and J. G. Snijders, *J. Chem. Phys.*, 1993, **99**, 4597.
[11] E. van Lenthe, J. G. Snijders and E. J. Baerends, *J. Chem. Phys.*, 1996, **105**, 6505.
[12] K. G. Dyall, *J. Chem. Phys.*, 1994, **100**, 2118.
[13] L. Visscher and T. Saue, *J. Chem. Phys.*, 2000, **113**, 3996.
[14] D. H. Whiffen, *Pure Appl. Chem.*, 1978, **50**, 75.
[15] W. Kutzelnigg, in *Calculation of NMR and EPR Parameters* (eds M. Kaupp, M. Bühl and V. G. Malkin), Wiley-VCH, Weinheim, 2004, p. 43.
[16] B. A. Hess, C. M. Marian and S. D. Peyerimhoff, D. R. Yarkony (ed.) *Modern Electronic Structure Theory – Part I. Advanced Series in Physical Chemistry,* World Scientific Singapore, 1995, Vol. 2, p. 152.
[17] C. M. Marian, in *Reviews in Computational Chemistry*, (eds K. B. Lipkowitz and D. B. Boyd), Wiley-VCH, New York, 2001, Vol. 17, p. 99.
[18] D. G. Fedorov, S. Koseki, M. W. Schmidt and M. S. Gordon, *Rev. Phys. Chem.*, 2003, **22**, 551.
[19] H. A. Bethe and E. E. Salpeter, *Quantum Mechanics of One- and Two-Electron Atoms*, Plenum/Rosetta, New York, 1977.
[20] J. D. Jackson and L. B. Okun, *Rev. Mod. Phys.*, 2001, **73**, 663.
[21] R. E. Moss, *Advanced Molecular Quantum Mechanics*, Chapmann & Hall, London, 1973.
[22] C. G. Darwin, *Philos. Mag.*, 1920, **39**, 537.
[23] L. H. Thomas, *Nature*, 1926, **117**, 514.
[24] L. H. Thomas, *Philos. Mag.*, 1927, **3**, 1.
[25] J. D. Jackson, *Classical Electrodynamics*, Wiley, New York, 1999.
[26] C. W. Misner, K. S. Thorne and J. A. Wheeler, *Gravitation*, Freeman, San Francisco, 1973.
[27] H. Zatzkis, *J. Franklin Inst.*, 1960, **269**, 268.

[28] D. Shelupsky, *Am. J. Phys.*, 1967, **35**, 650.

[29] K. R. MacKenzie, *Am. J. Phys.*, 1972, **40**, 1661.

[30] W. R. Theis, *Z. Phys. A*, 1979, **290**, 355.

[31] W. L. Kennedy, *Eur. J. Phys.*, 2002, **23**, 235.

[32] W. E. Baylis and G. Jones, *J. Math. Phys.*, 1988, **29**, 57.

[33] A. Pais, *Subtle is the Lord … The Science and the Life of Albert Einstein*, Oxford University Press, Oxford, 1982.

[34] J.-M. Lévy-Leblond, *Commun. Math. Phys.*, 1967, **6**, 286.

[35] W. Kutzelnigg, in *Relativistic Electronic Structure Theory – Part 1. Fundamentals* (ed. P. Schwerdtfeger), Elsevier, Amsterdam, 2002.

[36] T. Saue, in *Relativistic Electronic Structure Theory. Part 1. Fundamentals* (ed. P. Schwerdtfeger), Elsevier, Amsterdam, 2002, p. 332.

[37] K. Schwarzschild, *Gött. Nach., Math.-Phys. Kl.*, 1903, 126.

[38] M. Gell-Mann, *Nuovo Cim. Suppl.*, 1956, **4**, 848.

[39] G. Breit, *Phys. Rev.*, 1929, **34**, 553.

[40] T. Itoh, *Rev. Mod. Phys.*, 1965, **37**, 159.

[41] T. Saue, Ph.D. Thesis, University of Oslo, 1996.

[42] L. Visscher and K. G. Dyall, *At. Data Nucl. Data Tables*, 1997, **67**, 207.

[43] J.-M. Lèvy-Leblond, *Nuovo Cim.*, 1974, **4**, 99.

[44] L. Visscher and E. van Lenthe, *Chem. Phys. Lett.*, 1999, **306**, 357.

[45] K. Faegri and T. Saue, *J. Chem. Phys.*, 2001, **115**, 2456.

[46] J. N. P. van Stralen, L. Visscher and J. F. Ogilvie, *Phys. Chem. Chem. Phys.*, 2004, **6**, 3779.

[47] I. Infante and L. Visscher, *J. Chem. Phys.*, 2004, **121**, 5783.

[48] T. Saue and H. J. A. Jensen, *J. Chem. Phys.*, 2003, **118**, 522.

[49] P. Salek, T. Helgaker and T. Saue, *Chem. Phys.*, 2005, **311**, 187.

[50] O. Christiansen, P. Jørgensen and C. Hättig, *Int. J. Quantum Chem.*, 1998, **68**, 1.

[51] J. Oddershede, *Adv. Chem. Phys.*, 1987, **67**, 201.

[52] J. Oddershede, in *Methods in Computational Molecular Physics* (eds S. Wilson and G. H. F. Diercksen), Plenum Press, New York, 1992.

[53] W. H. Flygare, *Chem. Rev.*, 1974, **74**, 655.

[54] T. Enevoldsen, L. Visscher, T. Saue, H. J. Aa. Jensen and J. Oddershede, *J. Chem. Phys.*, 2000, **112**, 3493.

[55] T. Enevoldsen, T. Rasmussen and S. P. A. Sauer, *J. Chem. Phys.*, 2001, **114**, 84.

[56] B. Mashhoon, *Phys. Rev. Lett.*, 1988, **61**, 2639.

[57] G. Aucar, T. Saue, H. J. A. Jensen and L. Visscher, *J. Chem. Phys.*, 1999, **110**, 6208.

[58] W. Gordon, *Z. Phys.*, 1928, **50**, 630.

[59] J. J. Sakurai, *Advanced Quantum Mechanics*, Addison-Wesley, Reading, MA, 1967.

[60] W. Kutzelnigg, *Phys. Rev. A*, 2003, **67**, 032109.

[61] J.-M. Levy-Leblond in *Group Theory and Its Applications*, (ed. E. M. Loebl), Academic Press, New York, 1971, Vol. II, p. 221.

[62] DIRAC, a relativistic *ab initio* electronic structure program, Release DIRAC04.0 (2004), written by H. J. Aa. Jensen, T. Saue and L. Visscher with contributions from V. Bakken, E. Eliav, T. Enevoldsen, T. Fleig, O. Fossgaard, T. Helgaker, J. Laerdahl, C. V. Larsen, P. Norman, J. Olsen, M. Pernpointner, J. K. Pedersen, K. Ruud, P. Salek, J. N. P. van Stralen, J. Thyssen, O. Visser and T. Winther (http://dirac.chem.sdu.dk).

[63] A. D. Becke, *Phys. Rev. A*, 1988, **38**, 3098.

[64] C. Lee, W. Yang and R. G. Parr, *Phys. Rev. B*, 1988, **37**, 785.

[65] K. G. Dyall, *Theor. Chem. Acc.*, 2004, **112**, 403. The basis sets are available from the DIRAC web site http://dirac.chem.sdu.dk

[66] D. Goebel and U. Hohm, *J. Phys. Chem.*, 1996, **100**, 7729.

[67] C. E. Moore, *Atomic Energy Levels. Circ. 467*, National Bureau of Standards, Washington, DC, 1958, Vol. III.

[68] T. H. Dunning, *J. Chem. Phys.*, 1989, **90**, 1007.

[69] Dalton, a molecular electronic structure program, Release 1.2 (2001), written by T. Helgaker, H. J. Aa. Jensen, P. Jørgensen, J. Olsen, K. Ruud, H. Ågren, A. A. Auer, K. L. Bak, V. Bakken, O. Christiansen, S. Coriani, P. Dahle, E. K. Dalskov, T. Enevoldsen, B. Fernandez, C. Hättig,

K. Hald, A. Halkier, H. Heiberg, H. Hettema, D. Jonsson, S. Kirpekar, R. Kobayashi, H. Koch, K. V. Mikkelsen, P. Norman, M. J. Packer, T. B. Pedersen, T. A. Ruden, A. Sanchez, T. Saue, S. P. A. Sauer, B. Schimmelpfennig, K. O. Sylvester-Hvid, P. R. Taylor and O. Vahtras (http://www.kjemi.uio.no/software/dalton/dalton.html).

[70] M. Pecul, T. Saue, K. Ruud and A. Rizzo, *J. Chem. Phys.*, 2004, **121**, 3051.

[71] P. Manninen, P. Lantto, J. Vaara and K. Ruud, *J. Chem. Phys.*, 2003, **119**, 2623.

[72] J. Vaara and P. Pyykkö, *J. Chem. Phys.*, 2003, **118**, 2973.

[73] M. M. Sternheim, *Phys. Rev.*, 1962, **128**, 676.

Highly Compact Wavefunctions for Two-Electron Systems

Frank E. Harris[1,2] and Vedene H. Smith, Jr.[3]

[1]*Department of Physics, University of Utah, Salt Lake City, UT, USA*
[2]*Quantum Theory Project, University of Florida, Gainesville, FL, USA*
[3]*Department of Chemistry, Queen's University, Kingston, Ont., Canada*

Abstract

There is particular value in having wavefunctions for multielectron systems which are compact but nevertheless have the features needed to capture the essence of electron correlation effects. For few-electron systems, explicit use of the interelectron distances has proved to be an indispensible component of highly accurate wavefunctions, but such wavefunctions contain hundreds or thousands of terms (configurations). We show here that for two-electron systems (the He isoelectronic series), expansions in which all the interparticle distances occur exponentially converge extremely rapidly if the nonlinear parameters occurring therein are very carefully optimized. Compact expansions of this kind give excellent values of the total energy (four-configuration functions exhibiting energy errors between 32 and 38 microhartree), and give other properties, including those arising entirely from electron correlation, with very small errors. These functions are highly suitable for visualizing the wavefunctions and for performing other analyses.

Contents

1. INTRODUCTION

Two-electron systems, i.e. the He atom and its isoelectronic ions, are the simplest species exhibiting electron correlation, and ever since the earliest days of quantum mechanics there has been interest in finding simple, yet accurate descriptions of correlation effects in such systems. Independent-particle

methods are of course inherently incapable of treating electron correlation, and expansions based on orbitals do not converge rapidly. The first significant contribution toward an efficient treatment of electron correlation was the introduction by Hylleraas, in 1929 [1], of a basis that included the interelectron distance r_{12} as an explicit coordinate in He. This was a precursor to more accurate studies on He in terms of r_{12} and the electron–nuclear distances r_1, r_2; the study that gained the most attention was that of Pekeris [2], who formed basis functions by appending powers of r_1, r_2, and r_{12} to an orbital product $\exp(-\varepsilon[r_1+r_2])$. His most accurate wavefunction of this type consisted of 1078 terms. A few years later Frankowski and Pekeris [3] investigated basis sets that also included powers of $(r_1^2 + r_2^2)^{1/2}$ and $\ln(r_1+r_2)$; with 246 terms of this sort they obtained a wavefunction with even less error in the energy than before.

Much more recently, extremely accurate studies on He-like systems have been reported, including that of Frolov [4] on H^- and He, an even more precise study of He by Schwartz [5], and computations on the He-like positive ions with nuclear charges $Z=3$–10 by Frolov and Smith [6]. While these investigations quantitatively reproduced the energy and other properties of He-like systems, the wavefunctions which did so contained thousands of terms, making an understanding of their features less than apparent. The situation corresponds well to an observation made by Mulliken [7] (and resuscitated in a recent paper by Scully *et al.* [8]):

> …the more accurate the calculations become the more the concepts tend to vanish into thin air.

An early attempt to find more compact, but still accurate He-like wavefunctions was reported in 1977 by Thakkar and Smith [9]. An interesting feature of that work was the use of basis functions that depended exponentially on all three interparticle distances, of the generic form $\exp(-\alpha r_1 - \beta r_2 - \gamma r_{12})$. They showed that the essential features of the He-like systems could be reproduced using as few as 66 exponential-basis terms; such wavefunctions typically gave the energy to within about 1 microhartree, and yielded excellent values of other properties as well. These wavefunctions were certainly more compact than those mentioned in the previous paragraph, but were hardly simple enough to address Mulliken's concern.

More recently, Kleinekathöfer, Patil, Tang, and Toennies (KPTT) [10] proposed a far more compact wavefunction for He-like systems, based on the use of a functional form that is essentially completely determined by requiring proper behavior of the wavefunction at small and large-r limits. The KPTT wavefunction is more complicated to use than the functions entering the large-scale accurate computations and from the perspective of the present authors is comparable in utility to a moderate-length configuration expansion. Its virtue is its lack of arbitrary parameters.

The present contribution investigates compact wavefunctions for the He isoelectronic series from a more pragmatic viewpoint, with the goal of finding functional forms that are easy both to use and to understand.

2. PROBLEM FORMULATION

We consider systems consisting of two electrons and an infinitely massive nucleus of charge Z, moving subject to the nonrelativistic Hamiltonian (in hartree atomic units, $m_e = \hbar = e = 4\pi\varepsilon_0 = 1$)

$$H = -\frac{1}{2}(\nabla_1^2 + \nabla_2^2) - \frac{Z}{r_1} - \frac{Z}{r_2} + \frac{1}{r_{12}}. \tag{1}$$

Here $\mathbf{r}_i$ (with magnitude r_i) describes the position of electron i relative to the nucleus, r_{12} is the interelectron distance $|\mathbf{r}_1 - \mathbf{r}_2|$, and ∇_i is with respect to the coordinates of $\mathbf{r}_i$. We will later refer to the momentum operators $\mathbf{p}_i = -i\nabla_i$.

2.1. Basis set

The ground-state wavefunction will be antisymmetric in the spin coordinates of the two electrons and symmetric in their spatial coordinates. It will also have zero orbital angular momentum (an S state); the most general S state can be shown to depend only on the interparticle distances $\mathbf{r}_1$, $\mathbf{r}_2$, and $\mathbf{r}_{12}$ [11]. We construct it from a basis of functions ϕ_i of the form

$$\phi_i = (1 + P_{12})e^{-\alpha_i r_1 - \beta_i r_2 - \gamma_i r_{12}}, \tag{2}$$

where P_{12} is an operator interchanging $\mathbf{r}_1$ and $\mathbf{r}_2$. We have chosen to restrict the parameters α_i, β_i, γ_i to real values. These parameters need not all be nonnegative, but they must satisfy $\alpha_i + \beta_i > 0$, $\alpha_i + \gamma_i > 0$, and $\beta_i + \gamma_i > 0$.

The basis we have chosen is not that which has been used in the majority of the studies of three-body systems. The most-used basis, often called a Hylleraas basis, consists of functions of the form

$$\phi_i = r_1^{m_i} r_2^{n_i} r_{12}^{p_i}\, e^{-\varepsilon(r_1 + r_2)}, \tag{3}$$

where ε is a real parameter that may (or may not) have been optimized, and m_i, n_i, p_i are nonnegative integers associated with basis function ϕ_i. In that basis, our parameter γ is zero, and the explicit dependence on the interelectron separation consists of the powers of r_{12}. Hylleraas wavefunctions usually have the same value of ε for all basis functions, and the needed flexibility is obtained by taking many sets of the m, n, and p. By contrast, in our basis one does not have powers of r_i or r_{12}, but instead takes individual values of α, β, and γ for each basis function.

2.2. Determination of wavefunction

For given values of the α_i, β_i, γ_i, the coefficients C_i in a wavefunction of the form

$$\Psi = \sum_i C_i \phi_i \tag{4}$$

Table 1. Two He wavefunctions

	Ψ_1	Ψ_2
α_1	2.101867	2.373380
β_1	1.986105	1.823092
γ_1	0.263687	0.190160
α_2	2.049014	2.508922
β_2	2.034074	1.767881
γ_2	0.266048	0.130290
α_3	2.109173	2.068456
β_3	1.395636	2.022847
γ_3	-0.096823	0.264301
α_4	2.735322	2.106416
β_4	1.696751	1.395785
γ_4	-0.004567	-0.096228
E	-2.903687899	-2.903688012

Configurations in descending order of importance.

were determined variationally, minimizing the energy expectation value $E = \langle \Psi | H | \Psi \rangle$ by standard methods. The matrix elements needed for this purpose have been extensively studied, appearing as long ago as 1962 in a paper by Calais and Löwdin [12]. Another important contribution from that era was by Sack *et al.* [13]. A compact and convenient formulation is available in a paper by Abbott and Maslen [14]; see also Ref. [6].

Optimum values of the α_i, β_i, γ_i were then determined variationally, minimizing E (obtained as described above) with respect to these parameters by application of a conjugate gradient method. This task is not without its problems; even when taking as few as two configurations (containing six nonlinear parameters) the energy surface exhibits multiple relative minima, some of which are above the global minimum by very small amounts. This phenomenon is reflective of the fact that as a basis becomes more complete, the dependence of the computed energy on the basis weakens, disappearing entirely when completeness is achieved.

An indication of the severity of this problem is illustrated by some data for four-configuration wavefunctions of He. Table 1 shows two such wavefunctions and the energy obtained from each. The first of these is near a local minimum; the second can be further refined to move toward what we believe to be the global minimum, ultimately yielding a wavefunction of energy -2.903688260 hartree, and with the parameters shown in Table 5.

2.3. Wavefunction properties

For the analysis of the wavefunctions we computed the expectation values of a number of operators, using formulas in the works already cited. The quantities $\langle \delta(\mathbf{r}_1) \rangle$ and $\langle \delta(\mathbf{r}_{12}) \rangle$ give probability densities for pairwise particle coincidences; $\langle \delta(\mathbf{r}_1)\delta(\mathbf{r}_{12}) \rangle$ gives the same data for the triple coincidence. The quantity ν_1 is

a measure of the electron–nuclear cusp strength, with formal definition

$$\nu_1 = \frac{\langle \delta(\mathbf{r}_1) \partial/\partial r_1 \rangle}{\langle \delta(\mathbf{r}_1) \rangle};$$

(5)

the electron–electron cusp, ν_{12}, is defined analogously.

For visualization purposes we have made plots of pair distribution functions, defining the electron–nuclear radial probability distribution function $D(r_1)$ by the formula

$$D(r_1) = 2(4\pi r_1^2)\int dr_2 |\Psi(r_1, r_2, r_{12})|^2.$$

(6)

We follow here the notation of Thakkar and Smith [15], and evaluated this and the other distribution functions mentioned below using the formulas given by them. The prefactor "2" in the definition of $D(r_1)$ causes it to describe the pair density contributions of the entire electron distribution (rather than that of one of the two electrons).

In addition to $D(r_1)$, we have plotted the charge density $\rho(r_1) = D(r_1)/4\pi r_1^2$, the electron–electron probability distribution function $P(r_{12})$ (defined similarly to $D(r_1)$ but with omission of the prefactor "2"), and the electron–electron density $h(r_{12}) = P(r_{12})/4\pi r_{12}^2$ (sometimes referred to as the *intracule function*).

3. COMPACT WAVEFUNCTIONS

3.1. Single-configuration wavefunctions

Taking He as an example, we start by examining various single-configuration wavefunctions. In Table 2 we compare the optimum-energy "closed-shell" simple exponential wavefunction, $\exp(-\alpha[r_1 + r_2])$, with α assigned the well-known value 27/16, the optimum-energy "split-shell" wavefunction, and the optimum-energy single-configuration wavefunction of the type given in equation (2). All these wavefunctions (and in fact all studied herein) exactly satisfy the virial theorem, a consequence of the optimization of the chosen functional form. We see that relaxing the closed-shell condition $\alpha = \beta$ cuts the energy error in half and causes the delta-function properties to move significantly closer to their exact values. However, the absence of r_{12} from the wavefunction (and of equivalent functional dependence obtained from multiple configurations) causes the properties whose origin is correlation to remain at zero values. Thus, $\mathbf{r}_1 \cdot \mathbf{r}_2$ and $\mathbf{p}_1 \cdot \mathbf{p}_2$ both have vanishing expectation values, and there is no electron–electron cusp ν_{12}. The third data column of Table 2 shows that substantial improvement is gained by including $\exp(-\gamma r_{12})$ in the wavefunction. We note a decrease of nearly an order of magnitude in the energy error, and all the computed properties move closer to their exact values. Those arising solely from correlation are now nonzero and of correct orders of magnitude.

Looking next at the pair distribution functions, we find very little difference among the three single-configuration wavefunctions in the quantities describing the electronic distribution relative to the nucleus. The probability distributions

Table 2. Energy (E) and other properties of He, computed from optimized single-configuration wavefunctions of the form given in equation (2)

	$\alpha=\beta,\ \gamma=0$[a]	$\alpha\neq\beta,\ \gamma=0$[b]	$\alpha\neq\beta,\ \gamma=0$[c]	Exact[d]
E	-2.847656	-2.875661	-2.899534	-2.903724
$E-E_{\text{exact}}$	0.055618	0.028063	0.004190	
$\langle \mathbf{r}_1\cdot\mathbf{r}_2\rangle$	0.000000	0.000000	-0.085010	-0.064737
$\langle \mathbf{p}_1\cdot\mathbf{p}_2\rangle$	0.000000	0.000000	0.192818	0.159069
$\langle \delta(\mathbf{r}_1)\rangle$	1.529613	1.751235	1.777836	1.810429
$\langle \delta(\mathbf{r}_{12})\rangle$	0.191202	0.164767	0.129494	0.106345
$\langle \delta(\mathbf{r}_1)\delta(\mathbf{r}_2)\rangle$	2.340	2.010	2.000	1.869
ν_1	-1.688	-1.910	-1.962	-2.000
ν_{12}	0.000	0.000	$+0.207$	$+0.500$

Data are in hartree atomic units; ν is defined in equation (5).
[a] Closed-shell, $\alpha=\beta=27/16$.
[b] Split-shell, $\alpha=2.183171$, $\beta=1.188531$.
[c] General, parameter values given in Table 4.
[d] From Ref. [4].

$D(r_1)$ of these wavefunctions are so similar that little insight would be gained by studying their graphs; the densities $\rho(r_1)$ are also similar except in the immediate vicinity of the nucleus, where they approach different intercepts (as shown adequately from the $\langle \delta(\mathbf{r}_1)\rangle$ data in Table 2).

Larger differences are observed in the electron–electron distributions; the radial probability density, $P(r_{12})$, is shown for the three single-configuration wavefunctions in Fig. 1. Improvement in the energy occurs concurrently with a spreading of the electron-pair probability distribution; a majority of the spread occurs with passage from the closed-shell to the split-shell wavefunction. A small further spreading is associated with the inclusion of the factor $\exp(-\gamma r_{12})$.
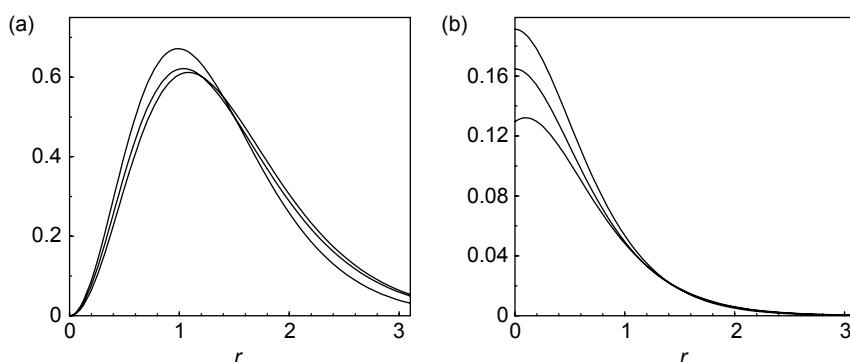
Fig. 1. Electron–electron distribution functions for single-configuration He wavefunction: (a) radial probability distribution $P(r_{12})$; (b) intracule function $h(r_{12})$. In both graphs, the curve with largest maximum is for the closed-shell wavefunction; that of intermediate maximum is for the split-shell wavefunction; that of smallest maximum is for the wavefunction containing $\exp(-\gamma r_{12})$.

The differences between the single-configuration wavefunctions are more clearly illustrated by comparing their plots of the intracule function $h(r_{12})$, also shown in Fig. 1. This plot reveals the absence of an electron–electron cusp for both the closed and split-shell functions, but shows that the inclusion of $\exp(-\gamma r_{12})$ causes the distribution to have a minimum at $r_{12}=0$, forming a cusp (of the correct sign) at that point. This feature will be important for the description of phenomena that depend upon the coincidence probability.

It is of interest to compare the data in Table 2 with the results of the investigation by KPTT. Only the tabulated function with nonzero γ is qualitatively comparable with the KPTT wavefunction for He; these two wavefunctions have about the same energy (that of KPTT is -2.9000). Our wavefunction has the exact virial ratio ($-$potential energy/kinetic energy$=2$ *vs.* the KPTT value of 2.074); this may be interpreted as an indication that it is at a better overall scaling than the KPTT function. That function, however, gives better results than ours for $\langle \mathbf{p}_1 \cdot \mathbf{p}_2 \rangle$: KPTT, 0.1545 *vs.* our 0.1928 and the exact value of 0.1591.

3.2. Two and three-configuration wavefunctions

Next we look at small multiconfiguration results for He; wavefunctions of two and three optimized configurations are compared with the single-configuration and exact results in Table 3; the nonlinear parameters of these wavefunctions are given in Table 4. It is apparent that the second and third configurations cause major improvements in the energy; the second configuration reduces the energy error by about an order of magnitude and the third reduces it further to less than one-quarter of the two-configuration error. Both the two- and three-configuration results render $\langle \mathbf{p}_1 \cdot \mathbf{p}_2 \rangle$, as well as the energy, more accurately than the KPTT wavefunction; the delta-function properties have also moved close to the exact results. The cusps, which are forced to have exact values in the KPTT formulation, are also moving near to correct values.

Table 3. Energy (E) and other properties of He, computed from optimized one, two, and three-configuration wavefunction (nonlinear parameters given in Table 4)

	1 cfg	2 cfg	3 cfg	Exact[a]
E	-2.899534	-2.903270	-2.903629	-2.903724
$E-E_{\text{exact}}$	0.004190	0.000454	0.000095	
$\langle \mathbf{r}_1 \cdot \mathbf{r}_2 \rangle$	-0.085010	-0.064522	-0.064373	-0.064737
$\langle \mathbf{p}_1 \cdot \mathbf{p}_2 \rangle$	0.192818	0.160746	0.158308	0.159069
$\langle \delta(\mathbf{r}_1) \rangle$	1.777836	1.783896	1.810488	1.810429
$\langle \delta(\mathbf{r}_{12}) \rangle$	0.129494	0.111481	0.108729	0.106345
$\langle \delta(\mathbf{r}_1)\delta(\mathbf{r}_2) \rangle$	2.000	1.803	1.849	1.869
ν_1	-1.962	-1.967	-2.001	-2.000
ν_{12}	$+0.207$	$+0.368$	$+0.427$	$+0.500$

Data are in hartree atomic units; ν is defined in equation (5).
[a] From Ref. [4].

Table 4. Nonlinear parameters (bohr^{-1}) of optimized one, two, and three-configuration wavefunctions for He

	Configuration no.	α	β	γ
1 cfg	1	2.206563	1.440579	-0.207329
2 cfg	1	1.802894	1.596886	0.127593
	2	1.705758	1.682329	0.145798
3 cfg	1	1.889806	1.765564	0.286883
	2	1.831361	1.819072	0.292634
	3	1.993570	1.365369	-0.102849

Configurations in descending order of importance.

It is interesting to note that the two-configuration wavefunction yields a positive electron–electron cusp ν_{12} even though neither of its configurations has a negative value of γ. What is occurring is that the two configurations enter the wavefunction with opposite signs, and their net "negative-cusp" contribution is of opposite sign to their net "$\delta(\mathbf{r}_{12})$" contribution.

Plots of the pair distribution functions also indicate a rapid convergence as the number of configurations increases. The main feature that undergoes a noticeable change is the intracule function. Figure 2 shows $h(r_{12})$ for these He wavefunctions. Addition of a second or third configuration lowers the pair density near $r_{12} = 0$ and intensifies the cusp, without making significant changes to the remainder of the pair distribution.

The trends observed here continue with the addition of more configurations; we decided that a point of diminishing returns was reached at four configurations, and therefore, established that degree of expansion for more exhaustive investigation.
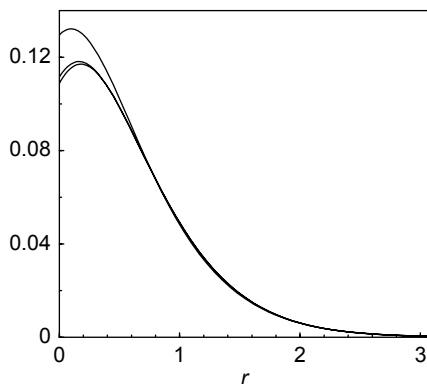
Fig. 2. Electron–electron distributions for optimized one, two, and three-configuration He wavefunctions: intracule function $h(r_{12})$. The curve can be identified by the heights of their maxima; larger maxima correspond to fewer configurations.

Table 5. Nonlinear parameters ($bohr^{-1}$) of optimized four-configuration wavefunctions

	Configuration no.	α	β	γ
H^-	1	0.857017	0.751909	0.101595
	2	0.841729	0.762291	0.105682
	3	1.021337	0.310090	-0.016292
	4	0.814655	0.814651	-0.212153
He	1	2.320734	1.854831	0.174222
	2	2.427973	1.804002	0.128539
	3	2.033598	2.066629	0.231423
	4	2.110861	1.397545	-0.096522
Li^+	1	3.889807	2.715842	0.467625
	2	4.058785	2.653114	0.400041
	3	3.235769	3.107544	0.633256
	4	3.172516	2.329155	-0.106053
Be^{2+}	1	5.266091	3.648710	0.740043
	2	5.412373	3.587088	0.685639
	3	4.288314	4.288312	0.956404
	4	4.234919	3.268605	-0.110674
B^{3+}	1	6.657537	4.630991	1.020850
	2	6.830580	4.556398	0.960249
	3	5.438123	5.438121	1.276809
	4	5.288535	4.216078	-0.113689
C^{4+}	1	7.999460	5.612951	1.319931
	2	8.227960	5.510309	1.244053
	3	6.575755	6.575753	1.602057
	4	6.337482	5.167592	-0.115545
N^{5+}	1	9.268894	6.669156	1.673238
	2	9.625883	6.501048	1.566561
	3	7.739251	7.739249	1.940929
	4	7.379939	6.124969	-0.116955
O^{6+}	1	10.564255	7.691253	1.996284
	2	11.017617	7.471464	1.867163
	3	8.886470	8.886468	2.272811
	4	8.421547	7.083665	-0.117972
F^{7+}	1	11.902890	8.692622	2.308089
	2	12.422627	8.437673	2.164073
	3	10.033120	10.033118	2.607577
	4	9.460889	8.044691	-0.118788
Ne^{8+}	1	13.283463	9.675289	2.615987
	2	13.850848	9.397064	2.461465
	3	11.180907	11.180904	2.949205
	4	10.497988	9.907933	-0.119465

Configurations in descending order of importance.

3.3. Four-configuration wavefunctions

As indicated in Section 3.2, we settled on an optimized four-configuration wavefunction using the basis described in equation (2) as a standard highly compact function for extensive study. These wavefunctions, for the members of the He isoelectronic series from $Z=1$ (H^-) to $Z=10$ (Ne^{8+}), have the parameter values given in Table 5.

Table 6. Exact [4,6] and compact-function properties, respectively labeled E and C, for Z from 1 to 6

	$^\infty H^-$	$^\infty He$	$^\infty Li^+$
E_C	-0.5277131	-2.9036883	-7.2798789
E_E	-0.5277510	-2.9037244	-7.2799134
$E_C - E_E$	0.0000379	0.0000361	0.0000345
$\langle \mathbf{r}_1 \cdot \mathbf{r}_2 \rangle_C$	-0.684555	-0.064662	-0.017248
$\langle \mathbf{r}_1 \cdot \mathbf{r}_2 \rangle_E$	-0.687313	-0.064737	-0.017253
$\langle \mathbf{p}_1 \cdot \mathbf{p}_2 \rangle_C$	0.032967	0.158902	0.288883
$\langle \mathbf{p}_1 \cdot \mathbf{p}_2 \rangle_E$	0.032880	0.159069	0.288976
$\langle \delta(\mathbf{r}_1) \rangle_C$	0.164154	1.807626	6.845013
$\langle \delta(\mathbf{r}_1) \rangle_E$	0.164553	1.810429	6.852009
$\langle \delta(\mathbf{r}_{12}) \rangle_C$	0.002865	0.108367	0.539470
$\langle \delta(\mathbf{r}_{12}) \rangle_E$	0.002738	0.106345	0.533723
$\langle \delta(\mathbf{r}_1)\delta(\mathbf{r}_2) \rangle_C$	0.005128	1.885	33.408
$\langle \delta(\mathbf{r}_1)\delta(\mathbf{r}_2) \rangle_E$	0.005064	1.869	33.321
$\nu_{1,C}$	-0.996	-1.993	-2.992
$\nu_{1,E}$	-1.000	-2.000	-3.000
$\nu_{12,C}$	$+0.437$	$+0.436$	$+0.441$
$\nu_{12,E}$	$+0.500$	$+0.500$	$+0.500$
	$^\infty Be^{2+}$	$^\infty Be^{3+}$	$^\infty C^{4+}$
E_C	-13.6555322	-22.0309380	-32.4062132
E_E	-13.6555662	-22.0309716	-32.4062466
$E_C - E_E$	0.0000340	0.0000336	0.0000334
$\langle \mathbf{r}_1 \cdot \mathbf{r}_2 \rangle_C$	-0.00690431	-0.00342637	-0.00194202
$\langle \mathbf{r}_1 \cdot \mathbf{r}_2 \rangle_E$	-0.00690595	-0.00342674	-0.00194226
$\langle \mathbf{p}_1 \cdot \mathbf{p}_2 \rangle_C$	0.420480	0.552814	0.685468
$\langle \mathbf{p}_1 \cdot \mathbf{p}_2 \rangle_E$	0.420520	0.552753	0.685335
$\langle \delta(\mathbf{r}_1) \rangle_C$	17.1873	34.7409	61.4178
$\langle \delta(\mathbf{r}_1) \rangle_E$	17.1982	34.7587	61.4436
$\langle \delta(\mathbf{r}_{12}) \rangle_C$	1.53465	3.33215	6.17079
$\langle \delta(\mathbf{r}_{12}) \rangle_E$	1.52290	3.31244	6.14104
$\langle \delta(\mathbf{r}_1)\delta(\mathbf{r}_2) \rangle_C$	231.34	996.8	3223
$\langle \delta(\mathbf{r}_1)\delta(\mathbf{r}_2) \rangle_E$	231.04	996.0	3221
$\nu_{1,C}$	-3.993	-4.993	-5.993
$\nu_{1,E}$	-4.000	-5.000	-6.000
$\nu_{12,C}$	$+0.442$	$+0.443$	$+0.443$
$\nu_{12,E}$	$+0.500$	$+0.500$	$+0.500$

Data are in hartree atomic units; ν is defined in equation (5).

Energies and other properties for the optimized four-configuration wavefunctions are presented in Tables 6 and 7. These wavefunctions yielded surprisingly accurate total energies, with errors ranging from 37.9 (for H^-) to 32.8 microhartrees (for Ne^{8+}). Not only are the energies almost incredibly precise for a wavefunction of this degree of compactness, but so also are the derived properties. The values of $\langle \mathbf{r}_1 \cdot \mathbf{r}_2 \rangle$ and $\langle \mathbf{p}_1 \cdot \mathbf{p}_2 \rangle$, both entirely dependent upon the description of electron correlation, are correct to within 1%, and in many cases to 0.1%. Similar agreement is found for the delta-function properties and for the electron–nuclear cusps. The only tabulated property not at the above level of accuracy was the electron–electron cusp strength, which is somewhat over 10% from its exact value $+0.5$. The energy and the values of $\langle \mathbf{p}_1 \cdot \mathbf{p}_2 \rangle$, the only properties available for comparison with KPTT, indicate errors about two orders of magnitude less than the corresponding KPTT values.

Looking next at the wavefunctions themselves, we see that there is a difference in character between that for H^- and those of the other species—the most obvious distinguishing feature is the occurrence of two H^- configurations with negative γ, in contrast to a single negative γ for He through Ne^{8+}. Wavefunctions of these two types correspond to low-lying relative energy minima in the parameter space, with the H^--type minimum becoming less favored as Z increases. For He, the H^--type minimum corresponds to the wavefunction labelled Ψ_1 in Table 1; as shown in that table, its energy is only 0.4 microhartree above the global minimum. By the time Ne^{8+} is reached, the two minima are separated by more than 1 millihartree.

Table 7. Exact [4,6] and compact-function properties, respectively labelled E and C, for Z from 7 to 10

	∞N^{5+}	∞O^{6+}	∞F^{7+}	∞Ne^{8+}
E_C	-44.7814121	-59.1565622	-75.5316795	-93.9067737
E_E	-44.7814451	-59.1565951	-75.5317124	-93.9068065
$E_C - E_E$	0.0000330	0.0000329	0.0000329	0.0000328
$\langle \mathbf{r}_1 \cdot \mathbf{r}_2 \rangle_C$	-0.00120499	-0.00079835	-0.00055921	-0.00040250
$\langle \mathbf{r}_1 \cdot \mathbf{r}_2 \rangle_E$	-0.00120514	-0.00079846	-0.00055599	-0.00040254
$\langle \mathbf{p}_1 \cdot \mathbf{p}_2 \rangle_C$	0.818379	0.951381	1.084471	1.217620
$\langle \mathbf{p}_1 \cdot \mathbf{p}_2 \rangle_E$	0.818119	0.951029	1.084024	1.217079
$\langle \delta(\mathbf{r}_1) \rangle_C$	99.125	149.775	215.278	297.541
$\langle \delta(\mathbf{r}_1) \rangle_E$	99.162	149.825	215.342	297.623
$\langle \delta(\mathbf{r}_{12}) \rangle_C$	10.289	15.926	23.320	32.709
$\langle \delta(\mathbf{r}_{12}) \rangle_E$	10.247	15.870	23.248	32.620
$\langle \delta(\mathbf{r}_1)\delta(\mathbf{r}_2) \rangle_C$	8599	19980	41836	80775
$\langle \delta(\mathbf{r}_1)\delta(\mathbf{r}_2) \rangle_E$	8596	19975	41750	80763
$\nu_{1,C}$	-6.993	-7.993	-8.993	-9.992
$\nu_{1,E}$	-7.000	-8.000	-9.000	-10.000
$\nu_{12,C}$	$+0.444$	$+0.444$	$+0.445$	$+0.445$
$\nu_{12,E}$	$+0.500$	$+0.500$	$+0.500$	$+0.500$

Date are in hartree atomic units; ν is defined in equation (5).
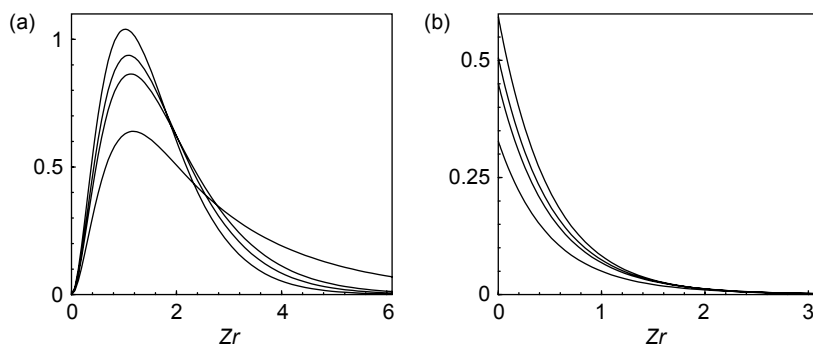
Fig. 3. Z-scaled electron–nuclear distribution functions for H^-, He, Li^+, and Ne^{8+}: (a) radial probability distribution $D(r_1)/Z$; (b) radial density $\rho(r_1)/Z^3$. The curves can be identified from the fact that higher maxima correspond to higher Z.

One of the desirable features of compact wavefunctions is the ability to use them to examine additional features of the electron distribution without the necessity of repeating extensive computations to recreate complicated wavefunctions. We illustrate this point, and also exhibit the similarity of our wavefunctions with those of the 66-configuration study of Thakkar and Smith [15] by looking at the pair distribution functions. It is most instructive to present these as Z-scaled quantities; Figure 3 contains the electron–nuclear distributions $D(r_1)$ and $\rho(r_1)$; for clarity we only plot data for H^-, He, Li^+, and Ne^{8+}. Even after Z scaling, a small but systematic narrowing of the distributions with increasing Z is still in process at $Z=10$.

The Z-scaled electron–electron distribution shows more pronounced differences for species of different Z. Values of $P(r_{12})$ and $h(r_{12})$ are given in Fig. 4. The Z-scaled intercepts (values of $\langle \delta(\mathbf{r}_{12}) \rangle$) change appreciably with Z, and even at $Z = 10$ the electron–electron cusp is clearly visible. None of these graphs exhibit
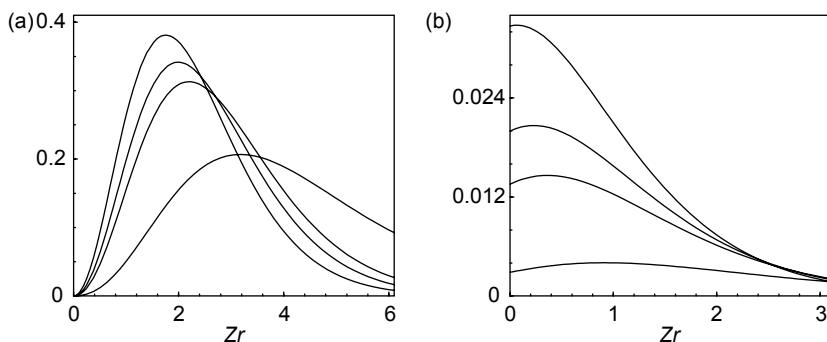
Fig. 4. Z-scaled electron distribution functions for H^-, He, Li^+, and Ne^{8+}: (a) radial probability distribution $P(r_{12})/Z$; (b) intracule function $h(r_{12})/Z^3$. Curve identification: same as Fig. 3.

perceptible differences from those from the 66-configuration Thakkar/Smith wavefunctions.

ACKNOWLEDGEMENTS

REFERENCES

[1]   E. Hylleraas, *Z. Phys.*, 1929, **54**, 347.

[2]   C. L. Pekeris, *Phys. Rev.*, 1962, **126**, 1470.

[3]   (a) K. Frankowski and C. L. Pekeris, *Phys. Rev.*, 1966, **146**, 46; (b) K. Frankowski and C. L. Pekeris, *Phys. Rev.*, 1996, **150**, 366(E).

[4]   A. M. Frolov, *Phys. Rev. A*, 1998, **57**, 2436.

[5]   C. Schwartz, *J. Comput. Methods Sci. Engng*, to appear.

[6]   (a) A. M. Frolov and V. H. Smith, Jr., *J. Phys. B*, 2004, **37**, 2917; (b) A. M. Frolov and V. H. Smith, Jr., *J. Phys. B*, 2004, **37**, 4037(E).

[7]   R. S. Mulliken, *J. Chem. Phys.*, 1965, **43**, S2.

[8]   M. O. Scully, R. E. Allen, Y. Dou, K. T. Kapale, M. Kim, G. Chen and A. Svidzinsky, *Chem. Phys. Lett.*, 2004, **389**, 385.

[9]   A. J. Thakkar and V. H. Smith Jr., *Phys. Rev. A*, 1977, **15**, 1.

[10] U. Kleinekathöfer, S. H. Patil, K. T. Tang and J. P. Toennies, *Phys. Rev. A*, 1996, **54**, 2840.

[11] C. Schwartz, *Phys. Rev.*, 1962, **128**, 1146.

[12] J. L. Calais and P.-O. Löwdin, *J. Mol. Spectrosc.*, 1962, **8**, 203.

[13] R. A. Sack, C. C. J. Roothaan and W. Kolos, *J. Math. Phys.*, 1967, **8**, 1093.

[14] P. C. Abbott and E. N. Maslen, *J. Phys. B*, 1986, **19**, 1595.

[15] A. J. Thakkar and V. H. Smith Jr., *J. Chem. Phys.*, 1977, **67**, 1191.

Excitation Energies for Transition Metal Atoms – A Comparison between Coupled Cluster Methods and Second-Order Perturbation Theory

Juraj Raab and Björn O. Roos

Department of Theoretical Chemistry, Chemical Center, P.O. Box 124,
S-221 00 Lund, Sweden

Abstract

Coupled cluster methods are compared to multiconfigurational second-order perturbation theory in a study of the high spin $d^x s^2 \rightarrow d^{x+1} s^1$ excitations in first, second, and third row transition metals. Large basis sets of the atomic natural orbital type are used. Scalar relativistic effects are included using the Douglas–Kroll–Hess Hamiltonian. The effect of spin–orbit coupling is demonstrated for third row atoms. The results show that the two methods give results of the same accuracy, with the exception of first row atoms with less than five 3d-electrons. The CASPT2 method here overestimates the effect of 3p correlation with about 0.1 eV.

Contents

1. INTRODUCTION

In this chapter we present the results from a study of the high spin $d^x s^2 \rightarrow d^{x+1} s^1$ excitation for the first, second, and third row transition metal (TM) atoms. Two methods have been used: coupled cluster with and without triples corrections (CCSD(T)) and multiconfigurational perturbation theory (CASSCF/CASPT2). The aim of the study has been to establish the accuracy of the latter approach, using CCSD(T) as the calibration point. Excitation energies for the first row TMs have, for a long time, been used to calibrate quantum chemical methods. It has been found particularly difficult to describe processes where the number of d-electrons changes, in particular, for atoms with more than half-filled d-shells. The reason is the strong electron repulsion, which apart from yielding strong effects of electron correlation, also affects the radial shapes of the d-orbitals.

It was shown in a study of the nickel atom that one had to use an active space extended with an extra d-shell (the *double shell* effect) when the MRCI or CASSCF/CASPT2 methods were used to compute the d^8s^2 $^3F \rightarrow d^9s^1$ ^3D and d^8s^2 $^3F \rightarrow d^{10}s^0$ ^1S excitation energies [1,2]. Raghavachari and Trucks (RT) presented in 1989 results from a study of all first row transition metals where the quadratic CI method was used (QCISD(T)) [3]. A rather limited basis set was used and relativistic effects were included only heuristically. Nevertheless, this study showed that a size-consistent method gives reasonable results for all first row TMs. A number of density functional studies have been performed [4–6]. Many functionals give large errors. Bauschlicher and Gutsev concluded in 2002 from a study of Ti, V, Fe, and Mn that the best functionals to use for transition metals were B3LYP and BP86 but deviation from experiment were in general larger than 0.5 eV [5]. Somewhat better results were obtained for the first row TMs in a recent application of a new functional called X3LYP [6]. An extensive CCSD(T) study of the Fe atom with a new basis set showed that this approach can give results in excellent agreement with experiment [7]. Similar results have been obtained for V, Cr, and Mn using the QCISD(T) method [8].

These single reference-based methods are limited to cases where the reference function can be written as a single determinant. This is most often not the case and it is then necessary to use a multiconfigurational approach. Multireference CI can possibly be used, but this method is only approximately size extensive, which may lead to large errors unless an extended reference space is used. For example, Osanai *et al.* [8] obtained for the $^6S \rightarrow {}^6D$ excitation energy in Mn 2.24 eV with the QCISD(T) method while SDCI with cluster corrections gave 2.64 eV. Extended basis sets were used. The experimental value is 2.15 eV.

Here, we are testing the possibilities of multiconfigurational second-order perturbation theory (CASPT2) [9,10]. It has been applied in a large number of studies of transition metal complexes (see, for example, Ref. [11]). However, no extensive test for the atoms has been performed, except a study of the contributions of core correlation to the excitation energies in first row TM ions [12]. It has recently been suggested in a study of the Cr dimer that the CASPT2 method overestimates the contribution from core–core and core–valence correlation to the binding energy [13]. This conclusion is somewhat alarming. If it is true, it will also affect the $d^xs^2 \rightarrow d^{x+1}s^1$ excitation energies in the atoms because core correlation favors electronic states with more d-electrons. It is therefore of interest to compare CASPT2 results for these excitation energies with results obtained with the CCSD(T) method that experience shows to give accurate results, at least for first row TMs.

We extend the method over all three rows of TMs. No systematic study is available for the heavier atoms, where relativistic effects are more prominent. Here, we use the Douglas–Kroll–Hess (DKH) Hamiltonian [14,15] to account for scalar relativistic effects. No systematic study of spin–orbit coupling has been performed but we show in a few examples how it will affect the results. A new basis set is used in these studies, which has been devised to be used with the DKH Hamiltonian.

2. METHODS

All calculations were carried out with the software MOLCAS-6.0 [16]. Scalar relativistic effects were included using a DKH Hamiltonian [14,15]. Specially designed basis sets of the atomic natural orbital type were used. These basis sets have been optimized with the scalar DKH Hamiltonian. They were generated using the CASSCF/CASPT2 method. The semi-core electrons (ns, np, $n = 3, 4, 5$) were included in the correlation treatment. More details can be found in Refs. [17–19]. The size of the basis sets is presented in Table 1. All atoms have been computed with basis sets including up to g-type function. For the first row TMs we also studied the effect of adding two h-type functions.

The CCSD(T) calculations were performed using the ROHF CCSD(T) code included in the MOLCAS program package. To preserve proper spin properties, the cluster amplitudes describing double excitations (t_{ij}^{ab}) were spin adapted (the DDVV approximation) [20]. We present results using the CCSD and CCSD(T) variants of the coupled cluster method. It is important in these calculations to find a representation where the reference function can be written as a single determinant. It was obtained by running the calculations in D_{2h} symmetry and select the open shell orbitals such that the determinant exactly represents a component of the given electronic state. As it turns out, this is possible for the lowest high spin states for all the atoms in both the $nd^x(n+1)s^2$ and the $nd^{x+1}(n+1)s^1$ electronic configurations. It will, in general, not be possible for low spin states (or for higher angular momentum than 3 when the calculations are run in D_{2h} symmetry). There will be some symmetry breaking in the coupled cluster amplitudes but we expect the effect to be small. Thus, CC wave functions give a correct, symmetry adapted, description of the electronic states. It would not be the case if an unrestricted version of the CC method was used.

The CASSCF/CASPT2 calculations were performed with an active space including the five nd, the $(n+1)$s, the three $(n+1)$p orbitals, and a second set of nd' orbitals to account for the *double shell* effect. The importance of including a second 3d shell in the active space was detected in an early study of the electronic spectrum of the nickel atom [2]. This had already been suggested from MRCI results [1]. The results obtained by RT at about the same time indicated that such effects are effectively accounted for when a method is used that includes cluster corrections to all orders, like the QCI method used by them [3]. This result will hold true also for the less approximate coupled cluster method CCSD(T).

Also the CASSCF/CASPT2 calculations were performed in D_{2h} symmetry and the orbitals rotations were restricted such that mixing between different angular

Table 1. ANO-RCC basis sets used for the transition metal atoms

Excitation atom	Primitive	Contracted
Sc–Cu	21s15p10d6f4g(2h)	10s9p8d5f4g(2h)
Y–Ag	21s18p13d6f4g	10s9p8d5f4g
La–Au	24s21p15d11f4g	11s10p9d8f4g

Calculations were performed with and without two h-type functions for the first row TMs.

momenta did not occur. This does not completely ensure spherical symmetry because orbitals in different irreps may have different radial shape, but the deviations should be small. In most cases separate calculations were made for each of the two electronic states. In some cases this was not possible because the two states have components in the same irreps and have the same spin. State average calculations were then made. An example is the ^{4}F $d^7s^2 \rightarrow ^4$F d^8s^1 excitation in Co, Rh, and Ir. The CASPT2 calculations used the new level shift technique that shifts active orbital energies in order to simulate ionization energies for orbitals excited out and electron affinities for orbitals excited into. The technique has recently been shown to reduce the systematic error in the CASPT2 approach for processes where the number of closed shell electron pairs changes [21].

3. RESULTS

3.1. All atoms

We present the results for all atoms in Table 2. Three sets of results are given: CCSD, CCSD(T), and CASPT2. For the first row atoms we have also performed calculations with two h-type basis functions added to the ANO-RCC basis set. Table 3 gives the root mean square (RMS) errors and also the maximum absolute error.

Comparison is made to experimental energies that have been averaged over the J quantum number. This works well for the first row atoms where the spin–orbit coupling is small and there is little interaction between different electronic states but becomes more questionable for the second and third row atoms. We shall return to this problem later.

The overall accuracy for all atoms is illustrated in Fig. 1, which gives the error in computed excitation energies for the three methods used (the $d^x s^2$ state is the reference state for all atoms). The RMS error is 0.21 for CCSD, 0.11 for CCSD(T), and 0.14 for CASPT2. The largest errors are found for the excitations to the ^{1}S $d^{10}s^0$ state in Ni and Pd. It is clear from the picture that the errors vary in an irregular way, but some general trends may be observed. CCSD and CCSD(T), in general, give too large excitation energies, at least for the first and second row atoms. The results for the third row are obscured by the large spin–orbit effects (see below). The triples corrections lead in most cases to improved results, in particular for the heavier first row atoms. Part of the error is certainly due to deficiencies in the basis set. We see that the addition of two h-type functions improves the results somewhat. The results of Ricca and Bauschlicher for Fe show that extrapolation from a quadruple basis set to the basis set limit decreases the excitation energy 0.13 eV at the CCSD(T) level [7]. Adding such a correction would also bring the present result close to experiment. The large triples corrections for atoms with more than a half-filled d-shell have most probably the same origin as the need to add a second d-shell to the active space in CASPT2 and MRSDCI calculations. We notice that the effect almost disappears for the second

Table 2. Coupled cluster and CASPT2 excitation energies (in eV)

Excitation	CCSD	CCSD(2h)	CCSD(T)	CCSD(T)(2h)	PT2	PT2(2h)	Expt[a]
Sc ^{2}D d^{1}s^2 → ^{4}F d^{2}s^1	1.44	1.40	1.50	1.46	1.47	1.43	1.43
Ti ^{3}F d^{2}s^2 → ^{5}F d^{3}s^1	0.83	0.79	0.87	0.83	0.71	0.67	0.81
V ^{4}F d^{3}s^2 → ^{6}D d^{4}s^1	0.28	0.25	0.30	0.26	0.10	0.07	0.25
Cr ^{7}S d^{5}s^1 → ^{5}D d^{4}s^2	0.98	1.02	0.96	1.00	1.21	1.24	1.00
Mn ^{6}S d^{5}s^2 → ^{6}S d^{6}s^1	2.40	2.35	2.28	2.23	2.30	2.25	2.15
Fe ^{5}D d^{6}s^2 → ^{5}F d^{7}s^1	1.13	1.07	1.01	0.95	1.11	1.04	0.88
Co ^{4}F d^{7}s^2 → ^{4}F d^{8}s^1	0.71	0.66	0.55	0.49	0.56	0.49	0.42
Ni ^{3}D d^{9}s^1 → ^{3}F d^{8}s^2	−0.27	−0.22	−0.07	−0.02	−0.04	0.04	0.03
Ni ^{3}D d^{9}s^1 → ^{3}D d^{10}s^0	2.23		1.80		1.85		1.74
Cu ^{2}S d^{10}s^1 → ^{2}D d^{9}s^2	1.26	1.31	1.46	1.51	1.48	1.53	1.49
Y ^{2}D d^{1}s^2 → ^{4}F d^{2}s^1	1.29		1.40		1.32		1.36
Zr ^{3}F d^{2}s^2 → ^{5}F d^{3}s^1	0.52		0.63		0.48		0.59
Nb ^{4}F d^{3}s^2 → ^{6}D d^{4}s^1	−0.29		−0.18		−0.32		−0.18
Mo ^{7}S d^{5}s^1 → ^{5}D d^{4}s^2	1.66		1.54		1.57		1.47
Tc ^{6}S d^{5}s^2 → ^{6}S d^{6}s^1	0.56		0.58		0.57		0.41
Ru ^{5}D d^{6}s^2 → ^{5}F d^{7}s^1	−0.71		−0.69		−0.78		−0.87
Rh ^{4}F d^{8}s^1 → ^{2}D d^{9}s^0	0.67		0.51		0.51		0.34
Pd ^{1}S d^{10}s^0 → ^{3}D d^{9}s^1	0.74		0.86		0.87		0.88
Pd ^{1}S d^{10}s^0 → ^{3}F d^{8}s^2	2.99		3.12		3.09		3.38
Ag ^{2}S d^{10}s^1 → ^{2}D d^{9}s^2	3.76		3.76		3.76		3.97

(*continued*)

Table 2. (*continued*)

Excitation	CCSD	CCSD(2h)	CCSD(T)	CCSD(T)(2h)	PT2	PT2(2h)	Expt[a]
La ^{2}D d^{1}s$^2 \rightarrow ^4$F d^{2}s^1	0.24		0.37		0.26		0.36
Hf ^{3}F d^{2}s$^2 \rightarrow ^5$F d^{3}s^1	1.50		1.65		1.54		1.69
Ta ^{4}F d^{3}s$^2 \rightarrow ^6$D d^{4}s^1	0.89		1.02		0.89		1.04
W ^{5}D d^{4}s$^2 \rightarrow ^7$S d^{5}s^1	−0.40		−0.25		−0.32		−0.19
Re ^{6}S d^{5}s$^2 \rightarrow ^6$D d^{6}s^1	1.82		1.84		1.93		1.76
Os ^{5}D d^{6}s$^2 \rightarrow ^5$F d^{7}s^1	0.79		0.82		0.89		0.75
Ir ^{4}F d^{7}s$^2 \rightarrow ^4$F d^{8}s^1	0.24		0.25		0.17		0.14
Pt ^{3}D d^{9}s$^1 \rightarrow ^3$F d^{8}s^2	0.35		0.35		0.46		0.40
Pt ^{3}D d^{9}s$^1 \rightarrow ^1$S d^{10}s^0	0.59		0.48		0.46		0.24
Au ^{2}S d^{10}s$^1 \rightarrow ^2$D d^{9}s^2	1.64		1.63		1.94		1.74

(2h) means that two h-type basis functions have been added to the basis set.
[a] Experimental data (*J*-averaged) from the NIST tables [24].

Table 3. RMS and maximum errors for the different calculations (in eV)

Method	RMS	Maximum error
All atoms		
CCSD	0.21	0.49 (Ni $d^9s^1 \rightarrow d^{10}s^0$)
CCSD(T)	0.11	0.26 (Pd $d^{10}s^0 \rightarrow d^8s^2$)
CASPT2	0.14	0.29 (Pd $d^{10}s^0 \rightarrow d^8s^2$)
First row TMs		
CCSD	0.24	0.49 (Ni $d^{10}s^0 \rightarrow d^8s^2$)
CCSD (frozen core)	0.31	0.44 (Mn)
CCSD (with 2h)	0.16	0.25 (Ni $d^9s^1 \rightarrow d^8s^2$)
CCSD(T)	0.09	0.14 (Mn)
CCSD(T) (frozen core)	0.24	0.34 (Mn)
CCSD(T) (with 2h)	0.05	0.09 (Mn)
CASPT2	0.14	0.23 (Fe)
CASPT2 (frozen core)	0.22	0.42 (Mn)
CASPT2 (with 2h)	0.13	0.24 (Cr)

and third row elements, where the d-orbitals are more diffuse and the d-electrons not so strongly correlated.

The errors obtained with the CCSD(T) method are, in general, smaller than 0.2 eV. There are some exceptions, however, in particular for palladium and silver.
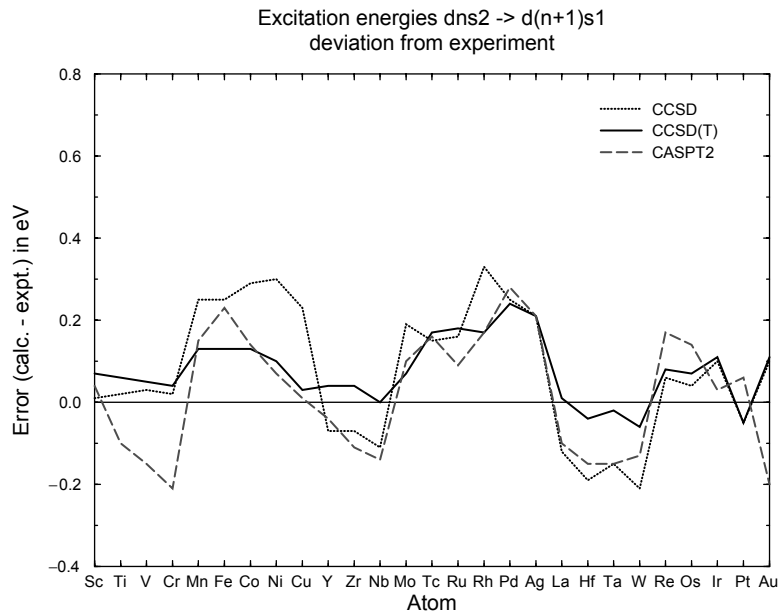
Fig. 1. Error in calculated energies (in eV) for the $d^x s^2 \rightarrow d^{x+1} s^1$ excitations (the electronic states are given in Table 2). Dotted line: CCSD; solid line: CCSD(T); dashed line: CASPT2.

Actually, triples corrections do not lead to much improvement for the heavier second row atoms. There is no obvious explanation for this behavior, except possibly deficiencies in the basis set. The CASPT2 errors are, in general, smaller than 0.2 eV and follow the CCSD(T) results in Fig. 1. For the first and second row we notice, however, that the CASPT2 method gives too low energies for atoms with less than five d-electrons and too large energies for the heavier atoms in each row. The behavior mimics the CCSD(T) results, so the conclusion is that CASPT2 gives too low excitations energies. The major part of this systematic error is due to an overestimate of the core correlation contribution to the excitation energy as we shall discuss below. Again, this is most pronounced for the first row atoms, while the CASPT2 and CCSD(T) errors are similar for second and third row atoms, indicating that most of the error is here due to basis set incompleteness.

Both CCSD(T) and CASPT2 results are generally in good agreement with experiment for the third row atoms. The behavior is somewhat irregular as seen in Fig. 1. The irregularity is partly due to spin–orbit coupling. We will give a more detailed discussion of the multiplet splittings in a forthcoming publication [19]. Here, we give just one example. In Table 4 we present the results from a CASPT2 calculation of the multiplets in the Pt atom. The calculation has been performed using the RASSI-SO method of MOLCAS-6. It has been described in detail in a recent publication [22]. CASSCF calculations are performed for all electronic states corresponding to the configurations d^8s^2, d^9s^1, and $d^{10}s^0$. A spin–orbit Hamiltonian is constructed in this basis with the diagonal elements shifted to the CASPT2 energies. The eigenvalues of this matrix give the multiplet levels. They are presented in Table 4. We notice that the separation of the levels does not at all follow the Landé interval rule. There is a strong mixing between different electronic states. If one computes the J-averaged $^3D \rightarrow {}^3F$ excitation energy using the results in the table, one obtains the CASPT2 value 0.38 eV. The spin–orbit free excitation energy is 0.46 eV, almost 0.1 eV larger. For the $^3D \rightarrow {}^1S$ excitation one obtains the J-averaged result 0.39 eV to be compared to the spin-free result in Table 2, 0.46 eV. It is a general result that corrections due to deviations for the Landé interval rule are of the order of 0.1 eV for third row TMs.

Table 4. CASPT2 excitation energies for the Pt atom including the effect of spin–orbit coupling

Excitation	CASPT2	Expt[a]
$^3D_3$ d^9s^1	0.00	0.00
$^3D_2$ d^9s^1	0.76	0.81
$^3D_1$ d^9s^1	1.27	1.26
$^3F_4$ d^8s^2	0.06	0.10
$^3F_3$ d^8s^2	1.23	1.25
$^3F_2$ d^8s^2	1.92	1.92
$^1S_0$ $d^{10}s^0$	0.90	0.76

[a] Experimental data from the NIST tables [24].

3.2. First row atoms

For the first row atoms we have also studied the effect of adding two h-type basis functions to the ANO-RCC basis set. We present in Fig. 2 the CCSD(T) and CASPT2 results. The effect of the increased basis set is to lower the excitation energies with about 0.04–0.06 eV for both methods. This leads to a general improvement, reducing the RMS error from 0.09 to 0.05 eV for CCSD(T) and from 0.14 to 0.13 eV for CASPT2. The maximum error is also improved for CCSD(T) but actually increases for CASPT2 (cf. Table 3) because CASPT2 energies are already too small for the lighter atoms.

In Table 5 and Fig. 3 we show the effect of not including the 3s,3p electrons in the correlation treatment. A comprehensive study of first row positive ions in 1993 showed that the effect of including the 3s,3p electrons in the correlation treatment was crucial with large differential effects for different electronic states [12]. It was shown that most of the differential effects derived from internal double excitations of the type 3p3d→3d3d and 3p3p→3d3d that are possible for some electronic states but not for others. On the other hand, some of the results indicated that the CASPT2 method may lead to an overestimation of the core correlation energy. This deficiency of the method has recently been emphasized in a study of the chromium dimer [13].

The present results show that there is a difference between CASPT2 and CCSD(T) for the lighter first row TMs. Freezing the 3s,3p orbitals in the CCSD(T)
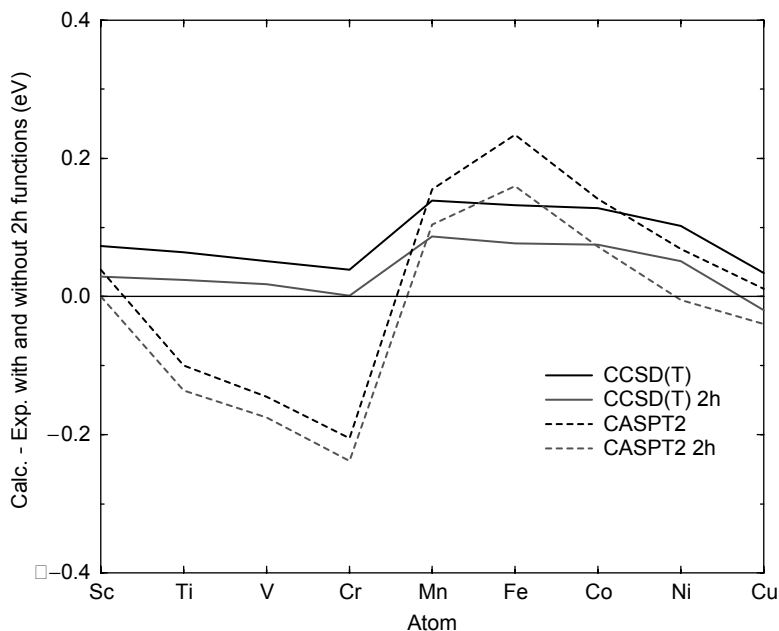
Fig. 2. The effect of adding two h-type functions to the basis set for first row atoms. Errors in computed excitation energies are shown (in eV). Solid lines: CCSD(T); dashed lines: CASPT2 (lower lines with h-type functions in both cases).

Table 5. Coupled cluster and CASPT2 excitation energies with (f.c.) and without the core electrons frozen (in eV)

Excitation	CCSD	f.c.	CCSD(T)	f.c.	CASPT2	f.c.	Expt[a]
Sc ^{2}D d^{1}s^2→^{4}F d^{2}s^1	1.44	1.69	1.50	1.72	1.47	1.73	1.43
Ti ^{3}F d^{2}s^2→^{5}F d^{3}s^1	0.83	1.05	0.87	1.07	0.71	1.04	0.81
V ^{4}F d^{3}s^2→^{6}D d^{4}s^1	0.28	0.45	0.30	0.47	0.10	0.40	0.25
Cr ^{5}D d^{4}s^2→^{7}S d^{5}s^1	−0.98	−0.89	−0.96	−0.87	−1.21	−0.96	−1.00
Mn ^{6}S d^{5}s^2→^{6}S d^{6}s^1	2.40	2.58	2.28	2.48	2.30	2.56	2.15
Fe ^{5}D d^{6}s^2→^{5}F d^{7}s^1	1.13	1.27	1.01	1.15	1.11	1.15	0.88
Co ^{4}F d^{7}s^2→^{4}F d^{8}s^1	0.71	0.82	0.55	0.66	0.56	0.54	0.42
Ni ^{3}F d^{8}s^2→^{3}D d^{9}s^1	0.27	0.37	0.07	0.18	0.04	−0.09	−0.03
Cu ^{2}D d^{9}s^2→^{2}S d^{10}s^1	−1.26	−1.21	−1.46	−1.42	−1.48	−1.43	−1.49

[a] Experimental data (*J*-averaged) from the NIST tables [24].
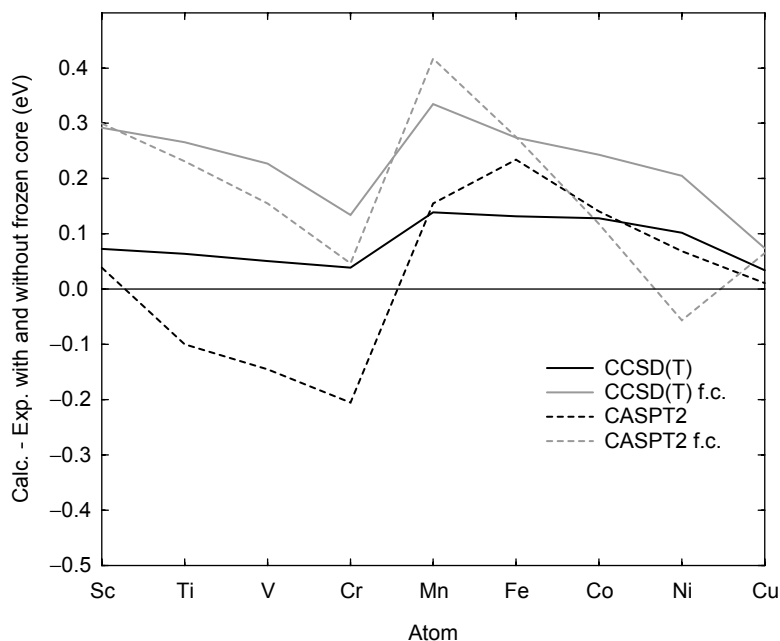
Fig. 3. The effect of freezing the 3s,3p core electrons. Errors in computed excitation energies are shown (in eV). Solid lines: CCSD(T); dashed lines: CASPT2 (upper lines with frozen core in both cases).

calculation leads to an increase of the excitation energies between 0.09 and 0.22 eV for the atoms Sc–Mn. For CASPT2, the effect varies between 0.25 and 0.33 eV. The difference is of the order 0.1 eV. The behavior for the heavier atoms is more irregular at the CASPT2 level. On the other hand are the CCSD(T) and CASPT2 results with the core frozen very similar, so it is clear that the difference is due to the correlation of the 3s,3p electrons. The difference between the CCSD(T) and CASPT2 results is largest for Ti. The effect of correlating 3s,3p is 0.33 eV with CASPT2 but only 0.20 eV with CCSD(T). In order to study this closer, we performed a CASPT2 calculation with also the 3p orbitals active. The crucial 3p to 3d excitations are then treated variationally. The resulting excitation energy was 0.79 eV. The effect of correlating the core is now 0.24 eV to be compared to the CCSD(T) value 0.20 eV. It is thus clear that the CASPT2 method will overestimate the core correlation for the early transition metals. The situation is different for the atoms with more than five 3d-electrons (Fe–Cu). Here it seems that CASPT2 underestimates the effect. Actually, for Co and Ni the correction changes sign. This behavior indicates that the reason for the error is an overestimate of the internal excitations from the 3p to the 3d shell. Such excitations are not possible for the heavier elements. A closer look shows that the interaction between the 3p and 3d shell is large. For example, the matrix element between the ground state and a $(3p)^2 \rightarrow (3d)^2$ excited state is 0.1 a.u. $= 2.7$ eV. It is possible that treating such large interactions using second-order perturbation theory will give rise to larger errors even if the denominators are large. This would

Table 6. Basis set dependence for the ^{7}S d^{5}s$^1 \rightarrow$ ^{5}D d^{4}s^2 excitation energy (CASPT2) for Cr, Mo, and W (eV)

Basis set	Cr	Mo	W[a]
MB	1.74	1.69	−0.00
DZP(1f)	1.21	1.73	−0.29
TZP(2f1g)	1.28	1.66	−0.40
QZP(3f2g)	1.22	1.60	−0.34
Large[b]	1.21	1.57	−0.32
Expt	1.00	1.47	−0.19

[a] The basis sets for W have one extra f- and g-type function.
[b] The basis set is given in Table 1.

also explain why the trend is the same for second and third row atoms but with smaller errors. Here, the interaction elements are smaller.

We finally show in Table 6 an example of the convergence of the results with the basis set for the atoms Cr, Mo, and W. Basis sets of quadruple zeta quality give results that are close to those obtained with the large basis sets given in Table 1. This is a general result for all atoms. The convergence is somewhat irregular. The basis sets have been generated with core correlation included. It is then not obvious what new correlation effects are included when the basis set is extended with a new set of ANOs. They are ordered after decreasing occupation number and account simultaneously for core and valence correlation. Similar tables are available for all atoms in the ANO-RCC basis set library of MOLCAS-6 (www.teokem.lu.se/molcas).

4. CONCLUSIONS

We have shown in this chapter what accuracy can be obtained in calculations of excitation energies for transition metal atoms using the CCSD(T) and CASPT2 methods, respectively. The purpose of the study has not been to achieve very accurate results for the atoms themselves. Instead, the interest is to calibrate methods and basis sets for use in transition metal containing molecules. The general result is that CCSD(T) and CASPT2 give similar absolute errors with the basis sets used here. The CASPT2 results also show that excitation energies, which converge within 0.1 eV, are obtained with basis sets of triple zeta quality. This result is quite general and many examples can be found in the ANO-RCC library, also for low spin excitations and ionization energies [23].

The largest difference between the CCSD(T) and CASPT2 results occurs for the first row TMs with less than five 3d-electrons. Here, it seems that the CASPT2 method will overestimate the contribution to the correlation energy from the 3p electrons. As a result, CASPT2 gives too low energies for the high spin d^{x}s$^2 \rightarrow$ d^{x+1}s^1 excitations. The deviation from the CCSD(T) energies varies between 0 and 0.2 eV. This does not mean that the CASPT2 error is this large because CCSD(T) tends to give slightly too large excitation energies. The error is smaller for the second and third row transition metals.

ACKNOWLEDGEMENTS

REFERENCES

[1] C. W. Bauschlicher Jr., P. E. M. Siegbahn and L. G. M. Petterson, *Theor. Chim. Acta*, 1988, **742**, 479.
[2] K. Andersson and B. O. Roos, *Chem. Phys. Lett.*, 1992, **191**, 507.
[3] K. Raghavachari and G. W. Trucks, *J. Chem. Phys.*, 1989, **91**, 1062.
[4] T. V. Russo, R. L. Martin and P. J. Hay, *J. Chem. Phys.*, 1994, **101**, 7729.
[5] C. W. Bauschlicher Jr. and G. L. Gutsev, *Theor. Chem. Acc.*, 2002, **108**, 27.
[6] X. Xu and W. A. Goddard III., *PNAS*, 2004, **101**, 2673.
[7] A. Ricca and C. W. Bauschlicher Jr., *Theor. Chem. Acc.*, 2001, **106**, 314.
[8] Y. Osanai, H. Ishikawa, N. Miura and T. Noro, *Theor. Chem. Acc.*, 2001, **105**, 437.
[9] K. Andersson, P.-Å. Malmqvist, B. O. Roos, A. J. Sadlej and K. J. Wolinski, *Phys. Chem.*, 1990, **94**, 5483–5488.
[10] K. Andersson, P.-Å. Malmqvist and B. O. Roos, *J. Chem. Phys.*, 1992, **96**, 1218–1226.
[11] B. O. Roos, K. Andersson, M. P. Fülscher, P.-Å. Malmqvist, L. Serrano-Andrés, K. Pierloot and M. Merchán, in *Advances in Chemical Physics: New Methods in Computational Quantum Mechanics, Vol. XCIII: 219–331*, (eds I. Prigogine and S. A. Rice), Wiley, New York, 1996, pp. 219–332.
[12] K. Pierloot, E. Tsokos and B. O. Roos, *Chem. Phys. Lett.*, 1993, **214**, 583–590.
[13] P. Celani, H. Stoll, H.-J. Werner and P. J. Knowles, *Mol. Phys.*, 2004, in press.
[14] N. Douglas and N. M. Kroll, *Ann. Phys.*, 1974, **82**, 89.
[15] B. Hess, *Phys. Rev. A*, 1986, **33**, 3742.
[16] G. Karlström, R. Lindh, P.-Å. Malmqvist, B. O. Roos, U. Ryde, V. Veryazov, P.-O. Widmark, M. Cossi, B. Schimmelpfennig, P. Neogrady and L. Seijo, *Comput. Mater. Sci.*, 2003, **28**, 222.
[17] B. O. Roos, V. Veryazov and P.-O. Widmark, *Theor. Chim. Acta*, 2004, **111**, 345.
[18] B. O. Roos, R. Lindh, P.-Å. Malmqvist, V. Veryazov and P.-O. Widmark, *J. Phys. Chem. A*, 2004, **108**, 2851.
[19] B. O. Roos, Basis sets for transition metals: private communication, 2004.
[20] P. Neogrady, M. Urban and I. Hubac, *J. Chem. Phys.*, 1994, **100**, 3706.
[21] G. Ghigo, B. O. Roos and P.-Å. Malmqvist, *Chem. Phys. Lett.*, 2004, **396**, 142–149.
[22] P.-Å. Malmqvist, B. O. Roos and B. Schimmelpfennig, *Chem. Phys. Lett.*, 2002, **357**, 230.
[23] B. O. Roos, The ANO-RCC basis sets are included in the MOLCAS-6 basis set library. They can be downloaded from the MOLCAS homepage (www.teokem.lu.se/molcas), 2004.
[24] J. Sansonetti, W. Martin and S. Young, *Handbook of Basic Atomic Spectroscopic Data (Version 1.00)*, National Institute of Standards and Technology, Gaithersburg, MD, 2003, [Online] Available: http://physics.nist.gov/Handbook

A Reinvestigation of Ramsey's Theory of NMR Coupling

S. Ajith Perera and Rodney J. Bartlett

*Quantum Theory Project, University of Florida, Gainesville,
FL 32611-8435, USA*

Abstract

A systematic development of relativistic molecular Hamiltonians and various non-relativistic approximations are presented. Our starting point is the Dirac one-fermion Hamiltonian in the presence of an external electromagnetic field. The problems associated with generalizing 'Dirac's one-fermion theory' smoothly to more than one fermion are discussed. The description of many-fermion systems within the framework of quantum electrodynamics (QED) will lead to Hamiltonians which do not suffer from the problems associated with the direct extension of 'Dirac's one-fermion theory' to many-fermion system. An exhaustive discussion of the recent QED developments in the relevant area is not presented, except for cursory remarks for completeness. The non-relativistic form (NRF) of the many-electron relativistic Hamiltonian is developed as the working Hamiltonian. It is used to extract operators for the observables, which represent the response of a molecule to an external electromagnetic radiation field. In this study, our focus is mainly on the operators which eventually were used to calculate the nuclear magnetic resonance (NMR) chemical shifts and indirect nuclear spin–spin coupling constants.

Contents

1. INTRODUCTION

Ever since the pioneering work of Ramsey [1] deriving the form of the nuclear magnetic resonance (NMR) spin–spin coupling operators based on phenomenological and electrostatic arguments laying the foundation for the numerous succeeding computational work on NMR spin–spin coupling constant calculations, a systematic derivation of the form of the NMR operators starting from the approximate relativistic many-electron Hamiltonian has not been presented. Considering the invaluable contribution that Ramsey's early work made toward the success of NMR spin–spin

calculations enjoy today, we believe that it would be an interesting exercise which would benefit both experts as well as non-experts, to revisit the Ramsey's derivation starting from the approximate four-component many-electron relativistic Hamiltonian and follow a systematic approach to arrive at a general form of the molecular Hamiltonian suitable for electronic structure calculations.

2. DIRAC'S ONE-FERMION THEORY

The relativistic one-fermion equation in the free field presented by Dirac in 1928 [2,3] is usually written in the contravariant form, which illustrates the relativistic equivalence of space and time in an elegant way

$$i\frac{\partial\psi}{\partial t} = [c(\boldsymbol{\alpha}\cdot\mathbf{P}) + \beta mc^2]\psi \tag{1}$$

where m and c are the rest mass of the particle and the velocity of light in atomic units, respectively. Here, the bold face letters represent both matrices and vectors interchangeably. The linear momentum operator $\mathbf{P}$ is given by

$$\mathbf{P} = -i\nabla = -i\left(\mathbf{i}\frac{\partial}{\partial x} + \mathbf{j}\frac{\partial}{\partial y} + \mathbf{k}\frac{\partial}{\partial z}\right) \tag{2}$$

The components of the $\boldsymbol{\alpha}$ and $\boldsymbol{\beta}$ operators are independent of space and time coordinates and satisfy the anticommutator relationship

$$[\boldsymbol{\alpha}_\mu, \boldsymbol{\alpha}_\nu]_+ = 2\delta_{\mu\nu} \qquad (\mu, \nu = 0, x, y, z) \tag{3}$$

where we have used

$$\boldsymbol{\beta} = \boldsymbol{\alpha}_0 \tag{4}$$

and x, y and z are the three components of the spatial coordinate vector $\mathbf{r}$. The components of $\boldsymbol{\alpha}$ and $\boldsymbol{\beta}$ operators in matrix representation are 4×4 matrices, and are usually written in the form

$$\boldsymbol{\alpha}_x = \begin{bmatrix} \mathbf{0} & \boldsymbol{\sigma}_x \\ \boldsymbol{\sigma}_x & \mathbf{0} \end{bmatrix} \quad \boldsymbol{\alpha}_y = \begin{bmatrix} \mathbf{0} & \boldsymbol{\sigma}_y \\ \boldsymbol{\sigma}_y & \mathbf{0} \end{bmatrix} \quad \boldsymbol{\alpha}_z = \begin{bmatrix} \mathbf{0} & \boldsymbol{\sigma}_z \\ \boldsymbol{\sigma}_z & \mathbf{0} \end{bmatrix}$$
$$\boldsymbol{\beta} = \boldsymbol{\alpha}_0 = \begin{bmatrix} \mathbf{I} & \mathbf{0} \\ \mathbf{0} & -\mathbf{I} \end{bmatrix} \tag{5}$$

where σ's are the Pauli spin matrices [4]; $\mathbf{I}$ and $\mathbf{0}$ are the 2×2 unit and null matrices, respectively. The Dirac spinor

$$\psi = \psi(\mathbf{r}, t) = \begin{pmatrix} \phi_1(\mathbf{r}, t) \\ \phi_2(\mathbf{r}, t) \\ \phi_3(\mathbf{r}, t) \\ \phi_4(\mathbf{r}, t) \end{pmatrix} \tag{6}$$

is a function of spatial ($\mathbf{r}$) and time (t) coordinates. Lengthy accounts of the properties and physical interpretation of the Dirac equation can be found in several standard textbooks [5–7], and will not be repeated here. However, some important points will be addressed below.

The Dirac equation is invariant to Lorentz transformations [8], a necessary requirement of a relativistic equation. In the limit of large quantum numbers the Dirac equation reduces to the Klein–Gordon equation [9,10]. The time-independent form of Dirac's Hamiltonian is given by

$$[c(\boldsymbol{\alpha}\cdot\mathbf{P}) + \boldsymbol{\beta}mc^2]\psi = E\psi \tag{7}$$

This can easily be derived from equation (1) by standard separation of variables technique (the quantity E is the total energy of the system). Note that in the time-independent Dirac equation the frame of reference is fixed. The energy spectrum of the Dirac equation is unbounded both from above and below, and has both positive and negative energy solutions. As an example, in the Dirac picture, a free fermion has both a positive and negative continuum of energies, above mc^2 and below $-mc^2$, respectively. However, in the presence of an external field, the Dirac equation has a discrete spectrum of bound state solutions for values of the total energy E in the range of $E < mc^2$, in addition to the continuum states above mc^2 and below $-mc^2$ [11]. The presence of a negative continuum of energies leads to conceptual difficulties: there is no ground-state energy as in the case of non-relativistic theory, which suggests that the fermion may fall into the negative continuum of energy and attain infinitely low energy. Dirac circumvented this problem by redefining the vacuum state as the situation in which all the negative energy states are fully occupied and all the positive energy states are unoccupied. The Pauli exclusion principle prevents additional fermions from occupying the fully occupied negative energy states. Excitation of a fermion from the negative energy state to a positive energy state implies a creation of a hole in the negative energy continuum and a particle in the positive energy continuum. The negative energy solutions are then interpreted as solutions for such hole particles having a positive charge, $+e$, positrons, while the positive energy solutions are interpreted as solutions for particles having an equal magnitude but opposite charge to the hole particles, $-e$, electrons. However, this interpretation is not free of problems either. One has to deal with the interaction of fermions with the background charge of an infinite 'sea of fermions'. This leads to infinities in the actual calculation of electron properties. On the other hand, Dirac's hypothesis does not apply to spinless particles, which do not obey the Pauli principle but which do have negative energy solutions. The problem was ultimately solved by renormalized quantum electrodynamics (QED) introduced in the late 1940s by Feynman, Dyson, Schwinger, Tomonaga and others [12–16].

In the presence of an external electromagnetic radiation field the Dirac equation for a fermion takes the form

$$\left[i\frac{\partial}{\partial t} - q\phi\right]\psi = [c(\boldsymbol{\alpha}\cdot\boldsymbol{\Pi}) + \boldsymbol{\beta}mc^2]\psi \tag{8}$$

where q is the charge of the fermion, $\phi = \phi(\mathbf{r}, t)$ is the scalar potential and $\mathbf{\Pi}$ is the modified canonical momentum of the fermion. The modified canonical momentum is given by

$$\mathbf{\Pi} = \mathbf{P} - \frac{q}{c}\mathbf{A} \qquad (9)$$

where $\mathbf{A} = \mathbf{A}(\mathbf{r}, t)$ is the vector potential. Thus, the introduction of coupling between particles and the radiation field corresponds to the substitution ($\mathbf{P} - \frac{q}{c}\mathbf{A}$) in equation (1) instead of $\mathbf{P}$, a relation which is often referred to as the principle of minimal electromagnetic coupling. This relationship can be derived rigorously using QED [17]. The attractive features of the free field Dirac Hamiltonian remain intact in the external electromagnetic radiation field Dirac equation. Alternatively, we can write the time-independent form of equation (8),

$$[\mathbf{h}_{\mathrm{D}} + \mathbf{V}_{\mathrm{ext}}]\psi = \mathbf{h}_{\mathrm{D,ext}}\psi = E\psi \qquad (10)$$

where, $\mathbf{h}_{\mathrm{D}} = [c(\boldsymbol{\alpha}\cdot\mathbf{P}) + \boldsymbol{\beta}mc^2]$ and $\mathbf{V}_{\mathrm{ext}} = q[\phi\mathbf{I} - (\boldsymbol{\alpha}\cdot\mathbf{A})]$, in which the external, field-dependent terms are grouped in $\mathbf{V}_{\mathrm{ext}}$ and $\mathbf{I}$ is the identity operator. As we will see later, the external electromagnetic field Dirac one-fermion equation as written in equation (10) is more convenient for the discussion of many-fermion relativistic Hamiltonians.

It is also common in the literature to write the time-independent Dirac equation in terms of Pauli-spin matrices

$$\begin{pmatrix} (mc^2 + q\phi)\mathbf{I} & c\boldsymbol{\sigma}\cdot\mathbf{\Pi} \\ c\boldsymbol{\sigma}\cdot\mathbf{\Pi} & (-mc^2 + q\phi)\mathbf{I} \end{pmatrix} \begin{pmatrix} \psi_{\mathrm{L}} \\ \psi_{\mathrm{S}} \end{pmatrix} = E \begin{pmatrix} \psi_{\mathrm{L}} \\ \psi_{\mathrm{S}} \end{pmatrix} \qquad (11)$$

Here,

$$\psi_{\mathrm{L}} = \begin{pmatrix} \phi_1^{\alpha}(\mathbf{r}, t) \\ \phi_2^{\beta}(\mathbf{r}, t) \end{pmatrix}$$

and

$$\psi_{\mathrm{S}} = \begin{pmatrix} \phi_3^{\alpha}(\mathbf{r}, t) \\ \phi_4^{\beta}(\mathbf{r}, t) \end{pmatrix}$$

are historically known as 'large' and 'small' components. They also are referred to as positive and negative energy components. The largest term in the Dirac Hamiltonian (equation (10)) is mc^2, the rest mass energy of the fermion. It will be useful to know an estimate of the magnitude of the other terms relative to this term. The order of magnitude of each of the other terms in the Hamiltonian, $c\boldsymbol{\alpha}\cdot\mathbf{P}$, $q\phi$ and $qc\boldsymbol{\alpha}\cdot\mathbf{A}$, can be expressed as $mc^2\alpha^n$, based on the magnitude of each of them in the ground state hydrogen atom [5]. As an example, the electron velocity (u) in the first Bohr radius is $c\alpha$ and the first Bohr radius (a_0) is given by $1/mc^2\alpha^2$. Thus, classically: $c\boldsymbol{\alpha}\cdot\mathbf{P} \sim mcu = mc^2\alpha$,

$q\phi \sim 1/a_0 = mc^2\alpha^2$ and $qc\boldsymbol{\alpha}\cdot\mathbf{A} \sim u/c^2 a_0 = mc^2\alpha^3$. Here α is the fine structure constant. The magnitude of the electric and magnetic field experienced by an electron in the first Bohr radius is much larger than the external electric or magnetic fields commonly encountered in the laboratory [5]. Hence, these qualitative estimates will not be altered materially in the presence of an applied external field. It will be seen later that the order of magnitude of any term arising in the relativistic many-fermion Hamiltonian can be estimated from these results as well as the order of magnitude of each term in the equivalent two-component form expanded in a power series.

So far our discussion is limited to a single fermion in the free field or in the presence of an electromagnetic radiation field. In the following section, we will generalize the discussion to relativistic many-fermion Hamiltonians.

2.1. Relativistic many-fermion Hamiltonians

Dirac's equation cannot be extended directly to many-fermion systems. The many-fermion Hamiltonians should be derived from first principles (QED). However, QED treatments of interacting many-fermion systems do not automatically lead to an eigenvalue problem. An eigenvalue problem has to be extracted from a perturbation expansion derived by QED for the frequency of the emitted radiation from a system. There is no universally accepted scheme for this process and consequently there is no unique, multi-purpose relativistic many-fermion Hamiltonian, but the Hamiltonians we are looking for should instead be 'reasonable'. To be 'reasonable', we would like our many-fermion relativistic Hamiltonian ($\mathbf{H}$) to satisfy criteria which are vital or desirable. The proper Hamiltonians should be based on sound theoretical concepts and should be amenable to systematic improvements. In the non-interacting limit they should be exact (i.e., reduce to a sum of independent external electromagnetic field Dirac Hamiltonians). Relativistic many-fermion Hamiltonians $\mathbf{H}$ can be regarded as linear Hermitian operators which act on configuration state functions (CS), $\boldsymbol{\Psi} = \boldsymbol{\Psi}(\mathbf{r}_1, \mathbf{r}_2, \ldots, \mathbf{r}_N, t)$ the multi-Dirac spinors, in the Hilbert space which refers to a definite number N ($N > 0$) of fermions. Here, the $\mathbf{r}_i$ ($i = 1, 2, \ldots, N$) are the position vector and the Dirac spin matrix of the ith particle. Moreover, the eigenvalue problem

$$\mathbf{H}\boldsymbol{\Psi} = E\boldsymbol{\Psi} \tag{12}$$

should have normalizable solutions, which can be associated with the energy levels of an N electron atomic or molecular system. An extensive list of criteria can be found in Ref. [18], and will not be repeated here.

The Dirac–Breit–Coulomb (DBC) Hamiltonian ($\mathbf{H}_{\mathrm{DBC}}$) is a good starting point for a discussion of many-fermion[1] relativistic Hamiltonians, not only because of its historical importance and widespread use in molecular relativistic calculations (in spite of its known failures) but also as an excellent example of a disastrous

---

[1] The original form of the DBC Hamiltonian was proposed for molecules. Here, we use it for general many-fermion systems.

failure of an attempt to directly extend a relativistic 'one-fermion theory' to a relativistic 'many-fermion theory' without sound theoretical justification. It has the form

$$i\frac{\partial \mathbf{\Psi}}{\partial t} = \left\{ \sum_{i=1}^{N} [\mathbf{h}_{\mathrm{D}}(i) + \mathbf{V}_{\mathrm{ext}}(i)] + \sum_{i<j}^{N} \mathbf{V}_{\mathrm{int}}(i,j) \right\} \mathbf{\Psi} = \mathbf{H}_{\mathrm{DBC}} \mathbf{\Psi} \qquad (13)$$

or for stationary states,

$$\mathbf{H}_{\mathrm{DBC}} \mathbf{\Psi} = E \mathbf{\Psi} \qquad (14)$$

where $\mathbf{h}_{\mathrm{D}}(i)$,

$$\mathbf{h}_{\mathrm{D}}(i) = [c(\boldsymbol{\alpha}_i \cdot \mathbf{P}_i) + \boldsymbol{\beta}_i m_i c^2] \qquad (15)$$

is the free field Dirac Hamiltonian for the ith particle and $\mathbf{V}_{\mathrm{ext}}(i)$,

$$\mathbf{V}_{\mathrm{ext}}(i) = q_i[\phi \mathbf{I} - (\boldsymbol{\alpha}_i \cdot \mathbf{A}_i)] \qquad (16)$$

is the external radiation field effects acting on the ith particle and $\mathbf{V}_{\mathrm{int}}(i,j)$, represents the particle–particle interactions. Note that the first part of the DBC Hamiltonian (equation (13)) is a sum of external field one-particle Dirac Hamiltonians. In the DBC Hamiltonian, the particle–particle interaction effects are approximated by an instantaneous Coulombic and Breit interaction [19],

$$\mathbf{V}_{\mathrm{int}}(i,j) = \frac{q_i q_j (\mathbf{I} + \mathbf{B}_{ij})}{|\mathbf{r}_i - \mathbf{r}_j|} \qquad (17)$$

where $\mathbf{B}_{ij}$,

$$\mathbf{B}_{ij} = -\frac{1}{2} \left[\boldsymbol{\alpha}_i \cdot \boldsymbol{\alpha}_j + \frac{(\boldsymbol{\alpha}_i \cdot \mathbf{r}_{ij})(\boldsymbol{\alpha}_j \cdot \mathbf{r}_{ij})}{\mathbf{r}_{ij}^2} \right] \qquad (18)$$

both of which are on the order of magnitude $mc^2\alpha^2$ in a molecular environment. The complete interaction cannot be written in a closed form but has to be obtained by (diagrammatic) perturbation theory. The Coulomb and the Breit interaction terms are the first two terms of an infinite series and the DBC Hamiltonian as written in equation (13) is only an approximation (not a closed form equation). The original derivation of the Breit interaction was based on the classical magnetic dipole interactions of moving charged particles [19]. Since then it has been rederived using QED arguments [11]. The higher order ($\gg mc^2\alpha^4$) terms in the series arise from the retarded interactions of particles *via* transverse virtual photons and, in principle, may be obtained to any order of accuracy based on QED arguments. The DBC Hamiltonian is not Lorentz invariant, but it can be systematically improved to any order and eventually in the limit it becomes Lorentz invariant. As we can see from equation (13), in the absence of particle–particle interactions the DBC Hamiltonian reduces to a sum of independent one-particle external radiation field Dirac equations. The DBC Hamiltonian is correct through order $mc^2\alpha^2$ and it can be shown that it is independent of the origin

of the coordinate system chosen to represent the electromagnetic potentials (gauge-origin invariant) [5].

At this point it is interesting to discuss the solutions of the DBC Hamiltonian briefly. As Brown and Ravenhall pointed out in 1951 [20], the DBC Hamiltonian does not have bound state solutions. To illustrate this point, let us consider the stationary state DBC Hamiltonian of two non-interacting fermions in an external potential given by

$$\left\{ \sum_{i=1}^{2} [\mathbf{h}_{\mathrm{D}}(i) + \mathbf{V}_{\mathrm{ext}}(i)] \right\} \mathbf{\Psi}_0 = \left\{ \sum_{i=1}^{2} \mathbf{h}_{\mathrm{D,ext}}(i) \right\} \tilde{\mathbf{\Psi}} = \tilde{E} \tilde{\mathbf{\Psi}} \tag{19}$$

As noted earlier, for each particle i, there is a discrete spectrum of positive energy bound states and positive and negative energy continuum states. Let us consider a product wave function of the form $\tilde{\mathbf{\Psi}} = \psi_1(1)\psi_2(2)$, a normalizable stationary bound-state eigenfunction of

$$\sum_{i=1}^{2} \mathbf{h}_{\mathrm{D,ext}}(i) \tag{20}$$

with energy

$$\tilde{E} = \sum_{i=1}^{2} \varepsilon_i(i) \cdot$$

Here, $\psi_i(i)$ for each i, are normalizable stationary state eigenfunctions of

$$\mathbf{h}_{\mathrm{D,ext}} \psi_i(i) = \varepsilon_i(i) \psi_i(i) \quad i = 1, 2 \tag{21}$$

To any bound state solution with energy $\tilde{E}$, we can associate an infinite number of states, one in the positive energy continuum and the other in the negative energy continuum having the same $\tilde{E}$ as the combined energy. As we turn on the particle–particle interaction, states from the negative energy continuum can mix with the positive energy continuum states so that their combined energy equal to $\tilde{E}$. This will add large contributions to the bound state wave function and extend it to infinite distances or dissolve into the continuum. This phenomenon is commonly known as 'Brown and Ravenhall disease' or 'continuum dissolution' (CD) [20]. As a consequence of the presence of negative energy continuum states, the positive energy bound state solutions of interest are highly excited, and the electrons that occupy the positive energy bound states can be excited to positive and negative energy continuum states. Thus, it can be easily shown by using perturbation theory arguments, following Sucher [18], that the first-order correction to the bound state wave function is not normalizable. However, it is important to note that the zeroth-order state is highly excited and for such a zeroth-order state, perturbation theory arguments break down. A solvable model problem has also been used to demonstrate the point in question, without relying on perturbation theory [21].

Obviously, the CD is related to the existence of unfilled negative energy (including rest mass energy) states, but arises only because fermions are

interacting with each other regardless of the mechanism of interaction. In the one-fermion case, Dirac conceptually avoided this problem by assuming completely filled negative energy states commonly known as Dirac's 'hole theory' but there is nothing explicitly in the Dirac equation itself to enforce this constraint. As noted earlier, the DBC Hamiltonian is not derived from first principles; it is merely an intuitive extension of Dirac's 'one-fermion' theory to many fermions. Hence, the DBC Hamiltonian does not incorporate the physical ideas of Dirac's 'hole theory' in which the Pauli exclusion principle prevents transitions to filled negative energy states. This dilemma calls for the derivation of many-fermion Hamiltonians from QED, the mathematical formulation of the Dirac's 'hole theory' which incorporates these ideas from the outset. As we will see later, such a derivation provides many-fermion Hamiltonians which are amenable to systematic improvements and do not suffer from CD.

The Dirac–Hartree–Fock (DHF) equation has been derived starting from the DBC Hamiltonian following similar arguments as was done in deriving its non-relativistic analogue, the Hartree–Fock (HF) equation [22–24]. The DHF equation has been severely numerically tested over the last few decades, and proven to be useful in a qualitative, and often quantitative, understanding of atomic structure and spectra of relativistic atoms, especially those involving inner-shell ionization in heavy atoms. It is not surprising that the DHF equation has bound state solutions, since the DHF equation is a one-body equation, which does not suffer from CD. However, CD undermines the interpretation of these solutions, because the exact wave function for which the DHF wave function is supposed to be an approximation does not exist. Any attempt to improve upon the DHF solutions by including electron correlation effects proved to be a dismal failure [25,26], just as one would expect since the DBC Hamiltonian does not have bound state solutions.

Apparently, a large number of successful relativistic configuration-interaction (RCI) and multi-reference Dirac–Hartree–Fock (MRDHF) calculations [27] reported over the last two decades are 'supposedly' based on the DBC Hamiltonian. This apparent success seems to contradict the earlier claims of the CD. As shown by Sucher [18,28], in fact the RCI and MRDHF calculations are not based on the DBC Hamiltonian, but on an approximation to a more fundamental Hamiltonian based on QED which does not suffer from the CD. At this point, let us defer further discussion until we review the many-fermion Hamiltonians derived from QED.

The underlying relativistic Hamiltonian for many-fermion systems is the Hamiltonian for QED, $\mathbf{H}_{QED}$. It acts on wave functions in Fock space and is capable of describing systems involving an arbitrarily large number of electrons, positrons and photons. $\mathbf{H}_{QED}$ conserves only the total charge of the system, not the total number of electrons, positrons or photons. Irrespective of a particular partitioning, $\mathbf{H}_{QED}$ will always have terms which couple different sectors of the Fock space with the same total electric charge but with different number of electrons, positrons and photons. The Fock-space wave function is an infinite-order column matrix, consists of electrons, positrons and photons consistent with the total charge and quantum numbers of the system [29]. For example, the Fock-space wave function for an electron consists of a one-electron wave

function, a one-electron and one-photon function, a one electron and electron–positron pair function, etc. The individual elements of the Fock-space wave function in a particular sector (Hilbert space) satisfy a set of infinite coupled linear partial differential equations and can be used to extract the form of the Fock-space wave function for the photons and electrons [29].

The first rigorous derivation of such a relativistic Hamiltonian for a two-fermion system that makes use of Feynman [13,14] formalism of QED was due to Bethe and Salpeter [30,31]. Recently, Broyles has extended it to many-electron atoms and molecules [32]. A detailed account of Broyle's derivation can be found elsewhere [32,33] and will not be repeated here. Following Broyles, the stationary state many-fermion Hamiltonian based on QED can be written as

$$\left\{ \sum_{i=1}^{N} \mathbf{h}_{\text{D,ext}}(i) + \left[\prod_{k=1}^{N} \mathbf{\Lambda}_{k+} - (-1)^N \prod_{k=1}^{N} \mathbf{\Lambda}_{k-} \right] \sum_{i<j} \mathbf{V}_{\text{int}}(i,j) \right\} \mathbf{\Psi} = E\mathbf{\Psi} \quad (22)$$

where $\mathbf{\Lambda}_{k\pm}$ are the projection operator into the positive and negative energy states of $\mathbf{h}_{\text{D,ext}}$ namely

$$\mathbf{\Lambda}_{k\pm}\psi_k(k) = \frac{1}{2}(\mathbf{p}^2 + m^2)^{-1/2}[(\mathbf{p}^2 + m^2)^{1/2} \pm \mathbf{h}_{\text{D,ext}}]|\psi_k(k)\rangle \quad (23)$$

where $\psi_k(k)$ is an eigenfunction of $\mathbf{h}_{\text{D,ext}}$. As we can see from equation (22), the form of the QED Hamiltonian is identical to that of the DBC Hamiltonian given in equation (13) except for the presence of projection operators. For potentials ($\mathbf{V}_{\text{int}}(i,j)$) which involve only pairwise interactions, Broyles has shown that the bound state wave functions of equation (22) separate into two components. This in mathematical terms can be written as

$$\mathbf{\Psi}_+ + \mathbf{\Psi}_- = \left[\prod_{k=1}^{N} \mathbf{\Lambda}_{k+} - (-1)^N \prod_{k=1}^{N} \mathbf{\Lambda}_{k-} \right] \mathbf{\Psi} \quad (24)$$

and consequently in no case does the wave function have a mixture of both positive and negative energy solutions. The positive and negative energy solutions correspond to two different equations. It is the presence of projection operators, which decouple the positive and negative energy states, that actually prevents the QED Hamiltonian from CD. As Broyles stated, if more than two-body interactions are present, this separation into two components still may hold, but in that case a more elaborate proof is required. The no-pair Hamiltonian derived from QED principles [26] is equivalent to the Broyles Hamiltonian. It may be obtained in a more simple and transparent manner, without invoking the perturbational four-dimensional machinery associated with Broyles or Bethe and Salpeter's derivation. However, it should be noted that this derivation is less rigorous. In the Coulomb gauge $\mathbf{H}_{\text{QED}}$ can be written in the form

$$\mathbf{H}_{\text{QED}} = \mathbf{H}_{\text{mat}} + \mathbf{H}_{\text{rad}} + \mathbf{H}_{\text{T}} \quad (25)$$

where $\mathbf{H}_{\text{mat}}$ is the external field Hamiltonian for the particles (electrons and positrons) in terms of the quantized Dirac field, the $\mathbf{H}_{\text{rad}}$ is the free Hamiltonian

for the radiation in terms of the quantized radiation field, and $\mathbf{H}_T$ is the Hamiltonian for the interaction of particles with the quantized transverse radiation field. The interaction term $\mathbf{H}_T$ is assumed to be small and is usually treated by perturbation theory. We can define a set of electron and positron creation and annihilation operators in terms of the solutions of the external field Dirac equation (equation (10)) or the free field Dirac equation (equation (7)). The two choices correspond to different definitions of creation and annihilation operators and hence lead to different 'no-pair' Hamiltonians. Expansion the quantized Dirac and the radiation field in terms of electron and positron field operators defined in terms of solution of the external field Dirac equation as in the *Furry* bound state picture or in terms of solution of the free field Dirac equation as in the *free* picture leads to analytical expressions for $\mathbf{H}_{mat}$, $\mathbf{H}_{rad}$ and $\mathbf{H}_T$ presented by Sucher [18,26,28]. The major difficulty with the operator $\mathbf{H}_{mat}$ is that it does not conserve the number of particles. However, it is possible to split off from $\mathbf{H}_{mat}$ a 'pair part' which involves the creation or destruction of virtual electron–positron pairs and which can in many cases be treated as perturbations, along with $\mathbf{H}_T$. The remaining part, the 'no-pair part', then has a fixed number of electrons and positrons (commute with electron and positron number operators) so that the eigenvalue problem it poses is equivalent to the problem of solving for the relativistic many-fermion wave equation. Thus, we can write

$$\mathbf{H}_{mat} = \mathbf{H}_{mat}^{np} + \mathbf{H}_{mat}^{pair} \tag{26}$$

The definition of the 'pair' part or, equivalently the 'no-pair part' of $\mathbf{H}_{mat}$ is not unique. The precise meaning of 'no-pair' implicitly depends on the choice of external potential, so that the operator $\mathbf{H}_{mat}^{np}$ depends implicitly on the external potential, whereas the sum $\mathbf{H}_{mat} = \mathbf{H}_{mat}^{np} + \mathbf{H}_{mat}^{pair}$ is independent of the choice of external potential. Since the no-pair part conserves the number of particles (electrons, positrons and photons) we can look for eigenstates $\mathbf{\Psi}$ of $\mathbf{H}_{mat}^{np}$ in the sector of Fock space with N fermions and no photons or positrons. Following Sucher [18,26,28], the resulting no-pair Hamiltonian in configuration space can be written as

$$\left\{ \sum_{i=1}^{N} \mathbf{h}_{D,ext}(i) + \prod_{k=1}^{N} \mathbf{L}_{k+}(k) \left(\sum_{i<j}^{N} \mathbf{V}_{int}(i,j) \right) \prod_{k=1}^{N} \mathbf{L}_{k+}(k) \right\} \mathbf{\Psi} = E\mathbf{\Psi} \tag{27}$$

where the positive energy projection operators are defined in terms of positive energy eigenfunctions $\psi_{k+}(k)$ of $\mathbf{h}_{D,ext}$ (both discrete and continuous) or $\mathbf{h}_D$ (continuous) such that

$$\mathbf{L}_{k+} = \sum_{k} |\psi_{k+}(k)\rangle\langle\psi_{k+}(k)| \tag{28}$$

Depending on the choice of $\psi_{k+}(k)$; eigenfunctions of the external field Dirac equation $\mathbf{h}_{D,ext}$ or the free field Dirac equation $\mathbf{h}_D$, equation (27) represents the *Furry* bound state molecular Hamiltonian or the *free* molecular Hamiltonian.

2.2. The non-relativistic form of the molecular relativistic Hamiltonian

Instead of a two-component equation as in the non-relativistic case, for fully relativistic calculations one has to solve a four-component equation. Conceptually, fully relativistic calculations are no more complicated than non-relativistic calculations, but they are computationally demanding, in particular, for correlated molecular relativistic calculations. Unless taken care of at the outset, spurious solutions can occur in variational four-component relativistic calculations. In practice, this problem is handled by employing kinetically balanced basis sets. The kinetic balance relation is

$$\psi_S = -\frac{1}{2mc}\boldsymbol{\sigma}\cdot\mathbf{P}\psi_L \tag{29}$$

This relation becomes exact only in the non-relativistic limit (NRL). If a basis set is chosen in which the small and large components do not fulfill this condition, convergence to the NRL upon enlarging the value of c is not possible. Such a lack of balance between the large and small components manifests itself by giving too small a value for the kinetic energy in that limit. Consequently, two different atomic orbital basis functions for the large and small components are required. This results in large storage requirements and expensive two electron integral evaluation. However, Dirac Hartree–Fock (DHF) (four component) calculations of atoms and simple diatomics are routine today and correlated fully relativistic molecular calculations are rapidly emerging [27].

An attractive alternative is to use a two-component equation derived from a decoupling of the 'large' and 'small' components of the four-component equation. By decoupling of the 'large' and 'small' components (equivalently positive and negative solutions) the Dirac equation would in effect be reduced to the non-relativistic form (NRF). Furthermore, the decoupling would allow us to focus on a particular component, basically the positive energy component, since the processes that we are interested in studying does not involve positrons or positron–electron pair creation. At least in principle, the decoupled equations can be expanded in terms of powers of α^2 which in turn can be used to obtain the NRL by taking the limit $\alpha \to 0$.

First, we consider the NRF and NRL of the one-electron external field Dirac equation. Before we continue any further, let us rewrite the equation (11), for a fermion in an external radiation field

$$\mathbf{h}_{D,ext}\psi = \begin{pmatrix} q\phi\mathbf{I} & c\boldsymbol{\alpha}\cdot\boldsymbol{\Pi} \\ c\boldsymbol{\alpha}\cdot\boldsymbol{\Pi} & (-2mc^2 + q\phi)\mathbf{I} \end{pmatrix}\psi = E\psi \tag{30}$$

where,

$$\psi = \begin{pmatrix} \psi_L \\ \psi_S \end{pmatrix},$$

$\langle\psi|\psi\rangle = \mathbf{I}$ and ψ_L and ψ_S are the large and small component, respectively. Note, that equation (30) is written for stationary states and also the whole energy spectrum is shifted by $-mc^2$, so that a direct comparison with the non-relativistic result is feasible. It is important to note that decomposition into small and large components is strictly valid only for the one-electron case.

Since the introduction of the Dirac equation [2,3], there have been numerous studies on the problem of decoupling it into a two-component equation and its NRL. The problem is that the Dirac equation does not have an obvious NRF or NRL. In order to write the Dirac equation in NRF or to establish the NRL one must first manipulate the Dirac equation. A recent review by Kutzelnigg [34,35] gives a detailed exposition of various approaches and the difficulties that arise in the form of divergent terms and singularities. In these approaches, usually, one first derives an effective Hamiltonian which acts on two-component wave functions and which is supposed to have the same eigenvalues as the original four-component Hamiltonian, before one takes the NRL or formulates a perturbation series in terms of α^2. We can classify all of these approaches into three broad categories.

First, the method for the large component of the Dirac spinor. In this category, the elimination of the small component (ESC) is the simplest and most straightforward [36]. It simply involves an elimination of the 'small' component in order to derive a Hamiltonian for the 'large' component. The resulting Hamiltonian is Hermitian, energy-dependent and acts on two-component spinors. Its eigenfunctions are identical to the large component ψ_L of the Dirac spinor ψ. In the second category, the Foldy–Wouthuysen (FW) or related transformations convert the Hamiltonian in equation (30) into a block diagonal form by a unitary transformation [37]. This results in an energy-independent, Hermitian Hamiltonian which acts on a two-component spinor, but the eigenfunctions of this Hamiltonian are no longer the large component of the Dirac spinor. The methods in the third category leave the four-component form of the equation intact, but treat the positive and negative energy states differently by different choices of the metric. They can be derived from the direct perturbation theory (DPT) approach of Kutzelnigg [34]. In the following discussion, all of the above three categories are presented as special cases of the general theory of effective Hamiltonians [38]. This procedure will help us to identify elements common in each method, problems, and possible solutions.

Let us rewrite the Dirac equation (equation (30)), with an added arbitrary real parameter z,

$$\mathbf{h}\psi = \begin{pmatrix} (q\phi + z)\mathbf{I} & c\boldsymbol{\sigma}\cdot\boldsymbol{\Pi} \\ c\boldsymbol{\sigma}\cdot\boldsymbol{\Pi} & [-2mc^2 + (q\phi + z)]\mathbf{I} \end{pmatrix}\psi = (E + z)\psi \qquad (31)$$

where the use of z will become clear later on. Now, consider an arbitrary but non-singular transformation $\mathbf{U}$, as yet unspecified, of the old basis ψ, into a new basis $\tilde{\psi}$, such that $\tilde{\psi} = \mathbf{U}^{-1}\psi$. Then equation (31) becomes

$$(\mathbf{U}^{\dagger}\mathbf{h}\mathbf{U})\mathbf{U}^{-1}\psi = E(\mathbf{U}^{\dagger}\mathbf{U})\mathbf{U}^{-1}\psi \qquad (32)$$

Let us define a transformed Hamiltonian as $\tilde{\mathbf{h}}$,

$$\tilde{\mathbf{h}} = \mathbf{U}^\dagger \mathbf{h} \mathbf{U} = \begin{pmatrix} \mathbf{h}_{11} & \mathbf{h}_{12} \\ \mathbf{h}_{21} & \mathbf{h}_{22} \end{pmatrix} \qquad (33)$$

and define the metric $\mathbf{S}$,

$$\mathbf{S} = \mathbf{U}^\dagger \mathbf{U} \qquad (34)$$

and rewrite equation (32),

$$\tilde{\mathbf{h}} \mathbf{U}^{-1} \psi = E \mathbf{S} \mathbf{U}^{-1} \psi \qquad (35)$$

As we can see from equation (35), $\tilde{\psi}$ is an eigenfunction of the transformed Hamiltonian $\tilde{\mathbf{h}}$ with the normalization $\langle \tilde{\psi} | \mathbf{S} | \tilde{\psi} \rangle$ and the eigenvalues remain unchanged. Basically this implies that instead of diagonalizing the full Hamiltonian for the whole energy spectrum, one can diagonalize the effective Hamiltonian to obtain a subset of eigenvalues. The form of $\mathbf{U}$ needs to be determined such that both $\tilde{\mathbf{h}}$ and $\mathbf{S}$ are block diagonal. The transformed Hamiltonian is Hermitian, but in general corresponds to a non-unit metric. Alternatively, we may use a similarity transformation

$$(\mathbf{U}^{-1} \mathbf{h} \mathbf{U}) \mathbf{U}^{-1} \psi = E \mathbf{U}^{-1} \psi \qquad (36)$$

and define a similarity transformation $\bar{\mathbf{h}}$, $\bar{\mathbf{h}} = \mathbf{U}^{-1} \mathbf{h} \mathbf{U}$ which does not involve a metric. The similarity transformed Hamiltonian is not necessarily Hermitian, but a Hermitian effective Hamiltonian can be derived from it by an additional transformation commonly known by the name des Cloizeaux [39]. When $\mathbf{U}$ is chosen to be unitary, the similarity transformed Hamiltonian is automatically Hermitian and the unitary similarity transformations are commonly known in the literature as Hermitian similarity transformations.

The FW transformation is in effect equivalent to a Hermitian similarity transformation. Following van Lenthe *et al.* [40], we can parameterize the unitary transformation $\mathbf{U}$, as follows

$$\mathbf{U} = \begin{pmatrix} (\mathbf{I} + \mathbf{X}^\dagger \mathbf{X})^{-1/2} & (\mathbf{I} + \mathbf{X}^\dagger \mathbf{X})^{-1/2} \mathbf{X}^\dagger \\ -\mathbf{X}(\mathbf{I} + \mathbf{X}\mathbf{X}^\dagger)^{-1/2} & (\mathbf{I} + \mathbf{X}\mathbf{X}^\dagger)^{-1/2} \end{pmatrix} \qquad (37)$$

Here, $\mathbf{X}$ is to be determined by imposing that the resulting transformed Dirac Hamiltonian is block diagonal. It is fairly easy to see that this leads to an equation for $\mathbf{X}$

$$\mathbf{X}(z) = \frac{1}{2mc^2} (c\mathbf{X}\boldsymbol{\sigma} \cdot \boldsymbol{\Pi}\mathbf{X} - c\boldsymbol{\sigma} \cdot \boldsymbol{\Pi} + [(q\phi + z)\mathbf{I}, \mathbf{X}]) \qquad (38)$$

and the effective Hamiltonian $\mathbf{h}_{11}$ and wave function ψ^{eff}

$$\mathbf{h}_{11} \psi^{\text{eff}} = [(\mathbf{I} + \mathbf{X}^\dagger \mathbf{X})^{1/2}((q\phi + z)\mathbf{I} - c\boldsymbol{\sigma} \cdot \mathbf{P}\mathbf{X})(\mathbf{I} + \mathbf{X}^\dagger \mathbf{X})^{-1/2}] \psi^{\text{eff}}$$

$$= (E + z)\psi^{\text{eff}} \qquad (39)$$

The FW Hamiltonian $\mathbf{h}^{FW}$,

$$\mathbf{h}^{FW}\psi^{FW} = [(\mathbf{I} + \mathbf{X}^\dagger\mathbf{X})^{1/2}(q\phi\mathbf{I} - c\boldsymbol{\sigma}\cdot\mathbf{PX})(\mathbf{I} + \mathbf{X}^\dagger\mathbf{X})^{-1/2}]\psi^{FW} = E\psi^{FW} \qquad (40)$$

follows directly from equations (38) and (39) by putting the arbitrary parameter z to zero. Here, ψ^{FW} is the FW two-component wave function. As we can see from equation (40), the FW Hamiltonian is energy independent and Hermitian. It is also important to note that the Hermiticity of $\mathbf{h}^{FW}$ is guaranteed only for exact $\mathbf{X}$. Now, we can write the FW wave function in terms of the solutions of the original Dirac Hamiltonian. Since

$$\begin{pmatrix} \psi^{FW} \\ \mathbf{0} \end{pmatrix}$$

is an eigenfunction of the similarity transformed Hamiltonian, one can write

$$\begin{pmatrix} \psi^{FW} \\ \mathbf{0} \end{pmatrix} = \begin{pmatrix} (\mathbf{I} + \mathbf{X}^\dagger\mathbf{X})^{-1/2} & -\mathbf{X}^\dagger(\mathbf{I} + \mathbf{X}^\dagger\mathbf{X})^{-1/2} \\ \mathbf{X}(\mathbf{I} + \mathbf{X}\mathbf{X}^\dagger)^{-1/2} & (\mathbf{I} + \mathbf{X}\mathbf{X}^\dagger)^{-1/2} \end{pmatrix} \begin{pmatrix} \psi_L \\ \psi_S \end{pmatrix} \qquad (41)$$

We can use the equation (41), to write an expression for ψ^{FW}, in terms of ψ_L as

$$\psi^{FW} = (\mathbf{I} + \mathbf{X}^\dagger\mathbf{X})^{1/2}\psi_L \qquad (42)$$

As we can see, the FW two-component wave function is not the large component of the Dirac spinor, but it is related to it by an expression involving $\mathbf{X}$. Consider a similarity transformation based on $\mathbf{U}$ parameterized as

$$\mathbf{U} = \begin{pmatrix} \mathbf{I} & \mathbf{0} \\ -\mathbf{X} & \mathbf{I} \end{pmatrix} \qquad \mathbf{U}^{-1} = \begin{pmatrix} \mathbf{I} & \mathbf{0} \\ \mathbf{X} & \mathbf{I} \end{pmatrix} \qquad (43)$$

In this case, $\mathbf{X}$ is to be determined by requiring that the off-diagonal blocks of the resulting transformed Dirac Hamiltonian vanishes. It can be shown that the equation for $\mathbf{X}$ is identical to the one we obtained in the case of a unitary transformation as given in equation (38). In this case, the effective Hamiltonian $\mathbf{h}_{11}$ and wave function ψ^{eff}, can be written as

$$\mathbf{h}_{11}\psi^{eff} = [((q\phi + z)\mathbf{I} - c\boldsymbol{\sigma}\cdot\mathbf{PX})]\psi^{eff} = (E + z)\psi^{eff} \qquad (44)$$

The ESC Hamiltonian is obtained by substituting $z = -E$ in equation (44)

$$\mathbf{h}^{ESC}\psi^{ESC} = (q\phi\mathbf{I} - c\boldsymbol{\sigma}\cdot\mathbf{PX})\psi^{ESC} = E\psi^{ESC} \qquad (45)$$

Similar to the FW case, one can write

$$\begin{pmatrix} \psi^{ESC} \\ \mathbf{0} \end{pmatrix} = \begin{pmatrix} \mathbf{I} & \mathbf{0} \\ \mathbf{X} & \mathbf{I} \end{pmatrix} \begin{pmatrix} \psi_L \\ \psi_S \end{pmatrix} \qquad (46)$$

resulting in $\psi^{ESC} = \psi_L$. That is, in contrast to the FW Hamiltonian, the large component of the Dirac spinor is an eigenfunction of the two-component ESC

Hamiltonian. Let us rewrite equation (38) when $z = -E$ and rearrange to obtain

$$\left(1 - \frac{(q\phi - E)}{2mc^2}\right)\mathbf{X} = \frac{1}{2mc^2}[c\mathbf{X}\boldsymbol{\sigma}\cdot\boldsymbol{\Pi}\mathbf{X} - c\boldsymbol{\sigma}\cdot\boldsymbol{\Pi} - \mathbf{X}(q\phi - E)\mathbf{I}] \qquad (47)$$

Rearranging equation (45) we get

$$(q\phi - E)\psi^{\text{ESC}} = c\boldsymbol{\sigma}\cdot\mathbf{PX}\psi^{\text{ESC}} \qquad (48)$$

Multiply equation (48) on left by $\mathbf{X}$. Then, the result is true for all ψ^{ESC}, we can substitute for $\mathbf{X}(q\phi - E)\mathbf{I}$ in equation (47) to get a simplified expression for $\mathbf{X}$,

$$\left(1 - \frac{(q\phi - E)}{2mc^2}\right)\mathbf{X} = \frac{-c\boldsymbol{\sigma}\cdot\boldsymbol{\Pi}}{2mc^2}, \quad \mathbf{X} = \frac{-ck\boldsymbol{\sigma}\cdot\boldsymbol{\Pi}}{2mc^2} \qquad (49)$$

where $k = (1 - (q\phi - E)/2mc^2)^{-1}$. Now substitute for $\mathbf{X}$ in equation (45) to get the ESC Hamiltonian $\mathbf{h}^{\text{ESC}}$

$$\mathbf{h}^{\text{ESC}}\psi_{\text{L}} = \left[q\phi\mathbf{I} + \frac{(\boldsymbol{\sigma}\cdot\boldsymbol{\Pi})k(\boldsymbol{\sigma}\cdot\boldsymbol{\Pi})}{2}\right]\psi_{\text{L}} = E\psi_{\text{L}} \qquad (50)$$

As seen from equation (50), the ESC Hamiltonian is energy dependent and Hermitian. For a fixed value of E, the ESC Hamiltonian can be diagonalized and the resulting solutions, in principle, form a complete orthonormal set. The eigenfunctions of $\mathbf{h}^{\text{ESC}}$ are identical to the large component of the Dirac spinor. When $z = 0$, equations (38) and (44) give us the similarity transformed Hamiltonian $\mathbf{h}^{\text{ST}}$

$$\mathbf{h}^{\text{ST}}\psi_{\text{L}} = (q\phi\mathbf{I} - c\boldsymbol{\sigma}\cdot\mathbf{PX})\psi_{\text{L}} \qquad (51)$$

Note that the $\mathbf{h}^{\text{ST}}$ is non-Hermitian and energy independent. Moreover, the large component of the Dirac spinor is an eigenfunction of $\mathbf{h}^{\text{ST}}$. The Hamiltonians $\mathbf{h}^{\text{ST}}$ and $\mathbf{h}^{\text{ESC}}$ are equivalent insofar as they have the same eigenvalues and eigenfunctions. They are indeed grouped together as derived from the methods for large components. The des Cloizeaux [39] transformation of $\mathbf{h}^{\text{ST}}$ will give us a Hermitian similarity transformed Hamiltonian which is identical to the FW Hamiltonian given in equation (40).

So far our derivations leading to the FW, ESC and ST Hamiltonians are formally rigorous. However, to be useful, the FW, ESC and ST Hamiltonians given in equations (40), (50) and (51) need to be rewritten with appropriate $\mathbf{X}$ given in equation (38). Conveniently, we can solve for $\mathbf{X}$ by iterating equation (38) with the outcome an expansion in terms of α^2:

$$\mathbf{X} = -\frac{\alpha}{2m}\boldsymbol{\sigma}\cdot\boldsymbol{\Pi} - \frac{\alpha^3}{4m}[q\phi\mathbf{I}, \boldsymbol{\sigma}\cdot\boldsymbol{\Pi}] + \frac{\alpha^3}{8m}(\boldsymbol{\sigma}\cdot\boldsymbol{\Pi})(\boldsymbol{\sigma}\cdot\boldsymbol{\Pi})(\boldsymbol{\sigma}\cdot\boldsymbol{\Pi}) + \cdots \qquad (52)$$

Now, substituting for $\mathbf{X}$ in equation (40) we get the FW or equivalent Hermitian similarity transformed Hamiltonian which is an expansion in terms of α^2

$$\mathbf{h}^{\text{FW}} = q\phi + \frac{1}{2m}(\boldsymbol{\sigma}\cdot\boldsymbol{\Pi})^2 - \frac{\alpha^2}{8m^3}(\boldsymbol{\sigma}\cdot\boldsymbol{\Pi})^4 + \frac{\alpha^2}{8m^2}[(\boldsymbol{\alpha}\cdot\boldsymbol{\Pi}), [q\phi, (\boldsymbol{\sigma}\cdot\boldsymbol{\Pi})]]$$

$$+ \mathcal{O}(mc^2\alpha^6) \qquad (53)$$

and the corresponding wave function

$$\psi^{\mathrm{FW}} = \psi_{\mathrm{L}} + \frac{\alpha^2}{4m^2}(\boldsymbol{\sigma}\cdot\boldsymbol{\Pi})^2\psi_{\mathrm{L}} + \cdots \tag{54}$$

Here, order of magnitude of the terms in the expansion being determined on the basis of orders of magnitude of $\phi \sim mc^2\alpha^2$ and $\boldsymbol{\sigma}\cdot\boldsymbol{\Pi} \sim mc^2\alpha^2$. We only retain the terms up to order of magnitude $mc^2\alpha^4$ or simply speaking expand through first order in α^2. Higher order terms quickly become cumbersome to evaluate. However, this is not a serious disadvantage, since higher order corrections are not very often observed to be important at present. In addition, at higher orders radiative corrections become important and QED treatments become essential.

In case of the Coulomb potential ($\phi \propto 1/|\mathbf{r}|$, where $\mathbf{r}$ is the position vector of the fermion with respect to an arbitrary origin) commutators such as $[\phi,(\boldsymbol{\sigma}\cdot\boldsymbol{\Pi})^2]$ would give us terms which are proportional to $1/|\mathbf{r}^n|$ (here n is an integer greater than 1) in the expansion for $\mathbf{h}^{\mathrm{FW}}$ in equation (53). When such operators act on well-behaved wave functions they may give terms which are proportional to $1/|\mathbf{r}|$, and singular when $|\mathbf{r}| \to 0$. Terms such as $(\boldsymbol{\sigma}\cdot\boldsymbol{\Pi})^4$ in the expansion lead to a higher order differential equations and there may not be enough constraints in the problem to find quantized solutions. These terms also become very large for the particles with higher momentum and for such cases the above expansion is not justified. Similar problems arise in the FW wave function too. As shown in equation (54), the FW wave function can also be written as an expansion in α^2 in terms of the large component of the Dirac spinor which is a well-behaved function. For Coulomb potentials, as in the case for the Hamiltonian, there will be terms in the expansion which are proportional to $(1/(|\mathbf{r}^n|))\psi_{\mathrm{L}}$ (n is a positive integer). This clearly shows that the FW wave function truncated at some finite order in α^2 can be divergent. The zeroth-order wave function is, of course, well behaved. In conclusion, the perturbation expansion in equation (53) is not valid for Coulomb potentials for small values of $\mathbf{r}$.

As shown by Chang, Pelissier and Durand (CPD) [41] a regular expansion, however, can be deduced by isolating the Coulomb singularity by infinite summations. Let us rewrite the equation (38), when $z=0$

$$\left(1 - \frac{q\phi}{2mc^2}\right)\mathbf{X} = \frac{1}{2mc^2}[c\mathbf{X}\boldsymbol{\sigma}\cdot\boldsymbol{\Pi}\mathbf{X} - c\boldsymbol{\sigma}\cdot\boldsymbol{\Pi} - \mathbf{X}q\phi],$$

$$\mathbf{X} = \frac{f}{2mc^2}[c\mathbf{X}\boldsymbol{\sigma}\cdot\boldsymbol{\Pi}\mathbf{X} - c\boldsymbol{\sigma}\cdot\boldsymbol{\Pi} - \mathbf{X}q\phi] \tag{55}$$

where $f = (1 - (q\phi/2mc^2))^{-1}$. An iterative solution of equation (55) leads to a regular expansion for $\mathbf{X}$ in terms of f

$$\mathbf{X} = \frac{f\alpha}{2m}\boldsymbol{\sigma}\cdot\boldsymbol{\Pi} - \frac{f^2\alpha^2}{4m}(\boldsymbol{\sigma}\cdot\boldsymbol{\Pi})q\phi - \frac{f^2\alpha^3}{8m}(\boldsymbol{\sigma}\cdot\boldsymbol{\Pi})(\boldsymbol{\sigma}\cdot\boldsymbol{\Pi})f(\boldsymbol{\sigma}\cdot\boldsymbol{\Pi}) + \cdots \tag{56}$$

It is clear from equation (56), that the CPD expansion is free from potentially problematic commutators in FW or ESC. Now, substituting for $\mathbf{X}$ in equation (40) we get an expansion similar to the one given in equation (53). Although the CPD

expansion is free from Coulombic singularities, it is divergent for particles with large momenta and should in principle only be used for slow moving particles. Application of CPD or related expansions to atomic and molecular relativistic calculations have been reported [40,42,43].

As we can see from equation (49), in the case of ESC the expression for $\mathbf{X}$ is much simpler and iterative solution gives an expansion in terms of α^2

$$\mathbf{X} = -\frac{\boldsymbol{\sigma}\cdot\boldsymbol{\Pi}}{2m}\alpha\mathbf{I} - \frac{(q\phi - E)\boldsymbol{\sigma}\cdot\boldsymbol{\Pi}}{4m^2}\alpha^3\mathbf{I} - \frac{(q\phi - E)^2\boldsymbol{\sigma}\cdot\boldsymbol{\Pi}}{8m^3}\alpha^5\mathbf{I} + \cdots \qquad (57)$$

This expansion is valid only when $(q\phi - E) < 2mc^2$. For the Coulomb potentials when $|\mathbf{r}| \to 0$ this assumption breaks down and the expansion is unjustified. Clearly, the expansion above is valid only for regular potentials such that the classical velocity of the particle is everywhere small compared to the velocity of light. On the assumption that such an expansion is justified, substitution in equation (50) gives the ESC Hamiltonian as an expansion of α^2

$$\mathbf{h}^{\mathrm{ESC}} = q\phi\mathbf{I} + \frac{(\boldsymbol{\sigma}\cdot\boldsymbol{\Pi})^2}{2m} + \frac{(\boldsymbol{\sigma}\cdot\boldsymbol{\Pi})(q\phi - E)(\boldsymbol{\sigma}\cdot\boldsymbol{\Pi})}{4m^2}\alpha^2$$

$$+ \frac{(\boldsymbol{\sigma}\cdot\boldsymbol{\Pi})(q\phi - E)^2(\boldsymbol{\sigma}\cdot\boldsymbol{\Pi})}{8m^3}\alpha^4 + \cdots \qquad (58)$$

The ESC Hamiltonian is energy dependent and not very useful for higher orders. The FW Hamiltonian (equation (53)) or identical Hermitian similarity transformed Hamiltonian truncated at order α^2 gives the widely used Pauli Hamiltonian. The resulting Hamiltonian has terms up to order of magnitude $mc^2\alpha^4$ as one can see from equation (53), since the order of magnitude of both $q\phi$ and $\boldsymbol{\sigma}\cdot\boldsymbol{\Pi}$ are proportional to $mc^2\alpha^2$. The Pauli Hamiltonian can also be derived from truncating the ESC Hamiltonian equation (58), at order α^2. The Pauli Hamiltonian often regarded as a valid approximation to the exact FW Hamiltonian (not expanded in powers of α^2). However, as we have already seen in the previous analysis, the expansion of the FW Hamiltonian in terms of α^2 is singular for small $|\mathbf{r}|$ and in fact the Pauli Hamiltonian is a very poor approximation to the exact FW Hamiltonian in this region. Consequently, an assessment of the accuracy of the Pauli Hamiltonian is necessary before it can be used in electronic structure calculations. This is usually done by comparison of the numerical results obtained by using the Pauli form with the full four-component relativistic calculations.

However, it is more appropriate to provide theoretical justifications for such use. In this respect, first, we introduce the third category of decoupling of positive and negative states commonly known as the 'direct perturbation theory'. This approach does not suffer from the singularity problems described previously. However, the four-component form of the Dirac equation remains intact. The new Hamiltonian requires identical computational effort as for the Dirac equation itself, hence it is not an attractive alternative to the Dirac equation. However, it is useful to assess the accuracy of approximate two-component forms derived from the Dirac equation such as Pauli Hamiltonian. Consider the transformation

matrix $\mathbf{U}$

$$\mathbf{U} = \begin{pmatrix} \mathbf{I} & \mathbf{0} \\ \mathbf{0} & c^{-1}\mathbf{I} \end{pmatrix} \tag{59}$$

and corresponding metric $\mathbf{S}$

$$\mathbf{S} = \mathbf{U}^\dagger \mathbf{U} = \begin{pmatrix} \mathbf{I} & \mathbf{0} \\ \mathbf{0} & c^{-2}\mathbf{I} \end{pmatrix} \tag{60}$$

and the transformed wave function $\tilde{\psi}$

$$\tilde{\psi} = \begin{pmatrix} \psi_{\mathrm{L}} \\ c\psi_{\mathrm{S}} \end{pmatrix} = \begin{pmatrix} \mathbf{I} & \mathbf{0} \\ \mathbf{0} & c\mathbf{I} \end{pmatrix} \begin{pmatrix} \psi_{\mathrm{L}} \\ \psi_{\mathrm{S}} \end{pmatrix} \tag{61}$$

Next, use the general transformation defined in equation (32), since we have a non-zero metric. Substituting for $\mathbf{U}^\dagger$, $\mathbf{U}$ and $\mathbf{S}$ in equation (32) with $z=0$ yields

$$\left[\begin{pmatrix} q\phi\mathbf{I} & \boldsymbol{\sigma}\cdot\boldsymbol{\Pi} \\ \boldsymbol{\sigma}\cdot\boldsymbol{\Pi} & -2m \end{pmatrix} + \frac{1}{c^2} \begin{pmatrix} \mathbf{0} & \mathbf{0} \\ \mathbf{0} & q\phi\mathbf{I} \end{pmatrix} \right] \begin{pmatrix} \psi_{\mathrm{L}} \\ c\psi_{\mathrm{S}} \end{pmatrix}$$
$$= E \begin{pmatrix} \mathbf{I} & \mathbf{0} \\ \mathbf{0} & \mathbf{0} \end{pmatrix} \begin{pmatrix} \psi_{\mathrm{L}} \\ c\psi_{\mathrm{S}} \end{pmatrix} + \frac{E}{c^2} \begin{pmatrix} \mathbf{0} & \mathbf{0} \\ \mathbf{0} & \mathbf{I} \end{pmatrix} \begin{pmatrix} \psi_{\mathrm{L}} \\ c\psi_{\mathrm{S}} \end{pmatrix} \tag{62}$$

Hence, the NRL of the Dirac equation with c-dependent metric is

$$\begin{pmatrix} q\phi\mathbf{I} & \boldsymbol{\sigma}\cdot\boldsymbol{\Pi} \\ \boldsymbol{\sigma}\cdot\boldsymbol{\Pi} & -2m \end{pmatrix} \begin{pmatrix} \psi_{\mathrm{L}} \\ c\psi_{\mathrm{S}} \end{pmatrix} = E \begin{pmatrix} \mathbf{I} & \mathbf{0} \\ \mathbf{0} & \mathbf{0} \end{pmatrix} \begin{pmatrix} \psi_{\mathrm{L}} \\ c\psi_{\mathrm{S}} \end{pmatrix} \tag{63}$$

This non-relativistic equation in terms of four-component spinors has been studied in detail by Lévy-Leblond [44,45], who has shown that it results automatically from a study of the irreducible representations of the Galilei group and that it gives a correct description of spin. It is easy to see that in the absence of an external magnetic field, equation (63) is equivalent to the Schrödinger equation in the sense that after elimination of the 'small component'

$$q\phi\psi_{\mathrm{L}} + c\boldsymbol{\sigma}\cdot\mathbf{P}\psi_{\mathrm{S}} = E\psi_{\mathrm{L}}, \quad \psi_{\mathrm{S}} = \frac{\boldsymbol{\sigma}\cdot\mathbf{P}\psi_{\mathrm{L}}}{2mc} \tag{64}$$

we get the Schrödinger equation

$$q\phi\psi_{\mathrm{L}} + \frac{(\boldsymbol{\sigma}\cdot\mathbf{P})^2\psi_{\mathrm{L}}}{2m} = E\psi_{\mathrm{L}} \tag{65}$$

Assuming $1/c^2$ as the perturbation parameter the first-order energy can be written as

$$E^{(1)}(\mathrm{DPT}) = \left\langle \begin{pmatrix} \psi_{\mathrm{L}}^{(0)} \\ c\psi_{\mathrm{S}}^{(0)} \end{pmatrix} \left| \begin{pmatrix} \mathbf{0} & \mathbf{0} \\ \mathbf{0} & (q\phi - E^{(0)})\mathbf{I} \end{pmatrix} \right| \begin{pmatrix} \psi_{\mathrm{L}}^{(0)} \\ c\psi_{\mathrm{S}}^{(0)} \end{pmatrix} \right\rangle \tag{66}$$

or in two-component form

$$E^{(1)}(\text{DPT}) = \left\langle \psi_L^{(0)} \frac{\boldsymbol{\sigma}\cdot\boldsymbol{\Pi}}{2m} \left| (q\phi - E^{(0)}) \right| \frac{\boldsymbol{\sigma}\cdot\boldsymbol{\Pi}}{2m} \psi_L^{(0)} \right\rangle. \tag{67}$$

We can use the relation

$$\left\{ \frac{(\boldsymbol{\sigma}\cdot\boldsymbol{\Pi})\cdot(\boldsymbol{\sigma}\cdot\boldsymbol{\Pi})}{2m} + q\phi \right\} |\psi_L^{(0)}\rangle = E^{(0)} |\psi_L^{(0)}\rangle \tag{68}$$

to rewrite equation (67)

$$\begin{aligned} E^{(1)}(\text{DPT}) &= \left\langle \psi_L^{(0)} \frac{\boldsymbol{\sigma}\cdot\boldsymbol{\Pi}}{2m} \left| \left(q\phi - \frac{(\boldsymbol{\sigma}\cdot\boldsymbol{\Pi})(\boldsymbol{\sigma}\cdot\boldsymbol{\Pi})}{2m} - q\phi \right) \right| \psi_L^{(0)} \right\rangle \\ &= \left\langle \psi_L^{(0)} \left| \frac{q(\boldsymbol{\sigma}\cdot\boldsymbol{\Pi})\phi(\boldsymbol{\sigma}\cdot\boldsymbol{\Pi})}{4m^2} - \frac{(\boldsymbol{\sigma}\cdot\boldsymbol{\Pi})^4}{8m^3} - \frac{q(\boldsymbol{\sigma}\cdot\boldsymbol{\Pi})^2\phi}{4m^2} \right| \psi_L^{(0)} \right\rangle \\ &= \langle \psi_L^{(0)} | \mathbf{h}_1^{\text{DPD}} | \psi_L^{(0)} \rangle \end{aligned} \tag{69}$$

where

$$\mathbf{h}_1^{\text{DPD}} = \frac{q(\boldsymbol{\sigma}\cdot\boldsymbol{\Pi})\phi(\boldsymbol{\sigma}\cdot\boldsymbol{\Pi})}{4m^2} - \frac{(\boldsymbol{\sigma}\cdot\boldsymbol{\Pi})^4}{8m^3} - \frac{q(\boldsymbol{\sigma}\cdot\boldsymbol{\Pi})^2\phi}{4m^2}.$$

Similarly, the first-order energy obtained from the Pauli Hamiltonian given in equation (53) can be written as

$$\begin{aligned} E^{(1)}(\text{FW}) &= \left\langle \psi_L^{(0)} \left| \frac{q(\boldsymbol{\sigma}\cdot\boldsymbol{\Pi})\phi(\boldsymbol{\sigma}\cdot\boldsymbol{\Pi})}{4m^2} - \frac{(\boldsymbol{\sigma}\cdot\boldsymbol{\Pi})^4}{8m^3} - \frac{q[(\boldsymbol{\sigma}\cdot\boldsymbol{\Pi})^2, \phi]_+}{8m^2} \right| \psi_L^{(0)} \right\rangle \\ &= \langle \psi_L^{(0)} | \mathbf{h}_1^{\text{FW}} | \psi_L^{(0)} \rangle \end{aligned} \tag{70}$$

where

$$\mathbf{h}_1^{\text{FW}} = \frac{q(\boldsymbol{\sigma}\cdot\boldsymbol{\Pi})\phi(\boldsymbol{\sigma}\cdot\boldsymbol{\Pi})}{4m^2} - \frac{(\boldsymbol{\sigma}\cdot\boldsymbol{\Pi})^4}{8m^3} - \frac{q[(\boldsymbol{\sigma}\cdot\boldsymbol{\Pi})^2, \phi]_+}{8m^2}.$$

The $\mathbf{h}_1^{\text{DPD}}$ is a non-Hermitian operator. Noting that the expectation value of a real non-Hermitian operator is equal to the expectation value of its Hermitian part, the equivalence of the two first-order energies is obvious. The difference in two Hamiltonians

$$\mathbf{h}_1^{\text{FW}} - \mathbf{h}_1^{\text{DPD}} = \frac{1}{4}[(\boldsymbol{\sigma}\cdot\boldsymbol{\Pi})^2, \phi]$$

is responsible for the singularities in $\mathbf{h}_1^{FW}$ higher orders of perturbation theory. But as shown above this fact does not affect the first-order energy in equation (70).

So far our discussion of the NRF and the NRL of the relativistic Hamiltonians has been limited to the one-fermion external field Dirac equation. For the many-fermion case the picture is not so simple. For example, in the case of two fermions, the wave function has 16 components: four components representing both particles having positive energy states, another eight components representing one particle having positive energy states and the other particle having negative energy states and the other four components representing both particles having negative energy states. Consequently, we cannot decompose the full wave function into two group of components, one having only positive energy states and the other having only negative energy states or equivalently, we cannot write the many-fermion Hamiltonian in the form given in equation (30) contrary to what has been done in the literature in some occasions [46]. The decoupling of positive energy components from negative and mixed (both positive and negative) components to establish the NRF or NRL of many-fermion Hamiltonian is conceptually similar to the one-fermion case but the mathematics involved is laborious. The two-fermion problem is manageable but tedious.

Consequently, we have to adopt an intelligent, and at the same time accurate, scheme to obtain the NRF of the many-electron Hamiltonian. Two such schemes have been used in the literature. The first one involves a rigorous derivation of the NRF of the two-fermion DBC Hamiltonian and directly extends the resulting non-relativistic Hamiltonian to many-fermion systems. The advantage of this scheme is that the order of each term in terms of $mc^2\alpha^n$ (n is a positive integer) can be determined without any ambiguities. However, the physical significance of the individual terms is not quite clear from the way they are derived. In the other scheme, the NRF of the one-fermion Hamiltonian (equation (53)) is extended directly to the many-fermion case. The Coulomb and Breit interaction terms are added later on recognizing the fact that they are formally of order $mc^2\alpha^2$ in a molecular environment. The effect of other moving charged particles to the vector potential has to be taken into account in the derivation. Contrary to the former procedure, there are ambiguities in the order of certain terms in the expansion [5]. For this reason the latter approach is not entirely satisfactory, but it does have the advantage of exhibiting the origin of the each term in the Hamiltonian and it allows physical interpretation to be given to each. Here, we adopt the first approach.

Both FW and ESC methods have been applied to decouple the positive energy states from the negative and mixed states of the two-fermion DBC Hamiltonian [47–49]. Since we are only interested in positive energy solutions, we may start from the original two-fermion DBC Hamiltonian without positive and negative energy projection operators. The two-fermion DBC Hamiltonian for stationary states can be written as

$$\left\{ \sum_{i=1}^{2} c\boldsymbol{\sigma}_i \cdot \boldsymbol{\Pi}_i + \sum_{i=1}^{2} q_i \phi_i \mathbf{I} + \frac{q_1 q_2 (\mathbf{I} + \mathbf{B}_{12})}{r_{12}} \right\} \boldsymbol{\Psi} = E\boldsymbol{\Psi} \qquad (71)$$

where

$$\mathbf{B}_{12} = -\frac{1}{2}\left[\boldsymbol{\alpha}_1\cdot\boldsymbol{\alpha}_2 + \frac{(\boldsymbol{\alpha}_1\cdot\mathbf{r}_{12})(\boldsymbol{\alpha}_2\cdot\mathbf{r}_{12})}{r_{12}^2}\right] \tag{72}$$

As in the one-fermion case, the whole energy spectrum is shifted by $-(m_1 + m_2)c^2$, so that the direct comparison with the non-relativistic results is feasible. Following the notation introduced by Foldy and Wouthuysen one can write

$$\mathcal{EE} = \sum_{i=1}^{2}q_i\phi_i\mathbf{I} + \frac{q_1q_2}{r_{12}}\mathbf{I}, \quad \mathcal{EO} = \boldsymbol{\alpha}_1\cdot\boldsymbol{\Pi}_1, \quad \mathcal{OE} = \boldsymbol{\alpha}_2\cdot\boldsymbol{\Pi}_2,$$

$$\mathcal{OO} = -\frac{1}{2}\left[\boldsymbol{\alpha}_1\cdot\boldsymbol{\alpha}_2 + \frac{(\boldsymbol{\alpha}_1\cdot\mathbf{r}_{12})(\boldsymbol{\alpha}_2\cdot\mathbf{r}_{12})}{r_{12}^2}\right] \tag{73}$$

Here, $\mathcal{E}$ represents an even operator, that is one that has no matrix elements between positive and negative energy components while $\mathcal{O}$ is an odd operator having only matrix elements between positive and negative energy components. The conditions for an operator to be even or odd can be expressed more formally; an even operator must commute with β: $[\mathcal{E},\beta]=0$ while an odd operator must anticommute with β: $[\mathcal{E},\beta]_+ =0$.

As mentioned earlier, the concepts involved in the two-fermion case are essentially the same and also the expansion in terms of α^2 have the similar problems as in the one-fermion case. Consequently, we have chosen to give only the final form of the Hamiltonian and refer to Barker and Glover [49] for mathematical details. The NRF of the two-fermion Hamiltonian can be written in terms of the operators defined in equation (73) as

$$\mathbf{H} = +\frac{1}{2m_1}(\mathcal{EO})^2 + \frac{1}{2m_2}(\mathcal{OE})^2 - \frac{\alpha^2}{8m_1^3}(\mathcal{EO})^4 - \frac{\alpha^2}{8m_2^3}(\mathcal{OE})^4 + (\mathcal{EE})$$

$$+ \frac{\alpha^2}{8m_1^2}\sum_i^N[\mathcal{OE},[\mathcal{EE},\mathcal{OE}]] + \frac{\alpha^2}{8m_1^2}\sum_i^N[\mathcal{EO},[\mathcal{EE},\mathcal{EO}]]$$

$$+ \frac{\alpha^2}{4m_1m_2}\sum_i^N[\mathcal{EO},[\mathcal{OE},\mathcal{OO}]_+]_+ + \mathcal{O}(mc^2\alpha^5) \tag{74}$$

Here, we only keep terms having order of magnitude $mc^2\alpha^4$. One can compare this expansion with the one-fermion Pauli expansion presented in equation (53), given the fact that in the one-fermion case $\mathcal{E}=q\phi\mathbf{I}$ and $\mathcal{O}=\boldsymbol{\sigma}\cdot\boldsymbol{\Pi}$. We can simplify this expression by expanding the commutators and with the extensive use of vector algebra. The resulting two-fermion Hamiltonian can be extended to many-fermions quite trivially and the NRF of the many-fermion Hamiltonian can

be written as

$$
\mathbf{H} = +\sum_i q_i \phi_i + \sum_i \frac{(\mathbf{\Pi}_i \cdot \mathbf{\Pi}_i)}{2m_i} + \frac{1}{2}\sum_{ij}\frac{q_i q_j}{r_{ij}} - \alpha \sum_i \frac{q_i \mathbf{S}_i \cdot (\nabla \times \mathbf{A}_i)}{m_i}
$$

$$
- \frac{\alpha^2}{8}\sum_i \frac{q_i(\nabla \cdot E_i)}{m_i^2} - \frac{\alpha^2}{8}\sum_i \frac{(\mathbf{\Pi}_i \cdot \mathbf{\Pi}_i)^4}{m_i^3} + \frac{\alpha^2}{2}\sum_i \frac{q_i \mathbf{S}_i \cdot (\nabla \times \mathbf{A}_i)(\mathbf{\Pi}_i \cdot \mathbf{\Pi}_i)}{m_i^3}
$$

$$
+ \frac{\alpha^2}{4}\sum_i \frac{q_i \mathbf{S}_i \cdot (\mathbf{\Pi}_i \times E_i - E_i \times \mathbf{\Pi}_i)}{m_i^2} - \frac{\alpha^2}{2}\sum_{i,j}\frac{q_i q_j \mathbf{S}_i \cdot (\mathbf{r}_{ij} \times \mathbf{\Pi}_i)}{m_i^2 r_{ij}^3}
$$

$$
- \alpha^2 \sum_{i,j}\frac{q_i q_j \mathbf{S}_i \cdot (\mathbf{r}_{ij} \times \mathbf{\Pi}_j)}{m_i^2 r_{ij}^3} - \frac{\alpha^2 \pi}{2}\sum_{i,j}\frac{q_i q_j}{m_i m_j}\delta(\mathbf{r}_{ij})
$$

$$
- \frac{\alpha^2}{4}\sum_{i,j} q_i q_j \left(\frac{\mathbf{\Pi}_i \cdot (r_{ij}^{-1}\mathbf{\Pi}_j + (\mathbf{\Pi}_i \cdot \mathbf{r}_{ij})r_{ij}^{-3}(\mathbf{r}_{ij} \cdot \mathbf{\Pi}_j))}{m_i m_j} \right)
$$

$$
+ \frac{\alpha^2}{2}\sum_{i,j}\frac{q_i q_j}{m_i m_j}\left(\frac{(\mathbf{S}_i \cdot \mathbf{S}_j)}{r_{ij}^3} - 3\frac{(\mathbf{S}_i \cdot \mathbf{r}_{ij})(\mathbf{S}_i \cdot \mathbf{r}_{ij})}{r_{ij}^5} - \frac{8\pi\delta(\mathbf{r}_{ij})(\mathbf{S}_i \cdot \mathbf{S}_j)}{3} \right) + O(mc^2\alpha^5)
$$

(75)

It is important to note once again that ϕ_i and $\mathbf{A}_i$ in equation (75) are the scalar and vector potential resulting from the external electromagnetic radiation field. Also note that here, $E_i = \nabla \phi_i$ and $\mathbf{S}_i$ is the spin of the ith particle. We can identify each term in equation (75) as corresponding to a certain type of physical interaction of moving charged particles. The list of physical interpretations of terms follows in the same order as the terms in equation (75).

1. Interaction of the charged particles with the external electric field.
2. Kinetic energy of the moving charged particle.
3. Particle–particle electrostatic interaction.
4. Interaction of particle spin magnetic moment with the external magnetic field (Zeeman term).
5. Relativistic correction to the first term (Darwin term).
6. Relativistic correction to the second term.
7. Relativistic correction to the third term.
8. Interaction of an electron's spin magnetic moment with the magnetic field it experiences by virtue of its motion relative to the external electric field (spin–orbit term).
9. Interaction of the spin magnetic moment of an electron with its own orbital motion due to the electric field of another electron.
10. Interaction of the spin magnetic moment of one electron with the orbital motion of another (spin–other orbit term).
11. Relativistic correction to the third term.

12. Retarded orbit–orbit interaction of one electron with the electromagnetic field due to the relative motion of another.
13. Dipole–dipole interaction between the spin magnetic moments of two electrons.

So far in the derivation of the Hamiltonian given in equation (75) we have not placed any restriction on the type of particles except that they are fermions. If we limit our many-fermion systems to be molecules whose nuclei are point charges with spin one-half entities with proper nuclear masses and charges, equation (75) describes a proper molecular Hamiltonian when we introduce the appropriate notation to distinguish the nuclei from electrons. In the case of electrons, the mass (m_e) and electronic charge (e) both are unity in terms of Hartree atomic units. The mass of nucleus N in atomic units is denoted by M_N. Similarly, the electron spin $\mathbf{S}_i$ is replaced by $\mathbf{I}_N$, the spin of the nucleus N and $Z_N e$ is used in place of charge q, where Z_N is the atomic number of nucleus N. However, this approach is not problem free either. It has been shown from QED arguments that the resulting molecular Hamiltonian is valid only if we neglect all the terms which involve M_N^{-2} and smaller [11]. As we can see from equation (75), in fact all these terms are formally of order $mc^2\alpha^4$ to begin with and at least 10^{-6} smaller than the corresponding electron terms.

Another potential problem which can arise can be seen by estimating the order of magnitude of the terms on the basis of an electron in a Bohr orbit of the hydrogen atom. In general, when higher nuclear charges ($Z_N e$) are involved it is no longer appropriate to express the magnitude of terms in the Hamiltonian in terms of $mc^2\alpha^n$. Instead the terms $c\boldsymbol{\alpha}\cdot\mathbf{P}$, $q\phi$ and $qc\boldsymbol{\alpha}\cdot\mathbf{A}$ in the Dirac Hamiltonian are of order $mc^2(Z_N\alpha)$, $mc^2(Z_N\alpha)^2$ and $mc^2(Z_N\alpha)^3$, respectively, so that $Z_N\alpha$ should be used as the expansion parameter rather than the fine structure constant itself. However, since α is a very small number, these comments only become important for atoms or molecules with large atomic numbers, and then only for the inner electrons, since the outer electrons are screened from the nuclei.

Another subtlety is that the assumption nuclei behave as Dirac particles, amounts to assuming that all nuclei have spin 1/2. However, it is not uncommon to have nuclei with spin as high as 9/2: worse nuclei with integer spins are bosons and do not obey Fermi–Dirac statistics. The only justification to use equation (75) for such a case is that the resulting theory agrees with experiment. Under the assumption, we are in a position to extend our many-fermion Hamiltonian to molecules assuming that the nuclei are Dirac particles with anomalous spin. The molecular Hamiltonian may then be written as

$$H = H_e + H_N + H_{eN} \tag{76}$$

where $H_e = H_e^1 + H_e^2 + H_e^3 + H_e^4 + H_e^5 + H_e^6 + H_e^7 + H_e^8 + H_e^9 + H_e^{10} + H_e^{11} + H_e^{12} + H_e^{13}$, $H_N = H_N^1 + H_N^2 + H_N^3 + H_N^4$ and $H_{Ne} = H_{Ne}^1 + H_{Ne}^2 + H_{Ne}^3 + H_{Ne}^4 + H_{Ne}^5 + H_{Ne}^6 + H_{Ne}^7$ are, respectively, the electronic, nuclear and the electron–nuclear interaction Hamiltonian. Expressions for individual terms in equation (76) can easily be written by substitution of appropriate masses and charges in equation (75). In doing so, it is helpful to keep in mind the interpretation of the individual terms

in equation (75) and which particle is responsible for quantities such as mass and charge in individual terms. The electronic terms

$$H_{\mathrm{e}}^1 = -\sum_i \phi_i$$

$$H_{\mathrm{e}}^2 = \sum_i \frac{(\mathbf{\Pi}_i \cdot \mathbf{\Pi}_i)}{2}$$

$$H_{\mathrm{e}}^3 = \frac{1}{2} \sum_{i,j} \frac{1}{r_{ij}}$$

$$H_{\mathrm{e}}^4 = \alpha \sum_i \mathbf{S}_i \cdot (\nabla \times \mathbf{A}_i)$$

$$H_{\mathrm{e}}^5 = \frac{\alpha^2}{8} \sum_i (\nabla \cdot \mathbf{E}_i)$$

$$H_{\mathrm{e}}^6 = -\frac{\alpha^2}{8} \sum_i (\mathbf{\Pi}_i \cdot \mathbf{\Pi}_i)^4$$

$$H_{\mathrm{e}}^7 = -\frac{\alpha^2}{2} \sum_i \mathbf{S}_i \cdot (\nabla \times \mathbf{A}_i)(\mathbf{\Pi}_i \cdot \mathbf{\Pi}_i)$$

$$H_{\mathrm{e}}^8 = -\frac{\alpha^2}{2} \sum_{i,j} \frac{\mathbf{S}_i \cdot (\mathbf{r}_{ij} \times \mathbf{\Pi}_i)}{\mathbf{r}_{ij}^3}$$

$$H_{\mathrm{e}}^9 = -\alpha^2 \sum_{i,j} \frac{\mathbf{S}_i \cdot (\mathbf{r}_{ij} \times \mathbf{\Pi}_j)}{\mathbf{r}_{ij}^3}$$

$$H_{\mathrm{e}}^{10} = -\frac{\alpha^2}{4} \sum_i \mathbf{S}_i \cdot (\mathbf{\Pi}_i \times \mathbf{E}_i - \mathbf{E}_i \times \mathbf{\Pi}_i)$$

$$H_{\mathrm{e}}^{11} = -\frac{\alpha^2}{4} \sum_{i,j} \mathbf{\Pi}_i \cdot (r_{ij}^{-1} \mathbf{\Pi}_j) + (\mathbf{\Pi}_i \cdot \mathbf{r}_{ij}) r_{ij}^{-3} (\mathbf{r}_{ij} \cdot \mathbf{\Pi}_j)$$

$$H_{\mathrm{e}}^{12} = \frac{\alpha^2}{2} \sum_{i,j} \left(\frac{(\mathbf{S}_i \cdot \mathbf{S}_j)}{r_{ij}^3} - 3 \frac{(\mathbf{S}_i \cdot \mathbf{r}_{ij})(\mathbf{S}_i \cdot \mathbf{r}_{ij})}{r_{ij}^5} - \frac{8\pi \delta(\mathbf{r}_{ij})(\mathbf{S}_i \cdot \mathbf{S}_j)}{3} \right)$$

$$H_{\mathrm{e}}^{13} = -\frac{\alpha^2 \pi}{2} \sum_{i,j} \delta(\mathbf{r}_{ij})$$

the nuclear terms

$$H_N^1 = \sum_N Z_N \phi_N$$

$$H_N^2 = \sum_N \frac{(\mathbf{\Pi}_N \cdot \mathbf{\Pi}_N)}{2}$$

$$H_N^3 = \frac{1}{2} \sum_{N,N'} \frac{Z_N Z_{N'}}{r_{NN'}} \tag{77}$$

$$H_N^4 = -\alpha \sum_N \frac{Z_N \mathbf{I}_N \cdot (\nabla \times \mathbf{A}_N)}{M_N}$$

and the electronic–nuclear coupling terms

$$H_{Ne}^1 = -\sum_{i,N} \frac{Z_N}{r_{iN}}$$

$$H_{Ne}^2 = \frac{\alpha^2}{2} \sum_{i,N} \frac{Z_N \mathbf{S}_i \cdot (\mathbf{r}_{iN} \times \mathbf{\Pi}_i)}{M_N r_{iN}^3}$$

$$H_{Ne}^3 = \frac{\alpha^2}{2} \sum_{i,N} \frac{Z_N \mathbf{S}_i \cdot (\mathbf{r}_{iN} \times \mathbf{\Pi}_N)}{M_N r_{iN}^3}$$

$$H_{Ne}^4 = \frac{\alpha^2}{2} \sum_{i,N} \frac{Z_N \mathbf{I}_N \cdot (\mathbf{r}_{iN} \times \mathbf{\Pi}_i)}{M_N r_{iN}^3} \tag{78}$$

$$H_{Ne}^5 = \frac{\alpha^2}{2} \sum_{i,N} \frac{Z_N [\mathbf{\Pi}_N \cdot (r_{iN}^{-1} \mathbf{\Pi}_N) + (\mathbf{\Pi}_N \cdot \mathbf{r}_{iN}) r_{iN}^{-3} (\mathbf{r}_{iN} \cdot \mathbf{\Pi}_N)]}{M_N}$$

$$H_{Ne}^6 = -\frac{\alpha^2}{2} \sum_{i,N} \frac{Z_N}{M_N} \left(\frac{(\mathbf{S}_i \cdot \mathbf{I}_N)}{r_{iN}^3} - 3 \frac{(\mathbf{S}_i \cdot \mathbf{r}_{iN})(\mathbf{I}_N \cdot \mathbf{r}_{iN})}{r_{iN}^5} - \frac{8\pi \delta(\mathbf{r}_{iN})(\mathbf{S}_i \cdot \mathbf{I}_N)}{3} \right)$$

$$H_{Ne}^7 = \frac{\alpha^2 \pi}{2} \sum_{i,N} Z_\alpha \delta(\mathbf{r}_{iN})$$

3. THE NMR CHEMICAL SHIFTS AND INDIRECT NUCLEAR SPIN–SPIN COUPLING OPERATORS

The preceding discussion was intended to present a general survey of molecular Hamiltonians, in both their relativistic and non-relativistic forms. We focused

mainly on the approximations involved in their derivations and also their limitations, with the hope that such a focus eventually will be helpful in using them intelligently for problems of interest and also in assessing the results obtained. In this respect, the Hamiltonian presented in equation (76) is general and can be used in non-relativistic or relativistic (within limitations) calculations of energetics, dynamics and spectra of molecules and atoms. Similarly, equation (27) can be used in four-component, fully relativistic calculations of such molecular properties.

We can make further approximations to simplify the NRF of the Hamiltonian presented in equation (75) for non-dynamical properties. For such properties, we can freeze the nuclear movements and study only the electronic problem. This is commonly known as the clamped nuclei approximation, and it usually is quite good because of the fact that the nuclei of a molecule are about 1836 times more massive than the electrons, so we can usually think of the nuclei moving slowly in the average field of the electrons, which are able to adapt almost instantaneously to the nuclear motion. Invocation of the clamped nuclei approximation to equation (75) causes all the nuclear contributions which involve the nuclear momentum operator to vanish and the others to become constants (nuclear repulsion, etc.). These constant terms will only shift the total energy of the system. The remaining terms in the Hamiltonian are electronic terms and nuclear–electronic interaction contributions which do not involve the nuclear momentum operator.

Generally, it is not required to retain all the terms in the resulting approximate Hamiltonian, except those operators which describe the actual physical processes involved in the problem. For example, in the absence of an external electromagnetic field, the non-relativistic energy calculations only requires retaining the terms H_e^1, H_e^2, H_e^3 and H_N^3. Perturbative relativistic energy calculations can be carried out by including H_e^5, H_e^6 in addition to the terms retained for non-relativistic energy calculations.

The electron coupled interaction of nuclear magnetic moments with themselves and also with an external magnetic field is responsible for NMR spectroscopy. Since the focus of this study is calculation of NMR spectra within the non-relativistic framework, we will take a closer look at the Hamiltonian derived from equation (76) to describe NMR processes. In this regard, we retain all the terms, which depend on nuclear magnetic moments of nuclei in the molecule and the external magnetic field through its vector potential in addition to the usual non-relativistic Hamiltonian. The result is

$$
\begin{aligned}
H = {} & \sum_i \frac{(\mathbf{\Pi}_i \cdot \mathbf{\Pi}_i)}{2} + \frac{1}{2}\sum_{i,j}\frac{1}{r_{ij}} - \sum_{i,N}\frac{Z_N}{r_{iN}} + \sum_{N,N'}\frac{Z_N Z_{N'}}{R_{NN'}} \\
& + \frac{1}{c}\sum_{i,N}\gamma_N \frac{\mathbf{I}_N \cdot (\mathbf{r}_{iN}\times\mathbf{\Pi}_i)}{r_{iN}^3} - \frac{1}{c}\sum_{i,N}\gamma_N\left(\frac{(\mathbf{S}_i\cdot\mathbf{I}_N)}{r_{iN}^3} - 3\frac{(\mathbf{S}_i\cdot\mathbf{r}_{iN})(\mathbf{I}_N\cdot\mathbf{r}_i)}{r_{iN}^5}\right) \\
& + \frac{8\pi}{3c}\sum_{i,N}\gamma_N\delta(\mathbf{r}_{iN})(\mathbf{S}_i\cdot\mathbf{I}_N)
\end{aligned}
\tag{79}
$$

Here, we have introduced the notation $\mu_N = \gamma_N \mathbf{I}_N = g_N \beta_N \mathbf{I}_N = (g Z_N m_p / M_N) \times (1/2 m_p c) \mathbf{I}_N$ and $\beta = 1/2c$ where β is the Bohr magneton and β_N, γ_N and μ_N are nuclear magneton, nuclear magnetogyric ratio and nuclear magnetic moments of the nuclei N, respectively. Substitute for $\mathbf{\Pi}_i$,

$$\mathbf{\Pi}_i = \mathbf{P}_i + \frac{\mathbf{A}_i}{c} = \mathbf{P}_i + \frac{1}{2c} \sum_i \mathbf{B} \times (\mathbf{r}_i - \mathbf{G}) \tag{80}$$

where $\mathbf{B}$ and $\mathbf{G}$ are the external magnetic fields, respectively. Substitute for $\mathbf{\Pi}_i$ in equation (79) and then simplify assuming the Coulomb gauge ($\nabla \cdot \mathbf{A} = 0$) to obtain

$$\begin{aligned}
\mathbf{H} = &-\sum_i \frac{\nabla_i^2}{2} + \frac{1}{2} \sum_{i,j} \frac{1}{r_{ij}} - \sum_{i,N} \frac{Z_N}{r_{iN}} + \sum_{N,N'} \frac{Z_N Z_{N'}}{R_{NN'}} \\
&+ \frac{1}{ic} \sum_i ((\mathbf{r}_i - \mathbf{G}) \times \nabla_i) \cdot \mathbf{B} + \frac{1}{ic} \sum_{i,N} \gamma_N \mathbf{I}_N \cdot \left(\frac{(\mathbf{r}_{iN} \times \nabla_i)}{\mathbf{r}_{iN}^3} \right) \\
&+ \frac{1}{2c^2} \sum \gamma_N \mathbf{I}_N \cdot \left(\frac{(\mathbf{r}_{iN} \cdot (\mathbf{r}_i - \mathbf{G}))(\mathbf{B})}{r_{iN}^3} - \frac{(\mathbf{r}_{iN} \cdot \mathbf{B})(\mathbf{r}_i - \mathbf{G})}{r_{iN}^3} \right) \\
&- \frac{1}{c} \sum_{i,N} \gamma_N \left(\frac{(\mathbf{S}_i \cdot \mathbf{I}_N)}{r_{iN}^3} - 3 \frac{(\mathbf{S}_i \cdot \mathbf{r}_{iN})(\mathbf{I}_N \cdot \mathbf{r}_{iN})}{r_{iN}^5} \right) \\
&+ \frac{8\pi}{3c} \sum_{i,N} \gamma_N \delta(\mathbf{r}_{iN})(\mathbf{S}_i \cdot \mathbf{I}_N) + \sum_i \frac{(\mathbf{B} \cdot \mathbf{B})[(\mathbf{r}_i - \mathbf{G}) \cdot (\mathbf{r}_i - \mathbf{G})]}{4c^2} \tag{81}
\end{aligned}$$

We can assign a formal order to each term in equation (81) assuming $\mathbf{B}$ and γ_N as ordering parameters. First, let us consider the first-order field independent terms in equation (81)

$$H(\text{FC}) = \frac{16\pi\beta}{3} \sum_{i,N} \gamma_N \delta(\mathbf{r}_{iN})(\mathbf{S}_i \cdot \mathbf{I}_N)$$

$$H(\text{SD}) = 2\beta \sum_{i,N} \gamma_N \left(\frac{3(\mathbf{S}_i \cdot \mathbf{r}_{iN})(\mathbf{I}_N \cdot \mathbf{r}_{iN})}{r_{iN}^5} - \frac{\mathbf{S}_i \cdot \mathbf{I}_N}{r_{iN}^5} \right) \tag{82}$$

$$H(\text{PSO}) = -2i\beta \sum_{i,N} \gamma_N \mathbf{I}_N \cdot \left(\frac{\mathbf{r}_{iN} \times \nabla_i}{\mathbf{r}_{iN}^3} \right)$$

where $\beta = 1/2c$. Historically, these operators are known as Fermi-contact (FC), spin-dipole (SD) and paramagnetic spin-orbit (PSO) operators and their forms were originally derived by Ramsey [1]. As we shall see, a collection of second-order properties, each of which involves a pair of the these various first-order external field independent operators, contributes to the indirect nuclear spin–spin

coupling constant tensor. According to Ramsey, the indirect nuclear spin-coupling tensor also consists of a second-order contribution involving the diamagnetic spin-orbit contribution (DSO) given by

$$H(\text{DSO}) = \frac{2\beta}{c} \sum_{N,N'} \gamma_N \gamma_{N'} \sum_i \frac{(\mathbf{I}_N \cdot \mathbf{I}_{N'})(\mathbf{r}_{kN} \cdot \mathbf{r}_{kN'}) - (\mathbf{I}_N \cdot \mathbf{r}_{kN'})(\mathbf{I}_{N'} \cdot \mathbf{r}_{kN})}{r_{kN}^3 r_{kN'}^3} \tag{83}$$

The DSO term involves a product of γ_N ordering parameters and formally a second-order term. As seen from equation (81), the DSO term does not arise in our derivation and requires further investigation. In this regard, first, we will present another derivation which will eventually lead to the DSO term in addition to all the other terms given in equation (81).

In principle, this additional derivation also starts from the many-fermion Hamiltonian given in equation (75). As discussed earlier, extension of this equation to molecules usually is done by imposing the requirement that some of these particles are nuclei which are assumed to be fermions. An alternative, but less rigorous approach to introduce nuclei is to consider them as an external perturbation which modifies the external vector and scalar potential in equation (75). Further approximations can be made for non-dynamical properties by invoking the clamped nuclei approximation. For such a situation the external vector potential $\mathbf{A}$ can be written as

$$\mathbf{A}_i = \frac{1}{2}\mathbf{B} \times (\mathbf{r}_i - \mathbf{G}) + \sum_N \frac{\boldsymbol{\mu}_N \times \mathbf{r}_{iN}}{r_{iN}^3} \tag{84}$$

Retain the following terms in equation (75),

$$H = \sum_i \frac{(\boldsymbol{\Pi}_i \cdot \boldsymbol{\Pi}_i)}{2} + \frac{1}{2}\sum_{i,j}\frac{1}{r_{ij}} - \sum_{i,N}\frac{Z_N}{r_{iN}} + \sum_{N,N'}\frac{Z_N Z_{N'}}{R_{NN'}}$$
$$+ \frac{1}{c}\sum_i \mathbf{S}_i \cdot (\nabla \times \mathbf{A}_i) \tag{85}$$

and substitute for $\boldsymbol{\Pi}_i$ where $\boldsymbol{\Pi}_i = \mathbf{P}_i + (\mathbf{A}_i/c)$ and $\mathbf{A}_i$ is given in equation (84). Expand the first term assuming the Coulomb gauge in order to obtain

$$\boldsymbol{\Pi}_i \cdot \boldsymbol{\Pi}_i = \left(\mathbf{P}_i + \frac{\mathbf{A}_i}{c}\right) \cdot \left(\mathbf{P}_i + \frac{\mathbf{A}_i}{c}\right) = \mathbf{P}_i^2 + \frac{2}{c}\mathbf{A}_i \cdot \mathbf{P}_i + \frac{1}{c^2}\mathbf{A}_i \cdot \mathbf{A}_i \tag{86}$$

and then the last two terms

$$\frac{2}{c}\mathbf{A}_i \cdot \mathbf{P}_i = \frac{1}{ci}\left[\sum_i \frac{\mathbf{B} \times (\mathbf{r}_i - \mathbf{G})}{2} + \sum_{i,N}\frac{\boldsymbol{\mu}_N \times \mathbf{r}_{iN}}{r_{iN}^3}\right] \cdot \nabla_i$$
$$= \frac{1}{ci}\sum_i ((\mathbf{r}_i - \mathbf{G}) \times \nabla_i) \cdot \mathbf{B} + \frac{1}{ic}\sum_{i,N}\frac{\boldsymbol{\mu}_N \cdot (\mathbf{r} \times \nabla_i)}{r_{iN}^3} \tag{87}$$

and

$$\frac{1}{c^2}\mathbf{A}_i \cdot \mathbf{A}_i = \frac{1}{4c^2}\sum_i (\mathbf{B}\cdot\mathbf{B})(\mathbf{r}_i - \mathbf{G})\cdot(\mathbf{r}_i - \mathbf{G})$$

$$+ \frac{1}{2c^2}\sum_{i,N}\frac{(\mathbf{B}\cdot\boldsymbol{\mu}_N)(\mathbf{r}_i - \mathbf{G})\cdot\mathbf{r}_i}{r_{iN}^3} - \frac{1}{2c^2}\sum_{i,N}\frac{(\mathbf{B}\cdot\mathbf{r}_i)(\mathbf{r}_i - \mathbf{G})\cdot\boldsymbol{\mu}_N}{r_{iN}^3}$$

$$+ \frac{1}{c^2}\sum_{N,N'}\sum_i\frac{(\boldsymbol{\mu}_N\cdot\boldsymbol{\mu}_{N'})(\mathbf{r}_{iN}\cdot\mathbf{r}_{iN'}) - (\boldsymbol{\mu}_N\cdot\mathbf{r}_{iN'})(\boldsymbol{\mu}_{N'}\cdot\mathbf{r}_{iN})}{r_{iN}^3 r_{iN'}^3} \qquad (88)$$

Substitute for $\mathbf{A}_i$ from equation (84), in the last term of equation (85) and then simplify to obtain

$$\frac{1}{c}\sum_i \mathbf{S}_i\cdot(\nabla\times\mathbf{A}_i) = \frac{1}{2c}\sum_i \mathbf{S}_i\cdot\nabla\times(\mathbf{B}\times(\mathbf{r}_i - \mathbf{G})) + \frac{1}{c}\sum_{i,N}\mathbf{S}_i\cdot\nabla\times\left(\frac{\boldsymbol{\mu}_N\times\mathbf{r}_{iN}}{r_{iN}^3}\right)$$

$$= \frac{1}{c}\sum_{i,N}\left(\frac{3(\mathbf{S}_i\cdot\mathbf{r}_{iN})(\boldsymbol{\mu}_N\cdot\mathbf{r}_{iN})}{r_{iN}^5} - \frac{(\mathbf{S}_i\cdot\boldsymbol{\mu}_N)}{r_{iN}^3}\right)$$

$$+ \frac{1}{c}\sum_{i,N}\frac{8\pi\delta(\mathbf{r}_{iN})(\mathbf{S}_i\cdot\boldsymbol{\mu}_N)}{3} \qquad (89)$$

The final molecular Hamiltonian

$$\mathbf{H} = -\sum_i\frac{\nabla_i^2}{2} + \frac{1}{2}\sum_{i,j}\frac{1}{r_{ij}} - \sum_{i,N}\frac{Z_N}{r_{iN}} + \sum_{N,N'}\frac{Z_N Z_{N'}}{R_{NN'}}$$

$$+ \frac{1}{ic}\sum_i ((\mathbf{r}_i - \mathbf{G})\times\nabla_i)\cdot\mathbf{B} + \frac{1}{ic}\sum_{i,N}\gamma_N\mathbf{I}_N\cdot\left(\frac{(\mathbf{r}_{iN}\times\nabla_i)}{r_{iN}^3}\right)$$

$$+ \frac{1}{2c^2}\sum_{i,N}\gamma_N\mathbf{I}_N\cdot\left(\frac{(\mathbf{r}_{iN}\cdot(\mathbf{r}_i - \mathbf{G}))(\mathbf{B})}{r_{iN}^3} - \frac{(\mathbf{r}_{iN}\cdot\mathbf{B})(\mathbf{r}_i - \mathbf{G})}{r_{iN}^3}\right)$$

$$- \frac{1}{c}\sum_{i,N}\gamma_N\left(\frac{(\mathbf{S}_i\cdot\mathbf{I}_N)}{r_{iN}^3} - 3\frac{(\mathbf{S}_i\cdot\mathbf{r}_{iN})(\mathbf{I}_N\cdot\mathbf{r}_{iN})}{r_{iN}^5}\right)$$

$$- \frac{8\pi}{3c}\sum_{i,N}\gamma_N\delta(\mathbf{r}_{iN})(\mathbf{S}_i\cdot\mathbf{I}_N) + \sum_i\frac{(\mathbf{B}\cdot\mathbf{B})[(\mathbf{r}_i - \mathbf{G})\cdot(\mathbf{r}_i - \mathbf{G})]}{4c^2}$$

$$+ \frac{1}{c^2}\sum_{N,N'}\gamma_N\gamma_{N'}\sum_i\frac{(\mathbf{I}_N\cdot\mathbf{I}_{N'})(\mathbf{r}_{iN}\cdot\mathbf{r}_{iN'}) - (\mathbf{I}_N\cdot\mathbf{r}_{iN'})(\mathbf{I}_{N'}\cdot\mathbf{r}_{iN})}{r_{iN}^3 r_{iN'}^3} \qquad (90)$$

is formulated by collecting the expressions derived in equations (86)–(89). The first-order field independent operators collected from this Hamiltonian are identical with the operators given in equation (82). The second-order field-independent contribution is identical to the DSO operator given in equation (83). As shown from this derivation, the DSO contribution arises from $\mathbf{A}\cdot\mathbf{A}$ type contributions to the molecular Hamiltonian. Formally, this term has an order of

magnitude $mc^2\alpha^8$ in a molecular environment. It is not all that surprising that the DSO term does not arise in our first derivation since it is based on a truncated Pauli expansion of the Hamiltonian in which the magnitude of all the terms is $mc^2\alpha^4$ or less. It seems, based on our estimation ($mc^2\alpha^8$), that the magnitude of the DSO term is very small. However, as we will see latter, the DSO contribution is significant for certain coupling constants and cannot be discarded. Note that our criterion to estimate the order of magnitude of the individual terms is based on an electron in a Bohr orbit of the hydrogen atom. On some occasions this estimate may not give a good indication of the actual magnitude.

For example, the DSO contribution involves a product of two gyromagnetic ratios of the pair of coupled nuclei which can be larger for lighter atoms and hence, can result in a large overall DSO contribution. Ultimately, these complications are results of the expansion of the Hamiltonian in terms of α^2 and terms which are supposedly higher order in the expansion and, can sometimes, be numerically significant. In such occasions the only guidance we have is the experimental results, and we arbitrarily incorporate higher order terms in the expansion to improve the agreement with experiment.

At this point, it is appropriate to present a brief discussion on the origin of the FC operator (δ function) in the two-component form (Pauli form) of the molecular relativistic Hamiltonian. Many textbooks adopt the point of view that the FC is a relativistic effect, which must be derived from the Dirac equation [50,51]. In other textbooks or review articles it is stressed that the FC is not a relativistic effect and that it can be derived from classical electrodynamics [52,53] disregarding the origin of the gyromagnetic factor $g=2$. In some textbooks both derivations are presented [54]. The relativistic derivations suffer from the inherent drawbacks in the Pauli expansion, in particular that the Pauli Hamiltonian can only be used in the context of the first-order perturbation theory. Moreover, the origin of the FC term appears to be different depending on whether one uses the ESC method or FW transformation.

Earlier we mentioned briefly that the electron spin is perfectly consistent with the non-relativistic four-component Levy-Leblond theory [44,45]. The FC type interaction does not manifest in Dirac or Levy-Leblond theory. We shall show that on reducing the four-component Levy-Leblond equation into a two-component form the FC contribution arises naturally. A non-relativistic electron in an electromagnetic radiation field is described by the Levy-Leblond equation given by

$$\begin{pmatrix} -\phi\mathbf{I} & \boldsymbol{\sigma}\cdot\boldsymbol{\Pi} \\ \boldsymbol{\sigma}\cdot\boldsymbol{\Pi} & -2m \end{pmatrix} \begin{pmatrix} \psi_{\mathrm{L}} \\ c\psi_{\mathrm{S}} \end{pmatrix} = E \begin{pmatrix} \mathbf{I} & \mathbf{0} \\ \mathbf{0} & \mathbf{0} \end{pmatrix} \begin{pmatrix} \psi_{\mathrm{L}} \\ c\psi_{\mathrm{S}} \end{pmatrix} \tag{91}$$

where ϕ is the scalar potential and $\boldsymbol{\Pi} = \mathbf{p} - \mathbf{A}/c$. We can rewrite equation (91) such that

$$\left[\begin{pmatrix} -\phi\mathbf{I} & \boldsymbol{\sigma}\cdot\mathbf{P} \\ \boldsymbol{\sigma}\cdot\mathbf{P} & -2m \end{pmatrix} - \frac{1}{c} \begin{pmatrix} \mathbf{0} & \boldsymbol{\sigma}\cdot\mathbf{A} \\ \boldsymbol{\sigma}\cdot\mathbf{A} & \mathbf{0} \end{pmatrix} \right] \begin{pmatrix} \psi_{\mathrm{L}} \\ c\psi_{\mathrm{S}} \end{pmatrix} = E \begin{pmatrix} \mathbf{I} & \mathbf{0} \\ \mathbf{0} & \mathbf{0} \end{pmatrix} \begin{pmatrix} \psi_{\mathrm{L}} \\ c\psi_{\mathrm{S}} \end{pmatrix} \tag{92}$$

which led to the perturbing operator

$$h_1 = -\frac{1}{c}\begin{pmatrix} \mathbf{0} & \boldsymbol{\sigma}\cdot\mathbf{A} \\ \boldsymbol{\sigma}\cdot\mathbf{A} & \mathbf{0} \end{pmatrix}.$$

Hence, the first-order perturbed energy can be written as

$$E^{(1)} = -\frac{1}{c}\left\langle \begin{pmatrix} \psi_{\mathrm{L}}^{(0)} \\ c\psi_{\mathrm{S}}^{(0)} \end{pmatrix} \middle| \begin{pmatrix} \mathbf{0} & \boldsymbol{\sigma}\cdot\mathbf{A} \\ \boldsymbol{\sigma}\cdot\mathbf{A} & \mathbf{0} \end{pmatrix} \middle| \begin{pmatrix} \psi_{\mathrm{L}}^{(0)} \\ c\psi_{\mathrm{S}}^{(0)} \end{pmatrix} \right\rangle \tag{93}$$

or in a two-component form

$$E^{(1)} = -\frac{1}{2mc}\{\langle \boldsymbol{\sigma}\cdot\mathbf{P}\psi_{\mathrm{L}}^{(0)}|\boldsymbol{\sigma}\cdot\mathbf{A}\psi_{\mathrm{L}}^{(0)}\rangle + \langle \psi_{\mathrm{L}}^{(0)}|(\boldsymbol{\sigma}\cdot\mathbf{A})(\boldsymbol{\sigma}\cdot\mathbf{P})|\psi_{\mathrm{L}}^{(0)}\rangle\} \tag{94}$$

One can use the 'turnover-rule' for $\boldsymbol{\sigma}\cdot\mathbf{P}$ and get

$$E^{(1)} = -\frac{1}{2mc}\{\langle \psi_{\mathrm{L}}^{(0)}|[\boldsymbol{\sigma}\cdot\mathbf{P},\boldsymbol{\sigma}\cdot\mathbf{A}]_+|\psi_{\mathrm{L}}^{(0)}\rangle\} \tag{95}$$

which is straightforward if $\mathbf{A}$ is regular at the origin, and which is still valid for singular $\mathbf{A}$ if the derivative implicit in $\mathbf{P}$ is taken in the 'distribution sense' [55]. This can be further simplified to obtain

$$E^{(1)} = -\frac{1}{2mc}\{\langle \psi_{\mathrm{L}}^{(0)}|\mathbf{P}\cdot\mathbf{A} + \mathbf{A}\cdot\mathbf{P} + i\boldsymbol{\sigma}\cdot(\mathbf{P}\times\mathbf{A}) + i\boldsymbol{\sigma}\cdot(\mathbf{A}\times\mathbf{P})|\psi_{\mathrm{L}}^{(0)}\rangle\} \tag{96}$$

The vector potential created by spin of a nucleus with a magnetic moment $\boldsymbol{\mu}$

$$\mathbf{A} = \frac{\boldsymbol{\mu}\times\mathbf{r}}{r^3} \tag{97}$$

is singular at the origin. As a result we must take the derivatives, implicit in equation (96), in the 'distribution sense'. This means that $\nabla\times\mathbf{A}$ consists of two terms, one in which the derivatives are taken in usual function sense, and an extra term

$$\nabla\times\mathbf{A} = -\frac{\boldsymbol{\mu}}{r^3} + \frac{3(\boldsymbol{\mu}\cdot\mathbf{r})\mathbf{r}}{r^3} + \frac{2\boldsymbol{\mu}\delta(\mathbf{r})}{3r^3} \tag{98}$$

This shows that the FC operator arises as an artifact if one wants to describe the hyperfine interaction by first-order perturbation theory in terms of two-component spinors. In other words, when singular functions are involved, the boundary conditions cannot be ignored. These give rise to the FC operator.

4. CONCLUSION

To summarize, a detailed discussion of relativistic and non-relativistic forms of molecular Hamiltonians is presented. Our starting point is the Dirac one-fermion Hamiltonian in the presence of an external electromagnetic radiation field.

We have focused on the problems associated with extending 'Dirac's one-fermion theory' smoothly to many-fermion systems. A brief discussion of QED many-fermion Hamiltonians also was given. A comprehensive account of the problem of decoupling Dirac's four-component equation into two-component form and the serious drawbacks of the Pauli expansion were presented. The origins of the DSO and FC operators have been addressed. The working Hamiltonian which describe NMR spectra is derived.

ACKNOWLEDGEMENTS

It is with great pleasure that we submit this paper to Prez Jens on this special occasion. In his previous life as a scientist, Jens was instrumental in our work with NMR coupling constants, as we first learned about them from his papers. One in particular, with Jan Geertsen, was the first I saw where quantum chemistry was able to get these quantities about right for HF, and that was accomplished by evaluating ALL the contributing terms from the Ramsay theory. Others tried to avoid such demanding terms in their studies. Having an excellent treatment of second-order properties from EOM-CC, Perera's dissertation was to develop this tool and the required integrals for all the terms in the NMR coupling constant to enable predictive and now we have made many such studies where theroy is able to lead experiment. So scientifically and socially – where Benta is even more important than Prez Jens – thanks for being friends.

REFERENCES

[1] N. F. Ramsey, *Phys. Rev.*, 1953, **91**, 303.
[2] P. A. M. Dirac, *Proc. R. Soc. Ser. A*, 1928, **117**, 610.
[3] P. A. M. Dirac, *Proc. R. Soc. Ser. A*, 1928, **117**, 351.
[4] W. v. Pauli Jr., *Z. Phys.*, 1927, **43**, 601.
[5] R. E. Moss, *Advanced molecular quantum mechanics. An Introduction to Relativistic Quantum Mechanics and the Quantum Theory of Radiation*, Chapman & Hall, London, 1973.
[6] E. Merzbacher, *Quantum Mechanics*, 2nd edn, Wiley, London, 1970.
[7] R. Shankar, *Principles of Quantum Mechanics*, Plenum Press, New York, 1985.
[8] P. A. M. Dirac, *The Principles of Quantum Mechanics*, 4th edn, Oxford University Press, New York, 1958.
[9] W. v. Gordon, *Z. Phys.*, 1927, **40**, 117.
[10] O. v. Klein, *Z. Phys.*, 1927, **41**, 407.
[11] H. A. Bethe and E. E. Salpeter, *Quantum Mechanics of One- and Two-Electron Atoms*, Academic Press, New York, 1958.
[12] S. Tomanaga, *Phys. Rev.*, 1948, **74**, 224.
[13] R. P. Feynman, *Phys. Rev.*, 1949, **76**, 749.
[14] R. P. Feynman, *Phys. Rev.*, 1949, **76**, 769.
[15] R. P. Feynman, *Phys. Rev.*, 1949, **76**, 790.
[16] F. J. Dyson, *Phys. Rev.*, 1949, **75**, 486.
[17] D. P. Craig and T. Thirunamachandran, *Molecular Quantum Electrodynamics: an Introduction to Radiation-Molecule Interactions*, Academic Press, London, 1984.

[18] J. Sucher, *Phys. Scr.*, 1987, **36**, 271.

[19] G. Breit, *Phys. Rev.*, 1929, **34**, 553.

[20] G. E. Brown and D. G. Ravenhall, *Proc. R. Soc. Ser. A*, 1951, **208**, 552.

[21] J. Sucher, *Phys. Rev. Lett.*, 1985, **55**, 1033.

[22] B. Swirles, *Proc. R. Soc. Ser. A*, 1935, **625**, 152.

[23] I. P. Grant, *Proc. R. Soc. Ser. A*, 1961, **162**, 555.

[24] G. Malli and J. Oreg, *J. Chem. Phys.*, 1975, **63**, 830.

[25] J. Sucher, Foundation of the relativistic theory of atomic structure, in *Workshop on the Foundation of the Relativistic Theory of Atomic Structure* (eds H. G. Berry, K. T. Cheng, W. R. Johnson and Y. K. Kim), Argonne National Laboratory, Argonne, IL, 1980, pp. 2–26.

[26] J. Sucher, *Phys. Rev. A*, 1980, **22**, 348.

[27] L. Visscher, *Relativity and Electron Correlation in Chemistry*, PhD thesis, Rijksuniversiteit Groningen, 1995.

[28] J. Sucher, *Int. J. Quantum Chem.*, 1984, **XXV**, 3.

[29] A. A. Broyles, *Phys. Rev. A*, 1982, **26**, 1181.

[30] E. E. Salpeter and H. A. Bethe, *Phys. Rev.*, 1951, **84**, 1232.

[31] E. E. Salpeter, *Phys. Rev.*, 1951, **87**, 328.

[32] A. A. Broyles, *Phys. Rev. A*, 1988, **38**, 1137.

[33] A. A. Broyles, *Int. J. Quantum Chem. Symp.*, 1995, **29**, 1181.

[34] W. Kutzelnigg, *Z. Phys.*, 1989, **11**, 15.

[35] W. Kutzelnigg, *Z. Phys.*, 1990, **15**, 27.

[36] P. O. Löwdin, *J. Mol. Spectrosc.*, 1964, **14**, 131.

[37] L. L. Foldy and S. A. Wouthuysen, *Phys. Rev.*, 1950, **78**, 29.

[38] I. Lindgren and J. Morrison, *Atomic Many-Body Theory*, Springer, Berlin, 1982.

[39] J. des Cloizeaux, *Nucl. Phys.*, 1960, **20**, 329.

[40] E. van Lenthe, E. J. Baerends and J. G. Snijders, *J. Chem. Phys.*, 1993, **99**, 4597.

[41] C. Chang, M. Pelissier and P. Durand, *Phys. Scr.*, 1986, **34**, 394.

[42] E. van Lenthe, R. van Leeuwen, E. J. Baerends and J. G. Snijders, Relativistic regular two-component hamiltonians, in *New Challenges in Computational Quantum Chemistry* (eds R. Broer, P. J. C. Aerts and P. S. Bagus), University of Groningen, Netherlands, 1994, pp. 93–111.

[43] R. van Leeuwen, E. van Lenthe, E. J. Baerends and J. G. Snijders, *J. Chem. Phys.*, 1994, **101**, 1272.

[44] J. M. Levy-Leblond, *Comm. Math. Phys.*, 1967, **6**, 286.

[45] J. M. Levy-Leblond, *Ann. Phys. (NY)*, 1970, **57**, 481.

[46] G. A. Aucar and J. Oddershede, *Int. J. Quantum Chem.*, 1993, **47**, 425.

[47] Z. V. Chraplyvy, *Phys. Rev.*, 1953, **91**, 388.

[48] Z. V. Chraplyvy, *Phys. Rev.*, 1953, **92**, 1310.

[49] W. A. Barker and F. N. Glover, *Phys. Rev.*, 1955, **99**, 317.

[50] D. W. Davies, *The Theory of the Electric and Magnetic Properties of Molecules*, Wiley, New York, 1967.

[51] J. E. Harriman, *Theoretical Foundations of Electron Spin Resonance*, Academic Press, New York, 1978.

[52] A. Messiah, *Quantum Mechanics II*, Wiley, New York, 1962.

[53] H. F. Hameka, *Advanced Quantum Chemistry*, Addison-Wesley, Reading, MA, 1965.

[54] T. P. Das, *Relativistic Quantum Mechanics and Electrons*, Harper and Row, New York, 1973.

[55] M. J. Lighthill, *Introduction to Fourier Analysis and Generalised Functions*, Cambridge University Press, London, 1958.

The Rotational g Tensor of HF, H_2O, NH_3, and CH_4: A Comparison of Correlated *Ab Initio* Methods

Stephan P. A. Sauer

Department of Chemistry, University of Copenhagen, Universitetsparken 5,
DK-2100 København Ø, Denmark

Abstract

The rotational g tensors of hydrogen fluoride, water, ammonia and methane are calculated at their equilibrium geometries with various correlated *ab initio* methods. Among the methods employed are the second order polarization propagator approximation (SOPPA), which was developed by Jens Oddershede and co-workers, the second order polarization propagator approximation with coupled cluster singles and doubles amplitudes (SOPPA(CCSD)), Møller–Plesset perturbation theory in second (MP2), third (MP3) and fourth order (MP4), the coupled cluster method (CCSD) and finally the multiconfigurational self-consistent field method (MCSCF) in the form of complete (CASSCF) and restricted active space (RASSCF) variant with several different active spaces. The results of calculations with the different methods using two large conventional basis sets are compared.

Contents

1. INTRODUCTION

The rotational g factor is the ratio of the rotational magnetic dipole moment of a molecule to its molecular rotational angular momentum [1–5]. Experimentally the rotational g factor was originally determined by measuring the rotational magnetic

dipole moment of small molecules in molecular beam experiments, in which a beam of molecules is deflected by an inhomogeneous magnetic field [6]. The precision of these measurements could be greatly enhanced when magnetic resonance techniques were introduced. The molecules in the beam then undergo a spectral transition from one orientational state to another [1,7]. Due to its relation to the rotation of molecules, the rotational g factor can also be measured in microwave spectra [3]. In the presence of an applied magnetic field, the rotational magnetic dipole moment interacts with the field leading to a splitting of spectral lines in a rotational spectrum. This rotational Zeeman effect was first applied to ammonia [8] and carbon monoxide [9] and was for many years the main source for experimental values of the rotational g factor [2,4]. In addition to a rotational magnetic moment, the rotational g factor is also related to a non-adiabatic correction to the rotational reduced mass [5,10,11]. An estimate for the rotational g factor can therefore also be obtained by fitting frequency data from ro-vibrational spectra without a magnetic field to an effective Hamiltonian [12–15].

The first theoretical treatment of the rotational g factor [16] based on quantum mechanics was presented only a couple of years after the first experimental measurements [6]. Alternative derivations were published in the following years [17–19]. The first series of calculations of the rotational g factor of diatomic molecules was performed by Lipscomb and co-workers at the level of Coupled-Hartree–Fock theory [20]. One of the first correlated calculations of the rotational g factor were the two studies on H_3^+ [21] and NH_3 [22] by Jens Oddershede and co-workers at the level of the second order polarization propagator approximation (SOPPA), a method which was mainly developed by Jens Oddershede and his co-workers [23–25]. In the following years other correlated calculations were presented using methods such as SOPPA [5,26], a coupled cluster polarization propagator approximation (CCSDPPA) [14,27], the second order polarization propagator approximation using coupled cluster singles and doubles amplitudes – SOPPA(CCSD) [28], Møller–Plesset perturbation theory to second order (MP2) [29,30], to third order (MP3) [30], a linearized coupled cluster doubles method (L-CCD) [30], multiconfigurational self-consistent field linear response theory (MCSCF) [5,15,31–36], the full configuration interaction CI method (full CI) [37,38] and finally density functional theory (DFT) [36,39].

However, until today no systematic comparison of methods based on Møller–Plesset perturbation (MP) and Coupled Cluster theory, the SOPPA or multi-configurational linear response theory has been presented. The present study is a first attempt to remedy this situation. Calculations of the rotational g factor of HF, H_2O, NH_3 and CH_4 were carried out at the level of Hartree–Fock (SCF) and multiconfigurational Hartree–Fock (MCSCF) linear response theory, the SOPPA and SOPPA(CCSD) [40], Møller–Plesset perturbation theory to second (MP2), third (MP3) and fourth order without the triples contributions (MP4SDQ) and finally coupled cluster singles and doubles theory. The same basis sets and geometries were employed in all calculations for a given molecule. The results obtained with the different methods are therefore for the first time direct comparable and consistent conclusions about the performance of the different methods can be made.

2. THEORY

2.1. The rotational g factor

Closed shell molecules in the rotational ground state have no net magnetic dipole moment $\vec{m}$ apart from nuclear magnetic dipole moments. However, when molecules rotate with angular momentum $\vec{J}$, they acquire a net rotational magnetic moment

$$\vec{m} = \frac{\mu_N}{\hbar} \mathbf{g} \vec{J} \tag{1}$$

in which $\mathbf{g}$ is the rotational g tensor, the trace of which is the rotational g factor, g.

In the derivation of quantum mechanical expressions for the rotational g tensor the nuclei are usually treated as classical rotating point charges, $Z_K e$, located at $\vec{R}_K$. Their contribution to the g tensor is then given as

$$g_{\alpha\beta}^{\text{nuc}} = \frac{m_{\text{p}}}{I_\beta} \sum_K Z_K((\vec{R}_K - \vec{R}_{\text{CM}})^2 \delta_{\alpha\beta} - (R_{K,\alpha} - R_{\text{CM},\alpha})(R_{K,\beta} - R_{\text{CM},\beta})) \tag{2}$$

Here $\mathbf{I}$ denotes the moment of inertia tensor defined with nuclear masses; $\vec{R}_{\text{CM}}$ is the position vector of the center of nuclear mass. The electrons, with position vectors $\vec{r}_i$, have to be treated quantum mechanically which implies that their contribution is obtained as expectation value of the corresponding electronic operator over the ground state wavefunction $\Psi_0^{(0)}$

$$g_{\alpha\beta}^{\text{el,rigid}} = \\ -\frac{m_{\text{p}}}{I_\beta} \left\langle \Psi_0^{(0)} \left| \sum_i ((\hat{\vec{r}}_i - \vec{R}_{\text{CM}})^2 \delta_{\alpha\beta} - (\hat{r}_{i,\alpha} - R_{\text{CM},\alpha})(\hat{r}_{i,\beta} - R_{\text{CM},\beta})) \right| \Psi_0^{(0)} \right\rangle \tag{3}$$

This is, however, only the contribution of a rigidly rotating distribution of electrons and predictions of the g factor based on this expression [41,42] do not agree with the experiment [42]. It is therefore necessary to take into account that the motion of the electrons is perturbed by the rotation of the molecule [16,17,42], i.e., electronic motion and molecular rotation couple through $\sum_i \vec{l}_i(\vec{R}_{\text{CM}}) \cdot \vec{J}$ which signifies a breakdown of the Born–Oppenheimer approximation. Treating this perturbation to first order one obtains two additional terms which combined with the rigid electron density distribution contribution in equation (4) gives a total electronic contribution to the rotational g tensor

$$
\begin{aligned}
g_{\alpha\beta}^{\text{el}} = \frac{m_{\text{p}}}{m_{\text{e}} I_{\beta}} \sum_{n \neq 0} & \left(\frac{\left\langle \Psi_0^{(0)} \left| \sum_i \hat{l}_{i,\alpha}(\vec{R}_{\text{o}}) \right| \Psi_n^{(0)} \right\rangle \left\langle \Psi_n^{(0)} \left| \sum_i \hat{l}_{i,\beta}(\vec{R}_{\text{CM}}) \right| \Psi_0^{(0)} \right\rangle}{E_0^{(0)} - E_n^{(0)}} \right. \\
& \left. + \frac{\left\langle \Psi_0^{(0)} \left| \sum_i \hat{l}_{i,\beta}(\vec{R}_{\text{CM}}) \right| \Psi_n^{(0)} \right\rangle \left\langle \Psi_n^{(0)} \left| \sum_i \hat{l}_{i,\alpha}(\vec{R}_{\text{o}}) \right| \Psi_0^{(0)} \right\rangle}{E_0^{(0)} - E_n^{(0)}} \right) \\
& - \frac{m_{\text{p}}}{I_{\beta}} \left\langle \Psi_0^{(0)} \left| \sum_i \left((\vec{R}_{\text{o}} - \vec{R}_{\text{CM}}) \cdot (\hat{\vec{r}}_i - \vec{R}_{\text{CM}}) \delta_{\alpha\beta} \right. \right. \right. \\
& \left. \left. \left. - (\hat{r}_{i,\alpha} - R_{\text{CM},\alpha})(R_{\text{o},\beta} - R_{\text{CM},\beta}) \right) \right| \Psi_0^{(0)} \right\rangle
\end{aligned}
\tag{4}
$$

Similar to other magnetic properties, such as the magnetizability and the nuclear magnetic shielding [43], the rotational g tensor has a 'paramagnetic' contribution, which arises from non-adiabatic coupling of excited states $|\Psi_n^{(0)}\rangle$ with energy $E_n^{(0)}$ with the ground state $|\Psi_0^{(0)}\rangle$ with energy $E_0^{(0)}$, and a 'diamagnetic' contribution which is a ground state average value. In analogy to the other magnetic properties [44,45] the diamagnetic contribution can be rewritten in a sum-over-excited-states form using a resolution of the identity $1 = \sum_n |\Psi_n^{(0)}\rangle\langle\Psi_n^{(0)}|$, and using the hypervirial relation $\langle \Psi_n^{(0)} | \sum_i \hat{\vec{p}}_i | \Psi_0^{(0)} \rangle = \frac{m_{\text{e}}}{i\hbar}(E_0^{(0)} - E_n^{(0)})\langle \Psi_n^{(0)} | \sum_i \hat{\vec{r}}_i | \Psi_0^{(0)} \rangle$ [5]. Combined with the paramagnetic contribution one obtains a slightly simpler expression for the electronic contribution to the rotational g tensor [18]

$$
\begin{aligned}
g_{\alpha\beta}^{\text{el}} = \frac{m_{\text{p}}}{m_{\text{e}} I_{\beta}} \sum_{n \neq 0} & \left(\frac{\left\langle \Psi_0^{(0)} \left| \sum_i \hat{l}_{i,\alpha}(\vec{R}_{\text{CM}}) \right| \Psi_n^{(0)} \right\rangle \left\langle \Psi_n^{(0)} \left| \sum_i \hat{l}_{i,\beta}(\vec{R}_{\text{CM}}) \right| \Psi_0^{(0)} \right\rangle}{E_0^{(0)} - E_n^{(0)}} \right. \\
& \left. + \frac{\left\langle \Psi_0^{(0)} \left| \sum_i \hat{l}_{i,\beta}(\vec{R}_{\text{CM}}) \right| \Psi_n^{(0)} \right\rangle \left\langle \Psi_n^{(0)} \left| \sum_i \hat{l}_{i,\alpha}(\vec{R}_{\text{CM}}) \right| \Psi_0^{(0)} \right\rangle}{E_0^{(0)} - E_n^{(0)}} \right)
\end{aligned}
\tag{5}
$$

From this expression one can see now that the electronic contribution $g_{\alpha\beta}^{\text{el}}$ is related to the paramagnetic contribution $\xi_{\alpha\beta}^{\text{p}}$ to magnetizability evaluated with the center of mass as gauge origin:

$$
g_{\alpha\beta}^{\text{el}} = -\frac{4 m_{\text{p}} m_{\text{e}}}{e^2 I_{\beta}} \xi_{\alpha\beta}^{\text{p}}(\vec{R}_{\text{CM}})
\tag{6}
$$

In practical applications of the expressions for the rotational g tensor, equations (2), (4), (5), or (6), the nuclear masses in the moment of inertia tensor $\mathbf{I}$ are generally approximated with atomic masses and $\vec{R}_{\text{CM}}$ is approximated with the center of atomic masses. This introduces a correction term to the moment of inertia tensor which is actually closely related to the nuclear contribution to the rotational g tensor [3,11,38]. Going to second order of perturbation theory for the electronic contributions one would obtain a further correction term to the moment of inertia tensor which is similar to the electronic contribution to the rotational g tensor [3,4].

All together one would obtain an effective moment of inertia tensor which includes the rotational *g* tensor again. This correction is normally ignored for polyatomic molecules, but allows to estimate the rotational *g* factor of diatomic molecules from field-free rotation–vibration spectra [5,10,11].

In the presence of an external magnetic flux density $\vec{B}$ the rotational magnetic moment $\vec{m}$, equation (1), causes a splitting of the energy levels

$$\Delta E = -\vec{m} \cdot \vec{B} = -\frac{\mu_N}{\hbar} \vec{B} \mathbf{g} \vec{J} \tag{7}$$

The electronic contribution to the rotational *g* tensor can therefore also be defined as second derivative of the electronic energy

$$g_{\alpha\beta}^{\text{el}} = -\frac{\hbar}{\mu_N} \frac{\partial^2 E(\vec{B}, \vec{J})}{\partial B_\alpha \partial J_\beta} \Big|_{\vec{B}, \vec{J}=0} \tag{8}$$

with respect to the rotational angular momentum and the magnetic flux density.

2.2. *Ab initio* methods

The nuclear contribution, equation (2) to the rotational *g* tensor is trivially calculated from the nuclear coordinates and atomic masses. The calculation of the electronic contribution, equation (5), requires in principle the calculation of all excited states $|\Psi_n^{(0)}\rangle$ of appropriate symmetry and the corresponding magnetic dipole transition moments $\langle\Psi_0^{(0)}| \sum_i \hat{l}_{i,\beta}(\vec{R}_{\text{CM}})|\Psi_n^{(0)}\rangle$. Recalling the spectral representation of the polarization propagator or linear response function [25,46]

$$\langle\langle \hat{P}; \hat{Q} \rangle\rangle_\omega = \sum_{n \neq 0} \frac{\langle\Psi_0^{(0)}|\hat{P}|\Psi_n^{(0)}\rangle\langle\Psi_n^{(0)}|\hat{Q}|\Psi_0^{(0)}\rangle}{\hbar\omega - (E_0 - E_n)} \tag{9}$$

$$- \sum_{n \neq 0} \frac{\langle\Psi_0^{(0)}|\hat{Q}|\Psi_n^{(0)}\rangle\langle\Psi_n^{(0)}|\hat{P}|\Psi_0^{(0)}\rangle}{\hbar\omega + (E_0 - E_n)} \tag{10}$$

it can be seen that the electronic contribution to the rotational *g* tensor can also be expressed as a polarization propagator

$$g_{\alpha\beta}^{\text{el}} = \frac{m_{\text{p}} m_{\text{e}}}{I_\beta} \left\langle\left\langle \sum_i \hat{l}_{i,\alpha}(\vec{R}_{\text{CM}}); \sum_i \hat{l}_{i,\beta}(\vec{R}_{\text{CM}}) \right\rangle\right\rangle_{\omega=0} \tag{11}$$

Polarization propagators or linear response functions are normally not calculated from their spectral representation but from an alternative matrix representation [25,46–48] which avoids the explicit calculation of the excited states.

$$\langle\langle \hat{P}; \hat{Q} \rangle\rangle_\omega = \langle \Psi_0^{(0)} | [\hat{P}, \tilde{\mathbf{h}}] | \Psi_0^{(0)} \rangle \langle \Psi_0^{(0)} | [\mathbf{h}^\dagger, \hbar\omega\tilde{\mathbf{h}} - [\hat{H}^{(0)}, \tilde{\mathbf{h}}]] | \Psi_0^{(0)} \rangle^{-1}$$

$$\times \langle \Psi_0^{(0)} | [\mathbf{h}^\dagger, \hat{Q}] | \Psi_0^{(0)} \rangle. \tag{12}$$

Here $\hat{H}^{(0)}$ is the unperturbed Hamiltonian of the system and $\{h_n\}$ denotes a complete set of excitation and de-excitation operators, arranged as column vector $\mathbf{h}$ or as row vector $\tilde{\mathbf{h}}$. Completeness of the set of operators $\{h_n\}$ means that all possible excited states $|\Psi_n^{(0)}\rangle$ of the system must be generated by operating on $|\Psi_0^{(0)}\rangle$, i.e., $h_n|\Psi_0^{(0)}\rangle = |\Psi_n^{(0)}\rangle$. Various polarization propagator methods are obtained by approximating the reference state $|\Psi_0^{(0)}\rangle$ and the complete set of operators $\{h_n\}$ [25,46,48].

In the self-consistent field linear response method [25,46,48] also known as random phase approximation (RPA) [49] or first order polarization propagator approximation [25,46], which is equivalent to the coupled Hartree–Fock theory [50], the reference state is approximated by the Hartree–Fock self-consistent field wavefunction $|\Phi_{SCF}\rangle$ and the set of operators $\{h_n\}$ consists of single excitation and de-excitation operators with respect to $|\Phi_{SCF}\rangle$, i.e., the so-called orbital rotation operators [51].

In SOPPA [24] a Møller–Plesset perturbation theory expansion of the wave function [52] is employed

$$|\Psi_0^{(0)}\rangle \approx N\big(|\Phi_{SCF}\rangle + |\Phi^{(1)}\rangle + |\Phi^{(2)}\rangle\cdots\big)$$

$$= N\left(|\Phi_{SCF}\rangle + \frac{1}{4}\sum_{\substack{ai\\bj}} {}^{(1)}\kappa_{ij}^{ab}|\Phi_{ij}^{ab}\rangle + \sum_{ai} {}^{(2)}\kappa_i^a|\Phi_i^a\rangle + \cdots\right) \tag{13}$$

and double excitation and de-excitation operators are added to the set of operators $\{h_n\}$. In equation (13) $|\Phi_i^a\rangle$ and $|\Phi_{ij}^{ab}\rangle$ are Slater determinants obtained by replacing the occupied orbitals i and j in $|\Phi_{SCF}\rangle$ by the virtual orbitals a and b, ${}^{(1)}\kappa_{ij}^{ab}$, ${}^{(2)}\kappa_i^a$, are the so-called Møller–Plesset correlation coefficients and N is a normalization constant. All matrix elements involving single (de-)excitation operators in equation (12) are then evaluated to second order in the fluctuation potential, which is the difference between the instantaneous interaction of the electrons and the averaged interaction as used in the Hartree–Fock approximation. Matrix elements with single and double (de-)excitation operators are evaluated to first order and pure double (de-)excitation matrix elements only to zeroth order. With this definition of SOPPA only the single excited terms in the second order correction to the wavefunction are needed. In the so-called SOPPA(CCSD) method [40], SOPPA with coupled cluster singles and doubles amplitudes, the Møller–Plesset correlation coefficients ${}^{(1)}\kappa_{ij}^{ab}$ and ${}^{(2)}\kappa_i^a$ are replaced in all SOPPA matrix elements by the corresponding coupled cluster singles and doubles amplitudes τ_{ij}^{ab} and τ_i^a. SOPPA(CCSD) is a generalization of the earlier CCSDPPA method [53], where only some of the Møller–Plesset correlation coefficients were replaced by coupled cluster amplitudes.

In the MCSCF linear response theory [48], also called multiconfigurational RPA [54], the reference state is approximated by a MCSCF wavefunction

$$|\Psi_0^{(0)}\rangle \approx |\Phi_{\text{MCSCF}}\rangle = \sum_i |\Phi_i\rangle C_{i0} \tag{14}$$

where $\{|\Phi_i\rangle\}$ are configuration state functions. The set of operators $\{h_n\}$ contains in addition to the non-redundant single excitation and de-excitation operators also state transfer operators $\{\mathbf{R}^\dagger, \mathbf{R}\}$, which are defined as

$$R_n^\dagger = |\Phi_n\rangle\langle\Phi_{\text{MCSCF}}| \tag{15}$$

where $|\Phi_n\rangle = \sum_i |\Phi_i\rangle C_{in}$ are the orthogonal complement states of the MCSCF state.

Based on equation (8) one can obtain alternative methods for the calculation of the electronic contribution to the *g* tensor by differentiating expressions for the electronic energy in the presence of an external magnetic flux density $\vec{B}$ and the coupling with the rotational motion $\sum_i \vec{l}_i(\vec{R}_{\text{CM}})\cdot\vec{J}$. Using equation (6) the rotational *g* tensor can also be obtained from the paramagnetic contribution of the magnetizability, which is the second derivative of the electronic energy with respect to an external magnetic flux density $\vec{B}$. This approach can be applied to any method for which an energy is defined. The calculation of magnetic properties as analytical derivatives of the MP2, MP3, MP4SDQ, and CCSD energies is well described in the literature [29,30,55,56] and is therefore not repeated here.

3. COMPUTATIONAL DETAILS

The calculations have been done using a local version of the Dalton 1.2 program package [57] and the ACESII program package [58,59].

3.1. Basis set and geometry

It is well known that the usage of perturbation dependent basis functions leads to a faster convergence towards the basis set limit in the calculation of magnetic properties [60,61]. However, not all the methods employed in this study have been modified for the use of perturbation dependent basis. Therefore, standard basis sets are used in this study. This implies that larger basis sets are required than would be the case for perturbation dependent basis sets, but this poses no problem for molecules of this size. The first basis set employed here is a modification of the $sp_{tt}d_{td}f_2/sp_td$ basis set used in previous studies of the magnetizability and nuclear magnetic shielding of small molecules [45]. This basis set was originally based on the 11s7p/7s basis set of van Duijneveldt [62] and the 3d2f/3p2d polarization basis set of Dunning [63] for non-hydrogen/hydrogen atoms. The same polarization functions are also used in the correlation consistent cc-pVQZ basis set. The $sp_{tt}d_{td}f_2$ basis

Table 1. vD+D basis set: exponents of the additional polarization functions included in the basis set

Atom	s-type	p-type	d-type	f-type
H	–	0.102	–	–
C	0.028099	0.030144	0.080; 0.0281	0.187
N	0.039255	0.0445396	0.116; 0.0401	0.245
O	0.0521357	0.0536415	0.152; 0.0518	0.324
F	0.0672366	0.0632794	0.199; 0.0676	0.460

sets had been optimized for the calculation of nuclear magnetic shielding constants and magnetizabilities and were further optimized for the rotational g tensor in this study. Starting from the sp_{tt}/s-subset of the $sp_{tt}d_{td}f_2/sp_td$ basis sets [45] the two additional tight p-type functions for the non-hydrogen atoms and the contraction of the s-type functions is removed. The s-functions with the three largest exponents for hydrogen and the six s-functions and three p-functions with the largest exponents for the non-hydrogen atoms were contracted with the SCF atomic orbital coefficients of van Duijneveldt [62]. Additional diffuse and polarization functions were then added as given in Table 1. This basis set is identified by the label 'vD+D' in the following. In total it consists of 7s-, 4p-, and 2d-type Gaussian functions contracted to 5s-, 4p-, and 2d-type Gaussian functions for hydrogen and 13s-, 8p-, 5d-, and 3f-type Gaussian functions contracted to 8s-, 6p-, 5d-, and 3f-type Gaussian functions for non-hydrogen atoms. It is expected to be well suited for the calculation of rotational g factors.

In addition to this, basis set calculations were also carried out with the daug-cc-pVTZ correlation consistent basis set by Dunning and co-workers [63,64]. This basis set consists of 7s-, 4p-, and 3d-type Gaussian functions contracted to 5s-, 4p-, and 3d-type Gaussian functions for hydrogen and 12s-, 7p-, 4d-, and 3f-type Gaussian functions contracted to 6s-, 5p-, 4d-, and 3f-type Gaussian functions for non-hydrogen atoms. The daug-cc-pVTZ basis set has thus one set of d-type functions more for the hydrogen atoms but is considerably smaller for the non-hydrogen atoms.

The internuclear distances and bond angles used in this study are the usual experimental equilibrium geometries. The details are given in Table 2.

Table 2. Experimental equilibrium geometries used in the calculations

Molecule	R_{H-X} (pm)	$\angle$ H–X–H	References
HF	91.68	–	[65]
H_2O	95.72	104.52°	[66]
NH_3	101.24	106.671°	[66]
CH_4	108.50	109.471°	[67]

3.2. Choice of the active space

The selection of configuration state functions to be included in MCSCF calculations is not a trivial task. Two approaches which can reduce the complexity of the problem are the complete active space self-consistent-field (CASSCF) [68] and the restricted active space self-consistent-field (RASSCF) [69] approach. Both are implemented in the Dalton program package [57] and are used in this study. Throughout the paper a CASSCF calculation is denoted by $^{inactive}CAS^{active}$ and a RASSCF calculation by $^{inactive}_{RAS1}RAS^{RAS2}_{RAS3}$. For the active spaces of HF, H_2O, and CH_4 a notation $(n_{A1}\,n_{B2}\,n_{B1}\,n_{A2})$ is used [70], where n_Γ is the number of orbitals in the irreducible representation Γ of the C_{2v} point group, and $(n_{A'}\,n_{A''})$ for NH_3 in terms of the irreducible representations of the C_s point group.

Three different types of CAS calculations and one RAS calculation were carried out for all molecules, where the 1s orbital on C, N, O, or F was always kept inactive (Table 3).

1. A valence CAS, which includes the molecular orbitals created from the 2s and 2p orbitals on C, N, O, or F and the 1s orbitals on the hydrogen atoms. Naturally the size of these valence CAS, (3110) for HF, (3210) for H_2O, (52) for NH_3 and (4220) for CH_4, increases from HF to CH_4 and thus the amount of correlation included in the respective calculations.
2. A CAS, (4220) or (62), which consists of the valence orbitals which would be occupied in a Hartree–Fock calculation, (2110) or (31), and exactly one unoccupied, so-called correlating, orbital for each of the occupied ones included in the active space. In CH_4 this is the same as the valence CAS.
3. A CAS, (6331) or (94), which was chosen according to the MP2 natural orbital occupation numbers [71]. They turn out to be slightly larger than a CAS which includes two correlating orbitals for each HF occupied orbital, (6330) or (93).

Table 3. Active spaces and corresponding number of determinants used in the MCSCF calculations. The notation of the spaces is $^{inactive}CAS^{active}$ or $^{inactive}_{RAS1}RAS^{RAS2}_{RAS3}$. SD indicates that single and double excitations out of RAS2 into RAS3 were allowed

Molecule	Active space	Number of determinants
HF, H_2O, CH_4	$^{1000}CAS^{3110}$	11
	$^{1000}CAS^{3210}$	65
	$^{1000}CAS^{4220}$	1284
	$^{1000}CAS^{6331}$	128,283
	$^{1000}RAS^{6331}_{3321}SD$	3,710,129
NH_3	$^{10}CAS^{52}$	625
	$^{10}CAS^{62}$	2500
	$^{10}CAS^{94}$	256,033
	$^{10}RAS^{94}_{33}SD$	3,792,373

The symmetry of the additional unoccupied orbital indicates that d-type orbitals are included in these active spaces.

4. A RAS, with the largest CAS, (6331) or (94), as RAS2 and single and double excitations to a RAS3, (3321) or (33).

4. RESULTS AND DISCUSSION

4.1. Basis sets

Before one can compare different correlated methods and their results for the rotational g tensor, one should discuss the quality of the employed basis set. Therefore, I have performed also calculations with rotational London orbitals for all the molecules at the SCF and the ^{1000}CAS^{4220}/^{10}CAS^{62} level of theory and compare them with the respective calculations with conventional basis sets in Tables 4–8.

Table 4. HF: the rotational g factor calculated with different *ab initio* methods and two basis sets. The nuclear contribution to the rotational g factor is 0.9731

| | g | | |
| | vD+D[a] | daug-cc-pVTZ | |
Method	99 functions	94 functions	Δ (%)
SCF London[b]	0.7624	0.7644	0.26
SCF	0.7632	0.7664	0.42
SOPPA	0.7479	0.7501	0.29
SOPPA(CCSD)	0.7465	0.7493	0.37
MP2	0.7628	0.7668	0.53
MP3	0.7443	0.7484	0.54
MP4SDQ	0.7433	0.7472	0.52
CCSD	0.7410	0.7450	0.53
^{1000}CAS^{3110}	0.7155	0.7189	0.47
^{1000}CAS^{4220} London[b]	0.7630	0.7662	0.41
^{1000}CAS^{4220}	0.7621	0.7654	0.43
^{1000}CAS^{6331}	0.7594	0.7626	0.42
^{1000}RAS$^{6331}_{3321}$SD	0.7521	0.7552	0.41
Experiment[c]	0.75449		
Experiment[d]	0.7523		
Experiment[e]	0.7538		

[a] Described in Section 3.1.
[b] Using perturbation dependent atomic orbitals (rotational London orbitals [61]) as basis functions.
[c] Extrapolated to a equilibrium geometry from the measured values in the $v=0$ and $v=1$ vibrational states [72].
[d] Experimental value for the $v=0$ state 0.741599 [72] minus a zero-point-vibrational correction -0.0107 calculated with a ^{1000}CAS^{6331} wavefunction [35].
[e] Experimental value for the $v=0$ state 0.741599 [72] minus a zero-point-vibrational correction -0.0122 calculated with a ^{1000}RAS$^{4220}_{6332}$ wavefunction [34].

Table 5. H_2O: the rotational g tensor calculated with different *ab initio* methods and two basis sets. The nuclear contributions to the rotational g factor are $g_{ip}^{nuc} = 0.9440$,[a] $g_{oop}^{nuc} = 0.9802$[a] and $g_{\parallel}^{nuc} = 0.9995$

Method	vD+D[b] 126 functions			daug-cc-pVTZ 126 functions		
	g_{ip}	g_{oop}	$g_{\parallel}$	g_{ip}	g_{oop}	$g_{\parallel}$
SCF London[c]	0.6821	0.6639	0.7346	0.6823	0.6639	0.7345
SCF	0.6833	0.6644	0.7353	0.6900	0.6670	0.7359
SOPPA	0.6689	0.6546	0.7295	0.6744	0.6559	0.7290
SOPPA(CCSD)	0.6667	0.6506	0.7252	0.6727	0.6524	0.7252
MP2	0.6821	0.6714	0.7555	0.6894	0.6746	0.7568
MP3	0.6649	0.6498	0.7310	0.6724	0.6527	0.7323
MP4SDQ	0.6603	0.6448	0.7274	0.6675	0.6479	0.7286
CCSD	0.6585	0.6430	0.7246	0.6656	0.6457	0.7254
$^{1000}CAS^{3210}$	0.6343	0.6298	0.7011	0.6408	0.6325	0.7017
$^{1000}CAS^{4220}$	0.6799	0.6526	0.7304	0.6850	0.6531	0.7279
London[c]						
$^{1000}CAS^{4220}$	0.6804	0.6526	0.7315	0.6869	0.6553	0.7321
$^{1000}CAS^{6331}$	0.6768	0.6589	0.7349	0.6835	0.6618	0.7357
$^{1000}RAS^{6331}_{3321}SD$	0.6664	0.6504	0.7291	0.6728	0.6533	0.7300
Experiment[d]	0.6920	0.6605	0.7335			
Experiment[e]	0.6902	0.6542	0.7279			
Experiment[f]	0.6964	0.6584	0.7348			

[a] The subscript *ip* stands for *in-plane* and *oop* for *out-of-plane*.
[b] Described in Section 3.1.
[c] Using perturbation dependent atomic orbitals (rotational London orbitals [61]) as basis functions.
[d] Experimental values for the $v=0$ state $g_{ip}=0.6650\pm0.002$, $g_{oop}=0.6465\pm0.002$ and $g_{\parallel}=0.7145\pm0.002$ [73] minus a ZPVC $\Delta g_{ip}=-0.0270$, $\Delta g_{oop}=-0.0140$ and $\Delta g_{\parallel}=-0.0190$ calculated with a $^{1000}RAS^{4220}_{6332}$ wavefunction [33].
[e] Experimental values (see footnote d) minus a ZPVC $\Delta g_{ip}=-0.0252$, $\Delta g_{oop}=-0.0077$ and $\Delta g_{\parallel}=-0.0134$ calculated with a $^{1000}CAS^{6331}$ wavefunction [35].
[f] Experimental values (see footnote d) minus a ZPVC $\Delta g_{ip}=-0.0314$, $\Delta g_{oop}=-0.0119$ and $\Delta g_{\parallel}=-0.0203$ calculated with a $^{1000}RAS^{4220}_{4221}$ wavefunction [36].

The differences between the results from the vD+D and daug-cc-pVTZ basis sets are smaller in rotational London orbital calculations than in conventional calculations, as one might expect [61]. Nevertheless, the differences between the vD+D and daug-cc-pVTZ results are not larger than 0.5% for all methods used here even without the usage of rotational London orbitals. Furthermore, the differences between the rotational London orbital results and conventional results for the vD+D basis set, 0.2% for CH_4 and 0.1% otherwise, are smaller than for the daug-cc-pVTZ basis set and often smaller than the differences between rotational London orbital results from the two basis sets.

I conclude therefore that the vD+D basis is closer to the basis set limit than the daug-cc-pVTZ basis set and that no important improvement could have been obtained by using rotational London orbitals in all calculations.

Table 6. H_2O: the rotational g factor calculated with different *ab initio* methods and two basis sets

Method	vD + D[a] 126 functions	daug-cc-pVTZ 126 functions	Δ (%)
SCF London[b]	0.6935	0.6936	0.01
SCF	0.6944	0.6976	0.47
SOPPA	0.6843	0.6864	0.31
SOPPA(CCSD)	0.6808	0.6835	0.39
MP2	0.7030	0.7069	0.56
MP3	0.6819	0.6858	0.56
MP4SDQ	0.6775	0.6813	0.56
CCSD	0.6753	0.6789	0.53
$^{1000}CAS^{3210}$	0.6551	0.6584	0.50
$^{1000}CAS^{4220}$	0.6876	0.6886	0.15
London[b] $^{1000}CAS^{4220}$	0.6882	0.6914	0.47
$^{1000}CAS^{6331}$	0.6902	0.6937	0.50
$^{1000}RAS^{6331}_{3321}SD$	0.6820	0.6854	0.50

[a] Described in Section 3.1.
[b] Using perturbation dependent atomic orbitals (rotational London orbitals [61]) as basis functions.

Another way to judge the quality of the basis sets employed here is to compare with the results of previous calculations. Cybulski and Bishop [29,30] have carried out SCF and correlated calculations of the rotational g tensor of the same molecules with a conventional basis set of comparable size. For HF their basis set is clearly larger than ours and their SCF result, 0.7624, is identical to our London orbital result with the vD + D basis set and very close to the conventional vD + D result. The same holds also at the MP2 level, where $g = 0.7619$. For the other three molecules they used a basis set which is larger in the s- and p-functions part but includes a smaller number of polarization functions than my vD + D basis set. Their SCF results (H_2O: $g_{ip} = 0.6830$, $g_{oop} = 0.6640$, $g_{\parallel} = 0.7355$; NH_3: $g_{\perp} = 0.5805$, $g_{\parallel} = 0.5061$ and CH_4: 0.3019) are still close to our conventional vD + D SCF results, but they are no longer identical to the London orbitals results. Furthermore, larger differences are also observed between the results at the MP2 level of theory (H_2O: $g_{ip} = 0.6822$, $g_{oop} = 0.6670$, $g_{\parallel} = 0.7453$; NH_3: $g_{\perp} = 0.5921$, $g_{\parallel} = 0.5224$ and CH_4: 0.3338) which must be a consequence of the smaller number of polarization functions in the basis set of Cybulski and Bishop.

Finally, I can compare my SCF and $^{1000}CAS^{6331}$ results with corresponding rotational London orbital calculations by Ruud and co-workers [32–36,61]. My SCF results for HF using the vD + D basis set and conventional or rotational London orbitals are almost identical to a rotational London orbital result 0.7627 using the daug-cc-pVQZ basis set [34,61] or a result 0.7626 obtained with a large ANO basis set [34,35]. Similarly the $^{1000}CAS^{4220}$ and $^{1000}CAS^{6331}$ results for HF

Table 7. NH$_3$: the rotational *g* tensor calculated with different *ab initio* methods and two basis sets. The nuclear contributions to the rotational *g* factor are $g_\perp^{nuc} = 0.9806$ and $g_\parallel^{nuc} = 0.9995$

| Method | vD+D[a] 153 functions | | | daug-cc-pVTZ 158 functions | | | Δ (%) |
	$g_\perp$	$g_\parallel$	g	$g_\perp$	$g_\parallel$	g	g
SCF London[b]	0.5798	0.5060	0.5552	0.5790	0.5059	0.5546	−0.10
SCF	0.5807	0.5065	0.5560	0.5832	0.5073	0.5579	0.34
SOPPA	0.5794	0.5097	0.5562	0.5803	0.5087	0.5564	0.05
SOPPA (CCSD)	0.5729	0.5024	0.5494	0.5743	0.5022	0.5503	0.17
MP2	0.6048	0.5395	0.5830	0.6070	0.5402	0.5848	0.30
MP3	0.5834	0.5157	0.5608	0.5854	0.5162	0.5623	0.27
MP4SDQ	0.5745	0.5064	0.5518	0.5766	0.5070	0.5534	0.29
CCSD	0.5723	0.5055	0.5501	0.5741	0.5059	0.5514	0.24
^{10}CAS^{52}	0.5494	0.4812	0.5266	0.5520	0.4822	0.5287	0.39
^{10}CAS^{62} London[b]	0.5615	0.4856	0.5362	0.5625	0.4857	0.5369	0.14
^{10}CAS^{62}	0.5624	0.4862	0.5370	0.5650	0.4871	0.5391	0.38
^{10}CAS^{94}	0.5807	0.5128	0.5581	0.5835	0.5140	0.5603	0.40
^{10}RAS$_{33}^{94}$SD	0.5754	0.5068	0.5525	0.5783	0.5082	0.5549	0.43
Experiment[c]	0.5789	0.5086					

[a] Described in Section 3.1.
[b] Using perturbation dependent atomic orbitals (rotational London orbitals [61]) as basis functions.
[c] Experimental values for the $v=0^\pm$ state $g_\perp = 0.5654 \pm 0.0007$ and $g_\parallel = 0.5024 \pm 0.0005$ [74] minus a zero-point-vibrational correction $\Delta g_\perp = -0.0135$ and $\Delta g_\parallel = -0.0062$ calculated with a ^{1000}CAS^{6331} wavefunction [35].

compare excellent with the corresponding results, 0.7621 and 0.7584, obtained with a large ANO basis set [34,35]. For the other molecules the comparison with the previous calculations using large ANO basis sets of rotational London orbitals [33,35,36] shows that my rotational London orbitals results with both basis sets and the conventional vD+D basis set results at the SCF level as well as the conventional vD+D basis set results at the ^{1000}CAS^{6331} level are in good agreement with the previous results, which indicates that the vD+D basis set is indeed close to the basis set limit for this property at the SCF and correlated level.

On the other hand, I observe larger differences between my SCF rotational London orbital results for HF, H₂O and NH₃ using both basis sets and the corresponding results in another study by Ruud *et al.* [32]. Similar larger deviations are found between the ^{1000}CAS^{6331} results. This is partly due to slightly different geometries but mostly to the fact that Ruud *et al.* used a smaller basis set, aug-cc-pVTZ, than I did.

4.2. Comparison with previous correlated calculations

The results of the correlated calculations in this paper can be compared with two different sets of calculations. There are on one side the MP2, MP3 and linearized

Table 8. CH_4: the rotational g factor calculated with different *ab initio* methods and two basis sets. The nuclear contribution to the rotational g factor is 0.9995

	g		
	vD+D[a]	daug-cc-pVTZ	
Method	180 functions	190 functions	Δ (%)
SCF London[b]	0.3031	0.3044	0.41
SCF	0.3039	0.3052	0.44
SOPPA	0.3201	0.3195	-0.19
SOPPA(CCSD)	0.3136	0.3139	0.08
MP2	0.3670	0.3674	0.11
MP3	0.3488	0.3491	0.06
MP4SDQ	0.3381	0.3386	0.14
CCSD	0.3365	0.3368	0.09
$^{1000}CAS^{4220}$ London[b]	0.2777	0.2795	0.65
$^{1000}CAS^{4220}$	0.2784	0.2800	0.58
$^{1000}CAS^{6331}$	0.3285	0.3301	0.50
$^{1000}RAS^{6331}_{3321}SD$	0.3097	0.3108	0.33
Experiment[c]	0.3220		

[a] Described in Section 3.1.
[b] Using perturbation dependent atomic orbitals (rotational London orbitals [61]) as basis functions.
[c] Experimental value for the $v=0$ state 0.31338 ± 0.0004 [75] minus a zero-point-vibrational correction -0.0086 calculated with a $^{1000}CAS^{6331}$ wavefunction [35].

coupled cluster doubles calculations by Cybulski and Bishop [29,30] and on the other hand a whole series of MCSCF calculations by Ruud and co-workers [32–36]. For NH_3 and CH_4, I am only aware of previous $^{1000}CAS^{6331}$ calculations [32,35], which are in good agreement with the equivalent results presented here as discussed in Section 4.1. My $^{10}RAS^{94}_{33}SD/^{1000}RAS^{6331}_{3321}SD$ results in Tables 7 and 8 are therefore the most accurate MCSCF results for the rotational g tensor of these molecules reported so far.

In the case of HF and H_2O, I can compare my MCSCF results in Tables 4 and 5 also with the results of other large RAS calculations [33,34,36]. Åstrand *et al.* [34] have conducted an extended basis set and correlation study of the magnetic properties of HF using much larger RASSCF wavefunctions than the ones employed in this study. They found, however, that the $^{1000}CAS^{6331}$ wavefunction accounted for almost all of the correlation effects obtainable with MCSCF wavefunctions. Ruud *et al.* [33] have similarly performed a extensive investigation of the dependence of the rotational g tensor in water on the size of the spaces in a RASSCF calculation. They used a smaller RAS2 space, (4220) than is used in this study, but performed also calculations with much larger RAS3 spaces (12;884). Nevertheless, their results show that the additional correlation effects included in calculations with larger active spaces than the $^{1000}RAS^{6331}_{3321}SD$ space employed here are negligible. Their best results are therefore also in excellent agreement with the $^{1000}RAS^{6331}_{3321}SD$ results from this study (Table 5).

Mohn *et al.* [36] employed in a very recent study an even larger RAS3 space (17;11;11;9), but the results are still in good agreement with the RAS calculation of this work.

In comparison with the MP2 and MP3 results of Cybulski and Bishop [29,30], I note a non-uniform picture. In most cases they predict smaller correlation effects than observed in this study whereas in individual cases such as HF at MP2, H_2O $g_\parallel$ at MP3, H_2O g_{ip} at MP2, NH_3 $g_\parallel$ and $g_\perp$ at MP3 level their results are in good agreement with my results. I believe that the differences are due to the smaller basis sets used by Cybulski and Bishop.

4.3. Comparison of *ab initio* methods

The first observation one can make is that the correlation effects for the rotational g tensor in HF, H_2O, and NH_3 are in general small, 1.5–3.5%, and negative, i.e., correlation reduces the values of the rotational g tensor and therefore the amount of coupling between the electronic and rotational motion. Methane is an exception in that respect, because correlation increases the value of the g factor and because some methods, MPn and CCSD, predict much larger correlation corrections.

In general, the results of the perturbation theory based methods, SOPPA, SOPPA(CCSD), MPn and CCSD become smaller with increasing level of theory, whereas the results of the CASSCF/RASSCF calculations go through a maximum for the $^{1000}CAS^{4220}$ or $^{1000}CAS^{6331}$ wavefunctions depending on the molecule. What slightly varies from molecule to molecule is the relative placement of the three series SOPPA–SOPPA(CCSD), MP2–CCSD and valence CAS to RAS calculation. Here methane clearly differs from the other molecules again. Nevertheless, some general statements can be made.

The valence CAS calculations overestimate the correlation corrections dramatically and predict rotational g tensor components which are much too small for all molecules. In CH_4 it predicts even the wrong sign for the correlation correction. Similarly, MP2 is not able to reproduce the sign or size of the correlation correction. For HF and the *in-plane* component in H_2O, the MP2 contribution is too small and for all the other molecules or tensor components the MP2 contribution is much too large and has even the wrong sign.

Comparing the SOPPA and SOPPA(CCSD) results one can see that both methods predict correlation corrections which are comparable to the results obtained at the CCSD or $^{1000}RAS^{6331}_{3321}SD$ level. However, it is clear that SOPPA(CCSD) is in better agreement with these more expensive methods. The SOPPA(CCSD) results for HF, for g_{ip} and g_{oop} in H_2O are close to the respective MP3 results. In case of NH_3 and the parallel component of the g tensor of H_2O, where the correlation corrections are somewhat smaller, $\sim 1.5\%$, SOPPA(CCSD) predicts values close to the CCSD numbers.

Overall, CCSD predicts larger correlation corrections than SOPPA(CCSD), which on the other hand predicts larger corrections than the $^{1000}RAS^{6331}_{3321}SD$ calculations. The only exceptions are $g_\parallel$ in NH_3, where SOPPA(CCSD) gives a larger correction than CCSD, and $g_{ip/oop}$ in H_2O where the order of
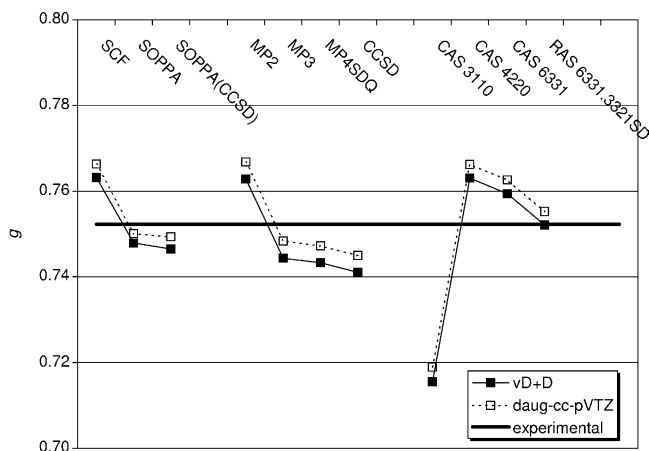
Fig. 1. HF: the rotational g factor as a function of *ab initio* methods for two basis sets.
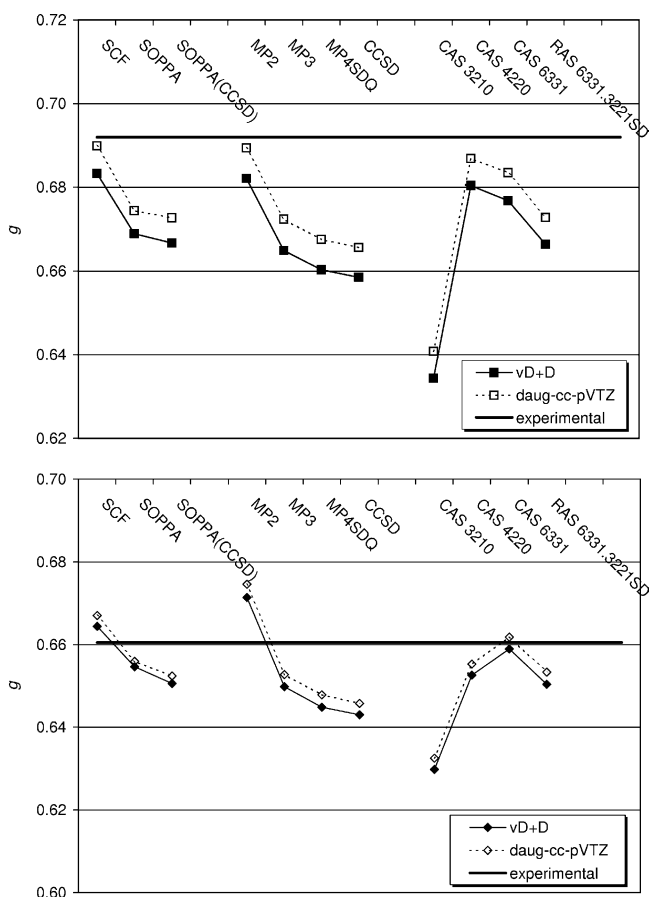
Fig. 2. H_2O: the g_{ip} (top) and g_{oop} (bottom) components of the rotational g tensor as a function of *ab initio* methods for two basis sets.
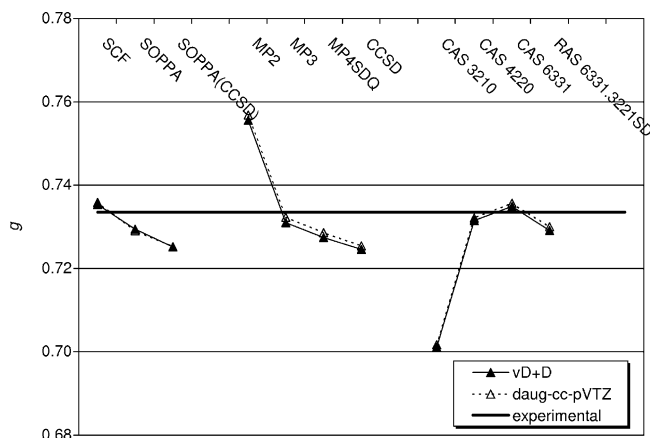
Fig. 3. H_2O: the $g_\parallel$ component of the rotational g tensor as a function of *ab initio* methods for two basis sets.

SOPPA(CCSD) and $^{1000}RAS^{6331}_{3321}SD$ is interchanged. One can therefore conclude that for the molecules studied here the results of SOPPA(CCSD) calculations are comparable to results of other state-of-the-art methods.

4.4. Comparison with experiment

Comparison with experiment is complicated by the fact that measurements can give the value of the rotational g tensor in one or several vibrational states and the rotational ground state, but not the value for a particular nuclear geometry. Since the results in this paper are calculated for a particular geometry, the alleged equilibrium geometry, it is in principle not possible to compare these results directly with the experimental values. One way to remedy this problem would be to vibrationally average the results of the various methods over appropriate nuclear vibrational wavefunctions. However, this is far beyond the scope of this paper. The other alternative is to compare with a value at a given nuclear geometry extracted or estimated from the experimental values. This is possible when the rotational g tensor was measured in more than one vibrational state [72]. From these values one can extrapolate to an equilibrium geometry. Another way is to combine the experimental vibrational state specific values with calculated vibrational corrections leading to 'empirical' equilibrium geometry values of the g tensor components. The experimental values listed in Tables 4–8 and shown in Figs 1–5 were obtained in this way from the experimental vibrational ground state values [72–75] and zero-point vibrational corrections calculated by Ruud and co-workers with CASSCF and RASSCF wavefunctions [33–36]. However, this approach becomes somewhat questionable, when the vibrational corrections are as large or even larger than the correlation corrections under investigation as it is the case for H_2O and NH_3 in this study. I will therefore not further discuss the different correlated
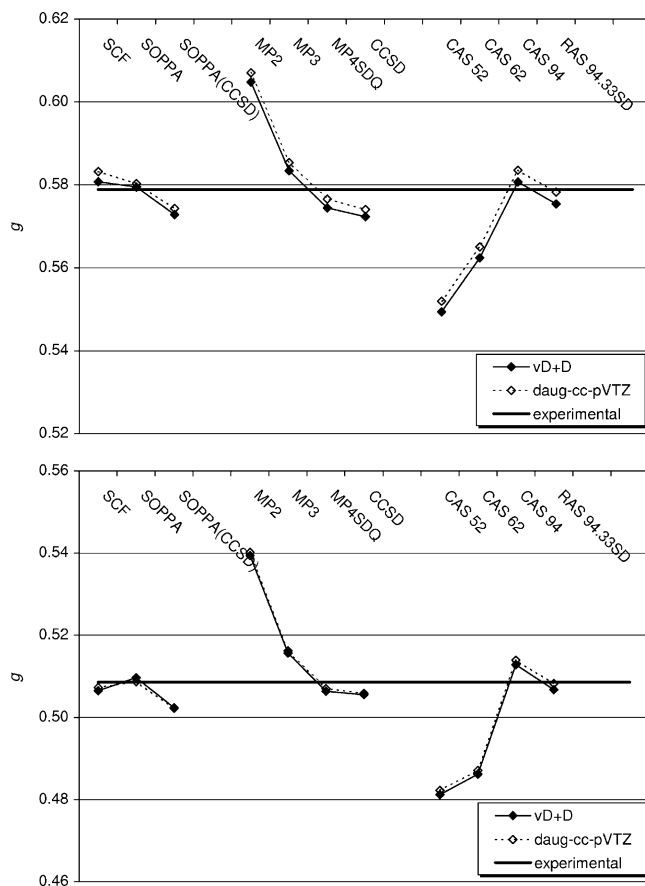
Fig. 4. NH_3: the $g_\perp$ (top) and $g_\parallel$ (bottom) components of the rotational g tensor as a function of *ab initio* methods for two basis sets.
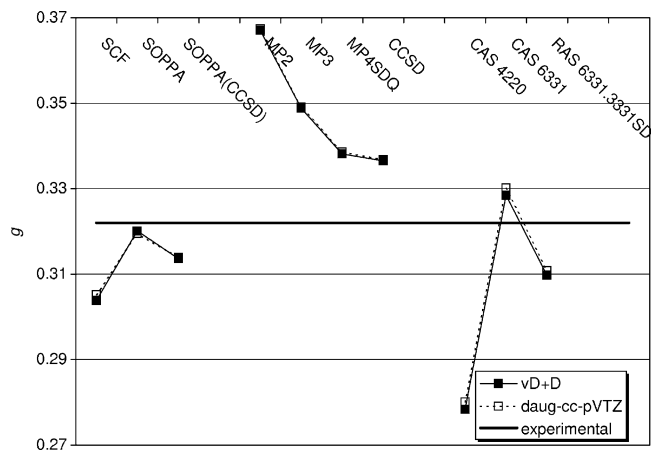
Fig. 5. CH_4: the rotational g factor as a function of *ab initio* methods for two basis sets.

results with respect to the experimental values because I believe that a complete investigation including the vibrational corrections is required in such a case [22,33–36].

5. FINAL REMARKS AND CONCLUSIONS

The components of the rotational *g* tensor of hydrogen fluoride, water, ammonia and methane have been calculated at their equilibrium geometries with different correlated *ab initio* methods and two large basis sets.

It is found that the basis sets employed are well converged even though no rotational London orbitals are used in the calculations. The correlation effects are rather small, in the range of 1.5–3.5%, and for all but methane the correlation corrections are negative.

Comparing the results of the different methods one sees that SOPPA gives a good indication of the size and sign of the correlation correction, but that SOPPA(CCSD) is always in better agreement with MPn/CCSD and the large RASSCF calculations than SOPPA. SOPPA(CCSD) gives results which are close to the results of MP3 calculations with the exception of CH$_4$. When the correlation effects are small, $\sim 1.5\%$, the SOPPA(CCSD) results are even close to the CCSD results.

On the other hand, the results of MP2 and valence CAS calculations are not useful. MP2 predicts correlation correction which are not only much too large but have also the wrong sign for most *g* tensor components studied here. In the remaining cases the correlation correction is either much too large (CH$_4$) or much too small (HF and H$_2$O g_{ip}). The valence CAS calculations similarly overestimate the correlation effects and predict in general much too small *g* tensor components. SOPPA and SOPPA(CCSD) performs thus clearly better than MP2 or valence CAS calculations for the rotational *g* tensor in the studied molecules.

The results of the three best methods employed here show for all but three cases the following ordering:

$$^{1000}\mathrm{RAS}^{6331}_{3321}\mathrm{SD} > \mathrm{SOPPA(CCSD)} > \mathrm{CCSD}$$

which implies that the SOPPA(CCSD) results can compete with the results from other state-of-the-art methods.

Finally, the results for CH$_4$ show quite a different pattern. The correlation corrections are positive and the results of MPn/CCSD calculations differ more from the results of SOPPA/SOPPA(CCSD) and the RASSCF calculations than for the other molecules. Further investigations of the correlation effects in this molecule are necessary.

the circle and contribute to this special issue on the occasion of his 60th birthday with a comparative study of calculations of the rotational g factor including NH_3.

REFERENCES

[1] N. F. Ramsey, *Molecular Beams*, Oxford University Press, London, 1969.

[2] (a) W. H. Flygare and R. C. Benson, *Mol. Phys.*, 1971, **20**, 225; (b) D. H. Sutter and W. H. Flygare, *Top. Curr. Chem.*, 1976, **63**, 89.

[3] C. H. Townes and A. L. Schawlow, *Microwave Spectroscopy*, Dover Publications, New York, 1975.

[4] W. H. Flygare, *Molecular Structure and Dynamics*, Prentice-Hall, Englewood Cliffs, 1978.

[5] J. F. Ogilvie, J. Oddershede and S. P. A. Sauer, *Adv. Chem. Phys.*, 2000, **111**, 475.

[6] F. Knauer and O. Stern, *Z. Phys.*, 1926, **39**, 780.

[7] N. J. Harrick and N. F. Ramsey, *Phys. Rev.*, 1952, **88**, 228.

[8] D. K. Coles and W. E. Good, *Phys. Rev.*, 1946, **70**, 979.

[9] J. T. Cox and W. Gordy, *Phys. Rev.*, 1956, **101**, 1298.

[10] (a) R. M. Herman and A. Asgharian, *J. Mol. Spectrosc.*, 1966, **19**, 305; (b) P. R. Bunker and R. E. Moss, *Mol. Phys.*, 1977, **33**, 417.

[11] R. M. Herman and J. F. Ogilvie, *Adv. Chem. Phys.*, 1998, **103**, 187.

[12] (a) J. F. Ogilvie, *J. Chin. Chem. Soc.,* 1992, **39**, 381; (b) J.-L. Teffo and J. F. Ogilvie, *Mol. Phys.,* 1993, **80**, 1507; (c) J. F. Ogilvie, *J. Phys. B: At. Mol. Opt. Phys.,* 1994, **27**, 47; (d) J. F. Ogilvie and S. C. Liao, *Chem. Phys. Lett.,* 1994, **226**, 281; (e) J. F. Ogilvie and S. C. Liao, *Acta Phys. Hung.,* 1994, **74**, 365; (f) J. F. Ogilvie, S. C. Liao, H. Uehara and K. Horiai, *Can. J. Phys.,* 1994, **72**, 930; (g) E. Tiemann and J. F. Ogilvie, *J. Mol. Spectrosc.,* 1994, **165**, 377; (h) J. F. Ogilvie, *J. Chem. Soc. Faraday Trans.,* 1995, **91**, 3005; (i) J. F. Ogilvie, H. Uehara and K. Horiai, *J. Chem. Soc. Faraday Trans.,* 1995, **91**, 3007; (j) J. F. Ogilvie, in *Fundamental Principles of Molecular Modeling* (eds W. Gans, A. Amman and J. C. A. Boeyens), Plenum Press, New York, 1996, pp. 41; (k) J. F. Ogilvie, *Mol. Phys.,* 1996, **88**, 1055.

[13] (a) M. Molski, *Acta Phys. Pol. A*, 1997, **92**, 1117; (b) M. Molski and J. Konarski, *Pol. J. Chem.*, 1998, **72**, 1398; (c) M. Molski, *J. Raman Spectrosc.*, 1999, **30**, 449; (d) J. F. Ogilvie and M. Molski, *Spectrochim. Acta A*, 1999, **55**, 1427; (e) M. Molski, *Chem. Phys. Lett.*, 1999, **306**, 88; (f) M. Molski, *J. Phys. Chem. A*, 1999, **103**, 5269; (g) M. Molski, *Mol. Phys.*, 2002, **100**, 3545; (h) J. A. Coxon and M. Molski, *Spectrochim. Acta A*, 2003, **59**, 13; (i) J. A. Coxon and M. Molski, *J. Mol. Spectrosc.*, 2004, **223**, 51.

[14] (a) S. P. A. Sauer and J. F. Ogilvie, *J. Phys. Chem.*, 1994, **98**, 8617; (b) J. F. Ogilvie, J. Oddershede and S. P. A. Sauer, *Chem. Phys. Lett.*, 1994, **228**, 183.

[15] J. F. Ogilvie, S.-L. Cheah, Y.-P. Lee and S. P. A. Sauer, *Theor. Chem. Acc.*, 2002, **108**, 85.

[16] (a) G. C. Wick, *Z. Phys.*, 1933, **85**, 25; (b) G. C. Wick, *Nuovo Cimento*, 1933, **10**, 118.

[17] G. C. Wick, *Phys. Rev.*, 1948, **73**, 51.

[18] J. R. Eshbach and M. W. P. Strandberg, *Phys. Rev.*, 1952, **85**, 24.

[19] (a) H. Brooks, *Phys. Rev.*, 1941, **59**, 925; (b) C. K. Jen, *Phys. Rev.*, 1951, **81**, 197; (c) N. F. Ramsey, *Phys. Rev.*, 1952, **87**, 1075; (d) C. H. Townes, G. C. Dousmanis, R. L. White and R. F. Schwarz, *Discuss. Faraday Soc.*, 1955, **19**, 56; (e) I. Espe, *Phys. Rev.*, 1956, **103**, 1254; (f) J. W. Cederberg and N. F. Ramsey, *Phys. Rev. A*, 1964, **135**, 39.

[20] (a) R. M. Stevens, R. M. Pitzer and W. N. Lipscomb, *J. Chem. Phys.*, 1963, **38**, 550; (b) R. A. Brooks, C. H. Anderson and N. F. Ramsey, *Phys. Rev. A*, 1964, **136**, 62; (c) R. M. Stevens and W. N. Lipscomb, *J. Chem. Phys.*, 1964, **40**, 2238; (d) R. M. Stevens and W. N. Lipscomb, *J. Chem. Phys.*, 1964, **41**, 184; (e) R. M. Stevens and W. N. Lipscomb, *J. Chem. Phys.*, 1964,

41, 3710; (f) R. M. Stevens and W. N. Lipscomb, *J. Chem. Phys.*, 1965, **42**, 3666; (g) R. M. Stevens and W. N. Lipscomb, *J. Chem. Phys.*, 1965, **42**, 4302; (h) R. A. Hegstrom and W. N. Lipscomb, *J. Chem. Phys.*, 1966, **45**, 2378; (i) R. A. Hegstrom and W. N. Lipscomb, *J. Chem. Phys.*, 1968, **48**, 809; (j) R. M. Stevens and M. Karplus, *J. Chem. Phys.*, 1968, **49**, 1094; (k) E. A. Laws, R. M. Stevens and W. N. Lipscomb, *J. Chem. Phys.*, 1971, **54**, 4269; (l) W. N. Lipscomb, *MTP Int. Rev. Sci. Phys. Chem.*, 1972, **1**, 167.

[21] J. Oddershede and J. R. Sabin, *Chem. Phys.*, 1988, **122**, 291.

[22] S. P. A. Sauer, V. Špirko and J. Oddershede, *Chem. Phys.*, 1991, **153**, 189.

[23] (a) J. Oddershede, P. Jørgensen and N. H. F. Beebe, *Chem. Phys.*, 1977, **25**, 451; (b) J. Oddershede, P. Jørgensen and N. H. F. Beebe, *Int. J. Quantum Chem.*, 1977, **12**, 655; (c) G. H. F. Diercksen, N. E. Grüner and J. Oddershede, *Comput. Phys. Commun.*, 1983, **30**, 349; (d) J. Geertsen and J. Oddershede, *Chem. Phys.*, 1984, **90**, 301; (e) M. J. Packer, E. K. Dalskov, T. Enevoldsen, H. J. Aa. Jensen and J. Oddershede, *J. Chem. Phys.*, 1996, **105**, 5886; (f) T. Enevoldsen, J. Oddershede and S. P. A. Sauer, *Theor. Chem. Acc.*, 1998, **100**, 275; (g) K. L. Bak, H. Koch, J. Oddershede, O. Christiansen and S. P. A. Sauer, *J. Chem. Phys.*, 2000, **112**, 4173.

[24] E. S. Nielsen, P. Jørgensen and J. Oddershede, *J. Chem. Phys.*, 1980, **73**, 6238.

[25] J. Oddershede, P. Jørgensen and D. L. Yeager, *Comput. Phys. Rep.*, 1984, **2**, 33.

[26] S. P. A. Sauer, V. Špirko, I. Paidarová and J. Oddershede, *Chem. Phys.*, 1994, **184**, 1.

[27] (a) J. Geertsen and G. E. Scuseria, *J. Chem. Phys.*, 1989, **90**, 6486; (b) S. P. A. Sauer, J. Oddershede and J. Geertsen, *Mol. Phys.*, 1992, **76**, 445.

[28] S. P. A. Sauer, *Chem. Phys. Lett.*, 1996, **260**, 271.

[29] S. M. Cybulski and D. M. Bishop, *J. Chem. Phys.*, 1994, **100**, 2019.

[30] S. M. Cybulski and D. M. Bishop, *J. Chem. Phys.*, 1997, **106**, 4082.

[31] P.-O. Åstrand, K. Ruud, K. V. Mikkelsen and T. Helgaker, *Mol. Phys.*, 1997, **92**, 89.

[32] K. Ruud, T. Helgaker and P. Jørgensen, *J. Chem. Phys.*, 1997, **107**, 10599.

[33] K. Ruud, J. Vaara, J. Lounila and T. Helgaker, *Chem. Phys. Lett.*, 1998, **297**, 467.

[34] P.-O. Åstrand, K. Ruud, K. V. Mikkelsen and T. Helgaker, *J. Chem. Phys.*, 1999, **110**, 9463.

[35] K. Ruud, P.-O. Åstrand and P. R. Taylor, *J. Chem. Phys.*, 2000, **112**, 2668.

[36] C. E. Mohn, J. D. Wilson, O. B. Lutnæs, T. Helgaker and K. Ruud, *Adv. Quantum Chem.* (in press).

[37] (a) K. Ruud, P.-O. Åstrand, T. Helgaker and K. V. Mikkelsen, *J. Mol. Struct. (THEOCHEM)*, 1996, **388**, 231; (b) P.-O. Åstrand, K. Ruud, K. V. Mikkelsen and T. Helgaker, *Chem. Phys. Lett.*, 1997, **271**, 163.

[38] K. L. Bak, S. P. A. Sauer, J. Oddershede and J. F. Ogilvie, *Phys. Chem. Chem. Phys.* 2005, DOI.10.1039/B500992H.

[39] P. J. Wilson, R. D. Amos and N. C. Handy, *J. Mol. Struct. (THEOCHEM)*, 2000, **506**, 335.

[40] S. P. A. Sauer, *J. Phys. B: At. Mol. Opt. Phys.*, 1997, **30**, 3773.

[41] (a) R. Frisch and O. Stern, *Z. Phys.*, 1933, **85**, 4; (b) E. U. Condon, *Phys. Rev.*, 1927, **30**, 781.

[42] N. F. Ramsey, *Phys. Rev.*, 1940, **58**, 226.

[43] S. P. A. Sauer and M. J. Packer, in *Computational Molecular Spectroscopy* (eds P. R. Bunker and P. Jensen), Wiley, London, 2000, pp. 221, Chap. 7.

[44] (a) J. Geertsen, *J. Chem. Phys.*, 1989, **90**, 4892; (b) J. Geertsen, *Chem. Phys. Lett.*, 1991, **179**, 479; (c) P. Lazzeretti, M. Malagoli and R. Zanasi, *Chem. Phys. Lett.*, 1994, **220**, 299; (d) S. P. A. Sauer, *J. Chem. Phys.*, 1993, **98**, 9220; (e) A. Ligabue, S. P. A. Sauer and P. Lazzeretti, *J. Chem. Phys.*, 2003, **118**, 6830.

[45] (a) S. P. A. Sauer and J. Oddershede, in *Nuclear Magnetic Shieldings and Molecular Structure* (ed. J. A. Tossel), Kluwer, Amsterdam, 1993, pp. 351; (b) S. P. A. Sauer, I. Paidarová and J. Oddershede, *Mol. Phys.,* 1994, **81**, 87; (c) S. P. A. Sauer, I. Paidarová and J. Oddershede, *Theor. Chim. Acta* 1994, **88**, 351.

[46] P. Jørgensen and J. Simons, *Second Quantization-Based Methods in Quantum Chemistry*, Academic Press, New York, 1981.

[47] B. T. Pickup and O. Goscinski, *Mol. Phys.*, 1973, **26**, 1013.

[48] J. Olsen and P. Jørgensen, *J. Chem. Phys.*, 1985, **82**, 3235.

[49] (a) A. D. McLachlan and M. A. Ball, *Rev. Mod. Phys.*, 1964, **36**, 844; (b) D. J. Rowe, *Rev. Mod. Phys.*, 1968, **40**, 153.

[50] H. W. Peng, *Proc. Roy. Soc. London A*, 1941, **178**, 499.

[51] T. Helgaker, P. Jørgensen and J. Olsen, *Molecular Electronic Structure Theory*, Wiley, Chichester, 2000.

[52] (a) C. Møller and M. S. Plesset, *Phys. Rev.*, 1934, **46**, 618; (b) J. A. Pople, J. S. Binkley and R. Seeger, *Int. J. Quantum Chem. Symp.*, 1976, **10**, 1.

[53] (a) J. Geertsen and J. Oddershede, *J. Chem. Phys.*, 1986, **85**, 2112; (b) J. Geertsen, S. Eriksen and J. Oddershede, *Adv. Quantum Chem.*, 1991, **22**, 167.

[54] D. L. Yeager and P. Jørgensen, *Chem. Phys. Lett.*, 1979, **65**, 77.

[55] (a) J. Gauss, *Chem. Phys. Lett.*, 1992, **191**, 614; (b) J. Gauss, *J. Chem. Phys.*, 1993, **99**, 3629; (c) J. Gauss, *Chem. Phys. Lett.*, 1994, **229**, 198; (d) J. Gauss and J. F. Stanton, *J. Chem. Phys.*, 1995, **103**, 3561; (e) J. Gauss and J. F. Stanton, *J. Chem. Phys.*, 1995, **102**, 251.

[56] (a) S. M. Cybulski and D. M. Bishop, *Mol. Phys.*, 1992, **76**, 1289; (b) S. M. Cybulski and D. M. Bishop, *Int. J. Quantum Chem.*, 1994, **49**, 371.

[57] T. Helgaker, H. J. Aa. Jensen, P. Jørgensen, J. Olsen, K. Ruud, H. Ågren, A. A. Auer, K. L. Bak, V. Bakken, O. Christiansen, S. Coriani, P. Dahle, E. K. Dalskov, T. Enevoldsen, B. Fernandez, C. Hättig, A. Hald, K. Halkier, H. Heiberg, H. Hettema, D. Jonsson, S. Kirpekar, R. Kobayashi, H. Koch, K. V. Mikkelsen, P. Norman, M. J. Packer, T. B. Pedersen, T. A. Ruden, A. Sanchez, T. Saue, S. P. A. Sauer, B. Schimmelpfennig, K. O. Sylvester-Hvid, P. R. Taylor and O. Vahtras, DALTON, an electronic structure program, Release 1.2, http://www.kjemi.uio.no/software/dalton/dalton.html, 2001.

[58] J. F. Stanton, J. Gauss, J. D. Watts, W. J. Lauderdale and R. J. Bartlett, ACES II, an ab initio program system. The package also contains modified versions of the MOLECULE Gaussian integral program of J. Almlöf and P. R. Taylor, the ABACUS integral derivative program written by T. Helgaker, H. J. Aa. Jensen, P. Jørgensen and P. R. Taylor, and the PROPS property integral code of P. R. Taylor.

[59] J. F. Stanton, J. Gauss, J. D. Watts, W. J. Lauderdale and R. J. Bartlett, *Int. J. Quantum Chem. Symp.*, 1992, **26**, 879.

[60] T. Helgaker and P. Jørgensen, *J. Chem. Phys.*, 1991, **95**, 2595.

[61] J. Gauss, K. Ruud and T. Helgaker, *J. Chem. Phys.*, 1996, **105**, 2804.

[62] F. B. van Duijneveldt, *IBM Tech. Rep.*, 1971, **RJ945**.

[63] T. H. Dunning Jr., *J. Chem. Phys.*, 1989, **90**, 1007.

[64] (a) R. A. Kendall, T. H. Dunning and R. J. Harrison, *J. Chem. Phys.*, 1992, **96**, 6796; (b) D. E. Woon and T. H. Dunning Jr., *J. Chem. Phys.*, 1994, **100**, 2975.

[65] K. P. Huber and G. Herzberg, *Molecular Spectra and Molecular Structure IV. Constants of Diatomic Molecules*, Van Nostrand Reinhold, New York, 1979.

[66] G. Herzberg, *Molecular Spectra and Molecular Structure III. Electronic Spectra and Electronic Structure of Polyatomic Molecules*, Van Nostrand Reinhold, New York, 1966.

[67] D. L. Gray and A. G. Robiette, *Mol. Phys.*, 1979, **37**, 1901.

[68] B. O. Roos, in *Ab Initio Methods in Quantum Chemistry – II. Advances in Chemical Physics* (ed. K. P. Lawley), Wiley, Chichester, 1987, pp. 399, Chap. 69.

[69] J. Olsen, B. O. Roos, P. Jørgensen and H. J. Aa. Jensen, *J. Chem. Phys.*, 1988, **89**, 2185.

[70] A. Rizzo, T. Helgaker, K. Ruud, A. Barszczewicz, M. Jaszuński and P. Jørgensen, *J. Chem. Phys.*, 1995, **102**, 8953.

[71] H. J. Aa. Jensen, P. Jørgensen, H. Ågren and J. Olsen, *J. Chem. Phys.*, 1988, **88**, 3834; H. J. Aa. Jensen, P. Jørgensen, H. Ågren and J. Olsen, *J. Chem. Phys.*, 1988, **89**, 5354.

[72] S. M. Bass, R. L. DeLeon and J. S. Muenter, *J. Chem. Phys.*, 1987, **86**, 4305.

[73] J. Verhoeven and A. Dymanus, *J. Chem. Phys.*, 1970, **52**, 3222.

[74] W. Hüttner, U. E. Frank, W. Majer, K. Mayer and V. Špirko, *Mol. Phys.*, 1988, **64**, 1233.

[75] I. Ozier, S. S. Lee and N. F. Ramsey, *J. Chem. Phys.*, 1976, **65**, 3985.

Subject Index